POLY(IONIC LIQUID)S: SYNTHESIS, STIMULI-RESPONSIVE PROPERTIES AND THEIR MATERIAL APPLICATIONS

Thesis submitted for the degree of

Doctor of Philosophy (Science)

of

JADAVPUR UNIVERSITY

2022

By

PALASH BANERJEE

SCHOOL OF CHEMICAL SCIENCES

INDIAN ASSOCIATION FOR THE CULTIVATION OF SCIENCE

JADAVPUR, KOLKATA-700032, INDIA

Indian Association for the Cultivation of Science

2A & 2B Raja S. C. Mullick Road, Jadavpur, Kolkata 700032, INDIA

Prof. Tarun K. Mandal
Sr. Professor
School of Chemical Sciences

CERTIFICATE FROM THE SUPERVISOR

This is to certify that this thesis entitled **"POLY(IONIC LIQUID)S: SYNTHESIS, STIMULI-RESPONSIVE PROPERTIES AND THEIR MATERIAL APPLICATIONS"** submitted by **PALASH BANERJEE**, who got his name registered on **10th September, 2018** for the award of **Ph.D. (Science) degree** of **Jadavpur University**, is absolutely based upon his own work under the supervision of **Prof. Tarun Kumar Mandal** and that neither this thesis nor any part of it has been submitted for either any degree/diploma or any other academic award anywhere before.

Tarun Kumar Mandal

Signature of the Supervisor

Date with official seal 17/10/2022

Dr. Tarun K. Mandal
Senior Professor
School of Chemical Sciences
Indian Association for the Cultivation of Science
Jadavpur, Kolkata - 700 032

Phone: +91-33-2473 4971 (Ext. 1562) **Fax: +91-33-2473 2805**
E-mail: psutkm@iacs.res.in

Dedicated

To

My Beloved Parents and All My Family Members…..

PREFACE

The present thesis embodies the obtained results of my research works towards the designing and synthesis of ionic liquids, ionic liquid monomers and poly (ionic liquid)s bearing different functional moieties and investigation of their stimuli-responsive behaviors in solution. I have mainly used conventional free radical and reversible addition-fragmentation chain transfer polymerization techniques to polymerize the ionic liquid monomers and also copolymerized these monomers with other conventional non-ionic monomers to synthesize various new poly(ionic liquid)-based copolymers. I then thoroughly examined the phase transition behavior of the synthesized polymers in aqueous and non-aqueous medium in response to two different external stimuli, temperature, and ion; and also investigated their stimuli responsive nanostructure formation. Further, I have also studied ionic conductivity and relaxation behaviors of several poly (ionic liquid)-based copolymers and investigated their potential applicabilities to be used as solid-state polymer electrolytes. Regarding other applications, I have demonstrated the capabilities of ionic liquids and poly(ionic liquid)s to be utilized as efficient photoinitiators for polymerization of different vinyl monomers in aqueous medium. Further I have shown the applicabilities of various ionic liquid-crosslinked polyionic hydrogels towards the removal of several charged organic dyes from aqueous media. The whole research work has been conducted at the School of Chemical Sciences, Indian Association for the Cultivation of Science, Jadavpur, Kolkata. I would like to express my sincere gratefulness to my advisor and mentor, Prof. Tarun Kumar Mandal, for his continuous encouragement, endless support, valuable ideas, freedom to work and help throughout my graduate career. It would have been really impossible to reach thus far without his tireless effort, invaluable guidance, and constant inspiration in this entire journey of my research work.

I would like to express my immense gratitude to Department of Science and Technology (DST), Govt. of India for providing me the financial assistance through DST-INSPIRE Fellowship programme during my research work. I express my deepest gratitude to Indian Association for the Cultivation of Science (IACS), Kolkata, India for providing me the essential fellowship to finish my research work. I would also like to express my sincere gratitude to Prof. Tapas Chakraborty, the Director of IACS; and Prof. Santanu Bhattacharya, Ex. Director

of IACS, Kolkata for giving me the facility of library and laboratory during the course of my research work. I would also like to express my wholehearted sincere thanks to Prof. Aswini Ghosh of School of Physical Sciences, Prof. Arun K. Nandi of School of Material Sciences; and Prof. Sudip Malik and Prof. Suhrit Ghosh of School of Applied and Interdisciplinary Sciences for their valuable suggestions and inspiration.

I am really indebted to Dr. Pulak Pal for his substantial contributions in my research work. Thanks are also to my seniors, Dr. Rama Ranjan Bhattacharjee, Dr. Satyabrata Si, Dr. Atanu Kotal, Dr. Md. Harunar Rashid, Dr. Enakshi Dinda, Dr. Manoj Raula, Dr. Tapas K. Paira, Dr. Sanjib Banerjee, Dr. Mrinmoy Biswas, Dr. Anupam Saha, Dr. Madhab Dule, Dr. Tanmoy Maji, Dr. Somdeb Jana, Dr. Yajnaseni Biswas, Dr. Tamalika Das, Avijit Bose, and Soumyajit Khan for their constant help and valuable guidance. I am tremendously grateful to all my colleagues and young friends, Md. Anas, Priyanka Dinda, Mahuya Kar, Ambuz Basak, Joy Das, Debabrata Kundu, Pratyush Ghosh, Suman Bhowmik, Sreshtha Nayek, Nadira Hassan, Ritobroto Sikdar, Amal Gayen, Rojalin Nayak, Pritha Chakraborty and Soumik Sarkar for their constant help and cooperation which made this long journey successful and memorable. I would also like to express my heartiest thanks to the staff members of School of Chemical sciences for their valuable help and cooperation.

My appreciation and thanks are also to other fellow scholars of IACS Dr. Anurag Mukherjee, Mahuya, Subhra, Anwesha, Puspendu, Avik, Aishik, Soumya, Prashanta, Ayan, and all other friends of IACS for their kind support and help.

Finally, I take this opportunity to express my gratitude to my family for their love, constant encouragement, support and blessing.

School of Chemical Sciences
Indian Association for the Cultivation of Science,
Jadavpur, Kolkata – 700032, India
October, 2022.

Palash Banerjee
17.10.2022
(**PALASH BANERJEE**)

TABLE OF CONTENTS

LIST OF ABBREVIATIONS AND SYMBOLS i

ABSTRACT ix

CHAPTER-1 ***Introduction***

1.1 Ionic liquids (ILs)..... 2

1.1.1 Overview..... 2

1.1.2 Synthetic strategies to ILs..... 4

1.1.2.1 Quaternization 5

1.1.2.2 Exchange of counter ion 7

1.2 Poly(ionic liquid)s (PILs) 10

1.2.1 Overview..... 10

1.2.2 Synthesis of imidazolium and phosphonium-based PILs 14

1.2.2.1 Direct chain growth polymerization of IL monomers 15

1.2.2.1.1 Conventional free radical polymerization (CFRP)..... 16

1.2.2.1.2 Controlled/living radical polymerization (CRP)..... 22

1.2.3 Polymerization of cross-linkable IL monomers..... 27

1.3 Thermo- and ion-responsive PILs 29

1.3.1 Thermoresponsive PILs..... 30

1.3.2 Dual thermo- and ion-responsive PILs..... 39

1.4 PILs as conductive materials..... 41

1.4.1 Background..... 41

1.4.1.1 Solid-state polymer electrolytes..... 41

1.4.1.2 Single-ion conducting polymer electrolytes (SICPEs) 44

1.4.2 Poly (ionic liquid)s as single ion-conducting polymer electrolytes 45

1.4.3 Different factors affecting the bulk ionic conductivity (σ_{dc}) of PILs 48

1.4.4 Mechanism of ion transport and conductivity in PILs 55

1.4.5 Ionic conductivity and polymer chain mobility in PILs 61

1.5. Photoinitiators for aqueous polymerization 65

1.5.1 General aspect 65

1.5.1.1 Photopolymerization 65

1.5.1.2 Free radical photopolymerization 66

1.5.1.3 Free radical photoinitiators 69

1.5.1.4 Water-soluble free radical photoinitiators 73

1.5.1.4.1 Type I photoinitiators for free-radical polymerization 75

1.5.1.4.2 Type II photoinitiators for free-radical polymerization 77

1.5.1.4.3 Two-photon photoinitiators 78

1.5.1.4.4 Ionic liquid-based photoinitiators 80

1.6. Polymeric hydrogels 81

1.6.1 Basic overview 81

1.6.2 Classification of Hydrogels 82

1.6.3 Typical polymerization techniques used for hydrogel synthesis 86

1.6.3.1 Chain-growth polymerization 87

1.6.3.2 Step-growth polymerization 91

1.6.4 Methods of crosslinking for hydrogel fabrication 91

1.6.4.1 Chemical crosslinking 93

1.6.5 Macroporous hydrogels 101

1.6.5.1 Overview 101
1.6.5.2 Classification 102
1.6.5.3 Fabrication of macroporous hydrogels 103
1.6.6 Swelling behaviour of hydrogels 110
1.6.7 Applications of hydrogels 111
1.7 Potential application of ionic liquids and poly(ionic liquid)s 115
1.7.1 Application of theroresponsive ILs/PILs as smart materials 115
1.7.2 Energy harvesting and storage 117
1.7.3 Sorbents and separation 121
1.7.4 Application of porous PILs 122
1.8 Objectives and scope of the present research work 123
1.9 References 127
CHAPTER-2 ***UCST-type phosphonium-based poly(ionic liquid) random copolymers***
2.1 Introduction 164
2.2 Objectives and scope of the present work 167
2.3 Experimental section 169
2.3.1 Materials 169
2.3.2 Synthesis of random PIL copolymers 170
2.3.2.1 Synthesis of P[VBTP][Cl]-*ran*-PMMA (**P1**-**P3**) copolymers 170
2.3.2.2 Synthesis of P[VBTP][Cl]-*ran*-PS (**P4**-**P6**) copolymers 173
2.3.2.3 Synthesis of P[VBTP][Cl]-*ran*-PHEMA (**P7**-**P9**) copolymers 176
2.3.2.4 Synthesis of P[VBTP][Cl]-*ran*-PNIPAM (**P10**-**P13**) copolymers 179
2.3.3 Cloud point measurements 183
2.3.4 Characterization 183
2.4 Results and Discussion 185
2.4.1 Synthesis and characterization of PIL copolymers 185

2.4.2 Thermoresponsiveness of P[VBTP][Cl]-*ran*-PMMA copolymers in MeOH/water 189

2.4.3 Thermoresponsiveness of P[VBTP][Cl]-*ran*-PS copolymers..... 196

2.4.4 Thermoresponsiveness of P[VBTP][Cl]-*ran*-PHEMA copolymers..... 202

2.4.5 Dual thermoresponsiveness of P[VBTP][Cl]-*ran*-PNIPAM copolymers..... 204

2.5 Conclusions 214

2.6 References 215

CHAPTER-3 ***Ion conductance in phosphonium poly(ionic liquid)-based homo- and co-polymers***

3.1 Introduction 222

3.2 Objectives and scope of the present work 224

3.3 Experimental 225

3.3.1 Materials..... 225

3.3.2 Synthesis..... 226

3.3.2.1 Synthesis of different random PIL copolymers 226

3.3.2.1.1 Synthesis of P[VBTP][Cl]-*ran*-PMMA copolymers (**P1**-**P3**) by CFRP technique..... 226

3.3.2.1.2 Preparation of P[VBTP][TFSI]$_{80}$-ran-PMMA$_{20}$ (**P4**) via anion metathesis 227

3.3.2.1.3 Synthesis of P[VBTP][Cl]-*ran*-PMMA copolymers (**P5**-**P7**)via RAFT polymerization technique..... 228

3.3.2.2 Synthesis of P[VBTP][Cl] and PMMA homopolymers 230

3.3.2.3 Preparation of binary polymer blends [[P[VBTP][Cl]/PMMA(20/80) (**P8**) and [P[VBTP][Cl]/PMMA(80/20) (**P9**)]]..... 230

3.3.3 Characterizations..... 230

3.4 Results and Discussion..... 232

3.4.1 Synthesis and characterization of PIL homo- and co-polymers 232
3.4.2 Thermal Properties 241
3.4.3 Dielectric Spectra of PIL Based Systems 245
3.4.4 Analysis of Conductivity Spectra 250
3.4.5 Ionic Conductivity and Relaxation Time 252
3.4.6 Conducting Ion Diffusivity and Number Density 258
3.5 Conclusions 266
3.6 References 267

CHAPTER-4 ***Ionic liquid and poly(ionic liquid) based photoinitiators for aqueous polymerization of vinyl monomers***

4.1 Introduction 274
4.2 Objectives and scope of the present work 275
4.3 Experimental 277
4.3.1 Materials 277
4.3.2 Synthesis 278
4.3.2.1 Synthesis of phosphonium IL-based photoinitiators (PIs) 278
4.3.2.2 Synthesis of imidazolium IL-based photoinitiator (PI) 280
4.3.2.3 Synthesis of PNIPAMs (**P1** and **P2**) via photopolymerization initiated by phosphonium-IL based PIs (**PI-1** and **PI-2**) 282
4.3.2.4 Synthesis of PNIPAM (**P3**) initiated by imidazolium IL-based PI (**PI-3**) 282
4.3.2.5 Synthesis of PDMAEMA (**P4** and **P5**) initiated by phosphonium/ imidazolium IL-based PIs 283

4.3.2.6 Synthesis of poly(triphenyl-4-vinylbenzylphosphonium chloride) (P[VBTP][Cl]) by CFRP 283

4.3.2.7 Synthesis of P[VBTP][Cl]-g-PNIPAM(**P6**)/P[VBTP][Cl]-g-PDMAEMA(**P7**) copolymers 284

4.3.2.8 Synthesis of PNIPAMs (**P′1** and **P′2**) and PDMAEMAs (**P′3** and **P′4**) initiated by conventional radical PIs 285

4.3.3 Characterization 286

4.4 Results and discussion 289

4.5 Conclusions 324

4.6 References 324

CHAPTER-5 ***Ionic liquid cross-linked polyionic hydrogels for removal of anionic dyes***

5.1 Introduction 330

5.2 Objectives and scope of the present work 331

5.3 Experimental section 334

5.3.1 Materials 334

5.3.2 Synthesis of ionic liquid cross-linkers [VIm-4VBC][Cl] and [DMAEMA-4VBC][Cl] 334

5.3.3 Preparation of IL crosslinked hydrogels (CPAam and CPHEMA Hydrogels) 336

5.3.4 Characterization of the IL cross-linkers and hydrogels 338

5.3.5. Swelling experiment 339

5.3.6 Dye adsorption study 339

5.4 Results and Discussion 342

5.4.1 Synthesis and structure characterization of the hydrogels 342

5.4.2 Thermal degradation study 345

5.4.3 Morphological investigation 348

5.4.4 Water swelling abilities and kinetics of absorption by the hydrogels 349
5.4.5 Dye uptake study 355
5.4.6 Adsorption kinetics 357
5.4.7 Adsorption mechanism 366
5.5 Conclusions 372
5.6 References 373
SUMMARY 377
LIST OF PUBLICATIONS 382

LIST OF ABBREVIATIONS AND SYMBOLS

AA	: Acrylic acid
AAm	: Acrylamide
ACN	: Acetonitrile
ACVA	: 4,4′-Azobis(4-cyanovaleric acid)
AEM	: Anion exchange membrane
AFM	: Atomic-force microscopy
$AgBF_4$	: Silver tetrafluoroborate
AgCl	: Silver chloride
$AgNO_3$	: Silver nitrate
A-HA	: Aldehyde hyaluronic acid
AIBN	: 2,2′-azobisisobutyronitrile
AKG	: α-Ketoglutaric acid
AlCl3	: Aluminum chloride
AMPS	: 2-Acrylamido-2-methyl-1-propanesulfonic acid
APS	: Ammonium persulfate
ARS	: Alizarin Red S
ATRP	: Atom transfer radical polymerization
BAPO	: Bisacylphosphine oxide
BCP	: Block copolymer
BDMB	: 2-Benzyl-2-(dimethylamino)-1-(4-morpholinophenyl)-1-butanone
$[BF_4]^-$	: Tetrafluoroborate
BPO	: Benzoyl peroxide
BTPPB	: Benzyltriphenylphosphonium bromide
BuBr	: n-Butyl bromide
[BzTP][Cl]	: Benzyltriphenylphosphonium chloride
CCPH	: Chemically crosslinked polymer hydrogel

CDP	: 4-Cyano-4-[(dodecylsulfanylthiocarbonyl) sulfanyl] pentanoic acid
CFRP	: Conventional radical polymerization
$CF_3SO_3^-$	: Trifluoromethanesulfonate
$(CF_3SO_2)_2N^-$	: Bis(trifluoromethane)sulfonimide
$(CF_3CF_2SO_2)_2N^-$	: Tricyanomethanide
CHT	: Chitosan
ClO_4^-	: Perchlorate
CLPN	: Cross-linked polymeric nano-gel
CMC	: Carboxymethyl cellulose
CMRP	: Cobalt mediated radical polymerization
CNT	: Carbon nanotube
CPAam	: Crosslinked poly(acrylamide)
CPHEMA	: Crosslinked poly(2-hydroxyethyl methacrylate)
CQ	: Camphorquinone
CRP	: Controlled radical polymerization
CSC	: Critical salt concentration
CTA	: Chain transfer agent
D	: Ion diffusivity
$Đ$	: Dispersity
D_h	: Hydrodynamic diameter
DCM	: Dichloromethane
DCTB	:Trans-2-[3-(4-t-butyl-phenyl)-2-methyl-2-propenylidene]malononitrile
DEGDMA	: Diethylene glycol dimethacrylate
DHB	: 2,5-Dihydroxybenzoic acid
DHBC	: Double hydrophilic block copolymer
DLS	: Dynamic light scattering
DMAEMA	: N,N-Dimethylaminoethyl methacrylate

DMBVA : N, N-Dimethylbenzylvinylamine

DMF : N,N-Dimethylformamide

DMOH : 4-Dimethylaminobenzyl alcohol

DMSO : Dimethyl sulfoxide

DP : Degree of polymerization

DRS : Dielectric resonance spectroscopy

DSC : Differential scanning calorimetry

DSSC : Dye-sensitized solar cell

DTG : Derivative thermogravimetry

DTT : Dithiothreitol

DVB : Divinylbenzene

ECA : Ethyl cyanoacrylate

EDL : Electric double-layer

EGDE : Ethyleneglycol diglycidyl ether

EGDMA : Ethyleneglycol dimethacrylate

[EMIm][BF_4] : 1-Ethyl-3-methylimidazolium tetrafluoroborate

EP : Electrode polarization

EPR : Electron paramagnetic resonance

ESI-MS : Electrospray ionisation mass spectrometry

[EtBzTP][Cl] : 4-Ethylbenzyltriphenylphosphonium chloride

[EtBzImBu][Br] : 4-Ethylbenzylimidazolium butyl bromide

EVImBr : 1-Ethyl-3-vinylimidazolium bromide

FESEM : Field emission scanning electron microscopy

FRSP : Free-radical solution polymerization

FTIR : Fourier-transform infrared

HDNPH : Hybrid double network polymer hydrogel

HEMA : Hydroxy ethyl methacrylate

$HFSI^-$: Bis(fluorosulfonyl)imide

HLB : Hydrophilic–lipophilic balance

HRMS : High-resolution mass spectrometry

HRP : Horseradish peroxidase

GMA : Glycerol methacrylate

GPC : Gel permeation chromatography

IC : Ionic content

IL : Ionic liquid

ILM : Ionic liquid monomer

KPS : Potassium persulfate

LAP : Lithium phenyl-2,4,6-trimethylbenzoylphosphinate

LCST : Lower critical solution temperature

$LiClO_4$: Lithium perchlorate

LMB : Lithium metal battery

LRP : Living radical polymerization

M_n : Number average molecular weight

M_p : Peak molecular weight

M_w : Weight average molecular weight

MADIX : Macromolecular design via the interchange of xanthate

MALDI-TOF-MS : Matrix-assisted laser desorption/ionization time-of-flight mass spectrometry

MAPO : Monoacylphosphine oxide

MBA : N,N′-Methylenebisacrylamide

MBS : Sodium 4-[2-(4-morpholino)benzoyl-2-dimethylamino] butylbenzenesulphone

MC : Methylcellulose

MeOH : Methanol

MHG : Macroporous hydrogel

MIPN : Microstructured interpenetrating network

Micro DSC : Micro differential scanning calorimetry

MMA : Methyl methacrylate

MMT : Montmorillonite

MOF : Metal-organic framework

MoS_2 : Molybdenum(IV) sulfide

$MoSe_2$: Molybdenum(IV) selenide

MWCNT : Multiwalled carbon nanotube

MWD : Molecular weight distribution

NfO^- : Nonafluorobutane sulfonate

NIPAM : N-isopropylacrylamide

NMP : Nitroxide-mediated polymerization

NMR : Nuclear magnetic resonance

NP : Nanoparticle

NVP : N-Vinylpyrrolidone

NTf_2^- : Bis(trifluoromethane)sulfonimide

P : Ion number density

PAAc : Poly(acrylic acid)

PAEM : Poly(2-aminoethyl methacrylate)

PAF : Porous aromatic framework

P[BMIM][PF_6] : Poly(1-butyl-3-vinylimidazolium-hexafluorophosphate)

PCA : Poly(crotonic acid)

PCPH : Physical crosslinked polymer hydrogel

PDI : Polydispersity index

PDMAEMA : Poly(N ,N -dimethylaminoethyl methacrylate)

PEG : Polyethylene glycol

PEMA : Poly(ethyl methacrylate)

PEMFC : Proton-exchange membrane fuel cell

PEO : Polyethylene oxide

PF_6^- : Hexafluorophosphate

$PFSI^-$: Bis(pentafluoroethanesulfonyl)imide

PGA : Phenylglyoxylic acid

PHEMA : Poly(2-hydroxyethyl methacrylate)

PI : Photoinitiator

PIA : Poly(itaconic acid)

PIL : Poly(ionic liquid)

PMA : Poly(maleic acid)

PMAA : Poly(methacrylic acid)

PMAAm : Poly(methacrylamide)

PMMA : Poly(methyl methacrylate)

PNAGA : Poly(N-acryloyl glycinamide)

PNIPAM : Poly(N-isopropylacrylamide)

P(OEtOxA) : Poly[oligo(2-ethyl-2-oxazoline)acrylate]

POx : Poly(2-oxazoline)

PS : Polystyrene

PSPP : Poly(3-[N-(3-methacrylamidopropyl)-N,N-dimethyl]ammoniopropane sulfonate)

PSSA : Poly(styrene sulfonic acid)

PTPSS : Poly(4-tetrabutylphosphonium styrene sulfonate)

PUA : Polyurethane acrylate

PUD : Polyurethane dispersion

PVA : Poly(vinyl alcohol)

P[VBTP][Cl] : Poly(triphenyl-4-vinylbenzylphosphonium chloride)

P[VBuIm][Br] : Poly(3-n-butyl-1-vinylimidazolium bromide)

PVDF : Poly (vinylidene fluoride)

PVME : Poly(vinyl methyl ether)

PZIL : Poly(zwitterionic ionic liquid)

RAFT : Reversible addition-fragmentation chain transfer

RBM : Random barrier model

ROMP : Ring opening metathesis polymerization

ROP : Ring opening polymerization

RTIL : Room temperature ionic liquid

Sac^- o-Benzoic sulfimide

SEC : Size exclusion chromatography

SICPE : Single-ion conducting polymer electrolytes

SPE : Solid polymer electrolyte

S_N2 : Bimolecular nucleophilic substitution

SS : 4-Styrenesulfonate

T_{cL} : LCST-type cloud point temperature

T_{cp} : Cloud point temperature

T_{cU} : UCST-type cloud point temperature

T_d : Decomposition temperature

T_g : Glass transition temperature

T_m : Melting temperature

TBAB : Tetrabutylammonium bromide

TBPPS : Tetrabutylphosphonium persulfate

TEM : Transmission electron microscopy

TEMED : Tetramethylethylenediamine

TEMPO : 2,2,6,6-Tetramethyl-1-piperidinyloxy

TETDPPS : Trihexyltetradecylphosphonium persulfate

TfO^- : Trifluoromethanesulfonate

$TFSI^-$: Bis(trifluoromethane)sulfonimide

TGA : Thermo gravimetric analysis

THF : Tetrahydrofuran

TMP : 4-Vinylbenzyltrimethylphosphonium chloride

TPB : Tetrabutylphosphonium bromide

TPO : Diphenyl (2,4,6 trimethylbenzoyl)phosphine oxide

TPP : Triphenylphosphine

TPPO : Triphenylphosphine oxide

UCST : Upper critical solution temperature

ULMP : Unfrozen liquid micro-phase

UPL : Universal power law

UV : Ultraviolet

V-501 : 4,4'-Azobis(4-cyanovaleric acid)

V-70 : 2,2’-Azobis-(2,4-dimethyl-4-methoxyvaleronitrile)

VA-086 : 2,2’-Azobis[2-methyl-N-(2-hydroxyethyl) promionamide]

VIm : Vinylimidazole

[VBTP][Cl] : Triphenyl-4-vinylbenzylphosphonium chloride

[VBuIm][Br] : 1-Vinyl-3-butylimidazolium bromide

([VMIm][I] : 1-Vinyl-3-methyl imidazolium iodide

VPT : Volume phase transition

VFT : Vogel–Fulcher–Tammann (equation)

WAXD : Wide-angle X-ray diffraction

XRD : X-ray diffraction

ZIL : Zwitterionic ionic liquid

ε : Molar extinction coefficient

λ_{max} : Maximum absorption wavelength

μ : Ionic mobility

σ : Ionic conductivity

σ_0 (or σ_{dc}) : DC-ionic conductivity

τ_M : Conductivity relaxation time

τ_s : Structural/segmental relaxation time

ω_H : Hopping frequency

Abstract

In recent years, the development of ionic liquids (ILs) and/or poly(ionic liquid)s (PILs) have enriched some areas in polymer science, material science and materials-engineering. PILs show the unique properties of ionic liquids with the benefits of macromolecular architectures and provide excellent physicochemical properties that are of immense potential for their applications as stimuli-responsive materials, solid electrolytes, dispersant and stabilizer, adsorbent materials, precursor for carbon materials and porous polymers, *etc*.

Thus, the present thesis describes the design and synthesize of new types of ionic liquids (ILs) and/or poly (ionic liquids) (PILs), their stimuli-responsive behaviours and explores the role of macromolecular engineering in the development of novel polymer materials with the desired combination of properties for advanced applications. The main aim of this thesis is to synthesize a series of new stimuli-responsive ionic liquid-based random copolymers of different architectures via RAFT polymerization of an ILM with a variety of hydrophilic or hydrophobic monomers followed by the investigation of these PILs with regards to their stimuli-responsiveness, particularly in solution under different external stimuli such as temperature and ionic strength. This follows by the polymerization of an ionic liquid monomer into nonionic-ionic type random copolymers with varying composition of monomers followed by the investigation of their ionic conductivities as a function of different parameters. Further development of new photoinitiating ILs and PILs along with the detailed study of the photoinitiation mechanism and comparative photoinitiating abilities in aqueous medium are described along with eexploration of PIL as macromolecular photoinitiator towards the development of different types of

thermoresponsive graft copolymers. Finally, new cross-linkable ILMs and their successive use to fabricate hydrogel adsorbents for the removal of dyes are described.

Chapter 1 provides a quick overview on the general aspects of ILs and PILs. This chapter also includes a brief overview of the design and synthesis strategies for different types of ILs, ionic liquid monomers (ILMs) in particular, PILs via conventional free radical or controlled radical polymerization (e.g. RAFT) of ILMs. The different properties of ILs/PILs, particularly in connection with their ionic conductivity and stimuli-responsiveness are described in detail. This section also concentrates on the recent developments on water-soluble photoinitiators and fabrication of polymeric hydrogel adsorbents which are potential for advanced applications. Finally, the chapter ends with precise descriptions of various potential applications of ILs/PILs.

Chapter 2 describes the synthesis of a series of PIL, P[VBTP][Cl]- based random copolymers containing conventional polymer segments namely, P[VBTP][Cl]-ran-PMMA, P[VBTP][Cl]-ran-PS, P[VBTP][Cl]-ran-PHEMA and P[VBTP][Cl]-ran-PNIPAM of varying compositions via RAFT polymerization technique. The incorporation of only a very small percentage of ionic P[VBTP][Cl] segment into these copolymers enable the solubilization of hydrophobic polymer PMMA/PS segments in MeOH/water and hydrophilic PHEMA segment in water regardless of their molecular weights. Further, the copolymeric solutions undergo aggregation resulting in turbidity in the presence of externally added halide ions and experience phase transitions from turbid suspension to transparent solution upon heating, revealing the appearance of UCST-type phase behaviours due to the insertion of PIL (P[VBTP][Cl]) segment. The cloud point of UCST transitions in these copolymers are tunable with respect to various parameters such as content of ionic segment (copolymer composition) as well as

concentrations of added halide anions. On the other hand, P[VBTP][Cl]-ran-PNIPAM copolymers show a composition dependent dual thermo- and ion-responsive phase behaviour. The copolymers with low ionic PIL contents show only inherent LCST behaviour of PNIPAM with tunable cloud points by the addition of varying amount of Cl^- anion. However, the copolymer with moderately high ionic PIL content exhibits both LCST-type behaviour, inherent to PNIPAM segment as well as UCST-type behaviour arising from PIL (P[VBTP][Cl]) segment simultaneously in the presence of halide anion. Overall, the development of a large varieties of dual ion- and thermo-responsive copolymers with tunable cloud point due to introducing the PIL segment with easily available and cheaper conventional polymer segments, opens up the possibility of making varieties of new smart materials towards sensor, drug delivery and other useful applications.

Chapter 3 describes the polymerization of an ionic liquid monomer [VBTP][Cl] with a hydrophobic monomer MMA using both free radical polymerization as well as reversible addition-fragmentation chain-transfer (RAFT) polymerization methods to synthesize a series of ionic-nonionic type random copolymers (namely P[VBTP][Cl]-*ran*-PMMA) comprising of ionic PIL, P[VBTP][Cl] segment and non-ionic PMMA segments. The influence of copolymer compositions, counter anions (Cl^- and $TFSI^-$) and molecular weight as well as physical mixing of copolymer segments on the ion transport and relaxation of these random copolymers are investigated using broadband dielectric spectroscopy followed by analyzing the data using several theoretical models. The free ion diffusivity and ion number density of these random copolymers are obtained by analyzing the contribution of electrode polarization. The temperature dependence of ionic conductivity, relaxation time and ion diffusivity exhibit Vogel-Tammann-Fulcher behavior in these copolymers indicating ion

transport controlled by segmental motion of polymer chains. With increasing ionic content of PIL, the ionic conductivity increases in the random copolymers. P[VBTP][Cl]$_{80}$-*ran*-PMMA$_{20}$ copolymer show the ionic conductivity of 1.95×10^{-7} S cm^{-1} while the neat P[VBTP][Cl] exhibits high ionic conductivity of 1.96×10^{-6} S cm^{-1} at room temperature. In spite of low ionic conductivity, the applicability of PIL copolymers as energy storage materials is higher because of their less moisture sensitivity due to incorporation of hydrophobic PMMA segment. The ionic conductivity decreases due to the introduction of larger counter anion $TFSI^-$ in the place of Cl^- ion in copolymer. Ionic conductivity increases with decreasing molecular weight of the polymers. The random PIL copolymers show a better thermal stability and a faster ion diffusion compared to physically mixing of two homopolymers. In comparison with other reported systems, these PIL copolymers show good thermal stability, less moisture sensitivity and high ionic conductivity which open up new opportunities for making advanced materials for energy storage applications.

Chapter 4 describes a series of phosphonium and imidazolium ionic liquids (ILs) with high water-solubility followed by their utilization as efficient photoinitiators (PIs) for the polymerization of vinyl monomers such as N-isopropylacrylamide (NIPAM) and 2-(dimethylamino)ethyl methacrylate (DMAEMA) upon UV irradiation (λ_{max} = 310 nm) in aqueous medium at ambient temperature and pressure. The photopolymerization proceeds through a free radical pathway systematically established by EPR and ^{1}H-NMR spectroscopy, MALDI-TOF-MS, SEC analysis, and other control experiments. The kinetic study demonstrates that this photopolymerization is fast enough to produce high-molecular-weight polymers with ~70% yield even after 30 mins of UV irradiation. Control experiments show that these IL-based PIs have high water solubility and capability of producing high-molecular-weight polymers compared to those

obtained by other commercially available water-based PIs. Additionally, poly(NIPAM) and poly(DMAEMA) are grafted from the photoactive pendent IL moiety of the poly(ionic liquid), poly(triphenyl-4-vinylbenzylphosphonium chloride) (P[VBTP][Cl]) backbone by the grafting-from copolymerization. The presence of either poly(NIPAM) or poly(DMAEMA) graft segment induces thermoresponsiveness to their P[VBTP][Cl]-based copolymers.

Chapter 5 describes the syntheses of two different types of cross-linkable ionic liquid monomers (ILMs) followed by their utilization as cross-linkers for the fabrication of acrylamide and 2-hydroxyethyl methacrylate-based hydrogels. FTIR and FESEM analyses are utilized to characterize the structures of the hydrogels. Investigation of the thermal stability of the hydrogels by TGA and DTG analyses shows that these hydrogels are thermally stable at high temperature. Swelling performance and diffusion mechanism of water within the hydrogels are investigated and pseudo Fickian mechanism is observed to be operated during transportation of water molecules into the hydrogel network. The introduction of ionic liquid into the hydrogel matrix as cross-linkages results in the incorporation of cationic binding sites which are further utilized to remove hazardous anion dyes from water through electrostatic interaction. The dye adsorption abilities of these hydrogels are investigated using Eosin B and Alizarin Red S as model dyes. The dye adsorption data of representative hydrogels fit well with three kinetic models: pseudo first-order, pseudo-second-order and Elovich kinetic models where pseudo second-order kinetic model gives the best fitting result indicating chemisorption to be the rate controlling step. To explain the dye adsorption mechanism, intra-particle diffusion model is further used which show multi-linearity behaviour confirming that the adsorption occurred through different steps. The intercepts of the intra-particle diffusion plots do not pass through origin indicating intra-particle diffusion is not only the rate

controlling step. Further fitting the experimental data to Boyd kinetic model shows straight lines, which do not pass through the origin, meaning that boundary layer diffusion is involved in the adsorption process and the adsorption system is not solely controlled by intra-particle diffusion. Therefore, neither intra-particle diffusion nor liquid film diffusion is the sole rate-determining step. This indicates that both liquid film diffusion and intra-particle diffusion jointly control the removal of anionic dyes from aqueous solution by the macroporous cationic hydrogels.

Chapter 1

INTRODUCTION

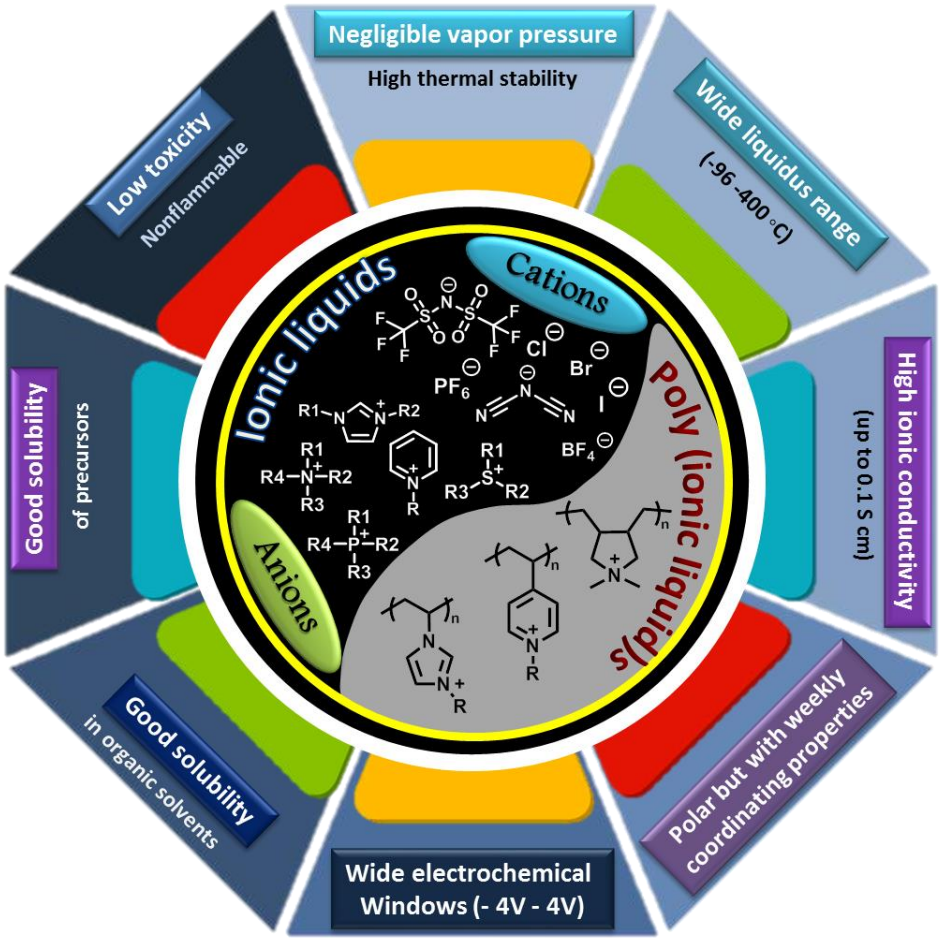

1.1 Ionic Liquids (ILs)

1.1.1 Overview

Ionic liquids (ILs) are generally defined as salts comprising of organic cations and organic /inorganic anions that are liquid at or below some arbitrary temperature, such as 100°C. It should also be noted that this temperature constraint is not always required for a substance to be termed as an IL. The history of ILs started in 1914 with the synthesis of the salt, ethylammonium nitrate ($[EtNH_3][NO_3]$), which is believed to be the first reported IL by Paul Walden and it was synthesized by the neutralization of ethyl amine with concentrated nitric acid and has a melting point of 13-14°C.[1] Though, his paper did not receive much appreciation at that time, IL has drawn great attention in past couple of decades and still remains as a topic of great curiosity even after a century. The reason of having lower melting point of an IL is mainly due to the bulky and unsymmetrical structure of the constituent ions. The large ions weaken the electrostatic interactions and the asymmetric structure lowers the lattice energy leading to lowering the melting points.[2] Cations and anions with different structure can be paired together in different combinations to tailor their thermo-physical properties which can end up with formation of innumerable types of 'task specific' ionic liquids.[3-4] Again by chemically modifying either the cationic or anionic component of an IL, the physical properties (e.g., melting point, viscosity, density, solubility, hydrophobicity etc.) of the IL can easily be fine-tuned.[5] These advantages make ionic liquids an appealing choice of solvent in many important areas such as catalysis,[6] biocatalysis,[7] synthetic chemistry,[8] and electrochemistry.[9] New types of ILs have actively been developed in the last two or three decades and the explorations are going on. Nowadays, ILs are in the cutting-edges of academic and industrial research because of their extraordinary

reactivity, solubility and miscibility properties.[10] Some of the commonly implemented cations and anions in the formation of ILs are shown in Figure 1**.** The electrostatic interaction between the constituent ions of an IL though weaker than that of the normal ionic salts but is still strong enough to give rise to very low vapour pressure under ambient condition. Readily biodegradable imidazolium and pyridinium-based ionic liquids have been developed by introducing ester functional groups which are susceptible to enzymatic hydrolysis.[3, 11] Low vapour pressure, low toxicity, high biodegradability, low bioaccumulation and low environment impact which can be achieved by suitable design and modification of these novel ILs make them as potential candidate for green solvent to replace the conventional volatile organic solvents.[4] Being environment friendly and depending on the nature of the ions, ILs can also act as a versatile solvents as they can dissolve a wide range of polar or nonpolar, organic or inorganic molecules providing new paths to chemical synthesis.[12] The ability of an IL to form a polar and non-polar domain nanostructure determines how other molecules and ions are solvated in these media.[12-13]

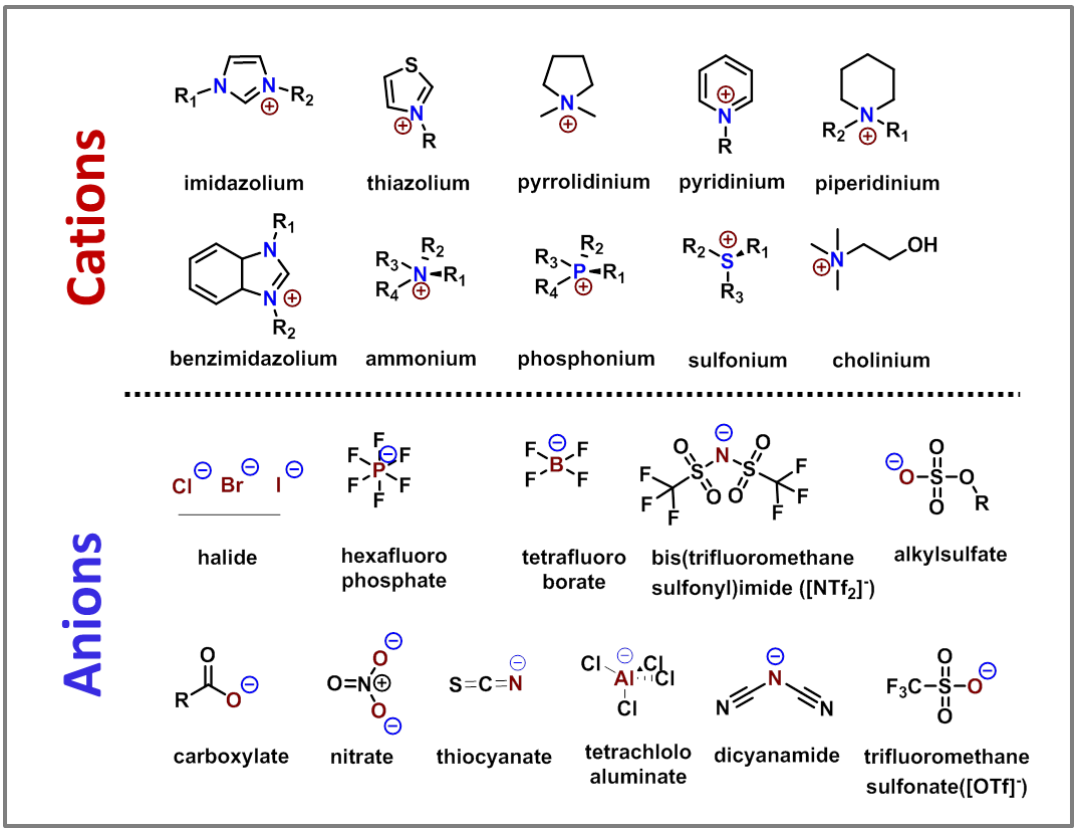

Figure 1. Commonly used cations and anions for the formation of ionic liquids.

1.1.2 Synthetic strategies to ILs

The synthesis of ILs can be simply described by two steps (Figure 2). The first step is the formation of the desired cation by quaternization reaction which occurs through an S_N2 pathway. The second step is anion exchange which is applicable only when the desired anion is not possible to be obtained directly. Now as exemplified in Figure 2, starting from a tertiary amine, NR_3, the desired cation can be easily synthesized either by the protonation of the amine by an acid or through quaternization reaction of the amine with an alkyl halide. Now the anion present in the as-synthesized ammonium halide, $[R'R_3N][X]$, can be further altered in two different ways. First, the halide $[R'R_3N][X]$ can be

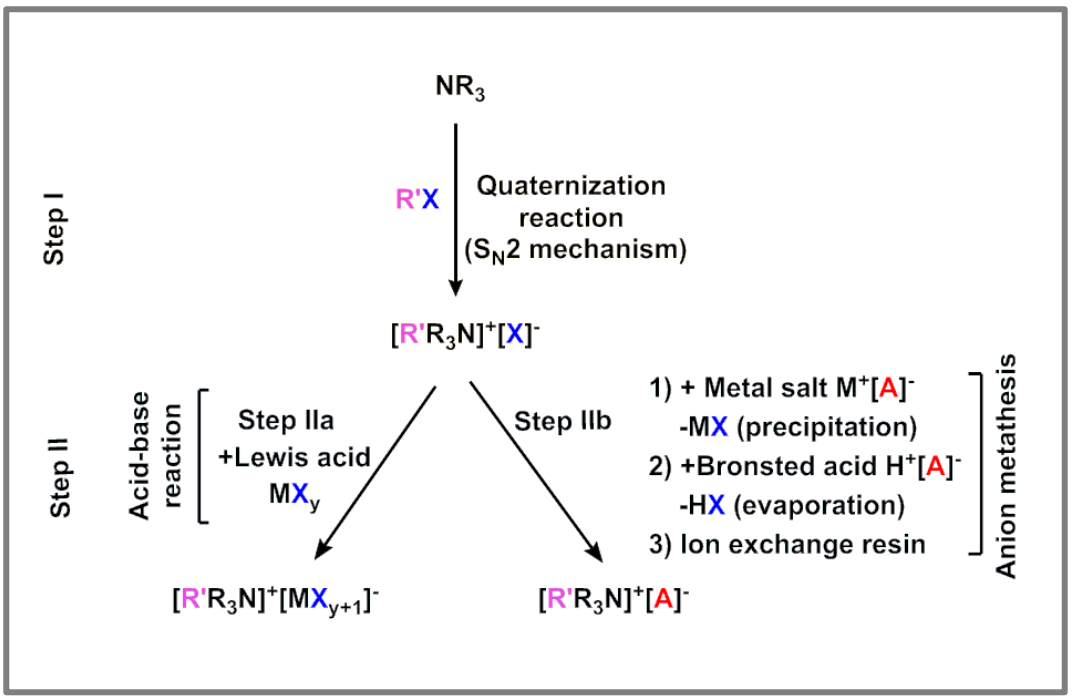

Figure 2. General synthetic pathway for the preparation of ammonium-based ionic liquid.[14]

treated with a Lewis acid MX_y (e.g. $AlCl_3$ for the chloride salt of IL) leading to the formation of an ionic liquid $[R'R_3N][MX_{y+1}]$ through simple Lewis acid-base reaction. Alternatively, anion exchange can also be carried out by anion metathesis. It is to be noted that highly purified starting materials are necessary to be used in each step to produce pure IL, since the presence of impurity can change not only the physical but also the chemical properties of the as-synthesized IL. The synthetic strategies and corresponding steps for the most useful ILs are described in more detail in the following section.

1.1.2.1 Quaternization

ILs are generally prepared by quaternization of heteroatoms for example nitrogen, phosphorous and sulphur of organic compounds through S_N2 mechanism. The direct alkylation of tertiary amines and phosphines, binary

sulphides, pyridine, pyrrolidine,[15] azoles or other quaternizable moieties with alkyl halides or other alkylating agents upon conventional heating[16-17] or microwave[18-19]/ultrasound irradiations[20] can produce various types of ILs. The anions of ILs come from the alkylating agents, for example, halides from alkyl halides, alkyl sulfates from dialkyl sulfates etc. The ILs obtained from this single step quaternization process are called first generation IL. Figure 3 represents the general method used for ionic liquid synthesis involving the alkylation of 1-alkylimidazole with an alkyl halide. This method is advantageous due to availability of low-priced alkyl halide and requirement of moderate reaction temperature. Alkyl fluorides are not used in ionic liquid synthesis due to the presence of strong C-F bonds. Other alkyl halides used in IL synthesis follow the reactivity order as: chloride < bromide < iodide, where alkyl iodides being very reactive should be used in low temperature and high dilution condition to avoid rapid formation of products leading to localized hot-spots formation and runaway reactions.[21] Again alkyl iodides are generally not used because of their photoactive nature which makes difficult in the purification step. However, the reaction time and temperature may vary

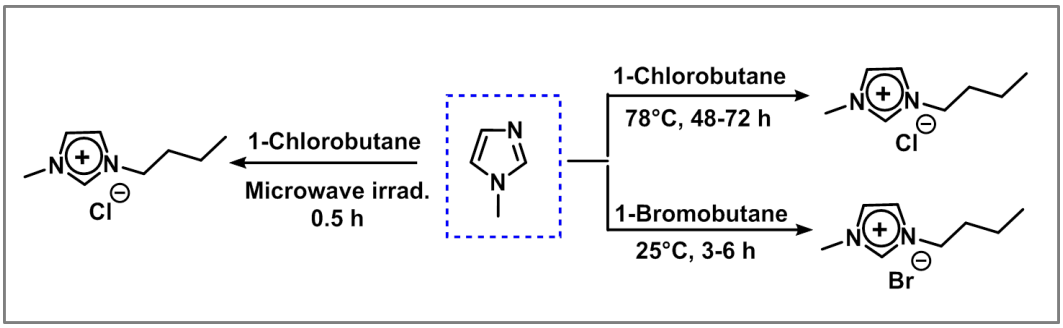

Figure 3. Synthesis of alkyl imidazolium ILs via quaternization reaction.

depending upon the nature of the alkylating agent and/or nucleophilic groups. Again, the reactivity of haloalkane generally decreases with increasing alkyl chain length. Alternative single step routes for halide-free ILs have also been reported

which requires the use of different alkylating reagents for the desired ILs. The halide-free ILs are formed via direct alkylation reaction of phosphine, amine, pyridine, or azole with, e.g., dialkyl sulfates, alkyl nitrate, dialkyl phosphonate, or alkyl triflates producing the corresponding alkyl sulfate, dialkyl phosphonate, or triflate ILs, etc.[22-23]

Solvent-free quaternization reaction can be achieved with the help of microwave (MW) irradiations,[24] or ultrasound[25] and a small excess of 1-haloalkane. Varma et al.[26] reported the first MW-assisted bulk synthesis of several imidazolium-based ILs where the reaction time was only few minutes. The IL that begins to form under MW irradiation increases the polarity of the reaction medium, and consequently the rate of MW absorption. Namboodiri and Varma [25] have also developed an efficient synthetic route for the preparation of ILs using ultrasound as the energy source by simple exposure of the reactant mixtures in a closed container for irradiation using a sonication bath.

However, first-generation ILs are usually hydrophilic and sensitive to air and moisture that restrict their use in many applications. Again, only a limited number of cation-anion combinations are possible to produce ILs by this method. In most of the cases, the quaternization step is followed by an anion exchange to obtain the desired cation-anion combination. The anion exchange procedure has been discussed in the next section.

1.1.2.2 Exchange of counter ion

As already mentioned, the halide-free ILs can be formed by direct alkylation reaction, however, the range of ionic liquids attainable through this route is very limited. Most of the ILs are synthesized in two steps, where an organic halide salt is formed via alkylation of a base by a haloalkane followed by an anion exchange reaction (Figure 4) involving either the direct acid-base reaction of a halide salt

with a strong Lewis acid (HY) like aluminium chloride to form complex anions or the formation of an ionic liquid with a different anion by the addition of a metal salt (MY) to the alkylated halide precursor while precipitating the unwanted ion (called anion metathesis).[27] Exchange of counter ions is also carried out by Brønsted acid and ion exchange resin.

- ***Anion metathesis***

In most of the cases, the syntheses of water and air stable ionic liquids involve a consecutive quaternization-anion metathesis procedure. The first step generates an alkylated halide precursor, which upon treatment with a metal salt having charge-delocalized soft anion (e.g. BF_4^-, PF_6^-, TfO^-, NTf_2^- etc.) or with the free acid of the appropriate anion generates the desired cation-anion combination for its material application, called second generation ILs.[27] The halide ion-containing by-product salts can be separated by extraction or precipitation followed by filtration. Anion-exchanged hydrophobic ILs can be easily separated from the reaction media if the metathesis reaction is carried out in water. However, for water-miscible ionic liquids, the extraction of the desired IL from aqueous media becomes challenging. To overcome this issue, an exchange reaction of the halide anion is usually carried out in the presence of a silver salt of various anions, e.g., dicyanamide, thiocyanate, or tetrafluoroborate.[28-30] Wilkes et al. first reported the air and water stable IL where the anion of 1-ethyl-3-methylimidazolium cation was replaced by anion of silver salts e.g., $AgBF_4$ and $AgNO_3$. Some other examples include IL with tetrafluoroborate anions synthesized in aqueous solution from halide-based IL and $AgBF_4$, precipitating silver halide, or IL with perchlorate anions synthesized from ethylsulfate-based IL and $LiClO_4$, precipitating lithium ethylsulfate in an organic solvent. Generally the group 1 metal, silver, or ammonium salts are mostly used for this metathesis. ILs with thiocyanate, nonafluoro-1-butanesulfonate,

bis((trifluoromethyl)sulfonyl)imide, tris((trifluoromethyl)sulfonyl)methide, trifluoroacetate, heptafluorobutanoate, nitrate, tetrafluoroborate, hexafluorophosphate counter anions have been easily prepared by metathesis reactions.[31-33] It is to be noted that the metathetic exchange of anions often produces halide by-products (MX), which may be difficult to remove by filtration especially for hydrophilic ILs.

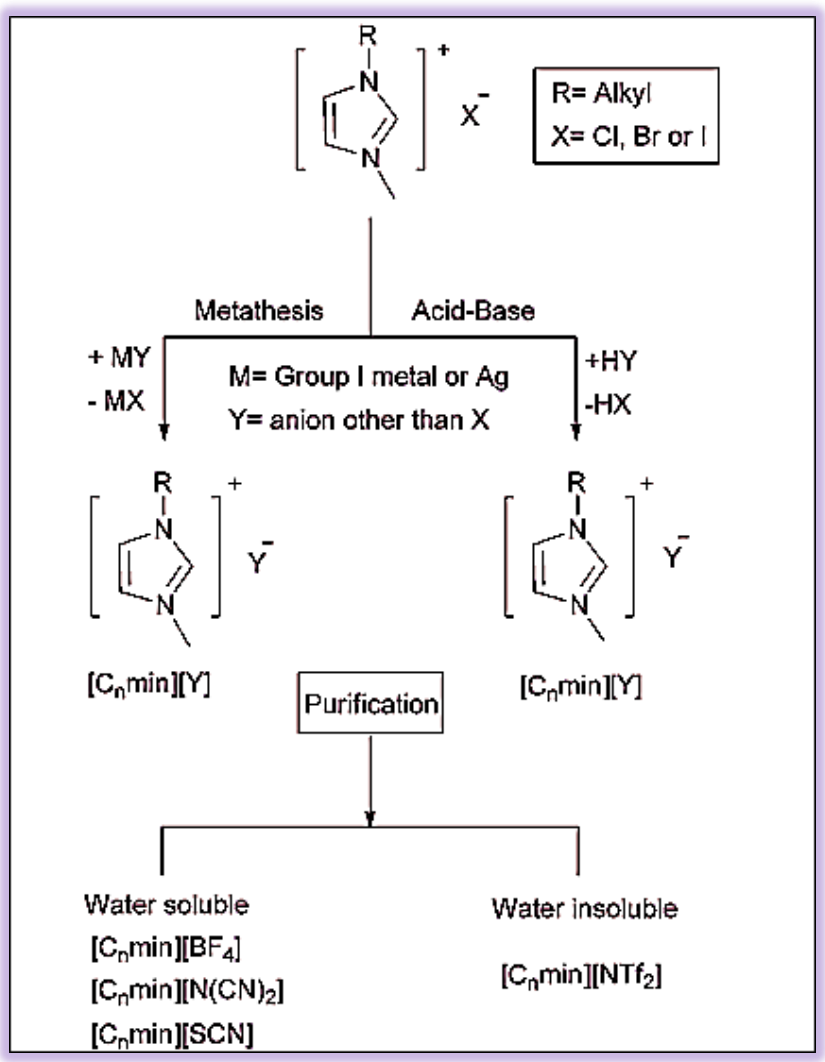

Figure 4. General anion-exchange procedure for the synthesis of imidazolium – based ionic liquids.[27]

1.2 Poly(ionic liquid)s (PILs)

1.2.1 Overview

Polymerized ILs or poly(ionic liquid)s (PILs) are typically considered as a special type of polyelectrolytes which carry an IL species in each of the repeating units (Figure 5).[34] Recently, PILs have received great interest in the fields of polymer chemistry and material sciences, not only because of the combination of the unique properties of ILs with the macromolecular architecture, but also due to generating materials of new properties and functions. Though, the first research on PILs started in 1970s,[35] later Ohno et al.[36] revitalized the field of PILs by designing PIL-based solid electrolytes which were able to replace ILs for electrochemical applications. PILs have several advantages over ILs such as enhanced

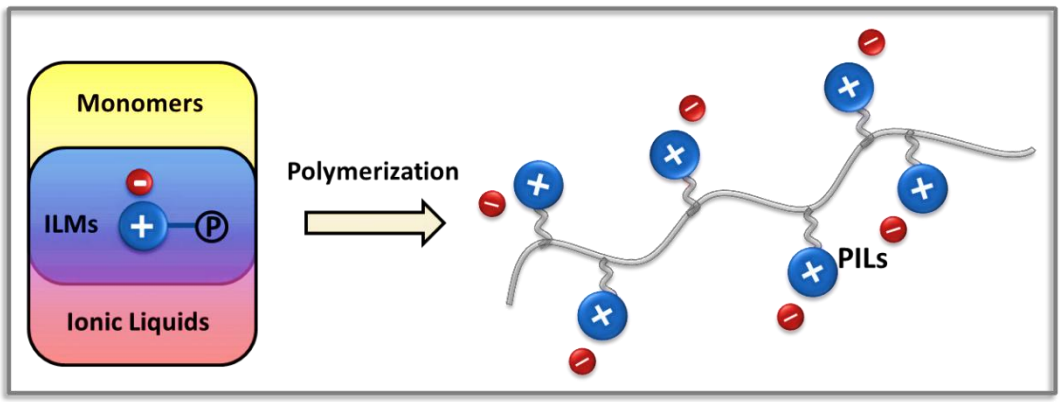

Figure 5. Schematic representation of the relationship between ionic liquid monomers (ILMs) and poly(ionic liquid)s (PILs). Here 'P' represents as 'polymerizable group' such as vinyl or acrylate group.[34]

mechanical stability, improved processability, durability and better control of their meso- to nano-structure. PILs also exhibit unique properties compared to common neutral polymers, such as high ion conductivity, chemical and thermal

stability, and tunable solubility. The structures and properties of PILs can be easily tuned by changing the type of counter-ion.[37-38] For instance, PILs can be tuned from being hydrophilic to hydrophobic via simple counter-ion exchange of a halide ion with $TFSI^-$ or PF_6^-. Mecerreyes et al.[38] reported the synthesis of poly(1-vinyl-3-alkylimidazolium) halides through radical polymerization of the corresponding ILMs and the solubility of the resulting polymers were tuned via anion exchange with excesses of various alkali salts of BF_4^-, PF_6^-, $CF_3SO_3^-$, $(CF_3SO_2)_2N^-$, $(CF_3CF_2SO_2)_2N^-$, and ClO_4^- to produce PILs ranging from hydrophilic to hydrophobic nature. Gnanou and co-workers[39] studied the of self-assembly for PIL block copolymers and examined how the size and shape of the self-assembled aggregates formed in water or organic media can be tuned by either changing the composition of the blocks or by a partial exchange of the counter anion. For instance, anion exchange of Br^- for NTf_2^- turned the solution properties of PIL blocks from hydrophilic to hydrophobic, resulting in their self-assembly into spherical polymeric micelles.

PILs in most cases are amorphous materials mainly due to the mobile nature of the counter anion which makes the crystallization processes difficult. PILs are much less hygroscopic and less fragile than the conventional polyelectrolytes. In spite of having a very high charge density, PILs are generally reported to have a lower and rather broad glass transition temperature (T_g), due to weak electrostatic ion pair interactions.[40] The nature of counter ion influences the T_g of these PILs, and substitution of one mobile ion with an appropriate one through an ion exchange process can result in decrease of T_g. Chen et al.[41] reported a significant reduction in T_g of the as-synthesized PIL-based copolymers by substituting the BF_4^- anion with larger $TFSI^-$ which was attributed to weaker ionic interactions. Tang et al.[42] synthesized a series of imidazolium-based PILs and showed that the anions strongly affected the T_gs of the polymers. The NTf_2^-

and o-benzoic sulphimide (Sac^-) anions substantially lower the T_g of the polymers because they plasticize the bulk polymer**.** Recently a PIL with a T_g of -57 °C was synthesized via free radical polymerization of an acrylate-type IL monomer containing 2-acrylamido-2-methyl-1-propanesulfonate anion and tris(2-[-[2-methoxyethoxy]ethyl)ammonium cation.[43-44] Even though these PILs possessed high charge density, they exhibited a low T_g by structurally shielding the coulombic interactions.

The thermal stability of PILs is also an important property considering their several applications such as (quasi-)solid-state electrolytes for electrochemical devices. PILs with a high thermal stability, ranging from 150°C to more than 400 °C can be achieved by the structural variation of the constituting cations and anions.[45-46] The nature of the PIL typically controls the onset of decomposition temperature (T_d). Aromatic PILs usually possess a higher T_d than PILs with aliphatic backbone structures. PILs with ammonium polycations exhibit lower thermal stability compared to that of imidazolium- and pyrrolidinium-based PILs, but better chemical stability than phosphonium and sulfonium-based PILs. The thermal stability of a PIL increases with the length of substituent in the cation.[47] Ionic conductivity is also an important property of PILs, particularly when applied as solid-state polymer electrolytes in electrochemical devices, which will be discussed in detailed later in the section 1.4.

In PILs, the ionic liquid moieties can be tethered to the polymer chain either as pendant groups (pendant PILs)[48-50] or directly in the polymer backbone (backbone PILs)[51-53] as shown in Figure 6. Although, PILs with pendants are, in general, easier to synthesize, backbone PILs (also termed as 'ionenes') may be synthesized via straightforward step growth polymerization of a diamine with a dibromoalkane and contain cationic charges located within the polymer main-

chain.[54] The huge majority of experimental reports have focused on pendant PILs where the charged group is hanging from the polymer backbone.

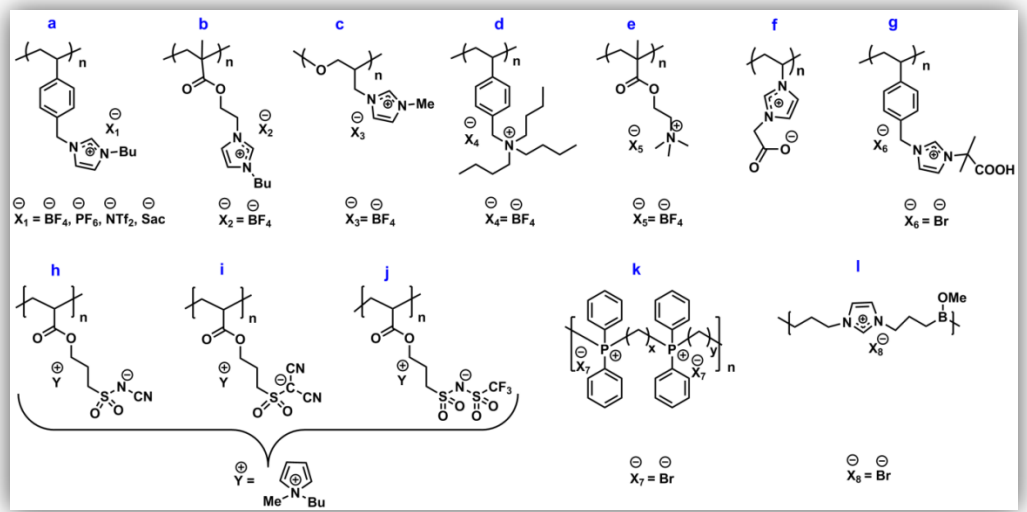

Figure 6. Chemical structures of cationic PILs (a-e), zwitterionic PILs (f-g), anionic PILs (h-j) and ionenes (k-l).[55]

Among the reported pendant PILs found in literatures, major part can be contributed to the PILs composed of polycations and free anion. The cationic PILs are mainly comprised of imidazolium,[38, 56-58] tetraalkyl ammonium,[59-61] phosphonium,[62-63] pyridinium,[59, 64] pyrrolidonium,[65-66] guanidinium,[67-68] and piperidinium[69] cations. The commonly used counter anions used in these PILs include chloride, bromide, iodide, thiocyanate, tetrafluoroborate, hexafluorophosphate and bis(trifluoromethane-sulfonyl)imide.[47, 70] The common polymerizable functional groups that present in a monomer are used to prepare these type of PILs include vinylic,[56, 64] styrenic,[71-72] (meth)acrylic[59-60]etc. On the other hand, the number of anionic PILs is much more limited as compared with cationic PILs. Ohno et al. first reported the synthesis of a new class of PILs with polyanion backbones containing anions such as vinyl carbonate, vinyl

sulphonate, vinyl phosphonate, styrenyl sulphonate, methacryloyl sulphonate etc and free imidazolium cations.[36] The anionic PIL of polystyrene sulfonate with tetrabutyl phosphonium as counter cation has been reported.[73] Apart from these, trifluoromethylsulfoimide (TFSI) PILs with a variety of counter cations including alkali metal cations is one of the few reported anionic PILs.[74-75] Among these different PILs, in this section, the discussion will be mainly focused on the synthesis, properties and application of imidazolium and phosphonium-based PILs. Other type of PIL architectures include crosslinked PIL network composed of polycations and polyanions. IL monomer units can also be covalently linked by an alkyl chain spacer to form various crosslinked PIL networks. Currently, cationic PILs dominate the PIL research. In this chapter, we will mainly discuss PILs consisting of phosphonium and imidazolium cationic units.

1.2.2 Synthesis of imidazolium- and phosphonium-based PILs

The manifold applications of PILs, such as, in solid state polymer electrolytes, electrochemical devices, smart materials, catalysts, porous materials, antibacterial materials etc., require different PIL structures and properties. Standard synthetic routes to PILs depend on three fundamental strategies: (1) direct sequential chain growth polymerization of ILMs, (2) post-modification of existing polymer chains, and (3) step growth polymerization of ILMs (Figure 7). The two synthetic strategies using chain-growth and step-growth mechanisms can be implemented by two different polymerization techniques, such as conventional free radical polymerization (CFRP) [76-78] and "controlled/living" free radical polymerization (reversible addition fragmentation chain transfer (RAFT),[79-81] atom transfer radical polymerization (ATRP),[82-83] cobalt-mediated radical polymerization (CMRP),[84] nitroxide-mediated polymerization(NMP)[85] or ring-opening metathesis polymerization (ROMP)[86]) technique. This chapter briefly covers recent developments, mainly regarding imidazolium- and

phosphonium-based PILs and their copolymers including their synthetic strategies and potential applications. In the next section, the synthetic strategies to imidazolium- and phosphonium-based PIL containing homo- and co-polymers via CFRP and RAFT polymerization technique will be discussed.

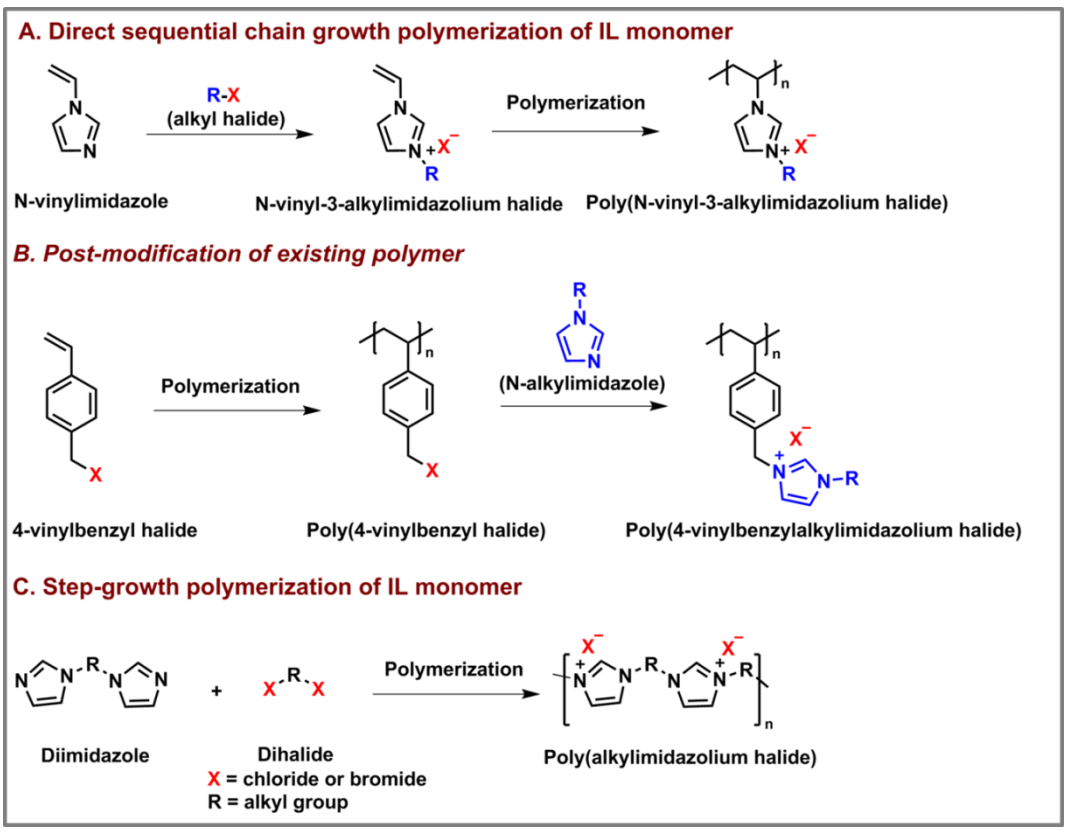

Figure 7. Synthetic strategies for the preparation of PILs considering synthesis of imidazolium-based PILs as examples.

1.2.2.1 Direct chain growth polymerization of IL monomers

An IL monomer (ILM) is an IL in which one or more polymerizable units are present. The polymerization of IL monomers is a conceptually simple and widely adopted strategy to prepare PILs in many research groups. Figure 8 illustrates five basic forms of ILMs. In an IL monomer, a polymerizable unit can be placed either on the cation (Figure 8A) or anion (Figure 8B), depending on the desired

polymeric architecture. The ILM with a polymerizable unit on the cation is so far the dominant form. IL monomers with two polymerizable units separated in the cation and anion (Figure 8C), or located on the cations (Figure 8D and E) have also been reported to build up PIL networks. The chain growth polymerization of an IL monomer results in a homologous polyelectrolyte (homopolymer) possessing the same type of IL moiety in each repeating unit. Copolymerization of an ILM with an ionic or non-ionic co-monomer is also applied to tune the distribution of the IL species along the polymer chain and modify the physical properties of PILs.

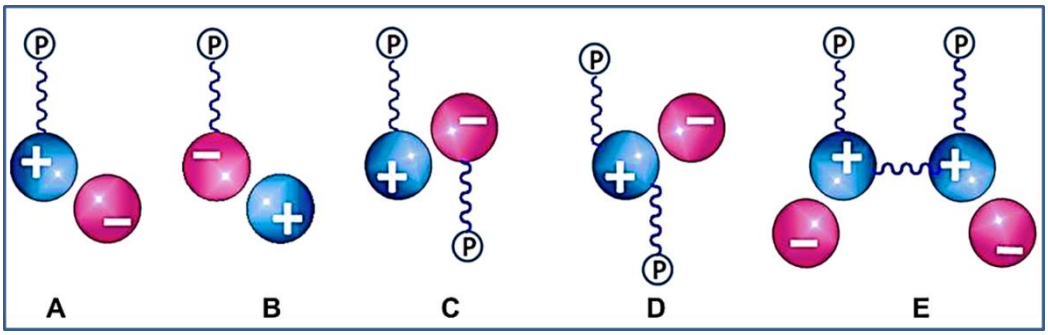

Figure 8. General illustration of the five basic structures of ionic liquid monomers (ILMs) where "P" represents a polymerizable group such as vinyl or acrylate group .[70]

1.2.2.1.1 Conventional free radical polymerization (CFRP)

Ohno and co-workers have devoted their research work on the synthesis of PILs via conventional free radical polymerization (CFRP) since 1900s aiming at a solid ionic conductor. Till date, CFRP is the common polymerization technique for obtaining PILs from the ionic liquid monomers (ILMs). As ILMs are hygroscopic, thus it is hard to polymerize them via conventional ionic polymerization techniques due to presence of moisture. ILMs may contain hard-to-separate impurities which cannot be separated by any means. As ILMs possess negligible

vapour pressure, distillation method cannot be used to separate them from the impurities. These are the main obstacle to polymerize ILMs via ionic polymerization techniques that are highly sensitive to impurities and moisture. This sensitivity is especially valid for hydrophilic ILMs, in which trace amount of moisture coexists even after careful purification. Therefore, the CFRP is the most feasible technique to prepare PILs in which the propagating species are tolerant to impurities and moisture. As disadvantage, the copolymers obtained via CFRP are, in general, heterogeneous with very limited control over the molar mass, constitution, and chain architecture.

ILMs used in CFRP usually contain (meth)acryloyl, styrenic , N-vinylimidazolium or phosphonium groups in the IL cation. Both imidazolium- and phosphonium-based PILs can be prepared by CFRP technique using conventional initiators [e.g. ammonium persulfate (APS), azobisisobutyronitrile (AIBN) or azoinitiators such as 4, 4'-azobis (4-cyanovaleric acid) (V-501) or 2, 2'-azobis(4-methoxy-2.4-dimethyl valeronitrile) (V-70)] either in solution or in bulk phase.[76-78, 87] In the following section, conventional free radical polymerization of imidazolium and phosphonium-based ILMs are introduced in detail.

- ***Polymerization of N-vinylimidazolium-based IL monomer***

Free radical polymerization of the N-vinylimidazolium-based ILMs was achieved by using a thermal initiator. The structural variation of this monomer can be achieved by varying the alkyl chain and the counter anion. Mecerreyes et al.[38] reported the synthesis of 1-vinyl-3-ethylimidazolium and 1-vinyl-3-butylimidazolum halide monomers and carried out their bulk polymerization in chloroform. The solubility characteristics of the polymers were tuned by anion exchange in the presence of excesses of salts (BF_4^-, PF_6^-, $CF_3SO_3^-$, $(CF_3SO_2)_2N^-$, $(CF_3CF_2SO_2)_2N^-$, ClO_4^-) producing polymers that ranged from hydrophilic to

hydrophobic. Ohno et al.[56] reported the synthesis of an imidazolium-based IL monomer with tetrafluoroborate anion by reacting N-vinyl imidazole with tetrafluoroboric acid in a mixture of water and ethanol. The preparation process is simple, generating no side product and can be extended to other acids, such as hexafluorophosphoric acid. Recently, Green et al.[88] reported the synthesis of a series of alkyl-substituted vinylimidazolium homopolymeric PILs with varying lengths of *n*-alkyl substituents and counter ions via a conventional free radical polymerization using AIBN as initiator (Figure 9). The variation of alkyl length and counter

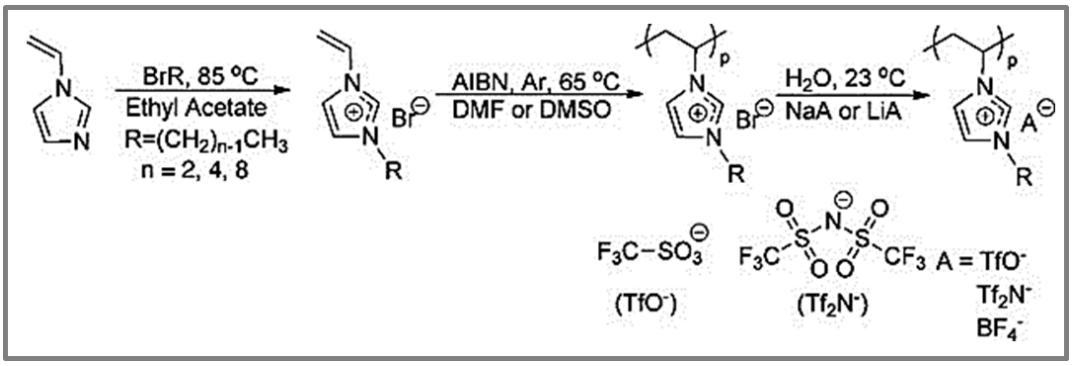

Figure 9. Synthesis and subsequent CFRP of N-vinylimidazolium-based IL monomers followed with anion exchange.[88]

anions provided systematic structural changes, which affected the thermal and ion conductive properties of the PILs. It was observed that longer alkyl chain lengths, ethyl < butyl<octyl decreased the T_g for Br^- and BF_4^- counter anions. On the other hand, for $TfO^-$and Tf_2N^- counter ions, T_g decreased from poly(EVIm-X) to poly(BVIm-X) and increased from poly(BVIM-X) to poly(OVIm-X). Thermal stability decreased with increasing the length of alkyl substituents. Exchanging the Br^-counter anion to BF_4^-, TfO^-, and Tf_2N^- reduced the T_g significantly and increased the thermal stability due to reduced anion basicity. The absolute ionic

conductivity of the PIL samples were analysed which showed an inverse dependence on T_g.

- ***Polymerization of phosphonium-based ILMs***

Phosphonium cation-based ionic liquids (ILs) offer a broad range of useful properties and in some applications offer superior properties as compared to nitrogen cation-based ILs. MacFarlane et al.[89] summarized the history, commercial synthesis, and several enhanced physical properties of phosphonium-based ILs compared to ammonium and imidazolium-based ILs. Phosphonium-based ILs have been much less studied compared but recently researchers have focused on development of phosphonium-containing PILs to examine the impact of cation structure on the macromolecular properties.[89-90] Phosphonium-based PILs have primarily been synthesized by conventional free radical polymerization of IL monomers containing a quaternary phosphonium cation with three attached alkyl chains and a vinylbenzyl polymerizable group, along with an associated free anion. Long et al.[50] performed a detailed study of structure-property relationships for high molecular weight ammonium and phosphonium-based PILs synthesized via conventional free radical polymerization with subsequent anion exchange (Figure 10).They studied the influence of cationic site, alkyl chain length of the substituent, and counter anion on thermal properties, ionic conductivity, and morphology of the as-synthesized PILs. The ammonium and phosphonium PILs showed significantly different thermal properties and ionic conductivities. Phosphonium PILs containing Cl^- counter anions displayed higher thermal stabilities (> 370 °C) compared with ammonium analogs (< 220 °C). Anion exchange with BF_4^-, TfO^-, and Tf_2N^- improved the thermal stability of all the PILs and depressed their T_gs. Moreover, phosphonium-based PILs exhibited only a single-step degradation

profile highlighting the advantageous use of phosphonium-based PILs for high temperature, conductive applications.

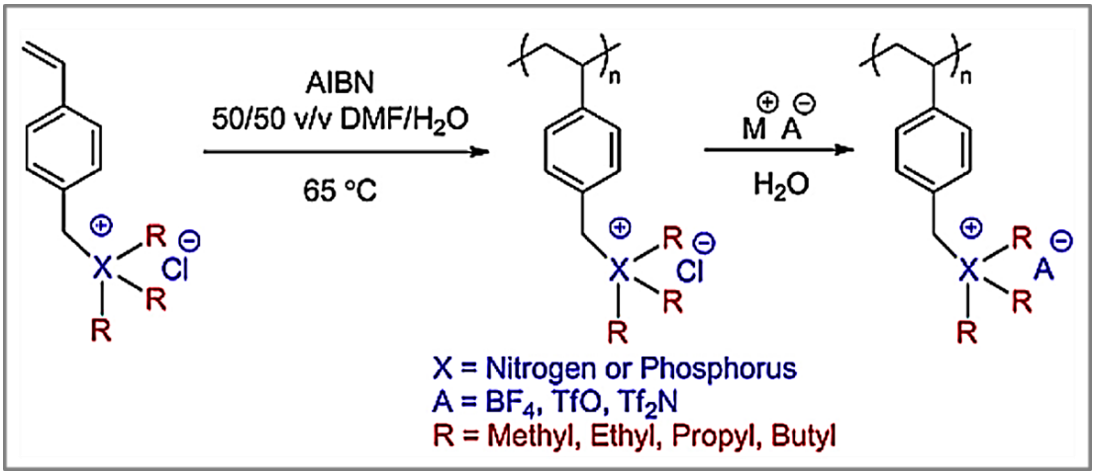

Figure 10. Synthesis of ammonium- and phosphonium-containing PILs using conventional free radical polymerization and anion exchange.[50]

The same group also reported the synthesis of copolymers of n-butyl acrylate and phosphonium ILMs possessing various alkyl substituents and counter anions through a combination of conventional free radical copolymerization using AIBN as the initiator and anion-exchange (Figure 11).[91] They investigated the influence of chemical structure on the thermo-mechanical behaviour of phosphonium-containing random copolymers with n-butyl acrylate bearing Cl^-, BF_4^- and $TFSI^-$ anions. Replacing Cl^- with large size counter ions, such as TFSI, plasticized the polymer and provided liquid-like, viscous behaviour. Additionally, their corresponding scattering peaks in wide-angle X-ray diffraction (WAXD) systematically shifted to lower q region, indicating an increase of ionic domain distance with the length of alkyl substituents.

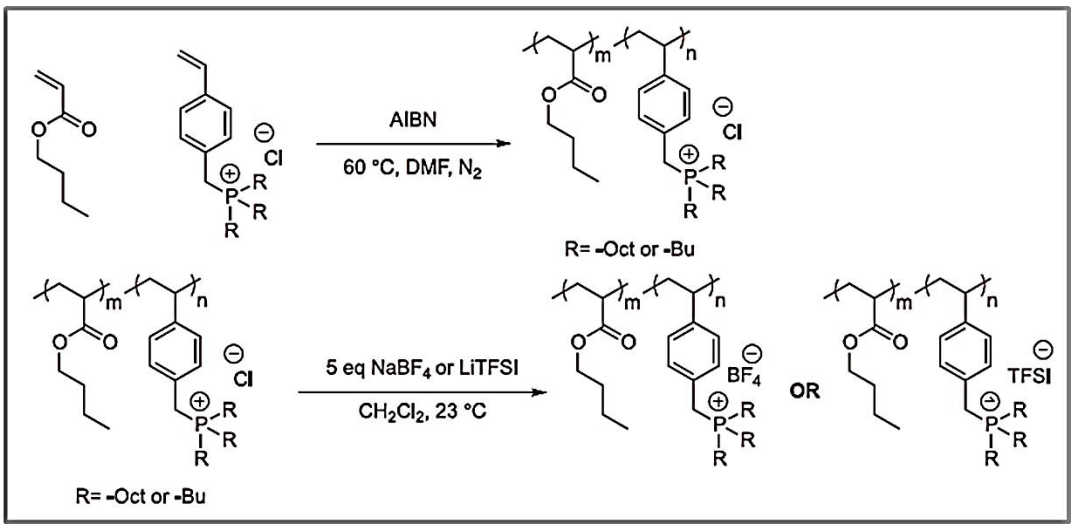

Figure 11. Synthesis of phosphonium-containing random copolymers via conventional free radical polymerization followed by anion-exchange.[91]

Endo and coworkers[92-93] pioneered structure-property analysis of ammonium- and phosphonium-containing polyelectrolytes, synthesized by thermal free radical polymerization, for antimicrobial applications. They reported that phosphonium based PILs exhibited enhanced antimicrobial properties compared to ammonium-based analogs. They also examined ammonium- and phosphonium-based random copolymers and polymer blends.[93] Polymer blends displayed a synergistic bactericidal effect, which resulted in improved efficacy. Random copolymers failed to display any synergistic effect and higher phosphonium concentrations in these copolymers resulted in higher antimicrobial efficacies.

Recently, Cowan et al.[94] reported the synthesis and characterization of PIL membranes, where a homologous series of (tri-n-alkyl)vinylbenzylphosphonium monomers with the bis(trifluoromethylsulfonyl) imide anion were polymerized via conventional free radical photopolymerization using 2-hydroxy-2-methylpropiophenone as radical photoinitiator. The resulting PIL materials (i.e.,

poly([P_{nnnVB}][Tf_2N]) where n= 4, 6, 8) (Figure 12) were further characterized for their single-gas transport properties and ionic conductivity. The gas permeability was found to increase approximately linearly with increasing alkyl chain length on the phosphonium group. The room temperature gas transport performance of phosphonium PIL materials offered advantages over the imidazolium- and ammonium-based PIL materials in terms of their thermal, chemical, and biological resistance.

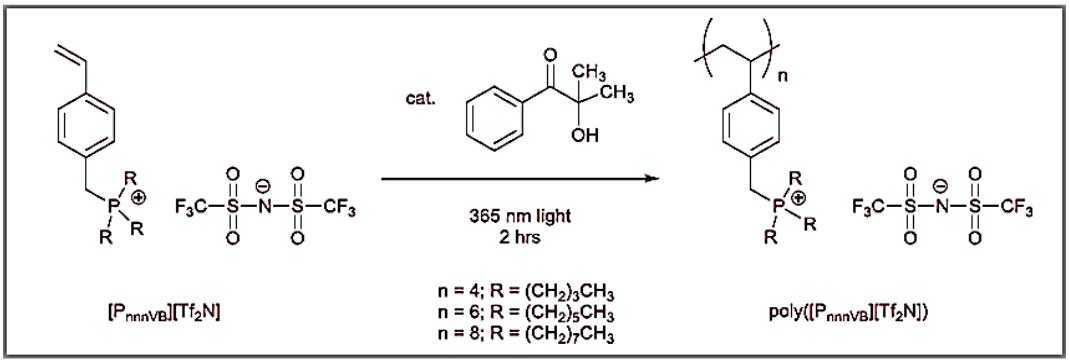

Figure 12. Free radical photopolymerization of neat [P_{nnnVB}][Tf_2N] monomers to form the poly([P_{nnnVB}][Tf_2N]) PILs.[94]

1.2.2.1.2 Controlled/living radical polymerization (CRP)

In order to optimize the performances of PIL–based materials, many efforts have been devoted to prepare PIL chains with predetermined molecular weights, narrow molecular weight distributions and ordered morphologies/architectures. The best possible way to achieve such tailor-made PILs is the polymerization of ILMs via controlled radical polymerization techniques such as ATRP, RAFT, cobalt CMRP, and organotellurium-mediated living radical polymerization (TERP). In the next section RAFT polymerization technique will be discussed in detail.

- ***Reversible addition fragmentation and chain transfer (RAFT) polymerization***

The reversible addition fragmentation chain transfer (RAFT) polymerization process was first reported in 1998 by Chiefari et al.[95] and since then this technique has become one of the most versatile polymerization techniques for the synthesis of complex polymeric architectures of predictable molecular weights with low dispersities (*Đ*s), high end-group accuracy, and ability for further chain growth.[96-98] The mechanism of RAFT polymerization (Figure 13) involves a reversible addition-fragmentation sequence in which the transfer of

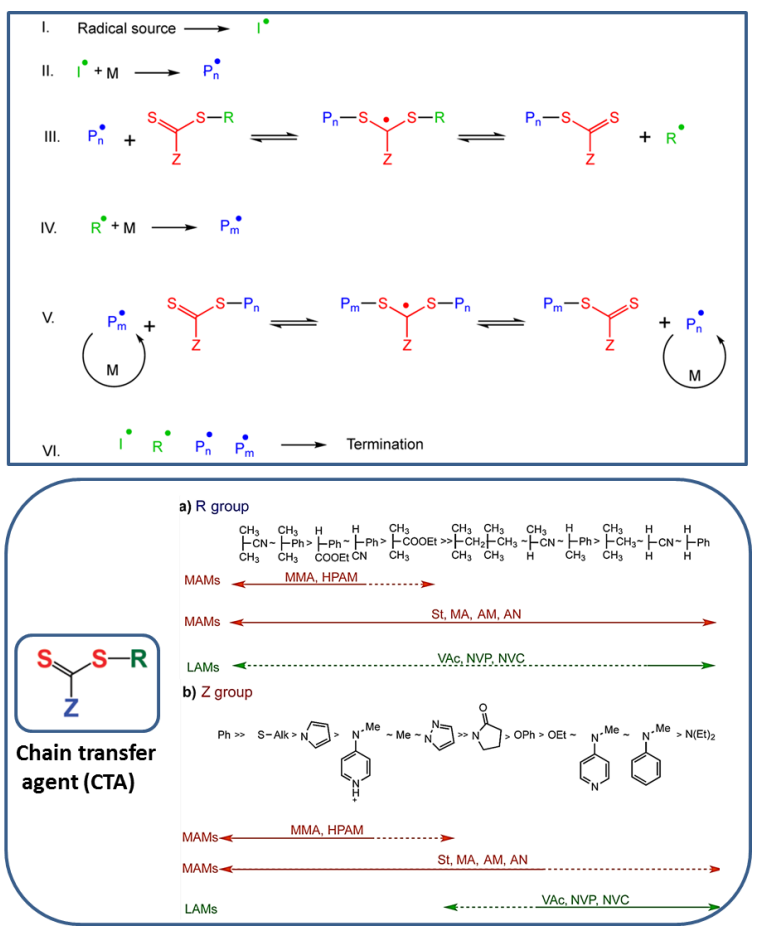

Figure 13. General mechanism of RAFT polymerization (above) and guidelines for selection of RAFT agents (Z-C(=S)S-R) for various polymerizations (below). For 'Z',

addition rates and transfer constants decrease and fragmentation rates increase from left to right. For 'R', fragmentation rates decrease from left to right. A dashed line indicates limited control (e.g., retardation, high dispersity etc.).

the S=C(Z)S- moiety between active and dormant chains is responsible to maintain the living character of the polymerization. Another important feature of the RAFT process is the high tolerance towards different functional monomers. RAFT polymerization is perhaps the most versatile method among the different CRP techniques applied to synthesize ionic polymers. The thiocarbonylthio groups, which play key role in the RAFT process, are surprisingly tolerant to water, if the pH of the reaction medium is below 6 or the reaction temperatures do not exceed 70 ^{o}C. It is to be noted that, RAFT method tolerates acidic conditions very well, but is highly sensitive towards base and other strong nucleophiles bearing a mobile hydrogen atom.[99]Consequently, the polymerization of anionic or acidic monomers and of quaternary ammonium monomers occurs normally without particular problems. However, the monomers with amine groups must be protonated before RAFT polymerization. Besides the functional group tolerance, high monomer-to-polymer conversion is also an important factor in RAFT polymerization of monomers with various functionalities. Taking advantage of the living character of the RAFT process, block copolymers with a PIL segment can be easily achieved.

- ***RAFT polymerization of imidazolium-based ILMs***

RAFT polymerization technique has been extensively used for the synthesis of imidazolium based PIL-homopolymers[100] of controllable molecular weights and the high end group precision of the living end groups affords the preparation of well-defined block copolymers (BCPs), either with ionic or neutral monomers.[39, 98, 101-103]For instance, Vijayakrishna et al. reported the RAFT polymerization of

different imidazolium-based ionic liquid (IL) monomers namely, 3-(1-ethyl imidazolium-3-yl)propylmethacrylamido bromide , 2-(1-methylimidazolium-3-yl)ethyl methacrylate bromide , and 2-(1-ethylimidazolium-3-yl)ethyl methacrylate bromide using 2-cyanopropyl dithiobenzoate or (4-cyanopentanoic acid)-4-dithiobenzoate as chain transfer agents (CTAs).[101] These hydrophilic PILs were further used as macro-CTAs in chain extension experiments acrylamide and methacrylic acid which resulted in synthesis of double hydrophilic block copolymers (DHBCs).N-vinyl imidazolium-based ILMs which can be easily polymerized by conventional free radical methods are often difficult to polymerize in a controlled manner since the generated N-vinyl propagating radicals are highly reactive, due to the lack of resonance stabilization, which ultimately increases the likelihood for chain transfer and chain termination events.[104] Recent progress of RAFT/MADIX (macromolecular design via the interchange of xanthate) process allows the successful synthesis of well-defined PILs by radical polymerization of non-conjugated monomers. Xanthate type CTAs are particularly useful for controlling the radical polymerization of N-vinyl monomers, because xanthate-type CTAs increase the electron density at the radical centre, which increase the fragmentation rate. Mori et al.[105] first demonstrated the synthesis of N-vinyl imidazolium PILs with controlled molecular weights and narrow dispersity (*Đ*) by RAFT/MADIX polymerization of three N-vinylimidazolium-based ILMs. Aqueous RAFT polymerization of hydrophilic narrowly dispersed imidazolium-based poly(ionic liquid)s has also been reported.[100] The resulting PIL macro-RAFT agents were finally used to synthesize well-defined block copolymers of various morphologies.

- ***RAFT polymerization of phosphonium-based ILMs***

RAFT polymerization of phosphonium-based ILMs was first reported by Wang and Lowe.[106-107]The authors carried out RAFT polymerizations of 4-

vinylbenzyl(trimethylphosphonium) chloride and 4-vinylbenzyl(triphenylphosphonium) chloride monomers under aqueous conditions at 80 °C employing 2-(2-carboxy-ethylsulfanylthiocarbonylsulfanyl) propionic acid trithiocarbonate as RAFT-CTA and 4,4′-Azobis(4-cyanovaleric acid) (V-501) as initiator.[106] The RAFT synthesis and aqueous solution properties of AB block copolymers of 4-vinylbenzyltrimethylphosphonium chloride (TMP) and N, N-dimethylbenzylvinylamine (DMBVA) was also reported.[107] The copolymers showed pH-induced self-assembly, resulting in formation of core-shell polymeric micelle-like structures. Recently, our group[108] reported the RAFT polymerization of the triphenyl-4-vinylbenzylphosphonium chloride ([VBTP][Cl]) monomer using 4-Cyano-4-[(dodecylsulfanylthiocarbonyl) sulfanyl]pentanoic acid (CDP) as a chain transfer agent (CTA) in combination with a radical initiator, AIBN at 65 °C (Figure 14).The synthesized cationic poly(ionic liquid), poly(triphenyl-4-vinylbenzylphosphonium chloride)s (P[VBTP][Cl]s) of varying and controllable molecular weights showed double responsiveness(insoluble to soluble) towards halide ions and temperature in aqueous solution.

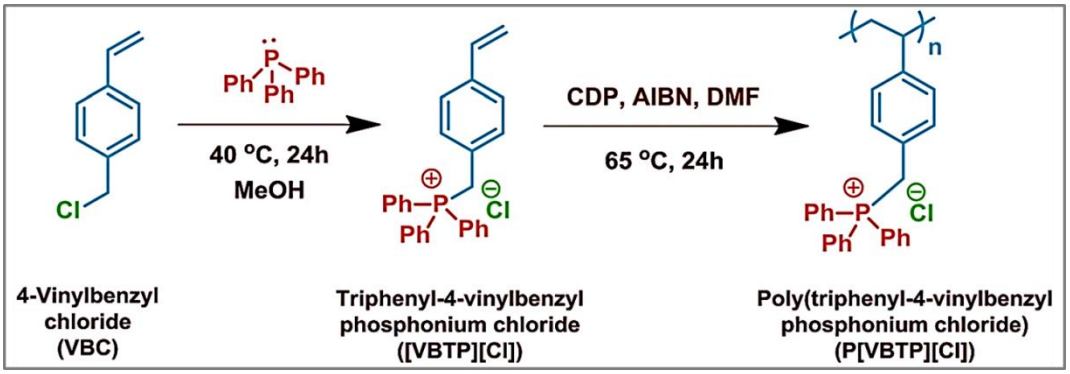

Figure 14. Synthesis of the [VBTP][Cl] monomer and its successive RAFT polymerization to obtain P[VBTP][Cl].[108]

1.2.3. Polymerization of cross-linkable IL monomers

From the structural point of view, ILMs which have two polymerizable groups can act as cross-linkers to prepare PIL networks, which are expected to be more stable than non-crosslinked PIL against moisture and solvents.[70] Such cross-linked PIL networks/nanoparticles can be synthesized via different CFRP techniques. Figure 15 depicted three common types of crosslinkable IL monomers. Ohno et al.[109] reported the introduction of two types of vinyl groups separated on the IL cation and anion via a simple synthetic strategy. In the first step, alkali metal cations of sodium vinylsulfonate and 3-sulfo-propyl acrylate potassium salt were exchanged by protons with the help of cation exchange resin to afford the corresponding acids. In the second step, aqueous solutions of these acids were slowly mixed with equi-molar amount of N-vinyl imidazole cooled by an ice bath. The formed IL monomers (Figure 15A) possessing an N-vinylimidazolium cation and a vinylsulfonate anion were further thermally polymerized in the presence of a radical initiator (AIBN) in ethanol to yield a cross-linked PIL network. Texter et al.[110] studied a unique IL monomer, 1-(2-acryloyloxyundecyl)-3-methylimidazolium 2-acrylamido-2-methylpropyl-sulfonate, which contained an acryloyl-type imidazolium cation and a sulfonyl-terminated acrylamide anion. Kadokawa et al.[111] synthesized a special type of cross-linkable IL monomers with two types of polymerizable groups connected to a single imidazolium ring (Figure 15B). For instance, the IL monomer N-vinyl-4-vinylbenzylimidazolium chloride obtained from N-vinyl imidazole and 4-chloromethyl styrene was polymerized via radical polymerization using AIBN initiator to produce a cross-linked PIL.

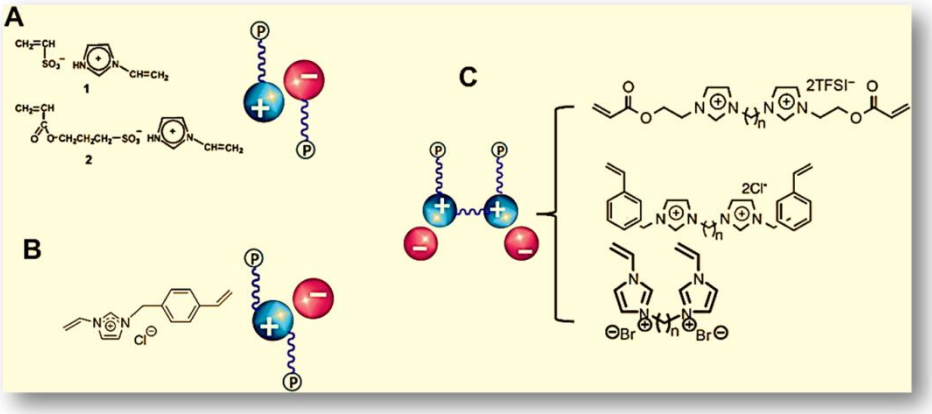

Figure 15. Chemical structures and sketches of three types of cross-linkable IL monomers.

Furthermore, radical polymerization was performed using cellulose and the as-synthesized cross-linked PIL to produce new type of composite materials. Yang et al.[112] reported the synthesis of crosslinked poly(1-butyl-3-vinylimidazolium bromide) microspheres with the diameter of about 200 nm via miniemulsion polymerization, in which 1,4-di(vinylimidazolium) butane bisbromide was used as the cross-linker. An imidazolium-based IL, reported by Das et al.[113], has been successfully utilized as cross-linker for dispersion polymerization of acrylamide in the presence of poly(vinyl methyl ether) (PVME) stabilizer (Figure 16), which produced water-friendly cationic cross-linked poly(acrylamide) (CPAAm) beads. Figure 15C represented the third type of frequently reported cross-linkable IL monomers, in which two monovalent IL monomers of the same type are covalently bridged through an alkyl chain. They are typically (meth)acryloyl-, styrenic or N-vinylimidazolium-based ILs. For example, an acryloyl-based monomer, 1,4-bis[3-[2-(acryloyloxy)ethyl]imidazolium-1-yl] butane bis[bis(trifluoromethylsulfonyl)imide],was prepared via an ester formation

between methacrylic acid and 1,4-bis[3-hydroxyethylimidazolium-1-yl] butane bis[bis(trifluoromethylsulfonyl)imide]; styrenic

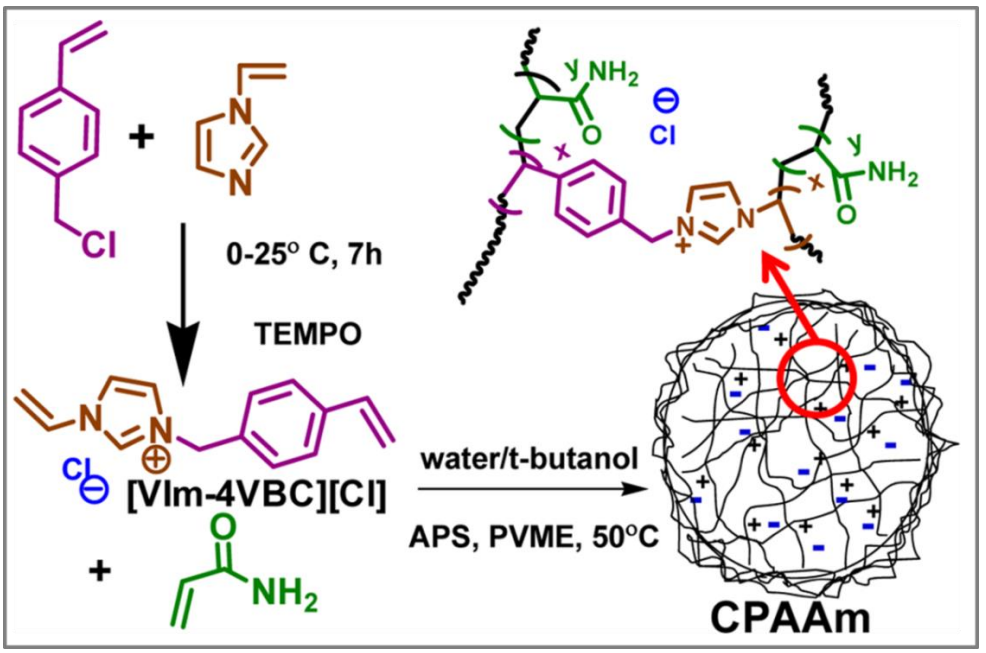

Figure 16. Schematic representation of dispersion polymerization of acrylamide using a cross-linkable ILM to prepare cross-linked poly(acrylamide) (CPAAm) beads.[113]

monomer with a hexyl bridge; 1,6-bis[3-(vinylbenzyl)imidazolium-1-yl]hexane chloride, was prepared via one step reaction of 4-chloromethyl styrene and 1,6-bis(imidazole-1-yl)hexane in a molar ratio of 2:1. [114] Armstrong et al. reported the preparation of N-vinylimidazolium-based cross-linkable monomer via one-step reaction between N-vinyl imidazole and dibromoalkane in a molar ratio of 2:1.[115-116]

1.3 Thermo- and ion-responsive PILs

Stimuli-responsive "smart" polymers of both ionic and non-ionic nature are of increasing interest due to their vast applications in drug delivery, fabrication of sensor-based materials and many more.[117-119] The reactive functional groups

present in these smart polymers show sharp responses to the changes of external environments. A very small change in the environmental conditions can cause substantial change in the properties of these polymeric materials including solubility, nature of surface, permeability, shape as well as mechanical, optical, electrical and chemical properties.[120] Polymers with different functional groups respond towards different stimuli such as temperature,[121] pH,[122] light,[123] redox reaction,[124] ionic strength,[125] glucose[126] and carbon dioxide (CO_2).[127] In the next section, the synthesis and properties of thermo-, ion- and dual thermo- and ion-responsive poly(ionic liquid)s will be discussed in detail.

1.3.1 Thermoresponsive PILs

Temperature-responsive polymers exhibit a phase transition due to a sudden change in their solvation behaviour at a particular temperature. The phase transition which is sometimes termed as "coil-globule transition" refers to the collapse of a macromolecule from an expanded coil state through an ideal coil state to a collapsed globule state in a particular solvent, or vice versa (Figure 17). Such polymers either become insoluble or soluble upon heating are known as lower critical solution temperature (LCST) or upper critical solution temperature (UCST) polymers. In case of LCST and UCST polymers, the collapse of polymer chains occurs with increasing and decreasing the temperature respectively. It is known that the extensive hydrogen bonding interactions between the molecules of LCST polymers and solvent molecules (such as water) are responsible for their solubilisation and restrict the intra−/inter-molecular interactions in a single polymer chain or between neighbouring polymer chains. Upon heating above the cloud point of a LCST polymer, the hydrogen bonding between the polymer chains and solvent molecules are broken and consequently the intra−/inter-molecular hydrogen bonding/hydrophobic interactions predominate resulting in an aggregation of enthalpically favoured polymer coil structure to a entropically

favoured dense globular structure.[128-129] This results in the development of a cloudy dispersion in a solvent due to the formation of insoluble macroscopic polymer aggregates upon heating.[130]

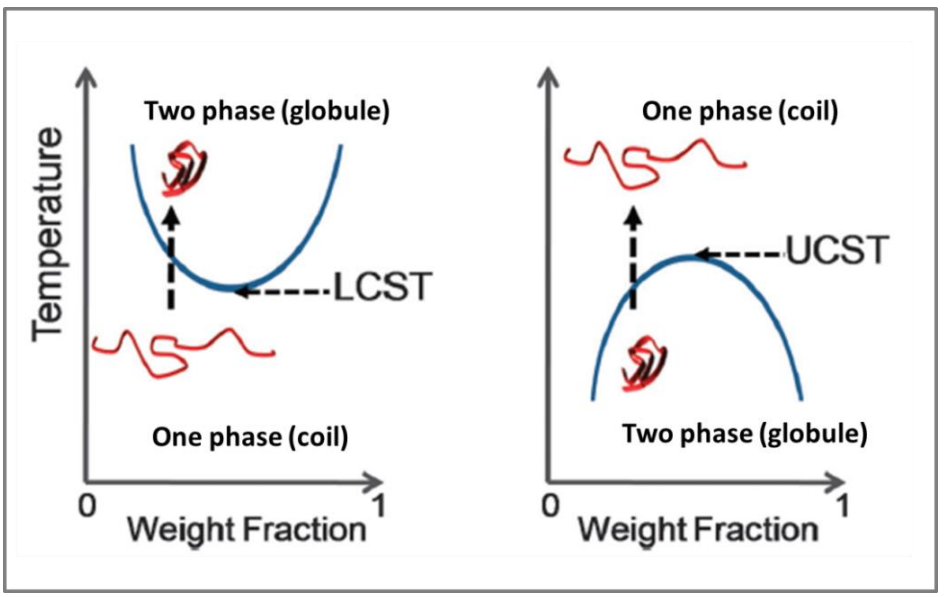

Figure 17. Schematic representation of phase transition associated with LCST (lower critical solution temperature) and UCST (upper critical solution temperature) type phase behaviour. Blue line represents the phase separation boundary, which produces a cloud point in solution.[129]

Most of the reported LCST polymers are non-ionic in nature. The examples of LCST polymers include poly(N-isopropyl acrylamide) (PNIPAM),[131] poly(2-oxazoline)s (POxs),[132] poly(N ,N -dimethylaminoethyl methacrylate) (PDMAEMA),[133] poly(vinyl methyl ether) (PVME),[134] poly(methacrylamide) (PMAAm),[135] etc., which are extensively studied for last two decades. On the other hand, reports on UCST type polymers showing globule-to-coil (insoluble-to-soluble) transitions in water are available but are much less compared to that of LCST polymers. However, considering their applications, it is equally important to develop UCST polymers. It is to be noted that polymers showing UCST-type phase behaviour is rarely observed under practically relevant conditions.[136]

UCST- or LCST-type phase transition depends on the free enthalpy of mixing which includes enthalpic and entropic contributions. It is noteworthy that an UCST-type phase transition arises from strong polymer−polymer and solvent−solvent interactions compared to weak polymer−solvent interactions.[136] Additionally, in UCST- polymer, the hydrophobic effect (entropic) is less dominant. Therefore UCST- behaviour is called enthalpy driven and it depends upon either hydrogen bonding (HB-UCST polymers) or Coulomb interactions (C-UCST polymers). Aqueous solution of non-ionic poly(N-acryloyl glycinamide) (poly(NAGA) shows UCST type phase behaviours in the presence of an electrolyte. [137] There are few other examples of non-ionic and zwitterionic UCST-type polymers,[138-139] the detailed discussion of those are not under this thesis work. In this section, thermoresponsive PIL systems will be discussed in a much elaborative way.

- ***PILs showing either LCST- or UCST-type phase transition***

Thermoresponsive PIL systems which show temperature-dependent phase transition (either LCST- or UCST-type) in water or in other solvents depending upon the hydrophobicity/hydrophilicity balance of the constituting ions of starting IL monomers can be achieved by manipulating the structure of cations/anions. Ritter and coworkers[140] reported that poly([1-butyl-3-vinylimidazolium][TFSI]) showed a pseudo-LCST type phase behaviour in the presence of cyclodextrin in water. The thermo-reversible complexation/decomplexation of the hydrophobic $TFSI^-$ ion of this PIL with the cyclodextrin was responsible for this type of phenomenon. At lower temperature, the hydrophobic PIL became water soluble due to the complexation between the cyclodextrin and the $TFSI^-$ ion. At higher temperature, the entropy driven decomplexation resulted the cyclodextrin to get out of hydrophobic anion which caused phase separation of aggregated PIL from water due to the dominance of hydrophobic component.[141] Seno et al.[142] reported

LCST-type phase transition of vinyl ether based polymers containing imidazolium or pyridinium cation pendants in organic solvent (Figure 18). The same group reported an UCST-type phase behaviour of the same vinyl ether based polymers with pendant cationic imidazolium moieties and BF_4^- counter anions.[143] They proposed that UCST-type phase behaviour was observed due to the presence of inter-polymer electrostatic interactions among the side chain ionic groups rather than intra-molecular polymer interactions. Ohno et al.[87] reported the first ever thermoresponsive PIL, namely poly(4-tetrabutylphosphonium styrene sulfonate), which showed LCST-type phase behaviour in aqueous solution. In their work, they prepared several tetraalkylphosphonium styrene sulfonate-based PILs that all showed LCST behaviour in aqueous solution. These PILs when dissolved in water precipitated out

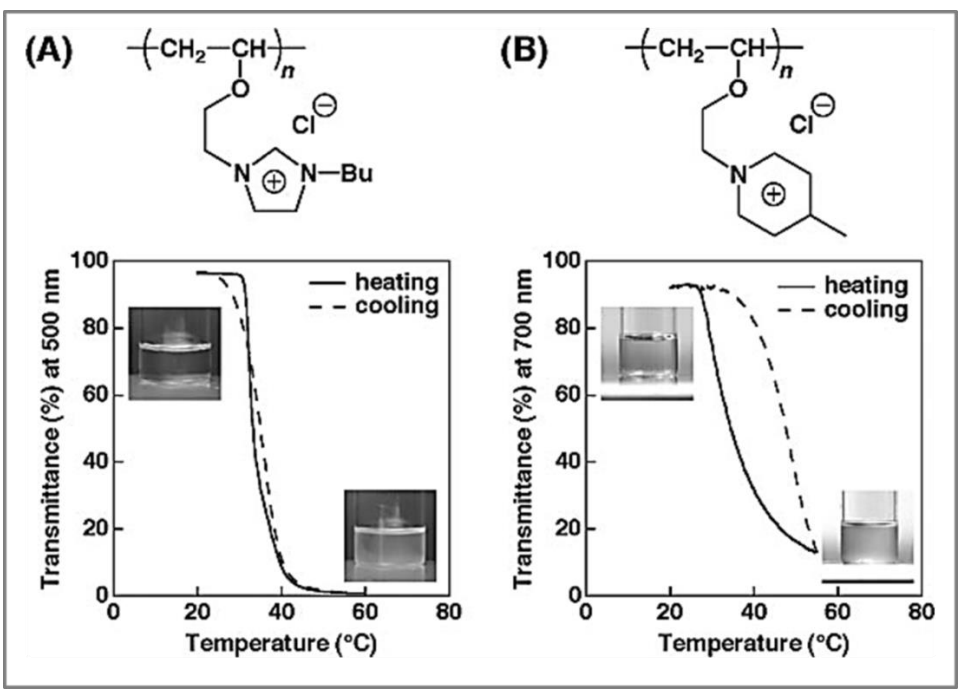

Figure 18. Structures and LCST-type phase transition of vinyl ether based polymers with (A) imidazolium and (B) pyridinium cation pendants in organic solvent.[142]

when heated above the LCST and re-dissolved when cooled below the LCST. They selected few polymerizable IL monomers containing 4-styrenesulfonate ([SS]) anion with two different phosphonium counter cations, $[P_{4444}]^+$ and $[P_{4446}]^+$ (Figure 19). Free radical polymerization of these ILs led to PILs of which the aqueous solution containing 10 wt. % poly ($[P_{4444}][SS]$) showed LCST-type phase transition with a cloud point (T_{cL}) at 57 °C.

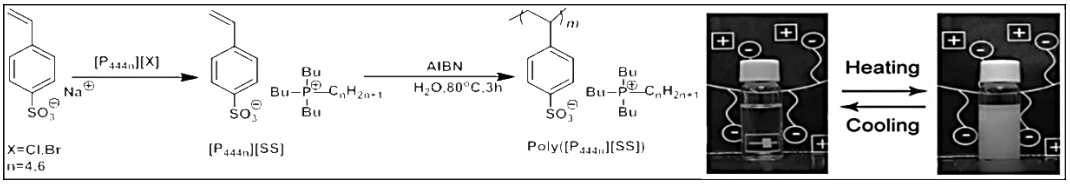

Figure 19. Synthetic procedure of $[P_{444n}][SS]$ monomer and its polymer along with the photographs showing the thermo-responsive behaviour of $[P_{4444}][SS]$ in water.[87]

Yuan et al. reported the synthesis (Figure 20) and tunable LCST-type phase behaviours of poly(4-tetrabutylphosphonium styrene sulfonate) (PTPSS) in aqueous solution.[144] They have demonstrated that the cloud point can be tuned to either higher or lower temperatures by adding different salts such as tetrabutylphosphonium bromide (TPB), potassium bromide, or TPSS monomer. The same group also reported the synthesis of a new type of gemini dicationic PIL, poly[(1,8-octanediyl-bis(tri-nbutylphosphonium) 4-styrenesulfonate] via conventional free radical polymerization.[76] The aqueous solution of this PIL showed LCST-type phase transition with tunable cloud point. Further copolymerization of this gemini dicationic ILM with divinyl benzene cross-linker

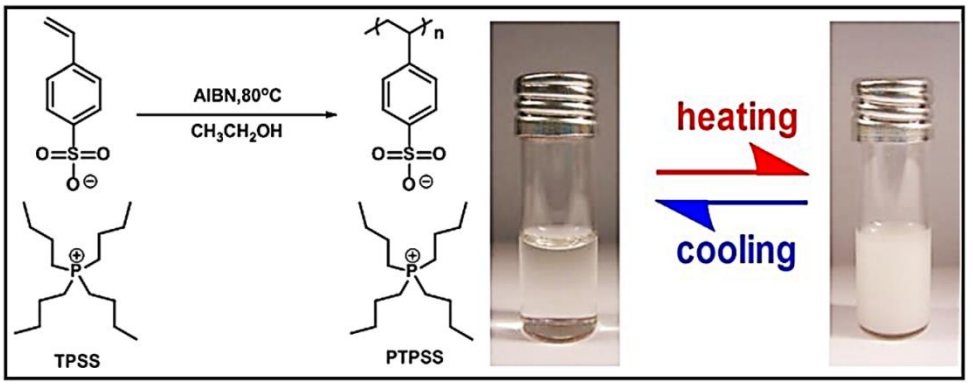

Figure 20. Chemical structure, synthesis and thermo-responsiveness of poly(4-tetrabutylphosphonium styrene sulfonate) (PTPSS) in aqueous solution.[144]

resulted in a hydrogel exhibiting temperature-induced volume change. The same group developed a LCST-type cationic PIL, poly(tributyl-4-vinylbenzylphosphonium pentanesulfonate) in water (Figure 21).[77] The phase transition temperature of the aqueous PIL solution was tuned within a wide range by varying the various parameters. According to them, the anion exchange and salting out effects are responsible for such types of flexible phase transitions.

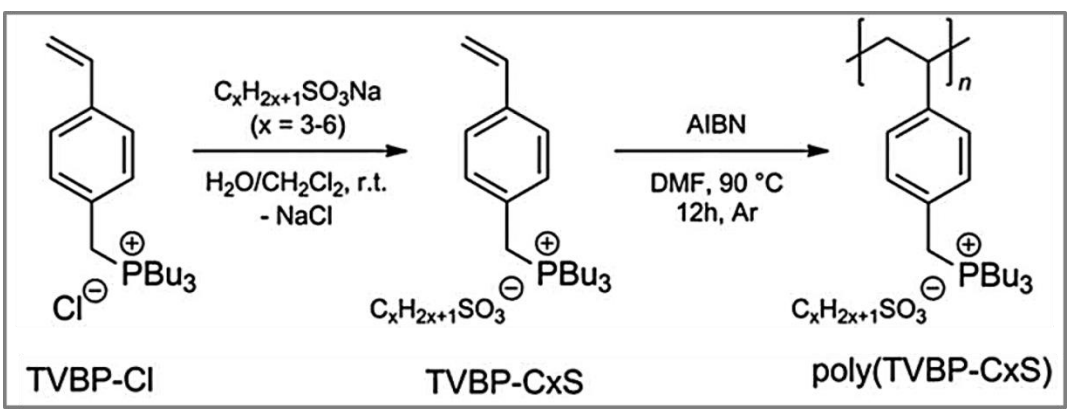

Figure 21. Synthesis of cationic PILs bearing a phosphonium sulfonate ion pair in each repeating unit (Bu = n-butyl).[77]

Xiong et al.[145] reported the synthetic strategy for the preparation of imidazolium IL (ImIL)-based thermoresponsive cross-linked polymeric nanogels

(CLPNs) by one-step copolymerization of geminal dicationic ILs, 1,4-butanediyl-3,3'-bis-1-vinylimidazolium halides (ImIL-X, X = Cl,Br) monomers with cross-linker, ethylene glycol dimethacrylate (EGDMA) or divinylbenzene (DVB) in selective solvent. The stable nanogel dispersion was found to be thermoresponsive and can be reversibly converted into a precipitate or macrogel in methanol by decreasing the temperature. Tenhu and coworkers[146] also reported UCST-type behaviours of imidazolium- and DMAEMA-based polycations in aqueous solution in the presence of both NTf_2^- and OTf^- ions while adjusting the ionic strength with sodium chloride. Moreover, PIL-based amphiphilic block copolymers (BCPs) with an ionic (cationic/anionic) polymer block[147-148] and thermoresponsive PIL hydrogels [149-150] are also reported.

- ***PILs showing simultaneous LCST- and UCST-type phase transition***

Very recently, our group reported the synthesis of various random copolymers from oligo(2-ethyl-2-oxazoline)acrylate (OEtOxA) and either triphenyl-4vinylbenzylphosphonium chloride ([VBTP][Cl]) or 3-n-butyl-1-vinylimidazolium bromide ([VBuIm][Br]) ILMs by RAFT polymerization (Figure 22), which showed simultaneous LCST and UCST-type thermoresponsiveness. Poly[oligo(2-ethyl-2-oxazoline)acrylate] [P(OEtOxA)] has already been reported to be a LCST polymer[151], whereas PILs such as P[VBTP][Cl] and P[VBuIm][Br] both show UCST behaviours in presence of halide ions in H_2O.[108, 152] It is to be noted that, the as-synthesized copolymers with low content of ionic PIL segments (either P[VBTP][Cl] or P[VBuIm][Br]) showed only LCST-type phase behaviour with a linear increase of their cloud point with the increase of amount of ionic PIL segments. The LCST-type cloud point (T_{cL}) was tuned by changing various parameters. On the other hand, the copolymers ($P(OEtOxA)_{10}$-ran-$P[VBTP][Cl]_{42}$)

with high content of ionic PIL segments showed simultaneous LCST- and UCST-type phase transitions in the presence of halide ions in water (Figure 23).

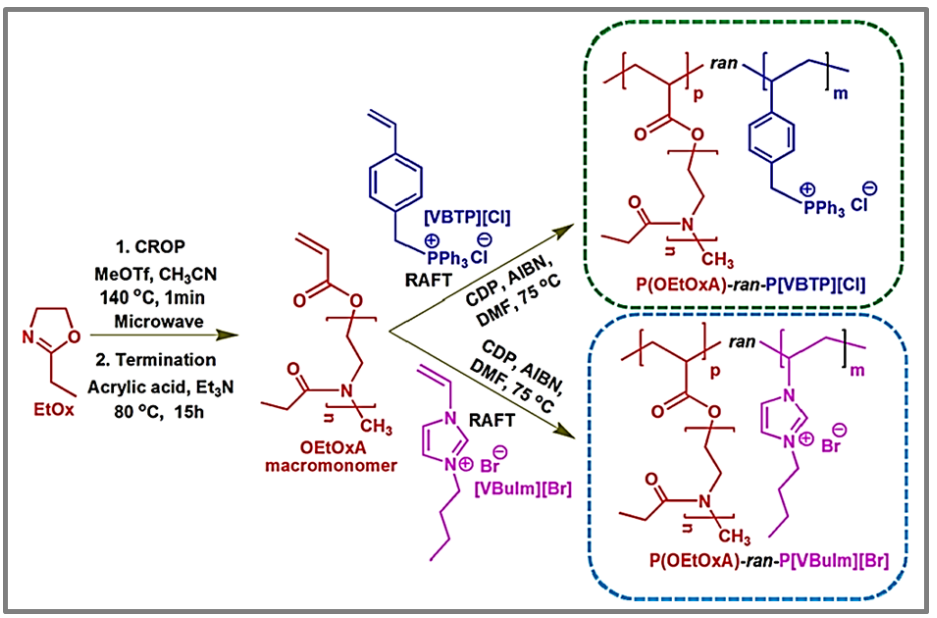

Figure 22. Synthetic strategies for P(OEtOxA)-ran-P[VBTP][Cl] and P(OEtOxA)-ran P[VBuIm][Br] copolymers. [153]

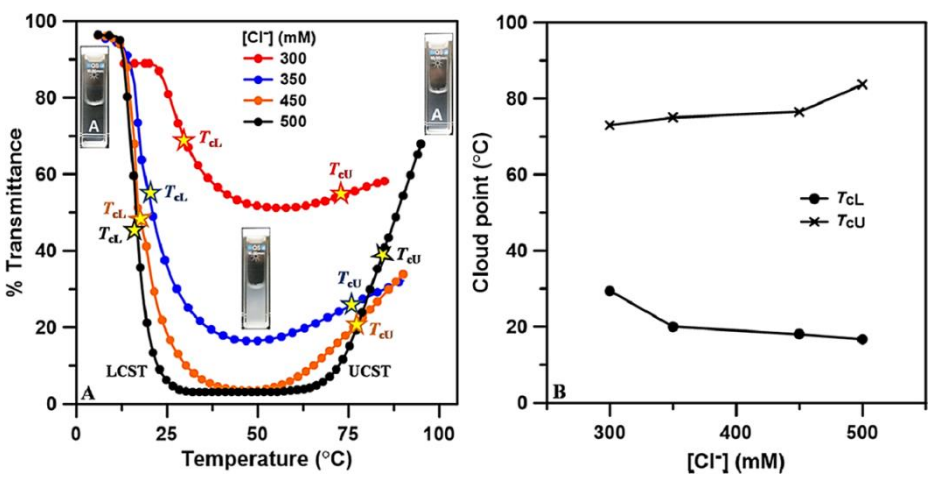

Figure 23. (A) Turbidity curves of aqueous solution of $P(OEtOxA)_{10}$-ran-$P[VBTP][Cl]_{42}$ copolymer at different concentrations of the Cl^- ion, and (B) the variations of LCST-/UCST-type cloud points of the same as a function of the $[Cl^-]$ ion. [153]

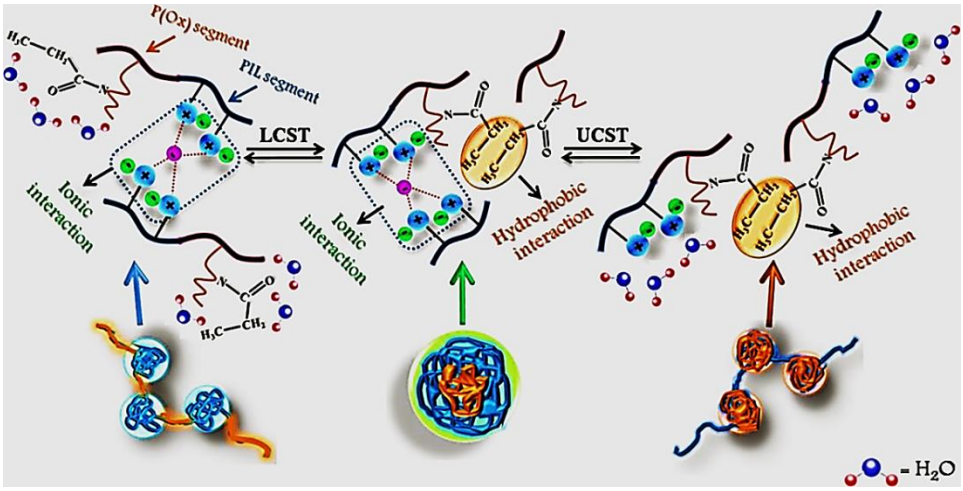

Figure 24. Schematic presentation of the aggregation behaviour shown by the PIL copolymers at the point of both LCST- and UCST- type phase transition. [153]

The explanation for the coexistence of both LCST- and UCST-type behaviours of PIL copolymer is shown in Figure 24. The ionic P[VBTP][Cl][153] segments of copolymer become hydrophobic in the presence of the Cl^- ion because of the halide anion bridging interactions, and therefore the T_{cL} of its P(OEtOxA) segments decreased to nearly 17 °C compared to that (56.9 °C) of neat P(OEtOxA). In addition to anion bridging interactions, the hydrophobic interactions among the pendent ethyl moieties of P(OEtOxA) segments also participated above its T_{cL}. The formation of insoluble large aggregates due to inter-/intra-molecular association of neighbouring copolymer chains can be attributed to both the ionic bridging and hydrophobic interactions resulting in the transformation of the transparent solution into a cloudy dispersion. Upon heating above $T_{cL,}$ breaking of the ionic interaction occurred and the ionic P[VBTP][Cl] segments became hydrophilic again and it predominated over the hydrophobically interacted P(OEtOxA) segments leading to the redissolution of aggregates present in cloudy dispersion. This is the reason behind the UCST-type phase transition with a cloud point (T_{cU}) at 83 °C. Moreover, both T_{cL} and T_{cU} were tunable with respect to various parameters. UCST-type phase behaviours

of both types of PIL copolymers with a very high ionic content (>90%) were similar to that of P[VBTP][Cl] or P[VBuIm][Br] homopolymers with halide ions.

1.3.2 Dual thermo- and ion-responsive PILs

Yuan and co-workers[154] reported a dual thermo- and ion- responsive copolymer by a single step free radical copolymerization of N-isopropylacrylamide and 1-ethyl-3-vinylimidazolium bromide. The poly(NIPAM-ran-EVImBr) copolymer exhibited temperature and ionic strength responsiveness in aqueous solution with a cloud point (T_{cL}) of 32 °C. The copolymer was further used as a stabilizer to stabilize multiwalled carbon nanotubes (MWCNTs) in aqueous solution to form "smart" dispersions. The presence of the PIL copolymer stabilizer facilitated the deagglomeration of the hydrophobic MWCNTs via sonication followed by its adsorption on the surface through PEVImBr PIL segment to form a homogeneous aqueous dispersion (Figure 25). The temperature-dependent turbidity measurements showed that the cloud point (T_{cL}) could be varied in a wide range of temperature by tuning the copolymer composition and ionic strength.

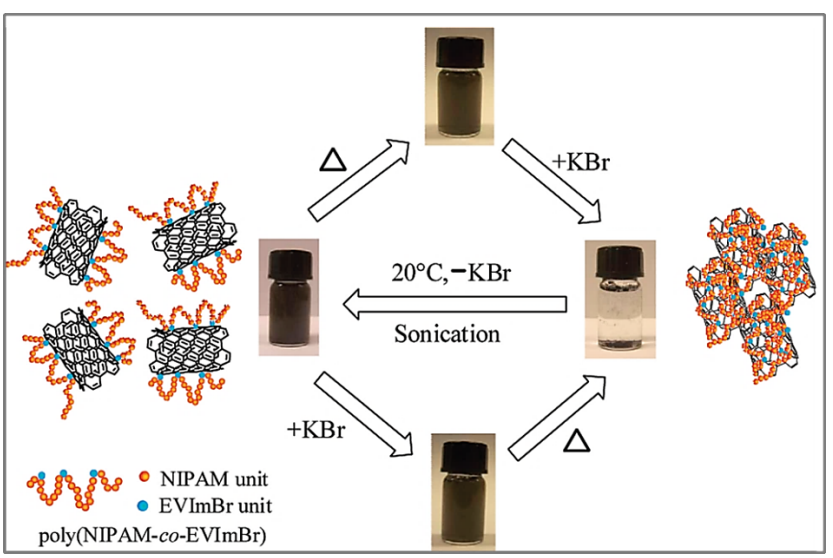

Figure 25. Schematic representation of temperature and ionic strength-responsive behaviours of poly(NIPAM-co-EVImBr) copolymer-stabilized MWCNT dispersion.[154]

Recently, our group have reported the synthesis of a dual temperature and ion-responsive cationic phosphonium PIL, poly(triphenyl-4-vinylbenzylphosphonium chloride) (P[VBTP][Cl]) by RAFT polymerization.[108] The synthetic strategy has earlier been discussed (Scheme 13). The clear aqueous solution of P[VBTP][Cl] turned into a cloudy dispersion due to the formation of insoluble microgel aggregates. The pendent positively charged phosphonium groups of PILs favoured the intra- and/or inter-chain cross-linking of PIL chains via coulomb interaction driven halide ion bridging. This cloudy dispersion upon heating experienced a UCST-type phase transition resulting in a transparent solution due to dissociation of ion bridges among PIL chains (Figure 26). The size of the externally added halide ions highly affected the UCST-type cloud point (T_{cU}) and increased almost linearly with increasing halide ion concentration and molecular weights of the PIL. The stabilizing power of this PIL towards MWCNT dispersion was also observed to be very good in water. The dispersion state of PIL-stabilized MWCNT was changed from dispersed to agglomerate state and vice versa by the addition of halide ions as well as increasing the dispersion temperature. The cross-linked hydrogel of P[VBTP][Cl] also found to show halide ion- and temperature-dependent UCST type phase transition. As an extension of this work, the authors prepared stable dispersion of single or few-layers MoS_2/$MoSe_2$ nano-sheets by a simple efficient exfoliation via sonication in presence of the cationic PILs (phosphonium- and imdazolium-PILs) in both aqueous and organic media.[152] These cation PILs served the dual purpose of an exfoliating-cum-stabilizing agent. The adsorption of PIL on MoS_2 nanosheet's surface made them responsive towards ions and temperature in aqueous solution.

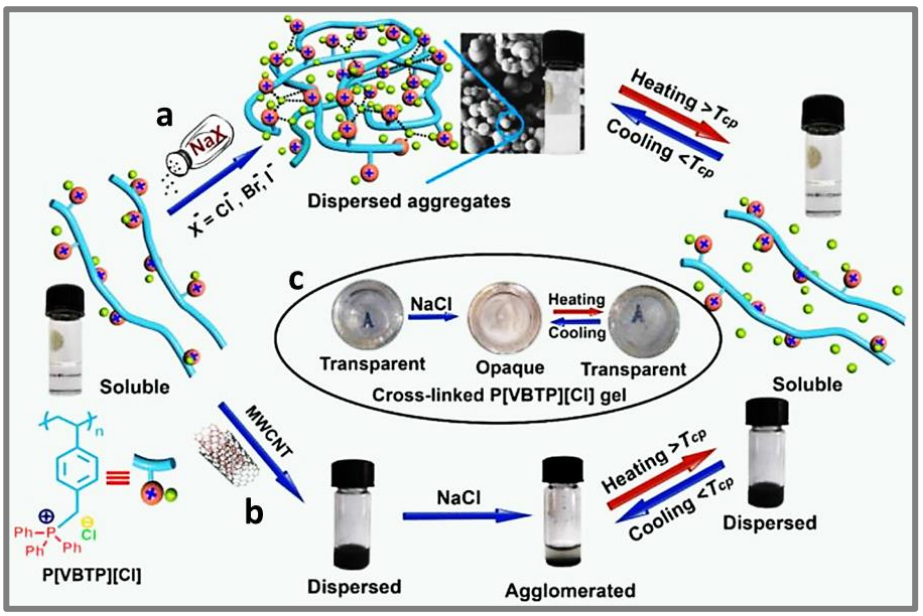

Figure 26. A cartoon representation of (a) UCST-type phase transitions of aqueous P[VBTP][Cl] solution in the presences of externally added halide ion. FESEM image showed the P[VBTP][Cl] aggregates and (b) photographs of P[VBTP][Cl]-stabilized MWCNT dispersion in water in the presence of added anion and with heating and (c)cross-linked hydrogel of P[VBTP][Cl] in H_2O showing ion-induced deswelling and temperature-induced reswelling. [Reproduced from ref.[108, 152]]

1.4 PILs as conductive materials

1.4.1 Background

1.4.1.1 Solid-state polymer electrolytes

In early days, liquid electrolytes which high ionic conductivities were extensively used as ion transport medium in lithium-ion batteries.[155] However, lithium metal electrode in contact with a liquid electrolyte forms metallic lithium electrodeposits (dendrites) during the charging/discharging processes and this dendrite growth is hazardous as it could cause internal short-circuiting and raise safety issues.[156] Hence, more recently, attention has been shifted towards solid-state electrolytes such as conductive ceramics and solid state-polymer

electrolytes to increase the safety and energy density of lithium batteries.[157-158] The very first ion conducting polymeric material was reported by Fenton et al.[159] in 1973 with the discovery of the polymer- salt complexes between polyethylene oxide (PEO) and alkali metal salts and the electrical properties of such systems ignited early interest in solid-state polymer electrolytes. The ability for alkali metal ions like lithium to coordinate with the ether oxygen atom present PEO chain facilitated the ion conduction in these polymeric materials. The ionic conductivity of solid-state electrolytes is expected to be lower than that of liquid electrolytes, but recently some polymer-based electrolytic materials have been developed with ionic conductivity values close to that of the liquid electrolytes. Such polymer electrolytes can offer multiple advantages over liquid electrolytes in terms of minimization of dendritic growth and safety along with attractive properties such as processability, flexibility and low cost. Polymer-based solid electrolyte system can be divided into three categories: polyelectrolytes, poly (ionic liquids) (PILs) and polymer-salt complexes (Figure 27). Both polyelectrolytes and PILs, which are characteristically same, are polymers having an electrolyte group in the repeating unit along the polymer backbone. The only difference is present in their synthetic approach: a polyelectrolyte is mainly achieved via post-polymerization coupling of an ionic group to the polymer backbone whereas PIL are obtained via the polymerization of an ionic liquid monomer. Polyelectrolytes dissociating in the solid-state (i.e., a thin film or pellet) produce charged polymer chains which are basically immobile due to their high mass and mobile counter-ions. Thus, polyelectrolytes in the solid-state are unique compared to other electrolytes as they only transport ions of one polarity. Current is carried by the movement of these free counter-ions. Polyelectrolytes that have a positively charged backbone (and negatively charged mobile ion) are termed as polycations, whereas polyelectrolytes with a

negatively charged backbone (and positively charged mobile ion) are termed as polyanions.

Polymer–salt complexes,[160] which are also termed as polymer electrolytes, are just like electrolyte solutions where a salt is dissolved in a solvating polymer matrix rather than a liquid solvent. Polymer electrolytes have been classified in two main families. The first one is 'solid polymer electrolytes' (SPEs) which are made by dissolving alkali metal salts into a coordinating polymer host and are usually created in thin-film form by solution casting or hot pressing. This is the case of the well-known combination of poly (ethylene oxide) (PEO) blended with a sodium or lithium salt. In conventional SPEs the ionic conductivity of the material is associated to both lithium/sodium cation and the salt anion which move through the PEO matrix. Such electrolytes are termed as "dual-ion" conductors, in which both cations and the anions are mobile. The alkali-metal cations are located at the -O- coordination sites in the polymer main chain, and the ether bridges of the backbone help the ionic species to hop from one coordination site to another.[161] This hopping occurs when free volume is created, which is typically above the glass transition temperature.

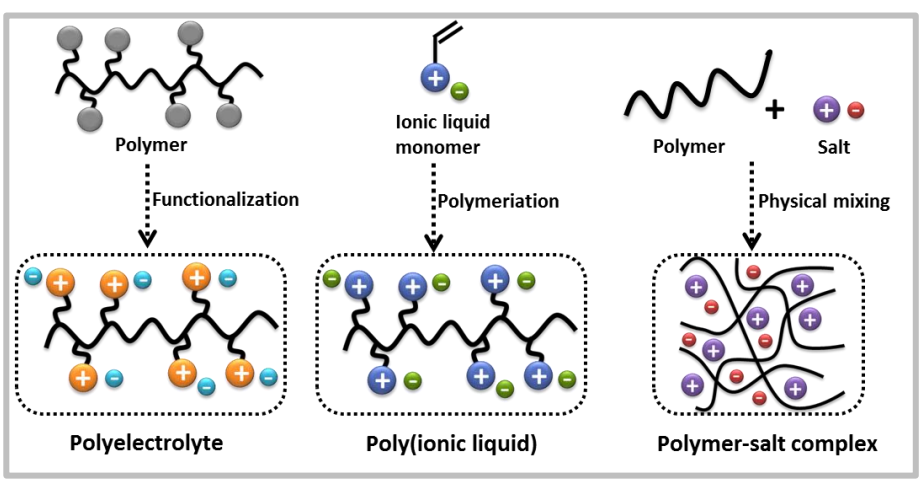

Figure 27. Structural illustration to understand the basic difference between polyelectrolytes, poly(ionic liquid)s and polymer-salt complexes.

The second family of polymer electrolytes is named as 'gel polymer electrolytes' which are composed of a polymer matrix, a salt and an organic solvent (plasticizer). In the case of gel electrolytes, the ionic conductivity is usually higher than in SPEs since the transport of the ions is favoured by the presence of the molecular organic solvent. The common example of gel polymer electrolytes that are generally used in lithium batteries is a combination of poly (vinylidene fluoride) (PVDF), a cyclic carbonate solvent and a lithium salt. As already mentioned, in polyelectrolytes and PILs, one ion is covalently bound to the polymer backbone but in polymer electrolytes, both ion species are free to diffuse through the system.

1.4.1.2 Single-ion conducting polymer electrolytes (SICPEs)

In case of conventional SPEs, the cations are solvated by polymer matrix and their motion is coupled to that of the polymer chain dynamics, and hence the cation mobilities are usually less than that of the anions. As a result, such systems exhibit a low cation transference number (a measure of the current contribution of the cation relative to the overall current). During the electrochemical cycling, the anions present in such systems accumulate at the anode and cause concentration gradients, a phenomenon termed as concentration polarization.[162] Such polarization leads to loss of voltages, higher internal impedance and eventually to cell failure. To overcome the concentration polarization issues "single-ion" conducting polymer electrolytes (SICPEs) with high ion transference number have been developed where mobility of anions are disabled by coupling them to the polymer backbone[163-165] or through the incorporation of additives which selectively complex with the anions.[166-167]Though, the innovative developments have occurred in the area of single ion conducting materials,[165] low mobility of lithium ions due to the low polarity of the polymer and strong ion pairing interactions leads to low conductivities

which has turned out to be a major issue. Additionally, as a result of the electrostatic interactions, these materials often possess high glass transition temperatures, which in turn contribute to a lower polymer chain mobility and ion conductivity. To overcome the above-mentioned issues regarding single ion conductors, polymerized ionic liquids (PILs) have turned out to be the best choice replacing conventional SICPEs. In the next section, we will discuss in detail about the recent development on PIL-based SICPE.

1.4.2 Poly(ionic liquid)s as single ion-conducting polymer electrolytes

Poly (ionic liquid)s (PILs) as already mentioned refer to a special type of polyelectrolyte which carry an ionic liquid (IL) moiety in each of the repeating units.[168-171] Ionic liquids (ILs), which are considered as low melting analogues of classical molten salts, have attracted huge attention due to their physicochemical properties such as high ion conductivity, chemical stability, non-flammability and very low vapour pressure.[172-174] By incorporating polymerizable groups, such as vinyl groups into the structure of ILs followed by polymerization, the produced PILs can be generated which combine both the high conductivity of ILs and good mechanical strength of polymers. There is an emerging trend in the development and application of PILs in the electrochemical devices not only because of the preservation of the unique properties of ILs with the macromolecular architecture, but also a matter of developing new properties and functions. The major advantages of using a PIL instead of an IL are the improved mechanical stability, processability, durability, and spatial controllability over the IL species which can be achieved through polymeric architectures (Figure 28). Ohno and co-workers[175] started the development of PILs for fast ion conductors in 1998 and since then many research groups have

conducted several studies to improve the conductivity and the overall performance of these materials.

PILs behave as single ion conductors, where one of the ionic species (either the cation or anion) is tethered to the polymer chain while the other is available to freely move.[176-178] The ion transference number which is defined as the ratio of the electric current carried by an ionic species of interest to the total current carried by all ionic species in the system is closely related to the power density of the energy storage devices. For many salt-polymer complexes, both the cation and anion contribute to the conductivity leading to a transference number much less than unity. But in case of PILs, one ionic species is anchored to the polymer chain which allows only the counters ion to move. Thus, a single-ion

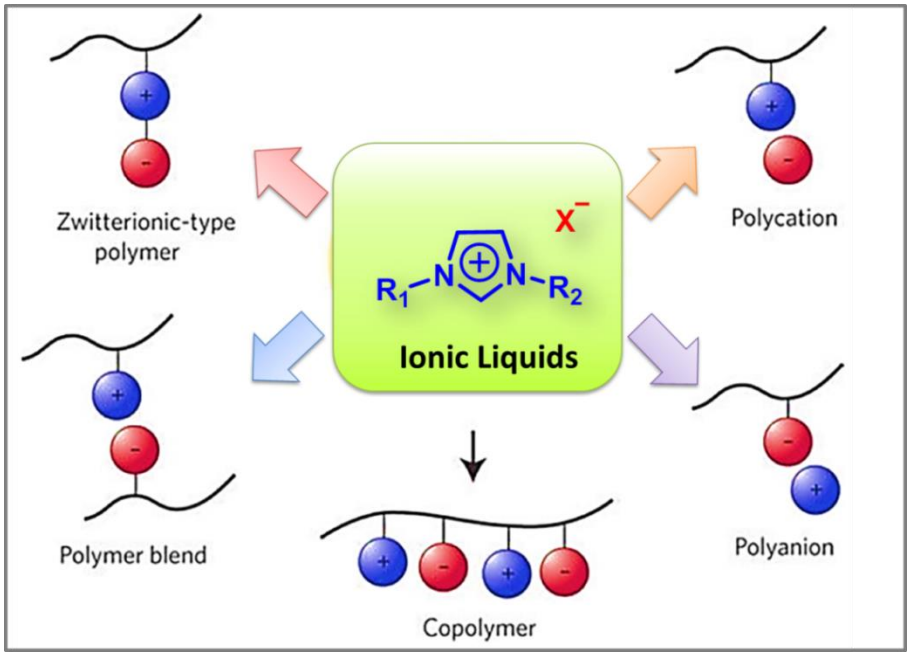

Figure 28. Different structures of poly(ionic liquid)-based electrolytes .[179]

conductor based on PILs can be achieved and the ion transference number becomes close to unity thereby improving the power density.[169, 180-181] Understanding the structure and glass transition properties of PILs is an

important key to understand how to improve the ionic conductivity in PIL based system. The conductive properties of PIL-based system vary significantly above and below the glass transition temperature. A glass transition temperature (T_g) is typically defined as the temperature at which an amorphous polymer experiences a reversible transition from a hard and relatively brittle state (in other words, a 'glassy' state) to a softer often rubbery or viscous state. It is the temperature at which polymer chains start to move and the free volume, or the gap between the polymer chains increases. Investigating PILs can allow us to understand the dependence of conductivity on polymer chain mobility and usually it is observed that a lower glass transition temperature (T_g) leads to higher ionic conductivity.[182] At temperatures greater than T_g, the conductivity in PILs is typically attained by hopping of counter-ions between ionic sites assisted by the segmental motion of the polymer chains. But below T_g, the motion of the polymer chains is 'frozen', and the transport of ions is attributed to the continued mobility of the counter-anions which is decoupled from the segmental motion.[183-185] Though diffusion of ions in the solid state below T_g is possible, substantial conductivity needed for practical applications is difficult to achieve without segmental motion of polymer chains . Hence, the influence of polymer structure on ion transport and enhancement of ionic conductivity even in glassy state has always been a topic of interest among researchers for PIL based systems.

There has been a continuous effort to improve the ionic conductivity of PIL-based system by manipulating the polymer structure. Ionic conductivity is immensely influenced by the structure and size of the cation or anion, nature and length of spacer between the main chain and IL moieties, morphology and glass transition temperature of the PIL.[54, 183, 186-189] In the next section it will be discussed in detail.

1.4.3 Different factors affecting the bulk ionic conductivity (σ_{dc}) of PILs

- **Effect of PIL architecture**

In common synthetic design of PILs, IL moieties can either be directly incorporated into the polymeric backbone (ionenes, or backbone-PILs) or can be placed in pendant groups on the side chain (pendant-PILs).[180, 183] There has been always a continuous effort on understanding the effect of molecular structure of backbone and pendant-PILs on the ion transport mechanism. Hall et al. performed molecular dynamics simulations on ionomer melts (polymers with a small fraction of charged groups and no solvent) and compared the scattering peak of ionomer melts, having periodically spaced charged beads either within the polymer chain (ionenes) or pendant to the polymer backbone.[190] Ionenes were found to have a more percolated path for charge transport, which can be attributed to the attachment of charges along the polymer chain. On the other hand, pendant -type ionomers were found to form discrete ionic aggregates that hindered the transport of ions leading to substantial lowering of ionic conductivity compared to the ionenes. Evans et al. investigated the effect of ion placement along the pendant positions and along the polymer backbone for imidazolium based PILs.[54] Both PILs were designed to have almost equal charge density and it was found that the backbone PIL showed much higher T_g-normalized ionic conductivity compared to the equivalent pendant PIL. The experimental results indicated an increase in the correlation length of ions which was consistent with the ion transport along a more percolated pathway following the polymer backbone. Recently, Kuray et al. have investigated the ionic conductivity of imidazolium-based pendant and backbone-PILs with different counter ions.[183] Figure 29 showed the structure of the reported PILs

and their ionic conductivities as a function of temperature. The authors have found that backbone-PILs have a considerably lower T_g than pendant-PILs with the same counter-anions and also exhibited a higher ionic conductivity on an absolute temperature scale. Pendant-PILs showed higher ionic conductivity, when scaled to T_g or below T_g. This is attributed to the movement of the counter-anions among the side chains in pendant-PILs (difference in the decoupling degree). Additionally, they found that the ion transport for backbone-PILs is linked to the segmental motions of polymer chains, whereas that for pendant-PILs is decoupled from the segmental dynamics at a temperature close to T_g.

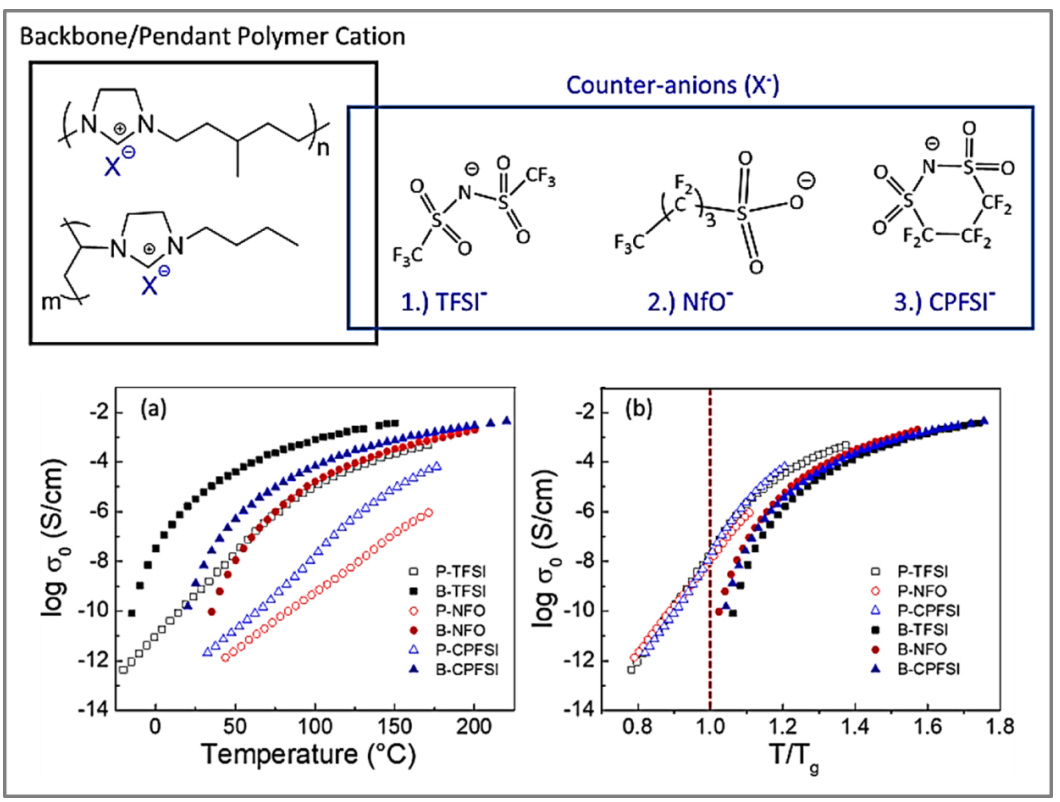

Figure 29. (**Top**) Chemical structures of aliphatic imidazolium-based backbone and pendant- PILs and varying counter anions; (**Bottom**) (a) conductivity profiles of backbone-PILs and pendant-PILs from DRS are shown as a function of

temperature and (b) scaled to each material's corresponding glass transition temperature.[183]

- **Effect of counter ion**

In general, the cationic groups in PILs include imidazolium, pyrrolidinium and phosphonium ions and are tethered to the polymer chain whereas the anionic groups are usually fluorinated sulfonic imides or tetrafluoroborates which are free for transport. Fluorinated sulfonimides such as $TFSI^-$ are favoured because the charge in this molecule is highly delocalized and less coordinative, which tends to increase the ionic conductivity.[191-193] The size of the counter-ion plays an important role in determining ion transport since smaller ions tend to exhibit higher mobility. Lacob et al. have reported that the size of the counter-anion strongly correlates with T_g-independent ionic conductivity for a broad series of imidazolium based PILs.[194] As shown in Figure 30, the variation of anion molecular volume is found to result in differences in the T_g-independent molar conductivity spanning ~3 orders of magnitude. The van der Waals volumes of the anions used in this work increases in the order: $BF_4^- < TfO^- < TFSI \cong NfO^- < PFSI^- < HFSI^-$ while the T_g-independent ionic conductivities were found to increase with decreasing counter-anion volume. The complex 3D network morphology and the related counter-anion volume were reported to be the principal factors in controlling the ionic conductivity in these PILs. Recently, Stacy et al. analysed the ionic conductivity spectra of several PILs with different chemical structure and different size of mobile ions.[195]. In these glassy PILs, the activation energy for the ion diffusion monotonously depends upon the size of the counter ions indicating the existence of two critical mechanisms in controlling the ion transport and its decoupling from the segmental dynamics. Coulombic (electrostatic) interactions dominate the ion diffusion for very small

ions whereas elastic forces dominate for larger ions and their contribution increases with the ion size.

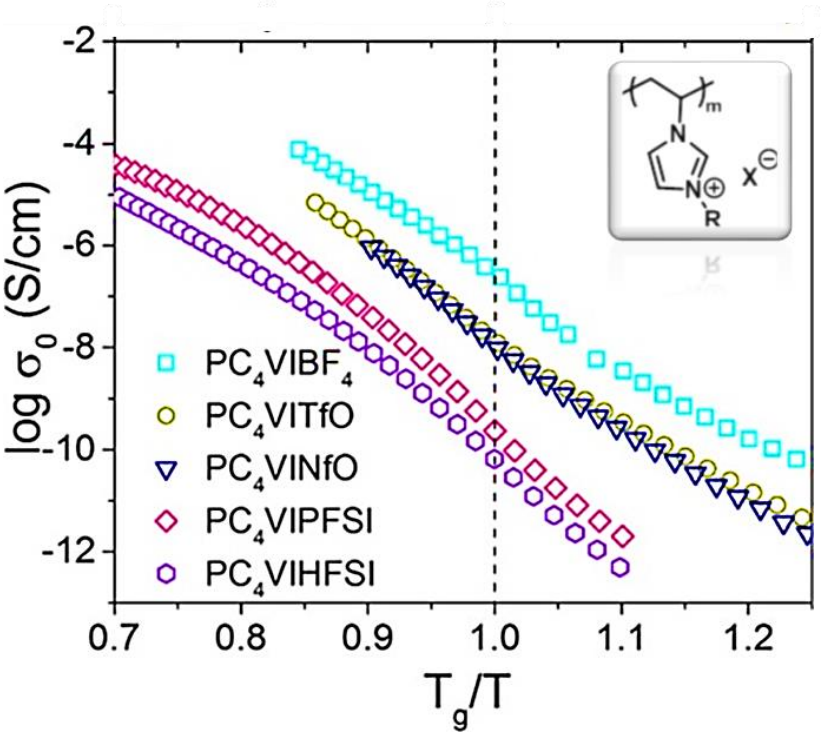

Figure 30. dc conductivity as a function of T_g/T for poly(1-butyl-3-vinylimidazolium-X^-), where X^- = BF_4^-, TfO^-, NfO^-, $PFSI^-$ and $HFSI^-$.[194]

- **Effect of spacer length**

The chemical composition and length of the spacer is also an important factor in understanding the conductivity of the PIL-based system. Spacers are usually alkyl chains connected to the polymer backbone and their length controls how far away the cationic group is from the polymer backbone. Typically, the longer the spacer, the farther the cationic group is from the polymer chain and the higher the conductivity. This occurs because long side chains tend to act as plasticizers, increasing the mobility of the counter-anion. Choi, et al. synthesized a series of imidazolium based PILs with varying spacer lengths.[196] These authors reported

the effect of the spacer length between the backbone and the imidazolium cation on the static dielectric constant and ion motion in these PILs. It was found that these PIL structure with the longest structure yielded the highest conductivity as the spacers plasticized the polymer chain. Delhorbe et al.[197] synthesized a series of 1-alkyl-3-vinylimidazolium bis(trifluoromethane) sulfonimide-derived homopolymers i.e., P(C_nVIm-TSI) with various alkyl chain lengths (n = 2, 4, 6, 8,10) and systematically investigated the effect of the spacer length on the physicochemical properties and ionic conductivity. The authors have found that the charge transport in PILs is determined by the segmental motion of the polymer backbone (i.e. the glass transition temperature, T_g), charge carrier density and the self-assembly nanostructure of such PILs, specifically the backbone-to-backbone correlation distance. The low viscosity and T_g favour the ion diffusion and the decrease in the backbone-to-backbone correlation distance increases ionic conductivity. Recently, Pipertzis et al.[198] reported the synthesis of a series of PILs based on polythiophene and both electronic and ionic conductivity as a function of the spacer length for a fixed anion. It was reported that increase of spacer length from butyl to decyl resulted in internal plasticization and in a decreased glass temperature (T_g). As a result, dc-conductivity at a fixed temperature increases with the increase of spacer length. Figure 31 depicted that the conductivities at a given temperature can vary by several orders of magnitude as a result of the distinctly different T_g values. Furthermore, dielectric permittivity being a decreasing function of the spacer length under T_g-scaled conditions further influenced the dc-conductivity.

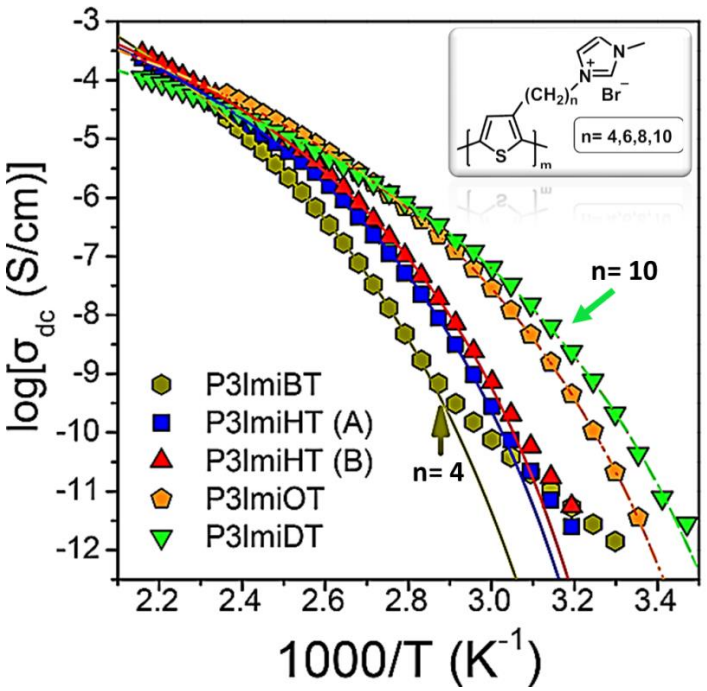

Figure 31. DC-conductivity as a function of inverse temperature for a series of PILs. Solid lines are fits to the VFT equation for conductivity.[198]

It is to be noted that, the effect of counter-anion on the ionic conductivity in PILs depends upon the delocalization of the counter-anion's charge, bulkiness and the ability to form hydrogen bonds with the polyelectrolyte. In order to attain high conductivity, the counter-anion should be small, delocalized and have minimum interactions with the polymeric backbone or spacer. Evans, et al.[199] recently synthesized a PIL–based homopolymer as well as a series of block copolymers with poly(styrene) and it has been found that the conductivity depends upon network structure and electrostatic interactions between the polymer matrix and counter-anion.

- **Effect of molecular weight**

There are several reports which describe the effect of molecular weight on ion transport in traditional polymer electrolytes, based on poly (ethylene oxide) and

poly(propylene glycol).[200-202] In these systems, ion transport has been found to be strongly coupled to the segmental relaxation of the polymer chain despite the change in molecular weight. However, a significant difference in the rate of ion transport and segmental relaxation (decoupling of the ion transport from the segmental relaxation) has been observed in several polymer electrolytes.[203-204]Recent studies revealed that ionic conductivity can be decoupled from structural (segmental) relaxation in PolyILs.[189, 205] However, the effect of molecular weight on ion transport in PILs has not been explored much. Recently Fan et al.[180] synthesized a series of PILs (represented as 'PolyIL-n') having degrees of polymerization (n) ranging from 1 to 333, corresponding to molecular weights from 482 to 160 400 g/mol respectively and studied the influence of molecular weight on the ion transport mechanism and segmental dynamics in these materials. The T_g of these PILs exhibited an increase with the increase of molecular weight and reached a plateau when n ≥ 72. The modified Walden plot analysis revealed that the ionic conductivity transformed from being closely coupled with structural relaxation to being strongly decoupled from it as molecular weight increases. The significant increase in decoupling of ionic conductivity from segmental motion of polymer chains was ascribed to the increase in chain packing frustration in these PILs. Figure 32a shows that as molecular weight increases from PolyIL-10 to PolyIL-333, the ionic conductivity values changes a little. This drop in conductivity is due to the changes in the glass transition temperature of the PILs. The temperature dependencies of the conductivity values of PolyIL-10, -72,-109, and -333 show a crossover from VFT to Arrhenius-type behavior as the temperature decreases. The influence of the shift in the T_gs was excluded by normalizing the temperature with T_g-BDS (T_g determined from broadband dielectric spectroscopy) as shown in Figure 32b. This revealed that PILs with higher molecular weight exhibited higher

conductivity than lower molecular weight samples when compared at the same T_g/T values. These results indicated that changes in molecular weight not only shift the T_g of the PILs, but they also strongly affect the conductivity mechanism. The authors speculated that frustration in the packing of the polymeric cation contributed to the decoupling of ion transport from segmental dynamics which resulted in higher ionic conductivity.

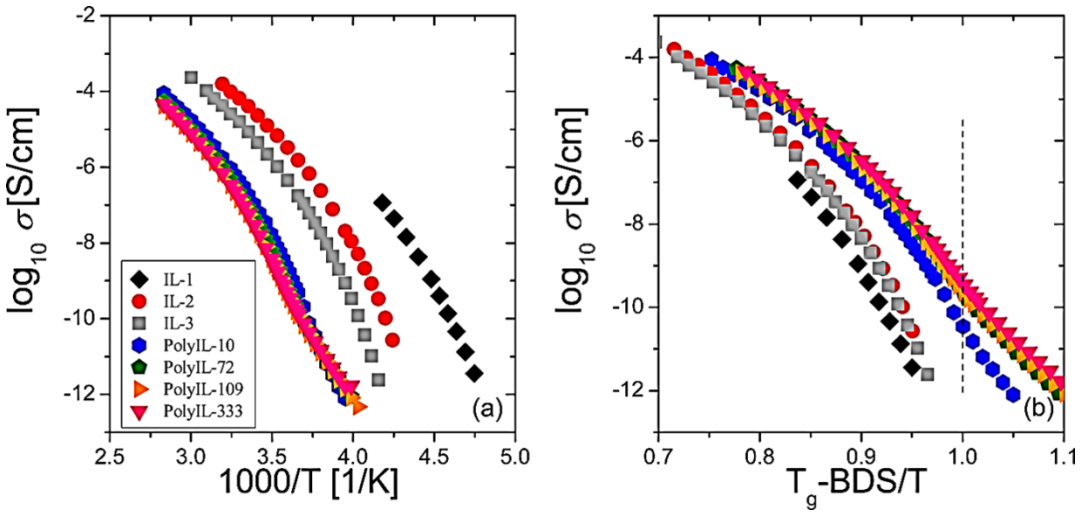

Figure 32. Conductivity values of the IL and PIL samples as a function of (a) 1000/T and (b) T_g-BDS/T.[180]

1.4.4 Mechanism of ion transport and conductivity in PILs

To understand the ion transport mechanism in PIL-based systems we need to understand the ion transport mechanism in some other related systems such as salt-doped polymer electrolytes, ionic liquids, and non-PIL based single-ion polymer electrolytes which have been explained briefly in the early of this section.

- ***Ion transport in salt-doped polymer electrolytes.***

Early studies of ion transport mechanisms in polymer electrolytes were primarily focused on PEO-based polymeric materials doped with a variety of alkali metal salts. The ion transport in such systems occurs through ion hopping mechanism mediated by polymer chain dynamics (Figure 33). The ionic conductivity of PEO membranes doped with different lithium salts has been reported to arise from three contributions: (a) intra-chain Li^+ ion motion along the polymer backbone; (b) co-operative motion of Li^+ ions coordinated with the PEO segments; and (c) the inter-segmental hopping of Li^+ ions from one chain to another

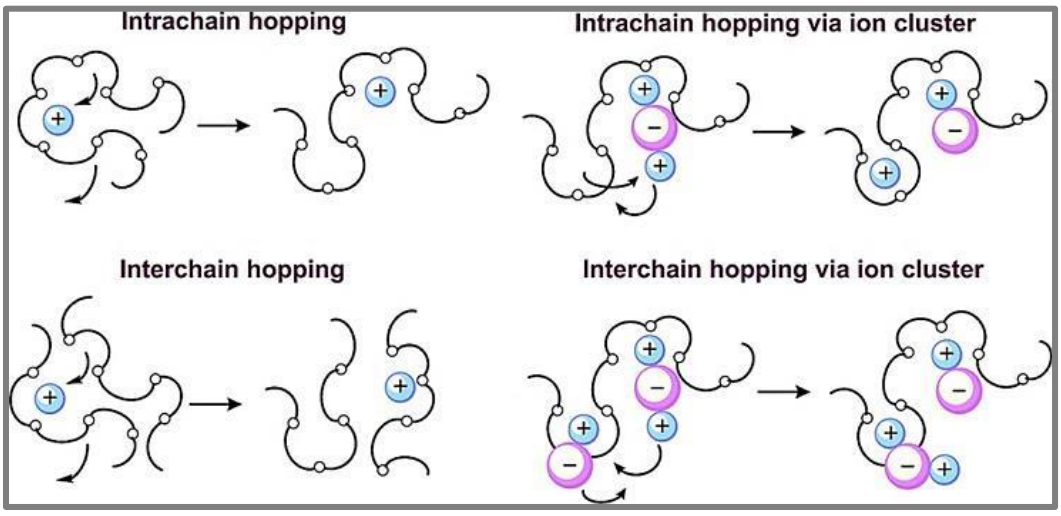

Figure 33. Ion transport mechanism in PEO-salt complexes via hopping and segmental motion.[206]

chain.[207-208] The diffusion of both the cations and the anions are coupled to the segmental motion of PEO chains and the glass transition temperature (T_g) of the polymer matrix. Recently, Ganesan et al.[209] investigated the role of ion solvation and polymer chain motion on the conductivity of such materials. These authors demonstrated that stronger cation–polymer interactions (relative to cation–anion interactions) lead to ion dissociation resulting in increased ionic

conductivity while overcoming the influence of the segmental motion of polymer chains and the glass transition temperature. Webb et al.[210] reported the occurrence of similar type of ion–polymer interactions which enabled the continuous pathway of solvation sites for the transport of Li^+ ions. The above-mentioned studies demonstrated that ion transport in salt-doped polymer electrolytes generally occurs through a mechanism involving a combination of intra- and inter-chain hopping motions. Such ion-transport depends upon two factors both of which depend on the ion–polymer interactions: (i) the solvation of Li^+ ions in the electrolyte which influences the ion dissociation and thus contributing ionic mobility to the overall conductivity and (ii) the polymer segmental dynamics.

- ***Ion transport in non-PIL-based single ion conducting polymer electrolytes.***

Non-PIL-based single ion conductors have attracted considerable attention as potential electrolytes for electrochemical devices, mainly batteries.[165] In this regard, a number of fundamental experimental studies have been carried out to identify the mechanisms and parameters underlying ion transport mechanism in PEO and other polymer-based single ion conductors.[211-214] Since the polarity of such materials is typically low; ions mostly get aggregated into neutral pairs. As a consequence, the ion diffusion occurs through the movement of ion pairs mediated by the segmental motion of the polymer chains. Hence, the mobilities of the ions are strongly coupled to the polymer segmental dynamics. Since ion transport involves neutral ion pairs, the resulting ionic conductivities are often much lower than expected.[213]Maranas et al. studied PEO-based single ion conducting polymeric systems to interpret the fundamental aspects of ion transport.[215-217] The authors observed clustered ion states, where cation hopping

occurs through a combination of pathways involving associated anions and/or the polymer backbone and they concluded that single ion conducting polymeric system should be designed with chemistries that can facilitate enhanced cation hopping through the polymer backbone.[218] In a different set of experimental studies; Frischknecht, Winey and co-workers have examined the effect of molecular architecture on the structure and dynamics of single ion conducting systems.[219-220] The authors illustrated that the architecture and spacing of ionic groups present on the SIC determined the morphology of the ion clusters and architectures which led with percolated ion clusters have faster counter-ion diffusion than systems with isolated clusters.[221] Milner et al. also studied single ion conductors using coarse-grained molecular dynamics simulations and showed that ion transport occurs through consecutive coordination with ion pairs.[222-223] Lin et al.[224] demonstrated the influence of ion–ion interactions on diffusion of cations in SICPEs and observed that decreased cation–anion interaction had almost no influence on cation mobility. This was attributed to the balance of cation–anion and cation–polymer interactions. In the case of weak cation–anion contacts, the cation–polymer interactions slowed the polymer chain motion which resulted in a compensation of the enhancement in cation mobilities achieved due to the reduction in cation–anion association.

In summary, the above mentioned studies on ion transport in non-PIL based SICPEs establish the formation of cation–anion aggregates which is driven by the low polarity of the medium and whose characteristics are influenced by the architecture of the SIC. Cation transport in such a medium occurs through a combination of ion hopping between the anion associated states and through the polymer backbone. As a consequence, ion dynamics in such systems is strongly coupled to polymer segmental dynamics.

- ***Mechanism of ion transport in poly (ionic liquid)s***

A fundamental understanding regarding the mechanism of ion transport in PILs is much needed to design highly conductive PILs. In case of pure ILs, ion diffusion is governed by the ion pair and ion cage formation and breaking mechanism[225]and by the polymer backbone segmental motion in polymer electrolytes such as poly(ethylene oxide).[208, 226]It should be noted that the ionic conductivity of a PIL is several orders of magnitude lower than its IL analogous.[193, 227]Ionic mobility is significantly reduced by the slower polymer chain relaxations in a PIL, indicating that polymer chain relaxations play an important role in ion conduction.[228] Choi et al.[229] reported ionic conductivities of PILs to be strongly related to the glass transition temperature and the segmental motion of the polymer chains. But this observation is in contradiction with some recent experiments where the decoupling between ionic conductivity and structural dynamics in PILs has been reported and also the dc conductivities of the PILs were observed to exceed that of their pure IL counterparts at their glass transition temperature.[189, 205, 230] Hence it is really very important to understand the fundamental ion transport mechanism prevailing in PILs, the origin of differences in ion- transport between PILs and pure ILs, and where the ion-diffusion phenomena is really decoupled from the segmental relaxations and glass transition temperatures in PILs or not.

Mogurampelly et al.[231] recently reported molecular level insights on the mechanisms underlying ion transport in an imidazolium-based PIL electrolyte, poly (1-butyl-3-vinylimidazolium-hexafluorophosphate). The authors used atomistic molecular dynamics simulations to characterize the ion diffusion in both the PIL-electrolyte and pure IL. The experimental results showed that in pure IL, structural relaxation processes served as the primary mechanism underlying ion transport, which significantly slowed upon approaching to the

glass transition temperature. In case of PIL, the authors have classified the different hopping events exhibited by anions into three main categories as represented in Figure 34: type1, intra-molecular anion hopping events along the polymer backbone occurring by means of the formation and breaking of ion-associations; (b) type2, inter-molecular ion hopping events between different polymer chains; (c) type3, anion hopping from polymer chains to free medium and vice-versa. It was observed that the type1 events were the dominant mechanism at all investigated temperatures. Ionic mobilities are also reported to be directly correlated to the average life times of the ion-associations. Such results establish the basis for experimental findings that reported ion transport in PILs to be decoupled from polymer segmental relaxations. This method of analysis was subsequently employed for

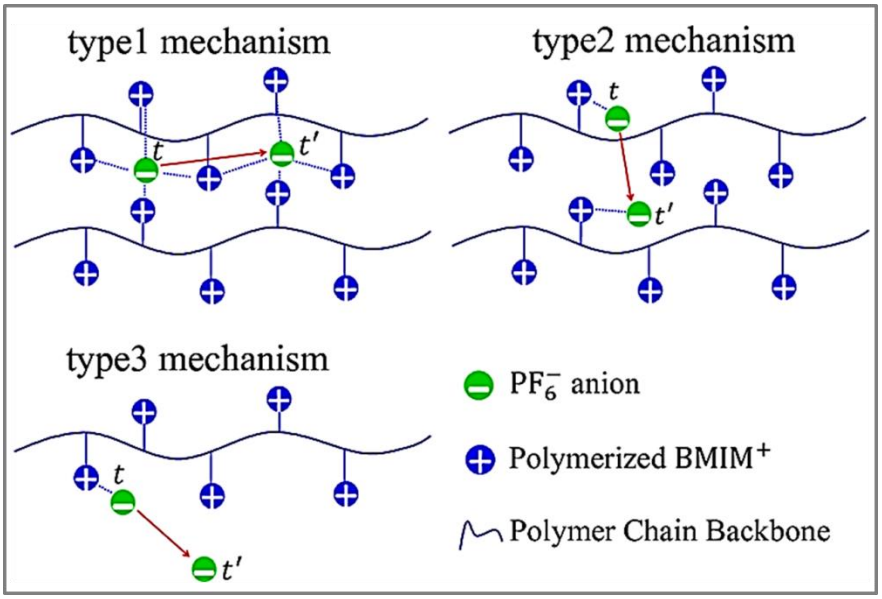

Figure 34. Different types of ion hopping events: intra-chain (type1), inter-chain (type2), and chain-to-free space (and vice versa) in poly(1-butyl-3-vinylimidazolium-hexafluorophosphate) (P[BMIM][PF_6]) electrolyte.[231]

various PILs which provided very crucial information about the rational design of novel PIL-based materials.[232-235] However, the existing ion hopping mechanism was limited to ion association and dissociation, which does not give a complete picture of the motion of a single ion. Later, Liu et al. [236] improved the methodology to understand the ion transport mechanism in a PIL, poly(n-ethylvinylimidazolium bistrifluoromethylsulfonylimide) [poly(C_2VIm)Tf_2N] at various temperatures. String-like cooperative motion of the mobile anions was observed. Effective hopping of the mobile ions contributed to the ion diffusivity which was dominated by inter-chain hopping and mainly facilitated with five associating pendant cation moieties from two different polymer chains.

1.4.5 Ionic conductivity and polymer chain mobility in PILs

To understand the ion dynamics in polymerized ionic liquids, it is necessary to understand the ionic conductivity of ionic liquid molecules which consist purely of ions. The motion of an ionic molecule is directly coupled to the motion of a charge. The ability of each ion to move is characterized by the diffusion coefficient (D). The ion mobility,μ which in electrostatics is the proportionality between the applied electric field ($\vec{E}$) and the average velocity of the ion, $\vec{v}_{\text{drift}}$ =μ $\vec{E}$. The drift velocity plays a crucial role in determining the current density, $\vec{J}$= nq$\vec{v}_{\text{drift}}$, which is a function of the number density of moving charges, n, their charge, q, and the drift velocity. Combining this relation with the current density formulation of Ohm's law, $\vec{J}=\sigma_0\vec{E}$, one can derive an expression for the overall DC-ionic conductivity,σ_0, as a sum over N number of ionic species present in the system:[237]

$$\sigma_0 = \sum_{i=1}^{N} q_i \mu_i \, n_i \qquad (1)$$

In case of ionic liquids, q_i is the charge on each ion, μ_i is the ionic mobility, and n_i is the number density of ions in the system. This is a fundamental equation when it comes to the strategic design of highly ion conducting electrolytes. To increase the ionic conductivity of any particular ionic liquid system, there are only two possible ways, either to increase the number density of charge carriers or the ion mobility. Ionic mobility and diffusivity are related by the Einstein relation as:

$$\mu_i = \frac{q_i D_i}{k_B T} \; ; \qquad (2)$$

where D is the diffusivity, T is the temperature, and k_B is the Boltzmann constant. From equations 1 and 2, it is very clear that ionic conductivity of an electrolyte is controlled by the free ion concentration, the diffusivity, and the charge of the ion. According to the Stokes−Einstein relation for ion diffusion in a liquid,

$$D = \frac{k_B T}{6\pi\eta r} \; ; \qquad (3)$$

where, η is the viscosity and r is the effective hydrodynamic radius of a molecule. Maxwell found that relaxation time and viscosity are inversely proportional and for small solvent molecules we can use Maxwell relation:

$$\eta = G\tau_s; \qquad (4)$$

where G is the glassy modulus and τ_s is the structural relaxation time.

Combination of Stokes−Einstein relation and Maxwell relation gives the relationship $D \propto T/\tau_s$; i.e., the diffusion of ions in liquid electrolytes is controlled by the viscosity (η) and the structural relaxation time (τ_s). Alternatively, combining the Maxwell relation (eq. 4) with the Stokes-Einstein relation (eq. 2) and plugging into the conductivity equation (eq. 1), it is possible to relate the DC-ionic conductivity (σ_0), which is a macromolecular material property, to the structural relaxation of ionic molecules: In the case of polymer electrolytes, ion

transport depends upon the local segmental (structural) dynamics,[238-239] while viscosity is controlled by the motion of the entire chain.

Ionic conductivity in solid-state polymer electrolytes can be enhanced either by increasing the number of ion-containing groups in the polymer or by lowering the glass transition temperature (T_g) of the polymer. In ion-conducting polymers, ionic mobility is influenced by the segmental motion of the polymeric chain above the glass transition temperature.[240] The polymer chains are frozen and unable to move below the T_g, but above that, the polymer chains have enough kinetic energy to start moving. This segmental motion of polymer chains creates free volume leading to generation of enough space for the "hopping" of ionic groups. An ion can hop from one coordination site to the other, which is accompanied by the segmental motion of the polymer chains. In the presence of an external electric field and above the T_g, ion transport is achieved by this continuous hopping of ions which is facilitated by the movement of the polymer main chain. For a plot of ionic conductivity(σ) versus inverse temperature , if the plot is non-linear then it indicates that conductivity is coupled with the segmental motion of polymer chains and this behaviour can be described by the Vogel–Fulcher–Tammann (VFT) equation as follows:[241]

$\sigma = \sigma_0 T \exp\left(-\frac{B}{T-T_0}\right)$;

where σ_0 is the pre-exponential factor related to the amount of charge carriers, B is the activation energy required for ion conduction, and T_0 is a reference temperature (also termed as Vogel temperature) which typically falls 10-50 K below the glass transition temperature. The VFT equation was initially developed to explain the ion diffusion process in glassy and amorphous polymeric material and it was derived from quasi-thermodynamic models of free volume and configurational entropy, and this type of behaviour can be seen in solid polymer electrolytes above the glass transition temperature. As already mentioned, VFT

behaviour in a polymer material indicates that ion motion is associated with the long-range motions of the polymer backbone or solvent molecules and the conductivity arises due to the diffusion of ions from one free volume to another. There is a strong 'coupling' between ion diffusion and polymeric relaxation. In general, diffusion of ions in a polymeric material cannot occur unless there is an associated relaxation process.[241-244] Polymeric materials with higher conductivity values usually relax more rapidly, or at a higher frequency than the insulating materials, and when temperature is scaled to the glass transition temperature, parameters fall on the same VFT curve which allows a direct comparison. When the relaxation of the host polymer or polymeric matrix occurs rapidly, the ionic conduction tends to increase, which is usually associated with the host polymer having a low glass transition temperature. However, when the temperature approaches below the T_g of the polymeric material, the segmental relaxation is significantly slowed down as the polymeric backbone does not have enough kinetic energy to move. As a result, free volume of the polymer decreases and diffusion of ion becomes more difficult. Below T_g, conductivity in polymer electrolytes displays Arrhenius-type behaviour and can be described as follows:[241]

$\sigma = \sigma_0 \exp\left(-\frac{E_a}{kT}\right)$;

where σ_0 is a pre-exponential factor, E_a is the activation energy, and k is Boltzmann's constant. In polymeric materials which show Arrhenius-type behaviour, ion diffusion occurs by a simple hopping mechanism that is decoupled from segmental motion or long-range motions of the polymer matrix. This can be due to the rotation or movement of pendant groups coming off the polymer chain.[180, 186, 245] The current focus in creating effective solid polymeric electrolytes lies in improving the conductivity as much as possible in the solid-state below the glass transition temperature.

1.5 Photoinitiators for aqueous polymerization

1.5.1 General aspect

1.5.1.1 Photopolymerization

The use of light to control the formation, structure and properties (chemical, mechanical or biological) of polymeric materials has always been one of the interesting topics of research in polymer science.[246] Photopolymerization (also termed as photoinitiated or photoinduced polymerization) is a technique that uses light (visible or ultraviolet) to initiate and propagate a polymerization reaction to form a linear or crosslinked polymer structure.[247] This technique plays a crucial role in polymer chemistry and shows a number of economic advantages over the conventional thermal polymerization, such as rapid curing, curing at spatially well-defined regions, low energy requirements, room-temperature treatment, non-polluting and solvent-free formulations and low cost.[248-250] Photopolymerization is applied in various fields which include industrial applications like coatings (on wood, plastic, paper or metal surfaces), adhesives, 3D printing (stereolithography), microelectronics, optics, as well as in biomedical applications (e.g. tissue engineering, dental fillings and ophthalmology).[248, 251-252]

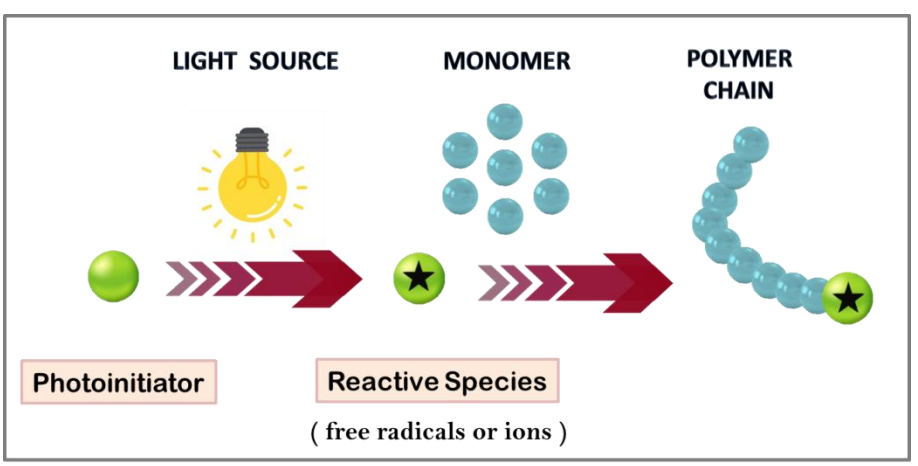

Figure 35. General representation of a photoinitiated polymerization reaction.[248]

Photoinitiator or photoinitiating system is a key component in every photopolymerization reaction. A photoinitiator can be defined as a single molecule or combination of molecules that upon absorption of light (visible or ultraviolet) generates reactive species which initiate the polymerization process (Figure 35).[253] These reactive species may be free radicals (in free radical photopolymerization) or ions (e.g. in cationic photopolymerization), the free radical process is though frequently applied.[254-255] The type and concentration of photoinitiator, irradiation time, the intensity and wavelength of the initiating light, reaction temperature, and monomer structure and concentration largely affect the reaction rate and grafting density.[256] The initiating systems based on one-component, two-component or multi-component photoinitiators play an important role in photopolymerization processes.[257-258] Photoinitiating systems not only determine the mechanism of the polymerization process, but also affect its performance, curing speed and final properties of the polymer such as hardness and viscosity. Thus, the selection of an appropriate photoinitiator is essential to achieve the desired photopolymerization reaction rate and polymer properties. The basic parameters determining the selection of the photoinitiator are maximum absorption wavelength (λ_{max}) and molar extinction coefficient (ε). The efficiency of the photoinitiator is directly related to its structure, which influences the range of absorption and quantum efficiency of the photochemical and photophysical processes that take place in the excited states.[259] Researchers are continuously trying to develop new type of photoinitiators and particular interest is paid on water-soluble photoinitiating systems, which are important for industrial as well as biomedical applications[260-261].[262]

1.5.1.2 Free radical photopolymerization

Free radical photopolymerization is an extensively used methodology for the preparation of polymeric materials especially where its unique features (spatial resolution, precise control of the process etc.) are particularly important.[263] The

photoinduced radical polymerization occurs according to the typical radical polymerization mechanism and consist of three main steps: initiation, chain propagation and chain termination.[255] The radical photopolymerization is initiated by the generation of a free radical (R•) by a photoexcited photoiniator through a unimolecular (Type 1) or bimolecular process (Type 2) (Figure 36) which may add to the first monomer unit. During the propagation step, the free radical reacts with the monomer/oligomer forming a radical bearing monomer or oligomer (RM•) which is termed as macroradical. The macroradical then starts to grow by addition to more monomer units. The reaction proceeds through the propagation step and the chain reaction is terminated (chain termination step) via combination of two polymer radicals or disproportionation reactions.[255] There are other possibilities like quenching of the active

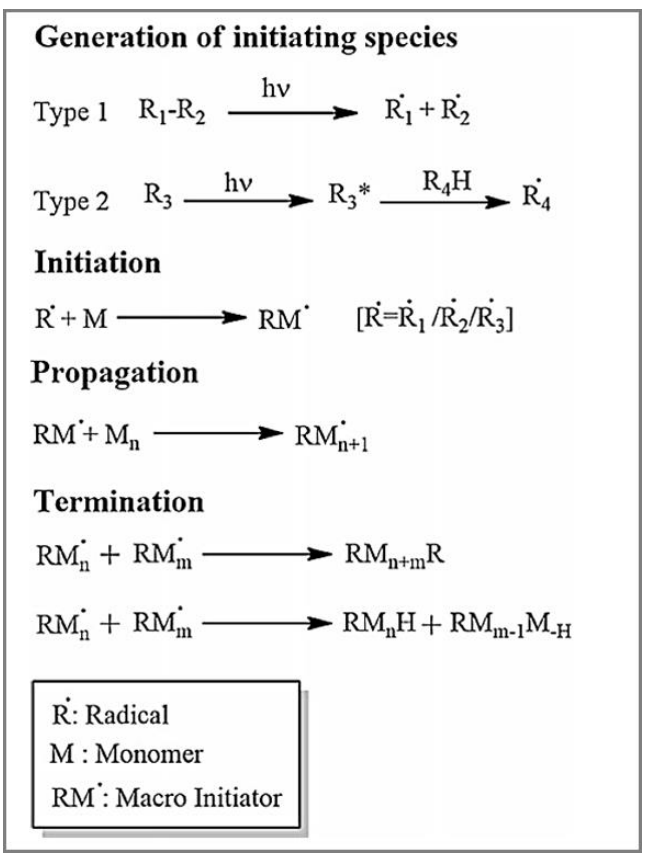

Figure 36. Different stages of photoinitiated free radical polymerization.[264]

radicals by molecular oxygen which can also terminate the polymerization process. Figure 37 showed a graphical representation of the progression of polymerization with time for any free radical photopolymerization reaction. The presence of inhibitors like dissolved oxygen or any other added components which are able to consume free radicals present in the polymerization medium has a destructive effect on the initiation process. The reactive species formed during the initiation step react with the inhibitors, leading to almost no polymerization reaction at the very beginning. This phase of the reaction is called the induction phase. The induction period is the relatively flat part at the initiation region. After complete consumption of the inhibitors through reactions, the initiating species start to react with monomer forming a macroradical. The diffusion of the macro radicals throughout the medium leads to a rapid increase in the rate of polymerization reaction until it reaches a maximum. The progress of the polymerization is associated with a change in viscosity and refractive index of the polymerization medium. The viscosity of the polymerizing medium continuously increases to the point where monomers are trapped between growing polymer chains. At this point, the polymerization reaction is terminated by the limited diffusion of the monomer. Due to this, photopolymerization reactions never yield 100% conversion of monomer.

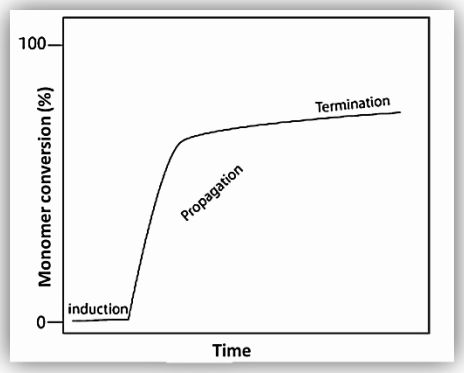

Figure 37. General representation of conversion of monomer (%) versus time during photopolymerization.[264]

1.5.1.3 Free radical photoinitiators

As already mentioned earlier, in radical photopolymerization, the photoinitiation starts when the photoinitiators upon absorption of photon generate free radicals. This process is controlled by the stability of the photoexcited state and the energy of the bonds within the

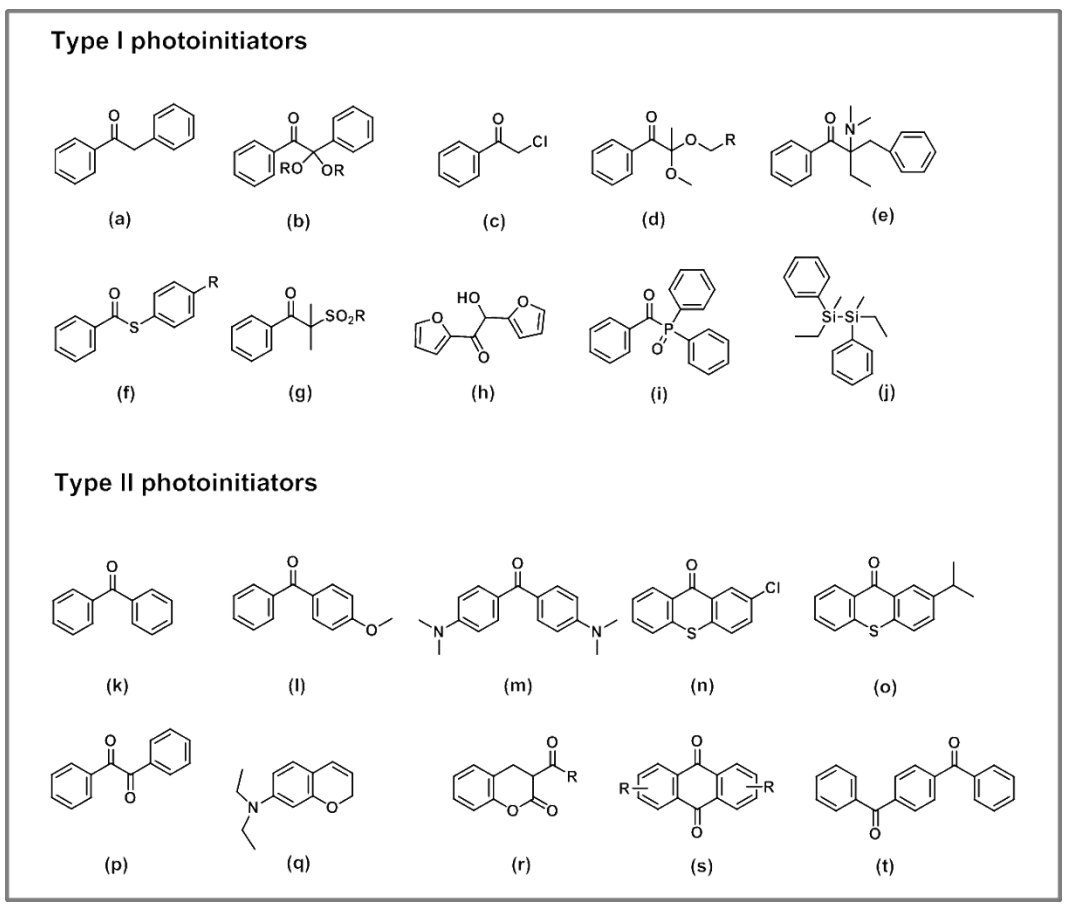

Figure 38. Different examples of Type I and Type II photoinitiators.

excited molecule. Free radical photoinitiators are divided into two main classes: cleavage (Norrish Type I) and H-abstraction type (Norrish Type II) initiators. Multicomponent initiating systems are also known.[254] The Norrish Type I PIs are aromatic carbonyl compounds such as benzoin derivatives, acetophenone derivatives, halogenated ketones, aminoketones, thiobenzoate derivatives,

sulfonylketones, 2,4,6-trimethylbenzoyl-diphenylphosphine, organosilanes etc. Some examples of Type I photoinitiators are shown in Figure 38. These compounds absorb light in the UV or near-UV range due to the $n \rightarrow \pi^*$ and $\pi \rightarrow \pi^*$ transition of the carbonyl group at around 320 – 360 nm and 280 – 300 nm respectively. The carbonyl groups of these initiators absorb a photon and are transformed into an excited state. Subsequent homolytic cleavage of the excited α-carbon bond (α-cleavage) produces two primary free radicals. Norrish Type II photoinitiators involve more than one molecule. A simple Type II photoinitiator consists of a bimolecular system involving an initiator and a co-initiator. Recently, one-component Type II systems, consisting of both the photoinitiator and the co-initiator within one molecule have been reported.[265] The initiator first absorbs photon and is excited into a long-lived triplet state, followed by an electron-transfer or a hydrogen-abstraction reaction with a co-initiator (e.g., alcohols, tertiary amines, or thiols). The co-initiator molecule then reacts with a monomer to initiate polymerization. Examples of Type II photoinitiators include benzophenone derivatives, thioxanthone derivatives, diketone (benzil) derivatives, coumarin, ketocoumarin, anthraquinone derivatives, terephthalophenone derivatives etc. Some examples of Type II photoinitiators are shown in Figure 38. Type I photoinitiators are more efficient than Type II, but produce more side products.[256] Type II photoinitiation process is usually slower and less efficient due to the bimolecular process, back electron transfer and more importantly the solvent cage effect in aqueous solutions.[266] On the contrary, the energy of photons in the visible range is generally lower than the dissociation energy of the individual bonds present in any organic compound. Therefore, it is particularly difficult to obtain a highly efficient photoinitiator operating in the visible range. Due to this, bimolecular systems are used as visible light photoinitiators.[267] The properties of the photoinitiator are crucial for

any photoinduced polymerization, having a substantial impact on the most important step, the initiation. Figure 39 depicts the general mechanisms of Type I and Type II photoinitiators.

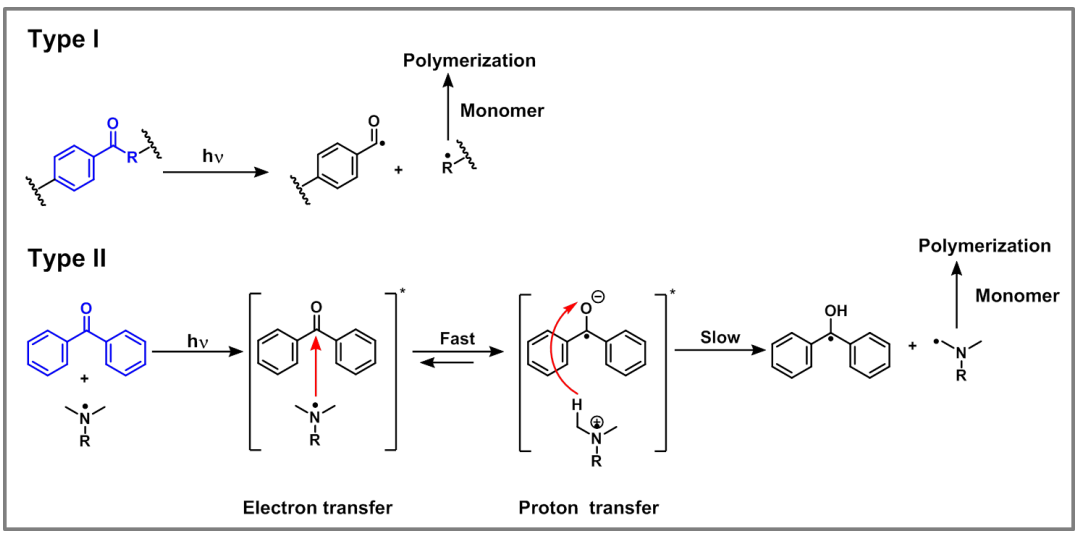

Figure 39. Photoinitiating mechanism of Type I and Type II initiators.

It is also noteworthy to discuss the photoinitiation mechanism of two-photon active initiators (Figure 40). These photoinitiators have highly conjugated π-systems with good coplanarity and strong donor/acceptor groups.[268] In case of radical photopolymerization, after the intra- and inter-molecular charge transfer interactions between the two-photon excited initiator and the monomer, radicals are formed by electron transfer which ultimately initiate the polymerization reaction.[269] [270] This type of polymerization process is an important tool to build a variety of 3D matrices for micro-and nano- scale 3D printing. However, two-photon initiating mechanism for more complex systems (e.g., thiol-ene polymerization) has still remained unexplored.

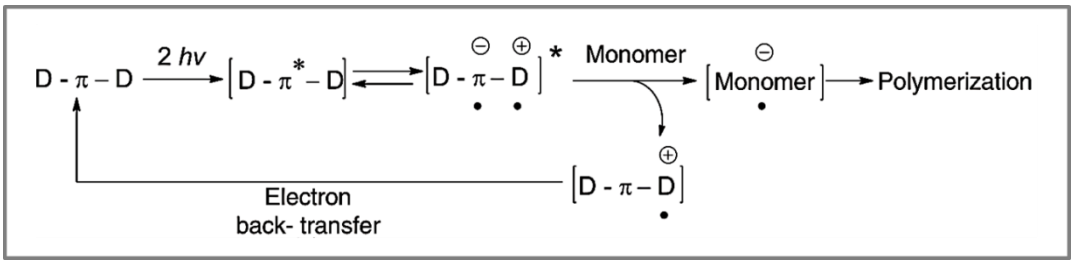

Figure 40. Schematic mechanism of photoinitiation by two-photon active initiators.[268]

Recently, multi-component photoinitiation systems, based on electron transfer and systems based on hydrogen abstraction are interesting alternatives. Electron transfer is based on the interaction between an excited electron donor or acceptor and a second component (electron acceptor or donor respectively) in the ground state, which is responsible for the photoinduced electron transfer process. The dual role of an excited photosensitiser molecule, which acts as the primary light absorber in a multiradical system,[271] can be understood as follows (Figure 41) :

- In first case, the photosensitiser acts as an electron donor and the transfer of the electron to the co-initiator leads to the formation of a cationic radical of the photosensitizer and an anionic radical of the co-initiator,
- In other case, the photosensitiser acts as an electron acceptor and electron transfer from co-initiator to photosensitizer generates anionic radical of the sensitizer molecule and cationic radical of the co-initiator.[267]

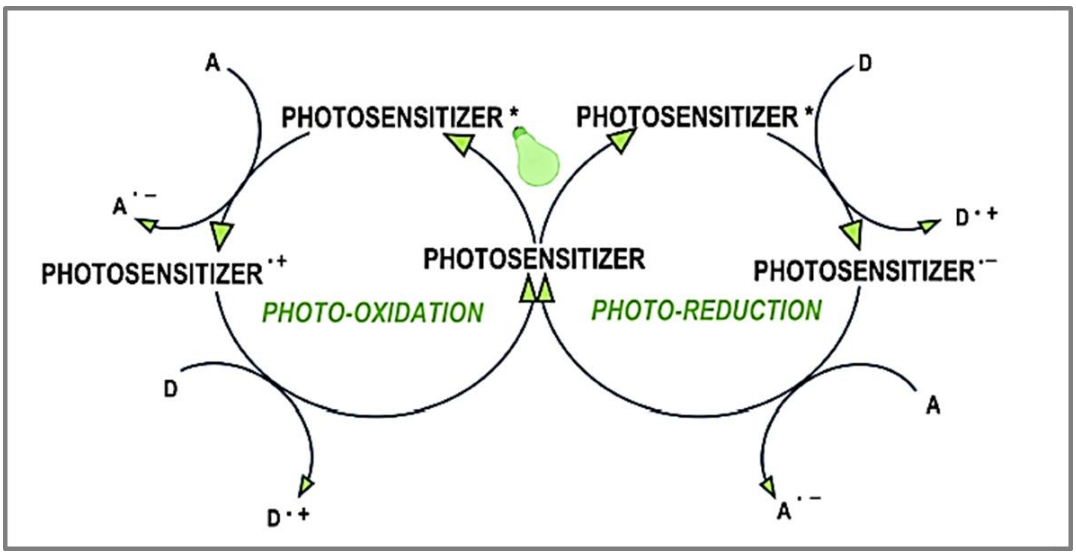

Figure 41. Initiation mechanism in multi-component systems. (Here D and A represent an electron donor and acceptor respectively).[267]

1.5.1.4 Water-soluble free radical photoinitiators

Water-soluble photoinitiators even though known for a long time have been less explored than the organo-soluble photoinitiators due to lack of demand from industry.[272-273] However this scenario has changed recently and water-soluble photoinitiators has gained popularity in the painting and coating industries. Recently, they are now in strong demand to polymerize water containing highly fluid resins for applications such as inks in graphic arts and food packaging.[273] Nowadays water-soluble photoinitiators are extensively used in biomedical application such as in the preparation of biodegradable polymer hydrogels which can be used as drug delivery systems.[274-276] Hence scientists are continuously trying to develop new type of water-soluble photoinitiators which can be used successfully in different waterborne compositions but it was always a great challenge because the increase in water solubility did not always follow the requisite lack of toxicity of these photoinitiators. The continuous growth of emerging water-soluble photoinitiators has been shown in Figure 42. The

breakthrough came in the beginning of 21st century when photoinitiators, like 2-hydroxy-1-[4-(2-hydroxyethoxy) phenyl]-2-methyl-1 propanone (Irgacure 2595) and water-soluble derivatives of acylphosphine oxides, e.g., monoacylphosphine oxide (MAPO) and bisacylphosphine oxide (BAPO) were developed and extensively used in hydrogel synthesis or in various biomedical applications. However, very little commercially available Type I photoinitiators are really water-soluble and only Irgacure 2959 is used for true water-phase photopolymerizations.[273, 277] Nowadays researchers have particularly focused on designing innovative photoinitiators by modifying the already known photoinitiators in order to increase their water solubility, absorption range and initiation efficiency to obtain a fast and efficient photoinitiating system. [262]

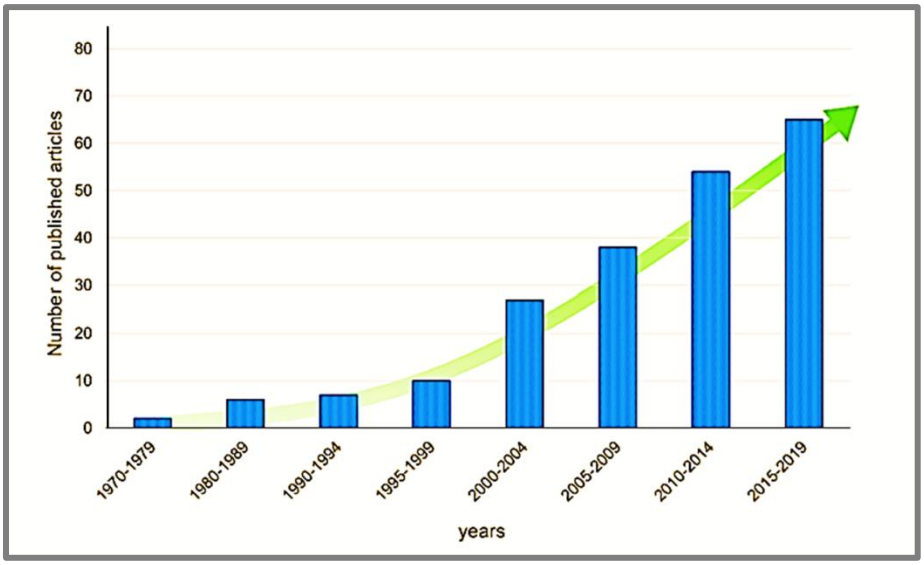

Figure 42. Number of published articles on water-soluble photoinitiators in the years 1970–2019.[267]

1.5.1.4.1. Type I photoinitiators for free-radical polymerization

- ***α-hydroxyketones and their derivatives***

The basic method to increase the water-solubility of conventional radical photoinitiators is to chemically modify their structure by adding appropriate groups to them.[278-279] These water-solubilising groups are: non-ionic ethers, polyethers, hydroxyethers, sulphonates, carboxylic acids, thiosulphates and ionic substitutes such as quaternary ammonium salts. [280-282] The most common solubilising group is the hydroxyl group, which can be found in the most accepted and one of the first commercially available water-soluble photoinitiators: 2-hydroxy-1-[4-(2 hydroxyethoxy)phenyl]-2-methyl-1-propanone (Irgacure 2959) (Figure 43). Irgacure 2959 ,a water-soluble α- hydroxyketone , is a Type I photoinitiator which upon photo-irradiation cleaves into two radicals, benzoyl and alkyl, which can both initiate a polymerization reaction.[267] Despite its drawbacks, such as low water solubility (< 2 wt. %), Irgacure 2959 has become widespread and a range of water-soluble initiators has been created on its core by simply modifying the primary carboxylic group.[283-284] One of the disadvantages of Irgacure 2959 and its derivatives is the need to use UV light. Its maximum absorption (λ_{max}) is at 276 nm and due to its poor absorption, Irgacure 2959 requires an extended exposure time.[267] Irgacure 2959 is widely used in preparation of hydrogel materials,[285-287]cell encapsulation[288-289] and for the targeted delivery of drugs and cells.[290] Liska et al. reported the syntheses of new water-soluble photoinitiators consisting of alkylphenones, benzophenones and thioxanthones and were accompanied by carbohydrate residues such as glucose and cellulose. These initiators showed high efficiency in the initiation process and considerably better water-solubility than Irgacure 2959.[291] Kojima et al. reported a novel water-soluble photoinitiator: sodium 4-[2-(4-

morpholino)benzoyl-2-dimethylamino] butylbenzenesulphone (MBS) which was synthesized by the sulfonation of 2-benzyl-2-(dimethylamino)-1-(4-morpholinophenyl)-1-butanone (BDMB).[292]and it has been used in many biomedical applications.[293-294]

- ***Phosphine Derivatives***

Mono-acylphosphine oxides (MAPO) and bi-sacylphosphine oxides (BAPO) are mainly water-insoluble initiators that absorb light range of 380–450 nm. Diphenyl (2,4,6 trimethylbenzoyl)phosphine oxide (TPO) is one of the first commercially available mono-acylphosphine initiators and this Type I photoinitiator was reported to be highly efficient in the polymerization process which offers advantages like good thermal stability and lack of colour and odour. However, major disadvantage is its very poor water-solubility.[295]Majima et al. reported the first water-soluble TPO derivative: lithium phenyl-2,4,6-trimethylbenzoylphosphinate (LAP), which showed good spectroscopic properties and high water solubility.[296] Later Fairbanks et al. improved the synthetic route for LAP photoinitiator.[297] LAP is a commercially available and widely used photoinitiator for obtaining hydrogel materials.[298-299] Recently, Pawar et al. have developed water-dispersible TPO nanoparticles, which showed high molar extinction coefficient and good water-solubility.[300] Benedikt et al. reported the comparative analyses of two bisacylphosphine oxide (BAPO) derivatives: BAPO-OLi and BAPO-ONa based on their spectroscopic characteristics, polymerization kinetics and cytotoxicity.[260, 262] Both derivatives were suitable as highly effective photoinitiators for obtaining hydrogel materials. Wang et al. reported a modification of BAPO by grafting its structure into a polyethylene glycol (PEG) chain, which improved its water-solubility.[301]

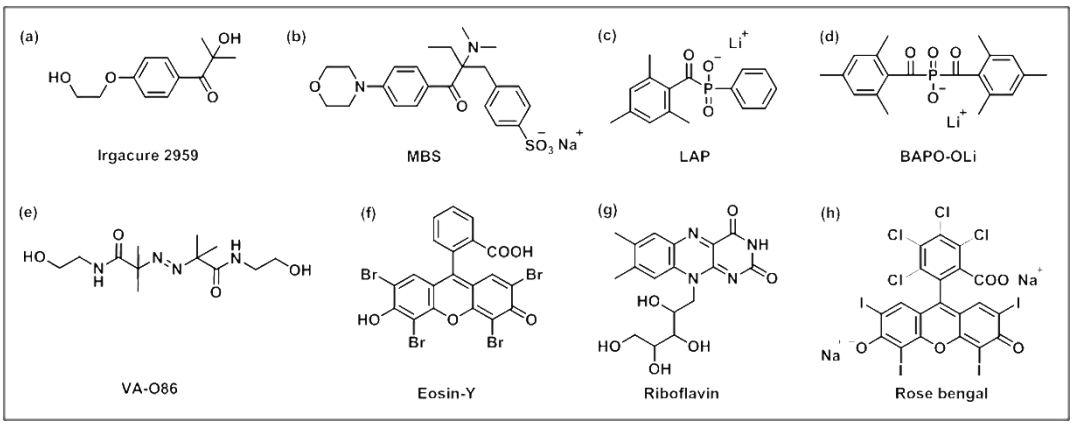

Figure 43. Examples of some commonly used water-soluble Type I (a-e), Type-II (f-g) and two-photon (h) photoinitiator.

- ***Azo-Initiators***

Commercially available water-soluble azo-initiator – 2,2'-azobis[2-methyl-N-(2-hydroxyethyl) promionamide] (VA-086) is most popular because of its low cytotoxicity, while its range of absorbance offers the possibility of using different light sources in the far UV range.[302] VA-086 initiator has successfully been used in the preparation of hydrogel microstructures and in tissue engineering.[303-304] Han et al. developed a two-component photoinitiating system by combining Irgacure 2959 and VA-086 photoinitiators, which was used in preparation of hydrogels with improved mechanical properties.[305]

1.5.1.4.2 Type II photoinitiators for free-radical polymerization

Eosin-Y is an example of the water-soluble Type II photoinitiator, which needs an electron-donor molecule (co-initiator) such as an amine to initiate a polymerization reaction. [306] This Type II photoinitiating system, Eosin-Y with an amine, has been used for the synthesis of hydrogels based on polyethylene glycol (PEG), [307] poly(ethylene glycol) diacrylate[308] and gelatin-methacryloyl.[309] It

has also been reported that Eosin-Y can act as a single-component photoinitiating system in a thiol-ene photo-click polymerization reaction.[310]

Riboflavin is also a highly water-soluble Type II photoinitiator, which in combination with a co-initiator can successfully initiate polymerization reaction. Bertolotti et al. used a combination of riboflavin and triethylamine as a photoinitiation system for the fabrication of methacrylate hydrogels.[311-312] Riboflavin with L-arginine as a co-initiator has also been used as a photoinitiating system to produce hydrogels.[313] Another water-soluble Type II photoinitiator is camphorquinone (CQ), which belongs to the class of aliphatic-ketone. This photoinitiator in the presence of tertiary amine as an electron donor is used for the cross-linking of tooth fillings based on methacrylate resins.[314] Camphorquinone, as a photoinitiator in the visible range, has some drawbacks like poor water-solubility and yellowing of cured product, which limits the possibility of using this photoinitiator to create hydrogel polymer networks.[315] To increase the water solubility of camphorquinone, carboxylated camphorquinone was developed, which showed good spectroscopic properties.[316] The most commonly used co-initiators with camphorquinone are amines such as triethylenamine and ethyl-4-(N, N-dimethylamino)benzoate.[317-318] The application of this photoinitiator includes production of hydrogels for targeted drug delivery and tissue engineering.[319-320]

1.5.1.4.3 Two-photon photoinitiators

Two-photon induced polymerization technique is considered to be a powerful tool for the microfabrication of 3D hydrogels.[321] Two-photon absorption occurs only within the small laser focal volume and hence this technique provides excellent spatial control with high resolution in the sub-micrometre range.[322] Moreover, the long wavelength of the excitation source (near-infrared region)

offers the advantages of deeper tissue penetration with reduced risk for unintended photodamage,[323-324] which make this technique suitable for various biological applications.[325-326] This technique requires an appropriate two-photon initiator which must be water-soluble, thermally and optically stable and should generate free radicals easily. The main challenge for two-photon initiators is to increase their water solubility. One of the strategies to increase the hydrophilicity is the addition of non-ionic surfactants. Jkaverii et al. carried out two-photon polymerization reaction using commercially available Irgacure 651 photoinitiator along with a surfactant, AF240.[327] Although, this approach facilitates the fabrication of hydrogel structures within an aqueous formulation, large amounts of surfactant are needed to ensure adequate initiation efficiency. The well-known UV photoinitiator Irgacure 2959 was also used in this technique for water-based formulations due to its reasonable hydrophilicity and low cytotoxicity[328] but it is only processable with 515 nm pulsed laser.[329] Till date, the most popular hydrophilic two-photon photoinitiating system is a dye–amine combination. Due to suitable absorption at desired wavelength and easy accessibility, commercially available hydrophilic xanthene dyes, such as rose bengal,[330] Eosin-Y[331] and erythrosine[332] in combination with amines are in two-photon induced polymerization. In these initiation system, the dye is excited by two-photon absorption and subsequently intermolecular electron transfer followed by hydrogen transfer from the amine to the excited dye molecule generates active amine radicals to initiate the polymerization reaction.[330] The main disadvantages of such initiation process are the requirements of high laser intensities and long exposure times.[333] Additionally, intrinsic limitations for bimolecular systems, such as limited electron transfer efficiency between the dye and co-initiator molecule or back transfer of electron can significantly decrease the initiation efficiency.[266] Another important and effective way to

produce efficient water-soluble two-photon initiators is to introduce water-borne functional groups, such as quaternary ammonium cations or carboxylic sodium salts, onto the known core structures possessing high two-photon absorption initiation efficiency.[334-335]

1.5.1.4.4 Ionic liquid-based photoinitiators

Phosphonium-based ionic liquids, tetrabutylphosphonium persulfate (TBPPS), and trihexyltetradecylphosphonium persulfate (TETDPPS) have earlier been reported as thermal free radical initiators by Mariani and coworkers.[336] However, the development of ionic liquid –based photoinitiators has lagged behind. Photoinitiators that contain an ionic liquid moiety can be termed as 'photoinitiating ILs' and researchers recently are trying to give focus on this particular area. Two acetophenone-imidazolium photoinitiators: 1-(p-hydroxy-acetophenone)-3-methyl imidazolium tetrafluoroborate and l-(p-hydroxy-acetophenone)-3-methyl imidazolium hexafluorophosphate were synthesized and their photopolymerization abilities were investigated.[337] These photoinitiators were able to initiate the polyurethane acrylate (PUA) polymerization in air or N_2 atmosphere within a minute. However, the photoinitiators were somewhat less efficient than commercially available photoinitiator Darocure 1173. The same group reported the syntheses of three acetophenone ammonium tetraorganylborate salts (Figure 44) and these salts were used as photoinitiators to polymerize B205 (bifunctionality PUA).[338] The experimental results indicated that they were efficient for the polymerization but less than Darocur 1173. Further, this group also synthesized two quaternary ammonium tetraphenyl borate salts, which were able to initiate the free radical photopolymerization under UV irradiation and cure an epoxy resin.[339]

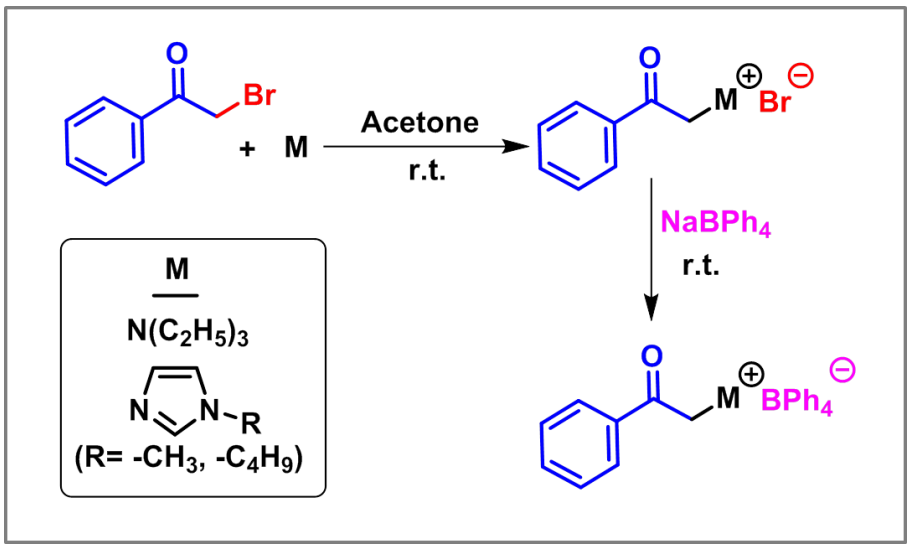

Figure 44. Synthesis of ammonium- or imidazolium-based ionic liquid photoinitiator.[338]

1.6 Polymeric hydrogels

1.6.1 Basic overview

The term 'Hydrogel' was first originated in 1894; then it was known as a colloidal gel of inorganic salts. Later, consecutive development in the field gave rise to newer discoveries. At the preliminary phases, cross-linked PVA hydrogel was constructed by gamma irradiation in the year 1958. Hydrogels are highly cross-linked 3D-network structures that are capable of absorbing enormous amount of water because of the presence of polar groups like carboxyl, hydroxyl, amide and sulphonic groups. Physical interactions or chemical cross-links are either of the two things that hold the hydrogels together. Hydrogels are regarded as novel polymers utilized for new material growth.[340-342] Hydrogels are also known as 'Smart Gels' depending upon how they respond to the external stimuli like ionic strength, temperature and pH that make them extremely efficient in several fields like biomedical, sensing and other applications in the industrial fields.[343-345]

Typically, hydrogels are prepared using either synthetic or natural polymers. Biopolymer-based hydrogels have been widely used in numerous fields like agriculture, biomedical materials, hygiene products, biosensors, heavy metal ions, dyes etc.[346-351] Several biopolymers such as sodium alginate, chitin, starch, cellulose, hemicelluloses and the derivatives of them have been used to originate hydrogels. The exemplary potentials of hydrogels have made them worthy of the synonyms as 'Smart' or 'Intelligent' materials, especially in the field of biomedical applications. Hydrogel's ability to respond to external stimuli like physical or chemical changes and appropriate phase transitions with time have focused the research in bio-implants, scaffolds, optics, drug delivery and others. The physical stimuli include temperature, solvent, intensity of light, electric potential, magnetic fields and pressure. The chemical stimuli include ions, pH and specific chemical compositions. The transition in hydrogels on exposure to the external stimuli is reversible in most of the cases. Nature of the monomer, charge density, cross-link density and the magnitude of external stimuli determine the response of hydrogel.[352-353]

1.6.2 Classification of Hydrogels

Hydrogels can be broadly categorized based on their origin, polymeric composition, configuration, physical appearance, type of cross-linking, network electrical change and response to external stimuli (Figure 45).[354]

- ***Based on Origin***

Hydrogels can be fabricated from polymers that have a natural/synthetic/semi-synthetic origin. Hydrogels based on natural polymers can be manufactured from sodium alginate, chitosan, cellulose or hemicellulose, whereas synthetic hydrogels are widely synthesized from vinyl monomers with the help of conventional polymerization methods.[355-356]

- ***Based on polymeric composition***

According to the composition of the polymer, hydrogels can be classified into three major categories: (i) homopolymer hydrogel, (ii) copolymer hydrogel (iii) multi inter-penetrating polymeric hydrogel and (iv) semi-interpenetrating polymeric hydrogels:[354]

(i) Homo-polymeric hydrogels are fabricated using a single species of monomer. The kind of monomer and the techniques of polymerization are the key points for the cross-linked structure of homopolymers.

(ii) Co-polymeric hydrogels can be synthesized by using two or more types of monomeric species, one of the components of which is hydrophilic. Copolymerization can lead to different kinds of configurations like random, alternate or block.

(iii) Interpenetrating polymeric hydrogels can be manufactured by using two different polymers that are cross-linked to form a 3D-network structure.

(iv) Semi-Interpenetrating polymeric hydrogels are fabricated having cross-linked polymers as one of the components and a non-cross-linked polymer as the other component.

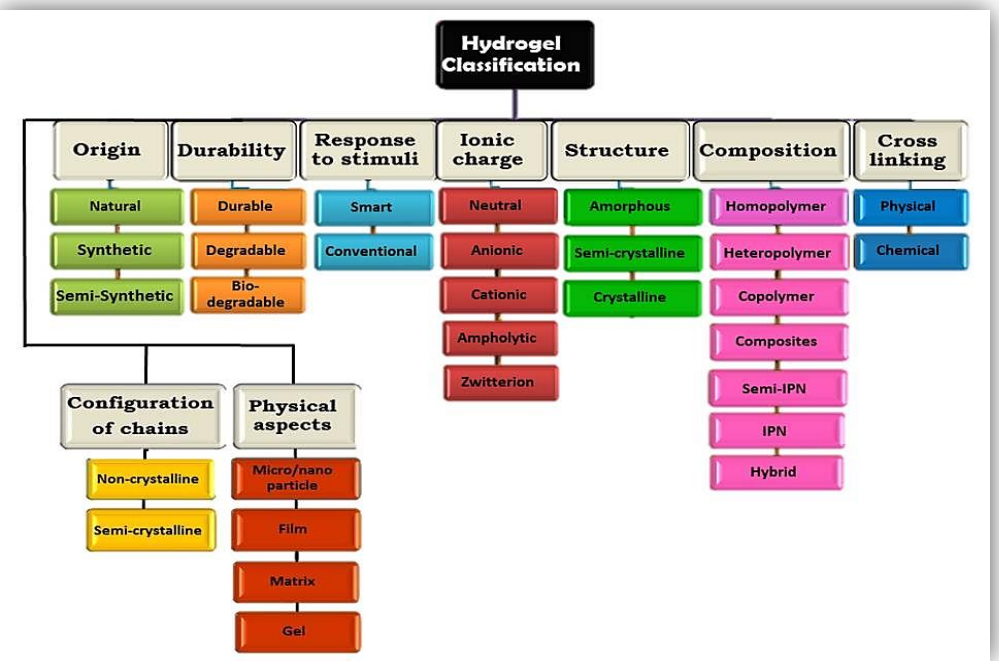

Figure 45 . Classification of hydrogels.

- ***Based on the configuration of polymer***

Based on the physical and chemical composition of the polymer used for hydrogel synthesis, hydrogels can be divided further into three types, (i) Amorphous i.e. non-crystalline, (ii) Semi-crystalline i.e. a mixture of amorphous and crystalline and (iii) Crystalline.

- ***Based on the type of cross-linking***

Depending upon the nature of cross-linking, hydrogels may be divided into two categories, (i) Chemically cross-linked hydrogels and (ii) Physically cross-linked hydrogels.[355]

(i) **Chemically cross-linked hydrogels** are formed by covalent bonding that result in strong cross-linked networks. These are permanent hydrogels and never get dissociated without complete degradation.

(ii) **Physically cross-linked hydrogels** are originated by secondary forces such as ionic, hydrogen bonding or hydrophobic interactions. All these physical interactions are reversible and can be disrupted by alterations in physical conditions or application of stress.

- ***Based on network electrical Charge***

Hydrogels can be further classified into three main groups on the basis of presence or absence of electrical charge that are located in the cross-linked polymer chains such as: neutral/non-ionic hydrogels, ionic hydrogels, and ampholytic hydrogels. [357] In neutral or non-ionic hydrogels, there is no charge on their backbone or side groups. Examples of non-ionic hydrogel include polyacrylamide (PAAm), poly(2-hydroxyethyl methacrylate) (PHEMA), poly (vinyl alcohol) (PVA), and polyethylene glycol (PEG). Ionic hydrogels represent both cationic (positive charge bearing) and anionic (negative charge bearing) hydrogels. Examples of cationic hydrogel include poly(4-vinylpyridine) (PVP), poly(2-aminoethyl methacrylate) (PAEM) and poly(N,N-dimethylaminoethyl methacrylate) (PDMAEMA), whereas anionic hydrogels include polyacrylic acid (PAA), poly(styrene sulfonic acid) (PSSA), poly(itaconic acid) (PIA), poly(crotonic acid) (PCA), poly(maleic acid) (PMA), and poly(methacrylic acid) (PMAA).[358] Ampholytic hydrogels carry negative as well as positive charges on the same polymer chain. This type of hydrogel contains polymer chains having both acidic and basic groups in each repeating unit. Poly(*N*-isopropylacrylamide)/poly((3-(methacryloylamino) propyl)dimethyl(3-sulfopropyl) ammonium hydroxide) (PNIPAM/PMPSA) copolymer hydrogel is an example of ampholytic hydrogel.[359] The presence of different ionic groups along the hydrogel backbone can affect the swelling properties of the hydrogels which has been discussed later. Electrostatic interactions between oppositely charged species can form inter or

intra-molecular interactions and therefore, consequently affect the different properties of hydrogels.[360]

- ***Based on external stimuli response***

Another type of hydrogel, which responds to the changes in pH, temperature, irradiation, pressure and chemical stimuli, is known as responsive or smart hydrogels. Smart hydrogels undergo very fast and reversible changes. These smart polymers may be used for various applications such as engineering and biomedical applications.[360]

1.6.3 Typical polymerization techniques used for hydrogel synthesis

As already mentioned, hydrogels are 3D- polymeric networks that typically can absorb and contain large amount of water molecules due to the presence of hydrophilic groups in the constituent polymeric networks.[361] The term 'network' suggests the presence of crosslinks within hydrogels matrix which provide pure elastic to viscoelastic properties. Though hydrophilic monomers are typically used to prepare hydrogels, but hydrophobic monomers are also incorporated to tune up the physical, mechanical, and chemical properties towards specific applications. Both synthetic and natural polymeric networks can be regarded as hydrogels. In general, synthetic polymers are hydrophobic and more chemically stronger than natural polymers and they provide a slow degradation rate and a mechanically robust structure when incorporated with natural polymers.[354, 362]Any technique which is suitable for synthesizing a cross-linked polymeric network can be applied to produce hydrogels. Free radical polymerization techniques are commonly applied to natural and/or synthetic hydrophilic monomers with multifunctional cross-linkers to produce hydrogels.[355] The choice of the polymerization process/ technique influences the properties of the resultant hydrogels greatly.[363] Hydrogels can be synthesized either through a

one-step process in the form of simultaneous polymerization and crosslinking of multifunctional monomers or by a stepwise process of producing polymers with reactive groups that can crosslink themselves or can react with appropriate crosslinkers.[355, 364-365] Composite hydrogel materials also can be developed by combining two or more types of organic, inorganic, and polymeric materials to generate the best combined effect of those materials for particular applications. For instance, to achieve desired mechanical strength and particular shape, hydrophobic polymer segments are incorporated in the presence of crosslinkers.[365]

The polymerization technique controls the functionality and properties of the resultant polymer hydrogel. The approaches used for the synthesis of polymer hydrogels, in general, are chain-growth and step-growth polymerization which have been discussed in the next section.

1.6.3.1 Chain-growth polymerization

Hydrogels can be synthesized in a number of ways, including single or multiple-step synthesis processes. The condensation of monomers or ingredients that have reactive functional groups with subsequent elimination of side products during the fabrication of polymeric hydrogels mostly follows the basics of polymerization chemistry. Chain growth polymerization with a free radical mechanism is frequently used to synthesize chemically crosslinked hydrogels. Hydrophilic monomers containing –C=C– bond mostly participate in free radical polymerization.[366] Various free radical polymerization techniques which are typically used for hydrogel synthesis are described below.

- ***Bulk polymerization***

This is a very simple and widely applied technique to produce hydrogels which involves the polymerization of liquid monomers and monomer-soluble initiators

with a small number of cross-linkers. The polymerization process is typically initiated using ultraviolet light, radiation, and/or chemical catalysts. Shin et al. synthesized pH-responsive hydrogels by bulk polymerization from sodium functionalized acrylic acid (NaAAc) and hydroxyethyl methacrylate (HEMA).[367]

The synthetic procedure follows two steps. AAc was initially neutralized by NaOH to obtain NaAAc. Afterward, required amount of the initiator (i.e.α,α'-azobisisobutyronitrile: AIBN), cross-linker (N,N'-methylenebisacrylamide: MBA) and HEMA were added to the reaction mixture. The polymerization was allowed to continue on a Petri dish for 30 minutes at 75°C in an oven. The unreacted reagents were removed by repeatedly washing the hydrogel with deionized (DI) water. Bulk polymerization shows high polymerization rate. However, the viscosity of the reaction mixture increases markedly with the conversion which generates heat during polymerization. These issues can be avoided by controlling the reaction at low conversions.[368] The resultant hydrogels exhibit a glassy and transparent polymer matrix, which swells and becomes flexible upon immersion into water.[355]When the reaction temperature and the initial concentration of the initiator is increased, the rate of polymerization and conversion is increased. Hence, it is possible to control the rate of conversion by manipulating the temperature and the concentration of the initiator.[369]

- ***Solution polymerization***

In solution polymerization, ionic or neutral monomers dissolved in a solvent (e.g., water, alcohol, or water–alcohol mixtures) are mixed with multifunctional cross-linkers and undergo polymerization by ultraviolet (UV) or redox initiation to form hydrogels. All unreacted reagents are removed completely by washing the hydrogel with distilled water. Solution polymerization is a very simple and low-cost process with for ease of synthesis and low-cost processing with better heat transfer control than bulk polymerization.[366, 370] Solution polymerization is

extensively used for synthesizing cellulose-based superabsorbent hydrogels. The rate of polymerization is high and the reaction can be conducted at room temperature. Typically, bulk and solution polymerization processes are homogenous with potential of becoming heterogeneous when the formed polymer is insoluble in the monomer and solvent in the respective processes.[370]

- ***Suspension polymerization***

Suspension polymerization generally involves insoluble monomers and initiators with a suspending agent having low hydrophilic–lipophilic balance (HLB) in aqueous solution. The reaction mixture is constantly agitated to create droplets of monomers having diameter 10-1000 μm.[371] As polymerization proceeds, the polymer hydrogel beads are formed, which can be filtered to separate from the reaction mixture. In this process, a protective colloidal agent [e.g., carboxymethyl cellulose (CMC) or methylcellulose (MC) and polyvinyl alcohol (PVA)] is often used to obstruct the coalescence of the droplets. Since water used as reaction medium, it works as an excellent heat transfer medium. Inverse-suspension polymerization is also widely used for hydrogel synthesis.[372]

- ***Emulsion polymerization***

A typical emulsion polymerization process involves a water-soluble initiator, a surfactant, cross-linkers, and slightly water-soluble or completely hydrophobic monomers.[361] In inverse emulsion polymerization, a hydrophilic monomer is used. Figure 46d shows a typical emulsion polymerization technique. It generates polymer particles with diameters 0.1–3 mm which is much smaller than those obtained in suspension polymerization. The suspension and emulsion polymerization processes can be easily controlled and heat transfer can be performed effectively over bulk polymerization.

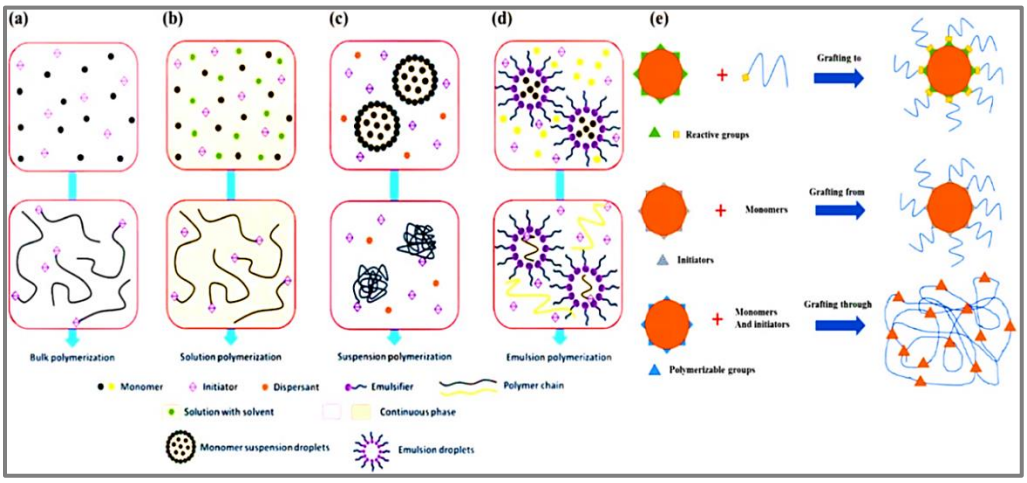

Figure 46. Schematic diagram of the common free-radical polymerization techniques used in hydrogel synthesis: (a) Bulk polymerization, (b) Solution polymerization, (c) Suspension polymerization, (d) Emulsion polymerization and (e) Graft polymerization.[361]

- ***Graft polymerization mechanism***

Hydrogels prepared by bulk polymerization technique have poor mechanical properties. To improve the mechanical properties of a hydrogel, it can be grafted onto the more robust support frames. This technique involves the generation of free radicals onto a stronger support surface and then polymerizing the monomers directly onto it resulting formation of polymer chains that are covalently bonded to the support. For example, grafting vinyl monomers onto polysaccharides is commonly observed.[355] Essawy et al.[373] reported the synthesis of grafted poly(acrylic acid) (PAAc) from hybridized chitosan (CHT) with cellulose via chemical bonding using thiourea formaldehyde resin which resulted in the formation of mechanically robust pH-responsive hydrogels.

1.6.3.2 Step-growth polymerization

In step-growth polymerization, monomers having distinct functional groups are utilized to synthesize hydrogels. These complementary functional groups react and form covalent bonds to propagate a one-step polymerization process.[366] Tibbitt et al.[374] studied the mechanical properties of photodegradable hydrogels synthesized via chain and step-growth polymerization processes. The mechanical integrity, tensile toughness, ductility, and shear strain of the hydrogels synthesized by step-growth polymerization were reported to be better than those obtained via chain growth polymerization due to network homogeneity and cooperativity.

1.6.4 Methods of crosslinking for hydrogel fabrication

Cross-linking is a stabilization process which leads to multidimensional extension of polymeric chain resulting in a network structure.[375] Cross-link is usually a bond which links one polymer chain to other. It can be ionic or covalent. Cross-linking can transform a liquid polymer (where the chains are freely flowing) into 'solid' or 'gel' by restricting the movement of polymer chains. On the other hand, as hydrogels contain hydrophilic segments, cross-linking is essential to avoid the dissolution of hydrophilic polymer segments in the aqueous medium. The presence of cross-links between polymer chains depending upon the degree of cross-linking can change the physical properties of the polymer including

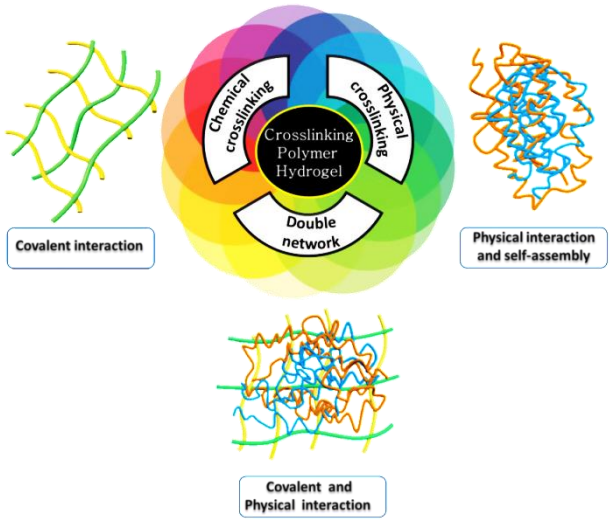

Figure 47. Schematic representation of polymer hydrogels fabricated through chemical crosslinking, physical crosslinking or double network.[376]

elasticity, viscosity, insolubility of the polymer, strength and toughness, thermal stability etc. [364] Water-soluble linear polymers of both natural and synthetic origin are typically cross-linked through chemical or physical interactions to form polymeric hydrogels. Polymer hydrogels can be classified into three categories depending upon their cross-linking mechanism as shown in Figure 47. Chemical or permanent hydrogels are made by covalent crosslinking of polymer chains whereas physical crosslinking hydrogel are not permanent in nature, as they are formed via hydrogen bonding, entangled chains, hydrophobic interaction, crystalline interaction, host–guest mechanism, etc. which give them a reversible nature.[376]There is an another category called double network hydrogel, which is made by the combination of chemical and physical crosslinking because of electrostatic interactions.[377] Chemically crosslinked polymer hydrogels (CCPHs) are formed by cross-linking through covalent bonds typically resulting in high mechanical strength. On the other hand, physical crosslinked polymer hydrogels (PCPH) are produced by non-covalent forces, crystallization, and molecular

entanglement, resulting in weak mechanical properties and viscoelastic behaviour.

Hybrid double network polymer hydrogels (HDNPH) contain two interpenetrating polymer networks; one is a strongly covalently cross-linked polymer network and the other one is a loosely crosslinked physical network. If these hydrogels are strongly deformed, their physical crosslinks can break such that strain energy is dissipated. So, these hydrogels show very high mechanical strength and toughness compared to CCPH and PCPH systems.

In this thesis, we will mainly focus on the synthesis and physico-chemical characterization of chemically crosslinked polymer hydrogels which has been discussed in the next section.

1.6.4.1 Chemical crosslinking

Chemical cross-linking method uses covalent bonding between polymer chains to produce permanent hydrogel. The cross-link formation is typically carried out by the addition of small cross-linkers molecules, photo-sensitive agents or by free-radical polymerization reaction in presence of cross-linking agent.

- ***Crosslinking by small molecules***

To prepare hydrogels in this method, the minimum requirement is one polymer and a small molecule as cross-linker dissolved in an appropriate solvent. Cross-linkers are typically molecules with at least two reactive functional groups that can allow the formation of bridges (linkages) between the polymeric chains.[378] Crosslinking of polymers using small molecules such as formaldehyde, glutaraldehyde, genipin, ethyleneglycol diglycidyl ether (EGDE) etc. has been reported and reviewed extensively. Covalently crosslinked polymers have an improved mechanical strength compared to physically crosslinked polymers. The

simplest form of this type of cross-linking is taken place between aldehyde and amino groups to form Schiff base. For example, dialdehyde such as glyoxal and particularly glutaraldehyde forms covalent imine bonds with the amino groups of chitosan via Schiff reaction.[379] Chitosan hydrogels have been synthesized through Schiff bases with other pre-functionalized polysaccharides, such as oxidized dextran and aldehyde hyaluronic acid (A-HA).[380] Other hydrogels of cellulose and alginate have also been prepared in a similar way.[381-382]In other cases, hydrogels formed by cross-linking of dextran-tyramine[383] and hyaluronic acid-tyramine conjugates in the presence of horseradish peroxidase (HRP) and hydrogen peroxide (H_2O_2) as cross-linkers showed improved controllable gelation times.[384] In spite of many advantages of this method, several disadvantages also exist. A general disadvantage of each of these small-molecule cross-linking methods is the potential cytotoxicity of residual unreacted cross-linker agents in vivo.[385] Preparation of hydrogels using this method requires multi-step preparation and purification.

- ***Crosslinking through ionizing radiation (Photo cross-linking)***

Formation of hydrogels based on photo cross-linking process depends upon the presence of photo-sensitive functional groups. This is done by linking a photo-sensitive functional group to a polymer which can form cross-linkages upon irradiation with light such as UV light.[385] Chitosan is one such polymer which has been investigated more compared to other polymers. Ono et al.[386] reported the synthesis of UV-light-irradiated chitosan hydrogels by introducing azide and lactose as light-sensitive moieties. In this work, a photo cross-linked chitosan hydrogel was prepared by incorporating azide group to the polymeric chain of chitosan. The azide group upon exposure to UV light was converted to nitrene group which binds free amino groups of chitosan resulting in the in-situ formation of hydrogel in a very short time. Photo cross-linked hydrogel can also

be formed between the polymers. For example, thermo-sensitive chitosan-pluronic hydrogel has been synthesized by UV irradiation of the physical gels above their gelation temperatures, where both the polymers were functionalized with photo sensitive acrylate groups.[387] Chitosan-PEG-based hydrogel was developed by modifying chitosan with photo-reactive azidobenzoic acid and PEG with arginylglycylaspartic acid (Arg-Gly-Asp) peptide.[388] Upon UV irradiation, a free-radical photo-initiated polymerization took place which led to the formation of hydrogel in situ. Recently, methacrylate-functionalized chitosan hydrogels have been synthesized with the help of UV irradiation by step growth or chain-growth polymerization using dithiothreitol (DTT).[389] This technique has several advantages, such as ease, fast gelation, and low cost of production compared to other chemical crosslinking methods.[390] However, this technique requires a photosensitizer and prolonged photo-irradiation, which result in local heating, thereby damaging adjacent cells and tissue when used in biological system.[385]

- ***Crosslinking through Free Radical Polymerization***

The development of chemically crosslinked hydrogels via free radical polymerization of low molecular weight vinyl monomers in the presence of crosslinking agent has attracted immense interests. Hydrogels are most commonly synthesized by free-radical chain polymerizations of hydrophilic monomers containing a >C=C< bond. As shown in Table 1, a variety of monomers may undergo free-radical polymerization reaction in presence of a crosslinking agent to form hydrogels. Some commonly used vinyl monomers in this technique include acrylic acid, acrylamide, vinyl chloride, styrene, epoxide, N-vinyl-2-pyrrolidone, and 2-hydroxyethyl methacrylate. Each of these monomers contains a >C=C< bond through which an active centre is generated which may propagate to produce polymer chains. The method for generating active centres

(initiation process) may be achieved by using heat, light, γ-radiation or electron beams. Each initiation process yields free radicals that initiate a chain reaction with the monomer molecules resulting in a polymerized gel. The water-soluble thermal initiators potassium persulfate (KPS) and ammonium persulfate (APS) or diazo compounds like 2-2′-azobisisobutyronitrile (AIBN) or peroxides like benzoylperoxide (BPO) are widely used in hydrogel synthesis. On the other hand, redox initiating system is also used which is comprised of reducing agent such as ferrous salts, sodium metabisulfite, or tetramethylenediamine (TEMED), in combination with an oxidizing agent such as ammonium persulfate or hydrogen peroxide.[371, 390] The crosslinking agents that are typically used in the free radical polymerization process are N, N′ -methylenebisacrylamide (MBA), ethyleneglycol dimethacrylate (EGDMA), melamine trimethylacrylamide, and melamine triacrylamide. Figure 48 shows the chemical structures of some di- and tri-functional cross-linkers that are widely used in the synthesis of hydrogels. The first polymeric hydrogel was introduced by Wichterle and Lim when they reported the radical polymerization of 2-hydroxyethyl methacrylate (HEMA) in the presence of ethylene glycol dimethacrylate (EGDMA) as a crosslinking agent.[391] Park et al. synthesized poly(N-isopropylacrylamide) (PNIPAM) hydrogel in the presence of N,N′-methylenebis(acrylamide) (MBA) as a cross-linker and N,N,N′,N′ tetramethyletyhlenediamine (TEMED) as an accelerator by chemical gelation process.[392] Devine et al.[393] reported the synthesis of chemically cross-linked copolymeric hydrogel of N-vinylpyrrolidone (NVP) and Acrylic acid (AA) by UV-light mediated free radical photo- polymerization using Irgacure 184 as photoinitiator, and ethylene glycol dimethacrylate and poly(ethylene glycol) dimethacrylate of variable molecular weights as cross-linkers.

Table 1. Some commonly used monomer in hydrogel synthesis via free radical polymerization.[394]

Monomer	Structure	R	Examples
Acrylic acids	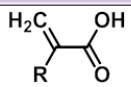	-H $-CH_3$	Acrylic acid Methacrylic acid
Acrylamides	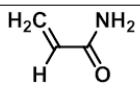	-H $-CH_3$	Acrylamide Methacrylamide
N-substituted acrylamides	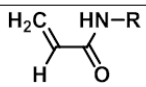		N-isopropylacrylamide
Acrylates	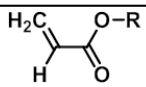	$-C_2H_4OH$ $CH_2(CH_2)_{16}CH_3$	2-Hydroxyethyl acrylate Octadecyl acrylate
Methacrylates	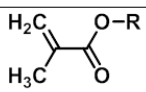	$-C_2H_4OCH_3$ $-C_2H_4OH$ $-C_4H_9$ 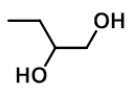	2-Methoxyethyl methacrylate 2-Hydroxyethyl methacrylate Butyl methacrylate 2,3-Dihydroxypropyl methacrylate
Glycols	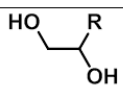	-H $-CH_3$	Ethylene glycol Propylene glycol
Vinyls	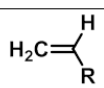	-OH   	Vinyl alcohol 4-Vinylpyridine N-Vinylcaprolactam N-Vinylpyrrolidone
Lactones		$-C_5H_{10}$	ε-caprolactone

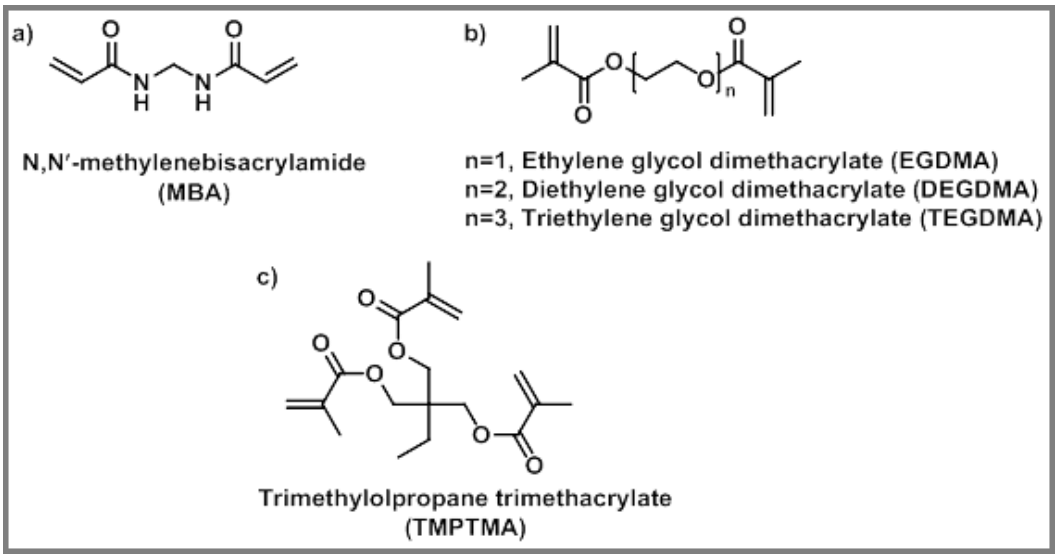

Figure 48. Some common di-functional (a, b) and tri-functional (c) vinyl cross-linkers used in the synthesis of hydrogels via free radical polymerization.

Crosslinked homopolymers, such as PHEMA and PNVP, and copolymers of NVP and HEMA have also been synthesized by free radical polymerization using melamine trimethylacrylamide and melamine triacrylamide as crosslinkers and AIBN as an initiator. Very recently Oucif et al.[395] reported the synthesis of poly (hydroxyethyl methacrylate-co -hydroxyethyl acrylate) [poly (HEMA-co-HEA)] hydrogels using potassium persulfate and MBA as a radical initiator and cross-linker respectively. The free radical polymerization mechanism proposed for the formation of cross-liked copolymer hydrogels has been shown in Figure 49. The study clearly demonstrated that adding HEA as a copolymer to HEMA enabled fine-tuning of the degree of swelling, drug loading, and release rate of the hydrogels to the desired level. Recently microstructured interpenetrating networks (MIPNs) consisting 2-hydroxyethyl methacrylate (HEMA) as the first network and glycerol methacrylate (GMA) as the second network has been reported.[396] The first PHEMA network was prepared by redox-initiated free-radical polymerization using diethylene glycol dimethacrylate (DEGDMA) as a

cross-linker and ammonium persulphate (APS) with N, N, N′, N′-tetramethylethylenediamine (TEMED) as redox-initiating system whereas the

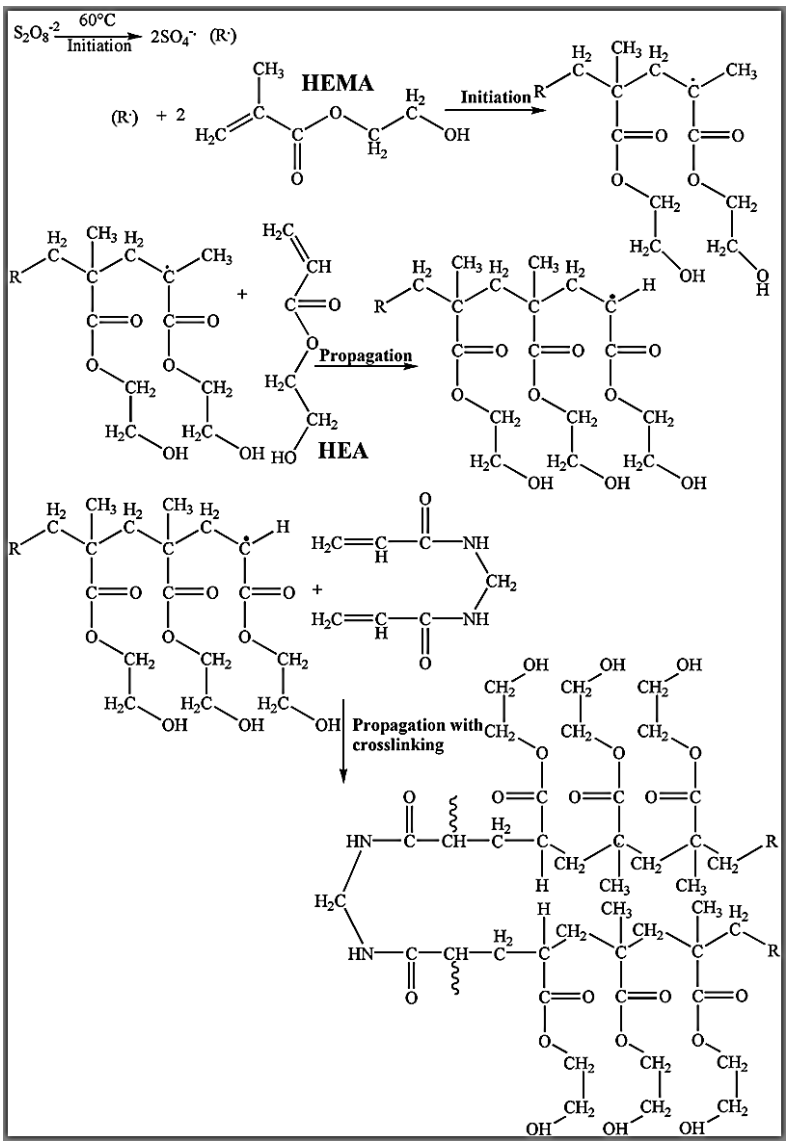

Figure 49. Mechanism of formation of the cross-linked poly (HEMA-co-HEA) copolymer via free radical polymerization.[395]

second network of PGMA was formed by UV polymerization using DEGDMA and 2-hydroxy-2-methyl-1-phenyl-propane-1-one (Darocur 1173) as cross-linker and photoinitiator respectively. The hydrogels showed high swelling capacity and

superior mechanical strength. Su et al. [397] reported a poly (N-isopropylacrylamide-co-2-hydroxyethyl methacrylate) (PNIPAM-co-HEMA) permanent hydrogel synthesized via free radical polymerization which showed micro dynamic mechanism of the volume phase transition (VPT) behaviour. In a similar fashion, Xu et al.[398] showed potential application in the drug delivery of biodegradable and pH-responsive poly(acrylic acid)-co-poly-(N isopropylacrylamide) hydrogel cross-linked by macromolecular cross-linker poly-(L-lactide)-co-polyethyleneglycol-copoly(L-lactide) dimethacrylates.[399] Moreover, free radical polymerization was also used to graft synthetic monomers over natural polysaccharides. Several hydrogels have been reported, in which natural polymers such as chitosan, cellulose, starch, pectin, alginate, hyaluronic acid, dextran, carrageenan, and gums, have been grafted by synthetic monomers in the presence of a crosslinking agent to improve their intrinsic properties. Pourjavadi et al.[400] reported the synthesis of pH-sensitive chitosan-graft-poly (acrylamide) hydrogels by using APS and MBA as an initiator and cross-linker respectively. Mahdivinia et al.[401] synthesized chitosan-graft- poly (acrylamide-co-acrylic acid) hydrogels using KPS as an initiator and MBA as a cross-linker and they studied the effect of pH and salt solution on the swelling properties of hydrogels. Moreover, the free radical mechanism is used to synthesize hydrogels by copolymerizing carboxymethyl chitosan and acrylic acid in the presence of vinyltriethoxysilane as a cross-linker and KPS as an initiator.[402] Elvira et al.[403] synthesized novel biodegradable hydrogels of acrylamide and acrylic acid in the presence of starch using the free radical polymerization which was initiated by benzoyl peroxide (BPO) /4-dimethylaminobenzyl alcohol (DMOH) redox system. The authors studied the thermal stability, mechanical strength and pH-dependent swelling behaviour of the hydrogels. Bao et al.[404] synthesized superabsorbent hydrogels by graft copolymerization of acrylic acid

(AA)/acrylamide (AAm)/2-acrylamido-2-methyl-1-propanesulfonic acid (AMPS) onto sodium carboxymethyl cellulose (CMC) and montmorillonite (MMT) by using potassium persulfate (KPS) as a free radical initiator, in the presence of N,N'-methylenebisacrylamide (MBA) as a crosslinking agent. These super porous hydrogels contained porous networks and showed pH-sensitivity to swelling behaviour.

The covalent bonds present in chemically cross-linked polymer hydrogels (CCPHs) are stable at ambient conditions due to their rigid and irreversible nature.[405] CCPHs have superior mechanical properties and good solvent resistance, which cause brittleness and make them suitable for various engineering applications.[376] The CCPHs are not homogeneous and contain both low water high swelling regions; the former is produced from high crosslink density, while the latter is produced from low crosslink density. The crosslinking does not take place isotropically because of viscosity and steric factor, which hinder the movement of reactants, thus restricting the cross-linking reaction at equal intervals of the main chain. Due to variation in the cross-link density, pores with different sizes are formed in the CCPH gels.

1.6.5 Macroporous hydrogels

1.6.5.1 Overview

Hydrogels having pore sizes in the range of 10 nm–10 μm are called microporous hydrogels while those with pores above 10 μm are usually termed macroporous hydrogels (MHGs).[406] MHGs due to presence of large interconnected pores can rapidly absorb water. The geometry of the polymeric network, porosity/ pore sizes can be easily tuned by controlling the chemical composition and cross-linking density, and structured into various geometries depending on the application requirements. MHGs are appropriate substrate for biomedical and

tissue engineering applications. The chemical composition and some physical properties of hydrogels can be easily modified for application specific purposes. The mechanical properties of MHGs mostly depend on the polymerization conditions, cross-linker concentrations, co-monomer ratios or the attachments of additional binding sites. Various stimuli-responsive or "smart" hydrogels have been reported which are able to change their shape and/or properties upon exposure to an external stimulus such as temperature, pH, ionic strength, light, electric and magnetic field, or a combination of them.[407] Stimuli-responsive MHGs can be synthesized by using sensitive polymers e.g., thermo-responsive MHGs can be prepared by using poly (N-isopropyl acrylamide) (PNIPAM) as polymer matrix. These MHGs are especially used as self-regulated and targeted drug delivery systems where the release of drug or other biological molecules from the loaded MHGs can be facilitated by using an appropriate stimulus (physical, chemical or mechanical).Some other application of MHGs include sorbents for separation techniques, or bioreactors in various biological and biomedical applications etc.

1.6.5.2 Classification

Depending on the nature of cross-linking mechanism, MHGs can be mainly classified into two categories: physical and chemical hydrogels. Physical hydrogels are nothing but non-covalently cross-linked polymer networks. Physical hydrogels are beneficial mainly because of their reversibility in nature and also the synthetic pathway requires no chemical reaction which leads to generation of no side products.[408] However, the weak physical interaction between the polymer chains leads to lower stability and weaker mechanical properties of the polymer network compared to the chemically cross-linked hydrogels. On contrary, better control over the network stability and mechanical properties can be achieved by preparing chemically cross-linked hydrogels

through formation of covalent bonds between polymer chains formed by coupling reactions, like 'click' chemistry, Michael-type addition, Schiff base coupling, disulphide bond formation, photo- and enzyme-mediated cross-linking reaction etc.[409-410] However, the use of chemically cross-linked hydrogels in biomedical applications is not favourable always because of the cytotoxicity and safety issues rendered due to the presence of un-reacted chemical reagents and side products in trace amount even after the purification of the synthesized hydrogels. To synthesize biocompatible MHGs for a wide range of biomedical applications, new approaches such as 3D printing and photolithography are now extensively used.[411-412]

1.6.5.3 Fabrication of macroporous hydrogels

MHGs are successfully synthesized by several techniques, such as cross-linking polymerization in the presence of pore-forming agents[413] and porogen gas-releasing inorganic compounds,[414] porogen leaching,[415-416] lyophilization of the water-swollen hydrogel,[417-418] cryogelation,[419-420] electrospinning,[421] colloidal particle templating,[422] 3D printing and photolithography.[411-412]Some of these methods are discussed in short as follows:

- ***Porogen leaching***

In this method, hydrogels are synthesized by free-radical polymerization in presence of water-soluble substances (termed as porogen) like sugar, salt , polymer etc. and are subsequently washed out from the hydrogel matrices after polymerization is over.[423] Facile control of pore size and overall porosity can be achieved by this technique by selecting appropriate particle size and concentration of porogen that is added during gelation. Different types of porogens are used , such as sodium chloride crystals,[423-424]sugar crystals,[425] poly(L-lactide) fibers,[426] polystyrene microspheres[427] etc. to obtain MHGs

especially for tissue engineering applications. PHEMA -based hydrogels are important materials for cell culture experiments. Přádný et al. reported the synthesis of MHGs based on cross-linked PHEMA with dual porosity(large and small pores) where addition of NaCl crystals to the reaction mixture resulted in the formation of large pores with pore diameters in the range of 10 -100 μm whereas in presence of 1-dodecanol (a poor solvent for PHEMA) , a phase separation occurs which resulted in the formation of small pores (pore diameter in the range of few microns). [424] It has been observed from cell experiments that the presence of two types of pores have significantly influenced the cell proliferation and adhesion. Difficulties regarding the complete removal of soluble unreacted reagents from hydrogel matrix and reduced control on the pore structure and degree of pore interconnectivity are among the major limitations associated with porogen leaching strategy.

- ***Lyophilization (freeze-drying technique)***

Lyophilization (Freeze-drying) is a simple and effective tool to create porous materials which is done by fast freezing of polymeric system in liquid nitrogen followed by sublimation of solvent (water) under reduced pressure. Synthesis of cross-linked pullulan/dextran, cross-linked chitosan (CS), CS–ZnO composite sponges, semi-IPN PAAm/CS composite hydrogels etc. have been reported using this technique.[414, 428-429] It has been observed that the degree of porosity of the hydrogels can be modulated by the freeze-drying pressure. Autissier et al. reported the synthesis of porous polysaccharide- based hydrogel scaffolds (cross-linked pullulan/dextran) by a combined freeze-drying/cross-linking process without using any organic solvent or porogen agent. It has been found that high freeze-drying pressure scaffolds contained pores with a mean pore diameter of 55 ± 4 μm and a porosity of 33 ± 12%, whereas low freeze-drying pressure scaffolds contained larger pores with a mean diameter of 243 ± 14 μm

and a porosity of 68 ± 3%. Polymer concentration also play an important role on the thickness of pore walls; a lower polymer concentration results in thinner walls and high pore interconnectivity[423]. In comparison with porogen leaching, lyophilization technique provides MHGs with higher specific pore area and thinner pore walls.[430] Ice crystals and also the formation of two different phases namely polymer-rich and polymer-poor phases are occurred during the freeze/thaw cycles which are eventually responsible for the development of porous structure in these hydrogels.[431]

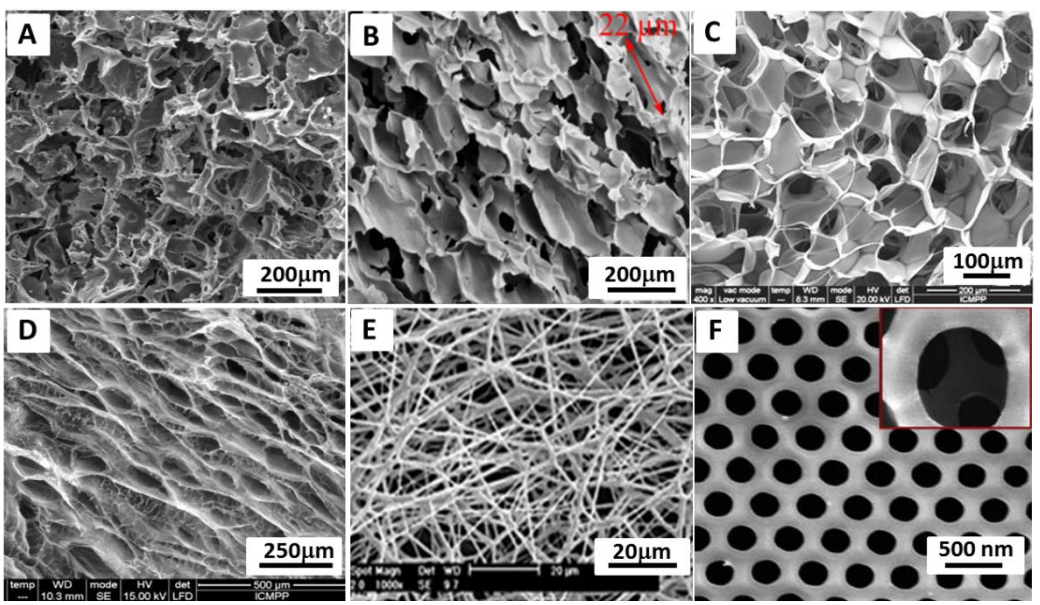

Figure 50. FESEM images revealing the porous structure of (A) 2-hydroxyethyl methacrylate (HEMA)-based hydrogel prepared by free radical polymerization in the presence of NaCl crystals[423],(B) starch hydrogel scaffold formed by freeze-drying technique[432], (C) cross-linked chitosan hydrogel synthesized by ice-templating process[433],(D) cross-linked chitosan hydrogel synthesized by unidirectional freezing in liquid nitrogen combined with porogen leaching technique[434], (E) electrospun salt-leached hyaluronic acid (HA)/collagen hybrid scaffolds [435], (F) PHEMA hydrogel synthesized by photo-patterning combined with colloidal templating method[436].

Interestingly freeze-drying technique is also applied to create pores within the non-porous hydrogels after their synthesis where hydrogel is first swollen in water followed by lyophilization.[417-418, 428, 437] A wide range of hydrogel materials based on natural and synthetic hydrophilic polymers with interconnected pores of various sizes are reported where the internal morphology and the pore size were mainly affected by changing the cross-linking degree. Higher cross-linking degree produces hydrogels with a more compact structure and smaller pore sizes[417-418] whereas higher polymer concentration affects the thickness of pore walls.[438] However, the porous materials generated by lyophilization are stiff and inelastic, while the swollen ones are soft, flexible, and elastic. The major drawbacks regarding this technique are the effect of thermal quenching to the architecture of the hydrogels, formation of MHGs with low mechanical strength , formation of a surface skin due to collapse of the hydrogel matrix at the scaffold–air interface during solvent evaporation etc. In spite of the requirement of longer processing time for a complete removal of the solvent, freeze-drying is a cost-effective technique.

- ***Cryogelation (Ice-Templating)***

Cryogelation or ice-templating is an easy, cost-effective and widely used technique for the preparation of porous materials based on natural and synthetic polymers or combination of both.[439-441] In cryogelation technique, macromolecular gels are formed under semi-frozen conditions, leading to the formation of cross-linked polymer network around ice crystals.[442-443] In this process, the precursors (initiators, activators, monomers, polymers etc.) are concentrated within the unfrozen liquid micro-phase (ULMP) between the ice crystals. The ice crystals behave as solid porogen and at the end of the polymerization process subsequent thawing of ice crystals (porogen removal) leaves behind a cross-linked polymeric material containing large and highly interconnected pores surrounded by a highly dense polymer wall. This material is

commonly called a cryogel.[443-445] Large and interconnected supermacropores provide elastic and spongy structure to the cryogels which imparts interesting properties like superfast water uptake, ability to resist different degree of deformations etc.[406, 440, 446] The shape and size of the pores depend on some factors such as concentration of monomer, polymerization temperature etc. The supermacropores in the structure of cryogels vary in size from 10 -200 µm whereas macropores formations are also observed in the polymeric phase of the cryogels.[446-447] A synthetic strategy combining porogen leaching and ice-templating process has been reported to create 3D polymeric networks with permeable walls for the diffusion of low-molecular weight particles when the large pores are filled with cells.[433-434] In cryogelation technique, the unidirectional freezing approach by different cooling agents like frozen acetic acid/diethylether mixture (−80 °C), frozen ethanol (−110 °C) or liquid nitrogen (−196 °C) at a controlled immersion rate provides a better control over the morphology of the resulting macroporous structures.[448-449] By unidirectional freezing approach various MHGs based on water-soluble polymers with aligned porous structures such as PVA,[450] poly(L-lactic acid),[451] PEG,[452] poly(NIPAM)[448] etc. and recently aligned porous zeolite/chitosan cryogels[453] (Zhang et al. 2015) and aligned chitosan/gelatin scaffolds[449] have also been prepared. Pore size and the thickness of the pore wall were also adjusted by varying the initial monomer or polymer concentration, the molecular weight of polymer as well as the crystallization speed.[434, 448-449]

- ***Gas Foaming***

In gas-foaming (or blowing) technique, the nucleation and growth of gas bubbles dispersed all over the polymer solution create pores within the 3D polymer network.[411, 454] The gas bubbles are generated by a foaming/blowing agent through chemical reactions or are expelled from a presaturated gas/polymer mixture prepared at high pressure. The foaming/blowing agent, which is

generally biocompatible, is a chemical compound which after mixing with the precursors generates a gas by chemical decomposition or some other technique. Sodium or ammonium bicarbonate, which can generate CO_2 gas in mild acidic solutions are commonly used as foaming agents to prepare poly(acrylic acid) or poly(/acrylamide) or PEG–based hydrogels with interconnected pores.[406, 454] Use of supercritical carbon dioxide has been also reported as "green" medium to induce porosity inside chitosan scaffolds[455] and hydrogels based on hydrophilic polymers such as PLA, PLGA, and PCL.[430, 454] To enhance the solubility of CO_2 in the hydrophilic polymers, various techniques, such as CO_2–water emulsion templating or the use of co-solvent systems have been developed.[411]

- ***Electrospinning***

Electrospinning is an another frequently used technique to prepare interconnected porous scaffolds mainly for tissue engineering applications.[421] A polymer solution held at the end of a capillary tube is charged by applying a high voltage and simultaneously a thin jet of solution is drawn from the tube by electrostatic forces toward an oppositely charged collector.[421, 456]During the jet flight of the polymer solution towards the collecting electrode, the solvent gets evaporated and fibres with lower diameter compared to the jet are finally formed.[457] A stationary ground plate or a rotating drum as required is used as collector. The morphology, porosity and fibre diameter of the hydrogels formed in this technique can be controlled by modulating the temperature, viscosity, solution conductivity, and applied voltage.[456] Porous fibres based on PHEMA or PVA and PAA in range of micro- and nanometre have been prepared by electrospinning.[423] Formation of macroporous HA/COL hydrogels as nanofibers are reported using a combination of electrospinning and porogen leaching. [435] However, the inability to prepare 3D hydrogel with various shapes, the poor mechanical properties of the hydrogel, and the low control over porosity and

pore size are some serious limitations of using this technique in development of macroporous materials.

- **Other Preparation Techniques**

(Templating, 3D Printing, Photolithography)

Colloidal crystal templating method is remarkably used to design 3D-ordered macroporous materials with interconnected pores and well-controlled pore size along with different architectures, such as films, monoliths, rods, and even hydrogels depending on material composition and preparation technique.[406, 422, 430] The resulted MHGs consist 3D ordered close-packed spherical cavities with sizes in the range of 1 μm to mm, surrounded by thin walls. The structural architecture can be described as the inverse replica of 3D assemblies of spherical colloidal particles closely packed like a face-cantered-cubic crystal, similar to that of natural opal gemstones. The 3D replica is obtained by back-filling the interparticle spaces with the material that will constitute the polymer matrix followed by the removal of colloids.

The 3D printing and photolithography processes have also been applied to design macroporous hydrogel scaffolds.[411-412, 436] In these techniques, the size and the distribution of the pores, pore wall composition and geometry can be properly controlled which make them potential candidate for the application of organ-specific 3D design and development. In 3D inkjet printing technique, a liquid precursor solution is drop wise expelled from a nozzle and accumulated on a support, where gets solidified.[411] Complex 3D porous structures could be built by layer-by-layer deposition of droplets and controlling their size. In photolithography technique, macroporous hydrogel scaffolds are synthesized by photo-polymerization of acrylic monomers or acrylate-based prepolymers or other vinyl functionalized macromolecules.[436, 458]

1.6.6 Swelling behaviour of hydrogels

Hydrogel, a cross-linked three-dimensional hydrophilic polymeric network, can swell in water as water molecules penetrate into the void space between the polymeric chain network and retain a large amount of water while maintaining its structure owing to cross-linking between the polymer chains.[390] The swelling can range from double to more than thousand times of their dry weight. Hydrogels possess some degree of flexibility quite similar to natural tissues due to their significant water content. The water absorbing nature of hydrogels is mainly because of the presence of hydrophilic functional groups such as -NH_2, -COOH, -OH, -$CONH_2$, - CONH -, and -SO_3H.The swelling of hydrogels in water generally takes place in three steps: (i) diffusion of water into the hydrogel network (water infiltrating is called primary bound water), (ii) relaxation of polymer chains (additional water infiltrating is called secondary bound water), and (iii) expansion of the hydrogel network (excess water infiltrating is called free water). According to the Flory–Reihner theory, swelling behaviour depends on the elastic nature of the polymer chains and their compatibility with water molecules.[390] Non-ionic hydrogels swell in aqueous medium entirely due to water–polymer interactions, whereas swelling of ionic hydrogel is influenced by the pH of the aqueous medium. Swelling is measured in terms of swelling ratio, which is the weight ratio of swollen gel to dry gel. The swelling of hydrogels The swelling kinetics and equilibrium swelling are controlled by many factors such as chemical structure of the polymer constituting the hydrogel, ionic charge, cross-linking density, hydrophilicity, hydrophobicity, and ionic strength of the swelling medium. Highly crosslinked structures usually have a lower swelling ratio and vice versa. Hydrogels containing more hydrophilic groups swell more as compared to hydrophobic groups. In some cases, swelling behaviour can also be influenced by the external factors such as pH, ionic strength, and temperature of the swelling medium. pH-sensitive hydrogels swell due to the ionization of

hydrophilic groups with variation of pH values.[459] Ionization produces electrostatic repulsion between similar charges on the polymer chains which breaks the secondary bonding between polymer chains resulting in higher swelling ratio.

1.6.7 Applications of hydrogels

Hydrogels have been widely used for different applications such as proteomic, bio-separation, electrophoresis, chromatography, tissue engineering, food, diaper, water remediation etc. because of their water absorption, non-toxicity and biocompatibility properties (Figure 51). Some of the applications of hydrogels are discussed in the next section.

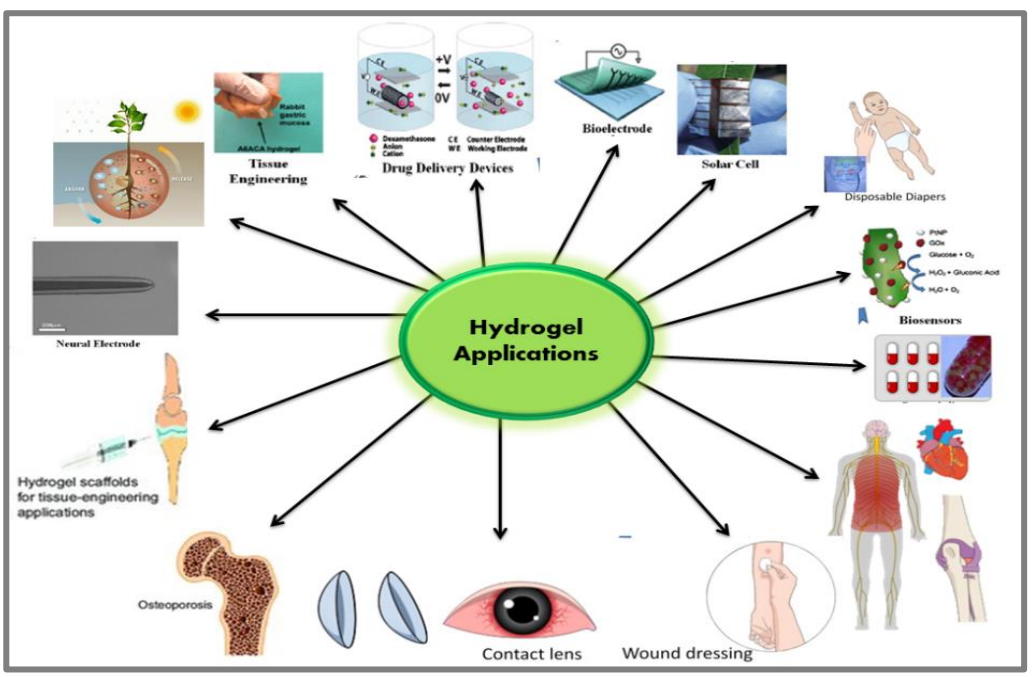

Figure 51. Potential application of hydrogels.

- ***Dyes and heavy metal ions removal***

Heavy metal pollution is usually observed in waste-water of many industrial processes whereas effluents from the textile and colouring paper industries

contain dyes in large amounts. These toxic dyes and heavy metal ions have become a serious threat to the public health and ecological systems. Hydrogels have an excellent swelling capacity under several external conditions which makes them a useful adsorbent material for the adsorption of water-soluble contaminants e.g. dyes, biomolecules, and metallic impurities.[355] It has been observed functional groups like –COOH, –OH, $–CONH_2$ and $–NH_2$ present in the hydrogel structures could be used as complexing agent for the removal of metal ions from aqueous solution.[460-462] The sorption mechanism and sorption capacity for the removal of heavy metal ions and/or dyes are greatly influenced by the functional groups of the hydrogel because of the participation of other processes like chelation and ion exchange rather than simple sorption.[463-464] Biopolymer-based hydrogels like chitosan, alginate, starch, and cellulose derivatives are widely used to remove metal ions from aqueous media. Primarily, the adsorptive and chelating features of maleic/itaconic acid-based hydrogels have been studied. The different ratio of maleic acid and itaconic acid was used to adsorb bovine serum albumin.[465] It was found that an increase in the content of these acids raises the bovine serum albumin adsorption. Karadag et al. produced acrylamide/ itaconic acid hydrogel adsorbents for the adsorption of nicotine and nicotine derivatives.[466] The complexation abilities of some hydrogels lend them to heavy metal adsorption. Chujo et al. successfully examined the complex formed between the polyoxazoline based hydrogel and metal ions such as iron (+2) and cobalt (+3).[467-468] Synthetic hydrogels like cross-linked polyacrylamide have also been used to remove heavy metal ions from aqueous media.[469] Güven et al developed poly(acrylamide)-based hydrogel as an adsorbent for uranium, iron and copper adsorption .[470-471] The presence of monomer-like maleic or itaconic acid added chelating characteristic into hydrogels which increased the adsorption capacity of hydrogels for heavy metal ions. Hydrogels can also be

used as efficient sorbents for the removal of many water-soluble organic dyes; owing to the ionic nature of the dyes, they interact with the hydrogel sorbents in the same manner as that for inorganic metal ions. For instance, chitosan-based hydrogel contains substantial amount of hydroxyl and primary amine groups which facilitate the chelation of various dyes.[472-473] Acrylamide-itaconic acid or acrylamide-maleic acid hydrogels have been investigated for the removal of cationic dyes like basic blue, basic red, basic violet, cresyl violet and basic green.[470, 474] Liu et al. have synthesized cationic hydrogels, poly (dimethyl diallyl ammonium chloride)/polyacrylamide (PDMDAAC/PAM), for the removal of anionic Congo red dye from aqueous solution.[475]

- ***Biomedical Applications***

Hydrogels' rubbery and soft nature makes them useful in the field of biomedical application.[353] Hydrogels can mimic the chemical, physical, and biological properties of biological organs and tissue, in response to changes in pH, temperature, enzymes and electric field.[476] Thus, hydrogels are used in artificial muscle formation, artificial organ preparations like in kidney, robotic grippers, bio-sensors, bio-adhesives, wound-healing, vocal cord replacement materials and artificial skin.[340, 477] Hydrogels are also ideal candidates for preparing contact lenses because they have a decent mechanical stability, very high oxygen permeability and favourable refractive index.[478] Gelatin–Carrageenan hydrogels' antimicrobial activity was performed by Padhi and coworkers.[479] A hybrid hydrogel methoxylpoly (ethylene glycol)-poly(caprolactone)-acryloyl chloride or Glycidylmethacrylated chitooligosaccharide or N-isopropylacrylamide or Acrylamide was reported for use in postoperative treatments of breast cancer patients.[480]

- ***Pharmaceutical Applications***

Hydrogels play an important role in the field of pharmaceutical applications. [481] Hydrogels have been widely used in several drug delivery systems for a long time because of their highly porous structure and swelling behaviour. Hydrogels are also known to have an important role in the rate of drug release; they increase drug solubility and limit drug degradation and toxicity.[482] Glycidyl methacrylate-b-cyclodextrin-based hydrogel was created for drug delivery in oculopathy therapy.[483] The copolymer hydrogel of methyl acrylic anhydride -modified β-cyclodextrin (MA-β-CD) and 2-hydroxyethyl methacrylate (HEMA) have been used for the delivery of Ofloxacin and Puerarin.[484] Das et al. synthesized dextrin or poly (acrylic acid) hydrogel for releasing Ciprofloxacin and Ornidazole.[399]

- ***Agricultural and horticultural applications***

Hydrogels are known to have several agricultural and horticultural applications. Super-absorbent polymers are crosslinked network of hydrophilic polymers that absorb a large amount of water and are generally used in horticulture and agriculture. The super-absorbent polymer influences the soil's permeability and improves its structure, density, texture and infiltration rate and therefore prevents soil erosion, enhances soil aeration, microbial activity and water holding capacity.[485] Various polysaccharides such as pectin, chitosan and carboxymethyl cellulose-based hydrogels are used as fertilizers to improve the quality of the soil.[486] Romero et al.[487] formulated an autonomous smart scheme of copolymer hydrogel tris[(hydroxymethyl) methyl]acrylamide–methyl methacrylate for agricultural irrigation and thus, successfully avoided the water wastage. Yan et al.[488] proposed starch-grafted-poly(acrylic acid) or organo-zeolite hydrogel for effective application in agriculture. Nano-copper

incorporated chitosan hydrogel has been used to enhance the plant growth and fruit quality.[489]

1.7 Potential application of ionic liquids and poly(ionic liquid)s

Ionic liquids find their application as high performance electrolytes in advanced electrochemical devices like batteries and capacitors,[179, 490] or as solvents for catalysis and chemical extraction.[491] Another advantage of ILs over conventional solvents lies in their tunable physicochemical properties such as selective solvation ability and miscibility depending upon the nature of cation and anion resulting in expansion of their applications from metal ions separation to chromatography. [492] On the other hand, the endless demands for versatile polymeric materials which can be employed in different specific conditions continuously motivate researchers to develop new types of functional polymers. The recently growing interest in PILs is due to their unique architecture - theoretically any type of functional groups can be tethered to their active nucleophilic sites (N, P, S etc.), and this creates endless possibilities for their physical properties, thermal behaviours, electrochemical performances and most importantly application scopes. Hence, PILs can serve as multifunctional platforms which provide a multitude of applications. There are many detailed review articles which mainly concentrate on the development and applications of PILs.[170, 177, 187] Here, we take some common applications as examples to describe the advantages of ILs and PILs.

1.7.1 Application of thermoresponsive ILs/PILs as smart materials

Thermoresponsive IL/solvent systems have several potential applications as liquid state materials due to their reversible phase transition between the homogeneous phase and liquid/liquid biphasic phase with change of temperature.[73] Both Ohno's group and Binnemans's group independently

developed energy-efficient extraction systems that are able to separate various compounds such as biopolymers[493] and metal ions[494] from the aqueous phase to IL-rich phase. Koo et al. utilized the LCST-type phase transition of amino acid based IL/water mixtures as reaction/product separation media for *in situ* enzymatic hydrolysis of penicillin.[495] On the other hand, thermoresponsive PILs, as solid state materials, hold great potential to be applied in several fields such as stabilisation, accumulation, extraction, and separation of charged molecules. Yuan et al. implemented thermoresponsive PILs as dispersion/accumulation agents for carbon materials[144] and gold nanoparticles.[77] Luis et al. reported thermoresponsive PIL-modified gold nanoparticles which show LCST-type phase behaviour in chloroform.[496] Ohno and co-workers developed chemically cross-linked PIL hydrogels which show LCST-type phase transition and proposed the utilization of these PIL gels in desalination applications.[497] Thermoresponsive PIL-based membranes would be useful for constructing novel separation systems for several compounds including biopolymers.[498] Tudor et al.[499] developed a thermoresponsive PIL hydrogel showing LCST –type phase transition. The hydrogel was further incorporated into a microfluidic device with the purpose of being used as temperature-controlled actuator. Thermoresponsive PIL-based nanoparticles can also be used for binding/release of target molecules in water. Thermoresponsive PIL-based hydrogels can also be implemented for desalination processes where reversible sorption/desorption of water molecules from salt water would occur by a slight temperature change. Figure 52 summarizes some potential applications of thermoresponsive PILs as solid-state materials.

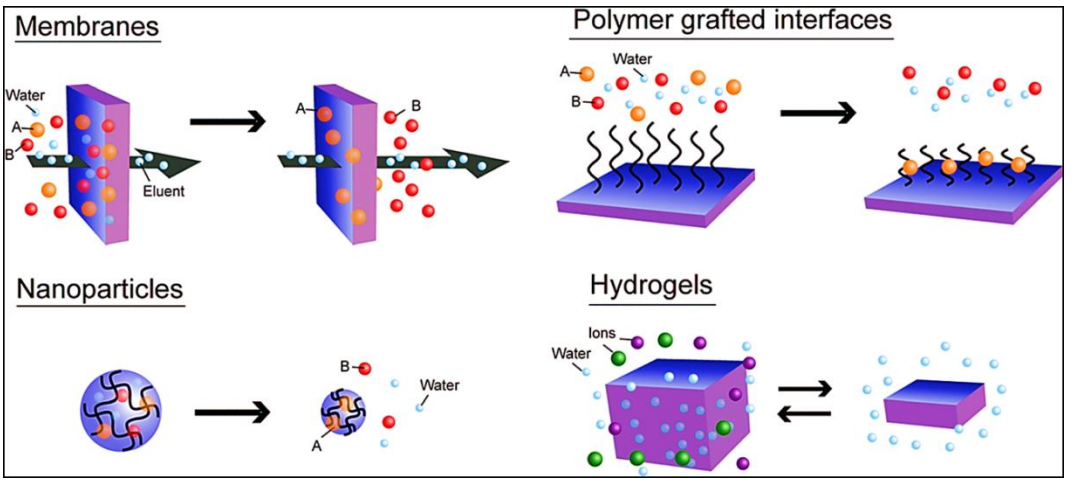

Figure 52. Potential applications of thermoresponsive PILs as solid-state materials. [73]

1.7.2 Energy harvesting and storage

The primary source of world's energy consumption is obtained from burning of fossil fuels (natural gas, oil, coal etc.), that results in global warming and environmental pollution due to emission of sulfur, nitrogen oxides and carbon dioxide. Consequently, several attempts have been made in order to develop electrochromic materials for renewable energy sources, energy storage and transformation devices. ILs have already gained popularity for their uses as electrolytes in electrochemical devices such as lithium batteries, dye sensitized solar cells, fuel cells, supercapacitors, light-emitting electrochemical cells and field effect transistors. However, liquid electrolytes have some serious drawbacks such as need of encapsulation due to leakage of the electrolyte. On the other hand, solid-state polymer electrolytes have advantages including mechanical stability, safety and simple processing, but their conductivity is still limited. For these reasons, there is an increasing interest in designing new types of solid-state polymer electrolytes with improved conductivity. Figure 53

summarizes some potential applications of PILs as ion-conducting solid-state polymer electrolytes.

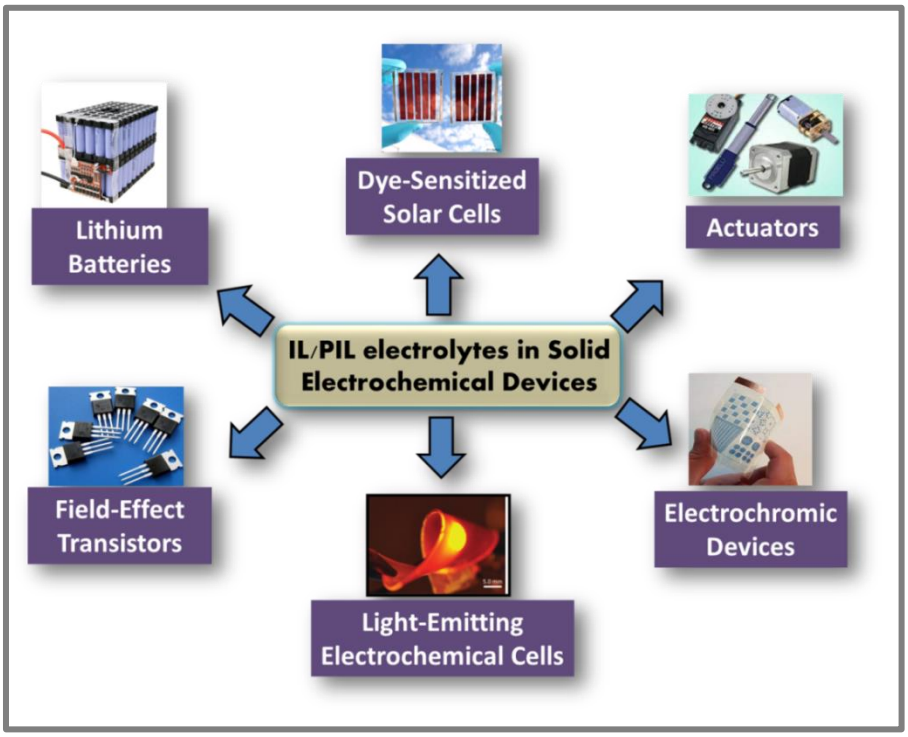

Figure 53. Application of poly(ionic liquid)s in various solid-state electrochemical devices (ECDs).[187]

a. Fuel cells

Fuel cell is a device that transforms chemical energy into electrical energy by a redox reaction. Presently, there is an increasing interest in fuel cells, which, contrary to classical Nafion membranes, function under alkaline conditions. Alkaline fuel cells are effortless to handle at low operating temperatures (e.g., 23–70 ^{o}C), where the reaction kinetics (at electrode surfaces) and cell voltages are upgraded. Protic ILs, made up of Brønsted acids and bases, that are capable of constituting hydrogen bonds and functioning as proton carriers, are known to be effective as proton transferring carriers for high temperature Proton-Exchange-Membrane-Fuel-Cell (PEMFC). Greenbaum et al.[500] have prepared a

free-standing, homogeneous and thermally stable gel-type PEM based on protic IL, 1-methyl-3-propyl imidazolium dihydrogen phosphate and phosphoric acid doped polybenzylimidazole. The PEM obtained had conductivity of up to 2.0 x 10^{-3} S cm^{-1} at 150 ^{o}C under anhydrous condition. But after some water vapor absorption, the conductivity rises even higher. Many groups have investigated PIL-based electrolyte membranes for its use in alkaline fuel-cell operation.[501-502] Yan et al. reported a facile synthetic route towards cross-linked anion exchange membranes (AEMs) based on alkaline PILs, without the use of chloromethyl ether and enabling the construction of simple processing membranes of desired dimensions.[503] In their fabrication procedure, an ILM, 1-vinyl-3-methyl imidazolium iodide ([VMIm][I]), was photopolymerized in situ with styrene and acrylonitrile in the presence of 2–10 wt.% of the cross-linker divinylbenzene. The same research group broadened this strategy to other IL monomers, such as 3-methyl-4-(1-vinybenzyl)imidazolium chloride and bis-imidazolium-type ILMs.[502, 504] The membrane built from these bis-imidazolium-type ILMs demonstrated superior chemical stability. Alkaline stability tests showed no obvious decrease in OH^- conductivity after immersing membrane samples in 1 M KOH solution at 60 ^{o}C for 30 days.

b. Dye-sensitized solar cells

Moreover, in case of fuel cells, there have also been reports on quasi-solid-state dye-sensitized solar cells (DSSCs) based on ILs and PILs. Grätzel et al. have constructed DSSCs based on mixtures of three different ILs, 1,3-dimethyl imidazolium iodide, 1-ethyl-3-methyl imidazolium iodide, and 1-ethyl-3-methyl imidazolium tetracyanoborate and achieved an efficiency of 8.2 %.[505] Furthermore, by consequent structure optimization of the ruthenium dye, higher efficiency (9.1 %) was achieved.[506] Also, a series of poly(1-vinyl-3 -alkylimidazolium) iodide PILs having different alkyl derivatives, e.g. methyl, propyl and perflurodecyl groups, have been synthesized as quasi-solid

electrolytes in a DSSC. The polymer electrolytes were formulated by mixing the PILs with an IL 1-methyl-3-propylimidazolium iodide, that showed IL-content-dependent ionic conductivities ranging from 10^{-3} to 10^{-7} S cm^{-1} at the room temperature. Solar cells having 1-cm^2 areas, prepared using poly(1-vinyl-3-propylimidazolium iodide) gel electrolyte, yielded a maximum light-to-electricity conversion efficiency of 3.73%. The value was later improved by Chen et al. [507] to 4.4% by using simulated solar illumination at 100 mW/cm and a poly(1-butyl-3-methylimidazolium TFSI) PIL. The efficiency was even further increased to 5.92% via a bis-imidazolium-based PIL.

c. *Lithium ion battery*

Because of high energy density and energy efficiency, lithium battery has been applied in various electronic devices e.g. digital cameras, laptops, cellular phones and even in vehicles and other large-scale power systems.[508] Although, the present lithium battery system has an innate safety issue because of its use of volatile and flammable organic solvents as electrolyte solvents.[509] Thus, it is highly necessary to construct new and safe electrolytes to replace organic solvent-based electrolytes. In present years, ILs and polymerized ILs have acquired substantial interests as electrolyte materials for lithium battery.[508-510] IL electrolytes have some unique characteristics making them promising applicants for lithium battery, e.g. non-flammability, non-volatility, wide electrochemical window, wide thermal operating range and high inherent conductivity.[508] The first report dealt with the electrochemical characteristics of solvent-free, ternary polymer electrolytes on the basis of the use of a novel poly(diallyldimethylammonium TFSI) PIL as a polymer host integrated with PYR14TFSI IL and LiTFSI salt.[66] Specifically, the PIL-based polymer electrolytes displayed room-temperature ionic conductivities above 10^{-4} S cm^{-1}, electrochemical stability windows of up to 5.0 V vs. Li^+/Li, time-stable interfacial resistance values and good lithium stripping/plating performance. Li et al.

constructed a similar ternary system based on a guanidinium-based PIL-containing copolymer.[511] Later, Yang et al. investigated a series of guanidinium PILs as electrolyte membranes for lithium batteries, obtaining maximum capacities of 130 and 140 mA/g at 0.2 and 0.1 C current rates, respectively.[68, 512] Recently, a trend has been observed to combine the ionic and electronic conductivities of conductive polymers by introducing a high density of IL species. This can be accomplished either by direct polymerization of an IL monomer with thiophene or by pyrrole units or by post-synthetic modifications.[513-514]

1.7.3 Sorbents and separation

The increase of CO_2 content in the atmosphere is broadly considered as one of the reasons of global warming. Chemical absorption and physical absorption are two main techniques used these days in industry for the removal of CO_2 from large point sources such as power plants. Due to their good solubility and selectivity to CO_2, non-volatility and thermal stability, ILs have been studied as a promising candidate in CO_2 absorption. The ability of ILs to physically absorb CO_2 was mainly affected by counter anions. A higher fluorination degree in counter anions causes a higher CO_2 absorption ratio, due to the interactions between Lewis basic fluorine atom and Lewis acidic CO_2.[515-516]

PILs have been proven as promising sorbents of CO_2 since they exhibit high CO_2 absorption capacity.[517] Tang et al. have investigated the CO_2 sorption ability of PILs for the first time, namely poly[1-(*p*-vinylbenzyl)-3-butylimidazolium tetrafluoroborate], poly[1-(*p*-vinylbenzyl)-3-butylimidazolium hexafluorophosphate] and poly[2-(methacryloyloxy)ethyl-3-butylimidazolium tetrafluoroborate] which gave CO_2 sorption values of 2.8 mol%, 2.27 mol% and 1.78 mol% respectively.[518] Later, the same group extended their research to prepare CO_2 absorbing tetraalkylammonium-based PILs, such as poly[p-vinyl benzyl trimethylammonium tetrafluoroborate], and poly[2-(methacryloyloxy)-

ethyl]trimethylammonium tetrafluoroborate.[519] The tetraalkylammonium-based PILs showed higher CO_2 sorption capacities than the imidazolium ones, due to the strong interaction of the tetraalkylammonium cation with CO_2 resulting in high positive charge density as compared to the imidazolium cation in which the positive charge is delocalized. . In addition, a cross-linkable ILM has been photopolymerized into a thin film, which is remarkably less permeable to gases than other types of PILs due to the higher cross-linking density.[520]

In the area of separation technology, PILs have been examined for use in solid phase extraction and chromatography. Hsieh and co-workers have constructed stationary phases depending upon imidazolium-derived PILs for use in gas chromatography, showing good reliability and structural selectivity.[521] These properties were attributed to the ordered arrangement of the PILs with octyl imidazolium side chains. PIL-based stationary coatings for solid-phase micro extraction have also been fabricated by free radical polymerization of vinyl-substituted imidazolium monomers and displayed sensitivity, good reproducibility, and yielded good detection limits.

1.7.4 *Application of porous PILs*

For past few years, several porous material with accessible pore channels and high surface area have been reported , like metal-organic frameworks (MOF),[522] porous organic polymers,[523] and porous aromatic frameworks (PAFs)[524]. Recently, some reports revealed that the ionic porous materials would offer more advantages over the natural analogues. The reasons behind such observations can be attributed to two factors. Firstly, the charged skeleton of the porous materials can strengthen the host-guest attraction/repulsion that is helpful for the application in selective separation. On the other hand, the counter ions of the charged pores can be easily exchanged.[525] Porous PILs combine the unique characteristics of both ILs and porous polymers or materials.

The charged pores present in porous PILs serve as the ion exchange materials for capturing ionic pollutants and hence make them potential candidates for extraction process, [526] storage and separation of analytes.[527-528] Recently Nayebi et al. developed imidazolium PIL-based porous polymers and utilized them as a sorbent for extraction and speciation of nitrite and nitrate ions. [525] Yan et al. developed porous PIL membranes as efficient and recyclable absorbents for heavy metal ions including Hg^{2+} , Pb^{2+} , Cu^{2+} , Cd^{2+} , and Zn^{2+} .[529] Weber et al. developed a mesoporous PIL network via hard-templating pathway which was used as an efficient adsorbent for CO_2 capture.[530] Zheng et al. reported a photo and humidity responsive mesoporous PIL membrane which showed excellent selective adsorption capability for cationic dye methylene blue. [531] Figure 54 summarizes some potential applications of porous PILs and their hybrids.

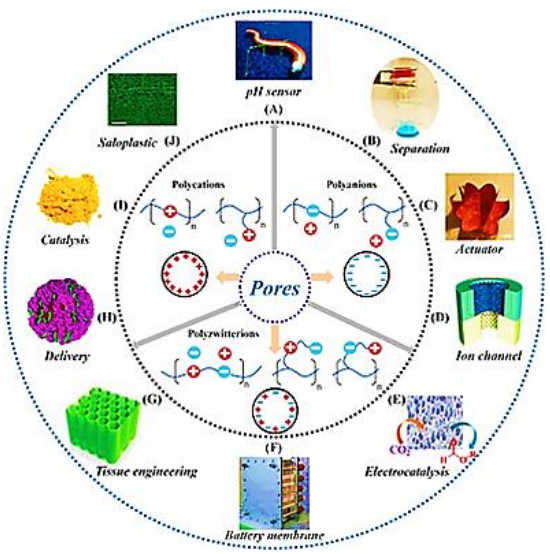

Figure 54. Application of porous PILs and their hybrids.[532]

1.8 Objectives and scope of the present research work

Poly (ionic liquid)s (PILs) have been a topic of great research interest among scientists because of their unique properties and wide range of applications as solid electrolyte, dispersant, stimuli-responsive polymer, porous polymeric

material and many more. In PILs, the unique properties of ILs are retained and due to polymerization, the mechanical performance, processability, and electrochemical and thermal stability of the materials get enhanced. Therefore, designing new class of IL as well as PIL having interesting functional properties is a current goal of research to the material scientists. The chemistry of stimuli responsive PILs or so-called 'smart PILs' has become a major focus nowadays because of the versatile application of these materials in smart devices, sensors, actuators etc. The nature of functionalities present in these polymers determines the type of external stimuli ranging from physical (temperature, light, electric or magnetic field, etc.) or chemical (pH, ligands, etc.) or biological (enzymes, etc.) to which they will be responded.

Furthermore, as discussed earlier in sections 1.3.1 and 1.7.1, the design of thermoresponsive PIL systems with water or organic solvents are rapidly growing because of their numerous applications including biomedical applications. The hydrophobicity/hydrophilicity balance of the starting IL monomers features the phase behaviour of the resulting PILs. Upper critical solution temperature (UCST)-type thermoresponsive phenomenon is not very common in conventional hydrophobic or hydrophilic polymers in aqueous solution. To address this issue, phosphonium PIL segment is coupled with either hydrophobic or polymer segments via RAFT copolymerization for introducing UCST property in their random copolymers. It is observed that the random PIL copolymers exhibited UCST-type behaviours in aqueous or in methanol solution depending on their compositions in the presence of externally added halide anions while the cloud points of these copolymers are tunable with respect to the copolymer compositions, molecular weight of polymers as well as concentrations of externally added anions. More interestingly, copolymerization of a PIL with a

LCST polymer results in the occurrence of a simultaneous LCST- and UCST-type phase behaviour in aqueous medium.

Moreover, PILs also belong to one of the most promising classes of materials in electrochemistry. PILs refer to a special type of polyelectrolyte where IL moieties are covalently bonded to a polymer backbone leaving the counter ions mobile. The major advantages of PILs including enhanced mechanical stability, improved processability and durability over the IL species allow them to be used in solid-state electrochemical devices (ECDs) such as batteries, fuel cells, supercapacitors and electrochromic devices. To develop new types of SPE, a PIL homopolymer and a series of PIL based random copolymers with a conventional hydrophobic polymer are synthesized by conventional free radical polymerization. Another series of PIL based copolymers with different molecular weights are synthesized by RAFT technique. The fundamental ion transport mechanism and relaxation in homo-PIL and PIL based random copolymers are investigated. The influences of copolymer compositions, nature of counter anions and molecular weights on ion transport and relaxation are studied to find the origin of the fast ion transport. It is observed that the precise molecular engineering of amphiphilic random copolymers influences the thermal and electrical properties of the copolymers.

Research on ionic liquids (ILs) has increased consistently over the last two decades. ILs have emerged as green solvents replacing traditional toxic, flammable and highly volatile solvents used in industries. Apart from this, there are other well-known applications of ILs such as in catalysis, electrochemistry, analytical uses, preparation of additives, etc. But unfortunately, there is no such report where ILs or their polymeric version are used as photoinitiators (PIs) for aqueous polymerization of vinyl monomers. Hence, the exploration of use of IL and PIL-based PI in aqueous medium becomes very important considering their

applications in industrial polymer synthesis, especially in replacing organic solvents with water. Thus, new phosphonium and imidazolium-based ILs are designed and synthesized which can act as novel PIs for polymerization of different vinyl monomers in aqueous medium. The kinetics and mechanism of this type of photopolymerization are also explored. Additionally, thermoresponsive polymers are grafted from the photoactive pendent IL moiety of the PIL by 'grafting-from' copolymerization, which results in the formation of thermoresponsive random graft copolymers.

Polymer hydrogels where hydrophilic polymeric chains are cross-linked with each other through chemical or physical interactions forming a three-dimensional fibrillar polymeric network are able to entrap a significant amount of water within its matrix and can provide clear advantages for removal of colour from effluents without dissolving in water. The development and devising of new types of chemically cross-linked polymer hydrogels (CCPHs) targeted mainly for waste-water treatment is still a challenging and interesting topic for researchers. CCPHs with ionic linkages are supposed to remove targeted anionic dyes from wastewater mainly through electrostatic interactions (physisorption) or chelation (chemisorption) between dye ions and hydrogel matrix. To develop new type of CCPHs, initially two different room temperature ionic liquids (RTILs) are synthesized. These two RTILs of varying concentrations are further utilized as cross-linkers for aqueous free radical solution polymerization of two hydrophilic monomers to produce different types of PIL-based hydrogels. Thermal stability and swelling ability of these hydrogels are investigated. Taking advantage of the anion exchange ability of these as-synthesized hydrogels, the dye uptake capacity, adsorption kinetics and adsorption mechanism of these hydrogels are thoroughly investigated.

1.9 References

1. Emel'yanenko, V. N.; Boeck, G.; Verevkin, S. P.; Ludwig, R., *Chem. Eur. J.* **2014**, *20*, 11640-11645.
2. Buszewski, B.; Studzińska, S., *Chromatographia* **2008**, *68*, 1-10.
3. Coleman, D.; Gathergood, N., *Chem. Soc. Rev.* **2010**, *39*, 600-637.
4. Plechkova, N. V.; Seddon, K. R., *Chem. Soc. Rev.* **2008**, *37*, 123-150.
5. Vekariya, R. L., *J. Mol. Liq.* **2017**, *227*, 44-60.
6. Pârvulescu, V. I.; Hardacre, C., *Chem. Rev.* **2007**, *107*, 2615-2665.
7. Van Rantwijk, F.; Sheldon, R. A., *Chem. Rev.* **2007**, *107*, 2757-2785.
8. Hallett, J. P.; Welton, T., *Chem. Rev.* **2011**, *111*, 3508-3576.
9. Armand, M.; Endres, F.; MacFarlane, D. R.; Ohno, H.; Scrosati, B., *Nat. Mater.* **2009**, *8*, 621-629.
10. Goel, K.; Bera, S.; Singh, M.; Mondal, D., *ChemistrySelect* **2019**, *4*, 6888-6895.
11. Gathergood, N.; Scammells, P. J., *Aust. J. Chem.* **2002**, *55*, 557-560.
12. JN, C. L.; MF, C. G.; Pádua, A., *J. Phys. Chem. B* **2006**, *110*, 16816-16818.
13. Greaves, T. L.; Drummond, C. J., *Chem. Soc. Rev.* **2013**, *42*, 1096-1120.
14. Wasserscheid, P.; Keim, W., *Angew. Chem. Int. Ed.* **2000**, *39*, 3772-3789.
15. Lethesh, K. C.; Van Hecke, K.; Van Meervelt, L.; Nockemann, P.; Kirchner, B.; Zahn, S.; Parac-Vogt, T. N.; Dehaen, W.; Binnemans, K., *J. Phys. Chem. B* **2011**, *115*, 8424-8438.
16. Zhang, H.; Li, M.; Yang, B., *J. Phys. Chem. C* **2018**, *122*, 2467-2474.

17. Fang, D.; Cheng, J.; Gong, K.; Shi, Q.-R.; Zhou, X.-L.; Liu, Z.-L., *J. Fluor. Chem.* **2008**, *129*, 108-111.

18. Deetlefs, M.; Seddon, K. R., *Green Chem.* **2003**, *5*, 181-186.

19. Martínez-Palou, R., *Mol. Divers.* **2010**, *14*, 3-25.

20. Cravotto, G.; Cintas, P., *Chem. Soc. Rev.* **2006**, *35*, 180-196.

21. Kuzmina, O.; Hallett, J., *Application, Purification, and Recovery of Ionic Liquids*; Elsevier, 2016.

22. Sachnov, S. J.; Schulz, P. S.; Wasserscheid, P., *Chem. Commun.* **2011**, *47*, 11234-11236.

23. Holbrey, J. D.; Reichert, W. M.; Swatloski, R. P.; Broker, G. A.; Pitner, W. R.; Seddon, K. R.; Rogers, R. D., *Green Chem.* **2002**, *4*, 407-413.

24. Boros, E.; Seddon, K. R.; Strauss, C. R., *Chim. Oggi* **2008**, *26*, 28-30.

25. Namboodiri, V. V.; Varma, R. S., *Org. Lett.* **2002**, *4*, 3161-3163.

26. Varma, R. S.; Namboodiri, V. V., *Chem. Commun.* **2001**, 643-644.

27. Srour, H.; Rouault, H.; Santini, C. C.; Chauvin, Y., *Green Chem.* **2013**, *15*, 1341-1347.

28. Wilkes, J. S.; Zaworotko, M. J., *J. Chem. Soc., Chem. Commun.* **1992**, 965-967.

29. Pringle, J. M.; Golding, J.; Forsyth, C. M.; Deacon, G. B.; Forsyth, M.; MacFarlane, D. R., *J. Mater. Chem.* **2002**, *12*, 3475-3480.

30. MacFarlane, D. R.; Golding, J.; Forsyth, S.; Forsyth, M.; Deacon, G. B., *Chem. Commun.* **2001**, 1430-1431.

31. Seddon, K. R.; Stark, A.; Torres, M.-J., *Pure Appl. Chem.* **2000**, *72*, 2275-2287.

32. Gordon, C. M.; Holbrey, J. D.; Kennedy, A. R.; Seddon, K. R., *J. Mater. Chem.* **1998**, *8*, 2627-2636.

33. Koch, V.; Nanjundiah, C.; Appetecchi, G. B.; Scrosati, B., *J. Electrochem. Soc.* **1995**, *142*, L116.

34. Patinha, D. J.; Silvestre, A. J.; Marrucho, I. M., *Prog. Polym. Sci.* **2019**, *98*, 101148.

35. Hoover, M. F., *J. Macromol. Sci. Chem.* **1970**, *4*, 1327-1418.

36. Ohno, H.; Yoshizawa, M.; Ogihara, W., *Electrochim. Acta* **2004**, *50*, 255-261.

37. João, K. G.; Tomé, L. C.; Isik, M.; Mecerreyes, D.; Marrucho, I. M., *Phys. Chem. Chem. Phys.* **2015**, *17*, 27462-27472.

38. Marcilla, R.; Alberto Blazquez, J.; Rodriguez, J.; Pomposo, J. A.; Mecerreyes, D., *J. Polym. Sci. Part A Polym. Chem.* **2004**, *42*, 208-212.

39. Vijayakrishna, K.; Mecerreyes, D.; Gnanou, Y.; Taton, D., *Macromolecules* **2009**, *42*, 5167-5174.

40. He, H.; Chung, H.; Roth, E.; Luebke, D.; Hopkinson, D.; Nulwala, H.; Matyjaszewski, K., *Polym. Adv. Technol.* **2015**, *26*, 823-828.

41. Chen, H.; Choi, J.-H.; Salas-de la Cruz, D.; Winey, K. I.; Elabd, Y. A., *Macromolecules* **2009**, *42*, 4809-4816.

42. Tang, J.; Tang, H.; Sun, W.; Radosz, M.; Shen, Y., *J. Polym. Sci. Part A Polym. Chem.* **2005**, *43*, 5477-5489.

43. Prescher, S.; Polzer, F.; Yang, Y.; Siebenbürger, M.; Ballauff, M.; Yuan, J., *J. Am. Chem. Soc.* **2014**, *136*, 12-15.

44. Ricks-Laskoski, H. L.; Snow, A. W., *J. Am. Chem. Soc.* **2006**, *128*, 12402-12403.

45. Dinda, E.; Si, S.; Kotal, A.; Mandal, T. K., *Chem. Eur. J.* **2008**, *14*, 5528-5537.

46. Vitz, J.; Erdmenger, T.; Haensch, C.; Schubert, U. S., *Green Chem.* **2009**, *11*, 417-424.

47. Shaplov, A.; Ponkratov, D.; Vygodskii, Y. S., *Polym. Sci. Ser. B* **2016**, *58*, 73-142.

48. Biswas, Y.; Mandal, T. K., *Macromolecules* **2017**, *50*, 9807-9820.

49. Tang, J.; Tang, H.; Sun, W.; Radosz, M.; Shen, Y., *Polymer* **2005**, *46*, 12460-12467.

50. Hemp, S. T.; Zhang, M.; Allen Jr, M. H.; Cheng, S.; Moore, R. B.; Long, T. E., *Macromol. Chem. Phys.* **2013**, *214*, 2099-2107.

51. Hemp, S. T.; Zhang, M.; Tamami, M.; Long, T. E., *Polym. Chem.* **2013**, *4*, 3582-3590.

52. Williams, S. R.; Salas-de la Cruz, D.; Winey, K. I.; Long, T. E., *Polymer* **2010**, *51*, 1252-1257.

53. Tamami, M.; Salas-de la Cruz, D.; Winey, K. I.; Long, T. E., *Macromol. Chem. Phys.* **2012**, *213*, 965-972.

54. Evans, C. M.; Bridges, C. R.; Sanoja, G. E.; Bartels, J.; Segalman, R. A., *ACS Macro Lett.* **2016**, *5*, 925-930.

55. Banerjee, P.; Anas, M.; Jana, S.; Mandal, T. K., *J. Polym. Res.* **2020**, *27*, 1-23.

56. Hirao, M.; Ito, K.; Ohno, H., *Electrochim. Acta* **2000**, *45*, 1291-1294.

57. Tang, J.; Sun, W.; Tang, H.; Radosz, M.; Shen, Y., *Macromolecules* **2005**, *38*, 2037-2039.

58. Blasig, A.; Tang, J.; Hu, X.; Tan, S. P.; Shen, Y.; Radosz, M., *Ind. Eng. Chem. Res.* **2007**, *46*, 5542-5547.

59. Marcilla, R.; Blazquez, J. A.; Fernandez, R.; Grande, H.; Pomposo, J. A.; Mecerreyes, D., *Macromol. Chem. Phys.* **2005**, *206*, 299-304.

60. Mineo, P. G.; Livoti, L.; Giannetto, M.; Gulino, A.; Schiavo, S. L.; Cardiano, P., *J. Mater. Chem. A* **2009**, *19*, 8861-8870.

61. Sato, T.; Marukane, S.; Narutomi, T.; Akao, T., *J. Power Sources* **2007**, *164*, 390-396.

62. Xiong, Y.; Wang, Y.; Wang, H.; Wang, R., *Polym. Chem.* **2011**, *2*, 2306-2315.

63. Godeau, G.; Navailles, L.; Nallet, F. d. r.; Lin, X.; McIntosh, T. J.; Grinstaff, M. W., *Macromolecules* **2012**, *45*, 2509-2513.

64. Xiao, S.; Lu, X.; Lu, Q., *Macromolecules* **2007**, *40*, 7944-7950.

65. Döbbelin, M.; Azcune, I.; Bedu, M. l.; Ruiz de Luzuriaga, A.; Genua, A.; Jovanovski, V.; Cabañero, G. n.; Odriozola, I., *Chem. Mater.* **2012**, *24*, 1583-1590.

66. Appetecchi, G.; Kim, G.-T.; Montanino, M.; Carewska, M.; Marcilla, R.; Mecerreyes, D.; De Meatza, I., *J. Power Sources* **2010**, *195*, 3668-3675.

67. Wang, J.; Li, S.; Zhang, S., *Macromolecules* **2010**, *43*, 3890-3896.

68. Li, M.; Yang, L.; Fang, S.; Dong, S., *J. Membr. Sci.* **2011**, *366*, 245-250.

69. Tsarevsky, N. V.; Matyjaszewski, K., *Chem. Rev.* **2007**, *107*, 2270-2299.

70. Yuan, J.; Antonietti, M., *Polymer* **2011**, *52*, 1469-1482.

71. Tang, J.; Tang, H.; Sun, W.; Plancher, H.; Radosz, M.; Shen, Y., *Chem. Commun.* **2005**, 3325-3327.

72. Bara, J. E.; Lessmann, S.; Gabriel, C. J.; Hatakeyama, E. S.; Noble, R. D.; Gin, D. L., *Ind. Eng. Chem. Res.* **2007**, *46*, 5397-5404.

73. Kohno, Y.; Saita, S.; Men, Y.; Yuan, J.; Ohno, H., *Polym. Chem.* **2015**, *6*, 2163-2178.

74. Meziane, R.; Bonnet, J.-P.; Courty, M.; Djellab, K.; Armand, M., *Electrochim. Acta* **2011**, *57*, 14-19.

75. Jangu, C.; Savage, A. M.; Zhang, Z.; Schultz, A. R.; Madsen, L. A.; Beyer, F. L.; Long, T. E., *Macromolecules* **2015**, *48*, 4520-4528.

76. Men, Y.; Schlaad, H.; Voelkel, A.; Yuan, J., *Polym. Chem.* **2014**, *5*, 3719-3724.

77. Men, Y.; Schlaad, H.; Yuan, J., *ACS. Macro. Lett.* **2013**, *2*, 456-459.

78. Zuo, Y.; Yu, J.; Liu, X.; Cao, P.; Song, P.; Wang, R.; Xiong, Y., *Polym. Chem.* **2017**, *8*, 1146-1154.

79. Destarac, M., *Polym. Rev.* **2011**, *51*, 163-187.

80. Perrier, S.; Takolpuckdee, P., *J. Polym. Sci. Part A Polym. Chem.* **2005**, *43*, 5347-5393.

81. Moad, G.; Rizzardo, E.; Thang, S. H., *Aust. J. Chem.* **2012**, *65*, 985-1076.

82. Matyjaszewski, K., *Macromolecules* **2012**, *45*, 4015-4039.

83. Matyjaszewski, K.; Xia, J., *Chem. Rev.* **2001**, *101*, 2921-2990.

84. Debuigne, A.; Caille, J. R.; Jérôme, R., *Angew. Chem. Int. Ed.* **2005**, *44*, 1101-1104.

85. Hawker, C. J.; Bosman, A. W.; Harth, E., *Chem. Rev.* **2001**, *101*, 3661-3688.

86. Bielawski, C. W.; Grubbs, R. H., *Prog. Polym. Sci.* **2007**, *32*, 1-29.

87. Kohno, Y.; Ohno, H., *Aust. J. Chem.* **2011**, *65*, 91-94.

88. Green, M. D.; Salas-de la Cruz, D.; Ye, Y.; Layman, J. M.; Elabd, Y. A.; Winey, K. I.; Long, T. E., *Macromol. Chem. Phys.* **2011**, *212*, 2522-2528.

89. Fraser, K. J.; MacFarlane, D. R., *Aust. J. Chem.* **2009**, *62*, 309-321.

90. Jangu, C.; Long, T. E., *Polymer* **2014**, *55*, 3298-3304.

91. Cheng, S.; Zhang, M.; Wu, T.; Hemp, S. T.; Mather, B. D.; Moore, R. B.; Long, T. E., *J. Polym. Sci. Part A Polym. Chem.* **2012**, *50*, 166-173.

92. Kanazawa, A.; Ikeda, T.; Endo, T., *J. Polym. Sci. Part A Polym. Chem.* **1994**, *32*, 1997-2001.

93. Kanazawa, A.; Ikeda, T.; Endo, T., *J. Polym. Sci. Part A Polym. Chem.* **1993**, *31*, 1467-1472.

94. Cowan, M. G.; Masuda, M.; McDanel, W. M.; Kohno, Y.; Gin, D. L.; Noble, R. D., *J. Membr. Sci.* **2016**, *498*, 408-413.

95. Chiefari, J.; Chong, Y.; Ercole, F.; Krstina, J.; Jeffery, J.; Le, T. P.; Mayadunne, R. T.; Meijs, G. F.; Moad, C. L.; Moad, G., *Macromolecules* **1998**, *31*, 5559-5562.

96. Moad, G., *Polym. Chem.* **2017**, *8*, 177-219.

97. Smith, A. E.; Xu, X.; McCormick, C. L., *Prog. Polym. Sci.* **2010**, *35*, 45-93.

98. Liu, C.; Wang, S.; Zhou, H.; Gao, C.; Zhang, W., *J. Polym. Sci. Part A Polym. Chem.* **2016**, *54*, 945-954.

99. Baussard, J.-F.; Habib-Jiwan, J.-L.; Laschewsky, A.; Mertoglu, M.; Storsberg, J., *Polymer* **2004**, *45*, 3615-3626.

100. Zhang, B.; Yan, X.; Alcouffe, P.; Charlot, A.; Fleury, E.; Bernard, J., *ACS Macro Lett.* **2015**, *4*, 1008-1011.

101. Vijayakrishna, K.; Jewrajka, S. K.; Ruiz, A.; Marcilla, R.; Pomposo, J. A.; Mecerreyes, D.; Taton, D.; Gnanou, Y., *Macromolecules* **2008**, *41*, 6299-6308.

102. Yang, Y.; Zheng, J.; Man, S.; Sun, X.; An, Z., *Polym. Chem.* **2018**, *9*, 824-827.

103. Nakabayashi, K.; Sato, Y.; Isawa, Y.; Lo, C.-T.; Mori, H., *Polymers* **2017**, *9*, 616.

104. Green, M. D.; Allen Jr, M. H.; Dennis, J. M.; Salas-de la Cruz, D.; Gao, R.; Winey, K. I.; Long, T. E., *Eur. Polym. J.* **2011**, *47*, 486-496.

105. Mori, H.; Yahagi, M.; Endo, T., *Macromolecules* **2009**, *42*, 8082-8092.

106. Wang, R.; Lowe, A. B., *J. Polym. Sci. Part A Polym. Chem.* **2007**, *45*, 2468-2483.

107. Lowe, A. B.; Wang, R.; Tiriveedhi, V.; Butko, P.; McCormick, C. L., *Macromol. Chem. Phys.* **2007**, *208*, 2339-2347.

108. Biswas, Y.; Maji, T.; Dule, M.; Mandal, T. K., *Polym. Chem.* **2016**, *7*, 867-877.

109. Yoshizawa, M.; Ogihara, W.; Ohno, H., *Polym. Adv. Technol.* **2002**, *13*, 589-594.

110. Gu, H.; England, D.; Yan, F.; Texter, J. In *New High Charge Density Polymers for Printable Electronics, Sensors, Batteries, and Fuel Cells*, 2008 2nd IEEE International Nanoelectronics Conference, IEEE: 2008; pp 863-868.

111. Kadokawa, J.-i.; Murakami, M.-a.; Kaneko, Y., *J. Compos. Sci.* **2008**, *68*, 493-498.

112. Yang, J.; Qiu, L.; Liu, B.; Peng, Y.; Yan, F.; Shang, S., *J. Polym. Sci. Part A Polym. Chem.* **2011**, *49*, 4531-4538.

113. Das, T.; Paira, T. K.; Biswas, M.; Mandal, T. K., *J. Phys. Chem. C.* **2015**, *119*, 4324-4332.

114. Nakajima, H.; Ohno, H., *Polymer* **2005**, *46*, 11499-11504.

115. Bao, Y.; Lantz, A. W.; Crank, J. A.; Huang, J.; Armstrong, D. W., *Electrophoresis* **2008**, *29*, 2587-2592.

116. Anderson, J. L.; Armstrong, D. W., *Anal. Chem.* **2005**, *77*, 6453-6462.

117. Pasparakis, G.; Vamvakaki, M., *Polym. Chem.* **2011**, *2*, 1234-1248.

118. Wei, M.; Gao, Y.; Li, X.; Serpe, M., *Polym. Chem.* **2017**, *8*, 127-143.

119. Zhang, A.; Jung, K.; Li, A.; Liu, J.; Boyer, C., *Prog. Polym. Sci.* **2019**, *99*, 101164.

120. Meng, H.; Li, G., *Polymer* **2013**, *54*, 2199-2221.

121. Dimitrov, I.; Trzebicka, B.; Müller, A. H.; Dworak, A.; Tsvetanov, C. B., *Prog. Polym. Sci.* **2007**, *32*, 1275-1343.

122. Dai, S.; Ravi, P.; Tam, K. C., *Soft Matter* **2008**, *4*, 435-449.

123. Ercole, F.; Davis, T. P.; Evans, R. A., *Polym. Chem.* **2010**, *1*, 37-54.

124. Akhoury, A.; Bromberg, L.; Hatton, T. A., *ACS Appl. Mater. Interfaces* **2011**, *3*, 1167-1174.

125. Magnusson, J. P.; Khan, A.; Pasparakis, G.; Saeed, A. O.; Wang, W.; Alexander, C., *J. Am. Chem. Soc.* **2008**, *130*, 10852-10853.

126. Ma, R.; Shi, L., *Polym. Chem.* **2014**, *5*, 1503-1518.

127. Liu, H.; Lin, S.; Feng, Y.; Theato, P., *Polym. Chem.* **2017**, *8*, 12-23.

128. Hocine, S.; Li, M.-H., *Soft Matter* **2013**, *9*, 5839-5861.

129. Gibson, M. I.; O'Reilly, R. K., *Chem. Soc. Rev.* **2013**, *42*, 7204-7213.

130. Fujishige, S.; Kubota, K.; Ando, I., *J. Phys. Chem.* **1989**, *93*, 3311-3313.

131. Li, Y.; Guo, H.; Gan, J.; Zheng, J.; Zhang, Y.; Wu, K.; Lu, M., *J. Polym. Res.* **2015**, *22*, 1-14.

132. Sivanantham, M.; Feng, H.; Winnik, F., *J. Polym. Res.* **2018**, *25*, 1-9.

133. Orakdogen, N., *J. Polym. Res.* **2012**, *19*, 1-10.

134. Bhattacharjee, R. R.; Chakraborty, M.; Mandal, T. K., *J. Phys. Chem. B* **2006**, *110*, 6768-6775.

135. Abbasi, S.; Yousefi, G.; Tamaddon, A.-M., *Colloids Surf. A Physicochem. Eng. Asp.* **2018**, *537*, 217-226.

136. Seuring, J.; Agarwal, S., *Macromol. Rapid Commun.* **2012**, *33*, 1898-1920.

137. Seuring, J.; Bayer, F. M.; Huber, K.; Agarwal, S., *Macromolecules* **2012**, *45*, 374-384.

138. Aliakseyeu, A.; Hlushko, R.; Sukhishvili, S. A., *Polym. Chem.* **2022**, *13*, 2637-2650.

139. Niskanen, J.; Tenhu, H., *Polym. Chem.* **2017**, *8*, 220-232.

140. Amajjahe, S.; Ritter, H., *Macromolecules* **2008**, *41*, 3250-3253.

141. Amajjahe, S.; Ritter, H., *Macromolecules* **2008**, *41*, 716-718.

142. Seno, K. I.; Kanaoka, S.; Aoshima, S., *J. Polym. Sci. Part A Polym. Chem.* **2008**, *46*, 5724-5733.

143. Yoshimitsu, H.; Kanazawa, A.; Kanaoka, S.; Aoshima, S., *Macromolecules* **2012**, *45*, 9427-9434.

144. Men, Y.; Li, X.-H.; Antonietti, M.; Yuan, J., *Polym. Chem.* **2012**, *3*, 871-873.

145. Xiong, Y.; Liu, J.; Wang, Y.; Wang, H.; Wang, R., *Angew. Chem. Int. Ed.* **2012**, *51*, 9114-9118.

146. Karjalainen, E.; Aseyev, V.; Tenhu, H., *Macromolecules* **2014**, *47*, 7581-7587.

147. Blanazs, A.; Armes, S. P.; Ryan, A. J., *Macromol. Rapid Commun.* **2009**, *30*, 267-277.

148. Moughton, A. O.; Patterson, J. P.; O'Reilly, R. K., *Chem. Commun.* **2011**, *47*, 355-357.

149. Li, J.; Cong, H.; Li, L.; Zheng, S., *ACS Appl. Mater. Interfaces* **2014**, *6*, 13677-13687.

150. Ziółkowski, B.; Diamond, D., *Chem. Commun.* **2013**, *49*, 10308-10310.

151. Jana, S.; Bose, A.; Saha, A.; Mandal, T. K., *J. Polym. Sci. Part A Polym. Chem.* **2017**, *55*, 1714-1729.

152. Biswas, Y.; Dule, M.; Mandal, T. K., *J. Phys. Chem. C* **2017**, *121*, 4747-4759.

153. Jana, S.; Biswas, Y.; Anas, M.; Saha, A.; Mandal, T. K., *Langmuir* **2018**, *34*, 12653-12663.

154. Soll, S.; Antonietti, M.; Yuan, J., *ACS Macro Lett.* **2012**, *1*, 84-87.

155. Goodenough, J. B., *Acc. Chem. Res.* **2013**, *46*, 1053-1061.

156. Etacheri, V.; Marom, R.; Elazari, R.; Salitra, G.; Aurbach, D., *Energy Environ. Sci.* **2011**, *4*, 3243-3262.

157. Agrawal, R.; Pandey, G., *J. Phys. D: Appl. Phys.* **2008**, *41*, 223001.

158. Zheng, F.; Kotobuki, M.; Song, S.; Lai, M. O.; Lu, L., *J. Power Sources* **2018**, *389*, 198-213.

159. Fenton, D., *Polymer* **1973**, *14*, 589.

160. Snyder, J.; Ratner, M.; Shriver, D., *Solid State Ion.* **2002**, *147*, 249-257.

161. Leuthner, S., Lithium-Ion Battery Overview. In *Lithium-Ion Batteries: Basics and Applications*, Springer: 2018; pp 13-19.

162. Maier, J., *Adv. Funct. Mater.* **2011**, *21*, 1448-1455.

163. Porcarelli, L.; Manojkumar, K.; Sardon, H.; Llorente, O.; Shaplov, A. S.; Vijayakrishna, K.; Gerbaldi, C.; Mecerreyes, D., *Electrochim. Acta* **2017**, *241*, 526-534.

164. Porcarelli, L.; Shaplov, A. S.; Bella, F.; Nair, J. R.; Mecerreyes, D.; Gerbaldi, C., *ACS Energy Lett.* **2016**, *1*, 678-682.

165. Zhang, H.; Li, C.; Piszcz, M.; Coya, E.; Rojo, T.; Rodriguez-Martinez, L. M.; Armand, M.; Zhou, Z., *Chem. Soc. Rev.* **2017**, *46*, 797-815.

166. Mehta, M. A.; Fujinami, T.; Inoue, S.; Matsushita, K.; Miwa, T.; Inoue, T., *Electrochim. Acta* **2000**, *45*, 1175-1180.

167. Blazejczyk, A.; Szczupak, M.; Wieczorek, W.; Cmoch, P.; Appetecchi, G.; Scrosati, B.; Kovarsky, R.; Golodnitsky, D.; Peled, E., *Chem. Mater.* **2005**, *17*, 1535-1547.

168. Nishimura, N.; Ohno, H., *Polymer* **2014**, *55*, 3289-3297.

169. Yu, Y.; Lu, F.; Sun, N.; Wu, A.; Pan, W.; Zheng, L., *Soft Matter* **2018**, *14*, 6313-6319.

170. Qian, W.; Texter, J.; Yan, F., *Chem. Soc. Rev.* **2017**, *46*, 1124-1159.

171. Matsumi, N.; Sugai, K.; Miyake, M.; Ohno, H., *Macromolecules* **2006**, *39*, 6924-6927.

172. Galiński, M.; Lewandowski, A.; Stępniak, I., *Electrochim. Acta* **2006**, *51*, 5567-5580.

173. Niu, H.; Wang, L.; Guan, P.; Zhang, N.; Yan, C.; Ding, M.; Guo, X.; Huang, T.; Hu, X., *J. Energy Storage* **2021**, *40*, 102659.

174. Zhao, Y.; Bostrom, T., *Curr. Org. Chem* **2015**, *19*, 556-566.

175. Ohno, H.; Ito, K., *Chem. Lett.* **1998**, *27*, 751-752.

176. Green, O.; Grubjesic, S.; Lee, S.; Firestone, M. A., *Polym. Rev.* **2009**, *49*, 339-360.

177. Yuan, J.; Mecerreyes, D.; Antonietti, M., *Prog. Polym. Sci.* **2013**, *38*, 1009-1036.

178. Shaplov, A. S.; Vlasov, P. S.; Lozinskaya, E. I.; Ponkratov, D. O.; Malyshkina, I. A.; Vidal, F.; Okatova, O. V.; Pavlov, G. M.; Wandrey, C.; Bhide, A., *Macromolecules* **2011**, *44*, 9792-9803.

179. Armand, M.; Endres, F.; MacFarlane, D. R.; Ohno, H.; Scrosati, B., Ionic-Liquid Materials for the Electrochemical Challenges of the Future. In *Materials for Sustainable Energy: A Collection of Peer-Reviewed Research Review Articles*, Nature Publishing Group: 2011; pp 129-137.

180. Fan, F.; Wang, W.; Holt, A. P.; Feng, H.; Uhrig, D.; Lu, X.; Hong, T.; Wang, Y.; Kang, N.-G.; Mays, J., *Macromolecules* **2016**, *49*, 4557-4570.

181. Bouchet, R.; Maria, S.; Meziane, R.; Aboulaich, A.; Lienafa, L.; Bonnet, J.-P.; Phan, T. N.; Bertin, D.; Gigmes, D.; Devaux, D., *Nat. Mater.* **2013**, *12*, 452-457.

182. Hu, H.; Yuan, W.; Jia, Z.; Baker, G. L., *RSC Adv.* **2015**, *5*, 3135-3140.

183. Kuray, P.; Noda, T.; Matsumoto, A.; Iacob, C.; Inoue, T.; Hickner, M. A.; Runt, J., *Macromolecules* **2019**, *52*, 6438-6448.

184. Shaplov, A. S.; Marcilla, R.; Mecerreyes, D., *Electrochim. Acta* **2015**, *175*, 18-34.

185. Hu, H.; Yuan, W.; Lu, L.; Zhao, H.; Jia, Z.; Baker, G. L., *J. Polym. Sci. Part A Polym. Chem.* **2014**, *52*, 2104-2110.

186. Wojnarowska, Z.; Knapik, J.; Jacquemin, J.; Berdzinski, S.; Strehmel, V.; Sangoro, J.; Paluch, M., *Macromolecules* **2015**, *48*, 8660-8666.

187. Mecerreyes, D., *Prog. Polym. Sci.* **2011**, *36*, 1629-1648.

188. Matsumoto, A.; Iacob, C.; Noda, T.; Urakawa, O.; Runt, J.; Inoue, T., *Macromolecules* **2018**, *51*, 4129-4142.

189. Sangoro, J. R.; Iacob, C.; Agapov, A.; Wang, Y.; Berdzinski, S.; Rexhausen, H.; Strehmel, V.; Friedrich, C.; Sokolov, A.; Kremer, F., *Soft Matter* **2014**, *10*, 3536-3540.

190. Hall, L. M.; Stevens, M. J.; Frischknecht, A. L., *Phys. Rev. Lett.* **2011**, *106*, 127801.

191. Nykaza, J. R.; Savage, A. M.; Pan, Q.; Wang, S.; Beyer, F. L.; Tang, M. H.; Li, C. Y.; Elabd, Y. A., *Polymer* **2016**, *101*, 311-318.

192. Pont, A.-L.; Marcilla, R.; De Meatza, I.; Grande, H.; Mecerreyes, D., *J. Power Sources* **2009**, *188*, 558-563.

193. Marcilla, R.; Alcaide, F.; Sardon, H.; Pomposo, J. A.; Pozo-Gonzalo, C.; Mecerreyes, D., *Electrochem. commun.* **2006**, *8*, 482-488.

194. Iacob, C.; Matsumoto, A.; Brennan, M.; Liu, H.; Paddison, S. J.; Urakawa, O.; Inoue, T.; Sangoro, J.; Runt, J., *ACS Macro Lett.* **2017**, *6*, 941-946.

195. Stacy, E. W.; Gainaru, C. P.; Gobet, M.; Wojnarowska, Z.; Bocharova, V.; Greenbaum, S. G.; Sokolov, A. P., *Macromolecules* **2018**, *51*, 8637-8645.

196. Choi, U. H.; Ye, Y.; Salas de la Cruz, D.; Liu, W.; Winey, K. I.; Elabd, Y. A.; Runt, J.; Colby, R. H., *Macromolecules* **2014**, *47*, 777-790.

197. Delhorbe, V.; Bresser, D.; Mendil-Jakani, H.; Rannou, P.; Bernard, L.; Gutel, T.; Lyonnard, S.; Picard, L., *Macromolecules* **2017**, *50*, 4309-4321.

198. Pipertzis, A.; Mühlinghaus, M.; Mezger, M.; Scherf, U.; Floudas, G., *Macromolecules* **2018**, *51*, 6440-6450.

199. Evans, C. M.; Sanoja, G. E.; Popere, B. C.; Segalman, R. A., *Macromolecules* **2016**, *49*, 395-404.

200. Fan, F.; Wang, Y.; Sokolov, A. P., *Macromolecules* **2013**, *46*, 9380-9389.

201. Wang, Y.; Fan, F.; Agapov, A. L.; Yu, X.; Hong, K.; Mays, J.; Sokolov, A. P., *Solid State Ion.* **2014**, *262*, 782-784.

202. Yoshida, K.; Manabe, H.; Takahashi, Y.; Furukawa, T., *Electrochim. Acta* **2011**, *57*, 139-146.

203. Wang, Y.; Agapov, A. L.; Fan, F.; Hong, K.; Yu, X.; Mays, J.; Sokolov, A. P., *Phys. Rev. Lett.* **2012**, *108*, 088303.

204. Wang, Y.; Fan, F.; Agapov, A. L.; Saito, T.; Yang, J.; Yu, X.; Hong, K.; Mays, J.; Sokolov, A. P., *Polymer* **2014**, *55*, 4067-4076.

205. Fan, F.; Wang, Y.; Hong, T.; Heres, M. F.; Saito, T.; Sokolov, A. P., *Macromolecules* **2015**, *48*, 4461-4470.

206. Xue, Z.; He, D.; Xie, X., *J. Mater. Chem. A* **2015**, *3*, 19218-19253.

207. Diddens, D.; Heuer, A.; Borodin, O., *Macromolecules* **2010**, *43*, 2028-2036.

208. Maitra, A.; Heuer, A., *Phys. Rev. Lett.* **2007**, *98*, 227802.

209. Wheatle, B. K.; Keith, J. R.; Mogurampelly, S.; Lynd, N. A.; Ganesan, V., *ACS Macro Lett.* **2017**, *6*, 1362-1367.

210. Pesko, D. M.; Webb, M. A.; Jung, Y.; Zheng, Q.; Miller III, T. F.; Coates, G. W.; Balsara, N. P., *Macromolecules* **2016**, *49*, 5244-5255.

211. Fragiadakis, D.; Dou, S.; Colby, R. H.; Runt, J., *Macromolecules* **2008**, *41*, 5723-5728.

212. Liang, S.; Choi, U. H.; Liu, W.; Runt, J.; Colby, R. H., *Chem. Mater.* **2012**, *24*, 2316-2323.

213. LaFemina, N. H.; Chen, Q.; Colby, R. H.; Mueller, K. T., *J. Chem. Phys.* **2016**, *145*, 114903.

214. Tudryn, G. J.; O'Reilly, M. V.; Dou, S.; King, D. R.; Winey, K. I.; Runt, J.; Colby, R. H., *Macromolecules* **2012**, *45*, 3962-3973.

215. Lin, K.-J.; Maranas, J. K., *Macromolecules* **2012**, *45*, 6230-6240.

216. Sinha, K.; Maranas, J., *Macromolecules* **2014**, *47*, 2718-2726.

217. Sinha, K.; Maranas, J. K., *Macromolecules* **2011**, *44*, 5381-5391.

218. Lin, K.-J.; Li, K.; Maranas, J. K., *RSC Adv.* **2013**, *3*, 1564-1571.

219. Ting, C. L.; Sorensen-Unruh, K. E.; Stevens, M. J.; Frischknecht, A. L., *J. Chem. Phys.* **2016**, *145*, 044902.

220. Middleton, L. R.; Tarver, J. D.; Cordaro, J.; Tyagi, M.; Soles, C. L.; Frischknecht, A. L.; Winey, K. I., *Macromolecules* **2016**, *49*, 9176-9185.

221. Hall, L. M.; Stevens, M. J.; Frischknecht, A. L., *Macromolecules* **2012**, *45*, 8097-8108.

222. Lu, K.; Rudzinski, J. F.; Noid, W. G.; Milner, S. T.; Maranas, J. K., *Soft Matter* **2014**, *10*, 978-989.

223. Lu, K.; Maranas, J. K.; Milner, S. T., *Soft matter* **2016**, *12*, 3943-3954.

224. Lin, K.-J.; Maranas, J. K., *Phys. Chem. Chem. Phys.* **2013**, *15*, 16143-16151.

225. Zhang, Y.; Maginn, E. J., *J. Phys. Chem. Lett.* **2015**, *6*, 700-705.

226. Mogurampelly, S.; Ganesan, V., *J. Chem. Phys* **2017**, *146*, 074902.

227. Ye, Y.; Elabd, Y. A., *Polymer* **2011**, *52*, 1309-1317.

228. la Cruz, D. S. d.; Green, M. D.; Ye, Y.; Elabd, Y. A.; Long, T. E.; Winey, K. I., *J. Polym. Sci. B Polym. Phys.* **2012**, *50*, 338-346.

229. Choi, U. H.; Mittal, A.; Price Jr, T. L.; Lee, M.; Gibson, H. W.; Runt, J.; Colby, R. H., *Electrochim. Acta* **2015**, *175*, 55-61.

230. Wojnarowska, Z.; Knapik, J.; Díaz, M.; Ortiz, A.; Ortiz, I.; Paluch, M., *Macromolecules* **2014**, *47*, 4056-4065.

231. Mogurampelly, S.; Keith, J. R.; Ganesan, V., *J. Am. Chem. Soc.* **2017**, *139*, 9511-9514.

232. Keith, J. R.; Mogurampelly, S.; Wheatle, B. K.; Ganesan, V., *J. Polym. Sci. Part B: Polym. Phys.* **2017**, *55*, 1718-1723.

233. Keith, J. R.; Mogurampelly, S.; Aldukhi, F.; Wheatle, B. K.; Ganesan, V., *Phys. Chem. Chem. Phys.* **2017**, *19*, 29134-29145.

234. Zhang, Z.; Krajniak, J.; Keith, J. R.; Ganesan, V., *ACS Macro Lett.* **2019**, *8*, 1096-1101.

235. Keith, J. R.; Rebello, N. J.; Cowen, B. J.; Ganesan, V., *ACS Macro Lett.* **2019**, *8*, 387-392.

236. Liu, H.; Luo, X.; Sokolov, A. P.; Paddison, S. J., *J. Phys. Chem. B* **2021**, *125*, 372-381.

237. DJ, G., Introduction to Electrodynamics. Prentice Hall: 1999.

238. Ratner, M. A.; Shriver, D. F., *Chem. Rev.* **1988**, *88*, 109-124.

239. McLin, M.; Angell, C., *Solid State Ion.* **1992**, *53*, 1027-1036.

240. Fragiadakis, D.; Dou, S.; Colby, R. H.; Runt, J., *Macromolecules* **2008**, *41*, 5723-5728.

241. Long, L.; Wang, S.; Xiao, M.; Meng, Y., *J. Mater. Chem. A* **2016**, *4*, 10038-10069.

242. Agrawal, R.; Pandey, G., *J.Phys. D Appl. Phys.* **2008**, *41*, 223001.

243. Nakamura, K.; Fukao, K.; Inoue, T., *Macromolecules* **2012**, *45*, 3850-3858.

244. Nakamura, K.; Fukao, K., *Polymer* **2013**, *54*, 3306-3313.

245. Angell, C., *Solid State Ion.* **1986**, *18*, 72-88.

246. Chatani, S.; Kloxin, C. J.; Bowman, C. N., *Polym. Chem.* **2014**, *5*, 2187-2201.

247. Bastiancich, C.; Danhier, P.; Préat, V.; Danhier, F., *J. Control. Release* **2016**, *243*, 29-42.

248. Yagci, Y.; Jockusch, S.; Turro, N. J., *Macromolecules* **2010**, *43*, 6245-6260.

249. Gruber, H. F., *Prog. Polym. Sci.* **1992**, *17*, 953-1044.

250. Sangermano, M.; Roppolo, I.; Chiappone, A., *Polymers* **2018**, *10*, 136.

251. Fouassier, J.-P.; Lalevée, J., *Photoinitiators for Polymer Synthesis: Scope, Reactivity, and Efficiency*; John Wiley & Sons, 2012.

252. Nesvadba, P., *Radical Polymerization in Industry*; John Wiley & Sons Inc, 2012.

253. Monroe, B. M.; Weed, G. C., *Chem. Rev.* **1993**, *93*, 435-448.

254. Fouassier, J. P.; Allonas, X.; Lalevée, J.; Dietlin, C., *Photoinitiators for Free Radical Polymerization Reactions*; John Wiley & Sons, 2010, p 351-419.

255. Moad, G.; Solomon, D. H., *The Chemistry of Radical Polymerization*; Elsevier, 2006.

256. Chiulan, I.; Heggset, E. B.; Voicu, S. I.; Chinga-Carrasco, G., *Biomacromolecules* **2021**, *22*, 1795-1814.

257. Dumur, F., *Eur. Polym. J.* **2020**, *125*, 109503.

258. Zhou, J.; Allonas, X.; Ibrahim, A.; Liu, X., *Prog. Polym. Sci.* **2019**, *99*, 101165.

259. Eibel, A.; Fast, D. E.; Gescheidt, G., *Polym. Chem.* **2018**, *9*, 5107-5115.

260. Müller, G.; Zalibera, M.; Gescheidt, G.; Rosenthal, A.; Santiso-Quinones, G.; Dietliker, K.; Grützmacher, H., *Macromol. Rapid Commun.* **2015**, *36*, 553-557.

261. Lalevée, J.; Fouassier, J.-P., *Photopolymerisation Initiating Systems*; Royal Society of Chemistry, 2018.

262. Benedikt, S.; Wang, J.; Markovic, M.; Moszner, N.; Dietliker, K.; Ovsianikov, A.; Grützmacher, H.; Liska, R., *J Polym. Sci. Part A Polym. Chem.* **2016**, *54*, 473-479.

263. Andrzejewska, E., Free Radical Photopolymerization of Multifunctional Monomers. In *Three-Dimensional Microfabrication Using Two-Photon Polymerization*, Elsevier: 2016; pp 62-81.

264. Prabhakaran, P.; Lee, K.-S., *Photo-Polymerization*; Springer, Cham, 2019, p 1-52.

265. Dadashi-Silab, S.; Doran, S.; Yagci, Y., *Chem. Rev.* **2016**, *116*, 10212-10275.

266. Ullrich, G.; Burtscher, P.; Salz, U.; Moszner, N.; Liska, R., *J. Polym. Sci. Part A Polym. Chem.* **2006**, *44*, 115-125.

267. Tomal, W.; Ortyl, J., *Polymers* **2020**, *12*, 1073.

268. Qin, X.-H.; Ovsianikov, A.; Stampfl, J.; Liska, R., *Bionanomaterials* **2014**, *15*, 49-70.

269. Woo, H. Y.; Hong, J. W.; Liu, B.; Mikhailovsky, A.; Korystov, D.; Bazan, G. C., *J. Am. Chem. Soc.* **2005**, *127*, 820-821.

270. Lu, Y.; Hasegawa, F.; Goto, T.; Ohkuma, S.; Fukuhara, S.; Kawazu, Y.; Totani, K.; Yamashita, T.; Watanabe, T., *J. Lumin.* **2004**, *110*, 1-10.

271. Dadashi-Silab, S.; Aydogan, C.; Yagci, Y., *Polym. Chem.* **2015**, *6*, 6595-6615.

272. Bonamy, A.; Fouassier, J.; Lougnot, D.; Green, P., *J. Polym. Sci., Polym. Lett. Ed.* **1982**, *20*, 315-320.

273. Aubry, B.; Dumur, F.; Lansalot, M.; Bourgeat-Lami, E.; Lacote, E.; Lalevée, J., *Macromol* **2022**, *2*, 131-140.

274. Bertz, A.; Wöhl-Bruhn, S.; Miethe, S.; Tiersch, B.; Koetz, J.; Hust, M.; Bunjes, H.; Menzel, H., *J. Biotechnol.* **2013**, *163*, 243-249.

275. Scott, R. A.; Peppas, N. A., *Biomaterials* **1999**, *20*, 1371-1380.

276. Wöhl-Bruhn, S.; Badar, M.; Bertz, A.; Tiersch, B.; Koetz, J.; Menzel, H.; Mueller, P. P.; Bunjes, H., *J. Control. Release* **2012**, *162*, 127-133.

277. Dietlin, C.; Schweizer, S.; Xiao, P.; Zhang, J.; Morlet-Savary, F.; Graff, B.; Fouassier, J.-P.; Lalevée, J., *Polym. Chem.* **2015**, *6*, 3895-3912.

278. Balta, D. K.; Temel, G.; Aydin, M.; Arsu, N., *Eur. Polym. J.* **2010**, *46*, 1374-1379.

279. Liska, R., *J. Polym. Sci. Part A Polym. Chem.* **2002**, *40*, 1504-1518.

280. Liang, Q.; Zhang, L.; Xiong, Y.; Wu, Q.; Tang, H., *J. Photochem. Photobiol. A Chem.* **2015**, *299*, 9-17.

281. Lougnot, D.; Fouassier, J., *J. Polym. Sci. Part A Polym. Chem.* **1988**, *26*, 1021-1033.

282. Knaus, S.; Gruber, H., *J. Polym. Sci. Part A Polym. Chem.* **1995**, *33*, 929-939.

283. Ma, Z.; Niu, X.; Xu, Z.; Guo, J., *J. Appl. Polym. Sci.* **2014**, *131*.

284. Rouillard, A. D.; Berglund, C. M.; Lee, J. Y.; Polacheck, W. J.; Tsui, Y.; Bonassar, L. J.; Kirby, B. J., *Tissue Eng. Part C Methods* **2011**, *17*, 173-179.

285. Assmann, A.; Vegh, A.; Ghasemi-Rad, M.; Bagherifard, S.; Cheng, G.; Sani, E. S.; Ruiz-Esparza, G. U.; Noshadi, I.; Lassaletta, A. D.; Gangadharan, S., *Biomaterials* **2017**, *140*, 115-127.

286. Marchioli, G.; Zellner, L.; Oliveira, C.; Engelse, M.; Koning, E. d.; Mano, J.; Apeldoorn, A. v.; Moroni, L., *J. Mater. Sci.: Mater. Med.* **2017**, *28*, 1-13.

287. Buwalda, S. J.; Perez, L. B.; Teixeira, S.; Calucci, L.; Forte, C.; Feijen, J.; Dijkstra, P. J., *Biomacromolecules* **2011**, *12*, 2746-2754.

288. Kamoun, E. A.; Omer, A. M.; Abu-Serie, M. M.; Khattab, S. N.; Ahmed, H. M.; Elbardan, A. A., *Arab. J. Sci. Eng.* **2018**, *43*, 3565-3575.

289. Chen, R. T.; Marchesan, S.; Evans, R. A.; Styan, K. E.; Such, G. K.; Postma, A.; McLean, K. M.; Muir, B. W.; Caruso, F., *Biomacromolecules* **2012**, *13*, 889-895.

290. Burdick, J. A.; Mason, M. N.; Hinman, A. D.; Thorne, K.; Anseth, K. S., *J. Control. Release* **2002**, *83*, 53-63.

291. Liska, R.; Knaus, S.; Gruber, H.; Wendrinsky, J., *Surf. Coat. Int.* **2000**, *83*, 297-303.

292. Kojima, K.; Ito, M.; Morishita, H.; Hayashi, N., *Chem. Mater.* **1998**, *10*, 3429-3433.

293. Serien, D.; Sugioka, K.; Engineering, *ACS Biomater. Sci. Eng.* **2020**, *6*, 1279-1287.

294. Serien, D.; Kawano, H.; Miyawaki, A.; Midorikawa, K.; Sugioka, K., *Appl. Sci.* **2018**, *8*, 147.

295. Sodré, C. S.; Albuquerque, P. P. A.; Isolan, C. P.; Moraes, R. R.; Schneider, L. F., *Int. J. Adhes. Adhes.* **2015**, *63*, 152-157.

296. Majima, T.; Schnabel, W.; Weber, W., *Makromol. Chemie* **1991**, *192*, 2307-2315.

297. Fairbanks, B. D.; Schwartz, M. P.; Bowman, C. N.; Anseth, K. S., *Biomaterials* **2009**, *30*, 6702-6707.

298. Calderon, G.; Thai, P.; Hsu, C.; Grigoryan, B.; Gibson, S.; Dickinson, M.; Miller, J., *Biomater. Sci.* **2017**, *5*, 1652-1660.

299. Raza, A.; Lin, C. C., *Macromol. Biosci.* **2013**, *13*, 1048-1058.

300. Pawar, A. A.; Saada, G.; Cooperstein, I.; Larush, L.; Jackman, J. A.; Tabaei, S. R.; Cho, N.-J.; Magdassi, S., *Sci. Adv.* **2016**, *2*, e1501381.

301. Wang, J.; Stanic, S.; Altun, A. A.; Schwentenwein, M.; Dietliker, K.; Jin, L.; Stampfl, J.; Baudis, S.; Liska, R.; Grützmacher, H., *Chem. Commun.* **2018**, *54*, 920-923.

302. Occhetta, P.; Sadr, N.; Piraino, F.; Redaelli, A.; Moretti, M.; Rasponi, M., *Biofabrication* **2013**, *5*, 035002.

303. Occhetta, P.; Visone, R.; Russo, L.; Cipolla, L.; Moretti, M.; Rasponi, M., *J. Biomed.*

Mater. Res. Part A **2015**, *103*, 2109-2117.

304. Wang, Z.; Jin, X.; Dai, R.; Holzman, J. F.; Kim, K., *RSC Adv.* **2016**, *6*, 21099-21104.

305. Han, W. T.; Jang, T.; Chen, S.; Chong, L. S. H.; Jung, H.-D.; Song, J., *Biomater.Sci.* **2020**, *8*, 450-461.

306. Encinas, M.; Rufs, A.; Bertolotti, S.; Previtali, C., *Polymer* **2009**, *50*, 2762-2767.

307. Sawhney, A. S.; Pathak, C. P.; Hubbell, J. A., *Biomaterials* **1993**, *14*, 1008-1016.

308. Nachlas, A. L.; Li, S.; Jha, R.; Singh, M.; Xu, C.; Davis, M. E., *Acta Biomater.* **2018**, *71*, 235-246.

309. Erkoc, P.; Seker, F.; Bagci-Onder, T.; Kizilel, S., *Macromol. Biosci.* **2018**, *18*, 1700369.

310. Shih, H.; Lin, C. C., *Macromol. Rapid Commun.* **2013**, *34*, 269-273.

311. Encinas, M.; Rufs, A.; Bertolotti, S.; Previtali, C., *Macromolecules* **2001**, *34*, 2845-2847.

312. Orellana, B.; Rufs, A.; Encinas, M.; Previtali, C.; Bertolotti, S., *Macromolecules* **1999**, *32*, 6570-6573.

313. Kim, S. H.; Chu, C. C., *J. Biomed. Mater. Res. Part B Appl.Biomater.* **2009**, *91*, 390-400.

314. Kamoun, E. A.; Menzel, H., *J. Polym. Res.* **2012**, *19*, 1-14.

315. Jakubiak, J.; Allonas, X.; Fouassier, J. P.; Sionkowska, A.; Andrzejewska, E.; Lindèn, L. Å.; Rabek, J. F., *Polymer* **2003**, *44*, 5219-5226.

316. Kamoun, E. A.; El-Betany, A.; Menzel, H.; Chen, X., *Int. J. Biol. Macromol.* **2018**, *120*, 1884-1892.

317. Declercq, H. A.; Gorski, T. L.; Tielens, S. P.; Schacht, E. H.; Cornelissen, M. J., *Biomacromolecules* **2005**, *6*, 1608-1614.

318. Wang, Y.; Spencer, P.; Yao, X.; Ye, Q., *J. Biomed. Mater. Res. Part A* **2006**, *78*, 721-728.

319. Matsuda, T.; Magoshi, T., *Biomacromolecules* **2002**, *3*, 942-950.

320. Okino, H.; Nakayama, Y.; Tanaka, M.; Matsuda, T., *J. Biomed. Mater. Res.* **2002**, *59*, 233-245.

321. Li, Z.; Torgersen, J.; Ajami, A.; Mühleder, S.; Qin, X.; Husinsky, W.; Holnthoner, W.; Ovsianikov, A.; Stampfl, J.; Liska, R., *RSC Adv.* **2013**, *3*, 15939-15946.

322. Maruo, S.; Nakamura, O.; Kawata, S., *Opt. Lett.* **1997**, *22*, 132-134.

323. Shen, X.; Li, L.; Min Chan, A. C.; Gao, N.; Yao, S. Q.; Xu, Q. H., *Adv. Opt. Mater.* **2013**, *1*, 92-99.

324. Tsai, C.-L.; Chen, J.-C.; Wang, W.-J., *J. Med. Biol. Eng.* **2001**, *21*, 7-14.

325. Hahn, M. S.; Miller, J. S.; West, J. L., *Adv. Mater.* **2005**, *17*, 2939-2942.

326. Ovsianikov, A.; Mironov, V.; Stampfl, J.; Liska, R., *Expert Rev. Med. Devices* **2012**, *9*, 613-633.

327. Jhaveri, S. J.; McMullen, J. D.; Sijbesma, R.; Tan, L.-S.; Zipfel, W.; Ober, C. K., *Chem. Mater.* **2009**, *21*, 2003-2006.

328. Ovsianikov, A.; Deiwick, A.; Van Vlierberghe, S.; Pflaum, M.; Wilhelmi, M.; Dubruel, P.; Chichkov, B., *Materials* **2011**, *4*, 288-299.

329. Vogel, A.; Venugopalan, V., *Chem. Rev.* **2003**, *103*, 577-644.

330. Pitts, J. D.; Campagnola, P. J.; Epling, G. A.; Goodman, S. L., *Macromolecules* **2000**, *33*, 1514-1523.

331. Farsari, M.; Filippidis, G.; Sambani, K.; Drakakis, T. S.; Fotakis, C., *J. Photochem. Photobiol. A Chem.* **2006**, *181*, 132-135.

332. Campagnola, P. J.; Delguidice, D. M.; Epling, G. A.; Hoffacker, K. D.; Howell, A. R.; Pitts, J. D.; Goodman, S. L., *Macromolecules* **2000**, *33*, 1511-1513.

333. Wan, X.; Zhao, Y.; Xue, J.; Wu, F.; Fang, X., *J. Photochem. Photobiol. A Chem.* **2009**, *202*, 74-79.

334. Woo, H. Y.; Liu, B.; Kohler, B.; Korystov, D.; Mikhailovsky, A.; Bazan, G. C., *J. Am. Chem. Soc.* **2005**, *127*, 14721-14729.

335. Cepraga, C.; Gallavardin, T.; Marotte, S.; Lanoe, P.-H.; Mulatier, J.-C.; Lerouge, F.; Parola, S.; Lindgren, M.; Baldeck, P. L.; Marvel, J., *Polym. Chem.* **2013**, *4*, 61-67.

336. Mariani, A.; Nuvoli, D.; Alzari, V.; Pini, M., *Macromolecules* **2008**, *41*, 5191-5196.

337. Zhong, R.; Xiong, F., Functional Ionic Liquids-a New Photoinitiator and Its Uv-Curing Properties. In *2011 International Conference on Materials for Renewable Energy & Environment*, IEEE: Shanghai, China, 2011; Vol. 2, pp 1946-1949.

338. Zhong, R.; Cao, C. G., *Adv. Mater. Res.* **2012**, *557*, 798-801.

339. Zhong, R.; Xiong, R. H.; Pang, L. X., *Adv. Mater. Res.* **2014**, *893*, 815-818.

340. Klouda, L.; Mikos, A. G., *Eur. J. Pharm. Biopharm.* **2008**, *68*, 34-45.

341. Killion, J. A.; Geever, L. M.; Devine, D. M.; Kennedy, J. E.; Higginbotham, C. L., *J. Mech. Behav. Biomed. Mater.* **2011**, *4*, 1219-1227.

342. Prettyman, J. B.; Eddington, D. T., *Sens. Actuators B: Chem.* **2011**, *157*, 722-726.

343. Vashist, A.; Vashist, A.; Gupta, Y.; Ahmad, S., *J. Mater. Chem. B* **2014**, *2*, 147-166.

344. Van Vlierberghe, S.; Dubruel, P.; Schacht, E., *Biomacromolecules* **2011**, *12*, 1387-1408.

345. Herrlich, S.; Spieth, S.; Messner, S.; Zengerle, R., *Adv. Drug Deliv. Rev.* **2012**, *64*, 1617-1627.

346. Zohuriaan-Mehr, M.; Pourjavadi, A.; Salimi, H.; Kurdtabar, M., *Polym. Adv. Technol.* **2009**, *20*, 655-671.

347. Arbona, V.; Iglesias, D. J.; Jacas, J.; Primo-Millo, E.; Talon, M.; Gómez-Cadenas, A., *Plant Soil* **2005**, *270*, 73-82.

348. Kulkarni, A. R.; Soppimath, K. S.; Aminabhavi, T. M.; Dave, A. M.; Mehta, M. H., *J. Control. Release* **2000**, *63*, 97-105.

349. Juang, R.-S.; Shiau, R.-C., *J. Membr. Sci.* **2000**, *165*, 159-167.

350. Abd-Elmohdy, F.; El Sayed, Z.; Essam, S.; Hebeish, A., *Carbohydr. Polym.* **2010**, *82*, 539-542.

351. Van Tran, V.; Park, D.; Lee, Y.-C., *Environ. Sci. Pollut. Res.* **2018**, *25*, 24569-24599.

352. Bahram, M.; Mohseni, N.; Moghtader, M., An Introduction to Hydrogels and Some Recent Applications. In *Emerging Concepts in Analysis and Applications of Hydrogels*, IntechOpen: 2016.

353. Hoffman, A. S., *Adv. Drug Deliv. Rev.* **2012**, *64*, 18-23.

354. Akhtar, M. F.; Hanif, M.; Ranjha, N. M., *Saudi Pharm. J.* **2016**, *24*, 554-559.

355. Ahmed, E. M., *J. Adv. Res.* **2015**, *6*, 105-121.

356. Ghosal, A.; Tiwari, S.; Mishra, A.; Vashist, A.; Rawat, N. K.; Ahmad, S.; Bhattacharya, J., Design and Engineering of Nanogels. In *Nanogels for Biomedical Applications*, 2017; pp 9-28.

357. Kabiri, K.; Omidian, H.; Zohuriaan-Mehr, M.; Doroudiani, S., *Polym. Compos.* **2011**, *32*, 277-289.

358. Singhal, R.; Gupta, K., *Polym.-Plast. Technol. Mater.* **2016**, *55*, 54-70.

359. Cai, W.; Gupta, R. B., *J. Appl. Polym. Sci.* **2003**, *88*, 2032-2037.

360. Nesrinne, S.; Djamel, A., *Arab. J. Chem.* **2017**, *10*, 539-547.

361. Sikdar, P.; Uddin, M. M.; Dip, T. M.; Islam, S.; Hoque, M. S.; Dhar, A. K.; Wu, S., *Mater. Adv.* **2021**, *2*, 4532-4573.

362. Annabi, N.; Tamayol, A.; Uquillas, J. A.; Akbari, M.; Bertassoni, L. E.; Cha, C.; Camci-Unal, G.; Dokmeci, M. R.; Peppas, N. A.; Khademhosseini, A., *Adv. Mater.* **2014**, *26*, 85-124.

363. Seidel, J. M.; Malmonge, S. M., *Mater. Res.* **2000**, *3*, 79-83.

364. Hennink, W. E.; van Nostrum, C. F., *Adv. Drug Deliv. Rev.* **2012**, *64*, 223-236.

365. Billiet, T.; Vandenhaute, M.; Schelfhout, J.; Van Vlierberghe, S.; Dubruel, P., *Biomaterials* **2012**, *33*, 6020-6041.

366. Ranganathan, N.; Bensingh, R. J.; Kader, M. A.; Nayak, S. K., *Synthesis and Properties of Hydrogels Prepared by Various Polymerization Reaction Systems*; Springer International Publishing, 2019, p 487-511.

367. Shin, B. M.; Kim, J.-H.; Chung, D. J., *Macromol. Res.* **2013**, *21*, 582-587.

368. Kiatkamjornwong, S., *Sci. Asia* **2007**, *33*, 39-43.

369. Achilias, D. S.; Verros, G. D., *J. Appl. Polym. Sci.* **2010**, *116*, 1842-1856.

370. Chanda, M., *Introduction to Polymer Science and Chemistry: A Problem-Solving Approach*; CRC Press, 2006.

371. Mathur, A. M.; Moorjani, S. K.; Scranton, A. B., *J. macromol. sci. Part C Polym. rev.* **1996**, *36*, 405-430.

372. Bajpai, S.; Bajpai, M.; Sharma, L., *Des. Monomers Polym.* **2007**, *10*, 181-192.

373. Essawy, H. A.; Ghazy, M. B.; Abd El-Hai, F.; Mohamed, M. F., *Int. J. Biol. Macromol.* **2016**, *89*, 144-151.

374. Tibbitt, M. W.; Kloxin, A. M.; Sawicki, L. A.; Anseth, K. S., *Macromolecules* **2013**, *46*, 2785-2792.

375. Maitra, J.; Shukla, V. K., *Am. j. polym. sci.* **2014**, *4*, 25-31.

376. Mondal, S.; Das, S.; Nandi, A. K., *Soft Matter* **2020**, *16*, 1404-1454.

377. Czarnecki, S.; Rossow, T.; Seiffert, S., *Polymers* **2016**, *8*, 82.

378. Berger, J.; Reist, M.; Mayer, J. M.; Felt, O.; Peppas, N.; Gurny, R., *Eur. J. Pharm. Biopharm.* **2004**, *57*, 19-34.

379. Liang, H.-F.; Hong, M.-H.; Ho, R.-M.; Chung, C.-K.; Lin, Y.-H.; Chen, C.-H.; Sung, H.-W., *Biomacromolecules* **2004**, *5*, 1917-1925.

380. Weng, L.; Chen, X.; Chen, W., *Biomacromolecules* **2007**, *8*, 1109-1115.

381. Ito, T.; Yeo, Y.; Highley, C. B.; Bellas, E.; Kohane, D. S., *Biomaterials* **2007**, *28*, 3418-3426.

382. Lee, K. Y.; Alsberg, E.; Mooney, D. J., *J. Biomed. Mater. Res.* **2001**, *56*, 228-233.

383. Jin, R.; Hiemstra, C.; Zhong, Z.; Feijen, J., *Biomaterials* **2007**, *28*, 2791-2800.

384. Kurisawa, M.; Chung, J. E.; Yang, Y. Y.; Gao, S. J.; Uyama, H., *Chem. Commun.* **2005**, 4312-4314.

385. Parhi, R., *Adv. Pharm. Bull.* **2017**, *7*, 515-530.

386. Ono, K.; Saito, Y.; Yura, H.; Ishikawa, K.; Kurita, A.; Akaike, T.; Ishihara, M., *J. Biomed. Mater. Res.* **2000**, *49*, 289-295.

387. Yoo, H. S., *J. Biomater. Sci. Polym. Ed.* **2007**, *18*, 1429-1441.

388. Yeo, Y.; Geng, W.; Ito, T.; Kohane, D. S.; Burdick, J. A.; Radisic, M., *J Biomed. Mater. Res. B Appl. Biomater.* **2007**, *81*, 312-322.

389. Ahn, J.; Ryu, J.; Song, G.; Whang, M.; Kim, J., *Carbohydr. Polym.* **2019**, *217*, 160-167.

390. Bashir, S.; Hina, M.; Iqbal, J.; Rajpar, A.; Mujtaba, M.; Alghamdi, N.; Wageh, S.; Ramesh, K.; Ramesh, S., *Polymers* **2020**, *12*, 2702.

391. Wichterle, O.; Lim, D., *Nature* **1960**, *185*, 117-118.

392. Park, Y.; Hashimoto, C.; Hashimoto, T.; Hirokawa, Y.; Jung, Y. M.; Ozaki, Y., *Macromolecules* **2013**, *46*, 3587-3602.

393. Devine, D. M.; Higginbotham, C. L., *Eur. Polym. J.* **2005**, *41*, 1272-1279.

394. Madduma-Bandarage, U. S.; Madihally, S. V., *J. Appl. Polym. Sci.* **2021**, *138*, 50376.

395. Oucif, A.; Haddadine, N.; Zakia, D.; Bouslah, N.; Benaboura, A.; Beyaz, K.; Guedouar, B.; El-Shall, M. S., *Polym. Bull.* **2022**, *79*, 1535-1554.

396. Sadakbayeva, Z.; Dušková-Smrčková, M.; Šturcová, A.; Pfleger, J.; Dušek, K., *Eur. Polym. J.* **2018**, *101*, 304-313.

397. Su, G.; Zhou, T.; Liu, X.; Ma, Y., *Polym. Chem.* **2017**, *8*, 865-878.

398. Xu, L.; Qiu, L.; Sheng, Y.; Sun, Y.; Deng, L.; Li, X.; Bradley, M.; Zhang, R., *J. Mater. Chem. B.* **2018**, *6*, 510-517.

399. Das, D.; Ghosh, P.; Dhara, S.; Panda, A. B.; Pal, S., *ACS Appl. Mater. Interfaces* **2015**, *7*, 4791-4803.

400. Pourjavadi, A.; Mahdavinia, G. R., *Turk. J. Chem.* **2006**, *30*, 595-608.

401. Mahdavinia, G.; Pourjavadi, A.; Hosseinzadeh, H.; Zohuriaan, M., *Eur. Polym. J.* **2004**, *40*, 1399-1407.

402. Yasin, T.; Rasool, N.; Akhter, Z., *E.Polym.* **2008**, *8*.

403. Elvira, C.; Mano, J.; San Roman, J.; Reis, R., *Biomaterials* **2002**, *23*, 1955-1966.

404. Bao, Y.; Ma, J.; Li, N., *Carbohydr. Polym.* **2011**, *84*, 76-82.

405. Imato, K.; Ohishi, T.; Nishihara, M.; Takahara, A.; Otsuka, H., *J. Am. Chem. Soc.* **2014**, *136*, 11839-11845.

406. Thakur, V. K.; Thakur, M. K., *Hydrogels: Recent Advances*; Springer, 2018.

407. Zhao, F.; Yao, D.; Guo, R.; Deng, L.; Dong, A.; Zhang, J., *Nanomaterials* **2015**, *5*, 2054-2130.

408. Suhag, D.; Bhatia, R.; Das, S.; Shakeel, A.; Ghosh, A.; Singh, A.; Sinha, O.; Chakrabarti, S.; Mukherjee, M., *RSC Adv.* **2015**, *5*, 53963-53972.

409. Guarino, V.; Galizia, M.; Alvarez-Perez, M.; Mensitieri, G.; Ambrosio, L., *J. Biomed. Mater. Res. A* **2015**, *103*, 1095-1105.

410. Lau, H. K.; Kiick, K. L., *Biomacromolecules* **2015**, *16*, 28-42.

411. Bajaj, P.; Schweller, R. M.; Khademhosseini, A.; West, J. L.; Bashir, R., *Annu. Rev. Biomed. Eng.* **2014**, *16*, 247.

412. Park, S.; Park, K. M., *Polymers* **2016**, *8*, 23.

413. Okay, O., *Prog. Polym. Sci.* **2000**, *25*, 711-779.

414. Croisier, F.; Jérôme, C., *Eur. Polym. J.* **2013**, *49*, 780-792.

415. Sato, R.; Noma, R.; Tokuyama, H., *Eur. Polym. J.* **2015**, *66*, 91-97.

416. Sokic, S.; Christenson, M.; Larson, J.; Papavasiliou, G., *Macromol. Biosci.* **2014**, *14*, 731-739.

417. Dash, R.; Foston, M.; Ragauskas, A. J., *Carbohydr. Polym.* **2013**, *91*, 638-645.

418. Wei, W.; Qi, X.; Liu, Y.; Li, J.; Hu, X.; Zuo, G.; Zhang, J.; Dong, W., *Colloids Surf. B: Biointerfaces* **2015**, *136*, 1182-1192.

419. Dragan, E. S.; Cocarta, A. I.; Gierszewska, M., *Colloids Surf. B: Biointerfaces* **2016**, *139*, 33-41.

420. Lozinsky, V. I., *A Brief History of Polymeric Cryogels*; Springer International Publishing: New York, 2014, p 1-48.

421. Rogina, A., *Appl. Surf. Sci.* **2014**, *296*, 221-230.

422. He, H.; Averick, S.; Mandal, P.; Ding, H.; Li, S.; Gelb, J.; Kotwal, N.; Merkle, A.; Litster, S.; Matyjaszewski, K., *Adv. Sci.* **2015**, *2*, 1500069.

423. Přádný, M.; Šlouf, M.; Martinová, L.; Michálek, J., *E-Polym.* **2010**, *10*.

424. Přádný, M.; Dušková-Smrčková, M.; Dušek, K.; Janoušková, O.; Sadakbayeva, Z.; Šlouf, M.; Michálek, J., *J. Polym. Res.* **2014**, *21*, 1-12.

425. Capes, J.; Ando, H.; Cameron, R., *J. Mater. Sci.: Mater. Med.* **2005**, *16*, 1069-1075.

426. Studenovská, H.; Šlouf, M.; Rypáček, F., *J. Mater. Sci.: Mater. Med.* **2008**, *19*, 615-621.

427. Kuo, Y.-C.; Wang, C.-C., *Colloids Surf. B: Biointerfaces* **2013**, *104*, 194-199.

428. Dragan, E. S.; Perju, M. M.; Dinu, M. V., *Carbohydr. Polym.* **2012**, *88*, 270-281.

429. Autissier, A.; Le Visage, C.; Pouzet, C.; Chaubet, F.; Letourneur, D., *Acta Biomater.* **2010**, *6*, 3640-3648.

430. Bencherif, S. A.; Braschler, T. M.; Renaud, P., *J. Periodontal Implant Sci.* **2013**, *43*, 251-261.

431. Ricciardi, R.; D'Errico, G.; Auriemma, F.; Ducouret, G.; Tedeschi, A. M.; De Rosa, C.; Lauprêtre, F.; Lafuma, F., *Macromolecules* **2005**, *38*, 6629-6639.

432. Baudron, V.; Gurikov, P.; Smirnova, I.; Whitehouse, S., *Gels* **2019**, *5*, 12.

433. Dinu, M. V.; Přádný, M.; Drăgan, E. S.; Michálek, J., *J. Polym. Res.* **2013**, *20*, 1-10.

434. Dinu, M. V.; Přádný, M.; Drăgan, E. S.; Michálek, J., *Carbohydr. Polym.* **2013**, *94*, 170-178.

435. Kim, T. G.; Chung, H. J.; Park, T. G., *Acta Biomater.* **2008**, *4*, 1611-1619.

436. Lee, Y.; Park, S.; Han, S. W.; Lim, T. G.; Koh, W.-G., *Biosens. Bioelectron.* **2012**, *35*, 243-250.

437. Fernandes, M.; Gonçalves, I. C.; Nardecchia, S.; Amaral, I. F.; Barbosa, M. A.; Martins, M. C. L., *Int. J. Pharm.* **2013**, *454*, 116-124.

438. Thein-Han, W.; Misra, R., *Acta Biomater.* **2009**, *5*, 1182-1197.

439. Apopei, D.; Dragan, E., *J.Nanostruct. Polym. Nanocompos.* **2013**, *9*, 16-20.

440. Berillo, D.; Volkova, N., *J. Mater. Sci.* **2014**, *49*, 4855-4868.

441. Dragan, E. S.; Cocarta, A. I., *ACS Appl. Mater. Interfaces* **2016**, *8*, 12018-12030.

442. Carvalho, B.; Da Silva, S.; Da Silva, L.; Minim, V.; Da Silva, M.; Carvalho, L.; Minim, L., *Sep. Purif. Rev.* **2014**, *43*, 241-262.

443. Rogers, Z. J.; Bencherif, S. A., *Gels* **2019**, *5*, 46.

444. Henderson, T. M.; Ladewig, K.; Haylock, D. N.; McLean, K. M.; O'Connor, A. J., *J. Mater. Chem. B* **2013**, *1*, 2682-2695.

445. Gun'ko, V. M.; Savina, I. N.; Mikhalovsky, S. V., *Adv. Colloid Interface Sci.* **2013**, *187*, 1-46.

446. Bakhshpour, M.; Idil, N.; Perçin, I.; Denizli, A., *Appl. Sci.* **2019**, *9*, 553.

447. Lozinsky, V. I.; Galaev, I. Y.; Plieva, F. M.; Savina, I. N.; Jungvid, H.; Mattiasson, B., *Trends Biotechnol* **2003**, *21*, 445-451.

448. Bai, H.; Polini, A.; Delattre, B.; Tomsia, A. P., *J. Mater. Chem. B* **2013**, *25*, 4551-4556.

449. Nieto-Suárez, M.; López-Quintela, M. A.; Lazzari, M., *Carbohydr. Polym.* **2016**, *141*, 175-183.

450. Gutiérrez, M. C.; Ferrer, M. L.; del Monte, F., *Chem. Mater.* **2008**, *20*, 634-648.

451. Kim, J.-W.; Taki, K.; Nagamine, S.; Ohshima, M., *Langmuir* **2009**, *25*, 5304-5312.

452. Wu, J.; Zhao, Q.; Sun, J.; Zhou, Q., *Soft Matter* **2012**, *8*, 3620-3626.

453. Zhang, Y.; Yan, W.; Sun, Z.; Pan, C.; Mi, X.; Zhao, G.; Gao, J., *Carbohydr. Polym.* **2015**, *117*, 657-665.

454. Annabi, N.; Nichol, J. W.; Zhong, X.; Ji, C.; Koshy, S.; Khademhosseini, A.; Dehghani, F., *Tissue Eng. Part B Rev.* **2010**, *16*, 371-383.

455. Ji, C.; Annabi, N.; Khademhosseini, A.; Dehghani, F., *Acta Biomater.* **2011**, *7*, 1653-1664.

456. Xu, S.; Deng, L.; Zhang, J.; Yin, L.; Dong, A., *J. Biomed. Mater. Res. Part B Appl. Biomater.* **2016**, *104*, 640-656.

457. Reneker, D. H.; Chun, I., *Nanotechnology* **1996**, *7*, 216.

458. Wu, Y.; Chen, Y. X.; Yan, J.; Yang, S.; Dong, P.; Soman, P., *J. Mater. Chem. B* **2015**, *3*, 5352-5360.

459. Rizwan, M.; Yahya, R.; Hassan, A.; Yar, M.; Azzahari, A. D.; Selvanathan, V.; Sonsudin, F.; Abouloula, C. N., *Polymers* **2017**, *9*, 137.

460. Kyzas, G. Z.; Lazaridis, N. K., *J. Colloid Interface Sci.* **2009**, *331*, 32-39.

461. Parasuraman, D.; Sarker, A. K.; Serpe, M. J., *Colloid Polym. Sci.* **2013**, *291*, 1795-1802.

462. Yetimoğlu, E. K.; Kahraman, M.; Ercan, Ö.; Akdemir, Z.; Apohan, N. K., *React. Funct. Polym.* **2007**, *67*, 451-460.

463. Dragan, E. S.; Apopei, D. F., *Chem. Eng. J.* **2011**, *178*, 252-263.

464. Ramesh, A.; Hasegawa, H.; Sugimoto, W.; Maki, T.; Ueda, K., *Bioresour. Technol.* **2008**, *99*, 3801-3809.

465. Karadağ, E.; Saraydin, D.; Öztop, H. N.; Güven, O., *Polym. Adv. Technol.* **1994**, *5*, 664-668.

466. Karadağ, E.; Saraydin, D.; Güven, O., *J. Appl. Polym. Sci.* **1997**, *66*, 733-739.

467. Chujo, Y.; Sada, K.; Saegusa, T., *Macromolecules* **1993**, *26*, 6320-6323.

468. Chujo, Y.; Sada, K.; Saegusa, T., *Macromolecules* **1993**, *26*, 6315-6319.

469. Kaşgöz, H.; Özgümüş, S.; Orbay, M., *Polymer* **2003**, *44*, 1785-1793.

470. Karadağ, E.; Saraydin, D.; Güven, O. J. J. o. a. p. s., *J. Appl. Polym. Sci.* **1996**, *61*, 2367-2372.

471. Saraydin, D.; Karadağ, E.; Güven, O., *Sep. Sci. Technol.* **1995**, *30*, 3287-3298.

472. Pakdel, P. M.; Peighambardoust, S. J., *Carbohydr. Polym.* **2018**, *201*, 264-279.

473. Liu, Y.; Zheng, Y.; Wang, A., *J. Environ. Sci.* **2010**, *22*, 486-493.

474. Saraydin, D.; Karadağ, E.; Güven, O., *Sep. Sci. Technol.* **1996**, *31*, 423-434.

475. Liu, Y.; Zheng, Y.; Huang, D.; Wang, A., *Sep. Sci. Technol.* **2012**, *47*, 1828-1836.

476. Kloxin, A. M.; Kloxin, C. J.; Bowman, C. N.; Anseth, K. S., *Adv. Mater.* **2010**, *22*, 3484-3494.

477. Aswathy, S.; Narendrakumar, U.; Manjubala, I., *Heliyon* **2020**, *6*, e03719.

478. Tighe, B. J., *Br. Polym. J.* **1976**, *8*, 71-77.

479. Padhi, J. R.; Nayak, D.; Nanda, A.; Rauta, P. R.; Ashe, S.; Nayak, B., *Carbohydr. Polym.* **2016**, *153*, 292-301.

480. Qu, Y.; Chu, B. Y.; Peng, J. R.; Liao, J. F.; Qi, T. T.; Shi, K.; Zhang, X. N.; Wei, Y. Q.; Qian, Z. Y., *NPG Asia Mater.* **2015**, *7*, e207-e207.

481. Tan, X.; Feldman, S. R.; Chang, J.; Balkrishnan, R., *Expert Opin. Drug Deliv.* **2012**, *9*, 1263-1271.

482. Narayanaswamy, R.; Torchilin, V. P., *Molecules* **2019**, *24*, 603.

483. Hu, X.; Tan, H.; Hao, L., *J. Mech. Behav. Biomed. Mater.* **2016**, *64*, 43-52.

484. Hu, X.; Gong, X., *J.Colloid Interface. Sci.* **2016**, *470*, 62-70.

485. El-Rehim, H. A.; Hegazy, E. S. A.; El-Mohdy, H. A., *J. Appl. Polym. Sci.* **2004**, *93*, 1360-1371.

486. Jamnongkan, T.; Kaewpirom, S., *J. Polym. Environ.* **2010**, *18*, 413-421.

487. Romero, M. R.; Wolfel, A.; Igarzabal, C. I. A., *Sens. Actuators B Chem.* **2016**, *234*, 53-62.

488. Zhang, Y.; Zhao, L.; Chen, Y., *J. Macromol. Sci. B* **2016**, *55*, 662-679.

489. Juarez-Maldonado, A.; Ortega-Ortíz, H.; Pérez-Labrada, F.; Cadenas-Pliego, G.; Benavides-Mendoza, A., *J. Appl. Bot. Food Qual.* **2016**, *89*.

490. Le Bideau, J.; Viau, L.; Vioux, A., *Chem. Soc. Rev.* **2011**, *40*, 907-925.

491. Zhang, Q.; Zhang, S.; Deng, Y., *Green Chem.* **2011**, *13*, 2619-2637.

492. Anderson, J. L.; Armstrong, D. W.; Wei, G.-T., *Anal. Chem.* **2006**, *78*, 2892-2902.

493. Kohno, Y.; Saita, S.; Murata, K.; Nakamura, N.; Ohno, H., *Polym. Chem.* **2011**, *2*, 862-867.

494. Vander Hoogerstraete, T.; Onghena, B.; Binnemans, K., *J. Phys. Chem. Lett.* **2013**, *4*, 1659-1663.

495. Mai, N. L.; Koo, Y.-M., *Enzyme Microb. Technol.* **2014**, *63*, 34-38.

496. Montolio, S.; Gonzáez, L.; Altava, B.; Tenhu, H.; Burguete, M. I.; García-Verdugo, E.; Luis, S. V., *Chem. Commun.* **2014**, *50*, 10683-10686.

497. Deguchi, Y.; Kohno, Y.; Ohno, H. J. A. J. o. C., *Aust. J. Chem.* **2014**, *67*, 1666-1670.

498. Kohno, Y.; Gin, D. L.; Noble, R. D.; Ohno, H., *Chem. Commun.* **2016**, *52*, 7497-7500.

499. Tudor, A.; Saez, J.; Florea, L.; Benito-Lopez, F.; Diamond, D., *Sens. Actuators B Chem.* **2017**, *247*, 749-755.

500. Ye, H.; Huang, J.; Xu, J.; Kodiweera, N.; Jayakody, J.; Greenbaum, S., *J. Power Sources* **2008**, *178*, 651-660.

501. Li, W.; Fang, J.; Lv, M.; Chen, C.; Chi, X.; Yang, Y.; Zhang, Y., *J. Mater. Chem.* **2011**, *21*, 11340-11346.

502. Qiu, B.; Lin, B.; Qiu, L.; Yan, F., *J. Mater. Chem.* **2012**, *22*, 1040-1045.

503. Lin, B.; Qiu, L.; Lu, J.; Yan, F., *Chem. Mater.* **2010**, *22*, 6718-6725.

504. Qiu, B.; Lin, B.; Si, Z.; Qiu, L.; Chu, F.; Zhao, J.; Yan, F., *J. Power Sources* **2012**, *217*, 329-335.

505. Bai, Y.; Cao, Y.; Zhang, J.; Wang, M.; Li, R.; Wang, P.; Zakeeruddin, S. M.; Grätzel, M., *Nat. Mater.* **2008**, *7*, 626-630.

506. Shi, D.; Pootrakulchote, N.; Li, R.; Guo, J.; Wang, Y.; Zakeeruddin, S. M.; Grätzel, M.; Wang, P., *J. Phys. Chem. C* **2008**, *112*, 17046-17050.

507. Chen, X.; Zhao, J.; Zhang, J.; Qiu, L.; Xu, D.; Zhang, H.; Han, X.; Sun, B.; Fu, G.; Zhang, Y., *J. Mater. Chem.* **2012**, *22*, 18018-18024.

508. Lee, J. S.; Bae, J. Y.; Lee, H.; Quan, N. D.; Kim, H. S.; Kim, H., *Ind. Eng. Chem.* **2004**, *10*, 1086-1089.

509. Lewandowski, A.; Świderska-Mocek, A., *J. Power Sources* **2009**, *194*, 601-609.

510. Seki, S.; Ohno, Y.; Kobayashi, Y.; Miyashiro, H.; Usami, A.; Mita, Y.; Tokuda, H.; Watanabe, M.; Hayamizu, K.; Tsuzuki, S., *J. Electrochem. Soc.* **2007**, *154*, A173.

511. Li, M.; Yang, L.; Fang, S.; Dong, S.; Hirano, S.-i.; Tachibana, K., *J. Power Sources* **2011**, *196*, 8662-8668.

512. Li, M.; Yang, L.; Fang, S.; Dong, S.; Hirano, S. i.; Tachibana, K., *Polym. Int.* **2012**, *61*, 259-264.

513. Richter, T. V.; Bühler, C.; Ludwigs, S., *J. Am. Chem. Soc.* **2012**, *134*, 43-46.

514. Zhao, J.; Yan, F.; Chen, Z.; Diao, H.; Chu, F.; Yu, S.; Lu, J., *J. Polym. Sci. Part A Polym. Chem.* **2009**, *47*, 746-753.

515. Anthony, J. L.; Anderson, J. L.; Maginn, E. J.; Brennecke, J. F., *J. Phys. Chem. B* **2005**, *109*, 6366-6374.

516. Huang, X.; Margulis, C. J.; Li, Y.; Berne, B. J., *J. Am. Chem. Soc.* **2005**, *127*, 17842-17851.

517. Zulfiqar, S.; Sarwar, M. I.; Mecerreyes, D., *Polym. Chem.* **2015**, *6*, 6435-6451.

518. Tang, J.; Sun, W.; Tang, H.; Radosz, M.; Shen, Y., *Macromolecules*

2005, *38*, 2037-2039.

519. Tang, J.; Tang, H.; Sun, W.; Plancher, H.; Radosz, M.; Shen, Y., *Chem. Commun.* **2005**, 3325-3327.

520. Bara, J. E.; Hatakeyama, E. S.; Gabriel, C. J.; Zeng, X.; Lessmann, S.; Gin, D. L.; Noble, R. D., *J. Membr. Sci.* **2008**, *316*, 186-191.

521. Hsieh, Y.-N.; Kuei, C.-H.; Chou, Y.-K.; Liu, C.-C.; Leu, K.-L.; Yang, T.-H.; Wang, M.-Y.; Ho, W.-Y., *Tetrahedron Lett.* **2010**, *51*, 3666-3669.

522. Elhussein, E. A. A.; Şahin, S.; Bayazit, Ş. S., *J. Mol. Liq.* **2018**, *255*, 10-17.

523. Liu, Z.-W.; Cao, C.-X.; Han, B.-H., *J. Hazard. Mater.* **2019**, *367*, 348-355.

524. Wang, T.; Xu, M.; Han, X.; Yang, S.; Hua, D., *J. Hazard. Mater.* **2019**, *368*, 214-220.

525. Nayebi, R.; Daneshvar Tarigh, G.; Shemirani, F., *Sci. Rep.* **2019**, *9*, 1-12.

526. Dai, X.; Wang, D.; Li, H.; Chen, Y.; Gong, Z.; Xiang, H.; Shi, S.; Chen, X., *J. Chromatogr. A* **2017**, *1484*, 7-13.

527. Zhang, S.; Dokko, K.; Watanabe, M., *Chem. Sci.* **2015**, *6*, 3684-3691.

528. Yan, A. X.; Yao, S.; Li, Y. G.; Zhang, Z. M.; Lu, Y.; Chen, W. L.; Wang, E. B., *Eur. J. Chem.* **2014**, *20*, 6927-6933.

529. Ren, Y.; Zhang, J.; Guo, J.; Chen, F.; Yan, F., *Macromol. Rapid Commun.* **2017**, *38*, 1700151.

530. Wilke, A.; Yuan, J.; Antonietti, M.; Weber, J., *ACS Macro Lett.* **2012**, *1*, 1028-1031.

531. Wu, A.; Lu, F.; Zhao, M.; Sun, N.; Shi, L.; Zheng, L., *ChemistrySelect* **2017**, *2*, 1878-1884.

532. Zhang, W.; Zhao, Q.; Yuan, J., *Angew. Chem., Int. Ed.* **2018**, *57*, 6754-6773.

Chapter 2

UCST-type phosphonium-based poly(ionic liquid) random copolymers

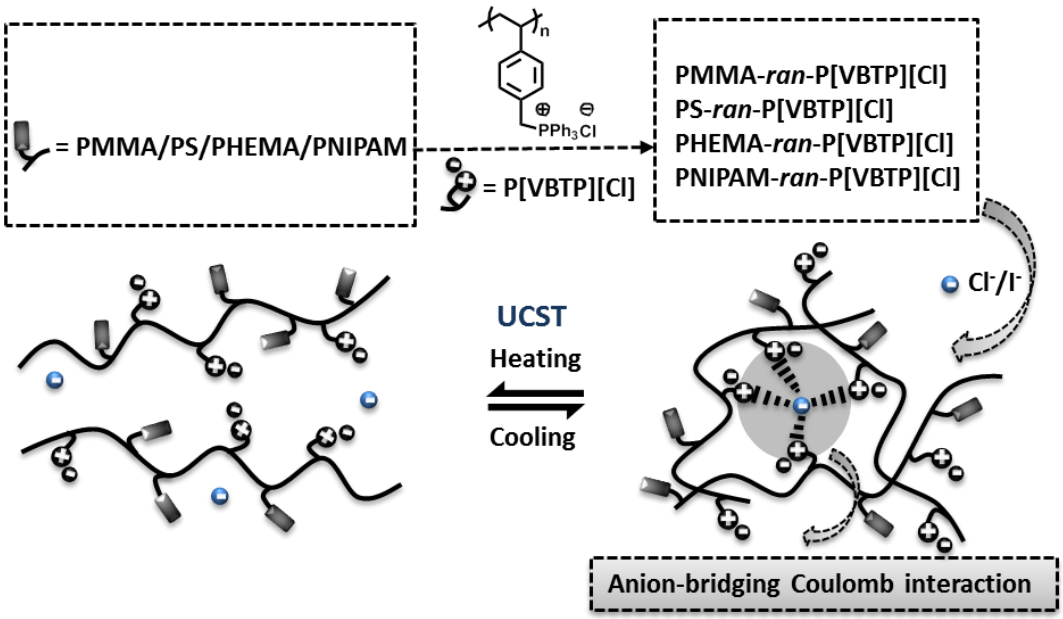

2.1 INTRODUCTION

Thermoresponsive polymers with lower and/or upper critical solution temperature (LCST or UCST) in solution show a significant miscibility gap at high temperatures and/or low temperatures, respectively. These polymers have particularly gained research interest due to their easy transition from the hydrophilic open coil state to hydrophobic globular state and vice versa in solution upon changing the temperature.[1-3] Consequently, a huge development has been observed in temperature sensitive macromolecules for generating new smart materials mainly for biomedical applications such as bioseparation,[4-5] drug delivery agents[6-7] substrates for cell culture[8] etc. One of the most extensively investigated thermoresponsive polymers include poly(N-isopropyl acrylamide) (PNIPAM) and the poly(meth)acrylamide derivatives whose aqueous solutions show a soluble to insoluble (S-I) transition, or lower critical solution temperature (LCST), when heated.[1-2, 9] A series of different bio-inspired polymers are also the important members of this LCST-type polymer family.[10-12] However, there are only few polymers whose aqueous solutions exhibit an insoluble to soluble (I-S) transition, or upper critical solution temperature (UCST), when heated. The non-ionic homopolymer of poly(N-acryloyl glycinamide) [poly(NAGA)] and poly(acrylamide-*co*-acrylonitrile) copolymers have been reported to exhibit a UCST-type phase behaviour in water as well as in electrolyte solution.[13-14] It is to be noted that most of these thermoresponsive polymers are non-ionic or weakly charged when dissolved in water and their phase transitions are mainly driven by H-bonding,[13, 15] except for zwitterionic polymers such as poly(sulfobetaine methacrylate)s which also showed UCST-type behaviour.[16-17] Thermoresponsive polymers that show two or more phase transitions upon heating or cooling are also interesting.[18-19] However, systems that exhibit both LCST- and UCST-type phase transitions (i.e., S-I-S or I-S-I) are much rarer.[20]

As already mentioned in Chapter 1, poly(ionic liquid) (PIL), an ionic polymer, possesses the unique properties of an ionic liquid (IL) along with the processability and durability of polymer materials.[21-23] These novel materials with new functions have been employed in different applications, such as nanocomposites,[24] gas separation membranes,[25] battery[26] and liquid crystal display.[21, 27] PILs also possess stimuli-responsive properties, but only a few are thermoresponsive. Earlier method of preparation of charged polymers exhibiting LCST-type phase behaviour were mainly obtained by copolymerizing thermally responsive non-ionic monomer with ionic monomer. Poly[1-butyl-3-vinylimidazolium bis(trifluoromethanesulfonyl)-imide] was the first reported thermoresponsive PIL which showed a pseudo-LCST behaviour in water in the presence of cyclodextrin because of temperature-sensitive formation/disruption of its inclusion complex.[28] Yuan et al. developed anionic and cationic PILs, poly(4-tetrabutylphosphonium styrene sulfonate) (PTPSS) and poly(tributyl-4-vinylbenzylphosphonium pentanesulfonate) respectively which showed LCST-type behaviours in water.[29-30] PILs showing thermoresponsive phase transition in water can be obtained by tailoring the hydrophilic/hydrophobic balance of the ionic components of the IL monomers, polymer concentration, and solvent. Thermal sensitivities of these PILs can also be tuned in the presence of cosolvents, salts, etc. in solution. On the other hand, UCST-type PIL homopolymers/copolymers are very rarely reported. One of such example is the UCST-type imidazolium- and DMAEMA-based polycations in aqueous solution in the presence of both $LiNTf_2$ and NaCl salts.[31] Another example of thermoresponsive PIL is poly(triphenyl-4-vinylbenzylphosphonium chloride) (P[VBTP][Cl]) (which has been mentioned in Chapter 1) which shows UCST-type phase behaviour in water in the presence of externally added halide anions.[32]

Poly(methyl methacrylate) (PMMA), being a bio-friendly polymer, has gained increasing interest as a particulate carrier in drug delivery.[33-35] There are also reports on the development of drug delivery systems based on PMMA containing copolymer micelles.[36-38] Polystyrene (PS)-based copolymers are able to influence the biological responses and those are established as interesting materials for fabrication of medical devices/drug delivery agents because of its bio-stability and vascular compatibility.[36, 39-41] There also exist handful of scientific reports regarding the drug release capabilities and biomedical applications of biodegradable poly(2-hydroxyethyl methacrylate) (PHEMA)-based[42-43] and poly(N-isopropyl acrylamide) (PNIPAM)-based[44-45] copolymers. However, in order to make PMMA/PS/PHEMA/PNIPAM based responsive copolymers suitable for biomedical applications including drug delivery and in other applications such as in paint or coating, it is important to keep their phase transition near physiological temperature. The cloud points of thermoresponsive polymers can be easily tuned by simple adjustment of the compositions through copolymerization along with the careful adjustment of other external factors such as varying counterions, redox potential, pH etc.[46-48] Thus, the development of stimuli-responsive random /block copolymers is highly essential for easy tuning of their switching behaviours. Statistical copolymers of different thermoresponsive polymer blocks furthermore offer the advantage of gradual change in their phase transition temperatures.[11, 49-50] Also, the incorporation of hydrophobic[51] or hydrophilic[52] comonomers can either decrease or increase the phase transition temperature, respectively. Weiss et al. employed RAFT polymerization to prepare a diblock copolymer, poly(N-n-propylacrylamide)-*b*-poly(N-ethylacrylamide) (PNPAM-*b*-PNEAM) of tunable thermoresponsiveness with two LCST-type cloud points for PNPAM (~20 ^{o}C) and PNEAM (~70 ^{o}C).[53] On the other hand, block copolymers comprising dual thermosensitivity of LCST- and

UCST-type behaviours can show so-called schizophrenic self-assembly in water, meaning that their micellar core–shell structure can be inverted under proper conditions.[54-55] However, there are only very few reports of thermoresponsive block/random copolymers comprising of one non-ionic and one ionic comonomer.[56-58] A block copolymer consisting of two hydrophilic blocks, PNIPAAm and the zwitterionic poly(3-[N-(3-methacrylamidopropyl)-N,N-dimethyl]ammoniopropane sulfonate) (PSPP) exhibiting double thermoresponsiveness in water is also reported.[59] Further, Dai et al. investigated the phase behavior, self-assembly process, and microdynamics of poly(tetrabutyl phosphonium styrene sulfonate)-*b*-(poly(2-(2-methoxyethoxy)ethyl methacrylate)) ($PMEO_2MA$-*b*-$P[P_{4,4,4,4}][SS]$) copolymers containing LCST-type non-ionic and PIL blocks.[56]

2.2 OBJECTIVES AND SCOPE OF THE PRESENT WORK

A detailed literature survey revealed that most of the studies have only been focused on the development of conventional non-ionic thermoresponsive homo- and co-polymers, but the thermoresponsiveness of copolymers of conventional hydrophobic/hydrophilic polymers and charged PILs has been rarely studied. Therefore, the interest to develop PIL based copolymers from an ionic liquid monomer and a non-ionic monomer (either hydrophilic or hydrophobic) is very obvious to grow. The incorporation of charged PIL blocks can lead to changes of the hydrophilic–hydrophobic balance and consequently the thermoresponsive behaviour, in particular UCST-type behaviour of the resultant copolymers. Another curiosity lies in the fact that whether random insertion of a PIL segment into a LCST-type polymer (such as PNIPAM) can lead to a copolymer showing simultaneous LCST- and UCST- type phase behaviour in aqueous medium in presence of externally added halide ions. On the other hand, copolymers based

on PMMA, PS, PHEMA and PNIPAM possess special features which made them attractive for various applications, including some in the biomedical field.Thus, the objectives of the present work are to synthesize various random copolymers comprising of a charged cationic PIL segment with various hydrophobic and hydrophilic polymer segments with the expectation that the copolymers would become soluble in water and would exhibit attractive thermoresponsive behaviour depending upon the nature of co-monomer and copolymer compositions.

Thus, in the present work, an attempt has been made to develop a series of random copolymers by the RAFT polymerization of either conventional hydrophobic monomers [methyl methacrylate (MMA) and styrene] or hydrophilic monomers [2-hydroxyethyl methacrylate (HEMA) and N-isopropyl acrylamide (NIPAM)] with previously mentioned (in Chapter 1) as-synthesised IL monomer, triphenyl-4-vinylbenzylphosphonium chloride ([VBTP][Cl]).[32] It is observed that the introduction of PIL segment made P[VBTP][Cl]-ran-PMMA, P[VBTP][Cl]-ran-PS and P[VBTP][Cl]-ran-PHEMA copolymers soluble in water or in methanol irrespective of their molecular weights. It is further observed that the transparent aqueous/MeOH solutions of these copolymers in presence of externally added halide ions transformed into a turbid suspension due to halide ion-induced aggregation followed by a transition to transparent solution due to temperature-induced disaggregation indicating a clear UCST-type phase behaviour. As already mentioned in Chapter 1, P[VBTP][Cl] homopolymer exhibits UCST-type behaviour in the presence of halide ions in water. The UCST-type phase behaviour is rarely observed in conventional hydrophobic or hydrophilic polymers in water. Thus, the main challenge is to introduce such property into both types of polymers. On the other hand, the solubility of hydrophobic polymers in aqueous medium is the main hindrance for showing

any UCST. Therefore, in this work, we have incorporated PIL segment with conventional hydrophobic polymers such as PMMA or PS via copolymerization to increase their solubility in water and also to bring down the UCST cloud point in the range of 0-100°C. These PIL copolymers showed UCST-type phase behaviour in a wide range of temperature window allowing them to use in various applications including drug delivery. On the other hand, P[VBTP][Cl]-ran-PNIPAM copolymer, expectedly, show either LCST-/UCST-type or simultaneously LCST- and UCST- type phase transition in the presence of halide ions in aqueous solution. The cloud points of these copolymers were tuned in a large temperature window with respect to different parameters such as copolymer composition, nature and concentration of externally added halide ion etc.

2.3 EXPERIMENTAL SECTION

2.3.1 Materials

Methyl methacrylate (MMA, >99%), styrene (St, ≥99.5%) and 2-hydroxyethyl methacrylate (HEMA, 98%) were purchased from Sigma-Aldrich and were purified by passing through basic alumina column to remove inhibitors prior to use. N-isopropyl acrylamide (NIPAM, ≥97%; Merck) was recrystallized twice from hexane before use. 2,2'-Azobis(2-methylpropionitrile) (AIBN, 98%) was obtained from Sigma-Aldrich and was recrystallized twice from ethanol. 4-Cyano-4-[(dodecylsulfanylthiocarbonyl) sulfanyl] pentanoic acid (CDP, ≥ 97%, HPLC), sodium iodide (NaI; 99.9%) and sodium chloride (NaCl ; > 99%) were used as received from Sigma-Aldrich. Dimethylformamide (DMF) and methanol (MeOH) were received from Merck, India. DMF was dried overnight with $CaCl_2$ and was distilled over CaH_2 under reduced pressure prior to use. Milli-Q water was used in preparation of various solutions.

2.3.2 Synthesis of random PIL copolymers

A series of different PIL-based AB type random copolymers of varying compositions were prepared from the A-type triphenyl-4-vinylbenzylphosphonium chloride ([VBTP][Cl]) ILM and a B-type either hydrophobic monomer or a hydrophilic monomer such as MMA/St or HEMA/NIPAM respectively via RAFT polymerization technique (Scheme 1) using CDP and AIBN as the chain transfer agent (CTA) and radical initiator respectively. It is to be noted that the synthesis of [VBTP][Cl] monomer was achieved by following a reported protocol.[32] The actual compositions of all the copolymers were obtained from ^{1}H-NMR analysis, which is given in Table 1.

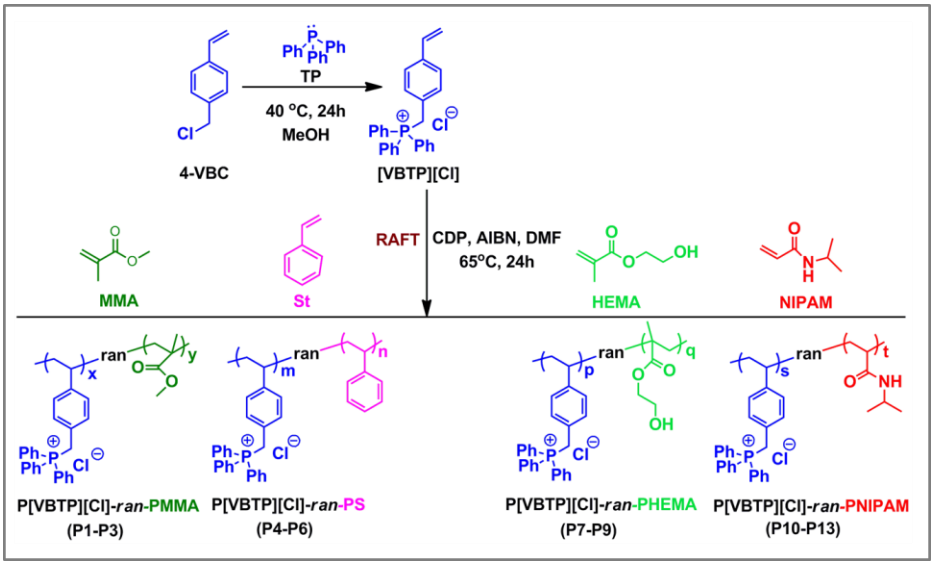

Scheme 1. Synthetic scheme for random copolymers, P[VBTP][Cl]-*ran*-PMMA /P[VBTP][Cl]-*ran*-PS/ P[VBTP][Cl]-*ran*-PHEMA/ P[VBTP][Cl]-*ran*-PNIPAM prepared via RAFT copolymerization.

2.3.2.1 Synthesis of P[VBTP][Cl]-ran-PMMA (P1-P3) copolymers

Typically, for **P1** (Table 1), MMA (0.832 g; 8.301 mmol), [VBTP][Cl] (0.350 g; 0.9224 mmol), CDP (0.0372 g; 0.0922 mmol) and AIBN (3.03 mg; 0.0184 mmol) were added to 12 mL dry DMF taken in a 25 mL long-neck RB flask. The mixture

was purged with argon gas for 45 mins before the flask was immediately sealed with a rubber septum. Finally, the sealed flask was placed in an oil bath preheated at 65 ^{o}C for 24h under magnetic stirring. After polymerization, the **P1** was precipitated in diethyl ether followed by further dissolution in DMF and re-precipitation in water and finally isolated by centrifugation to remove traces of unreacted [VBTP][Cl]. The purified **P1** was then dried in vacuum oven at 60 ^{o}C for overnight. Yield: 75 %. **P2** and **P3** of different compositions were also prepared following the same procedure as used for **P1,** while the molar feed ratios of [VBTP][Cl] and MMA were varied from 1:9 to 4:1 (Table 1).The actual compositions of **P1-P3** were determined by ^{1}H-NMR analysis (Table 1). The ^{1}H-NMR spectra of **P1**, **P2** and **P3** copolymer and their respective analysis are given in Figures 1 to 3 respectively.

^{1}H-NMR analysis of **P1** (500 MHz, $CDCl_3$, δ ppm)(Figure 1): 1.22-0.52 (-CH_2 and –CH and –CH_3 of polymer backbone, position ‘a’, ‘b’, ‘l’); 1.8 (-CH_2 protons of polymer backbone, position ‘k’); 5.26 (benzylic protons, position ‘f’); 6.91 (phenyl ring protons, position ‘d’); 6.75 (phenyl ring protons, position ‘e’); 7.62-7.73 (phenyl ring protons of TPP unit); 3.45 (-CH_3 protons, position ‘m’).

^{1}H-NMR analysis of **P2** (500 MHz, $CDCl_3$, δ ppm)(Figure 2) : 1.22-0.30 (-CH_2 and –CH and –CH_3 of polymer backbone, position ‘a’, ‘b’, ‘l’); 1.6 (-CH_2 protons of polymer backbone, position ‘k’); 5.24 (benzylic protons, position ‘f’); 6.8 (phenyl ring protons, position ‘d’; phenyl ring protons, position ‘e’); 7.66-7.84 (phenyl ring protons of TPP unit); 3.40 (-CH_3 protons, position ‘m’).

^{1}H-NMR analysis of **P3** (500 MHz, $CDCl_3$, δ ppm)(Figure 3) :1.14-1.24 (-CH_2 and –CH and –CH_3 of polymer backbone, position ‘a’, ‘b’, ‘l’); 1.8 (-CH_2 protons of polymer backbone, position ‘k’); 5.33 (benzylic protons, position ‘f’); 6.89 (phenyl ring protons, position ‘d’; phenyl ring protons, position ‘e’); 7.44-7.73 (phenyl ring protons of TPP unit); 3.44 (-CH_3 protons, position ‘m’).

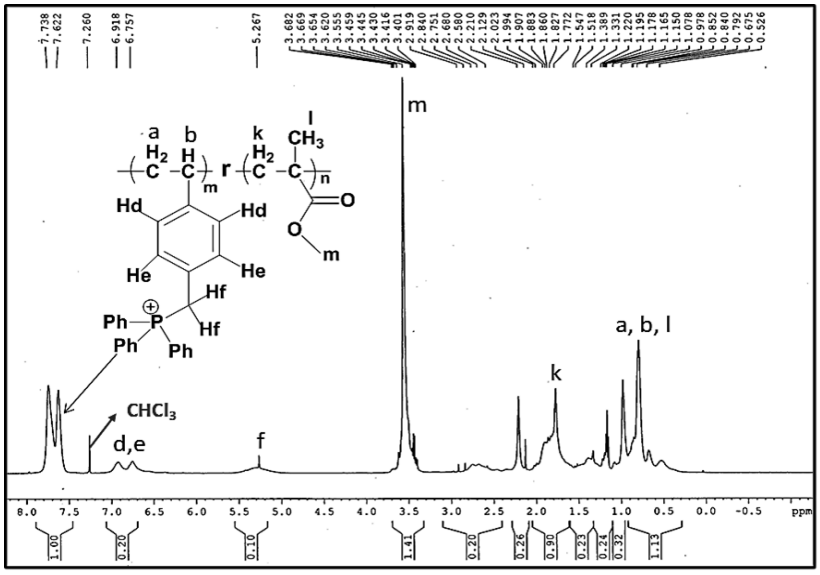

Figure 1. ^{1}H-NMR spectrum of **P1** in $CDCl_3$

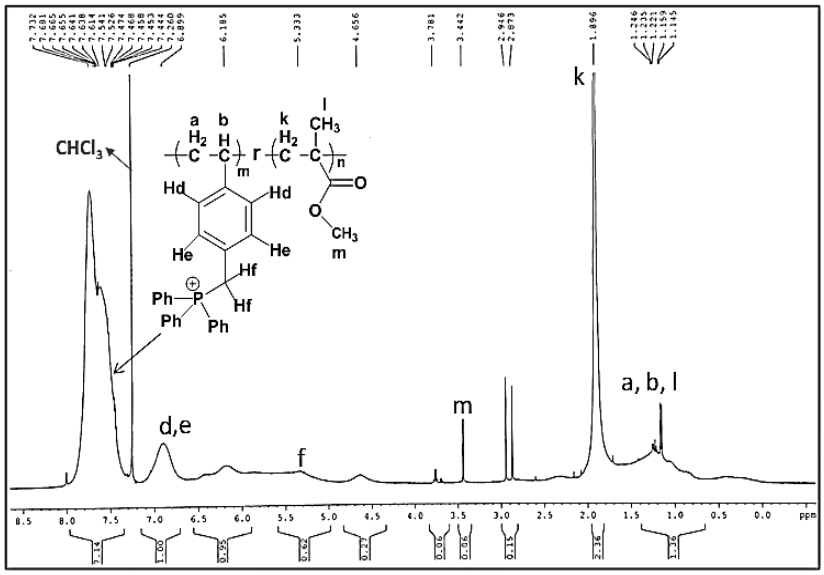

Figure 2. ^{1}H-NMR spectrum of **P2** in $CDCl_3$.

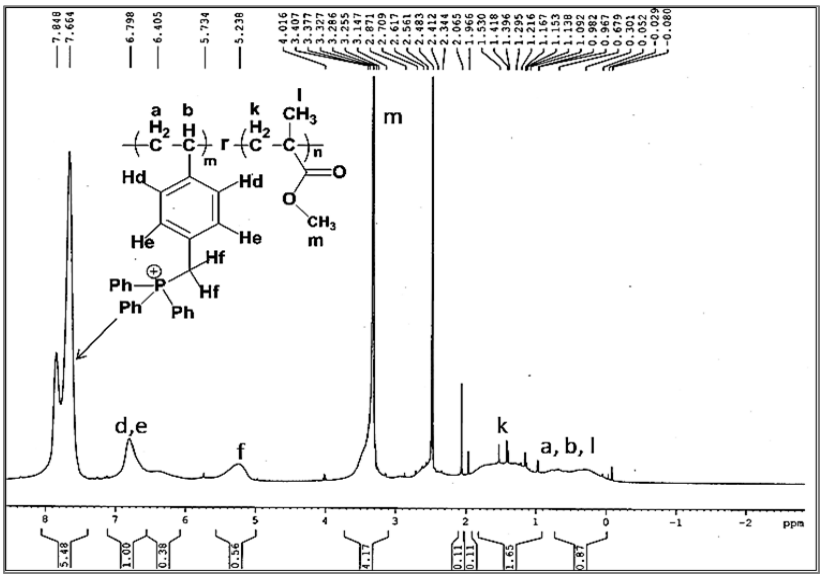

Figure 3. ^{1}H-NMR spectrum of **P3** in $CDCl_3$.

2.3.2.2 Synthesis of P[VBTP][Cl]-ran-PS (P4-P6) copolymers

The **P4-P6** copolymers were also synthesized by RAFT polymerization using monomer mixture: CDP: AIBN mole ratio of 100:1:0.2 with a concentration of monomer mixture of 10 wt. % (w/v) in DMF (Table 1). Note that these three copolymers were synthesized with [VBTP][Cl]/St monomer ratios of 1:4, 1:1, and 4:1. The polymerization of **P4** was carried out in a 25 mL long neck RB flask at 65 ^{o}C for 24h. Afterwards, the polymerization was quenched by cooling the flask quickly in ice-water and precipitated in diethyl ether. **P4** was re-dissolved in methanol and purified by precipitation in diethyl ether and was dried in vacuum oven at 50 °C for overnight (Yield = 68 %).

The **P5** and **P6** copolymers were re-dissolved in water and dialysed against DD water for 2 days using a membrane of molecular weight cut-off of 3000 g mole^{-1}. Finally, the purified **P5** and **P6** were collected by freeze drying and drying in vacuum oven at 50 °C for overnight (Yield ≈70%). The final compositions of P[VBTP][Cl]-*ran*-PS copolymers were determined from integration of the

appropriate signals of the respective ^{1}H-NMR spectra of **P4** (Figure 4), **P5** (Figure 5) and **P6** (Figure 6).

^{1}H-NMR analysis of **P4** (500 MHz, DMSO-d_6, δ ppm)(Figure 4): 1.53-0.82 (-CH_2 and -CH protons of polymer backbone, position 'a', 'b', 'h' and 'i'); 5.1 (benzylic protons, position 'f'); 7.0 (phenyl ring protons, position 'd'); 6.17 (phenyl ring protons, position 'e'); 7.63-7.87 (phenyl ring protons, position 'g' and 'j').

^{1}H-NMR analysis of **P5**(500 MHz, DMSO-d_6, δ ppm)(Figure 5): 1. 4-0.80 (-CH_2 and -CH protons of polymer backbone, position 'a', 'b', 'h' and 'i'); 5.26 (benzylic protons, position 'f'); 6.82 (phenyl ring protons, position 'd'); 6.08 (phenyl ring protons, position 'e'); 7.45-7.69 (phenyl ring protons, position 'g' and 'j').

^{1}H-NMR analysis of **P6** (500 MHz, DMSO-d_6, δ ppm)(Figure 6): 1.50-0.80 (-CH_2 and -CH protons of polymer backbone, position 'a', 'b', 'h' and 'i'); 5.14 (benzylic protons, position 'f'); 6.5-7.2(phenyl ring protons, position 'd';phenyl ring protons, position 'e'); 7.43-7.80 (phenyl ring protons, position 'g' and 'j').

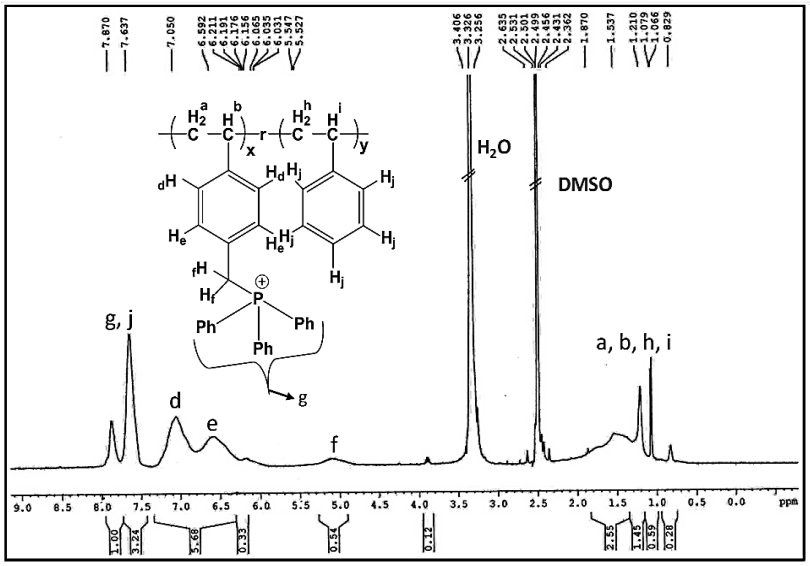

Figure 4. ^{1}H-NMR spectrum of **P4** in DMSO-d_6.

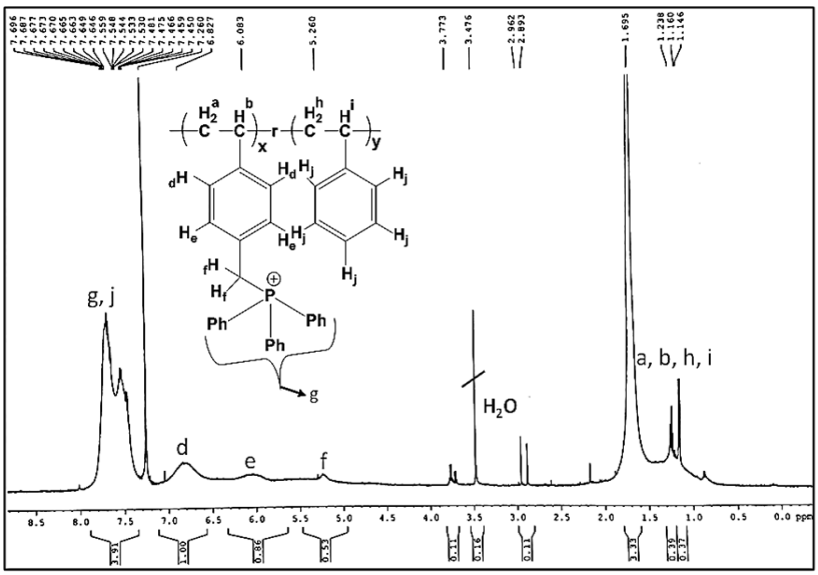

Figure 5. ^{1}H-NMR spectrum of **P5** in DMSO-d_6.

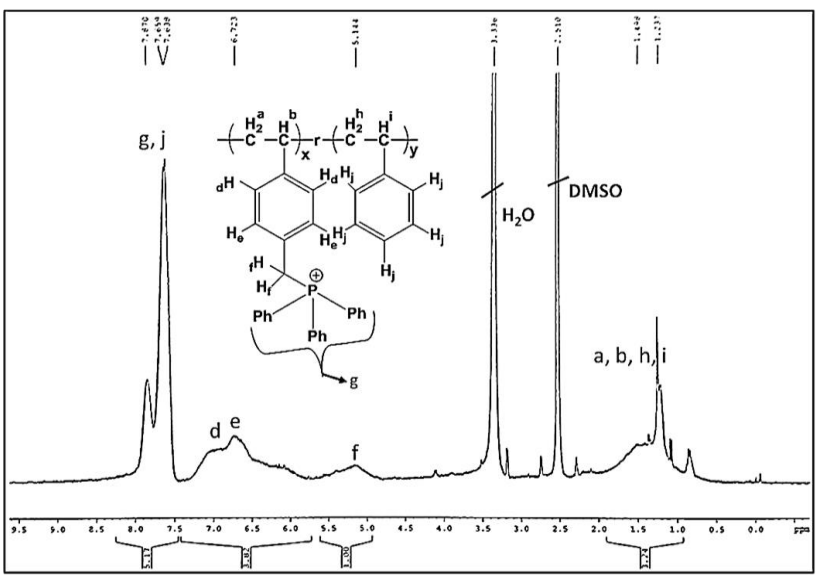

Figure 6. ^{1}H-NMR spectrum of **P6** in DMSO-d_6.

Table 1. Polymerization conditions and molecular characterization data of different copolymers.

Copolymer sample	*$[M_1:M_2]_o$:$[CDP]_o$:$[AIBN]_o$*	*% Yield*	*M_n (SEC) (kDa)*	*Đ (SEC)*	*IC[a] (wt. %)*
P[VBTP][Cl]$_{10}$-*ran*-PMMA$_{90}$ **(P1)**	[10:90]:1:0.2	75	12.01	1.40	10.0
P[VBTP][Cl]$_{18}$-*ran*-PMMA$_{82}$ **(P2)**	[50:50]:1:0.2	79	6.35	1.20	18.0
P[VBTP][Cl]$_{96}$-*ran*-PMMA$_{4}$ **(P3)**	[80:20]:1:0.2	74	6.20	1.20	96.0
P[VBTP][Cl]$_{22}$-*ran*-PS$_{78}$ **(P4)**	[20:80]:1:0.2	68	6.13	1.24	22.0
P[VBTP][Cl]$_{64.4}$-*ran*-PS$_{35.6}$ **(P5)**	[50:50]:1:0.2	70	9.18	1.20	64.4
P[VBTP][Cl]$_{90.3}$-*ran*-PS$_{9.7}$ **(P6)**	[80:20]:1:0.2	70	18.17	1.30	90.3
P[VBTP][Cl]$_{10.5}$-*ran*-PHEMA$_{89.5}$ **(P7)**	[10:90]:1:0.2	72	14.8	1.39	10.5
P[VBTP][Cl]$_{20}$-*ran*-PHEMA$_{80}$ **(P8)**	[20:80]:1:0.2	75	25.44	1.39	20.0
P[VBTP][Cl]$_{28.6}$-*ran*-PHEMA$_{71.4}$ **(P9)**	[50:50]:1:0.2	78	6.35	1.24	28.6
P[VBTP][Cl]$_{1.1}$-*ran*-PNIPAM$_{98.9}$ **(P10)**	[2:98]:1:0.2	65	11.42	1.28	1.13
P[VBTP][Cl]$_{2}$-*ran*-PNIPAM$_{98}$ **(P11)**	[5:95]:1:0.2	71	10.89	1.23	2.5
P[VBTP][Cl]$_{19.3}$-*ran*-PNIPAM$_{80.7}$ **(P12)**	[10:90]:1:0.2	69	5.12	1.20	19.3
P[VBTP][Cl]$_{34.5}$-*ran*-PNIPAM $_{66}$ **(P13)**	[20:80]:1:0.2	68	6.82	1.30	34.5

Reaction condition: Time = 24 h; Temperature = 65 ^{o}C; Solvent = DMF.

M_1= [VBTP][Cl];M_2= HEMA/MMA/Styrene/NIPAM; Monomer concentration = 10 wt. %(w/v); *IC*=Ionic content.

[a]Obtained from ^{1}H-NMR spectral analysis; The sample code represented actual copolymer compositions.

2.3.2.3 Synthesis of P[VBTP][Cl]-ran-PHEMA (P7-P9) copolymers

The **P7** copolymer was synthesized by a typical RAFT polymerization involving HEMA (1.08 g; 8.3 mmol) and [VBTP][Cl] (0.350 g; 0.922 mmol) in the presence of CDP (0.037 g; 0.0922 mmol) and AIBN (0.0302 mg; 0.018 mmol) in 14 mL dry DMF. The mixture was degassed and polymerized at 65 ^{o}C for 24h following the same procedure as described above. The **P7** was precipitated in acetone followed by dissolving the copolymer in water to remove unreacted [VBTP][Cl]

through dialysis against water for 2 days using a membrane of a molecular weight cut-off of 3000 g $mole^{-1}$. Finally, the purified **P7** was collected by freeze drying and also drying in vacuum oven at 50 °C for overnight (Yield ≈72 %). **P8** and **P9** of varying compositions were also synthesized under same reaction conditions with varying molar feed ratios of monomers as described in Table 1. The compositions of the copolymers (**P7-P9)** were determined from ^{1}H-NMR spectra which are given in Figures -7 to 9.

^{1}H-NMR analysis of **P7** (500 MHz, DMSO-d_6, δ ppm)(Figure 7): 0.94-0.77 (-CH_2 and -CH of polymer backbone, position 'a', 'b', 'h'); 1.79 (-CH_2 protons of polymer backbone, position 'g'); 4.84 (benzylic protons, position 'f'); 6.7 (phenyl ring protons, position 'd', 'e'); 7.65-7.91 (phenyl ring protons of TPP unit); 3.89 (-CH_2 protons, position 'i'); 3.58 (-CH_2 protons, position 'j').

^{1}H-NMR analysis of **P8** (500 MHz, DMSO-d_6, δ ppm)(Figure 8): 0.94-0.77 (-CH_2 and -CH of polymer backbone, position 'a', 'b', 'h'); 1.79 (-CH_2 protons of polymer backbone, position 'g'); 4.87 (benzylic protons, position 'f'); 6.8 (phenyl ring protons, position 'd', 'e'); 7.67-7.94 (phenyl ring protons of TPP unit); 3.89 (-CH_2 protons, position 'i'); 3.58 (-CH_2 protons, position 'j').

^{1}H-NMR analysis of **P9** (500 MHz, DMSO-d_6, δ ppm)(Figure 9): 0.90-0.60 (-CH_2 and -CH of polymer backbone, position 'a', 'b', 'h'); 1.40 (-CH_2 protons of polymer backbone, position 'g'); 5.2 (benzylic protons, position 'f'); 6.77 (phenyl ring protons, position 'd', 'e'); 7.67-7.94 (phenyl ring protons of TPP unit); 3.85(-CH_2 protons, position 'i'); 3.37 (-CH_2 protons, position 'j').

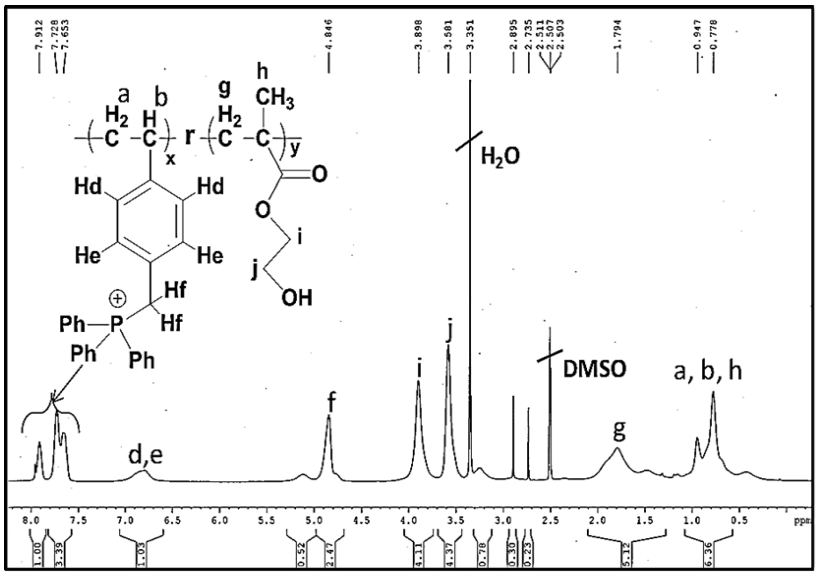

Figure 7. ^{1}H-NMR spectrum of **P7** in DMSO-d_6.

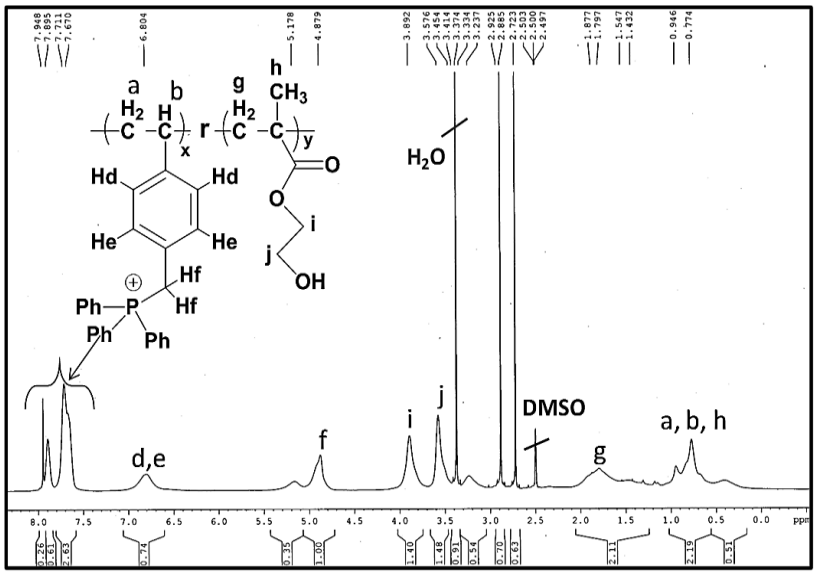

Figure 8. ^{1}H-NMR spectrum of **P8** in DMSO-d_6.

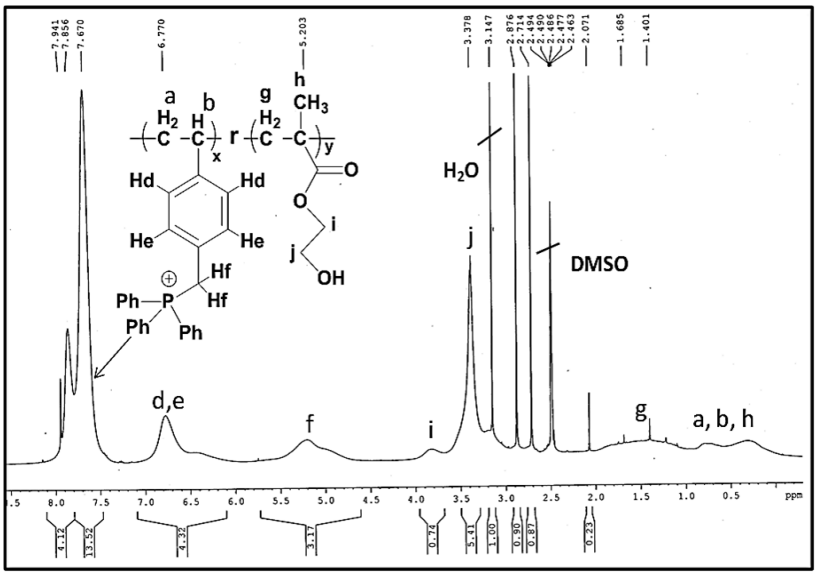

Figure 9. ^{1}H-NMR spectrum of **P9** in DMSO-d_6

2.3.2.4 Synthesis of P[VBTP][Cl]-ran-PNIPAM (P10-P13) copolymers

The RAFT copolymerization of [VBTP][Cl] and NIPAM monomers was also carried out to prepare four random copolymers, **P10-P13** (Table 1) of different compositions using the similar procedure as mentioned above. For **P10,** NIPAM (1.0 g; 8.8370 mmol), [VBTP][Cl] (0.068g; 0.180 mmol), AIBN (2.96mg; 0.018 mmol) and CDP (36.394mg; 0.090 mmol) were taken in a 50 mL long neck RB flask followed by addition of 10.7 mL dry DMF. The polymerization procedure, isolation of copolymer and purification procedures were similar to that used for the P[VBTP][Cl]-*ran*-PS copolymers. The resulting pale yellow coloured copolymer was stored in vacuum desiccator at room temperature (Yield = 65%). Similarly, three other copolymers were also prepared by varying the molar feed ratio of [VBTP][Cl] and NIPAM monomers as described in the Table 1. The compositions of the copolymers were determined from integration of the appropriate signals in the ^{1}H NMR spectra given in Figures 10 to 13.

^{1}H-NMR analysis of **P10** (500 MHz, DMSO-d_6, δ ppm)(Figure 10): 1.45-1.23 (-CH_2 and -CH of polymer backbone, position 'a', 'b', 'h'); 1.92 (-CH proton of polymer backbone, position 'i'); 3.82 (-CH proton, position 'j'); 1.04 (-CH_3 protons, position 'k'); 5.05 (benzylic protons, position 'f'); 7.16 (phenyl ring protons, position 'd'); 6.81 (phenyl ring protons, position 'e'); 7.63-7.88 (phenyl ring protons of TPP unit).

^{1}H-NMR analysis of **P11** (500 MHz, DMSO-d_6, δ ppm)(Figure 11): 1.45-1.23 (-CH_2 and -CH of polymer backbone, position 'a', 'b', 'h'); 1.94 (-CH proton of polymer backbone, position 'i'); 3.82 (-CH proton, position 'j'); 1.02 (-CH_3 protons, position 'k'); 5.03 (benzylic protons, position 'f'); 7.18 (phenyl ring protons, position 'd'); 6.80 (phenyl ring protons, position 'e'); 7.63-7.88 (phenyl ring protons of TPP unit).

^{1}H-NMR analysis of **P12** (500 MHz, DMSO-d_6, δ ppm)(Figure 12) : 1.45-1.23 (-CH_2 and -CH of polymer backbone, position 'a', 'b', 'h'); 1.92 (-CH proton of polymer backbone, position 'i'); 3.82 (-CH proton, position 'j'); 1.03 (-CH_3 protons, position 'k'); 5.05 (benzylic protons, position 'f'); 7.16 (phenyl ring protons, position 'd'); 6.81 (phenyl ring protons, position 'e'); 7.63-7.88 (phenyl ring protons of TPP unit).

^{1}H-NMR analysis of **P13** (500 MHz, DMSO-d_6, δ ppm)(Figure 13): 1.45-1.23 (-CH_2 and -CH of polymer backbone, position 'a', 'b', 'h'); 2.0 (-CH proton of polymer backbone, position 'i'); 3.83 (-CH proton, position 'j'); 1.03 (-CH_3 protons, position 'k'); 5.08 (benzylic protons, position 'f'); 6.82 (phenyl ring protons, position 'd';phenyl ring protons, position 'e'); 7.67-7.88 (phenyl ring protons of TPP unit).

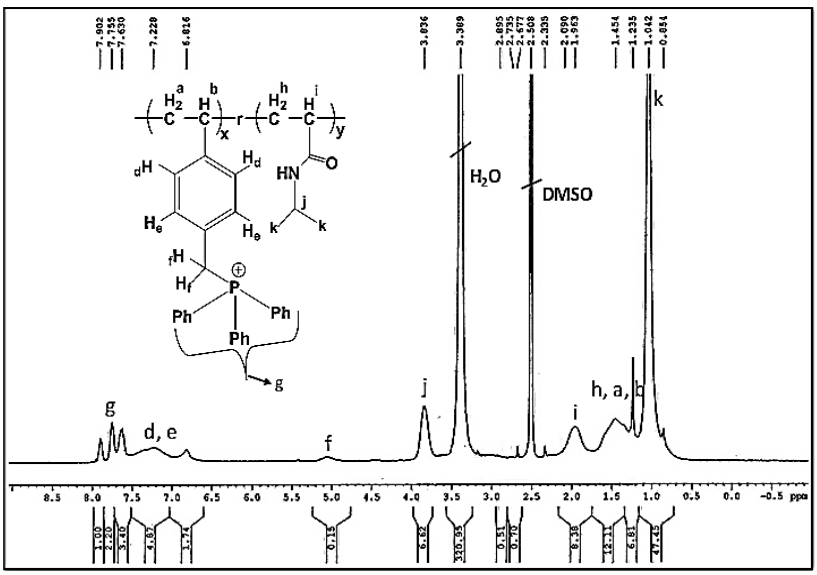

Figure 10. ^{1}H-NMR spectrum of **P10** in DMSO-d_6

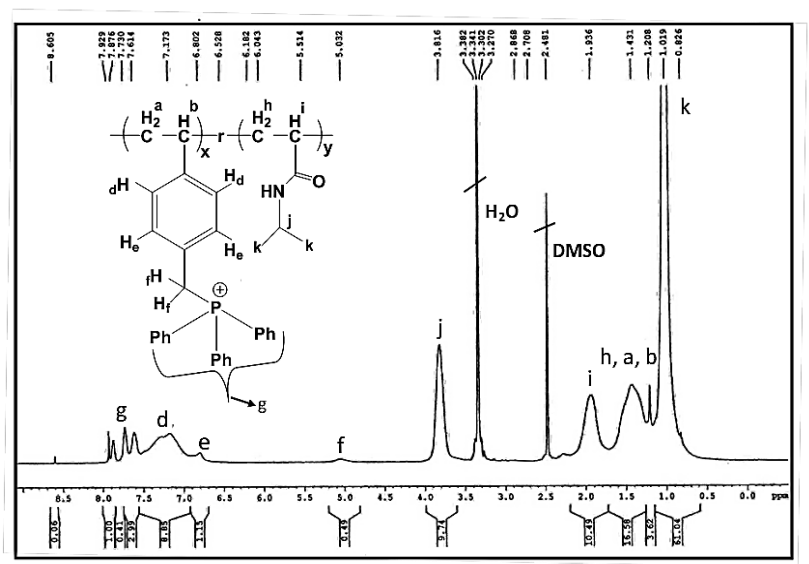

Figure 11. ^{1}H-NMR spectrum of **P11** in DMSO-d_6.

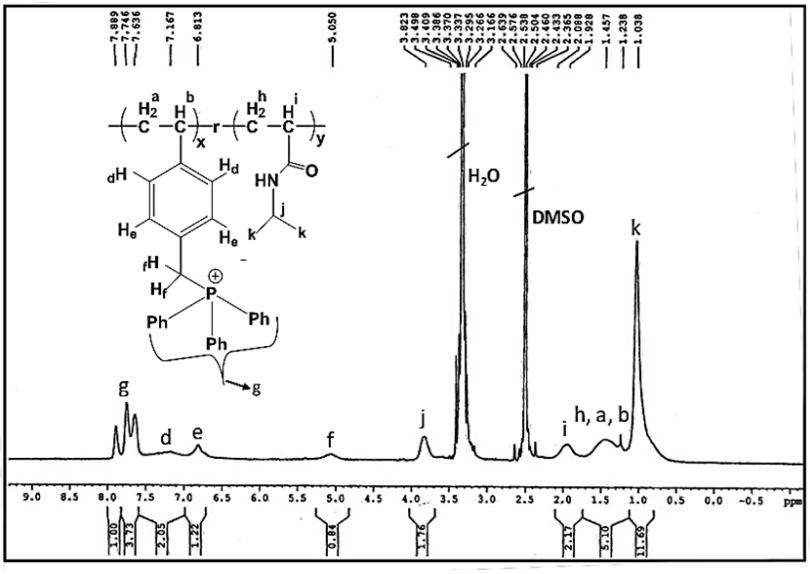

Figure 12. ^{1}H-NMR spectrum of **P12** in DMSO-d_6.

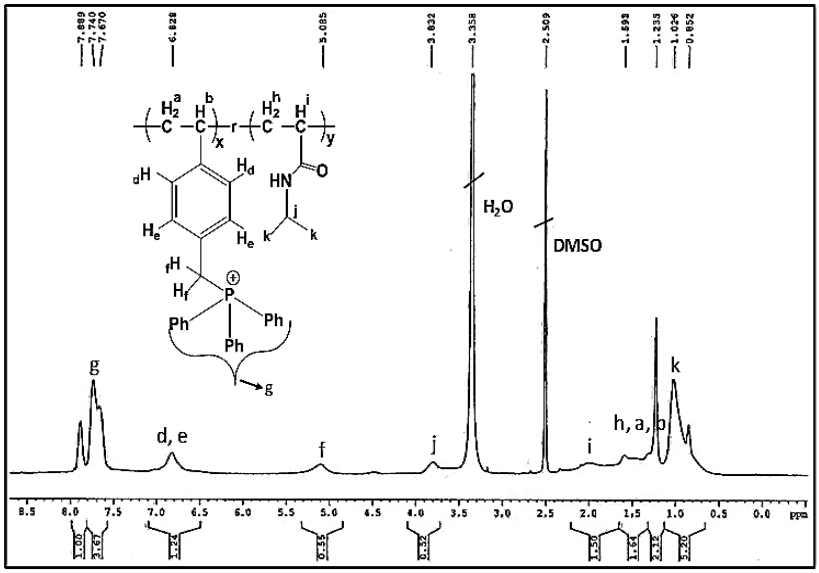

Figure 13. ^{1}H-NMR spectrum of **P13** in DMSO-d_6.

2.3.3 Cloud point measurements

Turbidimetry

Cloud point was measured by turbidimetry using a UV-vis spectrophotometer equipped with a temperature controller in the transmittance mode at a fixed wavelength of λ = 500 nm. For determination of LCST-type (T_{cL}) and UCST-type (T_{cU}) cloud points, solutions of copolymers in the presence different halide anions (e.g., Cl^- and I^-) were taken in a cuvette and were placed in the spectrophotometer. The % transmittances (%T) of these solutions were then measured in the temperature window of 10 to 90 ^oC upon increasing/decreasing the temperature at the rate of 1 °C/min after equilibration for 2 min at each temperature. Cloud point is considered to be the temperature at which the %T of a copolymer solution reached to exactly half of the difference of minimum and maximum transmittance. Note that, T_{cU}s of P[VBTP][Cl]-*ran*-PMMA/P[VBTP][Cl]-*ran*-PS copolymers with high hydrophobic PMMA/PS contents (**P1**, **P2** and **P7**) were measured in their MeOH solutions in the presence of I^- ion.

Dynamic light scattering

For comparison, cloud points of some of the copolymers solutions were also determined by dynamic light scattering (DLS). The change in the hydrodynamic diameter (D_h) of a copolymer in solution was due to coil-to-globule or globule-to-coil transitions for LCST- or UCST-type copolymers during heating or cooling, which was monitored by DLS. The temperature in which there was a sharp transition in hydrodynamic diameter was considered as the cloud point.

2.3.4 Characterization

^{1}H-NMR Study. A Bruker DPX 500 MHz spectrometer was used to acquire ^{1}H-NMR spectra of P[VBTP][Cl]-*ran*-PS, P[VBTP][Cl]-*ran*-PHEMA and P[VBTP][Cl]-

ran-PNIPAM copolymers in DMSO-d_6. But, the spectra of P[VBTP][Cl]-*ran*-PMMA copolymers were acquired from $CDCl_3$.

Size exclusion chromatography (SEC). The number average molecular weights (M_ns) and dispersities (*Đ*s) of the copolymers were determined by SEC technique using a Waters 1515 isocratic HPLC pump connected to three Waters Styragel HR1 (M_n = 100-5000), HR3 (M_n = 500-30,000) and HR4 (M_n = 5000-6,00,000) columns at 45 ^oC and a Waters 2414 RI detector at 35 ^oC. DMF with 50 mM LiBr was used as the eluent with a flow rate of 1 mL min^{-1}. The columns were calibrated against PMMA standards.

Field emission scanning electron microscopy (FESEM). The stable aqueous dispersions of **P6**, **P12**, **P9** and **P13** aggregates in the presence of Cl^- ion were drop casted on small pieces of glass and allowed to dry overnight in air. The piece of glass with the sample was then mounted on a metal stub, sputter coated with platinum and placed under a ZEISS JSM-6700F electron microscope operating at an accelerating voltage of 5 kV for imaging. The FESEM image of **P2** aggregates with I^- ion was acquired from MeOH suspension.

Transmission electron microscopy (TEM). The aqueous suspensions of **P6, P9** and **P12** aggregates with Cl^- ion were casted on carbon-coated copper grids and allowed to dry in air at room temperature for 24h. The grids were then observed by a JEOL JEM-2010 transmission electron microscope of accelerating voltage of 200 kV. The TEM specimen for **P2** was casted from MeOH in the presence of I^- ion.

Dynamic light scattering (DLS). Zetasizer NANO ZS 90, Malvern (Model ZEN 3690, Version 7.03) was used to measure D_h by DLS. Prior to the DLS experiment, the aqueous copolymer and the NaCl solutions were separately filtered through a membrane of 0.22 µm pore size to get rid of any large impurity particles. Afterwards, Cl^- ion was added to the copolymer solution to form turbid

suspension. The MeOH solution of copolymer and NaI were also filtered through a membrane of ~0.22 μm pore size prior to the measurement. Note that the turbid suspension has a tendency to get precipitated if the solution is kept for a long time. However, to avoid the possibility of precipitation in the bottom of the sample vial, the DLS experiment was performed just after the addition of anion to the PIL copolymer solution. The change of D_h of copolymer aggregates was then monitored with temperature at a rate of 4 °C min^{-1} followed by an equilibration for 2 mins at each temperature.

Turbidity measurements. The turbidity of aqueous/methanolic solutions/suspensions of copolymers were measured by UV-vis spectroscopy using a Hewlett Packard 8453 diode array UV-vis spectrometer (Agilent Technologies) equipped with a Peltier temperature controller.

2.4 RESULTS AND DISCUSSION

2.4.1 Synthesis and characterization of PIL copolymers

In Chapter 1, it has been already mentioned that P[VBTP][Cl] homopolymer shows UCST-type phase behaviour in the presence of halide ions in water. The ion-bridging Coulomb interactions between phosphonium cation of this PIL and externally added anion is the origin for existence of such UCST phenomenon.[32] The question is whether the insertion of this ionic [VBTP][Cl] monomer via random copolymerization with conventional hydrophobic MMA/St or hydrophilic HEMA/NIPAM monomers can introduce UCST properties to the final PIL copolymers. Thus, to have an answer, four different sets of copolymers (P[VBTP][Cl]-*ran*-PMMA, P[VBTP][Cl]-*ran*-PS, P[VBTP][Cl]-*ran*-PHEMA and P[VBTP][Cl]-*ran*-PNIPAM) of varying compositions were synthesized by RAFT polymerization (Scheme 1). Being hydrophobic, neat PMMA and PS are insoluble in both water and MeOH at ambient temperature. But, neat PMMA has been

reported to be soluble in ethanol/water mixtures.[60] Also, a UCST of T_{cU}~87 °C was also reported for PMMA in pure methanol/ethanol.[61-62] It is expected that the incorporation of ionic PIL segments leads to a significant hydrophilization of hydrophobic PMMA/PS that results in enhanced solubility in water/MeOH at ambient temperature. This modification also increases the potential applicability of these PIL copolymers in industry as well as in biology. On the other hand, the hydrophilic PHEMA with degree of polymerization (DP) < 20, is reported to be completely soluble in water without any LCST, while those with DP in the range of 20-45 exhibits LCST-type phase behaviour.[63] It is needless to mention that PNIPAM is a widely studied LCST polymer with a T_{cL} near to 32 °C.[2] Therefore, it is expected that copolymers of P[VBTP][Cl] with PHEMA and/or PNIPAM in solution would display interesting phase behaviours with UCST-type or LCST-type or coexistence of both types of transitions.

With these expectations, the as-synthesised [VBTP][Cl] monomer was employed for the preparation of a series of random copolymers with commercially available monomers such as MMA , St, HEMA and NIPAM by RAFT polymerization technique using AIBN as the radical initiator and CDP as chain transfer agent. Table 1 shows the list of random RAFT copolymers of different compositions that were synthesized by adjusting the molar feed ratios of the comonomers. The absence of ^{1}H-NMR signals corresponding to monomeric vinyl protons at δ 6.5, 5.6 and 5.2 ppm along with the appearance of signals corresponding to phenyl ring protons of VBC ('d' and 'e' near δ 6.8 ppm), three aromatic ring protons of TPP moiety of P[VBTP][Cl] segment (δ 7.62-7.73 ppm) and methyl protons ('m') of PMMA segment (δ 3.5 ppm) along with other signals confirmed the successful synthesis of P[VBTP]-*ran*-PMMA copolymer (**P1**) (Figure 1). The spectra of **P2** and **P3** (Figures 2 to 3) were almost identical to **P1.** The appearance of characteristic signals at δ 5.1 ppm for benzylic protons 'f' and

δ 7.63-7.87 ppm for phenyl ring protons ('g' and 'j') of both TPP and styrene moieties (δ 6.8 ppm) unambiguously confirmed the presence of P[VBTP][Cl] and PS segments in **P4**-**P6** (Figure 4 to 6). ^{1}H-NMR spectra of P[VBTP][Cl]-*ran*-PHEMA copolymers (**P7-P9**) (Figures 7 to 9) exhibited similar characteristic signals as of **P1**. Four phenyl ring protons of VBC ('d' and 'e') (δ 6.8 ppm) and three aromatic ring protons of TPP moiety of P[VBTP][Cl] segment (δ 7.65-7.73 ppm) along with signals at δ 3.89 and 3.58 ppm for methylene protons 'i' and 'j' respectively of HEMA unit confirmed the existence of both PHEMA and P[VBTP][Cl] segments in P[VBTP][Cl]-*ran*-PHEMA copolymer (**P7**) (Figure 7). Finally, in the cases of P[VBTP][Cl]-*ran*-PNIPAM (**P10-P13**) samples, the spectra showed signals of a secondary proton 'j' and six protons 'k' of two methyl groups of PNIPAM segments of isopropyl moiety at δ 3.82 and 1.03 ppm respectively in addition to the signals for P[VBTP][Cl] segments (Figures 10 to 13). The actual compositions, i.e., ionic P[VBTP][Cl] content (IC) of all the copolymers were then estimated from the ratios of peak area integrations of corresponding four phenyl ring protons ('d' and 'e') of [VBTP][Cl] at δ 6.8 ppm and the characteristics signals for PMMA, PHEMA, PS and PNIPAM segments (Figures 1 to 13) (Table 1).

FTIR spectra (Figure 14) of two representative samples P[VBTP][Cl]-*ran*-PMMA (**P2**) and P[VBTP][Cl]-*ran*-PHEMA (**P8**) revealed bands at 1659, 1510, and 1467 cm^{-1} (for C=C stretching of phenyl group of [VBTP][Cl]), 1720 cm^{-1} (for >C=O stretching of the ester groups of HEMA and MMA units), 1437cm^{-1} (for deformation of P-CH_2-Ph of $[VBTP]^+$), 1106 cm^{-1} (for three P-Ph stretching vibration) and 689 cm^{-1} (for typical benzene ring out of plane bending) further revealed the presence of P[VBTP][Cl] and PMMA segments in **P2** and P[VBTP][Cl] and PHEMA segments in **P8** respectively. Further, the spectra (Figure 14) of **P6** and **P11** also showed the similar characteristic bands of P[VBTP][Cl] segments along with bands at 1622 and 1508 cm^{-1} (for aromatic C=C stretching), 687 cm^{-1}

(for the typical benzene ring out of plane bending) for styrene moieties, 1547 cm^{-1} (for N–H bending of NIPAM) and 1650 cm^{-1} (C=O stretching of amide moiety) indicated the presence of P[VBTP][Cl]/PS or P[VBTP][Cl]/PNIPAM segments respectively (Table 1).

It is known that the molecular weight measurement of ionic polymers by SEC technique is little bit difficult because of their tendency to form aggregates due to the interactions between polymer and column materials. However, in this case, to avoid aggregation, DMF containing 50 mM LiBr was found to be the suitable eluent to run SEC for M_ns and dispersities (*Đs*) (Table 1). All the SEC traces (Figure 15) of **P1-P13** samples were unimodal in nature with calculated *Đ*s ranging from 1.2 to 1.4 (Table 1), indicating somewhat controlled nature of the RAFT polymerization in these cases. The obtained M_ns of copolymers were in the ranges from 5.12 to 25.44 kDa (Table 1).

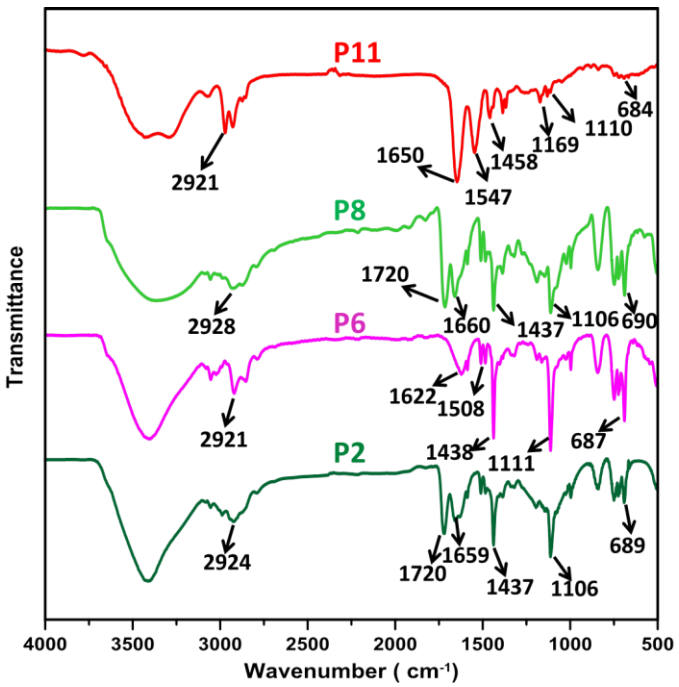

Figure 14. FTIR spectra of P[VBTP][Cl]-*ran*-PMMA (**P2**), P[VBTP][Cl]-*ran*-PS (**P6**) **,** P[VBTP][Cl]-*ran*-PHEMA (**P8**) and P[VBTP][Cl]-*ran*-PNIPAM (**P11**) copolymer.

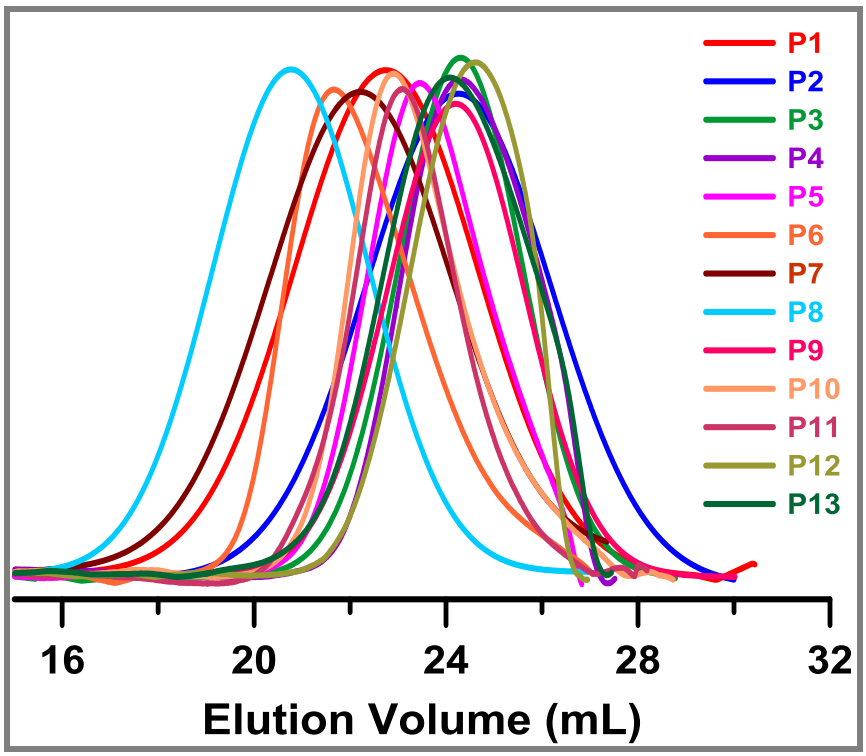

Figure 15. SEC traces of **P1-P13** copolymers.

2.4.2 Thermoresponsiveness of P[VBTP][Cl]-*ran*-PMMA copolymers in MeOH/water

It is known that PMMA homopolymers are insoluble in both water and MeOH at ambient temperature. Although, as mentioned above, it showed an UCST with T_{cU} ~ 87 °C in neat methanol/ethanol.[61-62] However, the random addition of ionic P[VBTP][Cl] segment with hydrophobic PMMA segment resulted copolymers (**P1-P3**) with substantial change in their solubility and the thermoresponsive behaviours. It was observed that the presence of low content of P[VBTP][Cl] segment (IC =10 and 18 wt. %, Table1) made **P1** and **P2** soluble in MeOH, but not in water. However, as expected, **P3** with IC = 96 wt. % (Table 1) became soluble in water. It should be noted that **P1-P3** did not show any UCST

behaviour either in methanol or in water, though they contend PMMA segments. In the cases of **P1** and **P2**, the NaI was added at a very low concentration to the 1 wt.% (w/v) transparent methanolic solution of the copolymers. Initially, a weakly interacted PIL aggregates were formed, but they got solubilized because of higher hydration energy. With the increase of concentration of iodide ion, the stable insoluble globular aggregates were formed through strong ionic-bridging Coulomb interactions (Scheme 2) among cationic PIL segments of copolymer resulting in the formation of stable cloudy/turbid suspension. It was observed the addition of I^- ion with minimum concentrations of 80 and 100 mM to the transparent 1 wt.% MeOH solutions of **P1** and **P2** respectively triggered a sharp jump in the transmittance due to the transformation of the transparent solution to cloudy suspension (~ 0% transmittance) (Figure 16). The inset photographs also clearly showed such phase transition. Note that the increase of ionic content in the copolymer required higher concentration of I^- ion to bring such turbidity. Such turbidity is due to the generation of anion (I^-)-induced copolymer micro/nanogel aggregates. The details of which will be explained in detail later in this section. DLS data also revealed the formation of **P2** aggregates with D_h of 2730 nm in the presence of 100 mM I^- (Figure 17A).It was further revealed that formation of mostly spherical aggregates of two distinctly different size distributions of average diameters of 330 and 630 nm as well as 100 and 970 nm as obtained from FESEM (Figure 18 A) and TEM (Figure 18E) images respectively occurred for **P2** in the presence of 100 mM I^-.

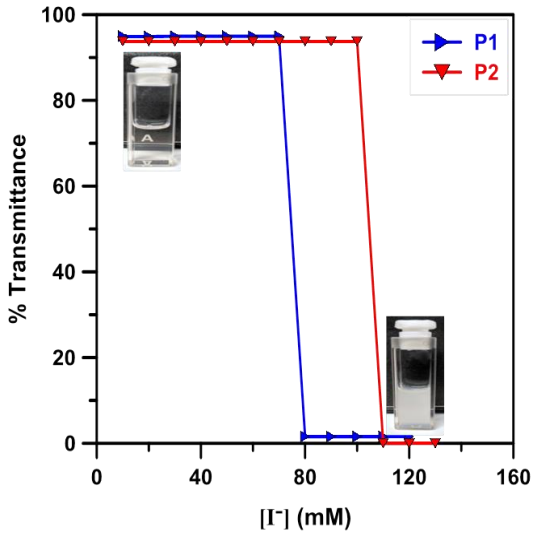

Figure 16. Variation of **%**transmittance against concentration of externally added iodide ion for 1 wt % MeOH solution of **P1** and **P2**.

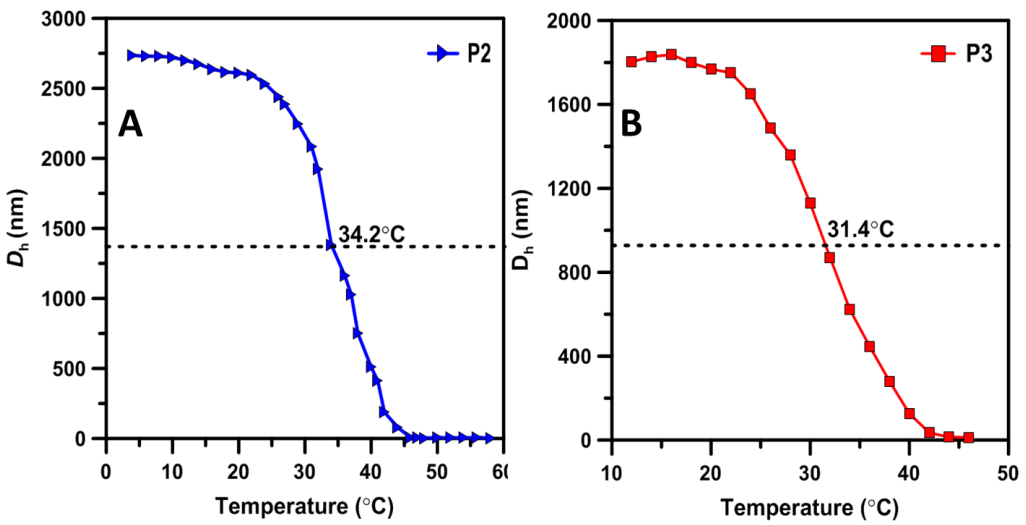

Figure 17. Plot of D_hs of A) **P2** in MeOH (1 wt %) in the presence of 100 mM I^- ion and B) **P3** in H_2O (1 wt %) in the presence of 250 mM Cl^- ion against temperature obtained from DLS.

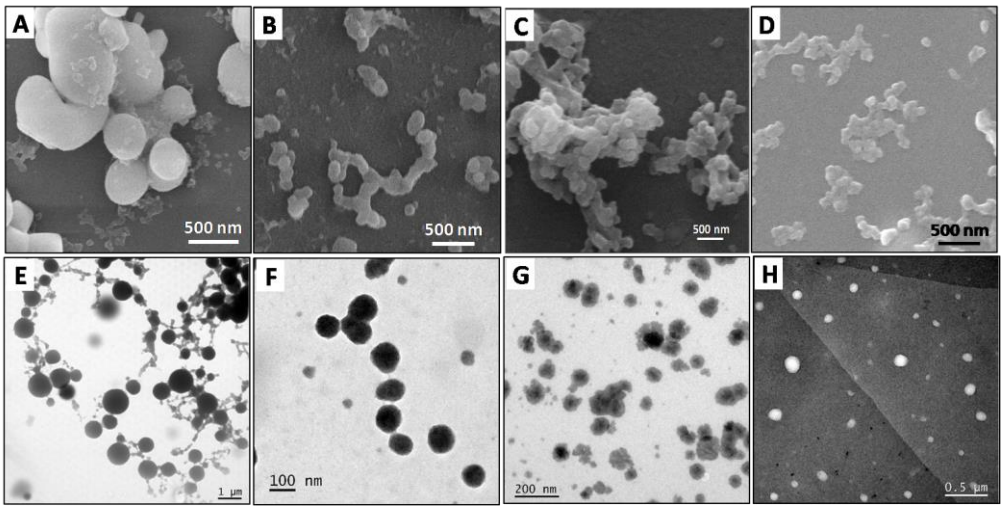

Figure 18. FESEM and TEM images of aggregates of **P2** (1 wt. %) with 100 mM I^- in methanol (A,E), **P6** (1 wt. %) with 375 mM Cl^- in water (B,F), **P9** (1 wt. %) with 75 mM Cl^- in water (C,G) and **P12** (1 wt. %) with 250 mM Cl^- in water (D, H) respectively.

These cloudy suspensions of **P1** and **P2** with I^- ion transformed into transparent and back to cloudy again upon heating above and cooling below the T_{cU} respectively (see photographs in Figure 19). Turbidity heating curve and cooling curve were almost reversible with slight hysteresis for **P1 and P2**(Figure 20A). The recorded T_{cU}s of **P1** and **P2** in methanol from cooling curve were 33.5 and 38.5 °C respectively (Figure 20A). But, these two copolymers did not show UCST-type transition in the presence of Cl^-/Br^- because of their insolubility in MeOH. Moreover, the DLS data of **P2** (Figure 17A) revealed that there was a rapid decrease in the D_h from 2730 to 10 nm as the temperature increased from 4 to 52 °C. T_{cU} obtained from DLS was 34.2 °C (Figure 17A), which agreed well with that (38.5 °C) obtained from turbidity measurement (Figure 20A).

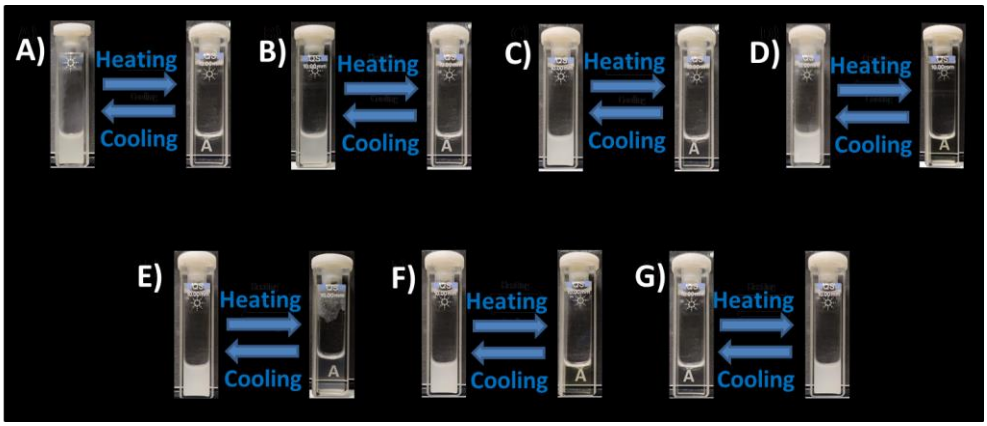

Figure 19. Photographs showing of halide ion-induced and temperature-induced solution phase transitions of copolymers in the presence of halide ions during their UCST-type behaviors: A) 1wt. % MeOH solutions of **P1** in the presence of 80 mM I^-; B) 1wt. % MeOH solution of **P2** in the presence of 100 mM I^- ion; (C) 1 wt. % aqueous solution of **P3** with 250 mM Cl^- ion; D) 1 wt. % MeOH solution of **P4** with 18 mM I^- ion; E) 1 wt. % aqueous solutions **P6** with 375 mM Cl^- ion and F) 1 wt. % aqueous solutions **P9** with 75 mM Cl^- ion. G) Photographs of phase transition behaviour for 1 wt. % aqueous solution of **P12** with 69 mM Cl^- ion during LCST-type behavior.

Furthermore, the UCST-type transition of the methanolic solution of P2, in the presence of I^- ion was found to be repeatable for at least six heating/cooling cycles (Figure 21). The aqueous solution of **P3** also showed similar reversible turbidity curves upon heating/cooling with a T_{cU} = 29.9 °C (cooling) in the presence of 250 mM of Cl^- ion (Figure 20B). The photographs also showed a clear transition of phase from turbid to transparent (Figure 22). DLS data also confirmed the formation of **P3** aggregates with D_h of 1837 nm in the presence of 250 mM Cl^- and T_{cU} was 31.4°C (Figure 17B). Therefore, the presence of UCST-type transition was further established as there is a transformation of two-phase

cloudy suspension to one-phase transparent solution with the increase of temperature.

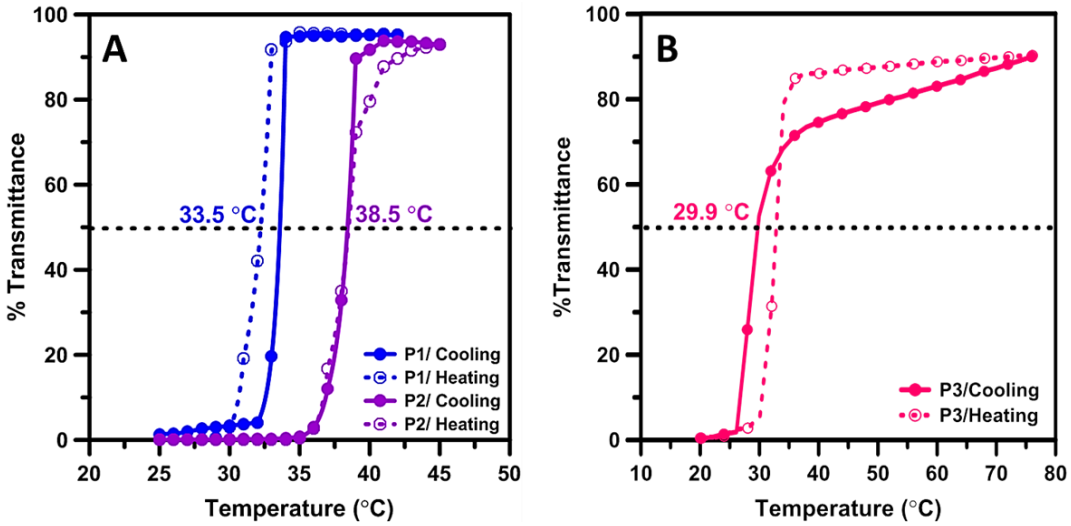

Figure 20. Turbidity [heating (dashed)/cooling (solid)] curves of P[VBTP][Cl]-*ran*-PMMA copolymers: (A) 1wt. % MeOH solutions of **P1** and **P2** in the presence of 80 mM and 100 mM I^- ion respectively and (B) 1 wt.% aqueous solution of **P3** with 250 mM Cl^- ion.

In Chapter 1, it has been explained that the P[VBTP][Cl] homopolymer chains interact through ionic bridging interactions between their positively charged phosphonium cations and excess foreign halide anions to form micro/nanogel aggregates.[32] Similarly, in this case, in spite of the presence of non-ionic PMMA segment, the cationic P[VBTP][Cl] segment of the P[VBTP][Cl]-*ran*-PMMA underwent anion-induced cross-linking of the copolymer chains in the presence of excess halide ions, which eventually forced the copolymer chain to collapse into globular micro-/nano-gel aggregates (Scheme 2). The formation of

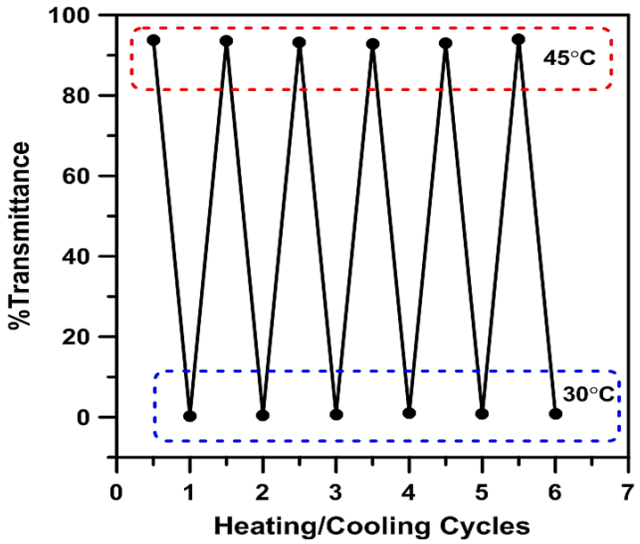

Figure 21. Temperature-dependent %transmittance of methanolic **P2** solution (1 wt. %) in the presence of 100 mM I^- during heating/cooling cycles (each data point was obtained after equilibrating the sample suspension for 2 min).

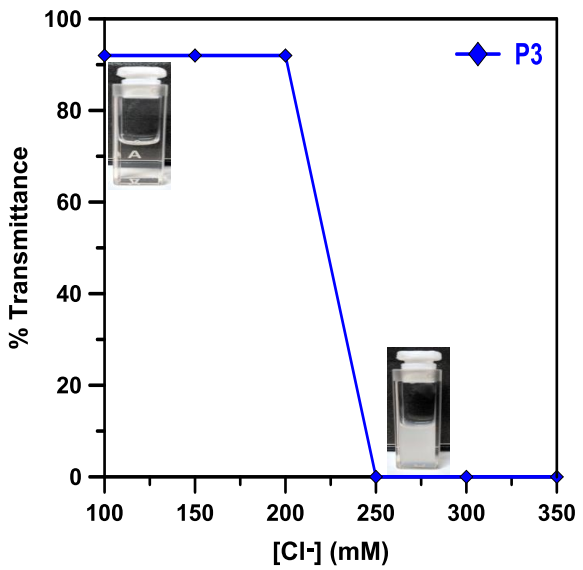

Figure 22. Variation of **%**transmittance against concentration of externally added chloride ion for 1 wt. % aqueous solution of **P3**.

insoluble aggregates resulted in the transformation of the transparent solution to cloudy suspension. These aggregates of copolymers are formed by weak anion-bridging interactions. Thus, heating would provide sufficient energy to

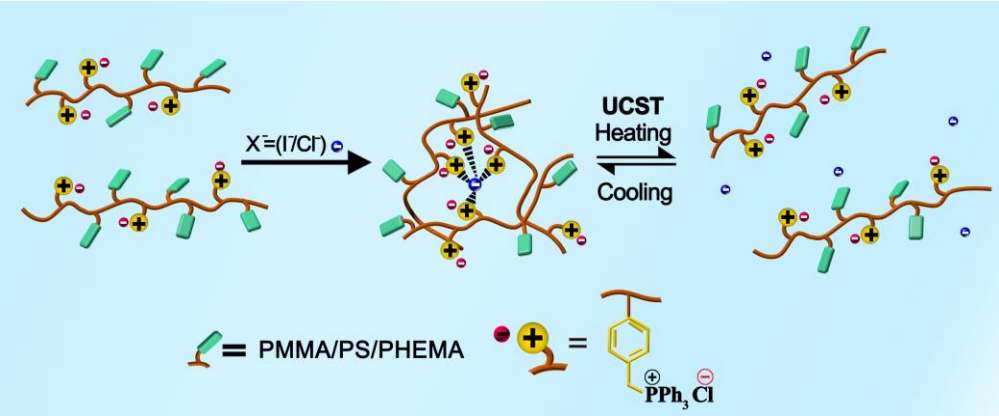

Scheme 2. Schematic representation for the anion-induced aggregation and temperature-induced dissociation of copolymer chains showing UCST-type phase behaviour.

rupture these ionic interactions and convert these globular copolymers aggregates into their coil chain conformation (Scheme 2), exhibiting a clear USCT-type behaviour as shown in Figures 16-22.

2.4.3 Thermoresponsiveness of P[VBTP][Cl]-*ran*-PS copolymers

Similar to the above-mentioned cases of **P1**-**P3**, the incorporation of 22 wt. % of P[VBTP][Cl] in **P4** (Table 1) also made it soluble in MeOH, in spite of insolubility of PS in methanol and in water. In this case, however, a minimum of 18 mM of I^- was required for transformation of the transparent methanol solution into turbid suspension containing insoluble micro-/nano-gel aggregates of **P4** (Figure 23).

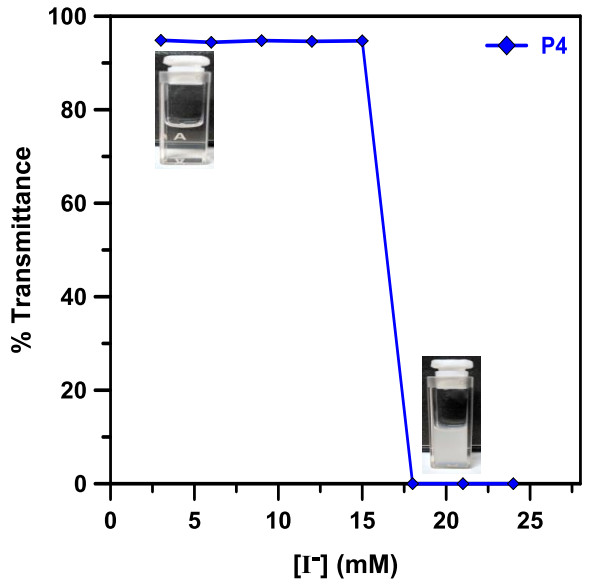

Figure 23. Variation of **%**transmittance against concentration of externally added iodide ion for 1 wt. % MeOH solution of **P4**.

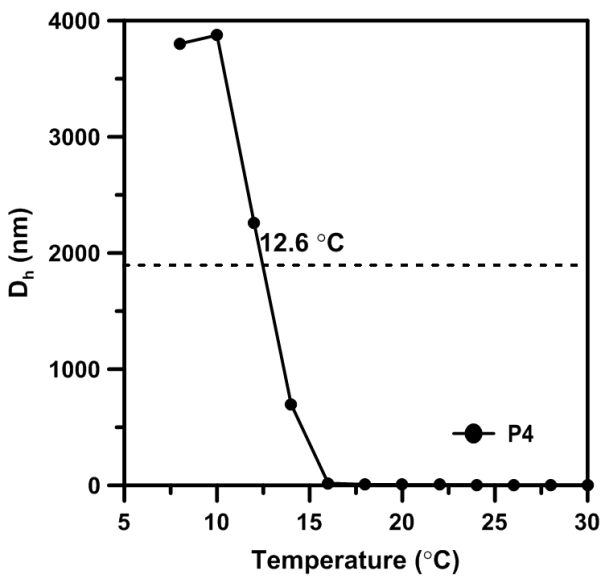

Figure 24. Plot of D_h of **P4** in MeOH (1 wt. %) in the presence of 18 mM I^- ion obtained from DLS.

The aggregate formation was evidenced from DLS curve showing formation of particles of D_h =3782 nm in the presence of 18 mM I^- ion (Figure 24). The

copolymer suspension upon heating above T_{cU} (18.3 °C) converted into transparent solution with very little hysteresis (Figure 25A). The T_{cU} measured in cooling condition was 17 °C (Figure 25A). Furthermore, **P5** and **P6** with IC of 64.4 and 90.3 wt. % respectively were soluble in water and formed aggregates in the presence of $[Cl^-]_{min}$ of 62.5 and 375 mM respectively (Figure 26). Note that the critical ion concentration to obtain turbidity increased with increasing IC (Table 1) in the copolymers. These solutions of **P5** and **P6** also exhibited UCST-type transitions with T_{cU}s of 40.4 and 47.5°C (cooling cycle) as well as 43.74 and 48.77°C (heating cycles) respectively (Figure 25B). The photographs also showed phase transformation due to UCST-type behaviour (Figure 19). Turbidity curves of **P4-P6** in the presence of different halide ions of varying concentrations in methanol and in water are given in Figure 27. T_{cU}s of **P4**, **P5** and **P6** solutions obtained from these turbidity curves revealed their increase with the increase of halide ion concentration (Figures 28), which is very much similar with the earlier reported observation on aqueous solution of P[VBTP][Cl] with halide ions.[32]

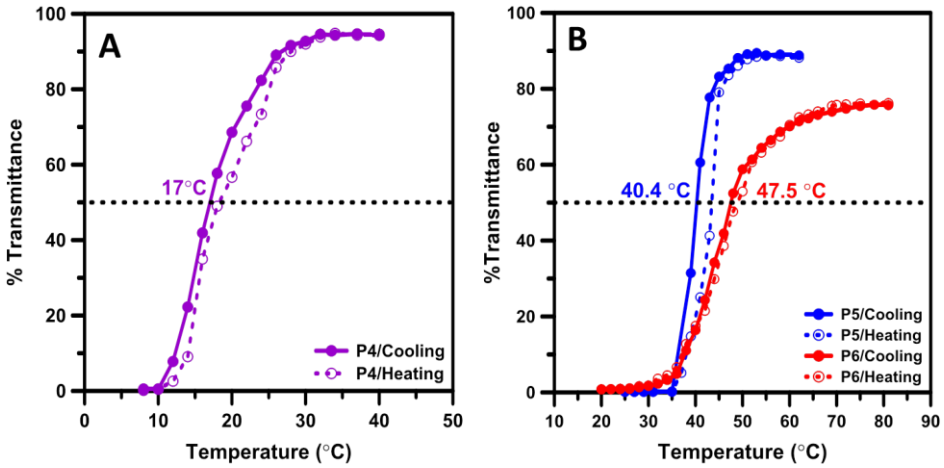

Figure 25. Turbidity [heating (dashed)/cooling (solid)] curves of P[VBTP][Cl]-*ran*-PS copolymers: (A) 1 wt.% MeOH solution of **P4** with 18mM I^- ion and (B) 1 wt. % aqueous solutions of **P5** and **P6** in the presence of 62.5 and 375 mM Cl^- ion respectively.

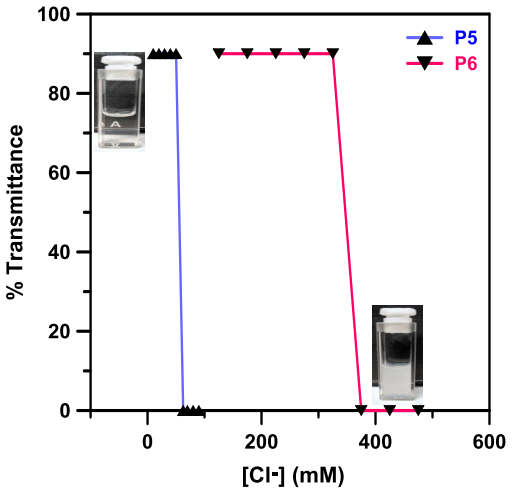

Figure 26. Variation of **%**transmittance against concentration of externally added chloride ion for 1 wt. % aqueous solutions of **P5** and **P6**.

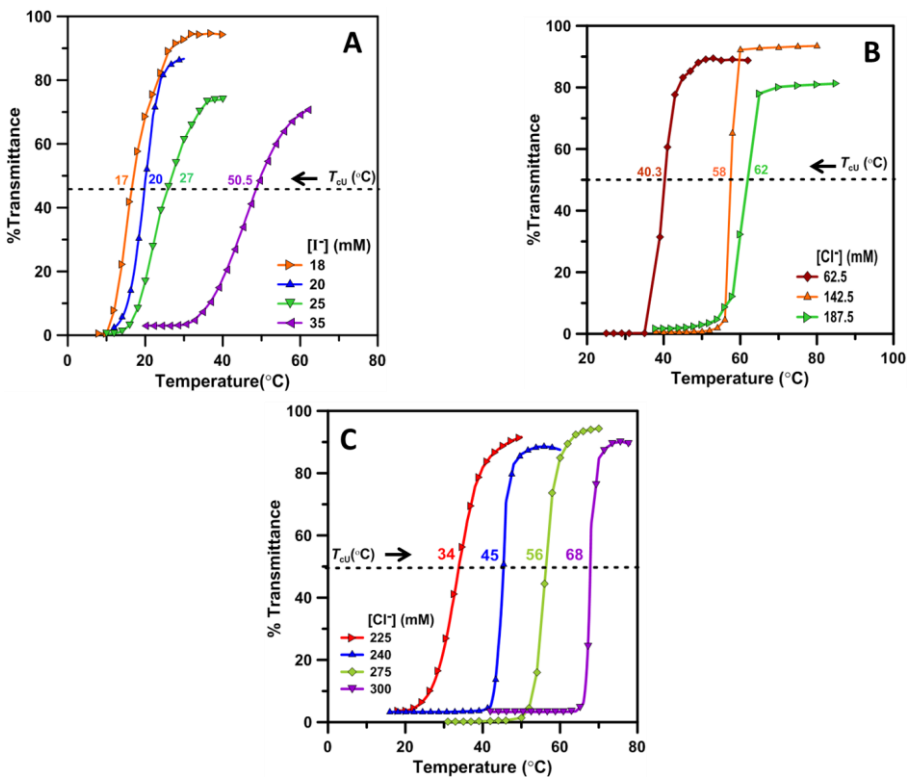

Figure 27. Turbidity cooling curves of (A) 1 wt. % MeOH solution of **P4** at different I^- ion concentrations, (B) 1 wt. % aqueous solution of **P5** at different Cl^- ion concentrations and (C) 0.5 wt. % aqueous solution of **P6** at different Cl^- ion.

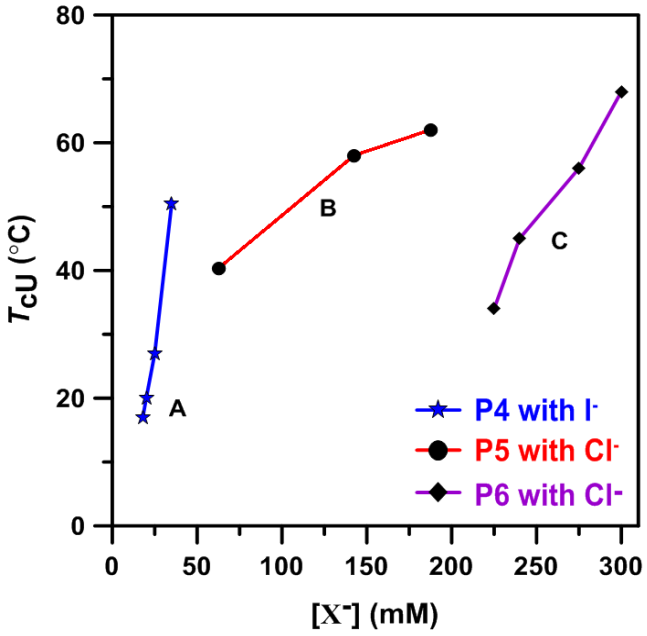

Figure 28. The variation of UCST-type cloud point measured from the turbidity cooling curves of P[VBTP][Cl]-*ran*-PS copolymers against concentrations of halide ions: (A) 1 wt. % MeOH solution of **P4** at varying I^- ion concentrations and (B, C) 1 and 0.5 wt. % aqueous solution of **P5** and **P6** respectively at different Cl^- ion concentrations respectively.

To support the turbidity measurement data, methanol solution of **P4** in the presence of I^- ion was also examined by DLS. The data showed a rapid decrease in the D_h of aggregate from 3782 to 16 nm with increase of temperature with a clear T_{cU} of 12.6 °C (Figure 24), which matched well with that (17°C) obtained from turbidity (Figure 25A). On the other hand T_{cU} obtained from the DLS data of **P6** in water with Cl^- (Figure 29) was 41.4 °C, which also matched well with that (40.4 °C) obtained from turbidity (Figure 25B). It was also observed that the UCST-type transition of P6 was reversible/repeatable for at least six heating/cooling cycles (Figure 30). FESEM (Figure 18B) and TEM (Figure 18F)

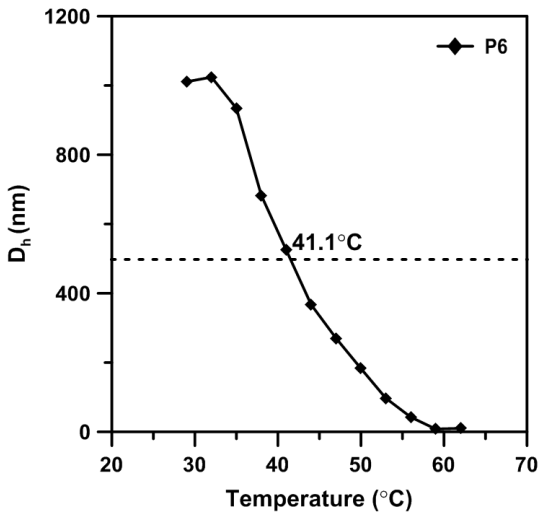

Figure 29. Plot of D_h of **P6** in H_2O (1 wt. %) in the presence of 375 mM of chloride ion against temperature obtained from DLS.

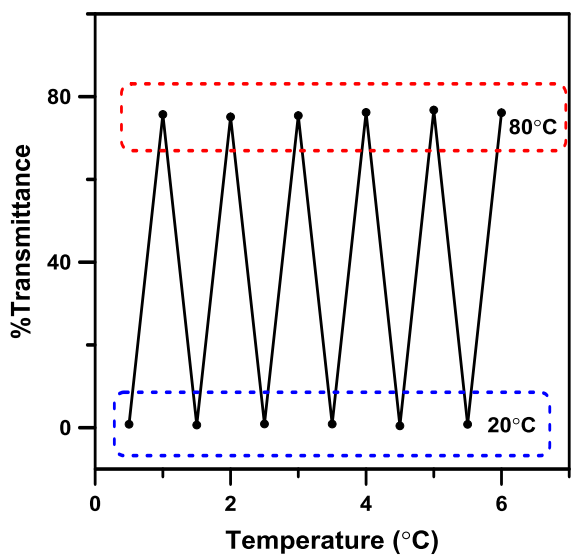

Figure 30. Temperature-dependent % transmittance of aqueous **P6** solution (1 wt. %) in the presence of 375mM Cl^- during heating/cooling cycles (each data point was obtained after equilibrating the sample suspension for 2 min).

images of **P6** further supported the formation of spherical aggregates with average diameters of 187 and 136 nm respectively.

As discussed for P[VBTP][Cl]-*ran*-PMMA (**P1-P3**), a similar explanation can also be applicable for these solution phase behaviours of P[VBTP][Cl]-*ran*-PS(s) (**P4-P6**) in the presence of halide ions (Scheme 2).

2.4.4 Thermoresponsiveness of P[VBTP][Cl]-*ran*-PHEMA copolymers

As per the report, PHEMA homopolymer behaved as thermoresponsive polymer below 0 and above 100 ^{o}C.[3] It is reported that PHEMA with DP < 20 is completely soluble in water without any LCST, while those with DP ≥ 20-45 exhibits LCST-type behaviour.[63] However, Longenecker et al.[20] reported a rather complex phase behaviour of both LCST- and UCST-type transitions for small molecular weight PHEMA (M_n = 4000 g mol^{-1}) and PHEMA copolymers in the presence of anion in water in between 0 to 100^{o}C. In this case, a series of P[VBTP][Cl]-*ran*-PHEMA copolymers (**P7-P9**) (Table 1) of varying compositions were thus prepared to examine their interesting thermoresponsiveness in water. **P7** containing only 10.5 wt.% of ionic P[VBTP][Cl] segment was soluble in water, even though its M_n was as high as 14.8 kDa (Table 1) . The aqueous solutions of **P7-P9** (ICs of 10.5, 20 and 28.6 wt. % respectively; Table 1) showed transparent-to-cloudy transition due to aggregate formation in the presence of Cl^- ion at critical concentrations ($[Cl^-]_{min}$) of 10, 25 and 75 mM respectively (Figure 31). The inset photographs also showed transformation from transparent to turbid phases. FESEM (Figure 18C) and TEM (Figure 18G) images of **P9** further supported the formation of spherical aggregates of D~ 200 and 150 nm respectively. Further, these turbid suspensions of **P7**-**P9** underwent UCST-type insoluble-to-soluble phase transition in water with T_{cU}s of 36.8, 45.8 and 52°C (in cooling cycles) respectively (Figure 32). Figure 32 further revealed the reversible nature of these UCST-type phase behaviours of these copolymers. It was very clear that the cloud point increased with increasing

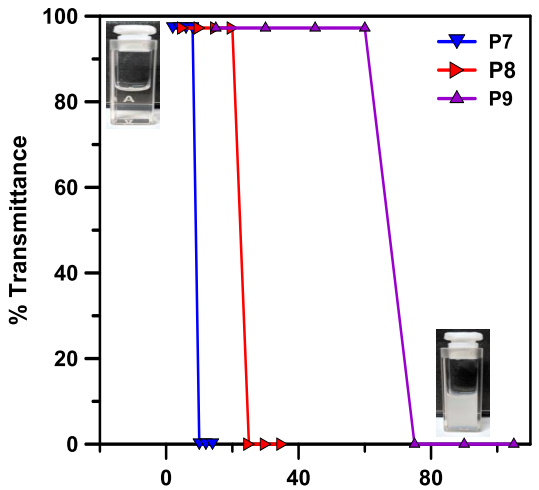

Figure 31. Variation of %transmittance against concentration of externally added chloride ion for 1 wt. % aqueous solutions of **P7**, **P8** and **P9**.

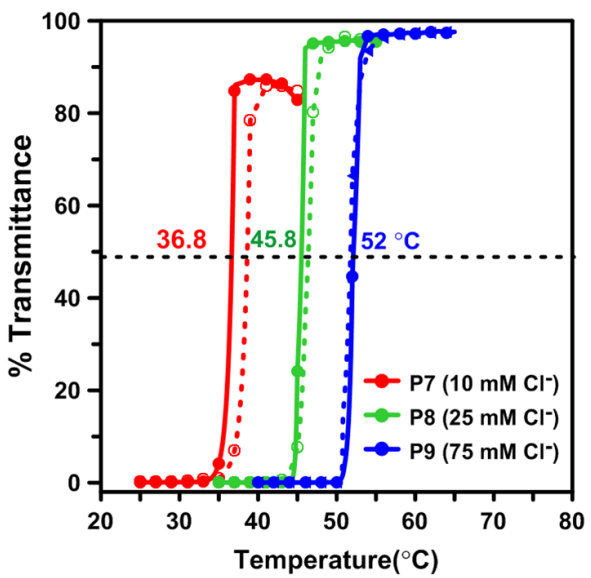

Figure 32. Turbidity [heating (dashed)/cooling (solid)] curves of 1 wt.% aqueous solutions of P[VBTP][Cl]-*ran*-PHEMA copolymers (**P7-P9**) in the presence of Cl^- ion.

ionic P[VBTP][Cl] segment content in the copolymers (Figure 32). DLS curve of **P9** in water with Cl^- ion also revealed the presence of UCST-type transition with a similar T_{cU} of 59.5°C (Figure 33). The explanations for such ion- and temperature-dependent phase behaviours of these copolymers in water are similar to those for P[VBTP][Cl]-*ran*-PMMA and P[VBTP][Cl]-*ran*-PS copolymers (Scheme 2).

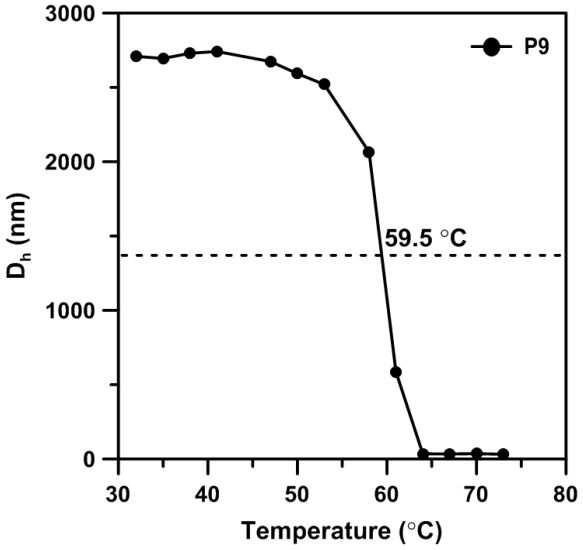

Figure 33. Plot of D_h of **P9** in H_2O (1 wt. %) in the presence of 75 mM of chloride ion against temperature as measured from DLS.

2.4.5 Dual thermoresponsiveness of P[VBTP][Cl]-*ran*-PNIPAM copolymers

PNIPAM is known to be a LCST polymer with a T_{cL} at ~32 °C.[64] Thus, the P[VBTP][Cl]-*ran*-PNIPAM copolymers (**P10**-**P13**) combining ionic P[VBTP][Cl] and PNIPAM segments would also expectedly show T_{cL} at round 32 °C, provided the lengths of the PNIPAM segments are sufficiently long. However, it was observed that T_{cLs} of **P10** and **P11** containing 1.13 and 2.5 wt. % of ionic P[VBTP][Cl] segments (Table 1) shifted to 36 and 45.3 °C respectively (Figure 34). Both these phase transitions were found to be reversible in nature with almost no hysteresis (Figure 34). For **P10** and **P11**, DLS curves also revealed the presence of LCST-type

transition with a similar T_{cL}s of 33.8 and 42°C (Figure 35) respectively. Moreover it was also observed that the LCST-type transition for **P10** was reversible/ repeatable for at least six heating/cooling cycles (Figure 36). These results substantiated that a very small increase (1.13 to 2.5 wt. %) of IC in **P10** to **P11**, induced a sharp increase of T_{cL} by (~9°C). The increase of ionic content increases their hydrophilicity in water which in turn increases the cloud point and the details of which will be discussed later.

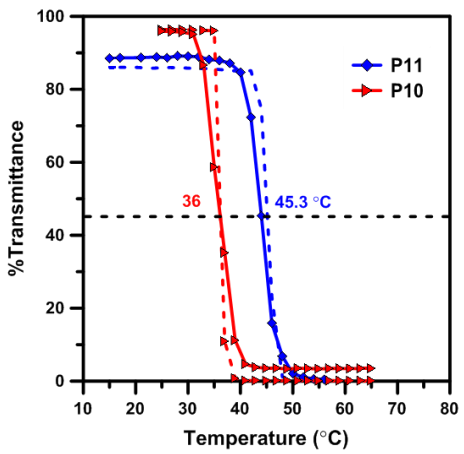

Figure 34. Turbidity curves of 1 wt. % aqueous solutions of **P10** and **P11** [heating (dashed curve)/cooling (solid curve)].

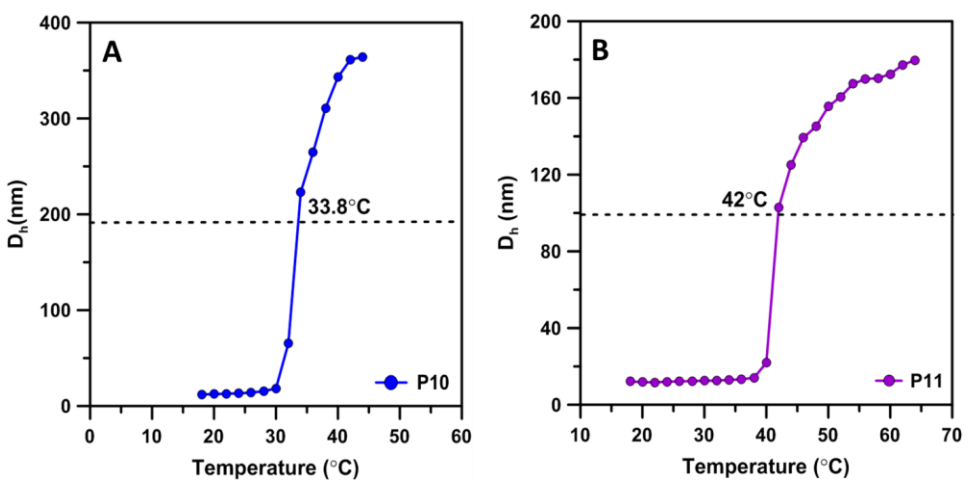

Figure 35. Plot of D_h of A) **P10** and B) **P11** in H_2O (1 wt. %) against temperature as measured from DLS.

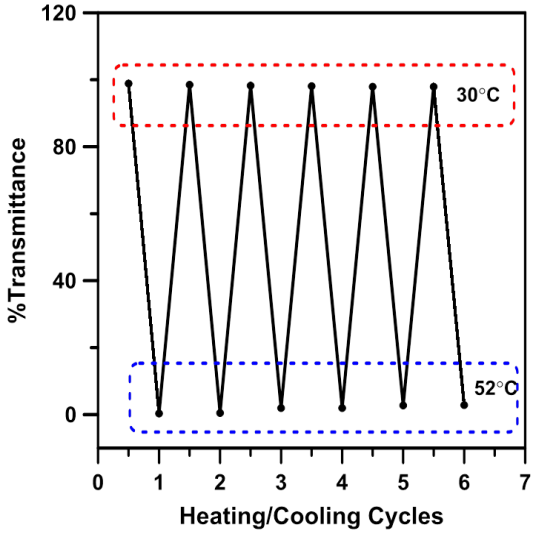

Figure 36. Temperature-dependent %transmittance of aqueous **P10** solution (1 wt. %) during heating/cooling cycles (each data point was obtained after equilibrating the sample solution for 2 min).

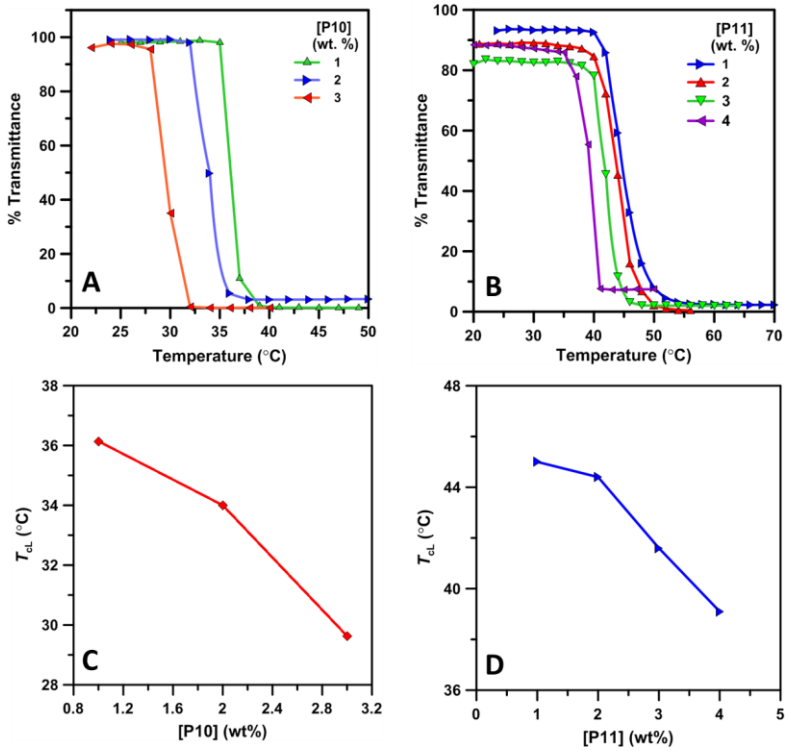

Figure 37. Turbidity cooling curves of aqueous solutions of A) **P10** and B) **P11** at their different concentrations. Plots of LCST-type cloud points (T_{cL}s) as a function

of (C) concentration of **P10** and (D) and concentration of **P11** measured from turbidity cooling curves.

Moreover, it can be seen from Figure 37 that the T_{cL}s of copolymers **P10** and **P11** initially decreases with increasing copolymer concentrations upto measureable limit. Above these concentrations, there was a precipitation instead of formation of colloidal copolymer aggregates. It should be noted that, in spite of having a UCST segment (P[VBTP][Cl] in the presence of Cl^-),[32, 57] **P10** and **P11** with low IC values (Table 1) showed only LCST-type behaviours in the presence of Cl^- ion. Further, T_{cL} of **P11** was found to be decreased with the increase of concentration of Cl^- ion (Figure 38) as also reported for other PIL copolymers .[57]

Surprisingly, no LCST-type transition was recorded in the temperature ranges of 10 to 90°C for **P12** and **P13** with PNIPAM contents of 80.7 and 65.5 wt. % (Table 1) respectively in the absence of Cl^- ion. The absence of LCST can be ascribed to shifting of T_{cL} to higher temperature and may be above 100°C due to the increase of hydrophilicities of **P12** and **P13** containing 19.3 and 34.5 wt. % of ionic P[VBTP][Cl] segments in comparison to those (1.13 and 2.5 wt. %) of **P10** and **P11** respectively (Table 1). However, **P12** solution exhibited T_{cL} at 44.8°C (cooling cycle) upon addition of 69 mM Cl^- ion, but there was no UCST transition (Figure 39).

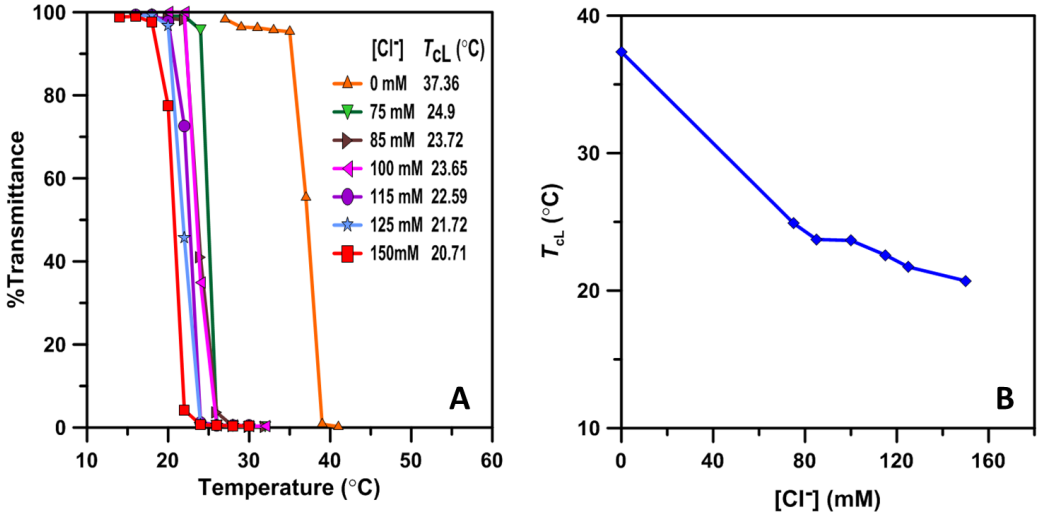

Figure 38. (A) Turbidity curves of 0.5 wt. % aqueous solution **P11** at different Cl^- ion concentrations. (B)The variation of T_{cL} of **P11** (0.5 wt.%) as a function of Cl^- ion concentration measured from turbidity cooling curves.

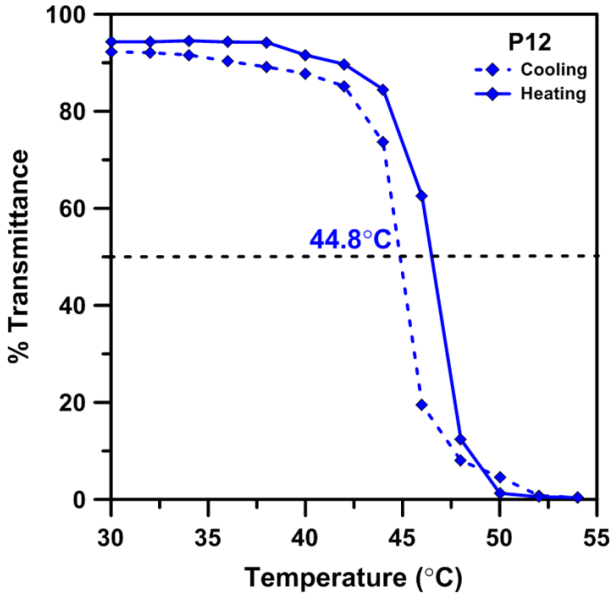

Figure 39. Turbidity curves of 1 wt.% aqueous solution of **P12** in presence of 69 mM Cl^- ion.

Interestingly, 0.25 wt.% aqueous solution of **P13** (IC = 34.5 wt. %, Table 1) exhibited both LCST- and UCST-type transitions with T_{cL} and T_{cU} of 21 and 69°C respectively in the presence of 160 mM Cl^- ion (Figure 40). Both of these transitions were reversible with little hysteresis in heating/cooling runs.The coexistence of both LCST-type (soluble-insoluble) and UCST-type (insoluble-soluble) transitions were clearly visible from the photographs given in the inset of Figure 41. It should be noted that the addition of Cl^- ion to 1wt.% **P13** (IC = 34.5 wt. %) led to irreversible coagulation of copolymers because of higher electrostatic interactions. This is the reason why the temperature dependency of **P13** was examined at a lower concentration (0.25wt.%) than those (1wt.%) used for similar measurement of **P10**-**P12**. Upon increasing the concentration of added Cl^- ion

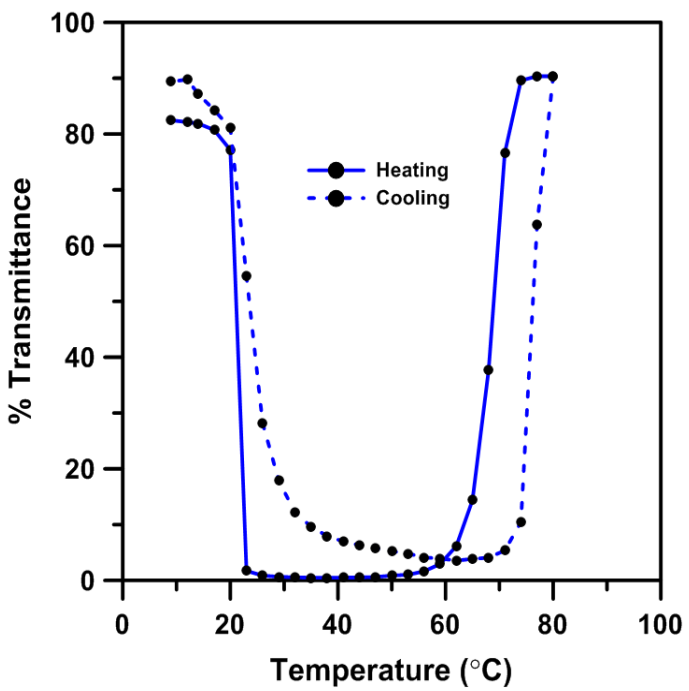

Figure 40. Turbidity curve of a **P13** in aqueous solution (0.25 wt. %) in the presence of 160 mM Cl^- during heating and cooling runs.

from 160 to 180mM in **P13** solution, there was a gradual decrease of T_{cL} followed by an increase of T_{cU} (Figure 41A and 41B). In the presence of Cl^- ion, the ionic P[VBTP][Cl] segment of **P13** become hydrophobic due to the presence of anion-induced intra- and/or inter-chain cross-linking/bridging interactions[32, 57] and therefore, there was a expected drop of T_{cL} of PNIPAM segment from 33 to 21 °C as usually reported for PNIPAM homopolymer (Figure 41B).

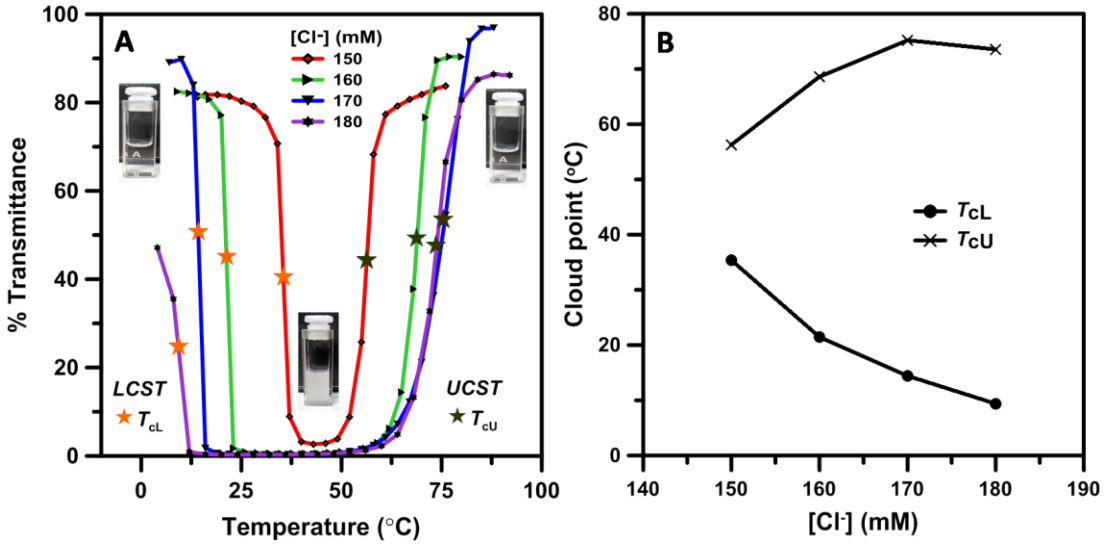

Figure 41. (A) Turbidity curves of aqueous **P13** solution (0.25 wt. %) at different concentration of Cl^- ion. Inset showed the snapshots of transparent solution (left one) below LCST, cloudy solution (middle one) in between LCST and UCST, and clear solution (right one) above UCST for the **P13** with 160 mM Cl^- ion (B) LCST-/UCST-type cloud points of **P13** (0.25 wt. %) as a function of [Cl^-] ion measured from the heating curves of given in Panel A.

DLS analysis of the aqueous **P13** (0.25 wt. %) in the presence of 160 mM Cl^- ion showed initially a sharp increase of D_h from 123 to 2990 nm with increase of temperature to 46°C and then a decrease to 234 nm upon further increase of temperature to 88 °C revealing coexistence of both LCST- and UCST-type transitions (Figure 42). T_{cL} and T_{cU} were measured to be 15 and 59.2 °C

respectively, while those were well-matched with those obtained from turbidity experiments (Figure 20). It was also observed that these LCST- and UCST-type transitions were reversible/repeatable for at least six heating/cooling cycles (Figure 43). The FESEM image further confirmed the formation of polydisperse spherical aggregates with a wide range of sizes from ~2 to10 µM in the turbid suspension of **P13** in the presence of 160 mM Cl^- at ~45 °C, a temperature in between the LCST and UCST-type cloud points (Figure 44).

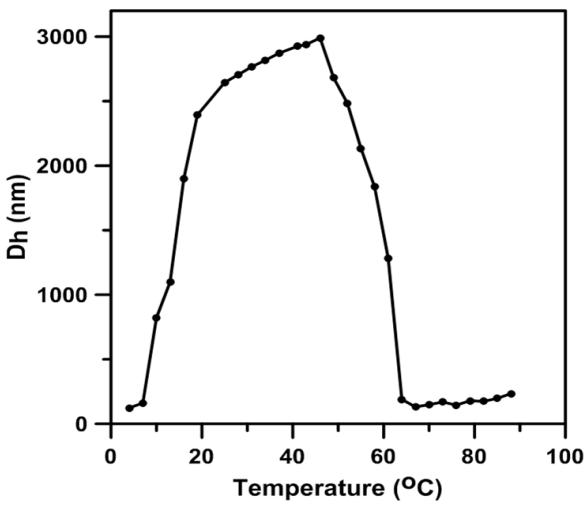

Figure 42. Plot of D_h of **P13** in H_2O (0.25 wt.%) in the presence of 160 mM Cl^- ion with temperature measured from DLS.

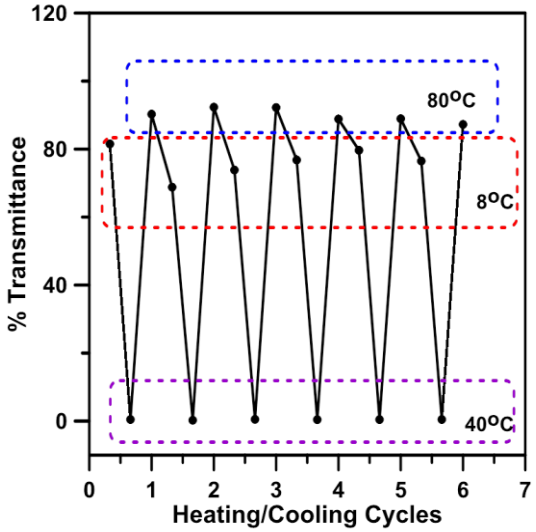

Figure 43. Temperature-dependent % transmittance of aqueous **P13** solution (0.25 wt.%) in the presence of 160 mM Cl^- during heating/cooling cycles (each data point was obtained after equilibrating the sample suspension for 2 min).

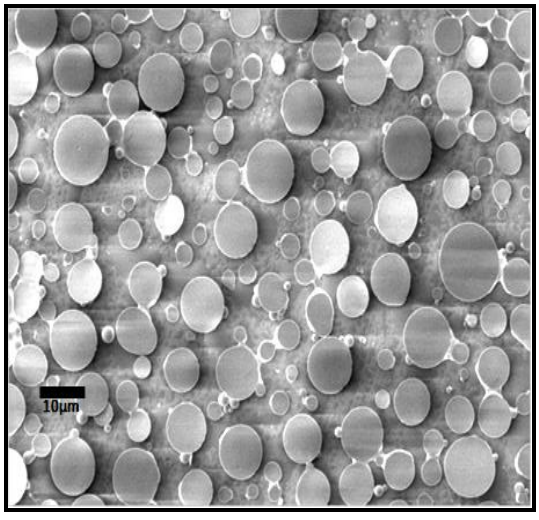

Figure 44. FESEM image of 0.25 wt. % aqueous solution of **P13** in the presence of 160mM Cl^- ion at 45 °C.

Both of the LCST- and UCST-type transitions were observed in the wide range of concentrations for **P13** at fixed Cl^- ion concentration of 160mM (Figure 45A). It was also clear that the T_{cL} gradually decreased and the T_{cU} gradually increased (Figure 45B) with increasing copolymer concentration because of the increase of extent of inter-/intra-molecular aggregation among the copolymer chains via hydrophobic and ionic-bridging interactions. The coexistence of such LCST- and UCST-type behaviours of **P13** could be explained in the following way as also discussed in our earlier report.[57] Above the T_{cL}, in addition to ionic-bridging interactions, the hydrophobic interactions among the pendent isopropyl moieties of PNIPAM segments come into play (Scheme 3). The combined ionic-bridging and hydrophobic interactions lead to the transformation from transparent solution to turbid suspension due to the formation of insoluble copolymer aggregates through inter-/intra-molecular association of neighbouring

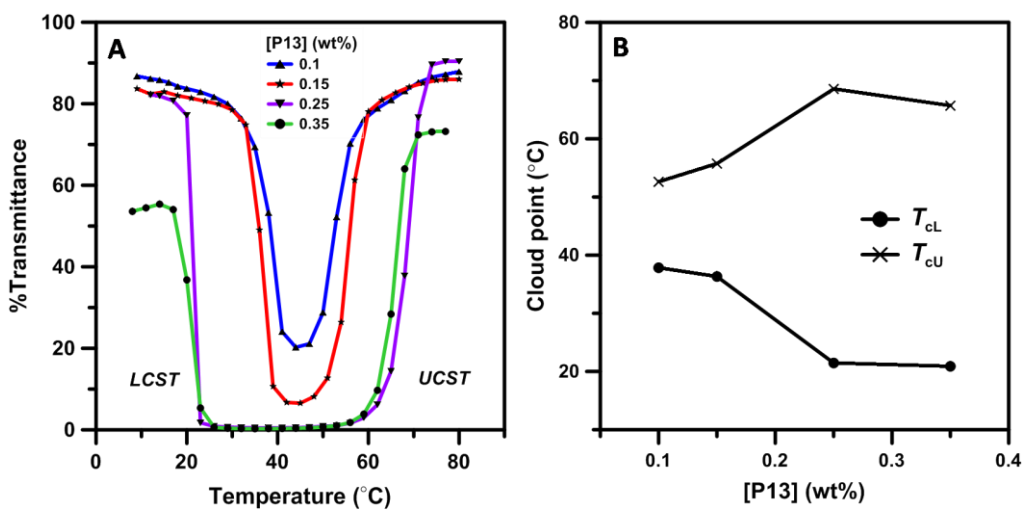

Figure 45. (A) Turbidity curves for aqueous **P13** solutions at different sample concentrations in presence of 160 mM Cl^- ion and **(B)** LCST-/UCST-type cloud points obtained from panel A as a function of concentration of **P13**.

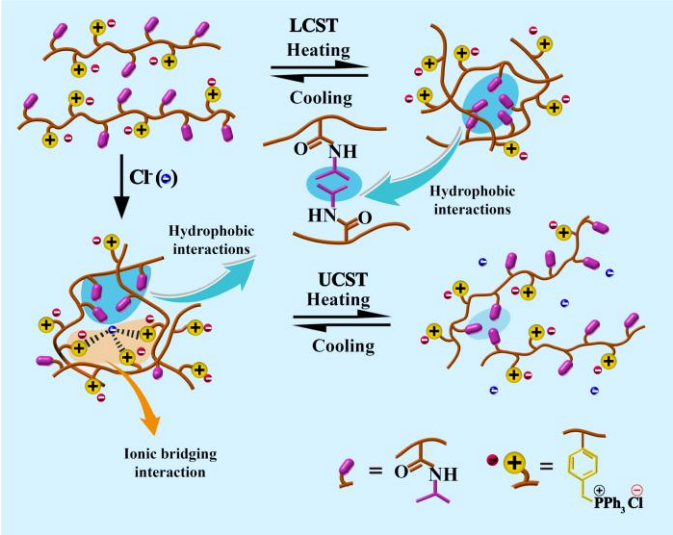

Scheme 3. Scheme showing different interactions for exhibiting LCST- and UCST-type transitions of P[VBTP][Cl]-*ran*-PNIPAM copolymer of high ionic content in the presence of chloride ion in water.

chains (Scheme 3). Heating above T_{cU} causes disruption of the ionic-bridging interactions and hence, the ionic P[VBTP][Cl] segments again become hydrophilic and predominates over the hydrophobically interacted PNIPAM segments of copolymer, which drives the redissolution of globular copolymer aggregates to coiled chain in a transparent solution.

2.5 CONCLUSIONS

In summary, a series of PIL, P[VBTP][Cl] based random copolymers containing conventional polymer segments namely, P[VBTP][Cl]-*ran*-PMMA, P[VBTP][Cl]-*ran*-PS, P[VBTP][Cl]-*ran*-PHEMA and P[VBTP][Cl]-*ran*-PNIPAM of varying compositions were synthesized by RAFT copolymerization. Indeed, the incorporation of only a very small percentage of ionic P[VBTP][Cl] segment into these copolymers enable solubilization of hydrophobic polymer PMMA/PS segments in MeOH/water and hydrophilic PHEMA segment in water irrespective

of their molecular weights. Further, the solutions of these copolymers underwent aggregation resulting in turbidity in the presence of externally added halide ions and experienced phase transitions from turbid suspension to transparent solution upon heating, indeed revealed the appearance of UCST-type phase behaviours due to the insertion of PIL (P[VBTP][Cl]) segment. The cloud point of UCST transitions in these copolymers were tunable with respect to various parameters such as ionic segment content, copolymer compositions as well as concentrations of added halide anions. On the other hand, P[VBTP][Cl]-*ran*-PNIPAM copolymers showed a composition dependent thermoresponsive behaviour. The copolymers with low ionic PIL contents showed only inherent LCST behaviour of PNIPAM with tunable cloud points by the addition of varying amount of Cl^- anion. However, the copolymer with moderately high ionic PIL content exhibited both LCST-type behaviour, inherent to PNIPAM segment as well as UCST-type behaviour arising from PIL (P[VBTP][Cl]) segment in the presence of halide anion. Overall, a large varieties of dual ion- and thermo-responsive copolymers with tunable cloud point and thermosensitivity were developed by introducing the PIL segment with easily available and cheaper conventional polymer segments, which opens up the possibility of making varieties of new smart materials towards sensor, drug delivery and other useful applications.

2.6 REFERENCES

1. Niskanen, J.; Wu, C.; Ostrowski, M.; Fuller, G. G.; Hietala, S.; Tenhu, H., *Macromolecules* **2013**, *46*, 2331-2340.

2. Schild, H. G., *Prog. Polym. Sci.* **1992**, *17*, 163-249.

3. Seuring, J.; Agarwal, S., *Macromol. Rapid Commun.* **2012**, *33*, 1898-1920.

4. Wu, Q.; Wang, R.; Chen, X.; Ghosh, R., *J. Membr. Sci.* **2014**, *471*, 56-64.

5. Xu, C.; Dong, W.; Wan, J.; Cao, X., *J. Chromatogr. A* **2016**, *1472*, 44-54.

6. Wei, H.; Cheng, S.-X.; Zhang, X.-Z.; Zhuo, R.-X., *Prog. Polym. Sci.* **2009**, *34*, 893-910.

7. Zhang, J.; Cui, Z.; Field, R.; Moloney, M. G.; Rimmer, S.; Ye, H., *Eur. Polym. J.* **2015**, *67*, 346-364.

8. Yamato, M.; Akiyama, Y.; Kobayashi, J.; Yang, J.; Kikuchi, A.; Okano, T., *Prog. Polym. Sci.* **2007**, *32*, 1123-1133.

9. Zhang, Y.; Furyk, S.; Bergbreiter, D. E.; Cremer, P. S., *J. Am. Chem. Soc.* **2005**, *127*, 14505-14510.

10. Hoogenboom, R.; Schlaad, H., *Polym. Chem.* **2017**, *8*, 24-40.

11. Lutz, J. F., *J. Polym. Sci. A: Polym. Chem.* **2008**, *46*, 3459-3470.

12. Weber, C.; Becer, C. R.; Hoogenboom, R.; Schubert, U. S., *Macromolecules* **2009**, *42*, 2965-2971.

13. Seuring, J.; Agarwal, S., *Macromolecules* **2012**, *45*, 3910-3918.

14. Seuring, J.; Bayer, F. M.; Huber, K.; Agarwal, S., *Macromolecules* **2011**, *45*, 374-384.

15. Makinen, L.; Varadharajan, D.; Tenhu, H.; Hietala, S., *Macromolecules* **2016**, *49*, 986-993.

16. Chang, Y.; Chen, W.-Y.; Yandi, W.; Shih, Y.-J.; Chu, W.-L.; Liu, Y.-L.; Chu, C.-W.; Ruaan, R.-C.; Higuchi, A., *Biomacromolecules* **2009**, *10*, 2092-2100.

17. Shih, Y.-J.; Chang, Y., *Langmuir* **2010**, *26*, 17286-17294.

18. Dimitrov, I.; Trzebicka, B.; Müller, A. H.; Dworak, A.; Tsvetanov, C. B., *Prog. Polym. Sci.* **2007**, *32*, 1275-1343.

19. Xie, D.; Ye, X.; Ding, Y.; Zhang, G.; Zhao, N.; Wu, K.; Cao, Y.; Zhu, X., *Macromolecules* **2009**, *42*, 2715-2720.

20. Longenecker, R.; Mu, T.; Hanna, M.; Burke, N. A.; Stöver, H. D., *Macromolecules* **2011**, *44*, 8962-8971.

21. Yuan, J.; Antonietti, M., *Polymer* **2011**, *52*, 1469-1482.

22. Mecerreyes, D., *Prog. Polym. Sci.* **2011**, *36*, 1629-1648.

23. Yuan, J.; Mecerreyes, D.; Antonietti, M., *Prog. Polym. Sci.* **2013**, *38*, 1009-1036.

24. Cheng, H.; Wang, P.; Luo, J.; Fransaer, J.; De Vos, D. E.; Luo, Z.-H., *Ind. Eng. Chem. Res.* **2015**, *54*, 3107-3115.

25. Bara, J. E.; Lessmann, S.; Gabriel, C. J.; Hatakeyama, E. S.; Noble, R. D.; Gin, D. L., *Ind. Eng. Chem. Res.* **2007**, *46*, 5397-5404.

26. Osada, I.; de Vries, H.; Scrosati, B.; Passerini, S., *Angew. Chem. Int. Ed.* **2016**, *55*, 500-513.

27. Tollan, C. M.; Marcilla, R.; Pomposo, J. A.; Rodriguez, J.; Aizpurua, J.; Molina, J.; Mecerreyes, D., *ACS Appl. Mater. Interfaces* **2008**, *1*, 348-352.

28. Amajjahe, S.; Ritter, H., *Macromolecules* **2008**, *41*, 3250-3253.

29. Men, Y.; Li, X.-H.; Antonietti, M.; Yuan, J., *Polym. Chem.* **2012**, *3*, 871-873.

30. Men, Y.; Schlaad, H.; Yuan, J., *ACS Macro Lett.* **2013**, *2*, 456-459.

31. Karjalainen, E.; Aseyev, V.; Tenhu, H., *Macromolecules* **2014**, *47*, 7581-7587.

32. Biswas, Y.; Maji, T.; Dule, M.; Mandal, T. K., *Polym. Chem.* **2016**, *7*, 867-877.

33. Nandi, S. K.; Mukherjee, P.; Roy, S.; Kundu, B.; De, D. K.; Basu, D., *Materials Science and Engineering: C* **2009**, *29*, 2478-2485.

34. Sealy, P. I.; Nguyen, C.; Tucci, M.; Benghuzzi, H.; Cleary, J. D., *Ann. Pharmacother.* **2009**, *43*, 1606-1615.

35. Weiss, B. D.; Weiss, E. C.; Haggard, W. O.; Evans, R. P.; McLaren, S. G.; Smeltzer, M. S., *Antimicrob. Agents Chemother.* **2009**, *53*, 264-266.

36. Henry, S. M.; El-Sayed, M. E. H.; Pirie, C. M.; Hoffman, A. S.; Stayton, P. S., *Biomacromolecules* **2006**, *7*, 2407-2414.

37. Li, Y. Y.; Zhang, X. Z.; Zhu, J. L.; Cheng, H.; Cheng, S. X.; Zhuo, R. X., *Nanotechnology* **2007**, *18*, 215605.

38. Maeda, H.; Sawa, T.; Konno, T., *J. Control. Release* **2001**, *74*, 47-61.

39. El Fray, M.; Prowans, P.; Puskas, J. E.; Altstädt, V., *Biomacromolecules* **2006**, *7*, 844-850.

40. Maeda, H.; Ueda, M.; Morinaga, T.; Matsumoto, T. J. J. o. m. c., *J. Med. Chem.* **1985**, *28*, 455-461.

41. Ranade, S. V.; Richard, R. E.; Helmus, M. N., *Acta Biomaterialia* **2005**, *1*, 137-144.

42. Tsai, H.-C.; Chang, W.-H.; Lo, C.-L.; Tsai, C.-H.; Chang, C.-H.; Ou, T.-W.; Yen, T.-C.; Hsiue, G.-H., *Biomaterials* **2010**, *31*, 2293-2301.

43. Zhang, Y.; Chu, D.; Zheng, M.; Kissel, T.; Agarwal, S., *Polym. Chem.* **2012**, *3*, 2752-2759.

44. Antoniraj, M. G.; Kumar, C. S.; Kandasamy, R., *Colloid and Polym. Sci.* **2016**, *294*, 527-535.

45. Schmaljohann, D., *Adv. Drug Deliv. Rev.* **2006**, *58*, 1655-1670.

46. Sun, W.; An, Z.; Wu, P., *Macromolecules* **2017**, *50*, 2175-2182.

47. Maji, T.; Banerjee, S.; Biswas, Y.; Mandal, T. K., *Macromolecules* **2015**, *48*, 4957-4966.

48. Cai, X.; Zhong, L.; Su, Y.; Lin, S.; He, X., *Polymer Chemistry* **2015**, *6*, 3875-3884.

49. Lucht, N.; Eggers, S.; Abetz, V., *Polym. Chem.* **2017**, *8*, 1196-1205.

50. Lutz, J.-F.; Hoth, A., *Macromolecules* **2006**, *39*, 893-896.

51. Osváth, Z.; Tóth, T.; Iván, B., *Polymer* **2017**, *108*, 395-399.

52. De, P.; Sumerlin, B. S., *Macromol. Chem. Phys.* **2013**, *214*, 272-279.

53. Weiss, J.; Böttcher, C.; Laschewsky, A., *Soft Matter* **2011**, *7*, 483-492.

54. Butun, V.; Liu, S.; Weaver, J.; Bories-Azeau, X.; Cai, Y.; Armes, S., *React. Funct. Polym.* **2006**, *66*, 157-165.

55. Vishnevetskaya, N. S.; Hildebrand, V.; Niebuur, B.-J.; Grillo, I.; Filippov, S. K.; Laschewsky, A.; Müller-Buschbaum, P.; Papadakis, C. M., *Macromolecules* **2016**, *49*, 6655-6668.

56. Dai, Y.; Wu, P., *Phys.Chem.Chem.Phys.* **2017**, *19*, 18556-18564.

57. Jana, S.; Biswas, Y.; Anas, M.; Saha, A.; Mandal, T. K., *Langmuir* **2018**, *34*, 12653-12663.

58. Karjalainen, E.; Chenna, N.; Laurinmäki, P.; Butcher, S. J.; Tenhu, H., *Polym. Chem.* **2013**, *4*, 1014-1024.

59. Arotçaréna, M.; Heise, B.; Ishaya, S.; Laschewsky, A., *J. Am. Chem. Soc.* **2002**, *124*, 3787-3793.

60. Brandrup, J.; Immergut, E.; Grulke, E., Polymer Handbook 4th Edn 1999, Vol. 1. Wiley-Interscience: New York, NY.

61. Hoogenboom, R.; Becer, C. R.; Guerrero-Sanchez, C.; Hoeppener, S.; Schubert, U. S., *Aust. J. Chem.* **2010**, *63*, 1173-1178.

62. Zhang, Q.; Hoogenboom, R., *Prog. Polym. Sci.* **2015**, *48*, 122-142.

63. Weaver, J. V. M.; Bannister, I.; Robinson, K. L.; Bories-Azeau, X.; Armes, S. P.; Smallridge, M.; McKenna, P., *Macromolecules* **2004**, *37*, 2395-2403.

64. Hocine, S.; Li, M.-H., *Soft Matter* **2013**, *9*, 5839-5861.

Chapter 3

Ion conductance in phosphonium poly(ionic liquid)-based homo- and co-polymers

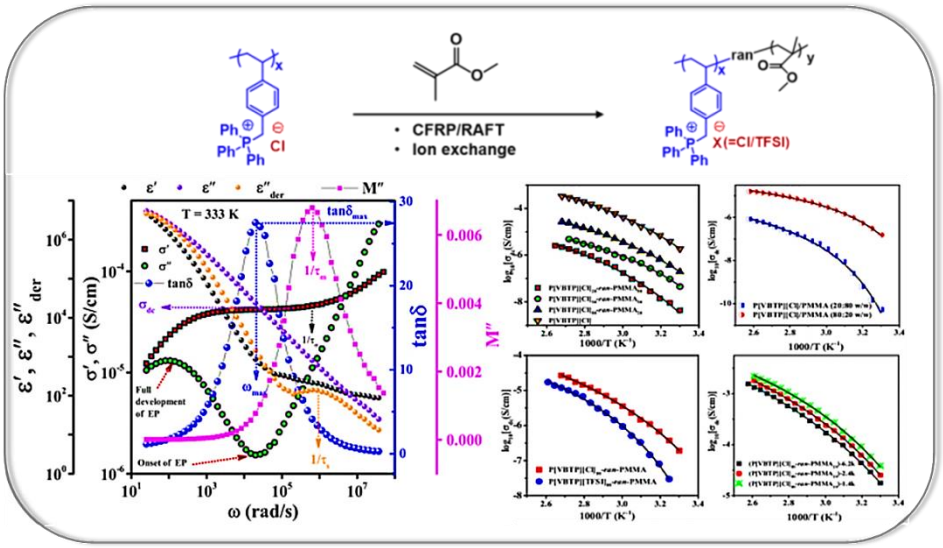

3.1 INTRODUCTION

The main advantages of using PILs (as already mentioned in Chapter 1) as conductive polymer electrolytes over ILs are that they combine all the novel properties related to ILs, while having the mechanical durability to form coatings, gels, films and membranes.[1] PILs are polyelectrolytes whose potential uses are being investigated for a variety of technologies, such as batteries, membranes, solar cells and switchable surfaces.[2] In recent years, a number of significant efforts have been made by the materials scientists to develop advanced functional materials to overcome the challenges in efficient energy storage and its utilization.[3-8] Recently, polymerized ionic liquids (PILs) have received significant attention for their use as solid-state polymer electrolytes in several energy storage and conversion devices including lithium-ion batteries, dye-sensitized solar cells, supercapacitors, fuel cells, supercapacitors, light-emitting electrochemical cells etc.[9-13] Actually, PILs belong to an interesting subclass of polymer electrolytes containing an ionic liquid (IL) species in each of the repeating monomer unit that constitutes the polymer backbone. Thus, PILs are also known as single ion conductors as they have non-conducting ions bound to the polymer backbone/side chain, while the counter ions conduct because of their mobile nature.[14-19] Fundamentally, the molecular level understanding of the charge carrier transport mechanism and relaxation in these types of ionic polymers are needed for rational designing of PILs for electrochemical applications.[15] However, the low ionic conductivity of polymer electrolytes at room temperature limits their applications in electrochemical devises. Therefore, it is highly important to have a clear understanding of the fundamental parameters[3, 16-17, 20-21] and how several factors such as chemical structure, morphologies, etc. influence the ion transport mechanism in PIL systems.

However, many of such reported studies remain controversial and require further exploration.

As per the Nernst-Einstein relation, $\sigma = \sum p_i q_i \mu_i$, the ionic conductivity (σ) of a liquid electrolyte is strongly controlled by the ion mobility (μ_i) (inversely proportional to ion diffusivity) and free ion number density (p_i).[22-23] Furthermore, the ion diffusivity in liquid electrolyte is largely controlled by medium viscosity (η) and structural relaxation time (τ_s). As reported in the literature, the classical mechanics assumes a strong coupling of charge carrier diffusion to structural relaxation (viscosity) for liquid electrolyte.[24] A similar mechanism has also been proposed for polymer electrolytes by different groups, where the charge carrier dynamics (diffusion) depends on local segmental motion of polymer chain.[25-26] In particular, in the cases of superionic glasses or crystal systems, a faster ion dynamics have been observed even in frozen condition of segmental dynamics, resulting in high ionic conductivity compared to ideal coupled system.[27-28] A similar decoupling of the charge carrier transport from segmental dynamics has also been reported for several PILs.[21, 29-31] It is hypothesized that the frustration in chain packing in PIL can cause such decoupling phenomenon.[3] Ultimately, the decoupling of ion dynamics from segmental motion is the most promising approach to achieve high ionic conductivity in polymer electrolytes at room temperature. In addition to mechanical properties,[32-33] the frequency dependent studies of the conductivity and dielectric response of the polymer electrolytes are useful tools to obtain the detailed information about the ionic conduction mechanism and differences in ion–polymer interactions in the polymer electrolytes. Moreover, there have been a series of studies to examine the effect of tuning of cation/anion size,[34-35] position of ions (either in the main chain or in the side chain) of PIL,[21, 31, 36-37] variation of molecular weight,[20] changing the space between neighboring PIL chains,[15] pressure exerted during conductivity

measurement,[3] variation of chain length,[38] glass transition temperature (T_g),[16, 34, 39] chain polarity,[40] etc., on the change of ionic transport in PIL systems.

3.2 OBJECTIVES AND SCOPE OF THE PRESENT WORK

PIL-based copolymers are potential candidates as solid-state polymer electrolytes since they combine the properties of both ionic liquids (ILs) and the copolymers and have the ability to offer several advantages such as high mechanical strength, flexibility, processability, less moisture sensitivity and high ionic conductivity. It is to be noted that, high mechanical strength and high ionic conductivity contradict with each other, as polymers with high mechanical strength are associated with a high glass transition temperature (T_g), which can remain in the glassy state during practical application, while high ionic conductivity requires amorphous polymers with low T_g values which enable the polymer segments to freely move resulting in an improved transportation of ions. Therefore, new investigations are urgently required to achieve PIL-based polymer materials as high-performance solid-state polymer electrolytes. Moisture sensitivity is also a major obstacle to the practical application of PILs in electrochemical devices. From the energy storage application point of view, the copolymers of PIL and hydrophobic polymer [such as poly(methyl methacrylate), PMMA] are of great importance because they are expected to offer high thermal stability and excellent resistance to both chemical and weather corrosion in comparison with homopolymeric PIL. Therefore, the exploration of ion transport properties in such type of PIL copolymers is necessary for their futuristic application in electrochemical devices. On the other hand, dielectric spectroscopic (DS) technique is reported to be the most popular method to investigate ionic conductivity, ion transport and relaxation mechanism in electrolyte systems.[31, 41-43] However, such studies have been reported for only limited number of PILs which are mostly homopolymers. In particular, there are

a very limited number of studies done on ion conduction in PIL-based copolymers.

Thus, this work is focused on the studies of ion transport and relaxation in PIL homo- and co-polymers as single ion conducting polymeric electrolytes using dielectric spectroscopy. In particular, this study puts special emphasis on examining how the composition of PIL copolymer, nature of counter anion and molecular weight (M_n) affects the ion transport properties in these PIL-based systems. For comparison, similar studies are also conducted on materials obtained by physical mixing of PIL and hydrophobic poly(methyl methacrylate) (PMMA) that actually constitute the copolymer. To do such experiment, poly(triphenyl-4-vinylbenzylphosphonium chloride) (P[VBTP][Cl]) homopolymer and a series of P[VBTP][Cl]-*ran*-PMMA PIL copolymers of varying compositions were synthesized by conventional free radical polymerization. Another series of PIL copolymers with varying molecular weights were also synthesized by reversible addition-fragmentation chain-transfer (RAFT) polymerization technique. This work further demonstrates that it is possible to enhance the thermal stability and electrical properties of the PIL copolymers compared to the physically mixed blend of two constituent polymer segments.

3.3 EXPERIMENTAL

3.3.1 Materials

Methyl methacrylate (MMA, >99%), 4-vinylbezyl chloride (VBC, 90%), 2'-azobis(2-methylpropionitrile) (AIBN, 98%), 4-cyano-4-[(dodecylsulfanylthiocarbonyl) sulfanyl] pentanoic acid (CDP, ≥ 97%) and bis(trifluoromethane)-sulfonimide lithium salt (LiTFSI, >99%) were used as received from Sigma-Aldrich. Triphenylphosphene (TPP) was obtained from TCI chemicals. Dimethylformamide (DMF) was received from Merck, India. MMA and

VBC monomers were passed through alumina columns for removal of inhibitors. AIBN and TPP were recrystallized twice from ethanol prior to use. DMF was kept overnight with anhydrous $CaCl_2$ and distilled over CaH_2 under reduced pressure prior to use. Milli-Q water was used in the preparation of various solutions.

3.3.2 Synthesis

3.3.2.1 Synthesis of different random PIL copolymers

A series of random PIL copolymers [P[VBTP][Cl]-*ran*-PMMA copolymers (**P1**-**P3**)] (Table 1) of varying compositions were prepared from an ionic liquid monomer (ILM), triphenyl-4-vinylbenzylphosphonium chloride ([VBTP][Cl]) and hydrophobic MMA monomer by conventional free radical polymerization (CFRP) technique using AIBN as the initiator (Scheme 1). The anion-exchange of chloride ion of **P3** ($P[VBTP][Cl]_{80}$-*ran*-$PMMA_{20}$) with bis(trifluoromethane) sulfonamide ($TFSI^-$) ion was done using a reported protocol[44] as shown in Scheme 1 which resulted in the formation of the ion exchanged copolymer, **P4** (Table 1). Low molecular weight copolymers (**P5**-**P7**, Table 1) (Scheme 1) were synthesized by reversible addition-fragmentation chain-transfer (RAFT) polymerization technique using the above mentioned two comonomers while CDP and AIBN was used as the chain transfer agent (CTA) and radical initiator respectively. Note that the synthesis protocol and the detailed characterization of the [VBTP][Cl] monomer has been already reported.[45] The detailed reaction recipe and the synthesis protocol are discussed below.

3.3.2.1.1 Synthesis of P[VBTP][Cl]-ran-PMMA copolymers (P1-P3) by CFRP technique

To synthesize **P1** copolymer (Table 1), MMA (0.832g; 8.3093 mmol), [VBTP][Cl] (0.788 g; 2.0772 mmol) and AIBN (34.11 mg; 0.207 mmol) were mixed together in 16 mL of dry DMF taken in a 50 mL long-neck round bottom flask. The reaction

mixture was purged by argon gas for 45 mins and the flask was immediately sealed with a rubber septum and placed in an oil bath preheated at 70 °C for 24 h under magnetic stirring. **P1** copolymer was finally isolated from DMF solution by precipitation in diethyl ether. Finally, **P1** was redissolved in DMF and reprecipitated in water followed by centrifugation to remove unreacted [VBTP][Cl] monomer. The **P1** was then dried in vacuum oven at 60 °C for overnight. Yield of **P1**: 75 %. **P2** and **P3** copolymers of varying compositions were also prepared by using the similar protocol at different molar feed ratios of the monomers (Table 1). The actual compositions of all the copolymers were determined from ^{1}H-NMR analysis (Table 1).

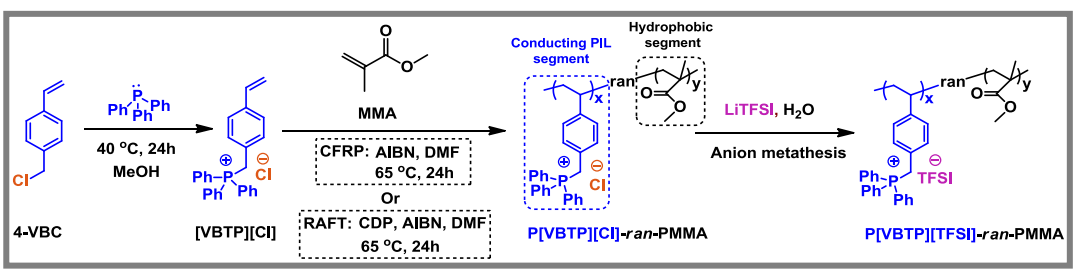

Scheme 1. Synthetic scheme for the preparation of a) P[VBTP][Cl]-*ran*-PMMA random copolymers via CFRP or RAFT polymerization and b) P[VBTP][TFSI]-*ran*-PMMA copolymer by anion metathesis of the chloride to bis(trifluoromethane)sulfonamide ($TFSI^-$) ion.

*Homopolymers P[VBTP][Cl] and PMMA are synthesized by the CFRP method using [VBTP][Cl] and MMA respectively as monomer and AIBN as initiator.

3.3.2.1.2 Preparation of P[VBTP][TFSI]$_{80}$-ran-PMMA$_{20}$ (P4) via anion metathesis

The anion-exchange of chloride ion of P[VBTP][Cl]$_{80}$-ran-PMMA$_{20}$ by bis(trifluoromethane) sulfonamide ($TFSI^-$) ion was done using a reported protocol.[46] 10 mL aqueous solution of **P3** copolymer [5 wt.%(w/v)) was added to 10 mL of 5 M LiTFSI solution drop wise and the mixture was stirred overnight at

ambient temperature. The mixture was then vigorously centrifuged to collect the crude anion-exchanged copolymer, which was further dialyzed against double distilled water for next 3 days. During dialysis, old solvent was exchanged with fresh solvent in every 6 h and 5 mL of 5 M LiTFSI solution was added to the dialysis tubing in every 12h. The **P4** solution was then dialyzed again against double distilled water for another 3 days with changing the solvent after every 6h to remove any excess, non-interacting $TFSI^-$ ion. Finally, the purified **P4** was collected by freeze drying, followed by drying in vacuum oven at 60 °C for overnight.

3.3.2.1.3 Synthesis of P[VBTP][Cl]-ran-PMMA copolymers (P5-P7) via RAFT polymerization technique

Another set of copolymers having lower molecular weights were synthesized via RAFT polymerization technique using CDP as the chain transfer agent and AIBN as the radical initiator. These copolymers (**P5**-**P7**) were achieved by using a molar feed ratio of [VBTP][Cl]:MMA of 4:1 and varying the $[Monomer]_0/[CDP]_0$ ratios as mentioned in Table 1. Typically, for **P5**, a 50 mL long neck RB flask was charged with MMA (0.823 g; 7.906 mmol), [VBTP][Cl] (0.750 g; 1.976 mmol), AIBN (3.24 mg; 0.019 mmol) and CDP (39.89 mg; 0.098 mmol) followed by addition of 15.7 mL dry DMF. The reaction mixture was then purged with argon gas for 45 min, sealed immediately with a silicone rubber septum and stirred magnetically in a preheated oil bath at 65 °C for 24h. The quenching of the polymerization reaction was done by quick cooling the flask in an ice-water bath. The mixture was precipitated in diethyl ether to isolate copolymer from DMF solution. The isolated copolymer was further dissolved in DMF and reprecipitated in water and collected by centrifugation to remove unreacted [VBTP][Cl] monomer. The purified **P5** was then dried in vacuum oven at 60 °C for overnight. Yield of **P5**: 74%. The other two copolymers, **P6** and **P7** were also synthesized just by varying

the $[Monomer]_0/[CDP]_0$ ratios following the same procedure as used for **P5**, while keeping $[CDP]_0/[AIBN]_0$ ratio as constant (Table 1).

Table 1: Polymerization conditions and molecular characterization data of P[VBTP][Cl], PMMA and different P[VBTP][Cl] based copolymers.

PIL systems[a]	$[M_1:M_2]_o:[CDP]_o:[AIBN]_o$	M_n (SEC) (kDa)	M_p (MALDI-TOF MS) (kDa)	Đ (SEC)	Ionic content (IC)[b] (wt%)
P[VBTP][Cl]	[100:0]:00:2	23.3	--	1.65	100
$P[VBTP][Cl]_{20}$-*ran*-$PMMA_{80}$ **(P1)**	[20:80]:00:2	28.9	--	1.92	18
$P[VBTP][Cl]_{50}$-*ran*-$PMMA_{50}$ **(P2)**	[50:50]:00:2	20.15	--	1.56	24.7
$P[VBTP][Cl]_{80}$-*ran*-$PMMA_{20}$ **(P3)**	[80:20]:00:2	19.1	--	1.69	88.34
$P[VBTP][TFSI]_{80}$-*ran*-$PMMA_{20}$ **(P4)**	[80:20]:00:2	19.1	--	1.69	88.34
$P[VBTP][Cl]_{80}$-*ran*-$PMMA_{20}$-6.2k[c] **(P5)**	[80:20]:1:0.2	6.2	--	1.20	89.1
$P[VBTP][Cl]_{80}$-*ran*-$PMMA_{20}$-2.4k[d] **(P6)**	[80:20]:10:2	--[e]	2378	--	50
$P[VBTP][Cl]_{80}$-*ran*-$PMMA_{20}$-1.4k[d] **(P7)**	[80:20]:20:4	--[e]	1391	--	66
PMMA	[00:100]:00:2	25.48	--	1.79	00

Reaction condition: Time = 24 h; Temperature = 65 °C; Solvent = DMF; M_1= [VBTP][Cl]; M_2= MMA; Monomer concentration = 10 wt%.

[a]The numerical value represents the feed ratios of the comonomers

[b]Obtained from ***^{1}H-NMR*** spectral analysis

[c]Molecular weight obtained from SEC analyses.

[d]Molecular weight obtained from MALDI-TOF Mass Spectrometry data.

[e]Not measurable

P5-P7 were the samples of molecular weights 6.2, 2.4 and 1.4 kDa respectively.

P8 and **P9** were the physical blends of P[VBTP][Cl] and PMMA homopolymers with a ratio of 1:4 and 4:1 (wt./wt.) respectively.

3.3.2.2 Synthesis of P[VBTP][Cl] and PMMA homopolymers

P[VBTP][Cl] and PMMA homopolymers were synthesized separately by the same polymerization procedure as used for **P1** at a concentration of 10 wt.% of [VBTP][Cl] and MMA monomers respectively using AIBN as the radical initiator.

3.3.2.3 Preparation of binary polymer blends [P[VBTP][Cl]/PMMA(20/80) (P8) and P[VBTP][Cl]/PMMA(80/20) (P9)]

The polymer blends of P[VBTP][Cl] and PMMA were prepared by solution-casting method. Two blend samples **P8** and **P9** were prepared by exactly weighing P[VBTP][Cl] (M_n = 23.3 kDa) and PMMA (M_n = 25.5 kDa) in the ratios of 1:4 and 4:1 (w/w) respectively. Each sample mixture was then dissolved in DMF at a concentration of 5 wt. % and vigorously stirred at 60 °C overnight to form a homogeneous mixture. The polymer blend samples were then isolated by precipitation in diethyl ether followed by drying overnight in vacuum oven at 70 °C and collected as white powder.

3.3.3 Characterizations

Molecular characterizations. ^{1}H-NMR spectra of all the homopolymers and copolymers (Figures 1 to 9) and ^{19}F-NMR spectrum of **P4** (Figure 10) were recorded on a Bruker DPX 500 MHz spectrometer. DMSO-d_6 was used as a solvent for P[VBTP][Cl], PMMA and P[VBTP][Cl/TFSI]-*ran*-PMMA copolymers of high molecular weights (**P1**-**P5**) whereas $CDCl_3$ was used as the same for P[VBTP][Cl]-*ran*-PMMA copolymers (**P6** and **P7**) with low molecular weights.

Size exclusion chromatography (SEC) technique was used to determine the number average molecular weights (M_ns) and dispersities (*Đ*s) of copolymers and homopolymers using a Waters GPC system connected with three Styragel columns, HR1 (M_n = 100-5000), HR3 (M_n = 500-30,000) and HR4 (M_n = 5000-6,00,000) columns. As already discussed in Chapter 2, the SEC analyses of these

cationic PILs using neat DMF as an eluent were not possible because of the tendency of these PILs to aggregate on the column materials due to the strong interaction between the ionic polymer and the SEC column.[47-48] However, to overcome this problem, as reported earlier,[45] DMF containing 50 mM LiBr was used as an eluent at a column temperature of 45 °C and at a flow rate of 1.0 mL min^{-1}. These columns were calibrated against PMMA standards.

Thermal analysis. The thermogravimetric analysis (TGA) of all the PIL samples were done in a TGA instrument (TA, model Q50) in argon atmosphere using a heating rate of 10 °C min^{-1}.

Differential scanning calorimetry (DSC) (Q2000, TA instrument) instrument was used to determine the thermal properties of the different PIL copolymers in N_2 atmosphere at a heating rate of 10°C min^{-1}.

Field emission scanning electron microscopy. Field emission scanning electron microscope (FESEM) images were taken using JEOL FESEM (Model: JSM 7500F) at an accelerating voltage of 5 kV to visualize and compare the phase morphologies of the PIL copolymer (**P1**) and the physical blend of its polymer component (**P8**).

Matrix-assisted laser desorption/ionization TOF mass spectrometry. MALDI-TOF-MS spectra were acquired in a Brucker instrument (Applied Biosystems) to determine the molecular weight of **P6** and **P7**. The samples were irradiated using 337 nm N_2 laser with an operating voltage of 25 kV. Trans-2-[3-(4-t-butyl-phenyl)-2-methyl-2-propeny- lidene]malononitrile (DCTB) was used as the matrix. The concentration of polymers was taken as 1 mg/mL in MeOH. For the measurement, 10 *μL* of polymer solution and 10 μL of matrix solution were mixed together and 1 μL of the solution mixture was spotted on the sample's plate and allowed to dry. The corresponding spectra of samples were acquired by summing the data obtained over 200 laser shots in a linear mode.

Dielectric spectroscopic measurements. The dielectric spectroscopic (DS) measurements at different temperatures was carried out using an LCR spectrometer (HIOKI, model: IM 3536) in the frequency range of 4 Hz - 8 MHz with a perturbation potential of 1.0 V. For dielectric measurements the powder PIL was pressed into pallet of 10 mm diameter using stainless steel dies by applying pressure. The thickness of the sample was varied from 0.7 mm to 0.8 mm. The pellet was sandwiched between a pair of stainless steel electrodes of 10 mm diameter and was then placed in the sample holder assembly kept inside the cryostat. Temperature of the sample pallet was controlled using a temperature controller (Lake Shore, Model: 331) with a temperature stability of ± 0.1 K using a vacuum nitrogen gas cryostat maintaining at a constant pressure of 0.01 mbar. The dielectric data were recorded in the heating mode from 303 to 388 K at every 5 K temperature interval, with 15 min of equilibration at each temperature.

Determination of saturated water content in PIL Systems. To understand the potentiality of these PIL systems to meet industrial and scientific applications, the saturated water content in the samples were determined. Typically, a polymer sample and a water-filled beaker were kept inside a desiccator for seven days for allowing the sample to absorb maximum amount of moisture. The water content was then calculated from the weight loss in TGA thermogram of the respective water-absorbed samples at and above 100 °C.

3.4 RESULTS AND DISCUSSION

3.4.1 Synthesis and characterization of PIL homo- and co-polymers

PMMA, P[VBTP][Cl] and **P1**-**P3** copolymers were synthesized via CFRP technique to obtain polymeric products having relatively high molecular weights with sufficient yields while low molecular weight PIL copolymers (**P5**-**P7**) were

synthesized by RAFT polymerization of [VBTP][Cl] and MMA using CDP and AIBN as chain transfer agent (CTA) and radical initiator respectively (Scheme 1, Table 1). The counter anion-exchange or metathesis reaction of the Cl^- ion of **P3** (Table 1) with bis(trifluoromethane)-sulfonamide ($TFSI^-$) ion to obtain **P4** has been achieved as shown in Scheme 1. ^{1}H-NMR spectral analysis (Figures 1 to 9) was used to determine the chemical compositions of PIL copolymers and that are summarized in Table 1. ^{19}F- NMR spectra of **P4** (Figure 10**)** were recorded relative to neat hexafluorobenzene (C_6F_6) at −164.9 ppm and the distinct signal at 81.02 ppm clearly referred to the presence of $TFSI^-$ anions in the copolymer. The absence of Cl^- ion in the anion-exchanged product (**P4)** was confirmed by titrating **P4** against silver nitrate. A 50 mg of **P4** copolymer was first leached with 1 mL of water followed by the drop wise addition of 1 M aqueous $AgNO_3$ solution in the presence of excess dilute nitric acid. No white precipitate of AgCl was observed which confirmed that the previous anion metatheses had been completed.The comparison of ^{1}H-NMR spectra of copolymer before (**P3**) and after exchange (**P4**) (Figure 11**)** clearly revealed a shift of signal of methylene protons adjacent to phosphonium cation from δ 5.32 to 5.02 ppm providing further evidence of complete exchange of Cl^- with $TFSI^-$ ion.

^{1}H-NMR analysis of **P[VBTP][Cl]** (500 MHz, DMSO-d_6, δ ppm)(Figure 1): 1.5-0.0.7 (-CH_2 and –CH of polymer backbone, position ‘a’, ‘b’); 5.74 (benzylic protons, position ‘f’); 6.75 (phenyl ring protons, position ‘d’ and phenyl ring protons, position ‘e’); 7.60 (phenyl ring protons of TPP unit).

^{1}H-NMR analysis of **P1** (500 MHz, DMSO-d_6, δ ppm)(Figure 2): 1.7-0.0.7 (-CH_2 and –CH and –CH_3 of polymer backbone, position ‘a’, ‘b’, ‘l’ and -CH_2 protons of polymer backbone, position ‘k’); 5.32 (benzylic protons, position ‘f’); 6.79 (phenyl ring protons, position ‘d’ and phenyl ring protons, position ‘e’); 7.60 (phenyl ring protons of TPP unit); 3.4 (-CH_3 protons, position ‘m’).

^{1}H-NMR analysis of **P2** (500 MHz, DMSO-d_6, δ ppm)(Figure 3) : 1.6-1.24 (-CH_2 and –CH and –CH_3 of polymer backbone at position 'a', 'b', 'l' and -CH_2 protons of polymer backbone at position 'k'); 5.18(benzylic protons, position 'f'); 6.82 (phenyl ring protons, position 'd'; phenyl ring protons, position 'e'); 7.35-7.92 (phenyl ring protons of TPP unit); 3.39 (-CH_3 protons, position 'm').

^{1}H-NMR analysis of **P3** (500 MHz, DMSO-d_6, δ ppm) (Figure 4) : 0.9-0.6 (-CH_2 and –CH and –CH_3 of polymer backbone, position 'a', 'b', 'l'); 1.7 (-CH_2 protons of polymer backbone, position 'k'); 5.17 (benzylic protons, position 'f'); 6.82 (phenyl ring protons, position 'd'; phenyl ring protons, position 'e'); 7.68-7.89 (phenyl ring protons of TPP unit); 3.44 (-CH_3 protons, position 'm').

^{1}H-NMR analysis of **PMMA** (500 MHz, DMSO-d_6, δ ppm) (Figure 5): 0.75 -0.95 (–CH_3 of polymer backbone, position 'a'); 1.84 (-CH_2 protons of polymer backbone, position 'b'); 3.57 (-CH_3 protons, position'd').

^{1}H-NMR analysis of **P4** (500 MHz, DMSO-d_6, δ ppm) (Figure 6) : 1.01 -0.41 (-CH_2 and –CH and –CH_3 of polymer backbone, position 'a', 'b', 'l'); 1.7 (-CH_2 protons of polymer backbone, position 'k'); 5.04 (benzylic protons, position 'f'); 6.79 (phenyl ring protons, position 'd'; phenyl ring protons, position 'e'); 7.62-7.89 (phenyl ring protons of TPP unit); 3.51 (-CH_3 protons, position 'm').

^{1}H-NMR analysis of **P5** (500 MHz, DMSO-d_6, δ ppm) (Figure 7): 1.2-0.8 (-CH_2 and –CH and –CH_3 of polymer backbone, position 'a', 'b', 'l'); 1.6 (-CH_2 protons of polymer backbone, position 'k'); 5.14 (benzylic protons, position 'f'); 6.87 (phenyl ring protons, position 'd'; phenyl ring protons, position 'e'); 7.69-7.88(phenyl ring protons of TPP unit); 3.43 (-CH_3 protons, position 'm').

^{1}H-NMR analysis of **P6** (500 MHz, $CDCl_3$, δ ppm) (Figure 8) : 1.3-0.8 (-CH_2 and –CH and –CH_3 of polymer backbone, position 'a', 'b', 'l'); 1.86 (-CH_2 protons of polymer backbone, position 'k'); 5.2-5.3 (benzylic protons, position 'f'); 6.56-6.65

(phenyl ring protons, position 'd'; phenyl ring protons, position 'e'); 7.60-7.76 (phenyl ring protons of TPP unit); 3.46 (-CH_3 protons, position 'm').

^{1}H-NMR analysis of **P7** (500 MHz, $CDCl_3$, δ ppm) (Figure 9) : 1.36-1.18 (-CH_2 and –CH and –CH_3 of polymer backbone, position 'a', 'b', 'l'); 2.03 (-CH_2 protons of polymer backbone, position 'k'); 5.2-5.4 (benzylic protons, position 'f'); 6.56-6.66 (phenyl ring protons, position 'd'; phenyl ring protons, position 'e'); 7.52-7.76 (phenyl ring protons of TPP unit); 3.46 (-CH_3 protons, position 'm').

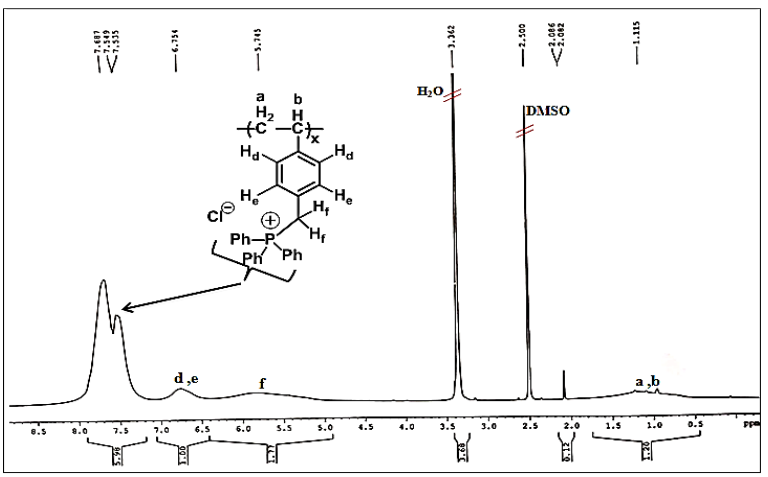

Figure 1. ^{1}H-NMR spectrum of **P[VBTP][Cl]** in DMSO-d_6.

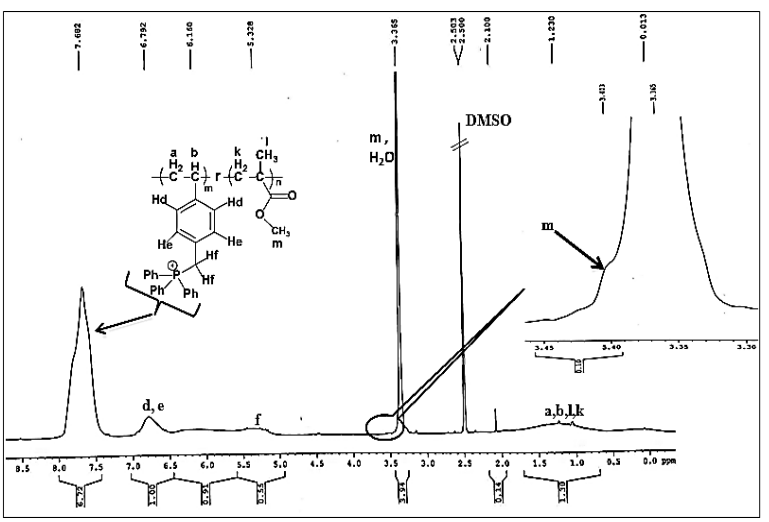

Figure 2. ^{1}H-NMR spectrum of **P1** in DMSO-d_6.

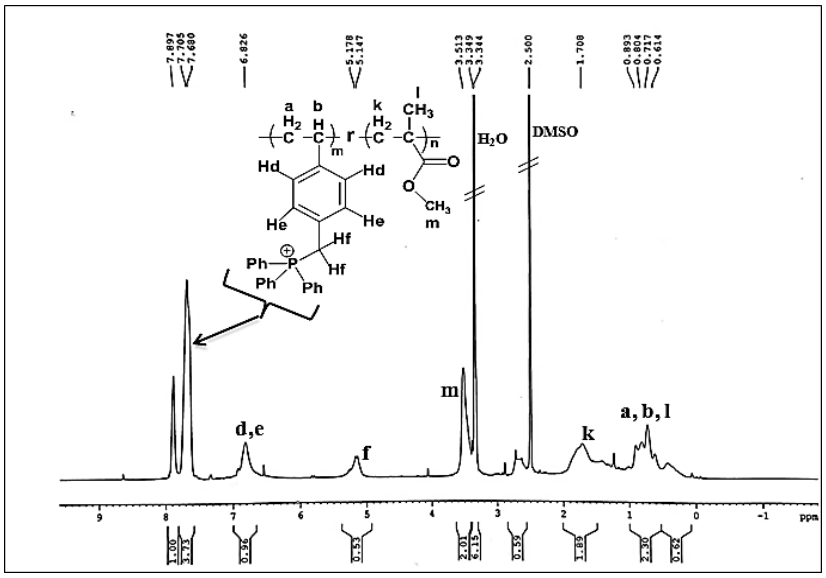

Figure 3. ^{1}H-NMR spectrum of **P2** in DMSO-d_6.

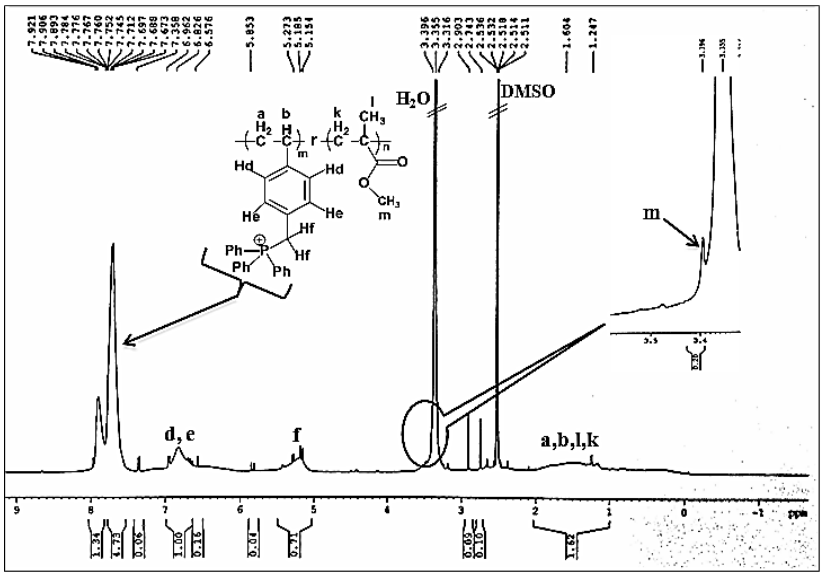

Figure 4. ^{1}H-NMR spectrum of **P3** in DMSO-d_6.

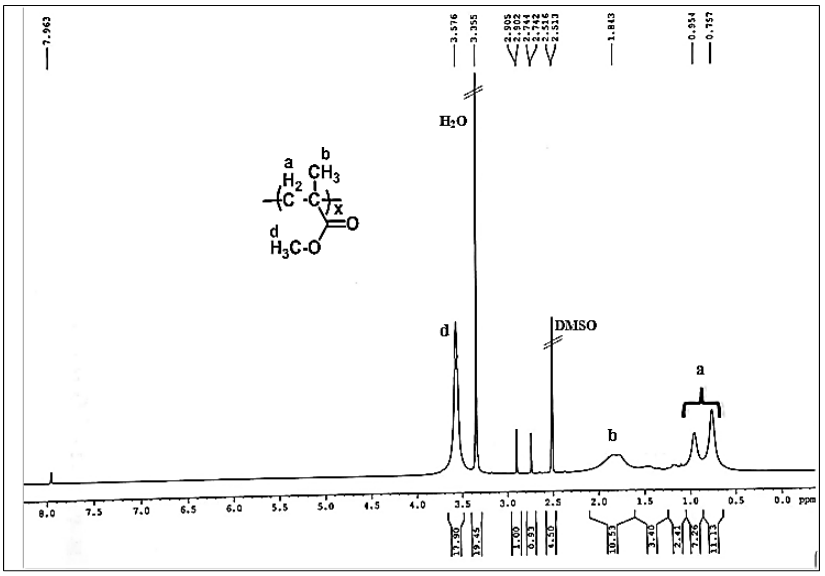

Figure 5. ^{1}H-NMR spectrum of **PMMA** in DMSO-d_6.

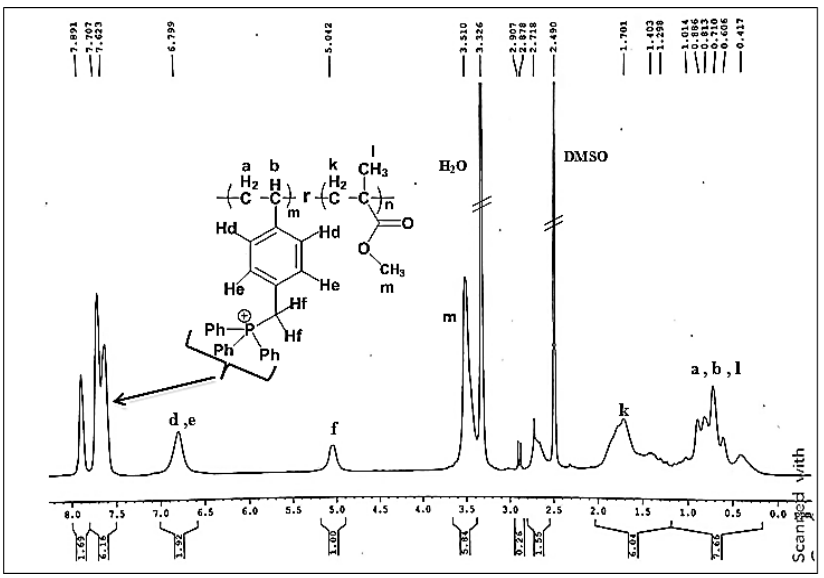

Figure 6. ^{1}H-NMR spectrum of **P4** in DMSO-d_6.

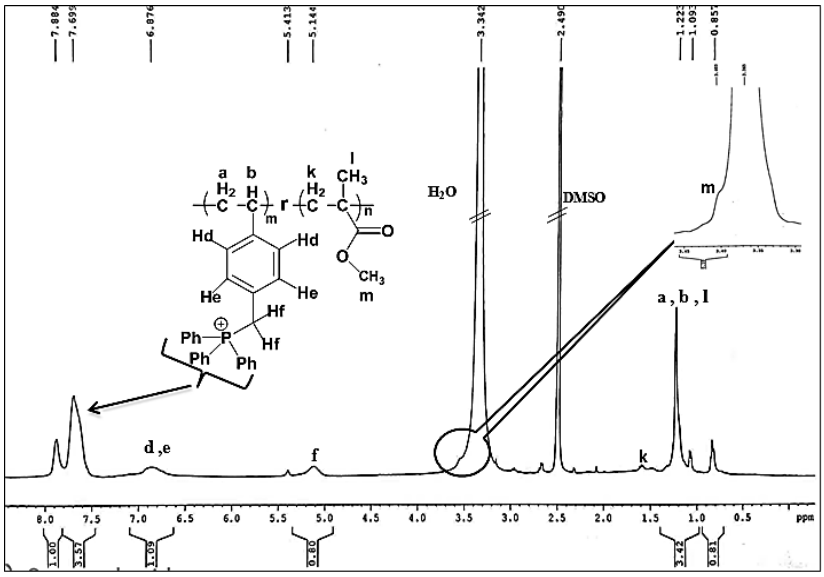

Figure 7. ^{1}H-NMR spectrum of **P5** in DMSO-d_6.

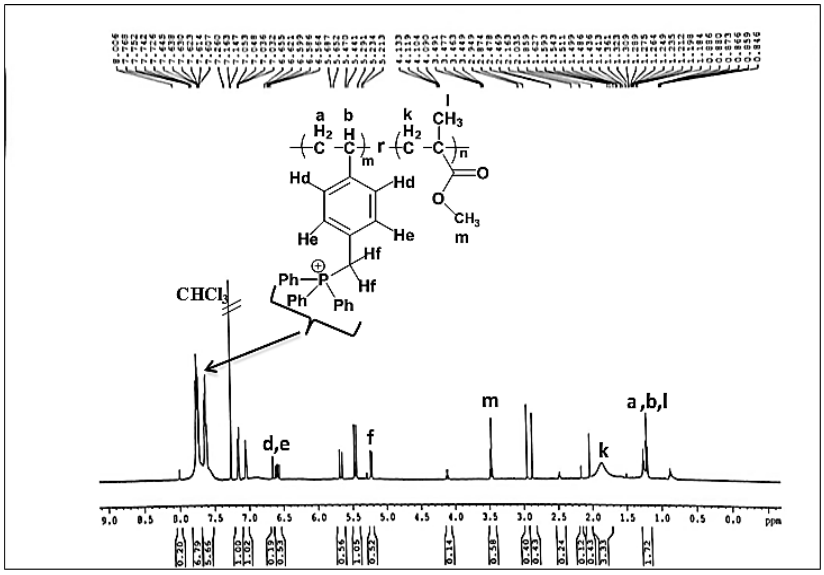

Figure 8. ^{1}H-NMR spectrum of **P6** in $CDCl_3$.

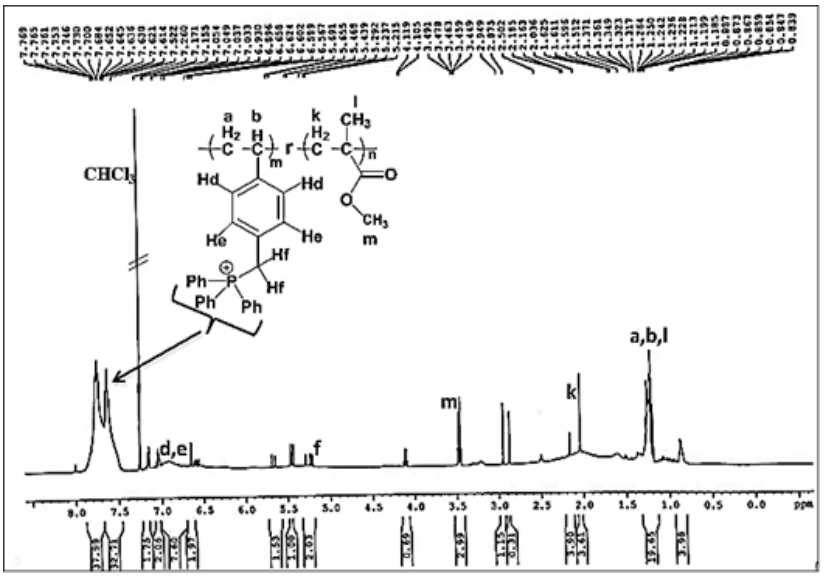

Figure 9. ^{1}H-NMR spectrum of **P7** in $CDCl_3$.

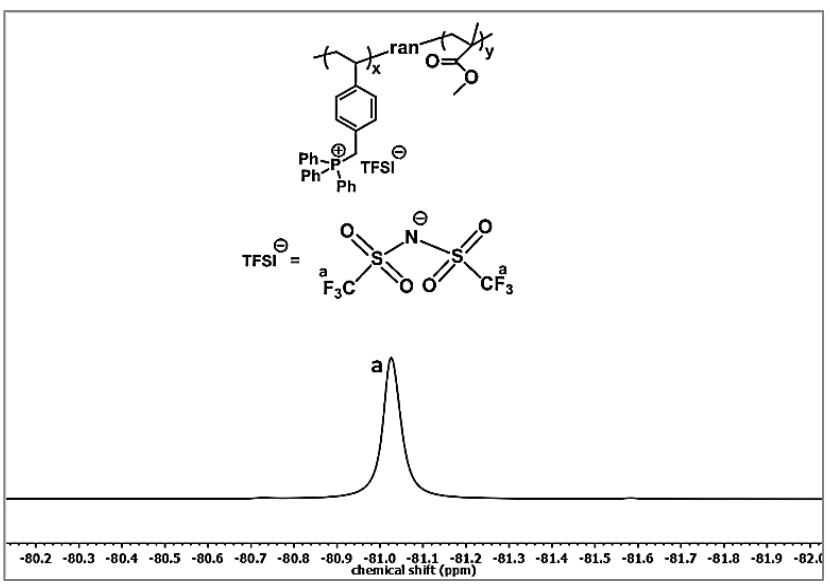

Figure 10: ^{19}F NMR spectra of **P4** in DMSO-d_6.

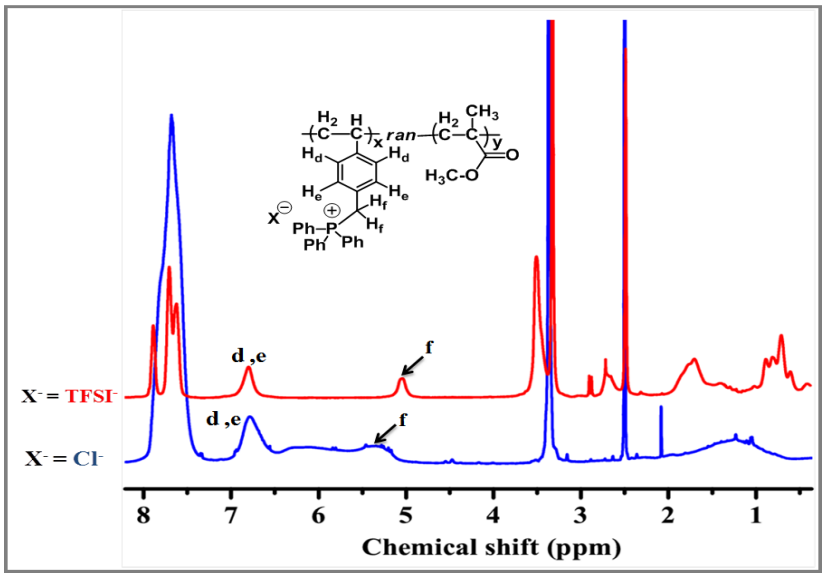

Figure 11: ^{1}H-NMR spectrum of **P3** (blue) and anion exchanged analog of **P3** i.e., **P4** (red) in DMSO-d_6.

The SEC traces of PMMA, P[VBTP][Cl] and PIL –copolymers are shown in Figure 12. The unimodal nature of the peaks indicated the absence of high and low molecular weight species. The results obtained from SEC analyses are summarized in Table 1 .In case of **P5** copolymer, the shifting of peak towards higher elution volume indicated the substantial lowering of molecular weight in the presence of a CTA. The average molecular weights of the copolymer samples, **P6** and **P7**, were determined from the analysis of the corresponding MALDI-TOF mass spectrum (Figure 13). The most probable molecular weights (M_ps) of the copolymer samples, **P6** and **P7**, were determined from the strong signals present in their corresponding MALDI-TOF-MS spectrum at 2378 and 1391 *Da* respectively.

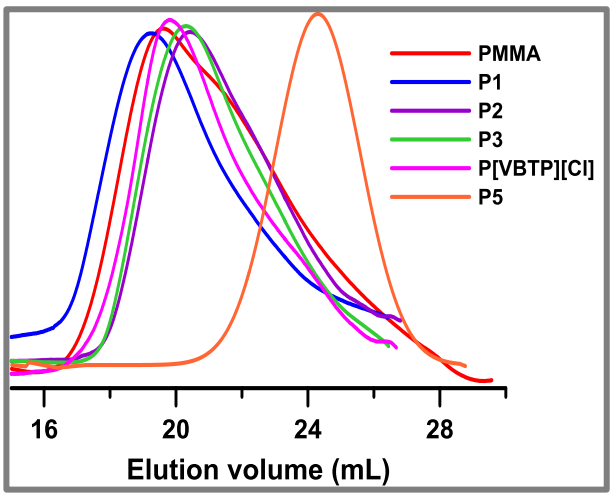

Figure 12. SEC traces of different homo and random PIL copolymers.

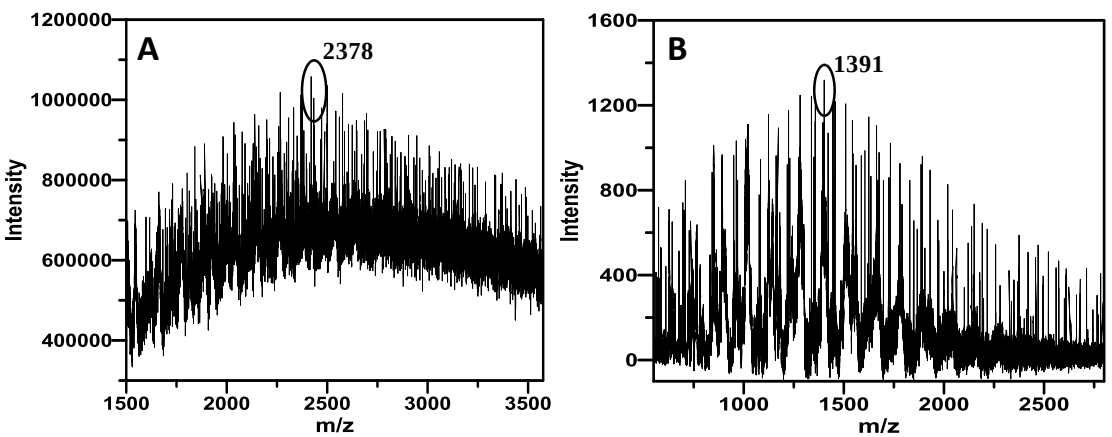

Figure 13. MALDI-TOF-MS spectrum of A) **P6** and B) **P7**.

3.4.2 Thermal Properties

PIL with higher thermal stability is one of the important factors for its application as an energy storage material. Thermal stability of any polymeric material mainly depends upon its chemical structure, degree of crystallinity, and molecular weight. On the other hand, thermal stability of polymer blends is strongly associated with their developed morphology which is a result of the compatibility and the composition ratio of the polymer components in the blend. The TGA traces of different PIL systems have been represented in Figure 14 and

the values of T_d of different PIL systems are listed in Table 2. The parameters obtained from TGA analysis, mainly the decomposition temperature (T_d), is controlled by the chemical structure of PIL backbone.[49] Measurement of thermal stability of samples **P2** and **P7** by TGA was not required as the major conclusion can be drawn without the analysis of these two samples. It can be seen from Table 2 that the PIL copolymers, **P1** and **P3,** showed decomposition temperatures above 316 °C which are much higher than those of neat P[VBTP][Cl] homo-PIL as well as physically mixed polymer blends of P[VBTP][Cl] and PMMA (**P8** and **P9**). The decomposition temperature is increased with the increase of non-ionic and hydrophobic poly(methyl methacrylate) (PMMA) segment in copolymers. On the other hand, the P[VBTP][TFSI]$_{80}$-*ran*-PMMA$_{20}$ (**P4**) showed higher value of T_d compared to that of P[VBTP][Cl]$_{80}$-ran-PMMA$_{20}$ (**P3)** which indicated that the

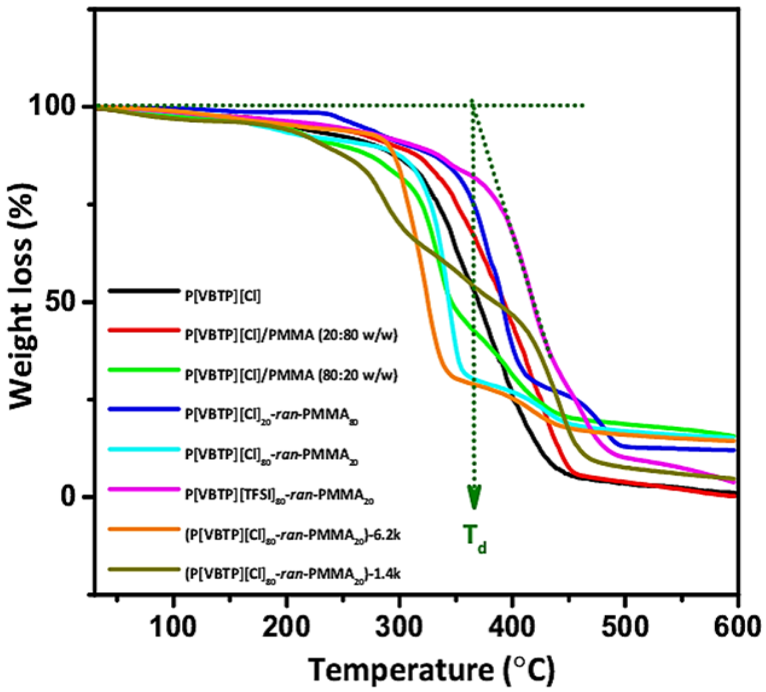

Figure 14. TGA traces of different PIL systems.

exchange of counter anion influenced the thermal stability of the PIL copolymers. The enhancement of thermal stability of PIL copolymer with $TFSI^-$ ion can be attributed to the higher nucleophilicity of the $TFSI^-$ ion.[50] As expected, Figure 14 also revealed that the thermal stability decreases with the decrease of M_n of PIL copolymers (**P5 and P7**) (Table 2). Moreover, the high thermal stabilities of PIL copolymers can enable them to use in high temperature electrochemical operation for energy storage applications such as Li-ion batteries, etc. Further, we have also measured the thermal stability of PMMA and PIL systems after their

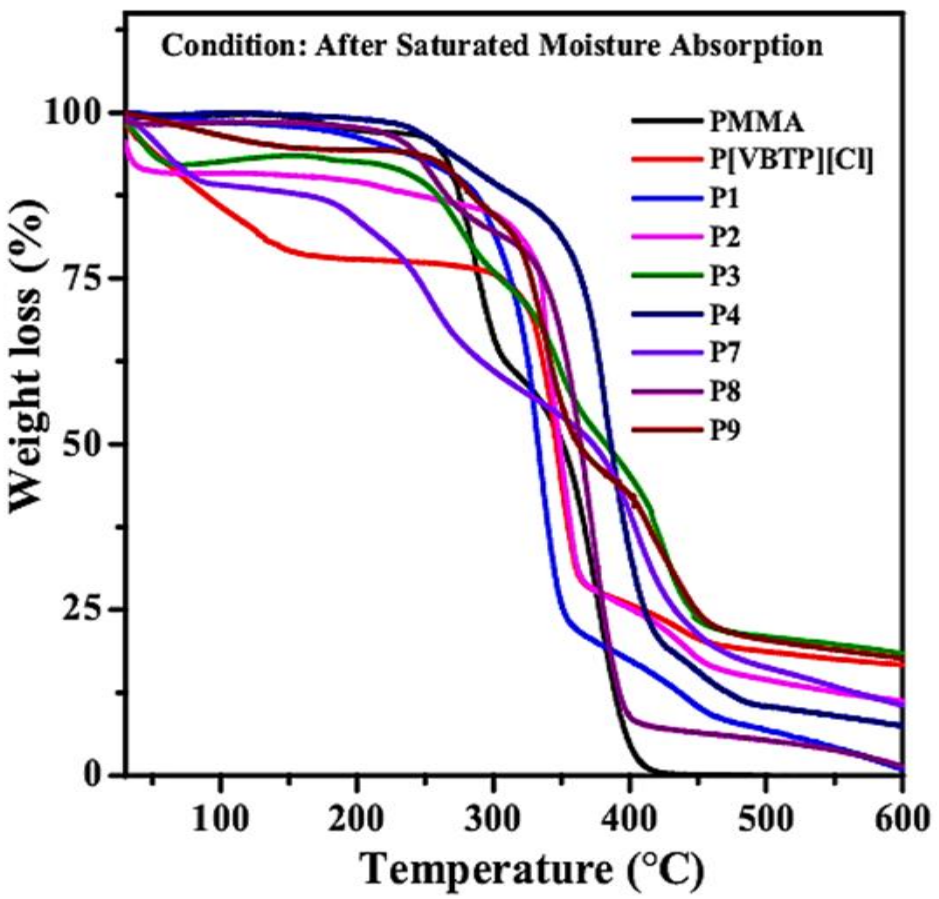

Figure 15. TGA traces of PIL copolymers after exposed with saturated water vapour.

complete exposure under saturated water vapor as shown in Figure 15. It was also observed from Figure 15 that the thermal stability of copolymers is still better than that of homo PIL after saturated amount of moisture absorption. The saturated water content of PMMA and different PIL systems such as PMMA, P[VBTP][Cl], **P1**, **P2**, **P3**, **P4**, **P7**, **P8** and **P9** were measured to be 0.24, 12.80, 1.13, 4.86, 6.41, 1.84, 10.45, 1.15 and 3.35 wt. % respectively. We found that the copolymers contain less amount of water than that of homopolymeric PIL due to the presence of hydrophobic PMMA segment in the copolymer. It should be noted that no glass transition temperature of the PIL copolymers could be detected by DSC (Figure 16). We have also measured the glass transition temperature for copolymers of other compositions and got similar results.

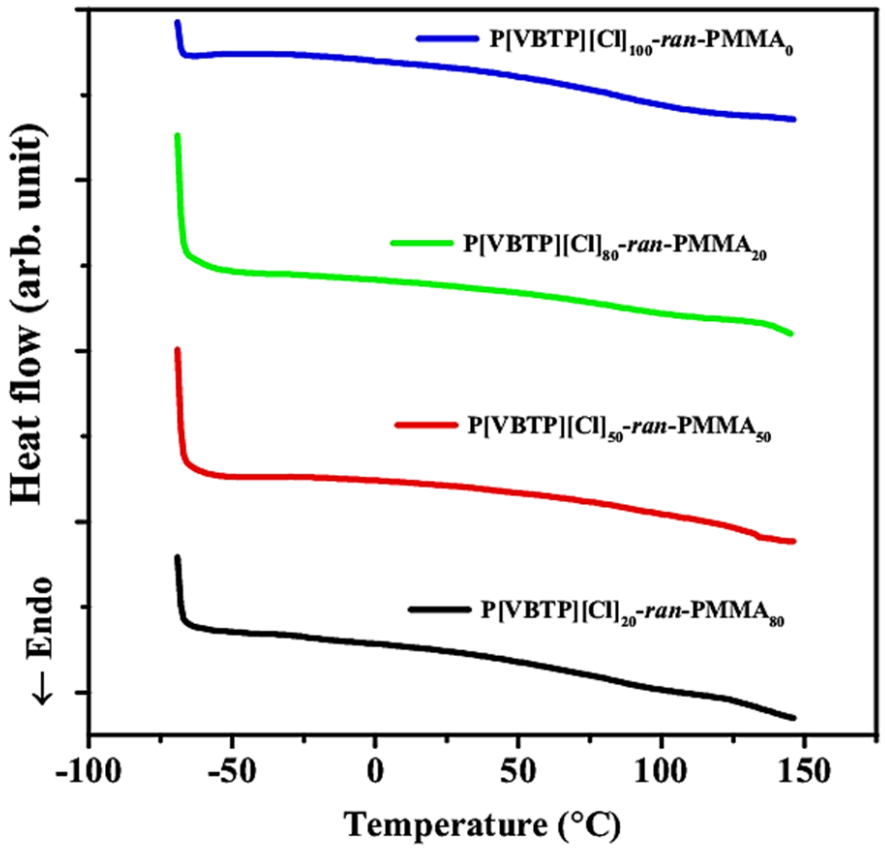

Figure 16: DSC traces of P[VBTP][Cl] copolymers.

Table 2: Decomposition temperature (T_d), ionic conductivity (σ_{dc}) at 303 K and power law exponent (n) at 333 K for the PIL and PIL based systems.

PIL systems	T_d (°C) (±4)	σ_{dc} (S cm^{-1})	n (±0.04)
P[VBTP][Cl]	301	1.96×10^{-6}	0.57
P[VBTP][Cl]$_{20}$-*ran*-PMMA$_{80}$(**P1**)	352	4.24×10^{-9}	0.62
P[VBTP][Cl]$_{50}$-*ran*-PMMA$_{50}$(**P2**)	NM	4.78×10^{-8}	0.55
P[VBTP][Cl]$_{80}$-*ran*-PMMA$_{20}$(**P3**)	316	1.95×10^{-7}	0.56
P[VBTP][TFSI]$_{80}$-*ran*-PMMA$_{20}$(**P4**)	365	2.96×10^{-8}	0.61
P[VBTP][Cl]$_{80}$-*ran*-PMMA$_{20}$-6.2k(**P5**)	288	1.77×10^{-5}	0.58
P[VBTP][Cl]$_{80}$-*ran*-PMMA$_{20}$-2.4k(**P6**)	NM	2.56×10^{-5}	0.56
P[VBTP][Cl]$_{80}$-*ran*-PMMA$_{20}$-1.4k(**P7**)	265	3.73×10^{-5}	0.54
P[VBTP][Cl]/PMMA (20:80 w/w) (**P8**)	324	5.32×10^{-11}	0.65
P[VBTP][Cl]/PMMA (80:20 w/w) (**P9**)	278	1.48×10^{-7}	0.58

NM ~ not measured

3.4.3 Dielectric Spectra of PIL Based Systems

Dielectric spectra, in general, can be represented in three frequency dependent complex quantities: the complex permittivity $\varepsilon^*(\omega) = \varepsilon'(\omega) - i\varepsilon''(\omega)$, the complex conductivity $\sigma^*(\omega) = \sigma'(\omega)+i\sigma''(\omega)$ and the complex electric modulus $M^*(\omega) = M'(\omega) + iM''(\omega)$, which are related to each other according to the following equation:[51]

$$M^*(\omega) = [M'(\omega)+iM''(\omega)] = 1/\varepsilon^*(\omega) = i\omega\varepsilon_0/\sigma^*(\omega) = i\omega\varepsilon_0/[\sigma'(\omega)-i\sigma''(\omega)],$$

where $\sigma'(\omega)$ and $\sigma''(\omega)$ are real and imaginary part of the complex conductivity respectively, and $M'(\omega)$ and $M''(\omega)$ respectively are real and imaginary part of complex electric modulus. It is to be noted that all these representations emphasize different aspects of the same process. Therefore, details which are not properly evident from one approach can be easily distinguished from the spectra in the other two representations.

In case of ionic compounds at low frequencies, ionic conductivity sharply increases in the dielectric loss function [$\varepsilon''(\omega)$] which completely masks the segmental relaxation present within the polymer chain. Accordingly, in order to understand the molecular dynamics of ionic polymers, such as PILs, the standard practice is to use the derivative formalism, which eliminates the conductivity contribution from the loss spectra. This issue can be avoided by analysing the dielectric properties using the complex electric modulus M*(ω) and complex electric conductivity σ*(ω) representations which are commonly used to represent dielectric data of conducting amorphous polymer materials.

Figure 17 represents a typical example of different representative forms of dielectric spectra for P[VBTP][Cl] at a temperature of 333 K. The dielectric constant $\varepsilon'(\omega)$ (orange), dielectric loss $\varepsilon''(\omega)$ (pink) and derivative of dielectric loss spectra (ε''_{der}) (green) of P[VBTP][Cl] are given in Figure 17a. The derivative of loss spectra ε''_{der} [= $(-\pi/2)\times(\partial\varepsilon'/\partial n\omega)$] which satisfies the Kramers-Kronig relation can reveal all other relaxation processes, which are actually suppressed by conductivity relaxation processes.[52-53]

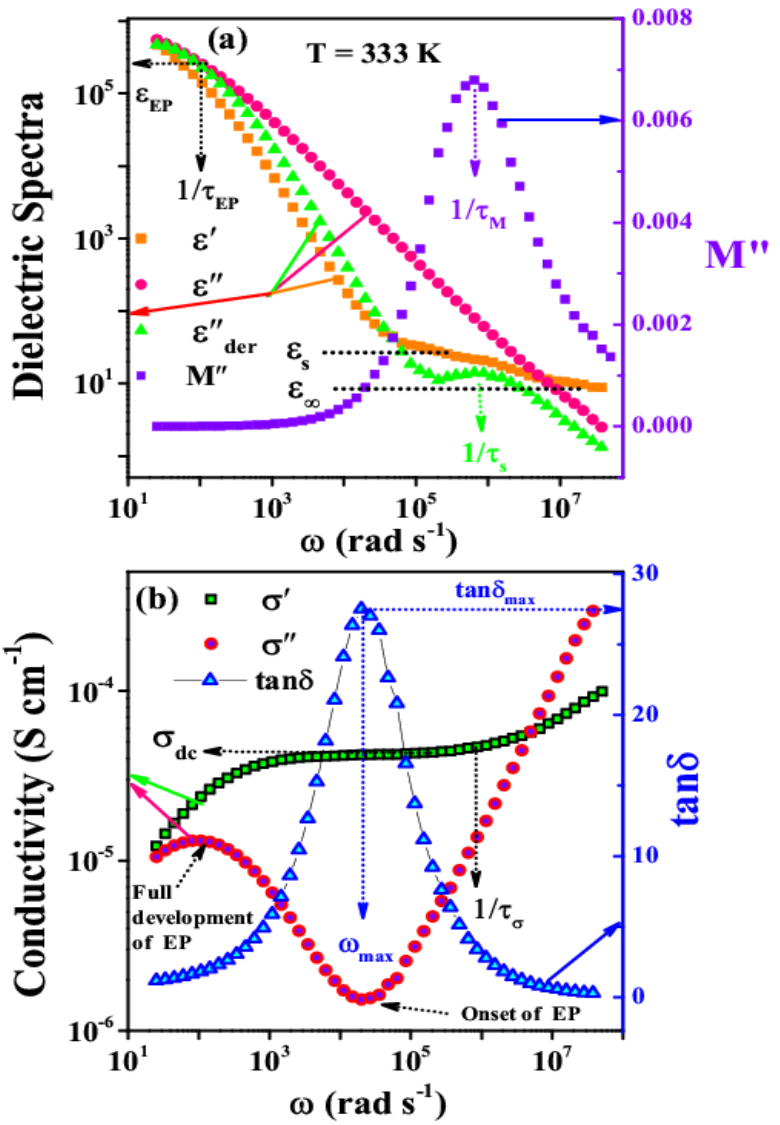

Figure 17. Dielectric spectroscopic data in several representations for P[VBTP][Cl]: (a) dielectric constant (ε') (orange solid squares), dielectric loss (ε'') (pink solid circles), derivative of dielectric loss (ε''_{der}) (green solid triangles) and modulus loss (M'') (violet diamonds) and (b) real part of complex conductivity (σ') (black open squares), imaginary part of complex conductivity (σ'') (red open circles) and loss tangent ($tan\delta$) (blue open triangles).

The M'' (imaginary part of M^* response) of P[VBTP][Cl] has been shown in Figure 17a. The real $\sigma'(\omega)$, imaginary $\sigma''(\omega)$ parts of the complex conductivity and $tan\delta$ are displayed in Figure 17b as a function of angular frequency ($\omega = 2\pi f$). The dielectric permittivity spectra of P[VBTP][Cl] showed three major mutually correlated phenomena: (i) electrode polarization (EP), (ii) dc conductivity and (iii) dielectric relaxation process in the low, medium and high frequency region respectively. A huge increase of dielectric constant (ε'), dielectric loss (ε'') and derivative spectra (ε''_{der}) with decreasing angular frequency including a small plateau in low frequency region was observed due to the formation of a space charge layer by the accumulation of charge carrier near metallic blocking electrodes (Figure 17a). Actually, the quick voltage drops due to the absence of ion drift in this region creates a large EP of the materials. This response was also reflected in the real and imaginary parts of the complex conductivity function and the value of conductivity decreased with decreasing angular frequency in the low frequency region as can be seen clearly in Figure 17b.[54] Generally, EP is an extrinsic and non-equilibrium phenomenon. It is directly linked to charge carrier dynamics as well as dependent on the thickness of the specimen, nature of the electrode interface and type of material of the electrode.[55-56] As shown in Figure 17a, a sharp increase in values ε' and ε''_{der} was observed at a certain angular frequency where the EP effect began corresponding to a minimum in the imaginary part [$\sigma''(\omega)$] of complex conductivity (Figure 17b). Such angular frequency (ω) was denoted as ω_{on} corresponding to onset of the EP process, i.e., ions reached the metal electrode and began to accumulate on the electrode surface. The full development of EP in the specimen occurred at a certain angular frequency, $\omega \approx \omega_{max}$, corresponding to a peak in imaginary part, $\sigma''(\omega)$ of complex conductivity where a slope in dielectric constant ($\varepsilon'(\omega)$) started towards low frequency in dielectric permittivity (Figure 17a). A frequency independent

plateau region (Figure 17b) was observed in the mid frequency region of $\sigma'(\omega)$ corresponding to ionic conductivity of the material representing long-range ion diffusion through successive hopping process from one favorable site to other neighboring site in a polymer network. A shoulder/plateau like feature (Figure 17a) was also observed in $\varepsilon'(\omega)$ in the same frequency region. Any value of dielectric constant in this region was denoted as static dielectric constant (ε_s), which is linked with long range ion hopping process. A leveling off was observed in the PILs under applied electric field towards the higher frequency region which is denoted as ε_∞ (high frequency limit value) in $\varepsilon'(\omega)$. However, the corresponding conductivity value significantly increased with the increase of frequency due to dipolar relaxation in the high frequency region, which is denoted as frequency dispersive region (Figure 17b). In spite of having bulk characteristics and EP features, the dielectric loss data sharply decreased with the increase of frequency (Figure 17a). However, ε''_{der} showed a prominent peak at high frequency region corresponding to segmental relaxation time (τ_s) of polymer chain as suggested by other research groups.[29] On the other hand, a crossover region, where a jump from frequency independent region to dispersive region occurred, is generally known as the onset of the so-called hopping regime and hopping frequency can be denoted as $\omega_H = 1/\tau_H = 1/\tau_\sigma = \varepsilon_s\varepsilon_0/\sigma_0$, ε_0 (= 8.85×10^{-12} F m^{-1}) is the dielectric permittivity of free space.[55, 57] Alternatively, the dielectric spectra can be appropriately analyzed in terms of electric modulus, in which EP is suppressed at low frequency regime. As shown in Figure 17a, electric modulus loss $M''(\omega)$ displayed a long tail in low frequency region associated with large capacitance due to the electrode-electrolyte interface and a distinct peak related with a transition from long to short range ionic motion. Such peak is correlated to the conductivity relaxation.[58] The time when diffusions of ions start is known as conductivity relaxation time (τ_M).[39] In

this context, it noteworthy that the dc-conductivity (σ_{dc}), which is typically defined as the product of the number of ions and their mobility, is inversely proportional to the conductivity relaxation times τ_M(or τ_σ or τ_H) determined from the angular frequency of M" peak maximum ($\tau_M = 1/\omega_M$).[59]It should also be noted that peak maxima in $\varepsilon''_{der}(\omega)$ response, conductivity relaxation in $M''(\omega)$ response and hopping frequency (ω_H) in conductivity response are very close to each other and also provide vital information for the origin of the dielectric relaxation peak. The peak maximum (ω_{max}) in frequency dependence of $tan\delta$ curve was situated at the onset of EP response (Figure 17b). The mobile ion diffusivity and number density can be estimated using the value of $tan\delta_{max}$ and ω_{max} obtained from $tan\delta$ spectroscopy employing the Macdonald-Trukhan model.[60-62] It is worth to mention that the diffusivity and number density of ions in electrolyte materials can also be estimated from this model, which are usually over estimated compared to that obtained from the PFG-NMR technique.[63] However, several authors have calculated the diffusivity and ion number density using the physical model proposed by the Macdonald-Coelho, which agreed well with the value obtained from the PFG-NMR.[39, 64-65]

3.4.4 Analysis of Conductivity Spectra

The real $\sigma'(\omega)$ part of complex conductivity $\sigma^*(\omega)$ spectra of the P[VBTP][Cl], P[VBTP][Cl]$_{80}$-*ran*-PMMA$_{20}$ and P[VBTP][TFSI]$_{80}$-*ran*-PMMA$_{20}$ in the frequency range of 4 Hz - 8 MHz at different temperatures are presented in Figure 18. The conductivity spectroscopy is often analyzed by using several physical model such as universal power law (UPL) model based upon non-uniform hopping distance with multidimensional arbitrarily varying potential barriers,[66] random barrier model (RBM) based on the uniform hopping distance with equal potential landscape,[67] etc.. As already discussed in Chapter 1, ions transport in polymer electrolyte occurs via hopping of ions from one favorable site to other site in

intra- and inter-polymer chains as well as thermal mobility of polymeric chains.[68] Due to thermal chain dynamics, a new favorable position is created by destroying their old accessible position in polymeric network. Thus, polymeric system represents a media where exists a non-uniform hopping distance with arbitrary potential landscape. There is a restriction of RBM applicability in the frequency range near dc to ac conductivity transition and significant deviations exist between model predictions and experimental data. Thus RBM is unable to describe the whole conductivity spectra of these PIL materials. Therefore, it is appropriate to analyze the conductivity spectra using UPL model.[42] At first**,** the conductivity spectra of P[VBTP][Cl] (Figure 18a) were analyzed using UPL model,[66, 69] as it is the best for describing polymer electrolyte systems. According to UPL model, the real conductivity $\sigma'(\omega)$ can be expressed in terms of dc conductivity σ_{dc} and hopping (diffusion) rate of ion ω_H ($\sim 1/\tau_H$) as:

$$\sigma'(\omega) = \sigma_{dc}\left[1+\left(\frac{\omega}{\omega_H}\right)^n\right] \quad , \qquad (1)$$

where n is an exponent ($0 < n \leq 1$), related to interactions between mobile ions and dimensionality of conduction pathway.[70] However, this relation is not applicable for materials with EP effect in low-frequency region at relatively high temperatures. Figure 18a shows the fitting of the real part $\sigma'(\omega)$ of complex conductivity spectra in the dispersive region to Eq. 1. The analyses of conductivity spectra of P[VBTP][Cl]$_{80}$-*ran*-PMMA$_{20}$ (Figure 18b) and P[VBTP][TFSI]$_{80}$-*ran*-PMMA$_{20}$ (Figure 18c) can also be done by applying the same UPL model as used for neat P[VBTP][Cl] (Figure 17a). Figure 18 also reveals that the UPL model can be fitted well with the real part of the conductivity spectra of P[VBTP][Cl] of PIL homopolymer, PIL copolymer and ion exchanged PIL copolymer.

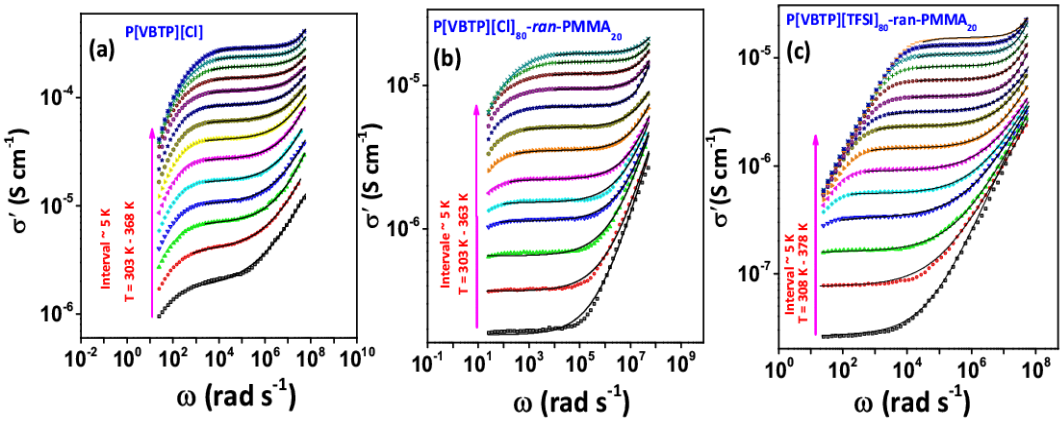

Figure 18. Real $\sigma'(\omega)$ part of complex conductivity spectra of P[VBTP][Cl] (a), P[VBTP][Cl]$_{80}$-*ran*-PMMA$_{20}$ (b) and P[VBTP][TFSI]$_{80}$-*ran*-PMMA$_{20}$ (c) respectively in the frequency ranges from 4Hz- 8MHz at different temperatures. The black lines in Figures 18a-18c were fitted to Eq. 1

3.4.5 Ionic Conductivity and Relaxation Time

Figure 19 reveals that the ionic conductivity which is the key factor for applications of the material, as obtained from the fitting of complex conductivity spectra, increased with the increase of temperature for each PIL system. It should be noted that the ionic conductivities of P[VBTP][Cl] and different PIL samples (**P1** to **P9**) at 303 K are given in Table 2. As shown in Figure 19a, the ionic conductivity of the PIL copolymers was high and increased with the increase of ionic content in these copolymers (**P1-P3**). It was also observed that the ionic conductivity of blend samples (**P8-P9**) was slightly lower than those of their corresponding copolymers (**P1** and **P3**) containing same ionic PIL content (Figure 19a). The cross-

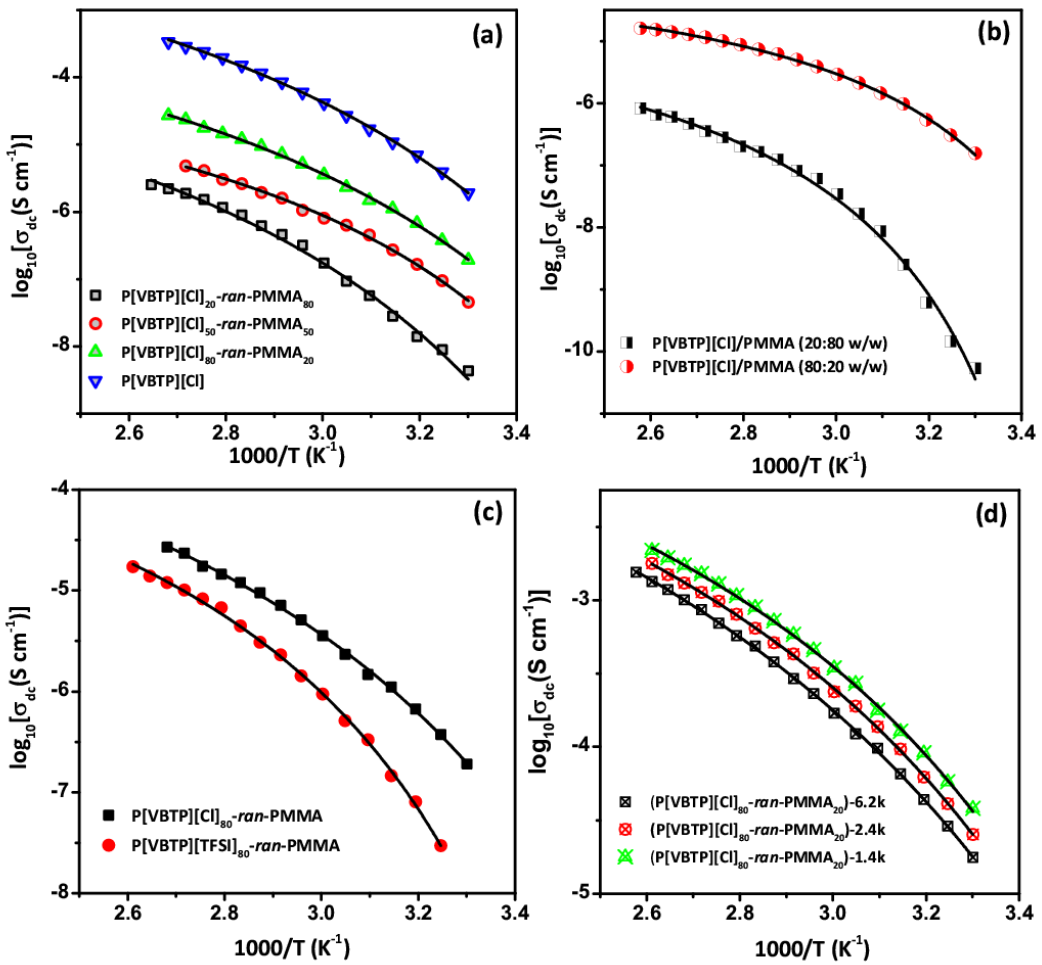

Figure 19. (a)-(d) Reciprocal temperature dependence of ionic conductivity, σ_{dc} for P[VBTP][Cl] and different P[VBTP][Cl] based systems. Solid black lines are best fits to VTF equation (Eq. 2).

sectional FESEM images (Figure 20) of physical blend of P[VBTP][Cl]/PMMA and P[VBTP][Cl]-*ran*-PMMA copolymer clearly revealed the heterogeneous phase separated structure for the former and homogeneous structure for the later. The phase separation in P[VBTP][Cl]/PMMA blend is attributable to the immiscibility of non-ionic PMMA and ionic P[VBTP][Cl] phases. It seems that the ionic

P[VBTP][Cl] phase dispersed into the continuous PMMA matrix. The phase separation between ionic and non-ionic components lengthens the ion transport pathway, resulting in a lowering of the overall ionic conductivity in physically mixed ionic PIL/non-ionic polymer system. Zhang and co-workers quantitatively established the correlation between ionic conductivity and extent of phase separation and observed that nano-scale phase separation rather than large micro or micro is more favorable to increase the ionic conductivity.[71] In case of our materials, micro phase separation occurred for PIL/PMMA (20:80 w/w), whereas for higher concentration of PIL and lower concentration of PMMA (PIL/PMMA (80:20 w/w)), ionic conductivity increases whose value is slightly lower than the corresponding copolymer sample. The nanoscale phase separation in the blend films is probably the reason behind this observation. The values of

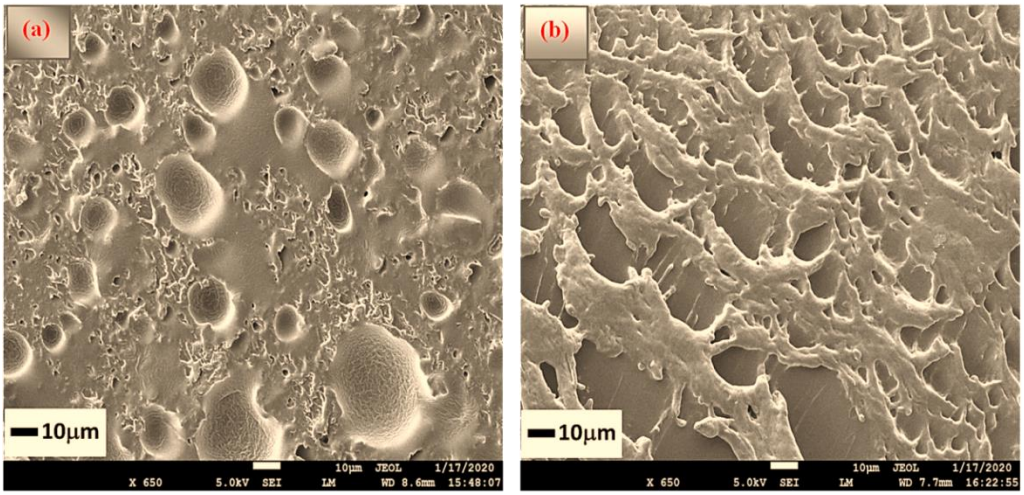

Figure 20. Cross-sectional field emission scanning electron microscopy (FESEM) images of freeze fractured samples: a**)** P[VBTP][Cl]/PMMA (20/80 w/w) binary homopolymer blend and b**)** P[VBTP][Cl]$_{20}$-*ran*-PMMA$_{80}$ copolymer.

ionic conductivity of **P4** copolymer (Table 2)with large-sized $TFSI^-$ anion showed lower value than that of PIL copolymer having same ionic content and small-sized Cl^- anion (Figure 19c). It is reported that the PIL chains are better packed when larger size counter anions are present while frustrated chain packing is observed for smaller size of counter anions.[72] The frustrated chain packing causes more disorder structure and leads to lower the energy barrier for ion transport from one site to another via hopping. The existence of smaller Cl^- anion in PIL copolymer (**P3**) leads to frustration chain packing compared to the corresponding large size $TFSI^-$ anion in **P4** copolymer.[72] However, there was a drastic increase of the ionic conductivity as the molecular weight (M_n) of PIL copolymer decreased from P[VBTP][Cl]-*ran*-PMMA-23k to P[VBTP][Cl]-*ran*-PMMA-6.2k (Table 2). When the decrease of molecular weight is less (PIL-*ran*-PMMA-6.2k to PIL-*ran*-PMMA-1.4k), the increase of conductivity was low. The enhancement of ionic conductivity with decrease of M_n occurred due to increase of ionic diffusivity which has been discussed later and ion motion becomes more correlated with structural relaxation at the same time.[73-74] It is also worth mentioning that the slight lower value of ionic content in **P6** and **P7** (Table 2) than that of PIL-ran-PMMA-6.2k (**P5**) did not influence the ionic conductivity values significantly. The ionic conductivity value followed the increasing trend after changing the M_n from 6.2 k to 1.4 k value due to faster segmental dynamics in **P6** and **P7** than that of **P5**. Table 2 revealed that the value of power law exponent *n* at a fixed temperature is almost independent of PIL and PIL related compositions and value of *n* lies between 0.54-0.65, indicating no change in correlation among PIL's compositional variation. Also, the average value of exponent $n \sim 0.57$ corresponds to a 3D conduction in the present PIL systems.[70]

Figure 19 shows that the temperature dependence of the ionic conductivity of PIL and PIL based systems exhibited the Vogel-Fulcher-Tammann (VTF)

behavior,[75-77] which has also been applied to understand the dynamical process of the various glassy and polymeric systems and is given by:

$$\sigma_{dc}(T) = \sigma_0' T^{-1/2} \exp\left[\frac{-E_\sigma}{k_B(T - T_0)}\right] , \quad (2)$$

where σ_0' is the pre-exponential factor, E_σ is the activation energy related to the critical free volume for ion transport and T_0 is the equilibrium Vogel scaling temperature. In this case, the σ_{dc} for all PILs and PIL copolymers has been fitted to Eq. 2 according to nonlinear least square fits and the results are shown in Figure 19. The values of fitting parameters E_σ and T_0 are displayed in Table 3.

To further advance our understanding of the ion transport mechanism in these PIL systems, we have explored the temperature dependence of conductivity relaxation time or hopping time (τ_H). The reciprocal temperature dependence of inverse hopping time ($1/\tau_H$) of P[VBTP][Cl] obtained from UPL model and that of its copolymers were obtained from the best fits of conductivity data (Figure 21), which also obeyed VTF behavior, given by

$$\tau_H(T) = \tau_0 \exp\left[\frac{E_H}{k_B(T - T_0')}\right] , \quad (3)$$

where τ_0, E_H, k_B and T_0' are constants.

The values of VTF fitting parameters E_H and T_0', obtained from the best fits, are given in Table 3, which revealed that the fit parameters E_σ, E_H, T_0 and T_0' obtained from both σ' and τ_H are very close to each other, indicating a common conduction and relaxation mechanism in this PIL and its random PIL copolymers. The VTF fits indicated that the ion conduction and relaxation is coupled with polymer segmental motion contributing to the conductivity.

Table 3: The parameters obtained from the fitting of VTF relation to the temperature dependence of ionic conductivity σ_{dc}, hopping time τ_H and free mobile ion diffusivity *D* and also Arrhenius fitting parameters to ion number density (*P*) for several PIL based systems.

PILs	Ionic conductivity		Hopping time		Ion diffusivity		Ion density	
	E_σ (eV) (±0.002)	T_0 (K) (±3)	E_H (eV) (±0.006)	T_0' (K) (±2)	E_D (eV) (±0.004)	T_0'' (K) (±4)	P_∞ (cm^{-3})	E_{dis}(meV) (±4)
P[VBTP][Cl]	0.025	224	0.031	223	0.022	235	1.6×10^{20}	65
P1	0.086	232	0.096	238	0.083	242	8.9×10^{18}	102
P2	0.065	238	0.062	234	0.073	231	1.2×10^{19}	90
P3	0.046	225	0.048	231	0.045	241	7.4×10^{19}	70
P4	0.049	252	0.054	240	0.061	243	4.2×10^{19}	86
P5	0.021	222	0.026	239	0.027	253	9.3×10^{20}	58
P6	0.018	218	0.021	235	0.021	243	1.1×10^{21}	53
P7	0.012	208	0.018	234	0.019	224	1.3×10^{21}	49
P8	0.095	250	0.11	255	0.094	227	6.9×10^{17}	124
P9	0.061	242	0.063	234	0.045	243	1.8×10^{19}	102

It has been observed that the increment of ionic content in PIL copolymers and lowering of molecular weight of PIL copolymers enhance the ionic conductivity. The size of counter ion and physical mixing of PIL and PMMA also influence the ionic conductivity. Ion conduction is also controlled by segmental motion of polymer chain. To analyze these effects, simultaneous determination of conducting ion number density and their diffusivity by using electrode polarization is more significant as mentioned below.

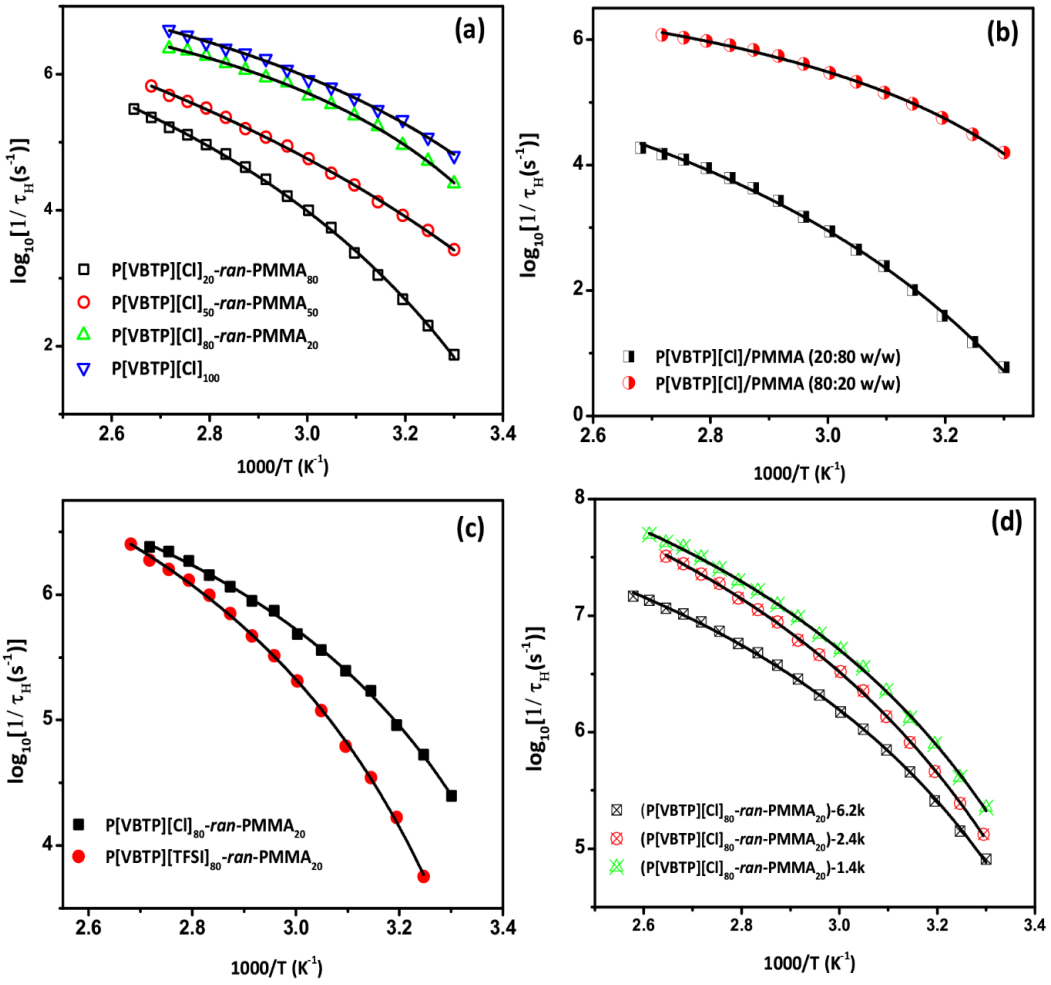

Figure 21. (a)-(d) Reciprocal temperature dependence of relaxation time $\tau_H(T)$ for PIL and different PIL copolymers. Solid black lines are the best fits to VTF equation (Eq. 3).

3.4.6 Conducting Ion Diffusivity and Number Density

We have simultaneously determined the free ion diffusivity (*D*) and ion number density (*P*) from the theoretical model for EP, occurring at the low frequency region of the dielectric spectra due to growth of ions at near metal electrode-PIL interface.[30, 78-79] According to Macdonald and Coelho model, the electrode

polarization can be described by loss tangent (*tan*δ), which can be expressed in terms of τ_σ and τ_{EP} as a simple case of Debye relaxation[80-81] as:

$$\tan\delta = \frac{\omega\tau_{EP}}{1+\omega^2\tau_\sigma\tau_{EP}} \quad , \tag{4}$$

where ω is the angular frequency, $\tau_{EP}(=\varepsilon_{EP}\varepsilon_0/\sigma_{dc})$ is the response of full development of polarization of conducting ions at the low frequency region and $\tau_\sigma(=\varepsilon_s\varepsilon_0/\sigma_{dc})$ is time scale for ion conduction, when ion motion becomes diffusive as described earlier in Figure 17.[78] The loss tangent spectra for a representative sample, P[VBTP][TFSI]$_{80}$-*ran*-PMMA$_{20}$ at different temperatures are presented in Figure 22a, where the solid black lines were obtained by fitting the data to Eq. 4 for temperatures 308 K and 368 K. The peak of loss tangent (*tan*δ) would usually occur at the geometric mean ($\omega = \tau_0^{-0.5}\tau_{EP}^{-0.5}$) of the τ_σ and τ_{EP} time scales.[18] For this sample, we observed that the *tan*δ peak shifted towards the higher frequency scale with increasing temperature.

The Macdonald and Coelho model, thus, can be used to simultaneously determine the free ion diffusivity (*D*) and ion number density (*P*) by τ_σ and τ_{EP}, obtained from *tan*δ fits with the help of the following equations:

$$D = \frac{L^2\tau_\sigma}{4\tau_{EP}^2} \text{ and } P = \frac{1}{\pi l_B L^2}\left(\frac{\tau_{EP}^2}{\tau_\sigma}\right), \tag{5a, 5b}$$

where *L* is thickness of the sample, $l_B\ (=e^2/4\pi\varepsilon_s\varepsilon_0 k_B T)$ is the Bjerrum length, k_B is Boltzmann constant and *T* is absolute temperature.

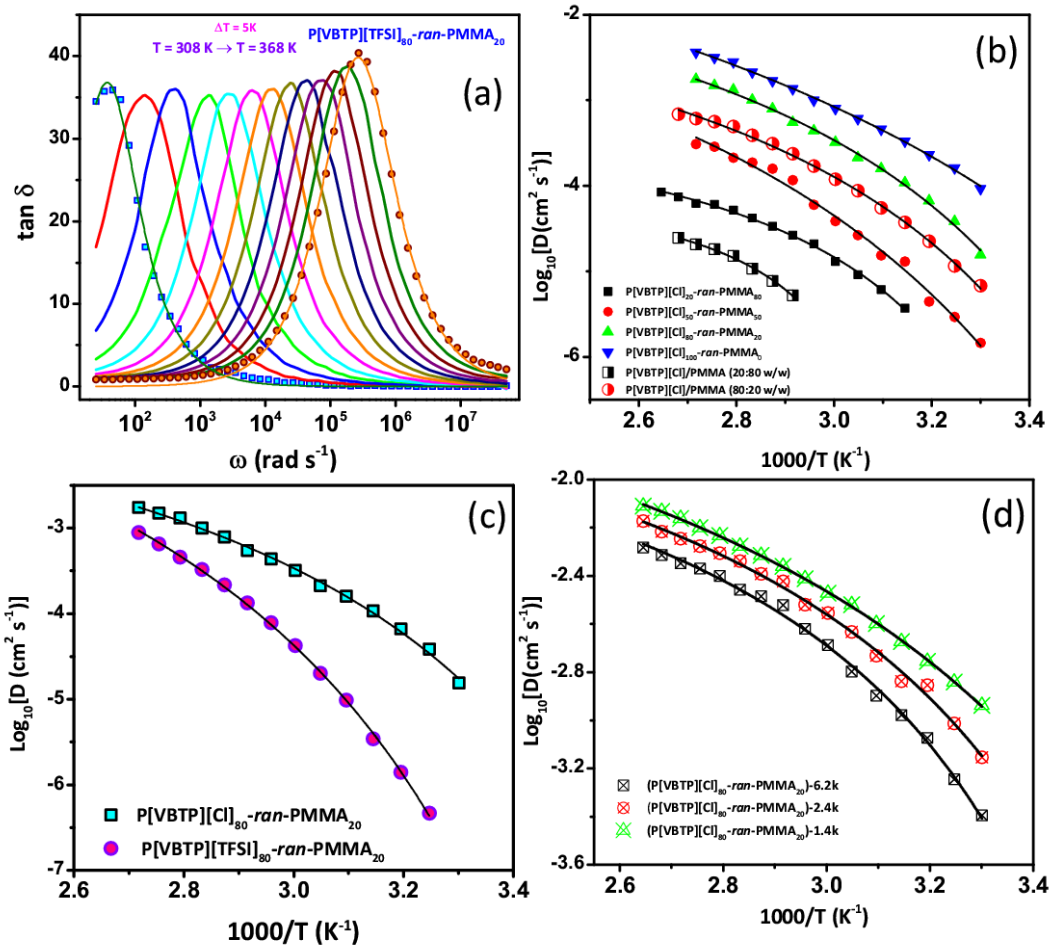

Figure 22: (a) A representative plot of angular frequency dependence of tan δ for P[VBTP][TFSI]$_{80}$-*ran*-PMMA$_{20}$ PIL (**P4**) at several temperatures and solid lines in Figure 10a for temperature 308 K and 368 K are fits to Eq. 4, **(b), (c)** and **(d)** Reciprocal temperature dependence of diffusivity, *D* obtained from Macdonald-Coelho model for different P[VBTP][Cl] copolymers, physical mixture of P[VBTP][Cl] and PMMA systems, TFSI-based PIL copolymer and P[VBTP][Cl] copolymers of different M_n.

The reciprocal temperature dependence of ion diffusivity for different PIL-based systems is given in Figures 22b-22d. It can be observed from Figure 22

that the ion diffusivity, *D* obeys the VTF behavior because *D* is controlled by polymer segmental motion and is expressed by the following equation:

$$D = D_{\alpha} \exp\left(\frac{-E_D}{k_B(T - T_0'')}\right), \quad (6)$$

where D_{∞} and T_0'' are the infinite temperature diffusivity and Vogel temperature respectively and E_D is the activation energy for the ion diffusivity. The solid black lines were the best fitted lines to Eq. 6 (Figures 22b-22d), and the fitting parameters are listed in Table 3. It is to be noted that the values of VTF fitting parameters for diffusivity were close to those obtained from the fits of σ_{dc} as well as τ_H. Thus, it can be concluded that the ion transport and relaxation were coupled with the polymer segmental motion and obeyed a common fundamental mechanism. Further, the ion diffusivity of different P[VBTP][Cl] copolymers increased with the increase of ionic PIL content in copolymer, while the ion diffusivity decreased when P[VBTP][Cl] was physically mixed with PMMA (Figure 22c). Figure 22c shows that the diffusivity of free conducting $TFSI^-$ ion decreased in P[VBTP][TFSI]$_{80}$-*ran*-PMMA$_{20}$ in comparison to that of Cl^- anion in P[VBTP][Cl]$_{80}$-*ran*-PMMA$_{20}$ PIL due to comparatively larger size of $TFSI^-$ ion. The enhancement of ion diffusivity (mobility) with lowering the molecular weight of PILs can also be clearly seen from Figure 22d. As per the earlier report, the ion transport (diffusivity) is directly linked with polymer segmental motion (structural relaxation) and the segmental motion increases with the decrease of molecular weight of PILs. Therefore, our result matched with what was reported earlier.[73]

The reciprocal temperature dependence of ion number density *P* for different PIL systems is presented in Figure 23. The data clearly shows that the value of *P* increased with the increase of temperature. However, the number

density followed a linear Arrhenius behavior at low temperature, which can be expressed as:

$$P = P_{\alpha} \exp\left(\frac{-E_{dis}}{k_B T}\right), \quad (7)$$

where P_{∞} and E_{dis} correspond to the total ion number density at infinite temperature ($T \rightarrow \infty$) and the dissociation energy. Figure 23 also indicated that the ion number density increased with the increase of ionic content in PIL copolymers (**P1**-**P3**), while its values were relatively lower for physical blends of P[VBTP][Cl]/PMMA (**P8** and **P9**). It is also worthy to note that the $TFSI^-$ ion number density in P[VBTP][TFSI]$_{80}$-*ran*-PMMA$_{20}$ is lower than that of Cl^- anion in P[VBTP][Cl]$_{80}$-*ran*-PMMA$_{20}$ due to larger size of $TFSI^-$ anion. On the other hand, number density increased with the decrease of molecular weight of the PIL copolymers (**P5**-**P7**). The number of ions that contribute to the conductivity in each of these PIL systems at any given instant is thus consistent with the variation of ionic conductivity. The values of P_{∞} and E_{dis} were obtained from the Arrhenius fits of the data shown in Figure 23 and the fitting parameters are listed in Table 3. It can be seen from Table 3 that the largest value of E_{dis} was observed for P[VBTP][TFSI]$_{80}$-*ran*-PMMA$_{20}$ in comparison to that of P[VBTP][Cl]$_{80}$-*ran*-PMMA$_{20}$ due to the large size of the $TFSI^-$ anion.

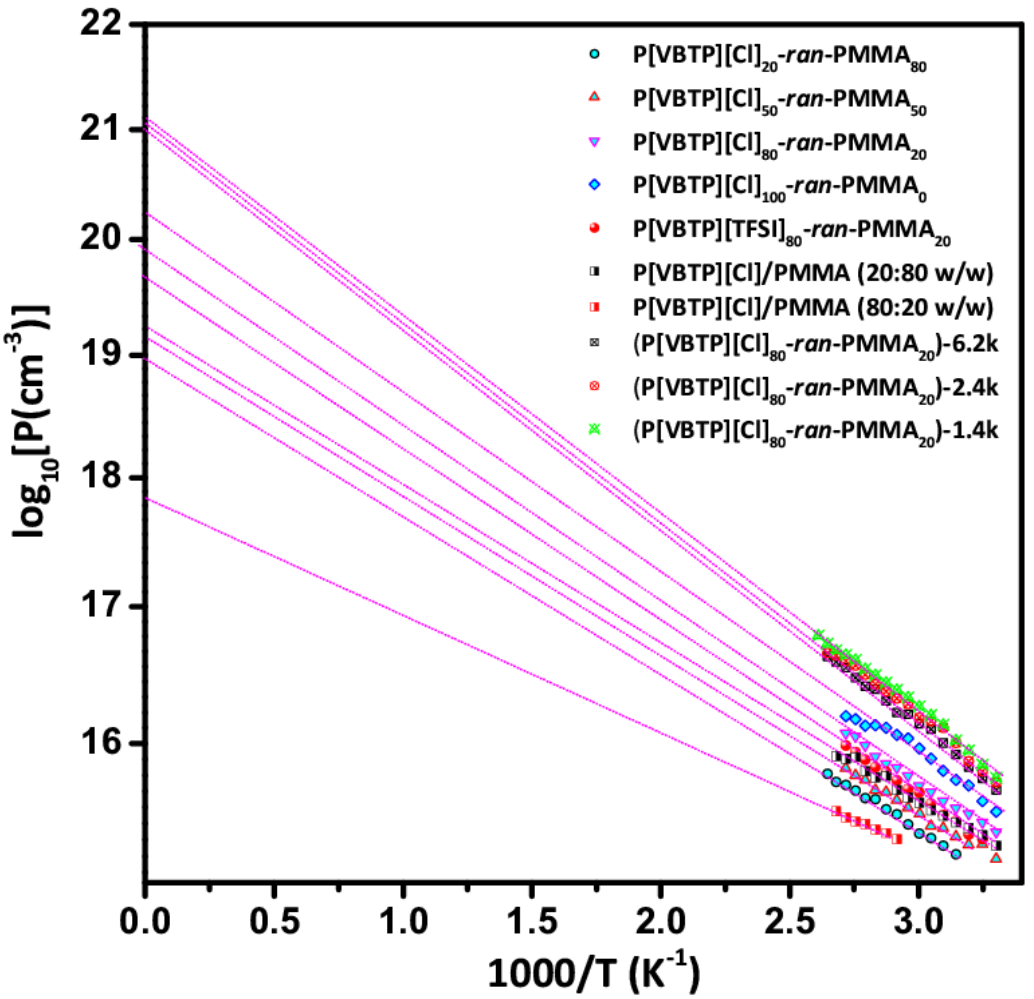

Figure 23: Reciprocal temperature dependence of free ion number density of different PIL based systems with the linear region at low temperature extrapolated to infinite temperature.

It is worth mentioning that PIL and PIL based materials have been developed enormously to understand some fundamental aspects of their ion transport and relaxation mechanism, but a question about the applications of these materials are still a challenge for the materials scientists. Recently, Peltekoff and co-workers[82] fabricated thin-film transistors (TFTs) by using the very similar type of copolymers (P[VBBI$^+$TFSI$^-$-ran-MMA]) forming an electric

double-layer (EDL) resulted in n-type TFT devices. More recently, Zhang and co-workers[71] demonstrated an alternating strategy to obtain solid polymer electrolytes having high mechanical strength, high ionic conductivity, high electrochemical stability and less Li dendrites growth by blending of copolymer based PIL (PPaB-MT) and P(VdF-HFP) containing 20% LiTFSI salt for Li-ion batteries. Cai and co-workers[83] also synthesized PIL based quasi-solid-state copolymers (PEGDA-P(BA-co-[EVIm]TFSI) QPE-IL) for lithium-sulfur batteries. Safa and coworkers[84-85] also synthesized a PIL (PDADMATFSI) based composite gel polymer electrolytes (PIL-EMIMTFSI-1 M LiTFSI) for lithium metal batteries (LMB). In this context, we have investigated the physicochemical properties such as thermal stability, moisture sensitivity and ion transport properties to know the applicability of our PIL based materials in energy storage applications. A comparison of such properties of some of the recently reported PILs and PIL based random copolymers along with our recent work is presented in Table 4. As observed from Table 4 that the PIL, P[VBTP][CL] and PIL based random copolymers showed good thermal stability, less moisture sensitivity and good ionic conductivity and that fundamental view ensures the potential use of these materials as polymer electrolytes in energy storage devices.

Table 4: A comparison of decomposition temperature, moisture content, ionic conductivity of some of the recently reported PILs and PIL based random copolymers.

PILs and PIL copolymers	Decomposition temperature (T_d) (°C)	Moisture content (wt%)	Ionic conductivity (S cm^{-1})	Ref.
Poly(VBBI$^+$TFSI$^-$-*ran*-MMA)-34.4	-	-	1.6×10^{-9}	82
Poly(MMA-*r*-MEBIm-TFSI-15.4)	268	-	2.5×10^{-9} @ 383 K	86
PIL-copolymer (PPaB-MT)	~ 270	-	-	71
Poly(HMA-*co*-MEBIm-BF_4)-34.5 mol% HMA	~ 300		~ 2.5×10^{-6} @ 360 K	50
Poly(MEBIm-TFSI-*co*-MEBIm -BF_4)-32.8 mol% TFSI	~ 350	-	~1×10^{-5} @ 360 K	50
Poly-EGIm TFSI	278	-	3.9×10^{-7} @ 300 K	3
SBMIm poly-SEM	260	13.8	2.5×10^{-5} @ 300 K	3
P[C_{18}Vim][Br]	~ 290	-	~5×10^{-8} @ 298 K	38
[PS-TAC][Cl]	-	-	~ 1×10^{-8} @ 303 K	16
P[VBTP][Cl]	301	12.8	1.96×10^{-6} @ 303 K	This work
P[VBTP][Cl]$_{80}$-*ran*-$PMMA_{20}$	316	6.41	1.95×10^{-7} @ 303 K	This work
P[VBTP][TFSI]$_{80}$-*ran*-$PMMA_{20}$	365	1.84	2.96×10^{-8} @ 303 K	This work
P[VBTP][Cl]$_{80}$-*ran*-$PMMA_{20}$-1.4k	265	10.45	3.73×10^{-5} @ 303 K	This work

3.5. CONCLUSIONS

A series of poly(ionic liquid) random copolymers comprising of ionic PIL and non-ionic PMMA segments were synthesized by using both free radical polymerization as well as reversible addition-fragmentation chain-transfer (RAFT) polymerization methods. The influence of copolymer compositions, counter anions (Cl^- and $TFSI^-$) and molecular weight as well as physical mixing of copolymer segments on ion transport and relaxation were investigated using broadband dielectric spectroscopy followed by analyzing the data using a theoretical model. The free ion diffusivity and ion number density of these random copolymers were obtained by analyzing the contribution of electrode polarization. The temperature dependence of ionic conductivity, relaxation time and ion diffusivity exhibited Vogel-Tammann-Fulcher behavior in these copolymers indicating ion transport controlled by segmental motion. With increasing ionic content of PIL, the ionic conductivity increased in the random copolymers. P[VBTP][Cl]$_{80}$-*ran*-PMMA$_{20}$ copolymer showed the ionic conductivity of 1.95×10^{-7} S cm^{-1} while the neat P[VBTP][Cl] exhibited the high ionic conductivity of 1.96×10^{-6} S cm^{-1} at room temperature. In spite of low ionic conductivity, the applicability of PIL copolymers as energy storage materials are higher because of their less moisture sensitivity due to incorporation of hydrophobic PMMA segment. The ionic conductivity decreased due to the introduction of larger counter anion $TFSI^-$ in the place of Cl^- ion in copolymer. Ionic conductivity increased with decreasing molecular weight. The random PIL copolymers showed a better thermal stability and a faster ion transport (ion diffusion) compared to physically mixing of two homopolymers. In comparison with other reported systems (Table 4), these PIL copolymers with good thermal stability, less moisture sensitivity and good ionic conductivity are more attractive materials for energy storage applications.

3.6 REFERENCES

1. Rozik, N. N.; Ward, A. A., *Polym. Bull.* **2018**, *75*, 267-287.
2. Yuan, J.; Antonietti, M., *Polymer* **2011**, *52*, 1469-1482.
3. Wojnarowska, Z., et al., *Chem. Mater.* **2017**, *29*, 8082-8092.
4. Armand, M.; Endres, F.; MacFarlane, D. R.; Ohno, H.; Scrosati, B., *Nat. Mater.* **2009**, *8*, 621-629.
5. Xu, W., *Science* **2003**, *302*, 422-425.
6. Nakamura, K.; Fukao, K.; Inoue, T., *Macromolecules* **2012**, *45*, 3850-3858.
7. Yu, B.; Danielsen, S. P. O.; Patterson, A. L.; Davidson, E. C.; Segalman, R. A., *Macromolecules* **2019**, *52*, 2560-2568.
8. Bridges, C. R.; Ford, M. J.; Thomas, E. M.; Gomez, C.; Bazan, G. C.; Segalman, R. A., *Macromolecules* **2018**, *51*, 8597-8604.
9. Osada, I.; de Vries, H.; Scrosati, B.; Passerini, S., *Angew. Chem. Int. Ed.* **2016**, *55*, 500-513.
10. Kim, T. Y.; Lee, H. W.; Stoller, M.; Dreyer, D. R.; Bielawski, C. W.; Ruoff, R. S.; Suh, K. S., *ACS Nano* **2011**, *5*, 436-442.
11. Singh, P. K.; Kim, K.-I.; Park, N.-G.; Rhee, H.-W., *Macromol. Symp.* **2007**, *249-250*, 162-166.
12. Sen, S.; Goodwin, S. E.; Barbará, P. V.; Rance, G. A.; Wales, D.; Cameron, J. M.; Sans, V.; Mamlouk, M.; Scott, K.; Walsh, D. A., *ACS Appl. Polym. Mater.* **2021**, *3*, 200-208.
13. Miller, R. J.; Smith, V. M.; Love, S. A.; Byron, S. M.; la Cruz, D. S.-d.; Miller, K. M., *ACS Appl. Polym. Mater.* **2021**, *3*, 1097-1106.
14. Stacy, E. W.; Gainaru, C. P.; Gobet, M.; Wojnarowska, Z.; Bocharova, V.; Greenbaum, S. G.; Sokolov, A. P., *Macromolecules* **2018**, *51*, 8637-8645.

15. Iacob, C.; Matsumoto, A.; Brennan, M.; Liu, H.; Paddison, S. J.; Urakawa, O.; Inoue, T.; Sangoro, J.; Runt, J., *ACS Macro Lett.* **2017**, *6*, 941-946.

16. Griffin, P. J.; Freyer, J. L.; Han, N.; Geller, N.; Yin, X.; Gheewala, C. D.; Lambert, T. H.; Campos, L. M.; Winey, K. I., *Macromolecules* **2018**, *51*, 1681-1687.

17. Gainaru, C.; Stacy, E. W.; Bocharova, V.; Gobet, M.; Holt, A. P.; Saito, T.; Greenbaum, S.; Sokolov, A. P., *J. Phys. Chem. B* **2016**, *120*, 11074-11083.

18. Karlsson, C.; Jannasch, P., *ACS Appl. Energy Mater.* **2019**, *2*, 6841-6850.

19. Schauser, N. S.; Seshadri, R.; Segalman, R. A., *Mol. Syst. Des. Eng.* **2019**, *4*, 263-279.

20. Fan, F., et al., *Macromolecules* **2016**, *49*, 4557-4570.

21. Fan, F.; Wang, Y.; Hong, T.; Heres, M. F.; Saito, T.; Sokolov, A. P., *Macromolecules* **2015**, *48*, 4461-4470.

22. Ratner, M. A.; Shriver, D. F., *Chem. Rev.* **1988**, *88*, 109-124.

23. Hansen, J.-P.; McDonald, I. R., Introduction. In *Theory of Simple Liquids*, Elsevier: 1990; pp 1-11.

24. Wolynes, P. G., *Annl. Rev. Phys. Chem.* **1980**, *31*, 345-376.

25. McLin, M. G.; Angell, C. A., *Solid State Ion.* **1992**, *53-56*, 1027-1036.

26. Ratner, M. A.; Johansson, P.; Shriver, D. F., *MRS Bulletin* **2000**, *25*, 31-37.

27. Boyce, J. B.; Huberman, B. A., *Physics Reports* **1979**, *51*, 189-265.

28. Hull, S., *Rep. Prog. Phys.* **2004**, *67*, 1233-1314.

29. Wang, Y.; Agapov, A. L.; Fan, F.; Hong, K.; Yu, X.; Mays, J.; Sokolov, A. P., *Phys. Rev. Lett.* **2012**, *108*.

30. Choi, U. H.; Ye, Y.; Salas de la Cruz, D.; Liu, W.; Winey, K. I.; Elabd, Y. A.; Runt, J.; Colby, R. H., *Macromolecules* **2014**, *47*, 777-790.

31. Lee, M.; Choi, U. H.; Colby, R. H.; Gibson, H. W., *Chem. Mater.* **2010**, *22*, 5814-5822.

32. Fan, L.; Dang, Z.; Nan, C.-W.; Li, M., *Electrochim. Acta* **2002**, *48*, 205-209.

33. Tang, Z.; Qi, L.; Gao, G., *Solid State Ion.* **2008**, *179*, 1880-1884.

34. Mapesa, E. U.; Chen, M.; Heres, M. F.; Harris, M. A.; Kinsey, T.; Wang, Y.; Long, T. E.; Lokitz, B. S.; Sangoro, J. R., *Macromolecules* **2019**, *52*, 620-628.

35. Luo, X.; Liu, H.; Paddison, S. J., *ACS Appl. Polym. Mater.* **2020**.

36. Evans, C. M.; Bridges, C. R.; Sanoja, G. E.; Bartels, J.; Segalman, R. A., *ACS Macro Lett.* **2016**, *5*, 925-930.

37. Nakamura, K.; Saiwaki, T.; Fukao, K., *Macromolecules* **2010**, *43*, 6092-6098.

38. Biswas, Y.; Banerjee, P.; Mandal, T. K., *Macromolecules* **2019**, *52*, 945-958.

39. Choi, U. H.; Colby, R. H., *Macromolecules* **2017**, *50*, 5582-5591.

40. Choi, U. H.; Price, T. L.; Schoonover, D. V.; Xie, R.; Gibson, H. W.; Colby, R. H., *Macromolecules* **2020**, *53*, 10561-10573.

41. Dyre, J. C.; Maass, P.; Roling, B.; Sidebottom, D. L., *Rep. Prog. Phys.* **2009**, *72*, 046501.

42. Pal, P.; Ghosh, A., *J. Appl. Phys.* **2019**, *126*, 135102.

43. Nakamura, K.; Fukao, K., *Polymer* **2013**, *54*, 3306-3313.

44. Abdulahad, A. I.; Jangu, C.; Hemp, S. T.; Long, T. E., *Macromol. Symp.* **2014**, *342*, 56-66.

45. Biswas, Y.; Maji, T.; Dule, M.; Mandal, T. K., *Polym. Chem.* **2016**, *7*, 867-877.

46. Abdulahad, A. I.; Jangu, C.; Hemp, S. T.; Long, T. E. In *Influence of Counterion on Thermal, Viscoelastic, and Ion Conductive Properties of Phosphonium Ionenes*, Macromolecular Symposia, Wiley Online Library: 2014; pp 56-66.

47. He, H.; Zhong, M.; Adzima, B.; Luebke, D.; Nulwala, H.; Matyjaszewski, K., *J. Am. Chem. Soc.* **2013**, *135*, 4227-4230.

48. Longenecker, R.; Mu, T.; Hanna, M.; Burke, N. A.; Stöver, H. D., *Macromolecules* **2011**, *44*, 8962-8971.

49. Qian, W.; Texter, J.; Yan, F., *Chem. Soc. Rev.* **2017**, *46*, 1124-1159.

50. Chen, H.; Choi, J.-H.; Salas-de la Cruz, D.; Winey, K. I.; Elabd, Y. A., *Macromolecules* **2009**, *42*, 4809-4816.

51. Kremer, F.; Schönhals, A., *Broadband Dielectric Spectroscopy*; Springer Science & Business Media: Berlin, 2002.

52. Zhang, S.; Runt, J., *J. Phys. Chem. B* **2004**, *108*, 6295-6302.

53. Wubbenhorst, M.; van Turnhout, J., *J. Non-Crysta. Solids* **2002**, *305*, 40-49.

54. Pal, P.; Ghosh, A., *Phys. Rev. E* **2015**, *92*.

55. Khamzin, A. A.; Popov, I. I.; Nigmatullin, R. R., *Phys. Rev. E* **2014**, *89*.

56. Serghei, A.; Tress, M.; Sangoro, J. R.; Kremer, F., *Phys. Rev. B* **2009**, *80*.

57. Pitawala, J.; Scheers, J.; Jacobsson, P.; Matic, A., *J. Phys. Chem. B* **2013**, *117*, 8172-8179.

58. Sangoro, J. R.; Iacob, C.; Serghei, A.; Friedrich, C.; Kremer, F., *Phys. Chem. Chem. Phys.* **2009**, *11*, 913-916.

59. Wojnarowska, Z.; Knapik, J.; Díaz, M.; Ortiz, A.; Ortiz, I.; Paluch, M., *Macromolecules* **2014**, *47*, 4056-4065.

60. Sorensen, T. S.; Compan, V., *J. Chem. Soc. Faraday Trans.* **1995**, *91*, 4235-4250.

61. Trukhan, M. E., *Sov. Phys. Solid State* **1963**, *4*, 2560.

62. Munar, A.; Andrio, A.; Iserte, R.; Compan, V., *J. Non-Cryst. Solids* **2011**, *357*, 3064-3069.

63. Wang, Y.; Fan, F.; Agapov, A. L.; Saito, T.; Yang, J.; Yu, X.; Hong, K.; Mays, J.; Sokolov, A. P., *Polymer* **2014**, *55*, 4067-4076.

64. Choi, U. H.; Lee, M.; Wang, S.; Liu, W.; Winey, K. I.; Gibson, H. W.; Colby, R. H., *Macromolecules* **2012**, *45*, 3974-3985.

65. Gorecki, W.; Jeannin, M.; Belorizky, E.; Roux, C.; Armand, M., *J. Phys. Condens. Matter* **1995**, *7*, 6823-6832.

66. Almond, D. P.; West, A. R., *Nature* **1983**, *306*, 456-457.

67. Dyre, J. C., *J. Appl. Phys.* **1988**, *64*, 2456-2468.

68. Feldman, D., *J. Polym. Sci.: Polym. Lett. Ed.* **1988**, *26*, 371-372.

69. Jonscher, A. K., *Nature* **1977**, *267*, 673-679.

70. Sidebottom, D. L., *Phys. Rev. Lett.* **1999**, *83*, 983-986.

71. Zhang, M.; Zuo, Q.; Wang, L.; Yu, S.; Mai, Y.; Zhou, Y., *ChemComm* **2020**, *56*, 7929-7932.

72. Doughty, B., et al., *Phys. Chem. Chem. Phys.* **2019**, *21*, 14775-14785.

73. Keith, J. R.; Mogurampelly, S.; Aldukhi, F.; Wheatle, B. K.; Ganesan, V., *Phys. Chem. Chem. Phys.* **2017**, *19*, 29134-29145.

74. Mogurampelly, S.; Keith, J. R.; Ganesan, V., *J. Am. Chem. Soc.* **2017**, *139*, 9511-9514.

75. Vogel, H., *Physikalische Zeitschrift* **1921**, *22*, 645.

76. Tammann, G.; Hesse, W., *Zeitschrift für anorganische und allgemeine Chemie* **1926**, *156*, 245-257.

77. Fulcher, G. S., *J. Am. Ceram. Soc.* **1925**, *8*, 339-355.

78. Klein, R. J.; Zhang, S.; Dou, S.; Jones, B. H.; Colby, R. H.; Runt, J., *J. Chem. Phys.* **2006**, *124*, 144903.

79. Fragiadakis, D.; Dou, S.; Colby, R. H.; Runt, J., *J. Chem. Phys.* **2009**, *130*, 064907.

80. Macdonald, J. R., *Phys. Rev.* **1953**, *92*, 4-17.

81. Coelho, R., *Rev. Phys. Appl. (Paris)* **1983**, *18*, 137-146.

82. Peltekoff, A. J.; Hiller, V. E.; Lopinski, G. P.; Melville, O. A.; Lessard, B. H., *ACS Appl. Polym. Mater.* **2019**, *1*, 3210-3221.

83. Cai, X.; Cui, B.; Ye, B.; Wang, W.; Ding, J.; Wang, G., *ACS Appl. Mater. Interface* **2019**, *11*, 38136-38146.

84. Safa, M.; Adelowo, E.; Chamaani, A.; Chawla, N.; Baboukani, A. R.; Herndon, M.; Wang, C.; El-Zahab, B., *ChemElectroChem* **2019**, *6*, 3319-3326.

85. Safa, M.; Chamaani, A.; Chawla, N.; El-Zahab, B., *Electrochimica Acta* **2016**, *213*, 587-593.

86. Ye, Y.; Choi, J.-H.; Winey, K. I.; Elabd, Y. A., *Macromolecules* **2012**, *45*, 7027-7035.

Chapter 4

Ionic liquid and poly(ionic liquid) based photoinitiators for aqueous polymerization of vinyl monomers

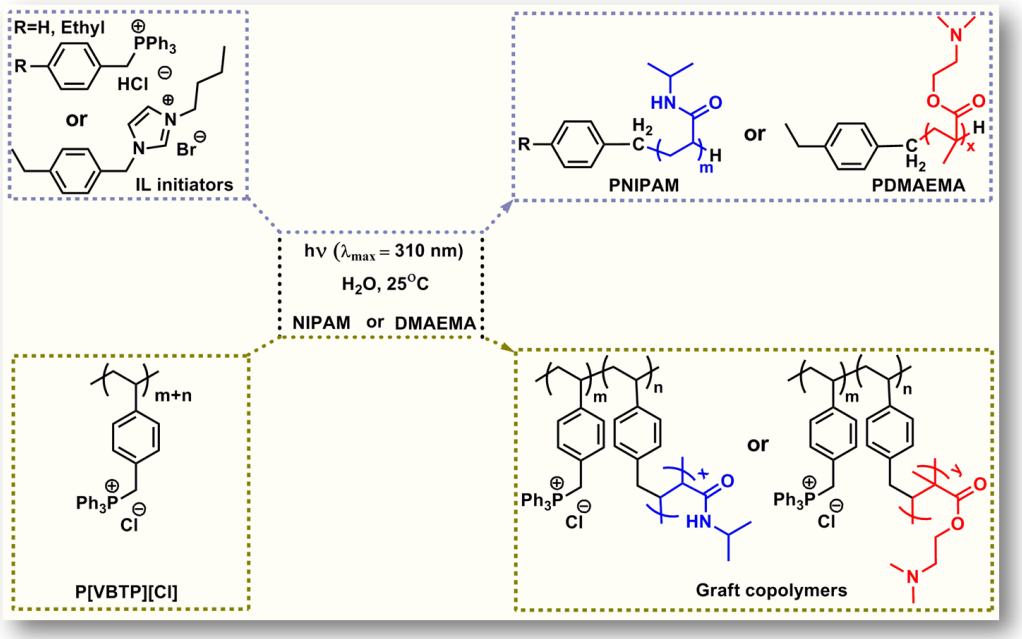

4.1 INTRODUCTION

Photopolymerization has sparked considerable interest in the field of polymer research for the last few decades and has its wide range of applications in industries such as varnishes, photoresists, composites, industrial coatings, adhesives, printing inks, sealants, fibre optics including biomaterials.[1-6] Besides the economic and environmental advantages, there are several other distinct advantages which drive the development of photopolymerization in academic research compared to thermal polymerization such as spatial control, possibility to turn on and off the polymerization, no leakage of solvent, high initiation rate, low energy input, and room temperature photocuring.[7-8] Furthermore, in the cases of curing without heating, such as dental fillings,[9] photopolymerization is the only technique to avoid thermal initiation and serve the purpose. Water-based photocuring of polymers have drawn attention in industrial research because of the use of non-toxic and low-cost water compared to the use of traditional organic solvents.[10] Water-borne formulations provide potential advantages in many applications which are not fulfilled by purely organic systems, such as better balance between hardness and flexibility, better adhesion and matting properties etc.[11] Water-borne UV-curable systems e.g., polyurethane dispersions (PUD) has its industrial application in cured coatings.[12] In all instances, a photoinitiator (PI) is one of the key components to control the polymerization efficiency and the properties of the final polymer product.[3, 11] The conventional radical photoinitiators (PIs) that are commonly found in literatures are non-ionic ethers, polyethers, hydroxyethers, etc..[13-14] Though the majority of radical PIs used in industrial applications are oil-soluble,[11] a recent change in the photopolymerization landscape has been observed with the emergence of new types of water-soluble PIs. For instance, 3D-printed hydrogels,[15] waterborne UV-LED inkjet inks,[16] or waterborne colloidal

dispersions[17] have raised a demand for the development of efficient water-soluble PIs. Till date, only a limited number of water-soluble PIs have been reported; among them, very few are commercially available. For example, Irgacure 2959 (1-[4-(2-hydroxyethoxy)-phenyl]-2-hydroxy-2-methyl-1-propanone) is the most used water-soluble type-I PI due to its commercial availability for a long period of time. However, this hydroxy-acetophenone derivative suffers from a limited water-solubility (<1.5 wt.%).[18] Therefore, the ionic PIs, containing quaternary ammonium, sulphonates, carboxylic acids and thiosulphates groups[19-21] are the alternatives to such non-ionic photoinitiators. Other radical PIs such as sodium 4-[2-(4-morpholino)benzoyl-2-dimethylamino] butylbenzenesulphone (MBS),[22] monoacylphosphine oxide (MAPO) salts (Na-TPO/Li-TPO (LAP)),[18] bisacylphosphine oxide (BAPO) salts,[18] azo-initiator–2,2'-azobis[2-methyl-N-(2-hydroxyethyl)propionamide] (VA-086),[23] etc. have also been developed to increase their solubility in water up to some extent. All these PIs have a higher water-solubility than Irgacure 2959. But, these PIs have complex structures and require complex chemistries for their syntheses. Thus, there is a challenge for polymer chemists to develop different types of PIs of simple chemical structures with improved water solubility such that they are capable of polymerizing different monomers in aqueous medium aiming for industrial applications.

4.2 OBJECTIVES AND SCOPE OF THE PRESENT WORK

In spite of the increasing interest in water-borne formulations, water-soluble photoinitiators (PIs) did not receive proper attention for a long period of time and new developments are urgently required. Although, several water-soluble PIs have been developed for industrial use [20, 24], but most of them suffered from poor water solubility.[11]Thus, the major concern of use of PIs for preparing polymers for various applications is their low extent of solubility in water.

Although, there are many commercially available radical[25-28] and cationic[29-32] PIs that are routinely used for the polymerization of vinyl monomers, but, the detailed survey of literature showed that there has not been any report of use of phosphonium or imidazolium salts/ionic liquids (ILs) as PIs for free radical polymerization of vinyl monomers in aqueous medium. However, Otsu et al. reported the photopolymerization of methyl methacrylate (MMA) using benzyltriphenylphosphonium bromide (BTPPB) in methanol.[33] They claimed that the polymerization followed a living free radical pathway. Yagci et al. reported photopolymerization of ethyl cyanoacrylate (ECA) by benzyltriphenylphosphonium hexafluoroantimonate (BP^+) and (anthracen-9-ylmethyl)-triphenylphosphonium hexafluoroantimonate (MAP^+) in CH_2Cl_2.[34] In these cases, it has been proposed that the reaction proceeded through both free radical and zwitterionic mechanisms with homolytic and heterolytic cleavage of carbon-phosphorous bond respectively. Photopolymerization of vinyl monomers initiated by quaternary ammonium salts and their corresponding binary mixtures have also been reported in nonaqueous medium.[35-36] There are several reports on synthesis of new types of phosphonium and imidazolium ILs, ionic liquid monomers (ILMs) and their polymerization to poly(ionic liquid)s (PILs) using conventional free radical or RAFT polymerizations.[37-41] The main motivation for their syntheses was to check the stimuli-responsive behaviors of those ILs/PILs in the absence or presence of various anions. In this context, as mentioned above, there are very few preliminary reports describing photopolymerization of vinyl monomers using organic phosphonium salts or ammonium salts in organic medium.[33-36] But, to-date there is no such report on the use of these phosphonium/imidazolium based salts/ILs as PIs for polymerization of vinyl monomers in aqueous medium. Hence, the exploration of use of these types of ILs as PIs in aqueous medium becomes very important considering their

applications in industrial polymer synthesis, especially in replacing organic solvents with green solvent like water because of numerous reasons.[7]

Thus in this work, a series of phosphonium and imidazolium ionic liquids (ILs) with high water-solubility have been synthesized and those have been utilized as efficient photoinitiators (PIs) for the polymerization of vinyl monomers such as N-isopropylacrylamide (NIPAM) and 2-(dimethylamino)ethyl methacrylate (DMAEMA) efficiently upon UV irradiation (λ_{max} = 310 nm) in aqueous medium at ambient temperature and pressure. The photopolymerization proceeds through free radical pathway which has been established by EPR and ^{1}H-NMR spectroscopy, MALDI-TOF-MS, SEC analysis, and other control experiments. The kinetic study demonstrates that this photopolymerization is fast enough to produce high-molecular-weight polymers with ~70% yield even after 30 mins of UV irradiation. Control experiments show that these IL-based PIs have high water solubility and capable of producing high-molecular-weight polymers compared to those of polymers obtained by other commercially available aqueous PIs. Additionally, poly(NIPAM) and poly(DMAEMA) are grafted from the photoactive pendent IL moiety of the poly(ionic liquid), poly(triphenyl-4-vinylbenzylphosphonium chloride) (P[VBTP][Cl]) backbone by the grafting-from copolymerization. The presence of either poly(NIPAM) or poly(DMAEMA) graft segment induces thermoresponsiveness to their P[VBTP][Cl]-based copolymers.

4.3 EXPERIMENTAL

4.3.1 Materials. Triphenylphosphine (TPP, ≥95%) was purchased from Sigma-Aldrich and recrystallized twice from ethanol prior to use. 4-Vinylbenzyl chloride (VBC) (Aldrich, 90%) was obtained from Sigma-Aldrich and purified by passing through a neutral alumina column to remove inhibitors before use. 4-Ethylbenzyl chloride (EtBzCl, >98%) and benzyl chloride (BzCl, >99.0%) were obtained from

TCI Chemicals and used as received. Lithium bromide (LiBr, >99%) was purchased from Spectrochem. 1-Bromobutane (99%), tetrabutylammonium bromide (TBAB, >99%), 2,2,6,6-tetramethyl-1-piperidinyloxyl (TEMPO) (99%), sodium azide (>99%), imidazole (Im, 99%), α-ketoglutaric acid (> 99%) and phenylglyoxylic acid (97%) were purchased from Sigma-Aldrich and were used as received. N-isopropylacrylamide (NIPAM) was obtained from TCI Chemicals and was recrystallized from hexane. 2-(Dimethylamino)ethyl methacrylate (DMAEMA) was obtained from Sigma-Aldrich and the inhibitor was removed by passing through basic alumina column. Dichloromethane (DCM), acetone, acetonitrile, hexane, methanol (MeOH), diethyl ether and dimethyl sulfoxide (DMSO) were used as received from Merck, India. Milli-Q water was used as solvent in the photopolymerization.

4.3.2 Synthesis

4.3.2.1 Synthesis of phosphonium IL-based photoinitiators (PIs)

Two PIs (**PI-1** and **PI-2**) of different chemical structures were synthesized by nucleophilic substitution reaction of triphenylphosphine (TPP) with two different aryl halides in a molar ratio of 1.5:1 at 40°C as shown in Scheme 1(a) following a previously reported protocol.[37] Typically, two 100 mL round-bottom (RB) flasks were separately charged with TPP (1.5 g; 5.72 mmol) followed by addition of required amount of corresponding aryl halides (8.58 mmol) (1.275 mL of EtBzCl or 0.987 mL of BzCl) and 15 mL of dry MeOH. The reaction mixtures were then placed in a preheated oil bath at 40°C and continued heating for 24h. After completion of the reaction, MeOH was evaporated in a rotary evaporator and the entire liquid mass was dissolved in DCM. Finally, PIs were isolated by precipitation in excess diethyl ether. The process was repeated twice for purification. The ESI-MS spectra of **PI-1** and **PI-2** are shown in Figures 1-2

respectively. The pure PIs were also characterized by FTIR and ^{1}H-NMR, which will be discussed later in the result and discussion section. % Yield for **PI-1** and **PI-2** were found to be 81 and 84 respectively.

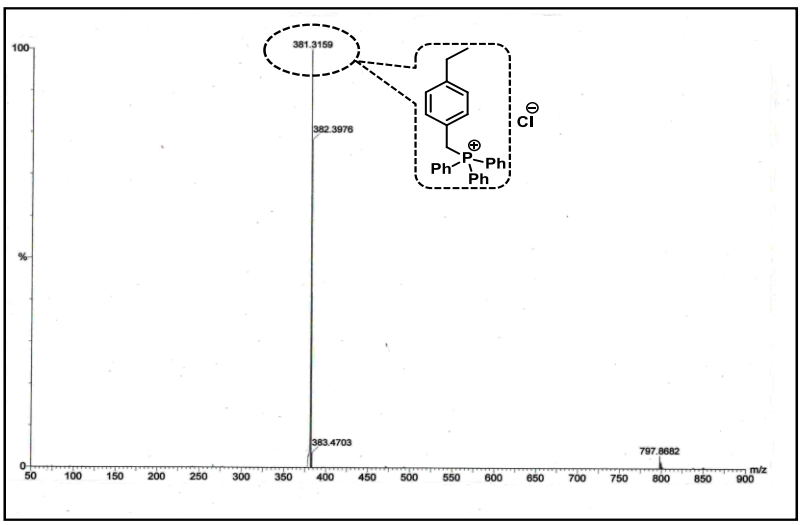

Figure 1. ESI-MS spectrum of **PI-1**.

PI-1: MS (ESI) (35 eV) m/z: 381.31 (theoretical mass: 381.18 g/mol)

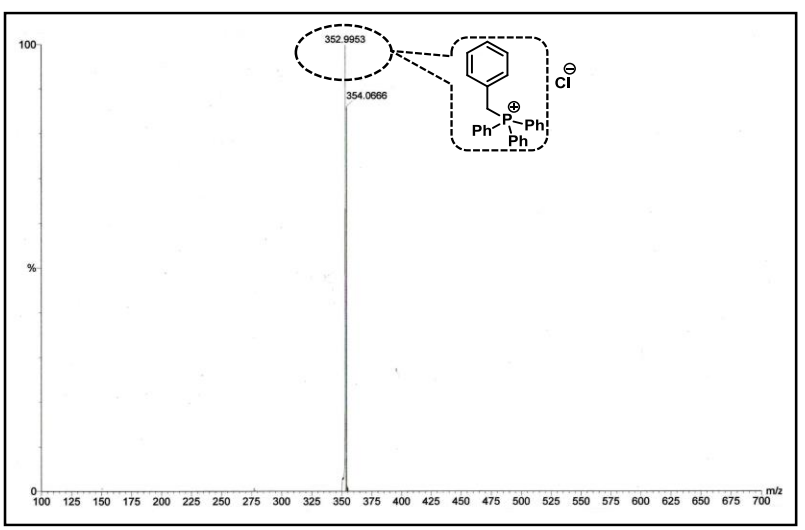

Figure 2. ESI-MS spectrum of **PI-2**.

PI-2: MS (ESI) (35 eV) m/z: 352.99 (theoretical mass: 353.15 g/mol)

4.3.2.2 Synthesis of imidazolium IL-based photoinitiator (PI)

In the first step of synthesis of **PI-3**, aryl substituted imidazole was synthesized by a nucleophilic substitution of imidazole with aryl halide (Scheme 1b) by following a reported protocol.[40] A two-neck RB flask (250 mL) was charged with imidazole (5.63 g, 82.66 mmol), $NaHCO_3$ (2.18 g; 25.86 mmol) and a 1:1 water/acetone mixture (44 mL). The mixture was stirred at 25°C for 1h for complete dissolution with continuous purging of N_2 gas. EtBzCl (3 mL; 20.68 mmol) was then separately added into the reaction mixture and was heated to reflux under N_2 atmosphere at 50°C for 20h. The reaction mixture was then cooled and filtered through gauze funnel to remove unreacted $NaHCO_3$. Acetone was evaporated in a rotary and the entire liquid mass was diluted with 300 mL of diethyl ether followed by washing with 450 (6×75) mL of water. The product and the unreacted imidazole were

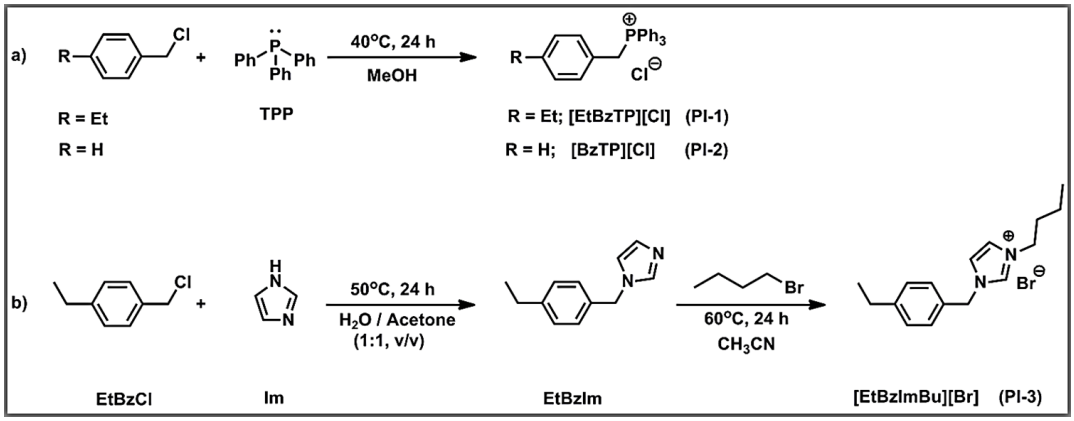

Scheme 1. Synthesis of (a) phosphonium IL-based PIs (**PI-1** and **PI-2**) and (b) imidazolium IL-based PI, **PI-3.**

extracted into aqueous phase by washing the organic phase with 75mL of 2.0 M HCl for three times. The partial neutralization with required volume of 4.0 M NaOH resulted in a white suspension along with an oily layer containing 4-ethylbenzyl imidazole and aqueous imidazolium chloride. The final product was

extracted into diethyl ether (300 mL) and was collected over anhydrous Na_2SO_4 using a separating funnel. Finally, ether was removed under reduced pressure resulting viscous yellow liquid [EtBzIm]. In the second step, the imidazolium-based photoinitiator was synthesized by nucleophilic substitution reaction between the as-synthesised aryl substituted imidazole and 1-bromobutane in a molar ratio of 2:1 at 60°C. EtBzIm (1.23 g; 7.75 mmol) was added to 1-bromobutane (0.418 mL; 3.87 mmol) in a 50 mL RB flask followed by the addition of 10 mL dry acetonitrile. The reaction mixture was placed in a pre-heated oil bath at 60°C with constant stirring for 24h. The product was then isolated by precipitation in diethyl ether. Finally, IL was washed with diethyl ether for four times for complete removal of unreacted components and was subjected to prolonged drying at 50°C for complete removal of diethyl ether. The final pure product was obtained as yellowish viscous liquid. ESI-MS was successfully applied to characterize **PI-3** and the spectrum is given in Figure 3.

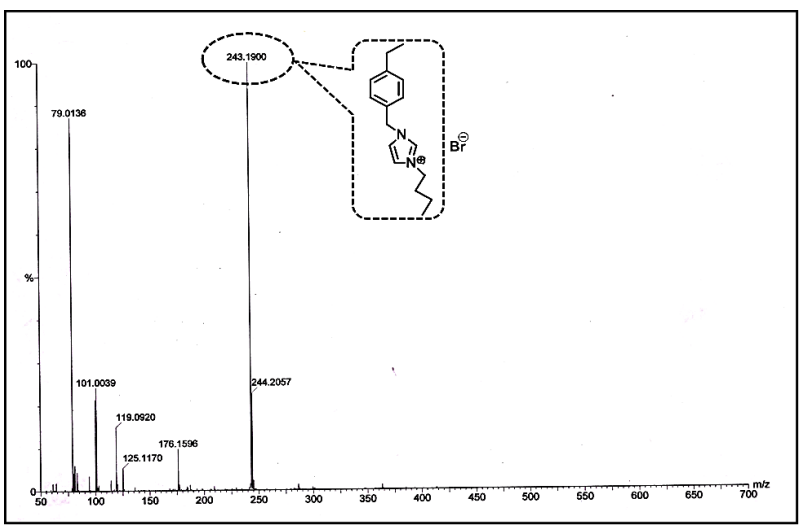

Figure 3. ESI-MS spectrum of **PI-3**.

PI-3: MS (ESI) (35 eV) m/z: 243.19 (theoretical mass: 243.19 g/mol)

PI-3 was also characterized by FTIR and ^{1}H-NMR analyses which will be discussed later. Yield (%) of **PI-3** was found to be 78.

4.3.2.3 Synthesis of PNIPAMs (P1 and P2) via photopolymerization initiated by phosphonium-IL based PIs (PI-1 and PI-2)

In a typical procedure (Table 1), 0.9 mmol (100 mg) NIPAM monomer was separately added to 0.09 mmol **PI-1** and **PI-2** (37.5 and 35.0 mg respectively) taken in two different quartz test tubes followed by the addition of 1 mL water to each of them (Scheme 2). The reaction mixtures were purged with argon gas for 45 min. The quartz test tubes were then immediately sealed with a silicone rubber septum and the photopolymerization was performed inside the photoreactor under UV light irradiation (λ_{max} = 310 nm) for 4h at room temperature. Finally, the reaction mixtures were precipitated in acetone, yielding **P1** and **P2**. Number average molecular weights (M_ns) and dispersities ($Đ$s) of the crude freeze-dried polymers were measured by size exclusion chromatography (SEC) before further purification. The obtained polymers were redissolved in water and precipitated again in acetone. Further, the aqueous solutions of these polymers were purified by extensive dialysis against double distilled water for 2 days. The aqueous polymer solutions were then lyophilized to obtain pure white polymers and were dried in vacuum oven. The final polymers were well characterized by different techniques as described later. Yields (%) for **P1** and **P2** were found to be 81 and 79 respectively (Table 1).

4.3.2.4 Synthesis of PNIPAM (P3) initiated by imidazolium IL-based PI (PI-3)

The photopolymerization procedure for synthesis of **P3** (Table 1, Scheme 2) was exactly similar to those used for the syntheses of **P1** and **P2**. NIPAM (100 mg; 0.9 mmol) and **PI-3** (29.1 mg; 0.09 mmol) were taken in a quartz test tube followed by the addition of 1 mL water. The reaction and work up procedure were same

as mentioned above for **P1** and **P2**. The final pure **P3** was characterized by FTIR, ^{1}H -NMR, and MALDI-TOF-MS as described later. %Yield = 76.

4.3.2.5 Synthesis of PDMAEMA (P4 and P5) initiated by phosphonium/ imidazolium IL-based PIs

In a typical procedure (Table 1, Scheme 2), DMAEMA (141.5 mg; 0.9 mmol) was separately added to 0.09 mmol of **PI-1** and **PI-3** (37.5 and 29.1mg respectively) taken in two different quartz test tubes followed by the addition of 1 mL water to each of them. The reaction mixtures were purged with argon gas for 45 min. The polymerization and work up procedure followed were same as mentioned above which yielded polymers **P4** and **P5**. The final pure polymers were characterized by FTIR, ^{1}H -NMR, and MALDI-TOF-MS as described later. Yield (%) for **P4** and **P5** were found to be 74 and 71 respectively.

4.3.2.6 Synthesis of poly(triphenyl-4-vinylbenzylphosphonium chloride) (P[VBTP][Cl]) by CFRP

The conventional free radical polymerization (CFRP) of triphenyl-4-vinylbenzylphosphonium chloride ([VBTP][Cl]) monomer produced **P[VBTP][Cl]**. Typically, [VBTP][Cl] (0.3 g; 0.8 mmol) and AIBN (3.89 mg; 0.024 mmol) were added to 16 mL of dry DMF taken in a 25 mL long-neck RB flask. Argon gas was purged through the reaction mixture for 45 min before the flask was sealed with a rubber septum. Finally, the sealed flask was placed in an oil bath preheated at 70°C for 6h under magnetic stirring. **P[VBTP][Cl]** was then immediately isolated from DMF solution by precipitation in diethyl ether. Finally, **P[VBTP][Cl]** was redissolved in DMF and reprecipitated in water followed by centrifugation to remove unreacted [VBTP][Cl]. The **P[VBTP][Cl]** was then dried in vacuum oven at 60°C for overnight. The final pure **P[VBTP][Cl]** polymer was characterized by ^{1}H – NMR as described later. Yield(%): 79 %.

Table 1: Photopolymerization of NIPAM and DMAEMA using different IL-/PIL-based PIs.

Entry	Monomer (concn.)	Photoinitiator (concn.)	Polymer	Conversion (%)[a]	M_n[b] (*kDa*)	$Đ$[b]
1	NIPAM (0.9 mM)	[EtBzTP][Cl] (**PI-1**) (0.09 mM)	EtBz-PNIPAM (**P1**)	81	45.7	1.48
2	NIPAM (0.9 mM)	[BzTP][Cl] (**PI-2**) (0.09 mM)	Bz-PNIPAM (**P2**)	79	53.6	1.41
3	NIPAM (0.9 mM)	[EtBzImBu][Br] (**PI-3**) (0.09 mM)	EtBz-PNIPAM (**P3**)	76	49.7	1.40
4	DMAEMA (0.9 mM)	[EtBzTP][Cl] (**PI-1**) (0.09 mM)	EtBz-PDMAEMA (**P4**	74	91.6	2.2
5	DMAEMA (0.9 mM)	[EtBzImBu][Br] (**PI-3**) (0.09 mM)	EtBz-PDMAEMA **(P5)**	71	163.3	1.54
6	NIPAM (0.9 mM)	P[VBTP][Cl] (2.5 wt %)	P[VBTP][Cl]-*g*-PNIPAM (**P6**)	76[c]	327.6	1.73
7	DMAEMA (0.9 mM)	P[VBTP][Cl] (2.5 wt %)	P[VBTP][Cl]-*g*-PDMAEMA (**P7**)	74[c]	269.3	1.64

In each of these cases, a total of 1 mL of reaction mixture was taken in a quartz tube and was irradiated for 240 min at 25°C and using UV-lamp (λ_{max}= 310 nm) with a light intensity of 13 mW cm^{-2}.

[a]Measured by gravimetric analysis.

[b]SEC traces were obtained from crude freeze-dried polymers..

[c] %Yield of grafted polymer

4.3.2.7 Synthesis of P[VBTP][Cl]-*g*-PNIPAM(P6)/P[VBTP][Cl]-*g*-PDMAEMA(P7) copolymers

The graft copolymers were also synthesized using the same technique but, the photopolymerizations were initiated from the pendant [VBTP][Cl] moiety of the as-synthesized **P[VBTP][Cl]** (Table 1, Scheme 3). A 25 mg of **P[VBTP][Cl]** was added separately to 0.9 mmol NIPAM (100 mg) and DMAEMA (141.5 mg) monomer (for **P6** and **P7** respectively) taken in two different quartz test tubes followed by the addition of 1 mL water to each of them and the reaction

mixtures were purged with argon gas for 45 min. The photopolymerization and purification procedure were exactly similar to those used for the preparation of polymers, **P1-P5.** % Yield: 76 and 74 for **P6** and **P7** respectively.

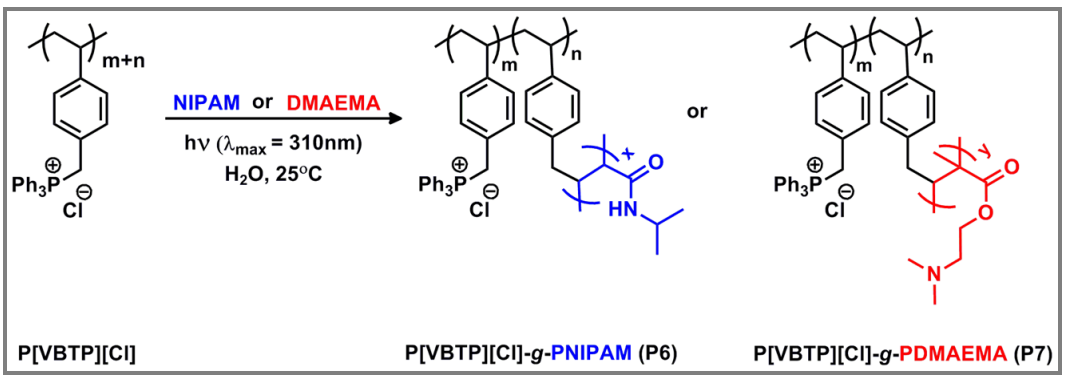

Scheme 3. The synthesis of P[VBTP][Cl]-*g*-PNIPAM(**P6**)/P[VBTP][Cl]-*g*-PDMAEMA (**P7**) by photopolymerization.

4.3.2.8 Synthesis of PNIPAMs (P′1 and P′2) and PDMAEMAs (P′3 and P′4) initiated by conventional radical PIs

NIPAM and DMAEMA were also polymerized using two commercially available conventional free radical PIs, α-ketoglutaric acid (AKG) and phenylglyoxylic acid (PGA) following the same reaction condition, irradiation source and purification procedure as mentioned for the syntheses of **P1**-**P6**. The obtained polymers were designated as **P′1, P′2, P′3** and **P′4** respectively with % Yield of 77, 72, 79 and 74.

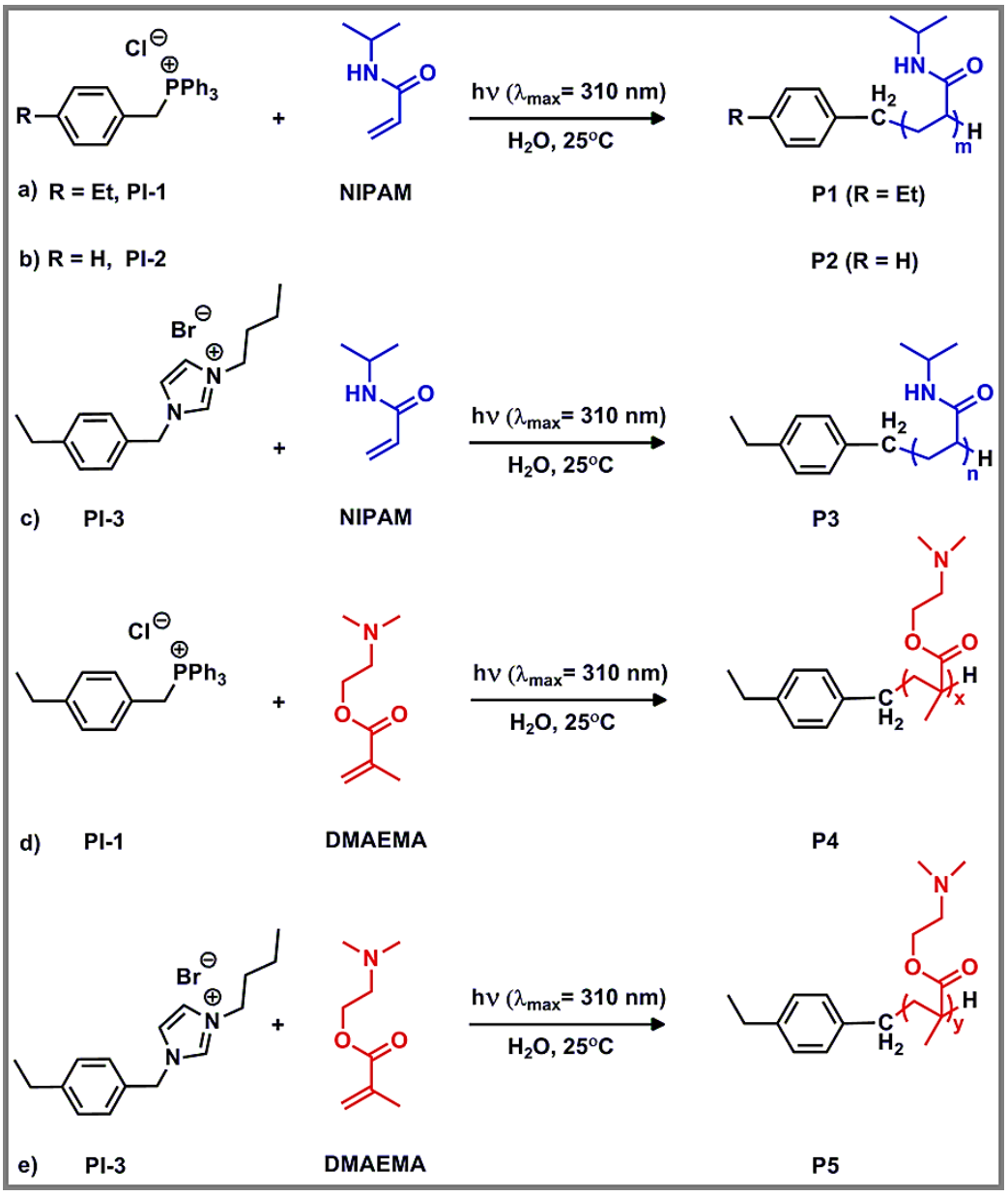

Scheme 2. Photopolymerizations of NIPAM (a, b and c) and DMAEMA (d and e) using IL-based PIs in water upon UV irradiation (λ_{max} = 310 nm).

4.3.3 Characterization

^{1}H-NMR study. ^{1}H-NMR spectra of IL-based PIs and polymers were acquired by using a Bruker DPX 500 MHz spectrometer. NMR spectra of all PIs and PNIPAMs

(**P1**-**P3**) were recorded in $CDCl_3$ whereas all the PDMAEMA polymers (**P4**, **P5**) were recorded in D_2O. The spectra of all types of **P[VBTP][Cl]** were recorded from $CDCl_3/CD_3OD$ (10/1) solvent mixtures.

ESI mass spectrometry. The ESI-MS spectra of the as-synthesized polymers were recorded by using a quadrupole time-of-flight (Q-TOF) Micro YA263 mass spectrometer. The samples were prepared at a concentration of 1 mg mL^{-1} in methanol.

Fourier transform infrared (FTIR) spectroscopy. FTIR spectra of PIs and polymers were recorded using pellets, prepared by mixing the corresponding dried samples with dried KBr in 1:100 (w/w) ratios in a Perkin Elmer FTIR Spectrum-400 spectrometer.

Size exclusion chromatography (SEC). The number average molecular weight (M_n) and dispersity (*Đ*) were measured by SEC using a Waters 1515 isocratic HPLC pump connected to three Waters columns and a Waters 2414 RI detector at 35°C. SEC analyses were performed on crude freeze-dried polymers obtained by photopolymerization. THF with 1wt% (w/v) TBAB as eluent and Styragel HR1 (M_n = 100−5000), HR3 (M_n = 500−30 000), HR4 (M_n = 5000−600000) and HR5 (M_n = 50000-4000000) columns were used for **P1-P3, P'1** and **P'2.** Whereas for **P[VBTP][Cl]** and **P6,** DMF with 50mM LiBr was passed through styragel HR1 (M_n = 100−5000), HR3 (M_n = 500−30 000), and HR4 (M_n = 5000−600000) columns as eluent at a flow rate of 1 mL/min at 45°C. A conventional calibration curve was constructed with narrow PMMA standards with molecular weights (M_p) between 2.58 and 1120 kDa. On the other hand, the M_ns and dispersities (*Đ*s*)* of **P4**, **P5, P7, P'3** and **P'4** were obtained using water as the eluent containing 0.30 M Na_2SO_4 and 0.1wt. % of NaN_3 at pH 7 with at a flow rate of 1.0 mL min^{-1} and at 30 °C. Styragel HR1 (M_n = 100−5000), HR3 (M_n = 500−30 000), and HR4 (M_n =

5000−600000) columns were used in this case. Narrow PEG standards with molecular weights (M_p) between 1.5 and 915 *kDa* were used for this calibration.

Matrix-assisted laser desorption/ionization TOF mass spectrometry. MALDI-TOF-MS spectra of all the polymers were acquired in a Brucker instrument. The sample was irradiated using 337 nm N_2 laser with an operating voltage of 25 kV. Trans-2-[3-(4-*tert*-Butylphenyl)-2-methyl-2-propenylidene]malononitrile (DCTB) (20 mg/mL in MeOH) was used as the matrix for **P1**, **P2** and **P3,** whereas 2,5-dihydroxybenzoic acid (DHB) (20 mg/mL in MeOH) was used as the matrix for **P4**. The concentration of polymer was taken as 1 mg/mL in methanol. For measurement, final sample was prepared by mixing 10 µL of polymer solution and 10 µL of matrix solution. Typically, 1 µL of the solution mixture was spotted on the sample's plate and allowed to dry to improve the crystallization. The corresponding spectra of samples were acquired by summing the data obtained over 200 laser shots in linear mode.

Turbidity measurement. The turbidity of aqueous solutions of the graft copolymers were measured using a Hewlett Packard 8453 diode array UV-vis spectrophotometer (Agilent Technologies) equipped with a Peltier temperature controller. The cloud point (T_{cp}) of the solution was determined by studying the solution %transmission (T) at 500 nm. T_{cp} of the copolymer was considered as temperature at which %T = 50.

Dynamic light scattering (DLS). Zetasizer NANO ZS 90, Malvern (Model ZEN 3690, Version 7.03) was used to measure the hydrodynamic diameter (D_h) by DLS. The aqueous graft copolymer solutions were filtered through a membrane of 0.22µ pore size prior to the DLS experiment. The change of D_h of the copolymer aggregates was then monitored with temperature at a rate of 4°C min^{-1} followed by an equilibration for 2 min at each temperature.

Photoreactor. The photopolymerization was performed in the Luzchem-ICH2 (Canada) photoreactor using a set of UV lamps (λ_{max} = 310 nm) with a light intensity of 13 mW cm^{-2}. The light intensity reading was obtained using a Digital Lux Meter (SMART SENSOR, AR823)

EPR spectroscopy. X-band EPR spectra of the reaction mixture was collected from a JEOL JES-FA 200 instrument.

4.4 RESULTS AND DISCUSSION

Interestingly, we have observed self-initiated photopolymerization, when a quartz tube containing an aqueous [VBTP][Cl][37] ILM solution (250 mg/mL) was placed in a photoreactor equipped with a set of UV lamps (λ_{max} = 310 nm) and was irradiated for 4h at 25°C (Scheme 4). The obtained gel-like polymeric

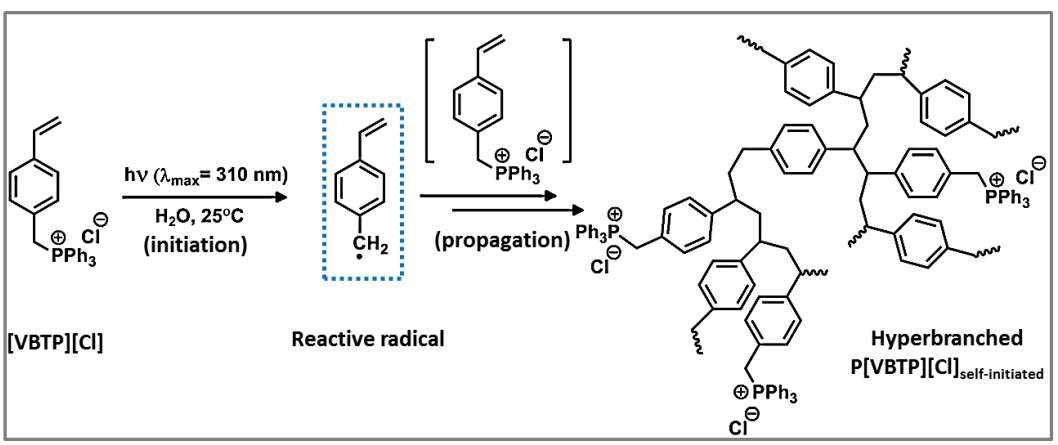

Scheme 4. Plausible reaction mechanism for the self-initiated photopolymerization of [VBTP][Cl] monomer under UV irradiation (λ_{max}=310 nm) in aqueous medium to form a hyperbranched polymer.

material was collected by freeze drying with a yield of about 77%. The gel-like nature of this polymer, **P[VBTP][Cl]$_{self\text{-}initiated}$** can be ascribed to its hyperbranched morphology, which is nothing but the consequence of generation of free radical at the benzylic position of [VBTP][Cl] monomer under UV

irradiation followed by its free radical self-condensing vinyl polymerization from all possible directions. In this case, [VBTP][Cl] played the dual role of a monomer as well as an initiator under UV irradiation (λ_{max} = 310 nm) in aqueous medium. The ^{1}H-NMR spectrum of **P[VBTP][Cl]$_{self\text{-}initiated}$** (Figure 4) did not show any signal corresponding to the vinyl protons of [VBTP][Cl] monomer in between δ 5.0-6.5 ppm [37], instead broad signals at δ 0.85-1.07 ppm due to the backbone methylene and methine protons were clearly visible indicating the successful self-initiating photopolymerization of the ILM, [VBTP][Cl]. M_n and $Đ$ of the **P[VBTP][Cl]$_{self\text{-}initiated}$**

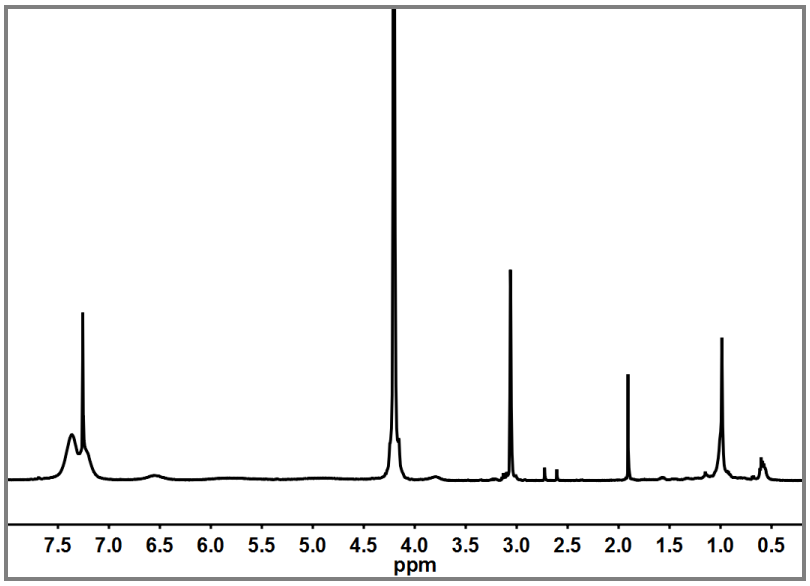

Figure 4. ^{1}H-NMR spectrum of **P[VBTP][Cl]$_{self\text{-}initiated}$** in $CDCl_3/CD_3OD$ (10 : 1) solvent mixture.

obtained from SEC chromatogram (Figure 5) were found to be 134.5 *kDa* and 1.66 respectively. However, in organic solvents such as methanol, chloroform, dichloromethane etc., there were no such self-initiated polymerization of [VBTP][Cl] upon irradiation with UV-light (λ_{max} = 310 nm). To explore the mechanism of this self-initiated photopolymerization, the end group analysis of

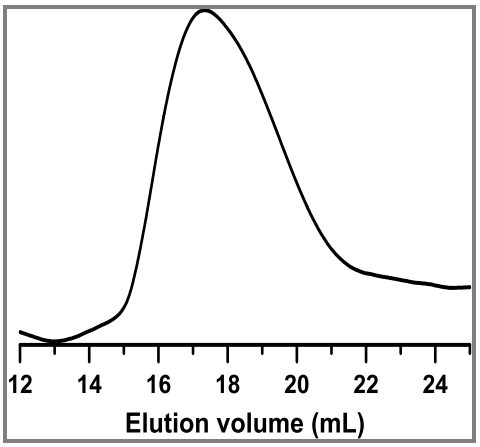

Figure 5. GPC trace of **P[VBTP][Cl]$_{self\text{-}initiated}$**. Eluent = DMF with 50 mM LiBr; column temperature = 45 °C.

the **P[VBTP][Cl]$_{self\text{-}initiated}$** was done by MALDI-TOF-MS, but no conclusion could be made from the spectrum. Thus, to elucidate the mechanism of this photopolymerization in detail, we have synthesized another IL, 4-ethylbenzyltriphenylphosphonium chloride (**PI-1**) (Scheme 1a) whose chemical structure is similar to that of [VBTP][Cl] (Scheme 4), but, without any polymerizable vinyl group and this led us to wonder whether **PI-1** might reveal a similar reactivity behaviour upon UV-irradiation. However, the control experiment of UV-irradiation of 10 wt.% aqueous solution of **PI-1** did not proceed with such type of self-initiated polymerization as the **PI-1** has no vinyl group. However, **PI-1** was capable to initiate the photopolymerization of NIPAM in water upon irradiation with UV light (Table 1, Scheme 2), the details of which will be discussed later in this section. For detailed study, a series of other IL-based PIs such as benzyltriphenylphosphonium chloride (**PI-2**) (Scheme 1a) and 4-ethylbenzylimidazolium butyl bromide (**PI-3**) (Scheme 1b) were synthesized following the general procedure given in the experimental section. ESI-MS spectra (Figures 1-3) of all three PIs showed signals corresponding to their molecular ions whose mass exactly matched with their theoretical mass,

indicating their successful syntheses. The characteristic ^{1}H-NMR signals for phenyl ring protons, benzylic -CH_2 protons next to the phosphonium cation and three phenyl ring protons belonging to triphenyl phosphonium cation appeared at δ 6.94, δ 5.34, δ 7.5–7.8 ppm and δ 7.06, δ 5.34, δ 7.5–7.8 ppm for **PI-1** and **PI-2** respectively (Figures 6a-6b). For **PI-1**, an additional signal appeared at δ 1.0-2.6 ppm for alkyl protons. Whereas for **PI-3**, the appearance of signals of imidazole ring protons at about δ 10.6, 7.4 and 7.3 ppm, phenyl ring protons (δ 7.17-7.27 ppm), benzylic-CH_2 protons (δ 5.53 ppm) or alkyl protons (δ 4.3-0.8 ppm) confirmed its successful synthesis (Figure 6c). FTIR spectra (Figures 7a-7b) of both **PI-1** and **PI-2** also confirmed their successful syntheses showing characteristic bands at 1434 cm^{-1} (for deformation of P–CH_2–Ph) and 1109 cm^{-1} (for P–Ph stretching). Whereas the spectrum for **PI-3** (Figure 7c) showed characteristic bands at 1453 cm^{-1} (N-CH_2- deformation), 1500-1620 cm^{-1} (imidazolium ring stretch), 2800-3000 cm^{-1} (aliphatic C-H stretching) and 3127 cm^{-1}(C=N deformation of imidazole ring).

The polymerization of NIPAM was achieved by PIs, **PI-1**, **PI-2** and **PI-3** in aqueous medium upon UV light irradiation (Scheme 2 and Table 1). The aqueous solution of NIPAM initiated by **PI-1** yielded EtBz-PNIPAM (**P1)** with high conversion (81%) (Table 1, entry 1). The FTIR spectrum of NIPAM (Figure 8a) showed a sharp peak at 1622 cm^{-1} and few peaks in the range of 800-1000 cm^{-1} due to >C=C< stretching, which were absent in the spectrum of **P1** (Figure 8b) confirming its complete polymerization. The spectrum of **P1** also showed other peaks of PNIPAM including the characteristic peak of >C=O at 1643 cm^{-1}. Figure 9a showed

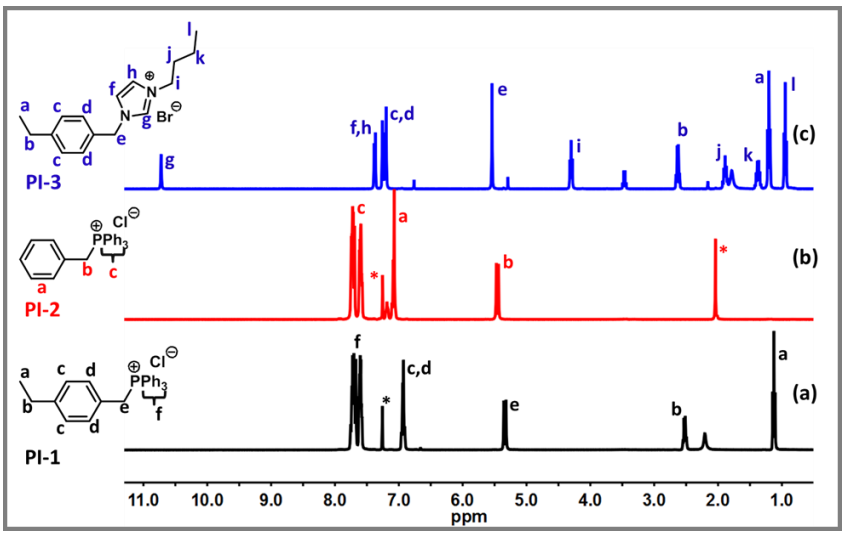

Figure 6. ^{1}H-NMR spectra of (a) **PI-1**, (b) **PI-2** and (c) **PI-3** in $CDCl_3$ (*signal at δ 7.26 ppm corresponds to $CHCl_3$ present).

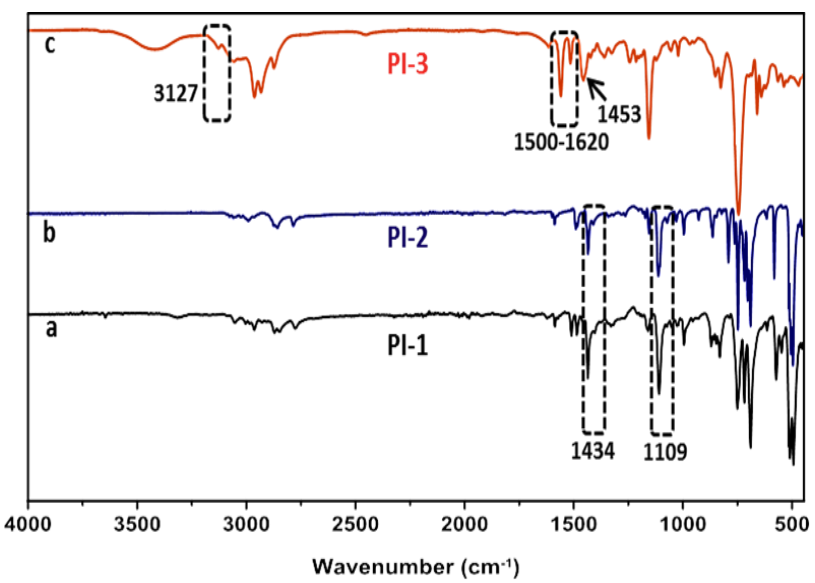

Figure 7. FTIR spectra of (a) **PI-1**, (b) **PI-2** and (c) **PI-3**.

that the vinyl protons signals of NIPAM at δ 5.58, 6.06, and 6.22 ppm completely disappeared after its photopolymerization and new broad signals of alkyl -CH

and -CH_2 of the PNIPAM main chain were appeared at δ 1.62 and 2.7 ppm respectively (Figure 9b). In addition, the ^{1}H-NMR spectrum of the **P1** (Figure 9b) also displayed the signature of the phenyl ring protons of the corresponding 4-ethylbenzyl moiety as two sharp peaks visible in the range of δ 7.0-7.2 ppm in magnified view, which further confirmed the attachment of the 4-ethylbenzyl moiety with PNIPAM chain.

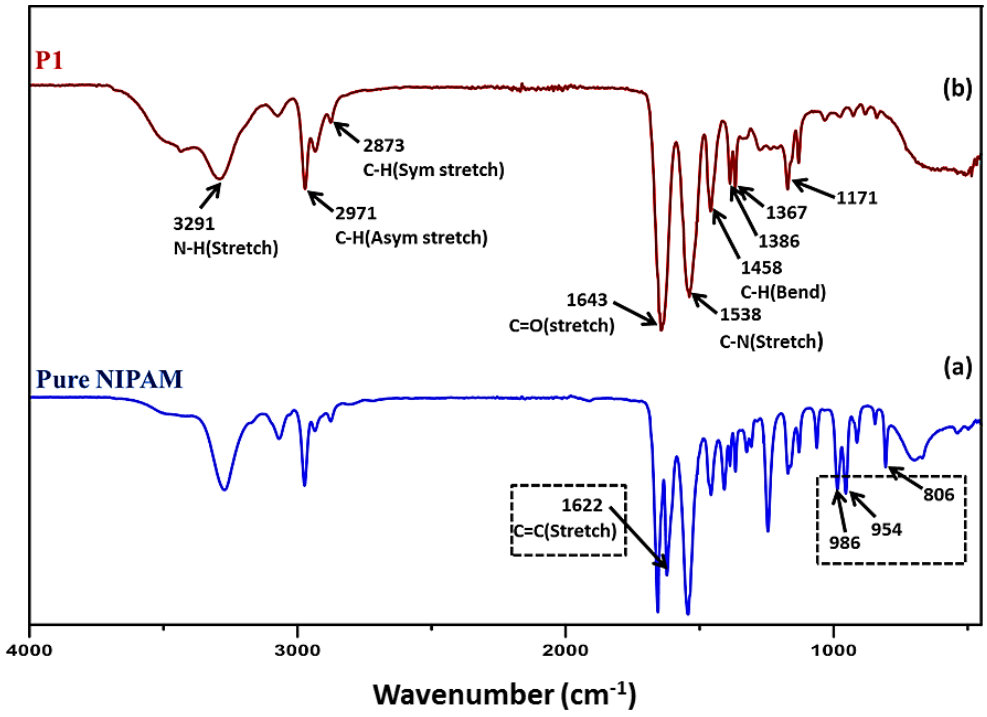

Figure 8. FTIR spectra of (a) NIPAM monomer and (b) **P1**.

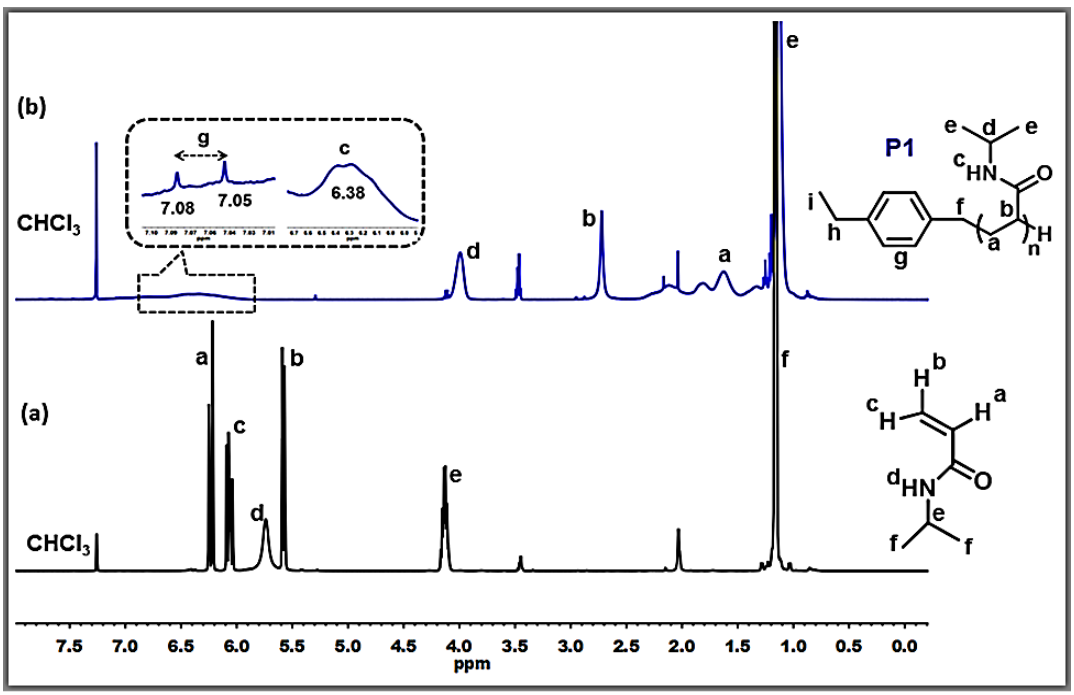

Figure 9. ^{1}H-NMR spectrum of a) NIPAM monomer and b) EtBz-PNIPAM (**P1**) (entry 1, Table 1) in $CDCl_3$.

The other IL-based PIs (**PI-2 and PI-3)** (Scheme 2 and Table 1) were also used to photopolymerize NIPAM to produce PNIPAMs, designated as **P2** and **P3** with high conversions of 79 and 76% respectively in water under similar reaction conditions. ^{1}H-NMR and FTIR spectra of **P2** and **P3** also confirmed the complete conversion of monomeric NIPAM to PNIPAM (Figures 10-11). The SEC analyses showed M_ns of 45.7, 53.6, and 49.7 *kDa* with *Đ*s of 1.48, 1.41 and 1.40 for **P1**, **P2** and **P3** respectively (Figure 12). It should be noted that the broad molecular weight distribution (MWDs)(*Đ*s) of the as-synthesized crude polymers **P1**, **P2** and **P3** give us an initial indication that this photopolymerization followed a free-radical pathway, where it is difficult to control the rate of chain propagation during the

polymerization, ultimately leading to an uncontrolled polymer chain length with broad MWDs. To check further, the kinetics of this photopolymerization was studied, which will be discussed later in this section.

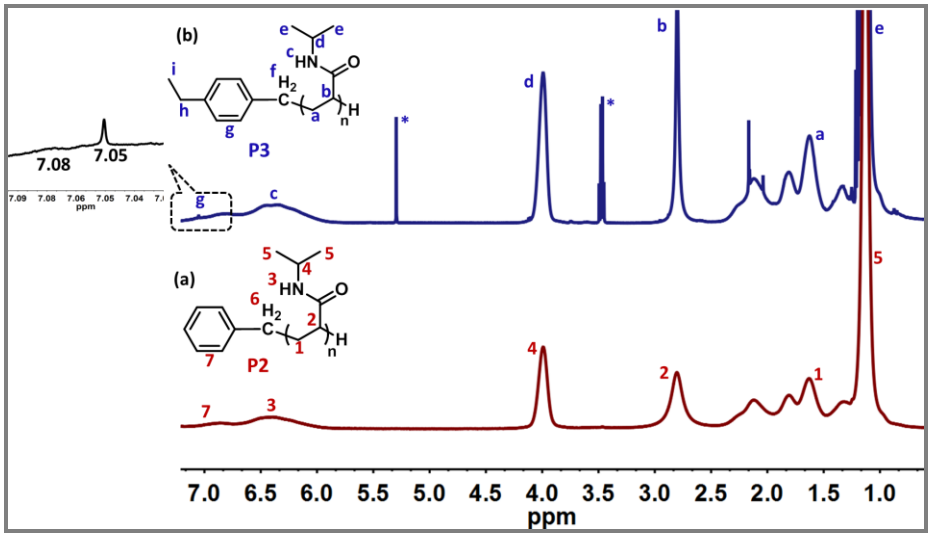

Figure 10. ^{1}H-NMR spectra of (a) **P2** and **(b) P3** polymer in $CDCl_3$. (*solvent peaks).

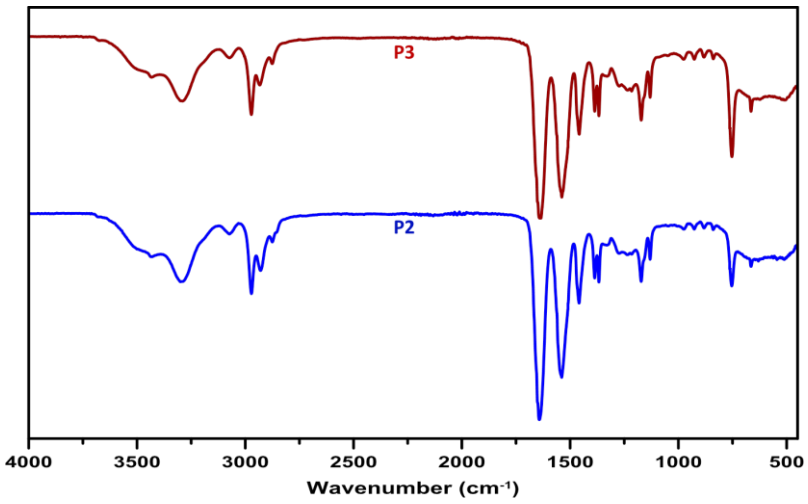

Figure 11. FTIR spectra of **P2** and **P3** polymer.

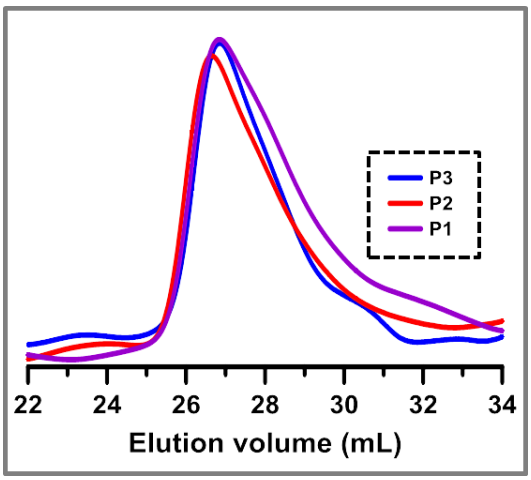

Figure 12. SEC traces of **P1**, **P2** and **P3.** Column temperature = 45 °C. THF with 1wt.% (w/v) TBAB as eluent and Styragel HR1 (M_n = 100−5000), HR3 (M_n = 500−30 000), HR4 (M_n = 5000−600000) and HR5 (50000-4000000) columns were used for **P1-P3.**

To check the versatility of these PIs, 2-(dimethylamino)ethyl methacrylate (DMAEMA) monomer was also subjected to photopolymerization using **PI-1** and **PI-3** (Scheme 2d, 2e and Table 1, entries 4-5). The obtained **P4** and **P5** did not show any vibration bands at around 1639 cm^{-1} for -C=C- bond in DMAEMA indicating its complete conversion to PDMAEMA (Figure 13). Further, FTIR spectra of **P4** and **P5** showed the characteristic band of the carboxylic (>C=O) group at 1728 cm^{-1} along with other bands. The absence of ^{1}H-NMR signal of vinylic protons of DMAEMA monomer in between δ 5.5- 6.5 ppm and the appearance of broad signal in between δ 0.7- 1.2 ppm for the backbone methylene protons in the ^{1}H-NMR spectra of **P4** and **P5** (Figure 14) clearly indicated the successful photopolymerization of DMAEMA.[42] SEC revealed M_ns of 91.6 and 163.3 *kDa* with *Đ*s of 2.2 and 1.54 respectively for **P4** and **P5** (Figure 15).

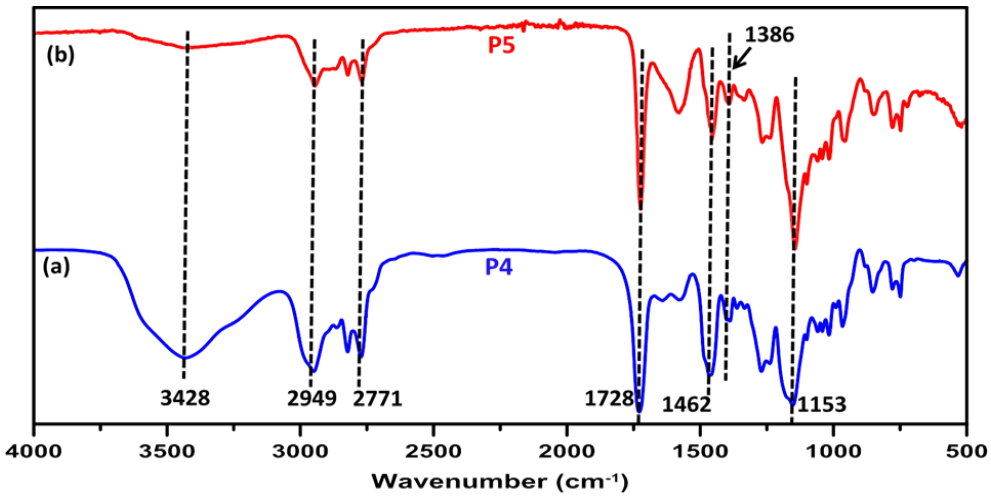

Figure 13. FTIR spectra of **P4** and **P5** polymer.

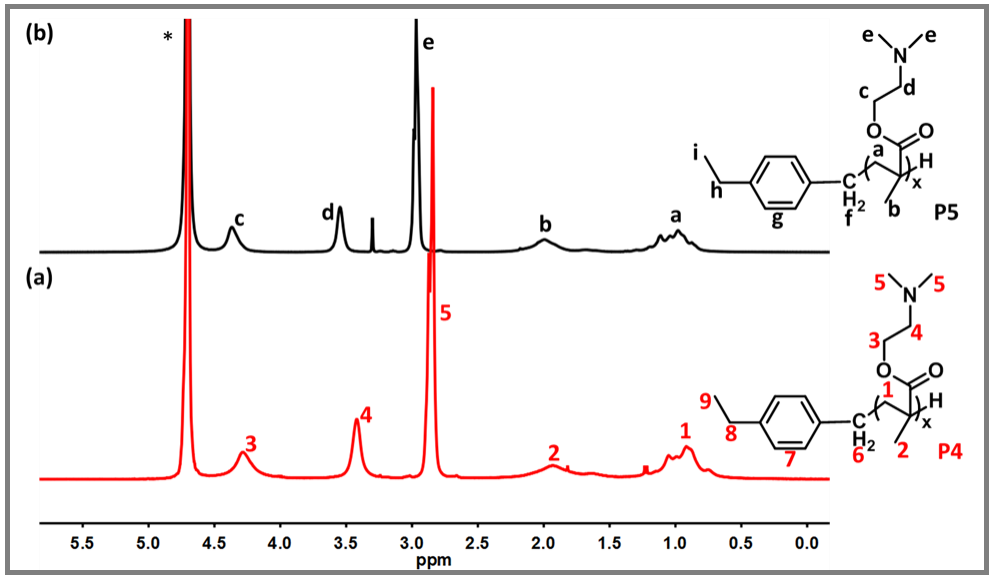

Figure 14. ^{1}H-NMR spectra of **P4** and **P5** polymer in D_2O (*solvent peaks).

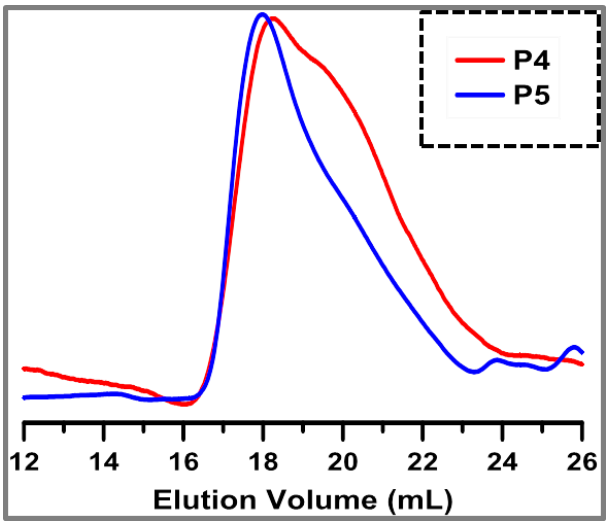

Figure 15. SEC traces of **P4** and **P5** polymer**.** Eluent: H_2O with 0.30 M Na_2SO_4 and 0.1% (w/v) NaN_3 at pH 7 at a flow rate of 1.0 mL min^{-1} and at 30 °C; column temperature = 30 °C. Styragel HR1 (M_n = 100–5000), HR3 (M_n = 500–30 000), and HR4 (M_n = 5000–600000) columns were used in this case.

To check the dependence of monomer conversion, M_n and *Đ*s with irradiation time, the kinetics of NIPAM polymerization was investigated using **PI-1** (Table 2) for different time intervals at ambient temperature. The SEC traces of PNIPAMs obtained at different time intervals are given in Figure 16 which clearly indicates that the retention time (RT) values of the chromatograms can hardly be correlated with the irradiation times. We have further plotted M_ns and *Đ*s as a function of irradiation time (Figure 17). Figure 17A represented the %conversion versus irradiation time for NIPAM polymerization using **PI-1**. We observed that %conversion initially increased with irradiation time and then it became constant, which is usually observed for CFRP. On the other hand, Figure 17B clearly revealed that M_ns of PNIPAMs changed randomly with irradiation time, whereas their *Đ*s were ranging from 1.44-1.67. Observing such irregular increase of M_ns with broad *Đ*s of obtained polymers at different time intervals, it can only

be concluded that M_ns and $Đ$s of the formed polymers did not depend on the irradiation time, which actually eliminates the possibility of any controlled/living nature of this photopolymerization.[43] From the above-mentioned results and discussion, it is understood that a free radical mechanism is most probably responsible for this IL-initiated photopolymerization (Scheme 5).

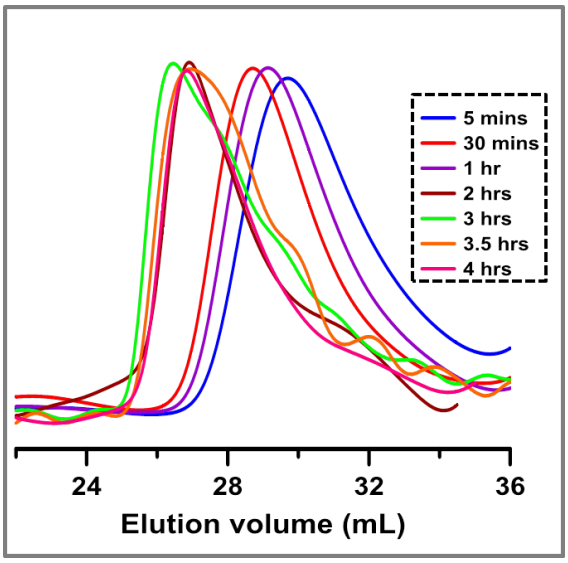

Figure 16. SEC traces of PNIPAMs obtained by photopolymerization of NIPAM using **PI-1** as initiator at different irradiation times. (Condition: [NIPAM]: [**PI-1**] =100:10; temperature= 25°C; and solvent = water).

Table 2. Kinetics of photopolymerization of NIPAM using **PI-1** under UV irradiation

Entry	Monomer (M)	Photonitiator (PI)	[M]:[PI]	Condition	Irrad. time (min)	% conversion	M_n (GPC) (KDa)	Đ
1	NIPAM	PI-1	100:10	hν (λ=310nm)	5	23.16	14.7	1.44
2	NIPAM	PI-1	100:10	hν (λ=310nm)	30	49.926	20.8	1.48
3	NIPAM	PI-1	100:10	hν (λ=310nm)	60	60.592	16.9	1.52
4	NIPAM	PI-1	100:10	hν (λ=310nm)	120	71.614	41.2	1.56
5	NIPAM	PI-1	100:10	hν (λ=310nm)	180	74.537	44.2	1.67
6	NIPAM	PI-1	100:10	hν (λ=310nm)	210	76.56	46.9	1.46
7	NIPAM	PI-1	100:10	hν (λ=310nm)	240	80.82	45.7	1.48

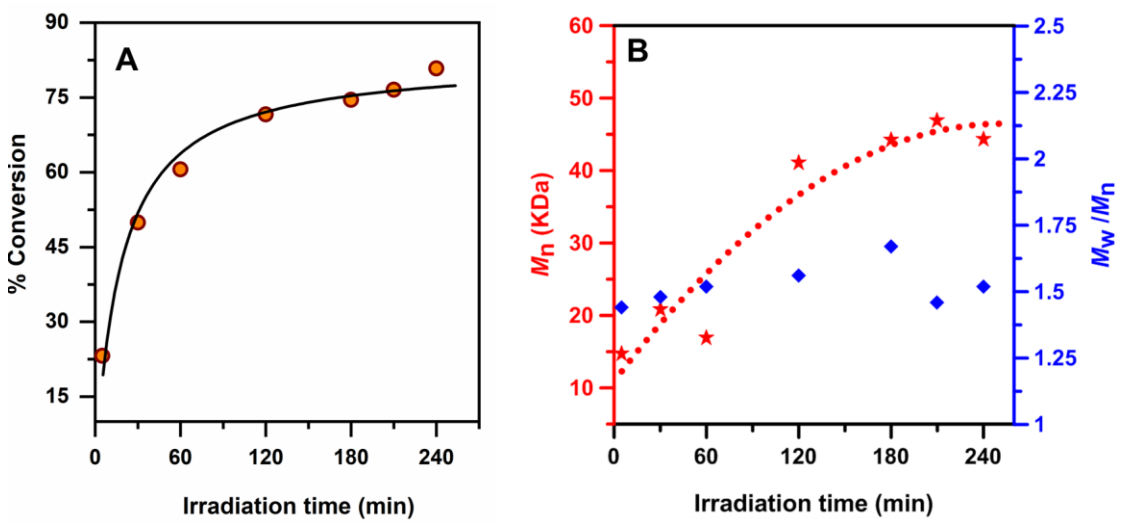

Figure 17. (A) Plot of monomer conversion (%) versus UV light irradiation time and (B) variations of M_n and Đ of **P1** with irradiation time. (Conditions:[NIPAM]:[PI-1] =100:10; Temperature = 25°C and Solvent = water).

To provide support to the proposed mechanism, radical trapping experiment was carried out by adding 0.009 mmol of radical scavenger 2,2,6,6-tetramethyl-1-piperidinyloxyl (TEMPO) into a set of reaction (entry 1, Table 1) (Figure 18A). A noticeable decrease of M_n of **P1** from 45.7 (without TEMPO) to 24.8 *kDa* (with TEMPO) was observed (Figure 18B), which indicated the radical pathway. This is obvious, because the free radicals generated in situ from the **PI-1** during the course of the polymerization are quenched partially by the TEMPO radical leading to lowering of molecular weight of the formed polymer. Therefore, in the presence of these IL-based PIs, the photopolymerization are actually initiated by either 4-ethylbenzyl or benzyl radical generated by the UV irradiation, which are not supposed to be very stable in aqueous medium. To provide further support in favour of this radical mechanism, an analogous radical-trapping experiment (Figure 18A) was performed where 0.265 mmol of **PI-1** and 0.398 mmol of TEMPO were added to 2 mL of water and subjected to UV irradiation (λ_{max} = 310 nm) under the optimized reaction conditions in the absence of any monomer. A mixture of (4-ethylbenzyl)-TEMPO adduct and triphenylphosphine oxide (TPPO) (designated as BP-1 in Scheme 5) were separated from the aqueous mixture after 4h of UV irradiation. The reaction mixture was first diluted with EtOAc (10 mL) and H_2O (10 mL) and then extracted with EtOAc (10 mL x 2). The combined organic phase was repeatedly washed with H_2O (4 x 30 mL), dried over anhydrous $MgSO_4$, and concentrated in vacuum. The presence of both (4-ethylbenzyl)-TEMPO adduct and triphenylphosphine oxide (TPPO) were confirmed from HRMS analysis (Figure 19). Furthermore, the dried ethyl acetate extract was examined by ^{31}P-NMR using H_3PO_4 as a standard and the signal at δ 25.9 ppm clearly indicated the formation of TPPO (Ph_3P=O) (Figure 20).[44] Therefore, as proposed, upon UV radiation, **PI-1** generates 4-ethylbenzyl radical through the direct homolytic cleavage of C–P bond followed by instantaneous

capture by TEMPO radical along with the generation of triphenylphosphonium radical cation ($Ph_3P^{\bullet+}$), which eventually transformed into TPPO as shown in Scheme 5, indicating the involvement of a radical sequence in this transformation.

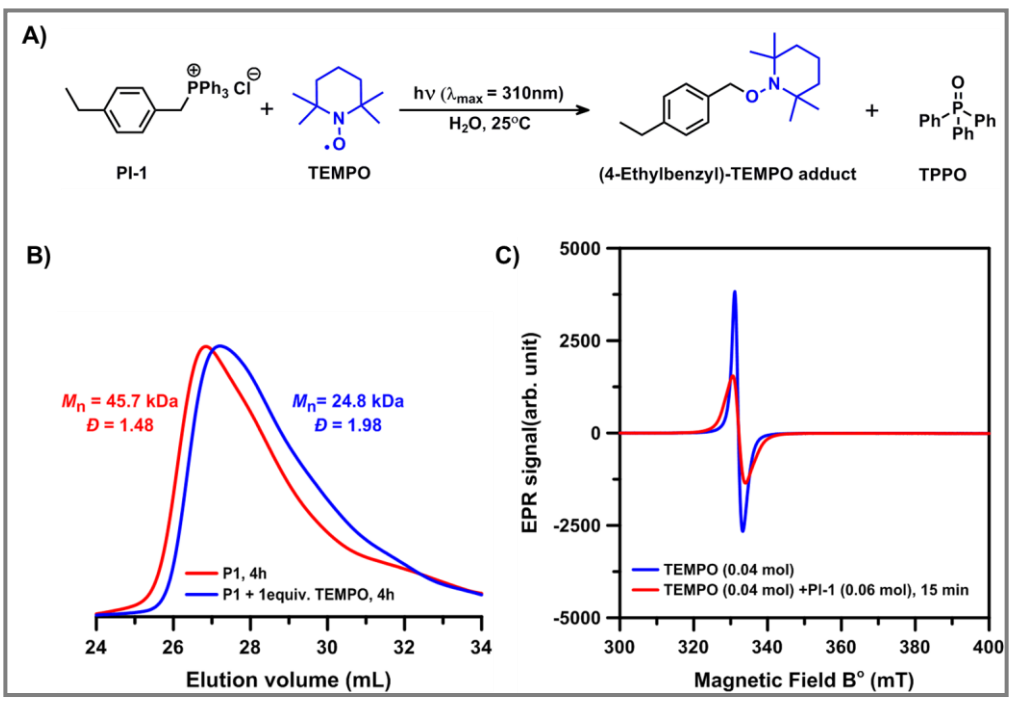

Figure 18. (A) Radical trap reaction of PI-1 with TEMPO; (B) SEC traces for PNIPAMs (Table 1, entry 1), synthesized in the absence (red) and in the presence (blue) of TEMPO (1 equiv.) under UV irradiation for 4h; (C) EPR spectra of TEMPO (0.04 mol/mL) radicals in water (blue line) and a mixture of TEMPO (0.04 mol/mL) radicals with **PI-1** (0.06 mol/mL) in water (red line).

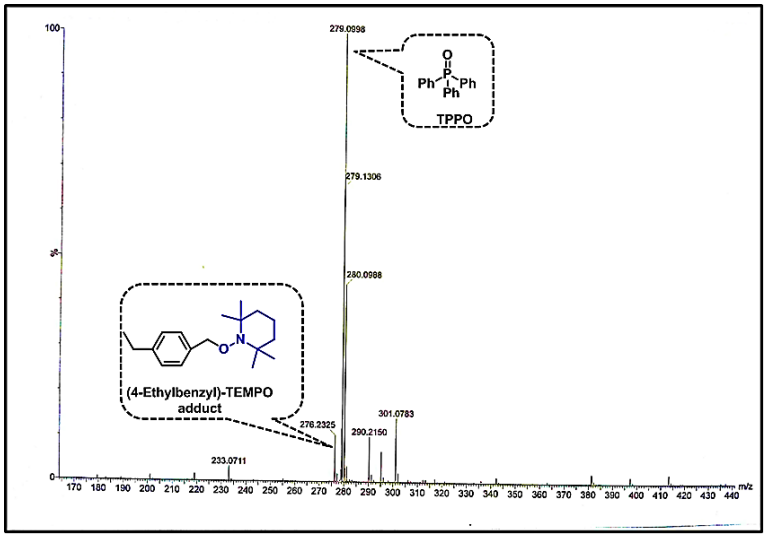

Figure 19. HRMS (ESI+) data of 4-ethylbenzyl-TEMPO adduct and TPPO obtained by radical trap reaction between **PI-1** and TEMPO.
HRMS (ESI+) m/z calculated for $C_{18}H_{29}NO$ $(M+H)^+$:276.228, found :276.2325.
HRMS (ESI+) m/z calculated for $C_{18}H_{15}OP$ $(M+H)^+$:279.098, found :279.0998.

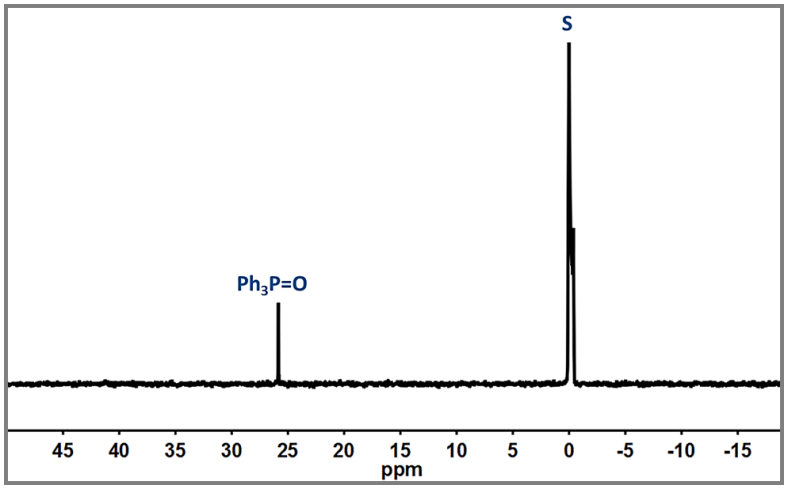

Figure 20. ^{31}P-NMR spectrum (DMSO-d_6) of the triphenylphosphine oxide generated after the reaction of **PI-1** with TEMPO in aqueous medium under UV-irradiation (λ_{max}=310nm). The peak was referenced to 88% H_3PO_4 (indicated as "S").

A similar radical trapping experiment was also performed using a mixture of 0.265 mmol of **PI-3** and 0.398 mmol of TEMPO in 2 mL of water and was irradiated with UV light (λ_{max} = 310 nm) for 4h in the absence of any monomer (Figure 21).The (4-ethylbenzyl)-TEMPO adduct and 1-butylimidazolium bromide

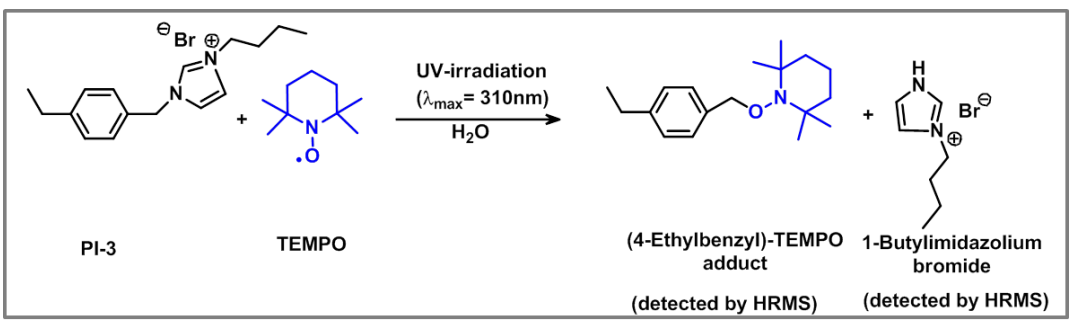

Figure 21. Radical trap reaction between **PI-3** and TEMPO.

(designated as BP-2 in Scheme 5) were isolated from the EtOAc and the aqueous extract respectively of the reaction mixture and their presence were confirmed by HRMS analysis (Figure 22). Furthermore, it is known that the photoinduced radical polymerization itself is very sensitive to oxygen inhibition, which makes it difficult to detect the radical by electron paramagnetic resonance (EPR) spectroscopy. We have also performed a parallel spin trapping experiment using EPR spectroscopy for further evidence.[45] EPR spectra of TEMPO (0.04 mol/mL) radicals in water (blue line in Figure 18 C) and a mixture of TEMPO (40 mmol/mL) radicals with **PI-1** (60 mmol/mL) in water (red line in Figure 3C) after 15 min of irradiation clearly showed the decrease in signal intensity by almost 60%**,** which indicated that some portion of TEMPO radials were quenched by the 4-ethylbenzyl free radicals generated from **PI-1** in situ, resulting in the decrease of its EPR signal intensity. This observation strongly supports the free radical pathway as shown in Scheme 5.

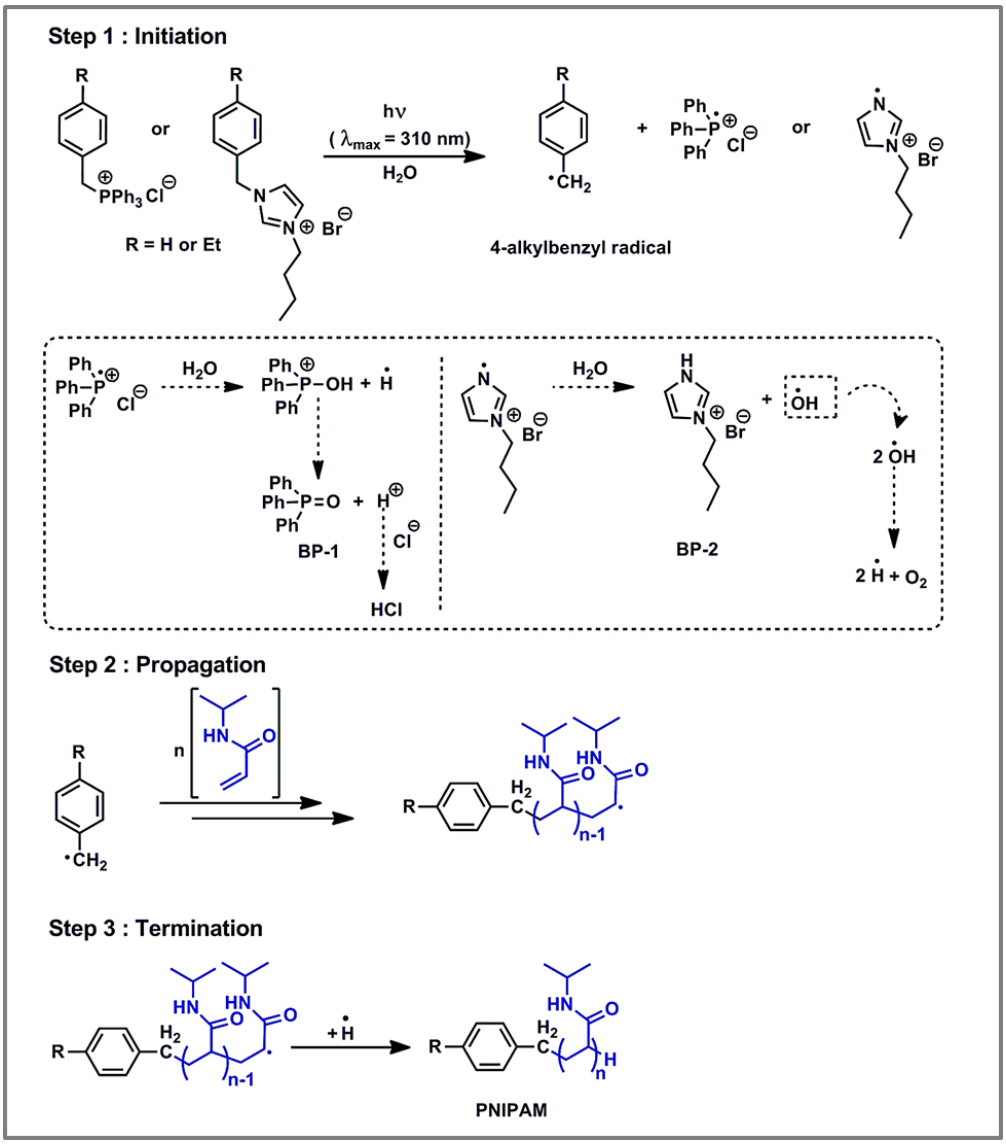

Scheme 5. Proposed mechanism for photoinduced free radical polymerization of NIPAM using phosphonium (**PI-1**, **PI-2**) and imidazolium (**PI-3**) IL-based PIs.

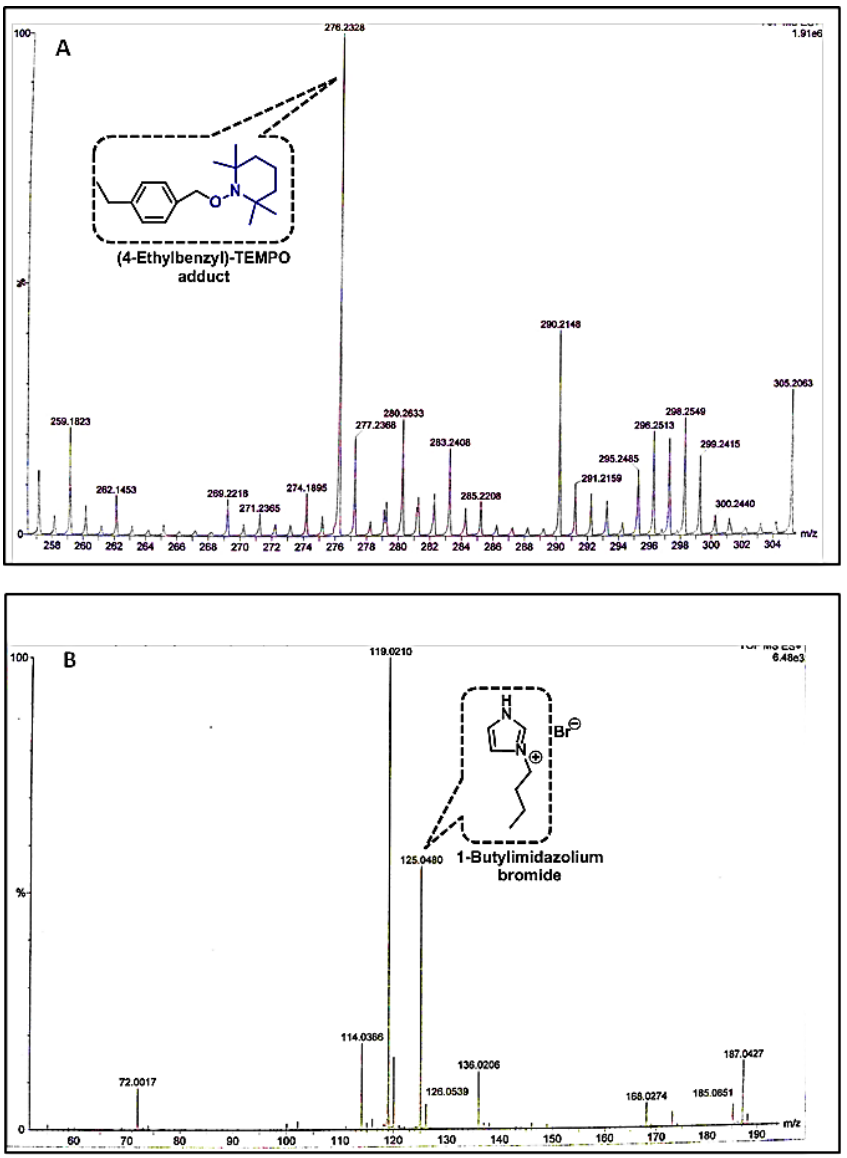

Figure 22. HRMS (ESI+) data of A) 4-ethylbenzyl-TEMPO adduct and B)1-Butylimidazolium bromide obtained by radical trap reaction between **PI-3** and TEMPO.

HRMS (ESI+) m/z calculated for $C_{18}H_{29}NO$ $(M+H)^+$:276.228, found: 276.2328.
HRMS (ESI+) m/z calculated for $C_7H_{13}N_2^+$ (M^+):125.11, found: 125.048

One may raise an issue that the benzyl/4-ethylbenzyl radicals (Scheme 5) may undergo electron transfer with the radical cations formed therein to form benzyl/4-ethylbenzyl cations, which eventually can combine with chloride ion

present in the medium to finally generate benzyl chloride/4-ethylbenzyl chloride. To check this, we have performed a control experiment, where a 10 wt.% aqueous solution of **PI-2** was subjected to UV irradiation (λ_{max} = 310 nm) for 4 h in the absence of any monomer. The crude reaction mixture was freeze-dried and subjected to HRMS analysis. The spectra (Figure 23) did not show any peak corresponding to the molecular ion of benzyl chloride, which eventually eliminates the possibility of its formation due to electron transfer.

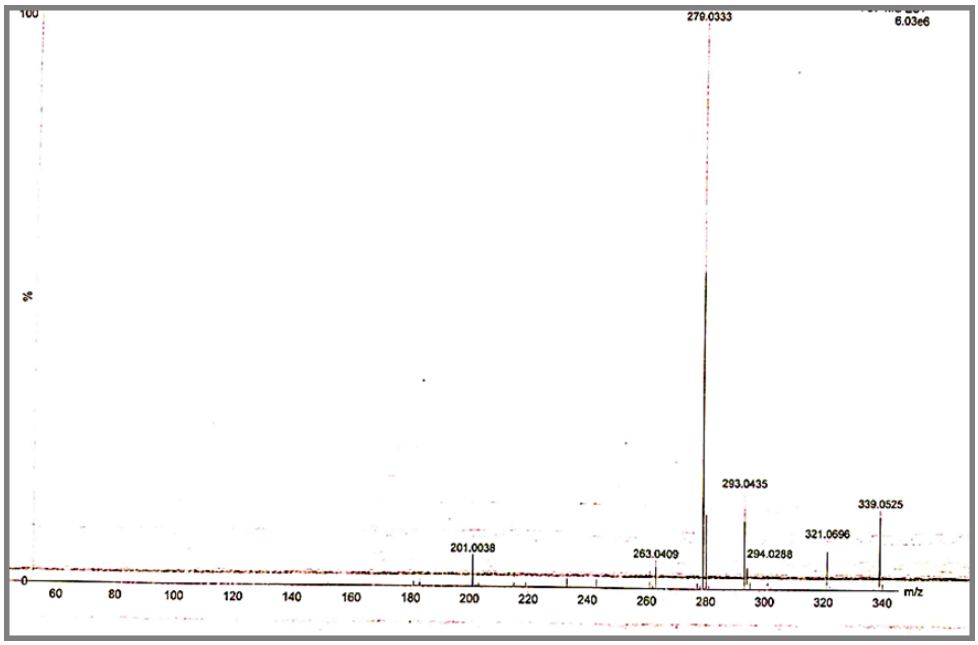

Figure 23. HRMS (ESI+) data of the crude freeze-dried reaction mixture obtained by irradiating (λ_{max}=310nm) **PI-2** in aqueous medium for 4h in absence of any monomer.

The proposed mechanism was finally confirmed via end-group analysis by MALDI-TOF-MS experiment. As shown in Scheme 2, it is expected that the 4-ethylbenzyl group would be present at the one end and H atom at the terminal end of PNIPAM chain. The enlarged middle portion of MALDI-TOF-MS spectrum of the **P1** (Figure 24) clearly revealed a series of equidistant (~113.3) molecular ion peaks

at m/z of 5257.62, 5370.9, 5484.19, and 5597.48. This value can be correlated to the molecular weight of NIPAM repeating unit of PNIPAM (**P1**). The experimental

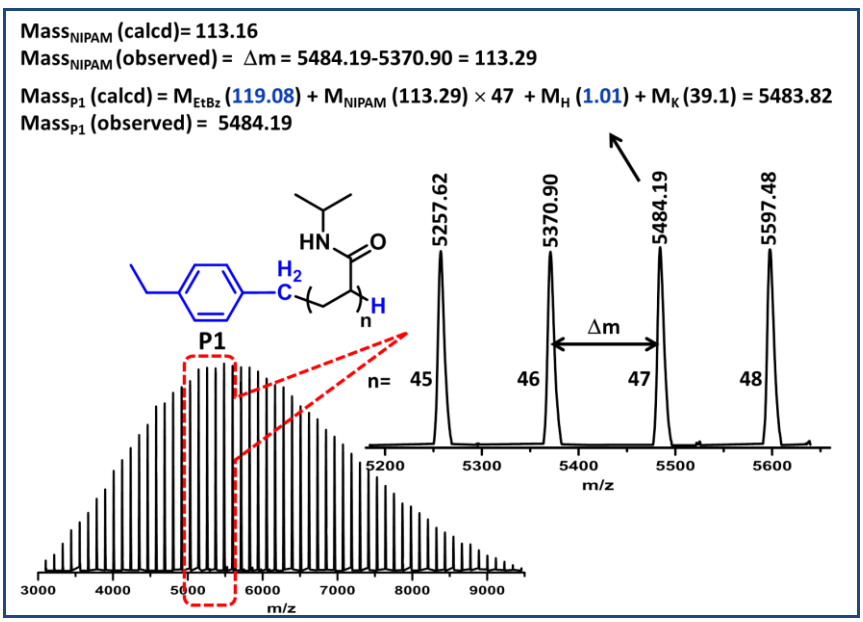

Figure 24. MALDI-TOF-MS spectrum of **P1** with 4-ethylbenzyl end group (entry 1 in Table 1).

peak at m/z = 5484.19 of **P1** can be correlated with EtBz-PNIPAM containing 47 units of NIPAM, one unit of 4-EtBz group, one hydrogen atom and one K^+ ion. Thus, the M_n (calculated) = (119.08 + 113.29×47 +1.01+39.1) almost exactly matched with the m/z peak value of 5484.19. These results confirmed the presence of 4-ethylbenzyl group at the one end and 'H' atom as terminal end of PNIPAM. Accordingly, the other highlighted peaks, 5257.62, 5370.9 and 5597.48, can also be correlated with PNIPAMs of 45, 46 and 48 NIPAM units respectively. The analyses of MALDI-TOF-MS spectra of **P2** (Figure 25a) and **P3** (Figure 25b) also revealed the incorporation of benzyl and 4-ethylbenzyl groups respectively at the ends of the corresponding polymers. The analysis of MALDI-TOF-MS

spectrum of **P4** also showed a series of peaks separated by ~156.5 Da which is almost equal to the molar mass of DMAEMA repeating unit (Figure 26). The enlarged middle portion of the spectrum showed two sharp molecular ion peaks at m/z of 2036.57 [=M_{EtBz} (119.08)+M_{DMAEMA} (156.5)×12+M_H (1.01) +M_K (39.1)] and 2193.07 [=M_{EtBz} (119.08)+M_{DMAEMA} (156.5)×13+M_H (1.01) +M_K (39.1)] corresponding to 4-ethylbenzyl moiety at the one end along with 12 and 13 units of DMAEMA respectively (Figure 26). Thus, the analysis of spectral data confirmed the attachment of 4-ethylbenzyl unit at the end of every growing PDMAEMA chain. MALDI analyses results of **P1**, **P2**, **P3** and **P4** clearly indicated the attachment of either 4-ethylbenzyl or benzyl group at the end of their chains confirming our proposed mechanism as shown in Scheme 4. In addition to this, ^{1}H-NMR spectra of **P1** and **P3** (Figure 1 and Figure 10b respectively) revealed the presence of aromatic benzene moiety. These results provided evidence of the incorporation of aromatic moiety at the polymer chain end and hereby support the proposed mechanism in Scheme 5.

There are some distinct advantages of these IL-based PIs compared to other commercially available PIs for aqueous or organic photopolymerization. As mentioned above, one of the basic requirements of photoinitiating systems for making speciality polymers in industrial applications is their partial or total solubility in water.[11] In fact, scientists have made serious efforts to improve PIs'

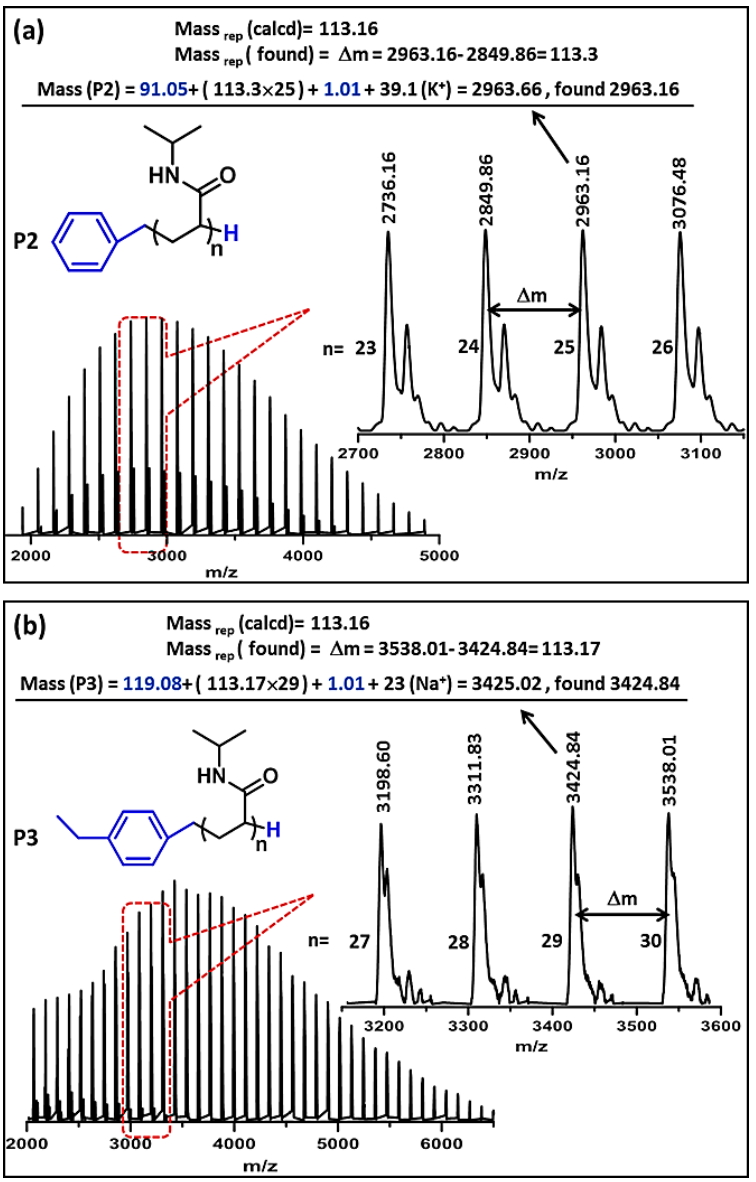

Figure 25. MALDI-TOF–MS spectrum of PNIPAM) with (a) benzyl end group (**P2**) (entry 2 in Table 1) and (b) 4-ethylbenzyl end group (**P3**) (entry 3 in Table 1).

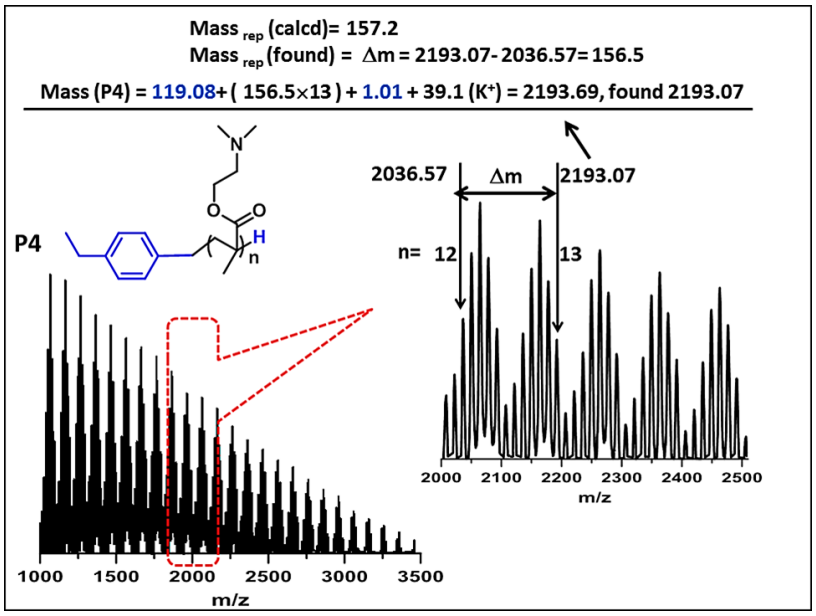

Figure 26. MALDI-TOF–MS spectrum of PDMAEMA with ethylbenzyl end group (**P4**).

water solubility for aqueous free radical photopolymerization.[18, 22, 46] In this context, ionic liquids, some special organic salts with unique physicochemical properties and high thermal stabilities are the interesting choice to use them as photoinitiating systems because of their higher solubility in water.[47-48]

Thus, we have checked the water solubility of these IL-based PIs by gravimetry[49] at ambient temperature and atmospheric pressure and compared them with those of other reported aqueous PIs (Table 3). The data clearly showed the higher water solubility of our IL-based PIs. Furthermore, the efforts have also been made to develop PIs that can be used for the photopolymerization of monomers by irradiating with lights of wide range of wavelengths.[14, 50] To check, the concentration dependent UV-vis spectra were recorded (Figure 27), which showed maximum absorbance peak (λ_{max}) at around 268 nm for **PI-1** and **PI-2** and 261nm for **PI-3**. But, the spectra also showed a

hump at around 310 nm when the concentration PIs were 0.05 M or more. Thus, their molar extinction coefficients (ε) are high enough to get initiated even upon exposure to relatively higher wavelength of UV-light source (310 nm with an intensity of 13 mW/cm^2). The molar extinction coefficients of all the PIs were determined from the slopes of the absorbance (at λ_{max}) vs. concentration plots as shown in Figure 28.

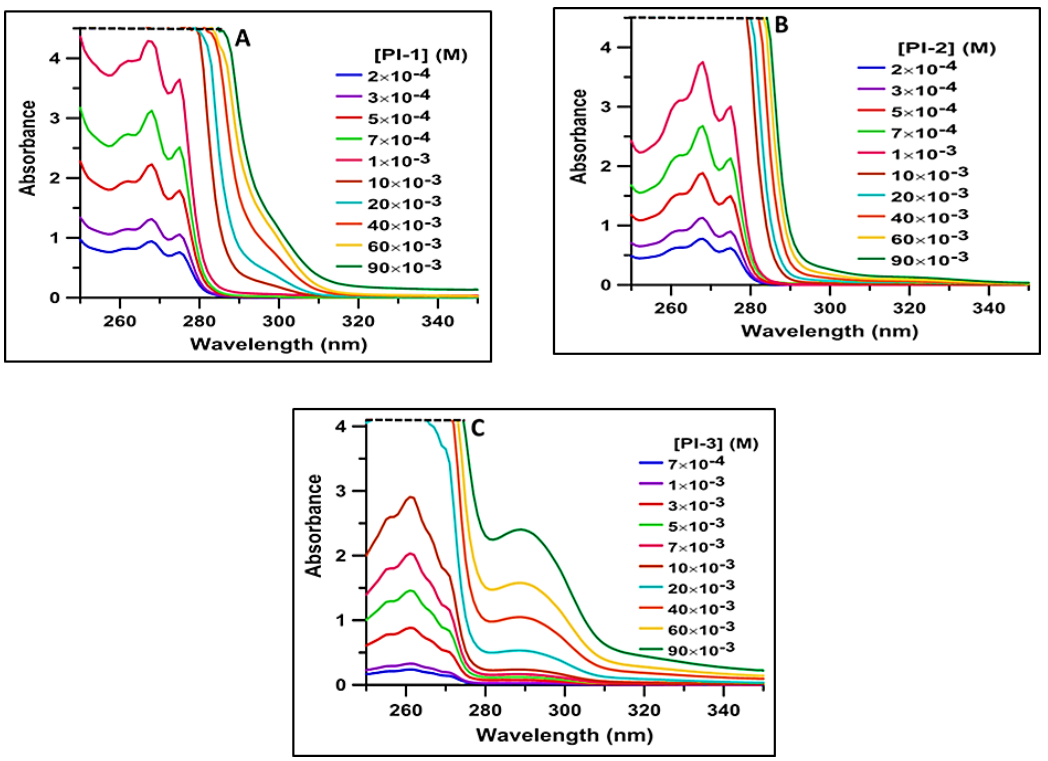

Figure 27. UV-vis absorption spectra of A) **PI-1** (2×10^{-4}-90×10^{-3} M); B) **PI-2** (2×10^{-4}-90×10^{-3} M) and C) **PI-3** (7×10^{-4}-90×10^{-3} M) in aqueous solution.

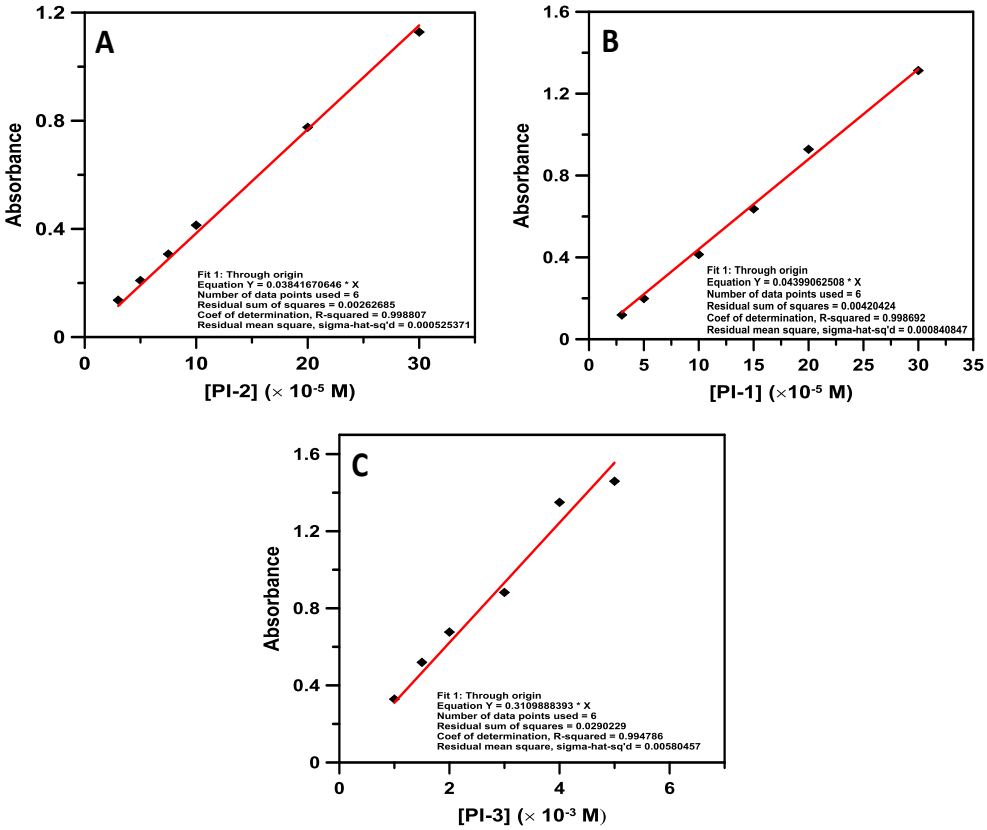

Figure 28.Calibration curves (concentrations vs absorbance measured at their λ_{max}s with the linear best-fit line) for the IL-based photoinitiators A) **PI-1**, B)**PI-2** and C)**PI-3** in aqueous solution.

It should be noted that the use of UV source of lower wavelength (λ = 250 nm) produced polymers, but the solution became yellow, which has also been noticed elsewhere for the use of shorter-wavelength UV irradiation.[51-52] Thus, in this case, a concentration of 0.09 M of PIs (**PI-1-PI-3**) and a 310 nm UV-source were used for successful polymerization of NIPAM and DMAEMA to obtain their high molecular weights with high % conversion without any yellowing of the solution.

Table 3. Comparison of spectroscopic properties and solubility of reported aqueous PIs along with the IL-based PIs used in this manuscript.

PI	Spectroscopic properties		Water solubility ($g.dm^{-3}$)	Reference
	λ_{max}/source of irradiation (nm)	$\varepsilon@\lambda_{max\text{-}ab}$ ($dm^3.mol^{-1}.cm^{-1}$)		
Irgacure 2959	276/365	--	<20	[14]
LAP	380/(320-395)	191	47	[14]
TPO-Na	380	250	29	[14]
BAPO-OLi	383/(320-420)	197	54	[14]
BAPO-ONa	383	256	60	[14]
PI-1	268,275/310	4399[a]	88[b]	This work
PI-2	268,275/310	3841[a]	125[b]	This work
PI-3	261,289/310	311[a]	>120[b]	This work

[a]Calculated from the calibration curves presented in Figure 28.

[b]Determined by gravimetry.

To further compare the efficiency of these IL-based PIs, we have polymerized NIPAM and DMAEMA using two commercially available conventional free radical photoinitiators, α-ketoglutaric acid (AKG)[53] and phenylglyoxylic acid (PGA)[54-55] keeping the same reaction conditions and irradiation source.The results have been provided in Table 4. M_ns of PNIPAMs, obtained by initiating with AKG and PGA (designated as P'1 and P'2 respectively) were 11.3 ($Đ$ = 1.5) and 10.7 *kDa* ($Đ$ = 1.4) respectively whereas PDMAEMAs initiated with AKG and PGA (P'3 and P'4 respectively) gave M_ns of 9.5 ($Đ$ = 1.45) and 36.5 *kDa* ($Đ$ = 2.91) respectively (Table 4, Figure 29). Table 3 clearly showed that M_ns of both PNIPAM and PDMAEMA initiated by either AKG or PGA were very low compared to those of same polymers obtained by our IL-based PIs in

aqueous medium. Thus, the IL-based PIs showed better performance in obtaining polymers of high molecular weights with respect to other commonly used water-soluble PIs.

Table 4. Comparison between % conversion, M_n*s* and *Đs* of PNIPAMs and PDMAEMAs initiated by commercially available aqueous photoinitiators AKG and PGA along with the present IL-based PIs.

Entry	Monomer	Photoinitiator	Polymer	Conversion (%)[a]	M_n[b] (*kDa*)	*Đ*[b]
1	NIPAM	PI-1	P1	81	45.7	1.48
2	NIPAM	PI-2	P2	79	53.6	1.41
3	NIPAM	PI-3	P3	76	49.7	1.40
4	NIPAM	AKG	P′1	77	11.3	1.51
5	NIPAM	PGA	P′2	72	10.8	1.41
6	DMAEMA	PI-1	P4	74	91.6	2.2
7	DMAEMA	PI-3	P5	71	163.3	1.54
8	DMAEMA	AKG	P′3	79	9.5	1.45
9	DMAEMA	PGA	P′4	74	36.5	2.91

Conditions: [Monomer]:[PI] =100 : 10; Total volume = 1 mL; Irradiation time = 4h and Temperature = 25°C.

[a]Determined by gravimetry.

[b]SEC traces of all freeze-dried crude polymers are shown in Figure 29**.**

To check the efficiency and applicability of this technique, the grafting of PNIPAM/PDMAEMA chains on preformed **P[VBTP][Cl]** backbone through the 'grafting from' process was carried out following the same photopolymerization procedure (entries 5-6 in Table 1). First, **P[VBTP][Cl]** (M_n =18.64 *kDa*) homopolymer was synthesized by CFRP technique. A 2.5 wt.% of aqueous

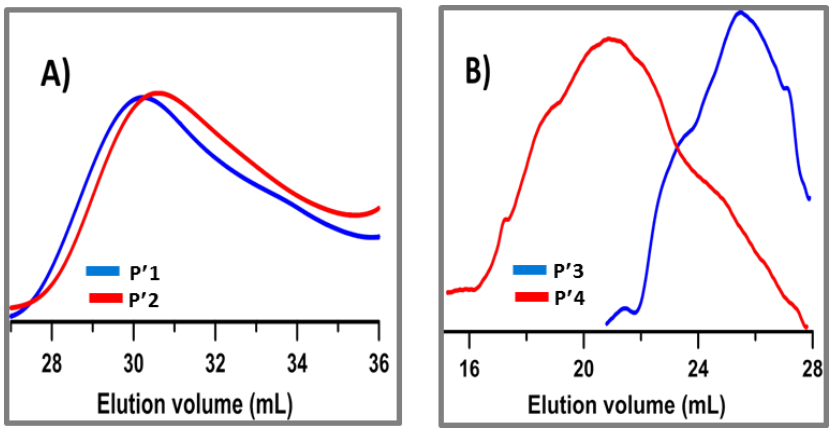

Figure 29. SEC traces of A) PNIPAM photoinitiated by α-Ketoglutaric acid **(**blue line) and phenylglyoxylic acid (red line). B) PDMAEMA photoinitiated by α-ketoglutaric acid **(**blue line) and phenylglyoxylic acid (red line).

P[VBTP][Cl] solution was mixed separately with 10 wt.% of either NIPAM or DMAEMA monomer and were subjected to UV irradiation. As expected, the PNIPAM or PDMAEMA chain was grown from the hanging benzylic end of the **P[VBTP][Cl] (**Scheme 3). The ^{1}H-NMR spectrum of P[VBTP][Cl]-*g*-PNIPAM (**P6**) (Figure 30) revealed the characteristic signals of **P[VBTP][Cl]** at δ (0.9-1.31), 5.22, 5.99, 6.75 and 7.58 ppm corresponding to '(a, b)', 'f', 'e', 'd' and 'g' protons respectively.[37] In addition to these signals for ungrafted **P[VBTP][Cl]**, signals at δ 1.48 and 3.88 ppm corresponding to the 'i' and 'k' protons respectively of NIPAM repeating unit were observed confirming the presence of grafted PNIPAM chains from the **P[VBTP][Cl]** backbone in **P6**. From the FTIR spectrum of **P6** copolymer (Figure 31), ungrafted **P[VBTP][Cl]** segment was identified from the characteristic bands at 1509 and 1483 cm^{-1}, corresponding to -C=C- stretching vibrations in the phenyl group, 1438 cm^{-1} for P-CH_2 deformation, 1110 cm^{-1} for P-Ph stretching

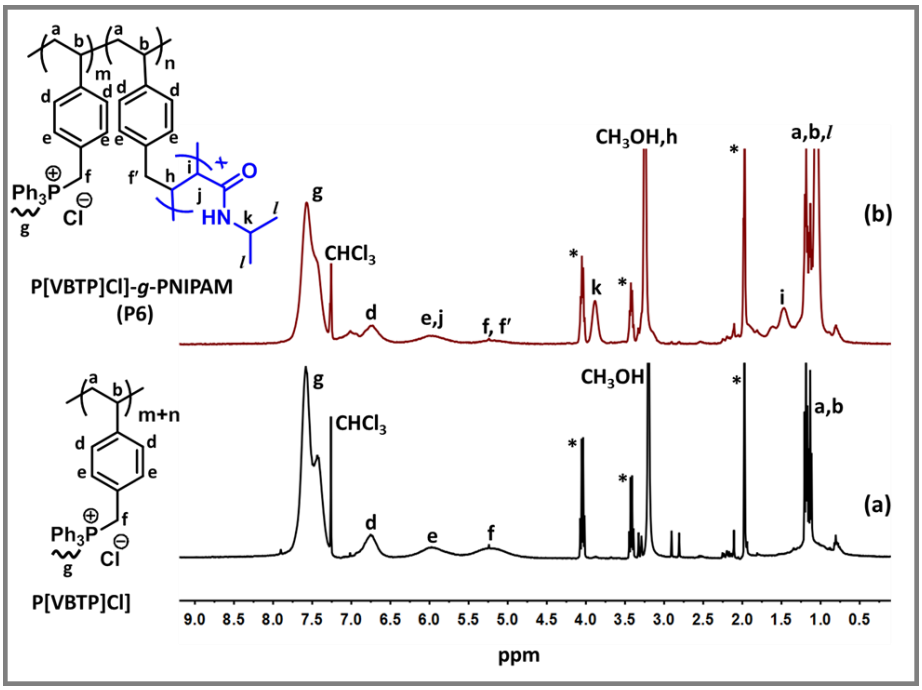

Figure 30. ^{1}H NMR spectra of a) **P[VBTP][Cl]** and b) P[VBTP][Cl]-*g*-PNIPAM (**P6)** in $CDCl_3/CD_3OD$(10/1) mixture (*Solvent peaks).

and 690 cm^{-1} for the typical benzene ring out of plane bending.[37] Whereas PNIPAM chains grafted from **P[VBTP][Cl]** backbone were characterized by a broad band at around 1643 cm^{-1} (amide I band, >C=O stretching vibration mode conjugated with –N–H groups on PNIPAM chains) and a band appearing at 1543 cm^{-1} (amide II band, N–H bending vibration).[56] Similarly, the grafting of PDMAEMA onto **P[VBTP][Cl]** backbone was carried out using the same photopolymerization of DMAEMA monomer and using above mentioned feed ratio (Table 1, Scheme 3). The ^{1}H-NMR spectrum of P[VBTP][Cl]-*g*-PDMAEMA (**P7**) (Figure 32) showed signals at δ 0.98, 6.46 and (7.1-7.8) ppm corresponding to the presence of ungrafted **P[VBTP][Cl]** unit[37], whereas the signals at δ 1.97, 2.94, 3.53

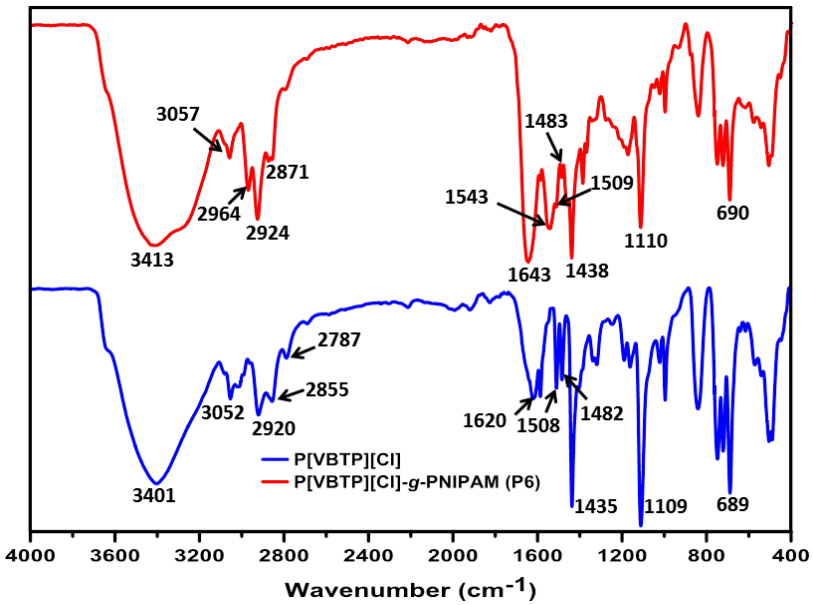

Figure 31. FTIR spectra of **P[VBTP][Cl]** (blue line) and P[VBTP][Cl]-*g*-PNIPAM (**P6**) (red line).

and 4.34 ppm correspond to the 'i', 'l', and 'k' protons respectively of DMAEMA repeating unit which further confirmed the presence of PDMAEMA that grafted from the **P[VBTP][Cl]** backbone in **P7.** The FTIR spectrum of **P7** (Figure 33) showed a sharp absorption band at 1726 cm^{-1} corresponding to the carbonyl stretching (>C=O), which was initially absent in neat **P[VBTP][Cl]**, which provided evidence for grafting of PDMAEMA onto the **P[VBTP][Cl]** backbone.

The SEC chromatogram (Figure 34A) clearly showed that the **P[VBTP][Cl]** having a low molecular weight elutes with a peak elution volume of about 22.2 mL (blue line), while the high-molecular-weight P[VBTP][Cl]-*g*-PNIPAM (**P6**) chains elute with much lower elution volume of about 15.7 mL (red line). Thus, it was a complete lateral shift in the chromatograms of **P[VBTP][Cl]** and **P6** copolymer with M_ns of 18.6 and 327.6 *kDa* respectively. The increase in M_n of the graft copolymer compared to that of homopolymer clearly suggested the

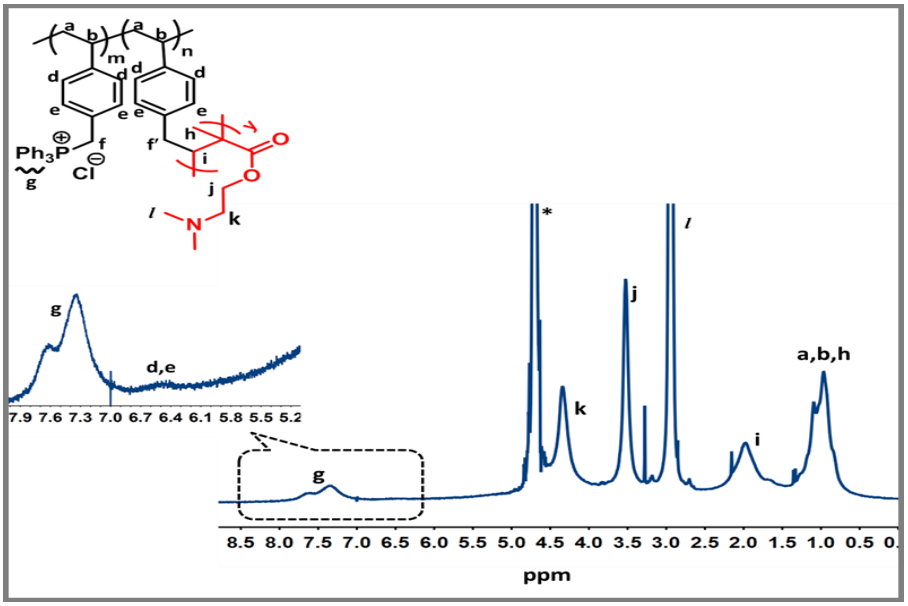

Figure 32. ^{1}H-NMR spectrum of P[VBTP][Cl]-*g*-PDMAEMA (**P7**) in D_2O (*Solvent peaks).

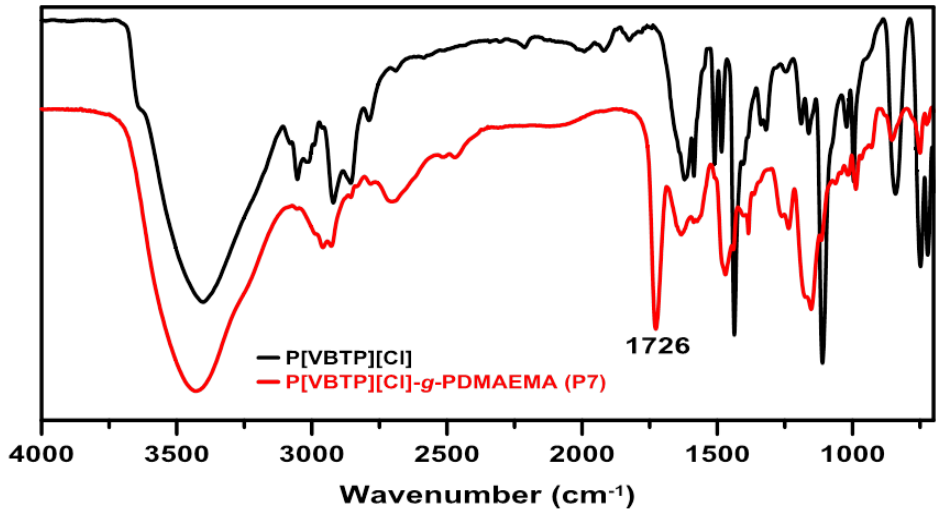

Figure 33. FTIR spectra of **P[VBTP][Cl]** (black line) and P[VBTP][Cl]-*g*-PDMAEMA (**P7**) (red line).

grafting of PNIPAM chain onto the **P[VBTP][Cl]** backbone upon irradiation with UV light. The grafting polymerization of NIPAM was initiated from the pendant benzylic radical of **P[VBTP][Cl]** chain under UV irradiation. The SEC chromatogram (Figure 34B, purple line) showed that M_n for **P7** was 269.3 kDa with a $Đ$ of 1.64. The molecular weight of P[VBTP][Cl]-*g*-PDMAEMA (**P7)** was much higher than that of neat **P[VBTP][Cl] (**Figure 34A, blue line**)**, which proved that **P[VBTP][Cl]** with hanging benzylic triphenyl phosphonium chloride moiety initiated the photopolymerization of DMAEMA, which resulted in formation of graft copolymer **P7**.

Further, as we know PNIPAM is a thermoresponsive polymer showing a lower critical solution temperature (LCST) phenomenon at around 32°C in aqueous solution.[57-60] Thus, we were interested to investigate the thermoresponsive behavior of **P6** graft copolymer in water by turbidimetry. As expected, the 0.5 wt.% aqueous **P6** solution showed an abrupt decrease of its %transmittance from 100 to almost 0 with increasing temperature (Figure 34C) due to the formation of insoluble macroscopic globules of P[VBTP][Cl]-*g*-PNIPAM. The cloud point (T_c) was measured to be 33.2°C. Upon heating, the phase separation of hanging PNIPAM chains occur resulting in a separation of whole graft copolymer from the aqueous solution due to the formation of insoluble globular copolymer aggregates above the cloud point.

PDMAEMA is also a LCST polymer and its T_c usually varied from 14 to 50 °C in water depending upon the pH of the medium.[61-63] Thus, we also examined the thermoresponsive behaviour of **P7** in water at pH 8.5 (Figure 34C). As PDMAEMA is a weak cationic polyelectrolyte, the aqueous solution of the **P7** is supposed to be in almost uncharged state at a pH of 8.5. At pH 8.5, the 0.5 wt.% aqueous **P7** solution showed an abrupt decrease in transmittance (%) from 100 to almost 0 with increasing temperature due to the formation of insoluble macroscopic

globules of P[VBTP][Cl]-*g*-PDMAEMA. The cloud point was measured to be 40°C. At this basic pH the solubility and stability of the graft copolymer in water

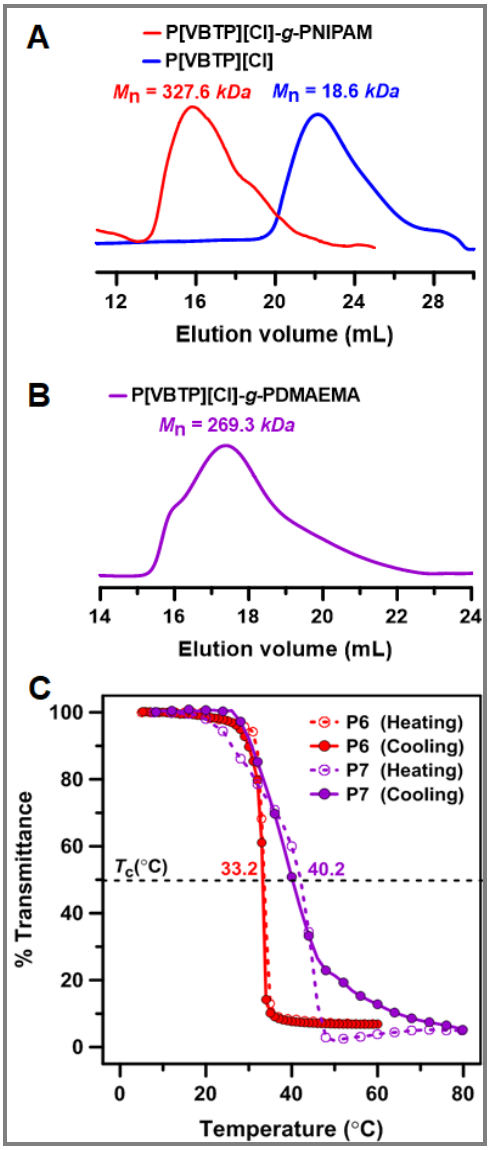

Figure 34: (A) SEC chromatograms of **P[VBTP][Cl]** homopolymer (blue line) and P[VBTP][Cl]-*g*-PNIPAM (**P6)** (red line) using DMF with 50 mM LiBr as eluent. (B) SEC trace of P[VBTP][Cl]-*g*-PDAMEMA (**P7)** (purple line) using H_2O with 0.3 M Na_2SO_4 and 0.1% (w/v) NaN_3 as eluent. (C) Turbidity [heating (dashed)/cooling (solid)] curves of 0.5 wt.% aqueous solution of **P6** (red line) and 0.5 wt.% aqueous solution of **P7** at pH 8.5 (purple line).

against aggregation and phase separation is due to effective hydrogen-bonding interactions with water molecules. When heated above the LCST, hydrogen-bonding interactions of the graft copolymer chains with water molecules are destroyed and the interchain hydrophobic interactions between hanging PDMAEMA moieties predominates resulting in the formation of insoluble globular aggregates and the graft copolymer completely phase-separated from aqueous medium at above 40°C. To support the turbidity measurement data, 0.5 wt. % aqueous solution of **P6** was also examined by DLS. The data showed a rapid increase in the D_h of aggregates from 60 to 185 nm with increase of temperature with a clear T_c of 33.8 °C (Figure 35 A), which matched well with that (33.2 °C) obtained from turbidity measurement. A 0.5 wt. % aqueous solution of **P7** at pH 8.5 was also examined by DLS. The data showed a rapid increase in the D_h of aggregate from 11 to 656 nm with the increase of temperature with a clear T_c of 39.6 °C (Figure 35B), which agreed well with that (40.2 °C) obtained from turbidity.

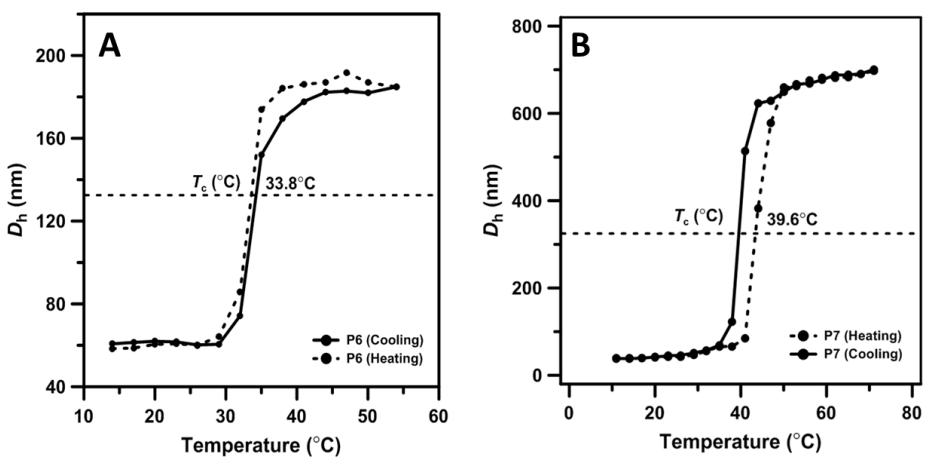

Figure 35. Changes in average hydrodynamic diameter (D_h) of 0.5 wt. % aqueous solution of (A) **P6** (B) **P7** (at pH 8.5) as plotted with temperature.

4.5 CONCLUSIONS

In summary, newly designed phosphonium- and imidazolium ionic liquids (ILs) of different chemical structures were successfully synthesized and were used for the first time as photoinitiators for polymerization of different vinyl monomers such as NIPAM and DMAEMA under UV irradiation (λ_{max} =310 nm) in aqueous medium. It has been established through end-group analysis by MALDI-TOF-MS, EPR and some control experiments that this photopolymerization proceed through free radical pathway. The kinetic and SEC data revealed no linear increase of %conversion and M_n with polymerization time as well as broad dispersities of the obtained polymers which eliminates the possibility of any kind of control in this photopolymerization, rather, as expected, it followed the conventional free radical pathway. Control experiments revealed that the water-solubility of these IL-based PIs were high and were capable of producing polymers with high molecular weights compared to those of polymers obtained by commercially available aqueous PIs. Further, as an extension of this photopolymerization technique, PNIPAM and PDMAEMA were successfully grafted onto **P[VBTP][Cl]** backbone by photoinduced grafting-from copolymerization.

4.6 REFERENCES

1. Pappas, S. P., *Radiat. Phys. Chem.* **1985**, *25*, 633-641.

2. Warson, H., *Uv & Eb Curing Formulation for Printing Inks, Coatings and Paints*; SITA Technology: London, 1988.

3. Fouassier, J. P.; Lalevée, J., *Photoinitiators for Polymer Synthesis: Scope, Reactivity, and Efficiency*; John Wiley & Sons: Munich, 2012.

4. Reetz, I.; Yagci, Y.; Mishra, M. K., *Plast. Eng.(N.Y.)* **1998**, *48*, 149-202.

5. Davidson, R. S., *Exploring the Science, Technology and Applications of Uv and Eb Curing*; Sita Technology: London, 1999.

6. Bagheri, A.; Jin, J., *ACS Appl. Polym. Mater.* **2019**, *1*, 593-611.

7. Tasdelen, M. A.; Karagoz, B.; Bicak, N.; Yagci, Y., *Polym. Bull.* **2008**, *59*, 759-766.

8. Yang, L.; Fan, X.; Zhang, J.; Ju, J., *Polymers* **2020**, *12*, 389.

9. Yagci, Y.; Jockusch, S.; Turro, N. J., *Macromolecules* **2010**, *43*, 6245-6260.

10. Barker, P.; Guthrie, J.; Davis, M.; Godfrey, A.; Green, P., *J. Appl. Polym. Sci.* **1981**, *26*, 521-527.

11. Lalevée, J.; Fouassier, J.-P., *Photopolymerisation Initiating Systems*; Royal Society of Chemistry, 2018.

12. Decker, C.; Masson, F.; Schwalm, R., *JCT Res.* **2004**, *1*, 127-136.

13. Liang, Q.; Zhang, L.; Xiong, Y.; Wu, Q.; Tang, H., *J. Photochem. Photobiol. A* **2015**, *299*, 9-17.

14. Tomal, W.; Ortyl, J., *Polymers* **2020**, *12*, 1073.

15. Yu, C.; Schimelman, J.; Wang, P.; Miller, K. L.; Ma, X.; You, S.; Guan, J.; Sun, B.; Zhu, W.; Chen, S., *Chem. Rev.* **2020**, *120*, 10695-10743.

16. Zapka, W., *Handbook of Industrial Inkjet Printing: A Full System Approach*; John Wiley & Sons, 2017.

17. Jasinski, F.; Zetterlund, P. B.; Braun, A. M.; Chemtob, A., *Prog. Polym. Sci.* **2018**, *84*, 47-88.

18. Benedikt, S.; Wang, J.; Markovic, M.; Moszner, N.; Dietliker, K.; Ovsianikov, A.; Grützmacher, H.; Liska, R., *J. Polym. Sci. A Polym. Chem.* **2016**, *54*, 473-479.

19. Lougnot, D.; Fouassier, J., *J Polym Sci A Polym Chem.* **1988**, *26*, 1021-1033.

20. Fouassier, J. P.; Burr, D.; Wieder, F., *J Polym Sci A Polym Chem.* **1991**, *29*, 1319-1327.

21. Knaus, S.; Gruber, H., *J Polym Sci A Polym Chem.* **1995**, *33*, 929-939.

22. Kojima, K.; Ito, M.; Morishita, H.; Hayashi, N., *Chem. Mater.* **1998**, *10*, 3429-3433.

23. Occhetta, P.; Sadr, N.; Piraino, F.; Redaelli, A.; Moretti, M.; Rasponi, M., *Biofabrication* **2013**, *5*, 035002.

24. Ikemura, K.; Endo, T., *Dent. Mater. J.* **2010**, *29*, 481-501.

25. Ganster, B.; Fischer, U. K.; Moszner, N.; Liska, R., *Macromolecules* **2008**, *41*, 2394-2400.

26. Benedikt, S.; Wang, J.; Markovic, M.; Moszner, N.; Dietliker, K.; Ovsianikov, A.; Grützmacher, H.; Liska, R., *J Polym Sci A Polym Chem.* **2016**, *54*, 473-479.

27. Wang, J.; Siqueira, G.; Müller, G.; Rentsch, D.; Huch, A.; Tingaut, P.; Levalois-Grützmacher, J.; Grützmacher, H., *Chem.Commun.* **2016**, *52*, 2823-2826.

28. Moszner, N.; Fischer, U. K.; Lamparth, I.; Fässler, P.; Radebner, J.; Eibel, A.; Haas, M.; Gescheidt, G.; Stueger, H., *J. Appl. Polym. Sci.* **2018**, *135*, 46115.

29. Crivello, J. V., *J. Polym Sci. A Polym. Chem.* **1999**, *37*, 4241-4254.

30. Ortyl, J.; Popielarz, R., *Polimery* **2012**, *57*, 510-517.

31. Sangermano, M., *Pure Appl. Chem.* **2012**, *84*, 2089-2101.

32. Sangermano, M.; Roppolo, I.; Chiappone, A., *Polymers* **2018**, *10*, 136.

33. Bajpai, U.; Otsu, T., *Eur. Polym. J.* **1993**, *29*, 517-521.

34. Onen, A.; Arsu, N.; Yagcı, Y., *Angew. Makromol. Chem.* **1999**, *264*, 56-59.

35. Fueno, T.; Okamoto, H.; Tsuruta, T.; Furukawa, J., *J. Polym. Sci* **1959**, *36*, 407-420.

36. Ko, M.; Sato, T.; Otsu, T., *J. Polym. Sci., Polym. Chem. Ed.* **1974**, *12*, 2943-2951.

37. Biswas, Y.; Maji, T.; Dule, M.; Mandal, T. K., *Polym. Chem.* **2016**, *7*, 867-877.

38. Biswas, Y.; Dule, M.; Mandal, T. K., *J. Phys. Chem. C* **2017**, *121*, 4747-4759.

39. Biswas, Y.; Mandal, T. K., *Macromolecules* **2017**, *50*, 9807-9820.

40. Biswas, Y.; Ghosh, P.; Mandal, T. K., *Chem. Eur. J.* **2018**, *24*, 13322-13335.

41. Banerjee, P.; Jana, S.; Mandal, T. K., *Eur. Polym. J.* **2020**, 109747.

42. Gao, J.; Zhai, G.; Song, Y.; Jiang, B., *J. Appl. Polym. Sci.* **2008**, *107*, 3548-3556.

43. Verros, G. D.; Achilias, D. S., *J. Appl. Polym. Sci.* **2009**, *111*, 2171-2185.

44. Rhine, M. A.; Rodrigues, A. V.; Urbauer, R. J. B.; Urbauer, J. L.; Stemmler, T. L.; Harrop, T. C., *J. Am. Chem. Soc.* **2014**, *136*, 12560-12563.

45. Perkins, M., Spin Trapping. In *Adv Phys Org Chem*, Elsevier: 1980; Vol. 17, pp 1-64.

46. Liska, R., *J. Polym. Sci. A Polym. Chem.* **2002**, *40*, 1504-1518.

47. Liu, B.; Jin, N., *Curr. Org. Chem.* **2016**, *20*, 2109-2116.

48. Brennecke, J. F.; Maginn, E. J., *AIChE J* **2001**, *47*, 2384.

49. Bhesaniya, K.; Baluja, S., *J. Appl. Chem.* **2014**, *2014*, 1-7.

50. Ullrich, G.; Ganster, B.; Salz, U.; Moszner, N.; Liska, R., *J. Polym. Sci. A Polym. Chem.* **2006**, *44*, 1686-1700.

51. Kowalska, A.; Sokolowski, J.; Bociong, K., *Polymers* **2021**, *13*, 470.

52. Yousif, E.; Haddad, R., *SpringerPlus* **2013**, *2*, 1-32.

53. Ghosh, S. K.; Mandal, B. M., *Polymer* **1993**, *34*, 4287-4290.

54. Papadopoulos, G. N.; Kokotou, M. G.; Spiliopoulou, N.; Nikitas, N. F.; Voutyritsa, E.; Tzaras, D. I.; Kaplaneris, N.; Kokotos, C. G., *ChemSusChem* **2020**, *13*, 5934-5944.

55. Defoin, A.; Defoin-Straatmann, R.; Hildenbrand, K.; Bittersmann, E.; Kreft, D.; Kuhn, H., *J. Photochem.* **1986**, *33*, 237-255.

56. Jin, S.; Liu, M.; Chen, S.; Gao, C., *Eur. Polym. J.* **2008**, *44*, 2162-2170.

57. Chumachenko, V.; Kutsevol, N.; Harahuts, I.; Soloviov, D.; Bulavin, L.; Yeshchenko, O.; Naumenko, A.; Nadtoka, O.; Marinin, A., *Int. J. Polym. Sci.* **2019**, *2019*.

58. Lanzalaco, S.; Armelin, E., *Gels* **2017**, *3*, 36.

59. Roy, D.; Brooks, W. L.; Sumerlin, B. S., *Chem Soc Rev* **2013**, *42*, 7214-7243.

60. Chee, C.-K.; Hunt, B. J.; Rimmer, S.; Rutkaite, R.; Soutar, I.; Swanson, L., *Soft Matter* **2009**, *5*, 3701-3712.

61. Plamper, F. A.; Ruppel, M.; Schmalz, A.; Borisov, O.; Ballauff, M.; Müller, A. H., *Macromolecules* **2007**, *40*, 8361-8366.

62. Fournier, D.; Hoogenboom, R.; Thijs, H. M.; Paulus, R. M.; Schubert, U. S., *Macromolecules* **2007**, *40*, 915-920.

63. Butun, V.; Armes, S.; Billingham, N., *Polymer* **2001**, *42*, 5993-6008.

Chapter 5

Ionic liquid cross-linked polyionic hydrogels for removal of anionic dyes

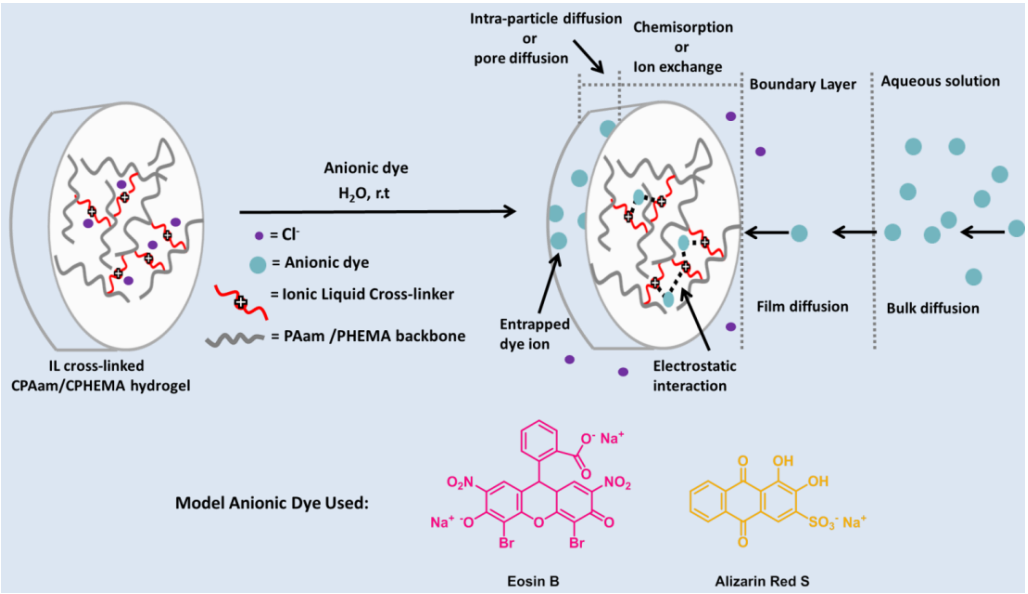

5.1 INTRODUCTION

Polymer hydrogels where hydrophilic polymeric chains are cross-linked with each other through chemical or physical interactions forming a three-dimensional fibrillar polymeric network are able to entrap a significant amount of water within its matrix and can provide clear advantages for removal of colour from effluents without dissolving in water.[1-3] Water molecules and ions can easily migrate within the swollen polymeric network leading to participation of most of the functional groups in ion exchange reactions. In recent years, a continuous increase in number of reports regarding the removal of dyes from aqueous media by polymer hydrogels has been observed.[2, 4]Among various types of polymer hydrogels, chemically cross-linked polymer hydrogels (CCPH) where a cross-linker is applied to interconnect the polymer chains via covalent interactions can be more useful in terms of practical application as they are stable at ambient conditions because of their rigid and irreversible nature.[3, 5] Some types of CCPHs impose special requirements for cross-linking agents. In general, the variation of cross-linkers does not change the properties of the functional groups of the polymeric backbone but it is done to change the structure and thermal as well as mechanical properties of the hydrogel matrix. The degree of cross-linking (expressed as percentage of the cross-linking reagent) also influences the structure of the matrix, its elasticity, swelling ability and mobility of the counter ions inside the polymeric network. Polymers with high degree of cross-linking though renders hardness and stability but show relatively slow diffusion rate. A good choice of the cross-linker density can produce materials with desirable stability and reactivity for some practical applications.[1] Furthermore, the widespread morphology from macroscopic to nanoscopic based upon porosity of the functional polymer hydrogels are very important parameters for controlling the diffusion of various types of solutes into the polymeric network.[6] The development and devising of new types of

CCPHs targeted mainly for waste-water treatment or more specifically for removal of hazardous dyes from aqueous media is still a challenging and interesting topic for researchers.

5.2 OBJECTIVE AND SCOPE OF THE PRESENT WORK

The effluents of the manufacturing and textile industries contaminated with synthetic and non-biodegradable organic dyes greatly harm the biological life of water bodies.[4, 7-10] Removal of colour from the effluents has always been a challenge because of the difficulty in treating such hazardous wastewaters by typical methods.[4] The removal of anionic dyes is considered to be the most challenging job because along with their high water solubility they bring out very bright colours in water with acidic properties.[11] Biodegradable, low-priced and easily accessible adsorbents are urgently required for the treatment of industrial and textile effluents to cut down the high-risk environmental impact.[4, 12-13] Several physico-chemical conventional methods such as flocculation,[14] floatation,[15] coagulation,[16] photodegradation,[17] oxidation,[18] ion exchange,[19] sorption[20] etc. are used for the treatment of such toxic waste-water. Among all of these separation methods, adsorption or sorption process using commercially available activated carbon is widely used for dye removal from aqueous solution but the main limitation of its usage is its high cost.[21] Hence a continuous effort by researchers has been observed for several years to develop cost- effective alternative to activated carbon adsorbents for the removal of different dyes.[11, 22-23] A detailed literature review has revealed that removal of natural organic materials[24] and many colorants[25] from water are now a days done by cost-effective ion exchange polymers which are cross-linked polymers carrying fixed functional groups or sites.[1] For instance, polystyrene sulfonate chemically cross-linked with divinylbenzene is most conventionally used because of its chemical and mechanical stability.[1]

Recently an emerging trend of using polyionic hydrogels has been observed for dye removal from aqueous solution. As already discussed in Chapter 1, one of the most important features of ILs and PILs is that their counter ions can be altered via ion exchange reaction. If IL or PIL moieties can be incorporated into the crosslinking network of the hydrogel matrix, the resultant hydrogel might possess both the characteristics of IL /PILs and hydrogel. Such synergetic properties might expand the scope of hydrogel applications and provide enhanced performance in their potential applications. For example, Yan et al. reported the applications of ILs for the synthesis of poly(ionic liquid) gels via host–guest interaction.[26]In a similar fashion, Zhou and co-workers introduced IL moieties into the cross-linked network of microgels, via the simultaneous quaternized cross-linking reaction during the surfactant-free emulsion copolymerization resulting in the synthesis of novel ionic microgels with synergetic properties of IL and microgel.[27] Very recently, the same group has reported the synthesis of PNIPAM-based ionic hydrogels by free-radical polymerization of NIPAM using imidazolium-based dicationic IL as the cross-linker.[28] The obtained polyionic hydrogels were further utilized for adsorption of anionic dyes from aqueous solution and the interfacial adsorption kinetic of anionic dyes onto the hydrogels was described by the pseudo-first-order kinetics. However similar types of polyionic hydrogels and their dye sorption capability/mechanism from aqueous medium have been rarely reported.

Thus in this work we have synthesized a new IL, [DMAEMA-4VBC][Cl] following a reported reaction procedure.[29] Further we have used this new IL along with a previously reported IL, [VIm-4VBC][Cl] [29] for aqueous free radical solution polymerization of acrylamide and 2-hydroxyethyl methacrylate at ambient temperature to synthesize cationic cross-linked poly(acrylamide) (CPAam) and poly(2-hydroxyethyl methacrylate) (CPHEMA) hydrogels using ammonium persulfate (APS) as initiator and tetramethylethylenediamine

(TEMED) as stabilizer. Due to ionic linkages present in the structure of the hydrogels, they are supposed to remove targeted anionic dyes from wastewater through mainly adsorption mechanism which is driven by electrostatic interactions between dye ions and hydrogel matrix. The syntheses, swelling properties, thermal stabilities and dye-removal abilities of a series of the as-synthesized cationic CPAam and CPHEMA hydrogels using different concentration of the IL cross-linkers have been described. High swelling behaviour in Milli-Q water was observed for these hydrogels at ambient temperature. The macroporous network structures of these hydrogels were investigated from FESEM analysis. The macroporous structures allowed the diffusion of solute dye molecules through the hydrogel structure. Thermogravimetric and differential thermogravimetric analysis data showed that these hydrogels are thermally stable even above 160 °C and hence can be applied for waste-water treatment even at elevated temperature. Diffusion of water within hydrogels was found to be of pseudo-Fickian in character. Diffusion coefficients were also calculated for these hydrogels in water. The ability of these hydrogels to remove anionic dyes from aqueous solution under several experimental conditions has been studied using Eosin B and Alizarin Red S as model dyes. The changes of adsorption capacities of these hydrogels on anionic dyes with the variation of concentration of IL cross-linkers were also investigated. Further the adsorption kinetics was investigated using three different kinetic models and pseudo second-order model best described the adsorption of the anionic dyes onto these hydrogels. The adsorption mechanism was also analysed by intra-particle diffusion model and Boyd kinetic model. All of these data clearly indicate that these hydrogels can be potentially applied in separation technology and water treatment.

5.3 EXPERIMENTAL SECTION

5.3.1 Materials.

Acrylamide (Aam, 98%) was purchased from TCI Chemicals (India) and recrystallized twice from hot chloroform prior to use. 2-(Dimethylamino)ethyl methacrylate (DMAEMA, 98%) 1-vinylimidazole (VIm, ≥ 99%), 4-vinylbenzyl chloride (VBC, 90%), 2-hydroxyethyl methacrylate (HEMA, ≥ 99%), ammonium persulfate (APS, ≥ 98%) and N,N,N',N'-tetramethylethylenediamine (TEMED) were purchased from Sigma. DMAEMA and VBC/HEMA were purified by passing through basic and neutral alumina column respectively. VIm was vacuum distilled in the presence of catalytic amount of 2,2,6,6-Tetramethylpiperidine-1-oxyl (TEMPO) prior to use. APS was recrystallized from lukewarm water whereas TEMED was used as received. Milli-Q water was used as solvent for polymerization and solution preparation.

5.3.2 Synthesis of Ionic Liquid (IL) Cross-linkers [VIm-4VBC][Cl] and [DMAEMA-4VBC][Cl]

Two different types of ionic liquid (IL)-based cross-linkers, [VIm-4VBC][Cl] (designated as ILA) and [DMAEMA-4VBC][Cl] (designated as ILB) were synthesized by nucleophilic substitution reaction of VBC with two different monomers, VIm and DMAEMA respectively in a molar ratio of 1:1 (Scheme 1).[29] Two 25 mL round-bottom (RB) flasks were separately charged with VBC (1.7mL; 12 mmol) followed by the addition of VIm (0.91 mL; 10 mmol) in one flask and DMAEMA (1.68 mL; 10 mmol) in another flask. . The reaction mixtures were then placed in an ice bath at 0-5 °C and kept for 7 h with magnetic stirring. RB flasks were then taken out from ice bath and continued stirring for another 15-17 h at 25 °C. After completion of the reaction, the reaction mixtures were dissolved in minimum amount of methanol and the products were isolated by precipitating in excess diethyl ether. The process was repeated twice for purification. The as-

synthesized IL cross-linkers were colourless liquid with high viscosity and were stored under refrigeration to avoid polymerization. The crosslinkers were characterized by ESI-MS analyses (Figures 1-2). % Yield for ILA and ILB were found to be 79 and 81 respectively.

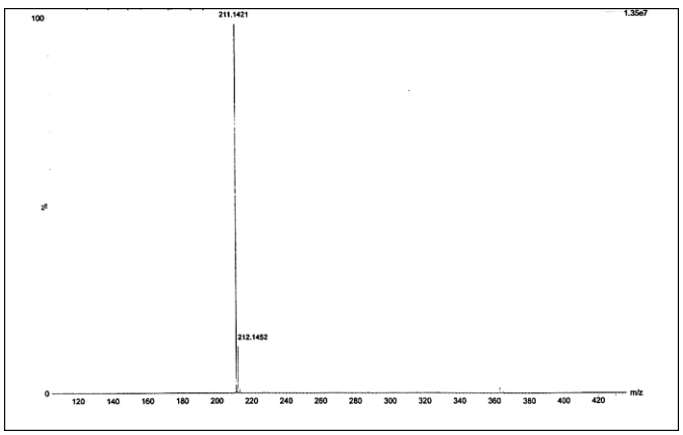

Figure 1. ESI mass spectrum of as-synthesized ionic liquid cross-linker [VIm-4VBC][Cl] (ILA).

[VIm-4VBC][Cl] : MS(ESI) (35 eV) : m/z: 211.14 ($[M]^+$), 212.14 ($[M+H]^+$)

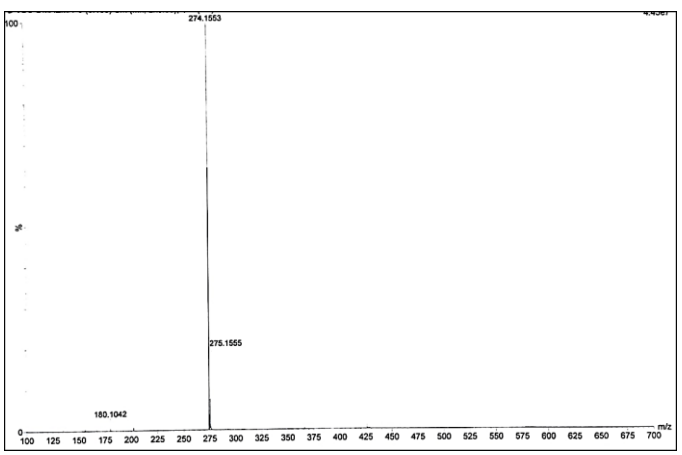

Figure 2. ESI mass spectrum of as-synthesized ionic liquid cross-linker [DMAEMA-4VBC][Cl] (ILB).

[DMAEMA-4VBC][Cl]: MS(ESI) (35 eV) : m/z: 274.15 ($[M^+]$), 275.15 ($[M+H]^+$)

The cross-linkers were also characterized by ^{1}H-NMR which will be discussed later.

5.3.3 Preparation of IL crosslinked Hydrogels (CPAam and CPHEMA Hydrogels).

A series of crosslinked poly(acrylamide) (CPAam) and poly(2-hydroxyethyl methacrylate**) (**CPHEMA**)** hydrogels were prepared using the free-radical solution polymerization (FRSP) technique by reacting 14 wt. % (w/v) of each of the Aam and HEMA monomers with 1 wt. % (w/w, w.r.t monomer) of APS as initiator and TEMED as stabilizer and two different types of ionic liquid (IL), ILA and ILB as cross-linkers with varying concentration [5, 10, 15, and 20 wt. % (w/w, w.r.t monomer)] (Table 1). In each case, monomer, initiator, stabilizer and IL cross-linkers with different concentrations (wt. %) were separately made soluble in a total 5 ml of Milli Q water (water was purged with argon gas for 45 min prior to use) and quickly mixed together to form a series of homogeneous aqueous solutions. The mixture solutions were gently vortexed by a vortex shaker for 2-3 min to prevent air bubbles. Afterward, the solutions were introduced into a petri dish having 2 cm width and kept for 12 h at ambient temperature to complete the polymerization. Finally the gels were sufficiently washed with Milli-Q water to remove unreacted components and sol parts .Finally the hydrogels were cut into thin rectangular slabs and freeze-dried followed by drying to constant weight in vacuum oven at 40 °C. The appearance of the fully polymerized CPAam and CPHEMA hydrogels strongly depend on their cross-linker concentration: it turned from transparent to semi-transparent to milky-white with increasing proportion of cross-linkers. In this work, as we have maintained the monomer concentration constant and varied the IL cross-linker concentration from a minimum of 5 wt. % to a maximum of 20 wt.% , hence the hydrogels are given

code names after their IL cross-linker content e.g. CPAam-ILA-5 to CPAam-ILA-20, CPAam-ILB-5 to

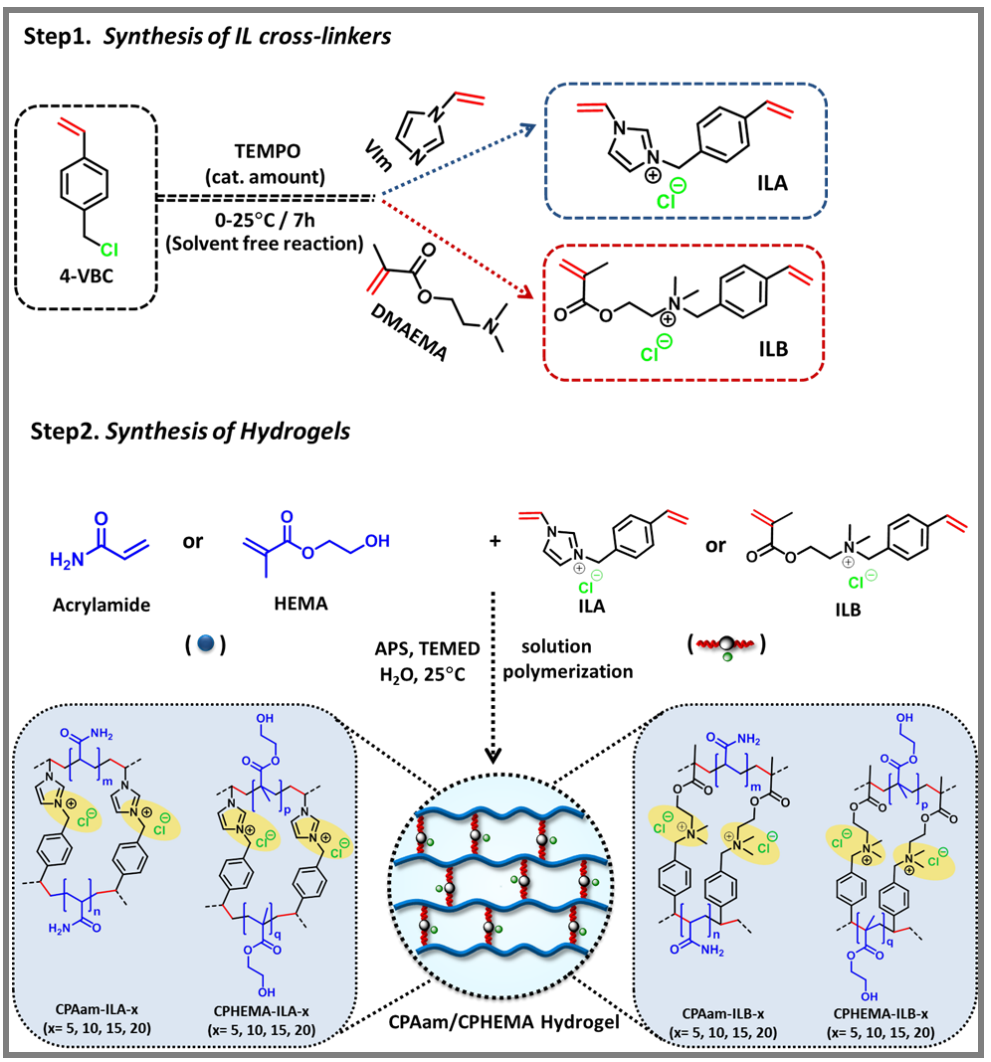

Scheme 1. Synthetic scheme and structure of IL cross-linkers ILA and ILB and the corresponding cross-linked poly(acrylamide) (CPAam) and poly(2-hydroxyethyl methacrylate) (CPHEMA) hydrogels.

CPAam-ILB-20, CPHEMA-ILA-5 to CPHEMA-ILA-20 and CPHEMA-ILB-5 to CPHEMA-ILB-20 throughout the manuscript. For comparative study, we have also synthesized CPAam and CPHEMA hydrogel using 10 wt. % of N,N'-

methylenebisacrylamide (MBA) as cross-linker. The polymerization and purification procedure are same as above. These two hydrogels have been designated as CPAam-MBA-10 and CPHEMA-MBA-10.

Table1. Composition of the reactants used in hydrogel synthesis

Hydrogel Code	Acrylamide wt.% (w/w)	HEMA wt.% (w/w)	ILA wt.% (w/w)	ILB wt.% (w/w)	MBA wt.% (w/w)	APS wt.% (w/w)	TEMED wt.% (w/w)
CPAam-ILA-5/10/15/20	100	-	5/10/15/20	-	-	1	1
CPAam-ILB-5/10/15/20	100	-	-	5/10/15/20		1	1
CPAam-MBA-10	100	-	-	-	10	1	1
CPHEMA-ILA-5/10/15/20	-	100	5/10/15/20	-	-	1	1
CPHEMA-MBA-10	-	100	-	-	10	1	1
CPHEMA-ILB-5/10/15/20	100	100	-	5/10/15/20	-	1	1

All solution polymerization reactions were occurred at ambient temperature and pressure.

5.3.4 Characterization of the IL Cross-linkers and Hydrogels.

Spectrum Two (Perkin Elmer) Fourier transform IR (FT-IR) spectrometer equipped with attenuated total reflection (ATR) accessory was used to record FTIR spectra of all the monomers and dried aerogels.

^{1}H- NMR spectra of all the IL-based crosslinkers were acquired in a Bruker DPX 400 MHz spectrometer at ambient temperature from their respective solvents.

For field emission scanning electron microscopy (FESEM), water-swollen hydrogels were freeze dried to convert them to xerogels. The morphology of the formed xerogels was then observed under JEOL JSM-7500F microscope. Prior to the scanning microscopy, the xerogels were sputter-coated with platinum and FESEM images were taken at an accelerating voltage of 5-10 kV.

Thermogravimetric analysis (TGA) was carried out using a PerkinElmer TGA 4000 thermogravimetric analyzer in the temperature range of 30°C–600°C. A total of 2-3 mg of the dry aerogel was taken in an aluminium crucible and was heating at a rate of 10°C/min under stream of N_2 purge.

5.3.5 Swelling experiment

Swelling kinetics was studied by conventional gravimetric method where a known mass (~50 mg) of aerogel was immersed into 15 mL of distilled water at room temperature. The swollen gels were weighted at different time intervals after wiping out the excess water from the surface of the hydrogels. Swelling readings were taken at different time intervals until it reaches equilibrium swelling mass. Swelling percentage (%S) and equilibrium swelling percentage (%ES) at different time intervals were determined from these two following the equations:

$$\%\text{Swelling (\%S)} = \frac{(W_s - W_d)}{W_d} \times 100 \qquad (1)$$

$$\text{and \% Equilibrium swelling (\%ES)} = \frac{(W_s^e - W_d)}{W_d} \times 100\ , \qquad (2)$$

where W_s and W_s^e are the weights of the swollen hydrogel at time t and 24 h respectively, whereas W_d is the weight of the dried hydrogel. For comparison of %S between different types of aerogels, all swelling experiments were repeated at least two times and the average values were plotted.

5.3.6 Dye adsorption study

Typically, an weighted amount of aerogel (20 ±1 mg) was immersed into aqueous solutions of Eosin B and Alizarin Red S (ARS) with different concentration for 24 h. Aliquots were withdrawn from the dye solutions at

different time intervals for determining the kinetics adsorption of dyes by the hydrogels. The concentration of the non-adsorbed dye was determined by measuring the absorbance of Eosin B and ARS at 519 and 423 nm respectively using a Cary 3500 spectrophotometer (Agilent Technologies) and quartz cuvettes (1 cm path length).

To determine the unknown dye concentrations at any time, a linear calibration curve was established between the dye concentration and their absorbance, as shown in Figures 3 -4, and the molar extinction coefficient value (ε) was determined using Beer–Lambert law (A = εcl), where A is the absorbance, ε is the molar absorptivity (mol^{-1} L cm^{-1}), l is the path length of the cuvette containing the sample (1 cm) and c is the concentration of dye solution (mol L^{-1}). The obtained molar absorbance coefficient (ε) for Eosin B and ARS was 48248 and 4857 mol^{-1} L cm^{-1} respectively.

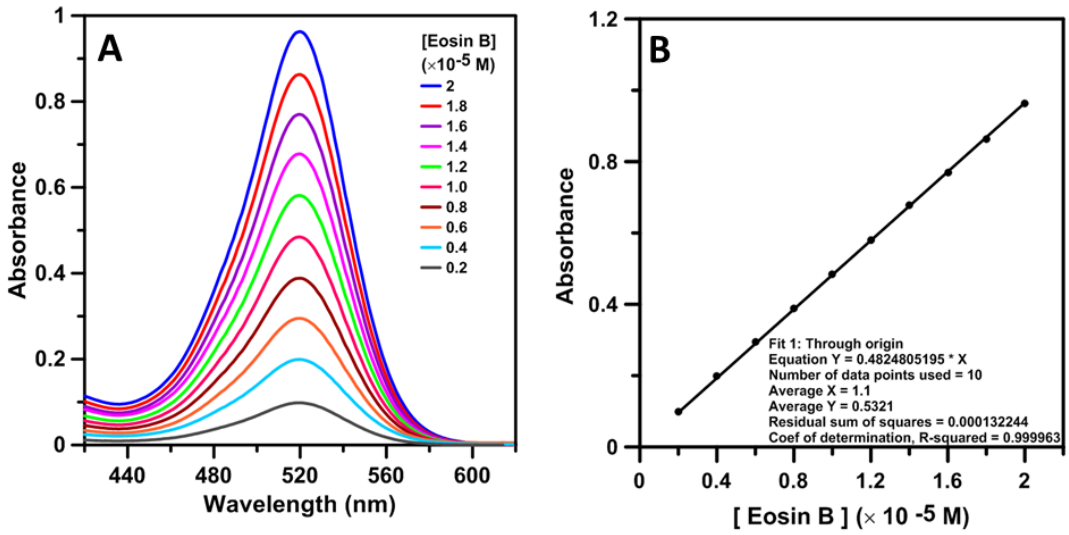

Figure 3. (A) Concentration dependent UV-Vis spectra of Eosin B dye. (B) Linearly fit calibration plot to determine absorption coefficient of Eosin B dye.

To determine the amount of the dye adsorbed by the hydrogels (mg of dye adsorbed per g of gel), we have calculated adsorption capacity and

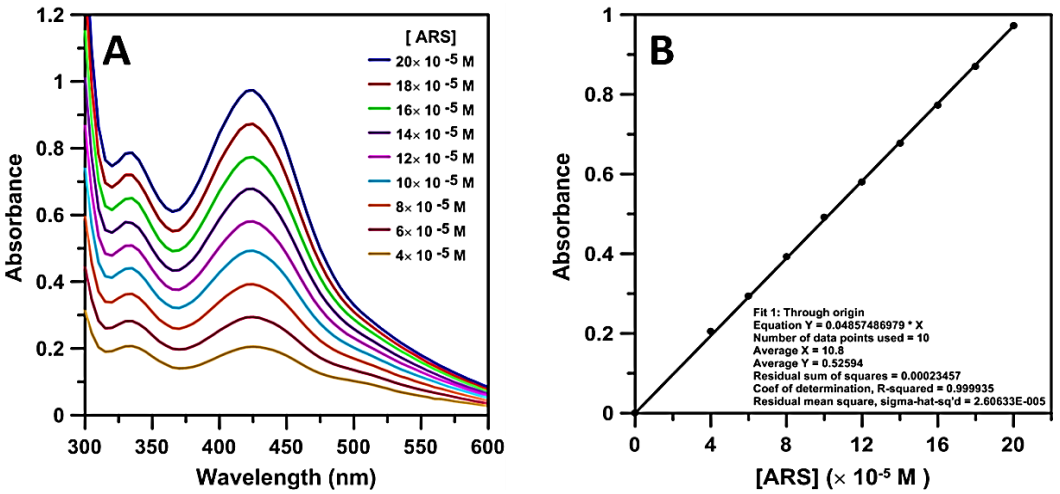

Figure 4. (A) Concentration dependent UV-Vis spectra of ARS dye. (B) Linearly fit calibration plot to determine absorption coefficient of ARS dye.

equilibrium adsorption capacity using the following equations:

$$q_t = \frac{C_0 - C_t}{W} \times V \quad (3)$$

$$q_e = \frac{C_0 - C_e}{W} \times V \quad (4)$$

where q_t and q_e (mg g−1) are the amount of dye adsorbed at a certain time t and at equilibrium, respectively. C_0 (mg L^{-1}) is the initial concentration of dye, C_t (mg L^{-1}) is the concentration of dye at time t, C_e (mg L^{-1}) is the equilibrium concentration of dye. V (L) is the volume of the dye solution, and W (g) is the mass of the dry gel. Note that C_t value for any particular time can be mathematically calculated from the corresponding A_t value, ε (mol^{-1} L cm^{-1}) and known molar mass (g mol^{-1}) of the dye.

5.4. RESULTS AND DISCUSSION

5.4.1 Synthesis and Structure Characterization of the Hydrogels.

The synthesis of IL crosslinker, [VIm-4VBC][Cl] (ILA) was carried out by coupling VIm with 4-VBC following a reported protocol.[29] Another IL-based crosslinker [DMAEMA-4VBC][Cl] (ILB) was also synthesized by coupling DMAEMA with 4-VBC following the similar synthetic protocol (Scheme 1). ILA and ILB were soluble in water. The ESI mass spectra of ILA and ILB (Figures 1 -2) showed the presence of sharp molecular ion peaks at m/z 211.14 and 274.15 respectively corresponding to the cationic part of these as-synthesized IL crosslinkers, which matched well with those of their theoretical values. The ^{1}H- NMR spectrum of ILA (Figure 5a) showed the characteristic signals of phenyl ring protons of 4-VBC at δ 7.2-7.47 ppm, ring protons of imidazolium cation at δ 7.53, 7.84 and 10.57 ppm and bridging methylene protons at δ 5.53 ppm. The spectrum of ILB (Figure 5b) also showed the characteristic signals of phenyl ring protons of 4-VBC at δ 7.28-7.63 ppm, methyl and methylene protons associated with the quaternized DMAEMA moiety at δ 3.30, 4.09 and 4.62 ppm along with that of bridging methylene protons at δ 5.1 ppm.

The FT-IR spectra of Aam and HEMA monomer are shown in Figure 6 whereas the spectra of the representative aerogels are given in Figure 7. In case of CPAam hydrogel, the FT-IR spectrum of CPAam-ILA-10 and CPAam-ILB-10 show complete disappearance of the characteristic C=C double bond stretching band (1610 cm^{-1}) of the Aam monomer (Figure 6) and exhibits the characteristic absorption bands at 1446 cm^{-1} , 1605 cm^{-1} ,1650 cm^{-1} and 3182 cm^{-1} corresponding to the C–N stretching, $–NH_2$ bending, >C=O stretching and N-H symmetric stretching vibration of the amide group respectively. The broad band at 3326 cm^{-1} may be attributed to the overlapping of bands of asymmetric N-H

stretching of amide group with O-H stretching of non-freezing bound water molecules that remain in aerogel structure that obtain after extensive drying. The spectrum also showed the presence of absorption bands at 2928 cm-^{1} which can be assigned to the -CH_2- groups present in the polymer main chains and crosslinking bridges. Similarly in the case of CPHEMA gel, the spectrum of CPHEMA-ILA-10 and CPHEMA-ILB-10 (Figure 7) showed complete disappearance of the C=C stretching band (1634 cm^{-1}) of the HEMA monomer (Figure 6) and

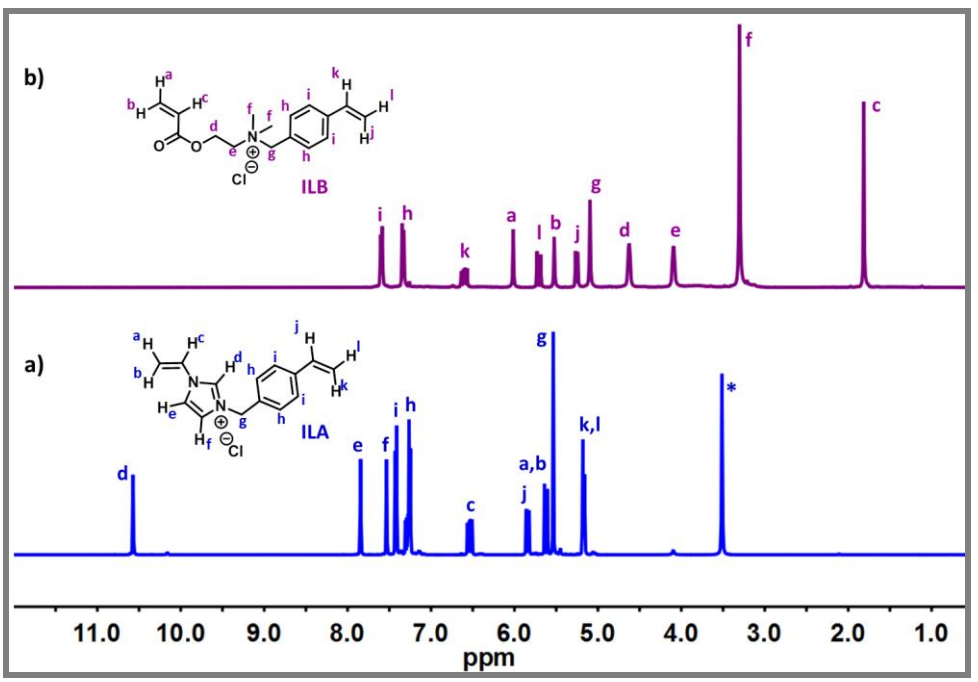

Figure 5. ^{1}H NMR spectra of the as-synthesized ionic liquid a) [VIm-4VBC][Cl] (ILA) and b) [DMAEMA-4VBC][Cl] (ILB) acquired in $CDCl_3$.(*Solvent impurity)

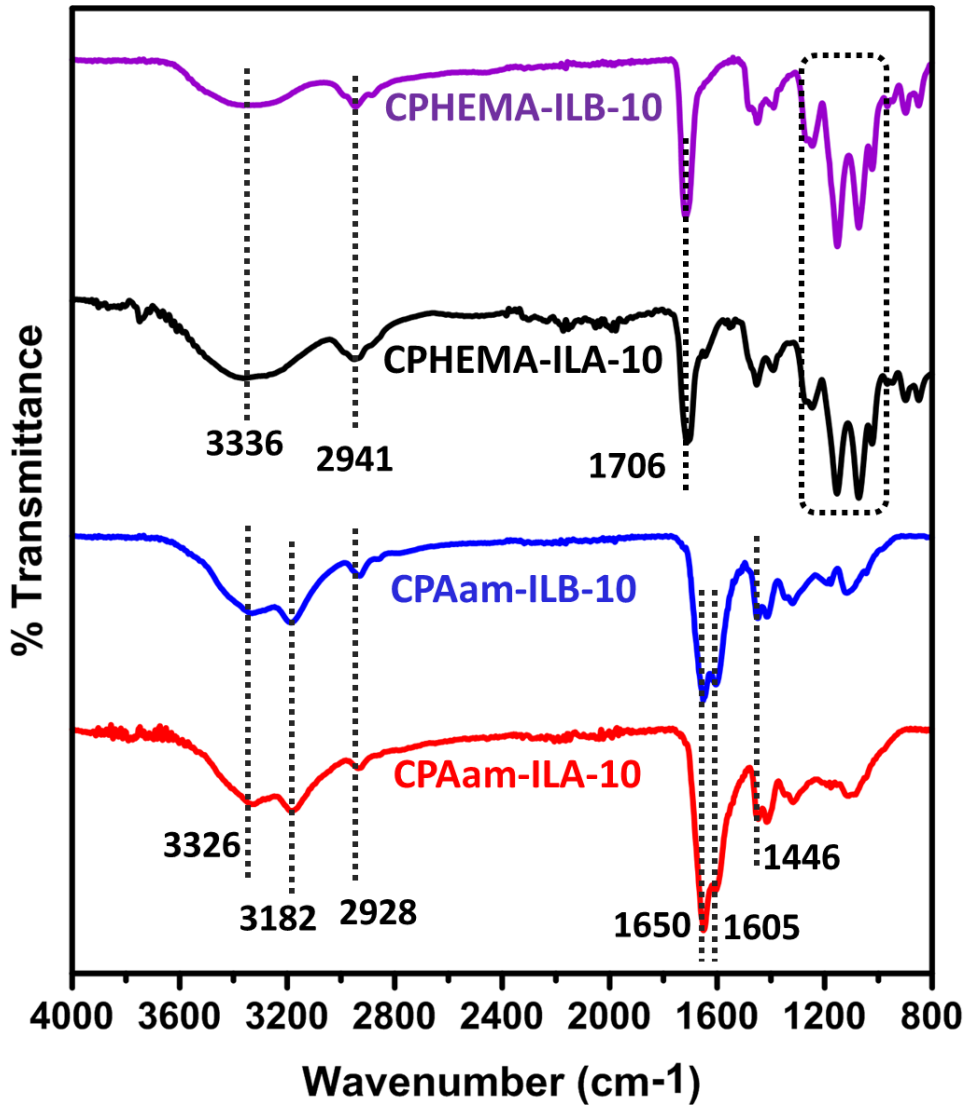

Figure 6. FT-IR spectra of Aam, NIPAM and HEMA monomer

exhibited several characteristic absorption bands at 1706 cm^{-1} for >C=O stretching, several characteristic signals in the region of 1020-1300 cm^{-1} for -C-O-C- stretching and a broad signal around 3310 cm^{-1} attributed to the stretching of hydrogen bonded hydroxyl group of HEMA unit. The spectra also showed absorption bands at 2941 cm^{-1} attributable to the $-CH_2$ groups present in the polymer chains and crosslinking bridges. FT-IR result confirmed the formation of crosslinked gels.

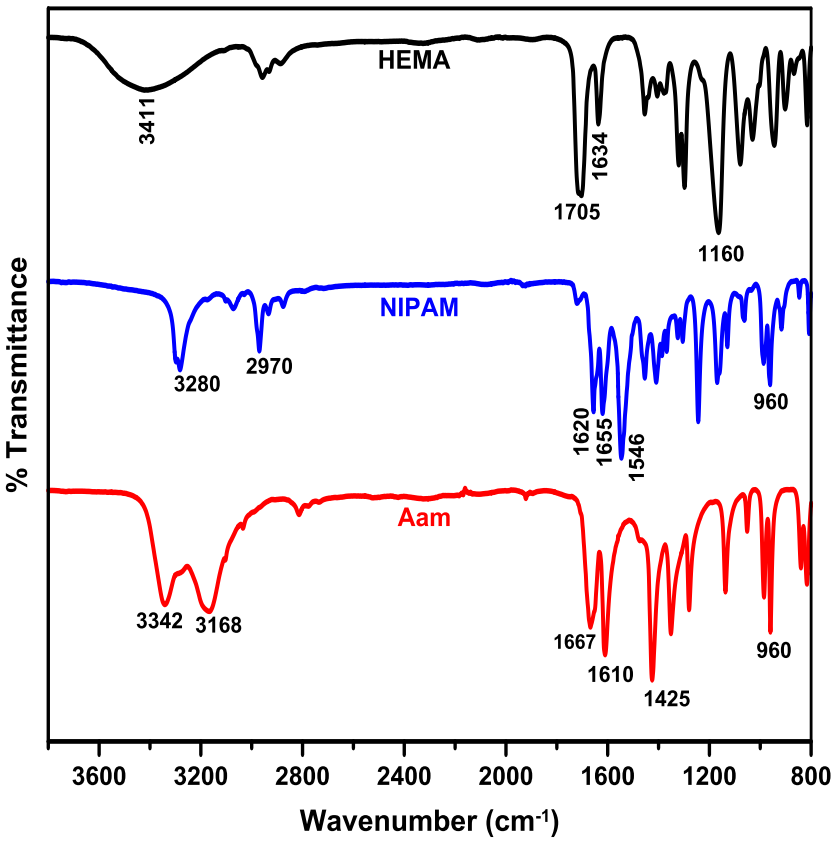

Figure 7. FT-IR spectra of CPAam and CPHEMA hydrogels cross-linked by 10 wt. % of ILA and ILB ionic liquids.

5.4.2 Thermal Degradation Study.

The thermal degradation of aerogels with three-dimensional network structures is a complex process and can be understood by the help of both the TGA and DTG.[30] The TGA and DTG curves [the plot of derivative thermogravimetric (dm/dT) (% $^{\circ}C^{-1}$) against temperature] of the aerogels, CPAam-ILA-10, CPAam-ILB-10, CPHEMA-ILA-10 and CPHEMA-ILB-10 were presented in Figure 8a and Figure 8b respectively. TGA curves showed several stages of decomposition of the dried aerogels. DTG curves in Figure 8b revealed that the IL crosslinked CPAam aerogels decomposed in three stages, whereas CPHEMA aerogels

decomposed in two stages. The T_{onset} and T_{endset} are the temperatures at which thermal decomposition starts and ends for each step. T_{peak} is the temperature at which maximal degradation occurred at any step. The mass loss in W_{loss} (%) and Residue (%) (percentage residual char) are equal to the amount of weight loss and the char remaining at an elevated temperature of 600°C (Table 2). The degradation curves showed that all the selected aerogels initially started to lose their weights around 100°C, in particular in the range of 30-145°C, where the expected dehydration of the hydrogels usually stars.[30] The weight loss was found to be less than 3%. The thermal degradation of the above mentioned CPAam hydrogels can be divided into three main stages. In the first stage, the breaking of the cross-linkages of the gels occurred where the weight loss were found to be 12.26 and 6.28 % for CPAam-ILA-10 and CPAam-ILB-10 respectively in the temperature region (160-245 °C) with a T_{peak} ~ 226°C and 227°C respectively. The second stage showed increase in weight loss (15.25 and 18.25%) in the temperature region (268-350°C) and (247-334°C) with T_{peak} ~ 317 and 307°C for samples CPAam-ILA-10 and CPAam-ILB-10 respectively. This region is probably due to the degradation of the polyacrylamide chains and eventually, the three-dimensional network. In the final stage, in the temperature range of 357-503°C and 340-498°C, the curves showed a pronounced increase of weight loss (37.75 and 45.37 % respectively) with a T_{peak} = 410 and 415°C which can be ascribed to the decomposition of the polymeric side and main chains (backbone) resulting in the formation of residual char. The char remained from the decomposition of CPAam-ILA-10 and CPAam-ILB-10 was found to be 28.5% and 23% respectively when heated above 600 °C.

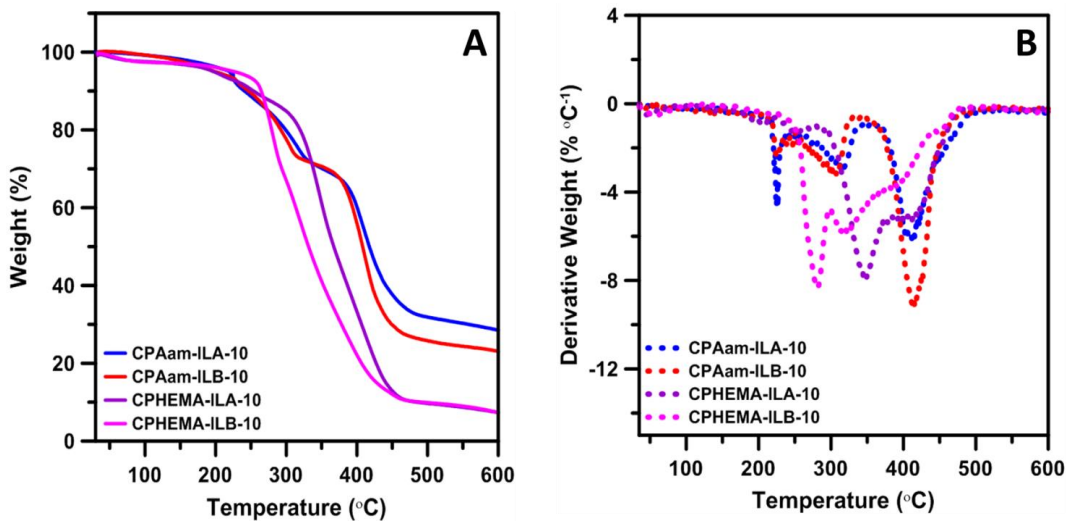

Figure 8. A) TGA and B) DTG curves showing thermal decomposition of the selected IL cross-linked CPAam and CPHEMA hydrogels.

On the other hand, CPHEMA-ILA-10 and CPHEMA-ILB-10 aerogels have two main weight loss regions; one in the temperature range of 160-382 °C (T_{peak} =348°C) and 163-298°C (T_{peak} =282°C) respectively (Table 2). The first loss is due to the degradation of the cross-linkers present in the gel network structures. The degradations of the poly(HEMA) backbone and side chains were occurred in the second region (388-492°C and 300-478 °C). In these cases, the char remained was found to be around 7.33 % for both the CPHEMA-ILA-10 and CPHEMA-ILB-10 aerogel samples after 600 °C. Note that these were much lesser than that of above mentioned CPAam aerogels indicating the higher thermal stability of IL-crosslinked CPAam than CPHEMA aerogels.

Table 2. Thermogravimetric analyses of CPAam and CPHEMA- hydrogels crosslinked by 10 wt. % of ILA and ILB.

Hydrogel code	Stage	T_{onset}(°C)	T_{peak}(°C)	T_{endset}(°C)	W_{loss} (%)	Residue (%)[a]	(%)[b]	DTA characteristic
CPAam-ILA-10	I	162	226	244	12.26	28.54	1.68	Endo
	II	268	317	350	15.85			
	III	357	410	503	37.75			
CPAam-ILB-10	I	160	227	240	6.28	23.06	2.05	Endo
	II	247	307	334	18.25			
	III	340	415	498	45.37			
CPHEMA-ILA-10	I	160	348	382	54.37	7.33	2.71	Endo
	II	388	413	492	29.46			
CPHEMA-ILB-10	I	163	282	298	28.96	7.34	2.67	Endo
	II	300	321	478	56.75			

[a] Weight (%) measured at 600°C from TGA plots.

[b] Weight loss (%) calculated from TGA plots at 145°C.

5.4.3 Morphological Investigation.

The equilibrium swollen hydrogels were frozen using liquid nitrogen, freeze-dried, sputtered with Pt, and finally the surface morphology was analyzed using field emission scanning electron microscopy (FESEM). Figure 9 showed the surface features of the CPAam and CPHEMA gels crosslinked by 10 wt. % of ILA and ILB. The hydrogels were first swollen in water and then freeze dried for 12 h. The freeze-dried and vacuum dried gels showed porous structures. All the samples showed fishing net like integrated pore structure and interconnected channels[31] with pore diameter of 1.2-5.3 μm , 0.5-5 μm, 1.4-11.2 μm and 0.15-1.2 μm for CPAam-ILA-10, CPAam-ILB-10, CPHEMA-ILA-10 and CPHEMA-ILB-10 hydrogels respectively. This type of pore size distributions are typically observed for macroporous networks obtained by the freeze-dried technique.[32] In aqueous

solution, these gels with such porous structures allowed them to absorb extensive amounts of solvent or dye molecules within their 3D-network. The solvent or dye molecules would be able to interact with the 3D-matrix of the hydrogel by intermolecular chemical forces. It was evident from Figure 9D that pore sizes of CPHEMA-ILB-10 aerogels were comparatively smaller than other aerogels indicating lower swelling ability as suggested by other researchers considering the correlation between water content and pore size, which will be discussed later.[33] Note that when cross-linker concentration was 20 wt. %, the pore size distribution of the aerogel was found to be much irregular and less well-defined. It is probably due to the fact that aerogels with high extent of crosslinking may have denser network meshes leading to smaller pores after swollen, and such smaller pores might got partially collapsed after freeze-drying.

5.4.4 Water Swelling Abilities and Kinetics of Absorption by the Hydrogels.

In general, when a dry aerogel sample is brought in contact with water, water molecules diffuse into gel matrix resulting in the expansion of polymer network.[34] The adsorption capacity, i.e., the swelling property is considered to be the most important for any dried gel.[35] Swelling property is also dependent on the nature of the chemical structure of the hydrogels because of the elasticity of the crosslinked covalent-bonded network.[36] We have examined the time dependent swelling behaviours of all the CPAam-ILA-x, CPAam-ILB-x, .CPHEMA-ILA-x and CPHEMA-ILB-x aerogels where x (= 5, 10, 15 and 20) represents the wt. % of IL cross-linker used with respect to monomer. We have also checked the effect of swelling behaviour of the CPAam hydrogel cross-linked with ionic type ([VIm-4VBC][Cl] (ILA) and other

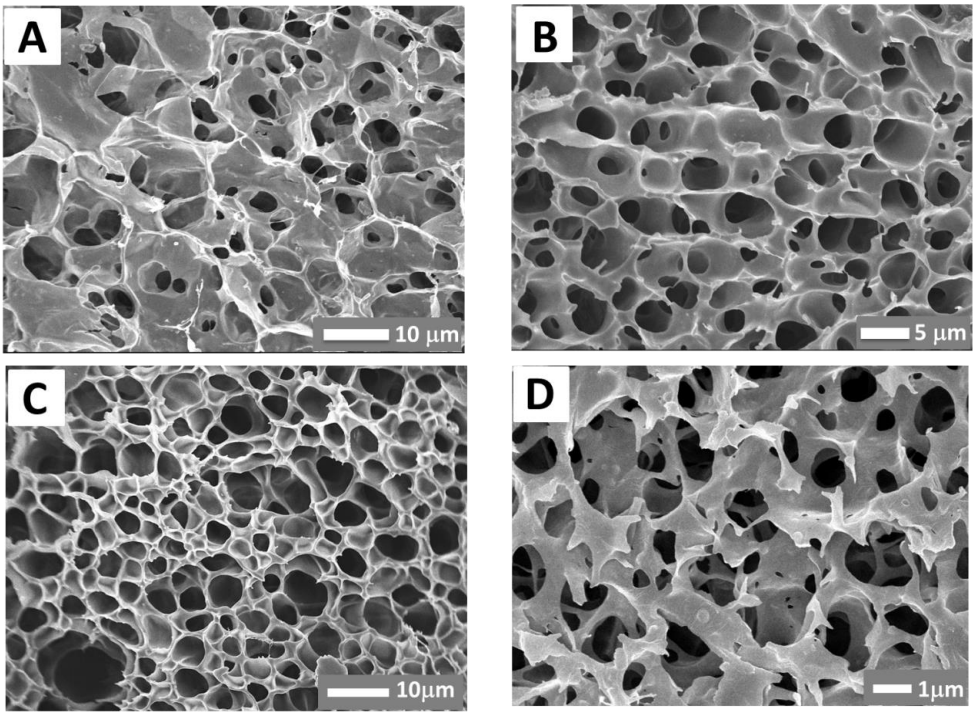

Figure 9. FESEM image of freeze-dried (A) CPAam-ILA-10, (B) CPAam-ILB-10, (C) CPHEMA-ILA-10 and (D) CPHEMA-ILB-10 hydrogel showing well-developed macroporous morphology.

non-ionic, N,N'-Methylenebisacrylamide (MBA). Figure 10 showed the % swelling in water of CPAam and CPHEMA hydrogels containing different wt. % of crosslinker, ILA or ILB. All the hydrogels showed similar swelling behaviour where the rate of water uptake increased sharply in the first 3-5 h and then started to level off and ultimately reached to the equilibrium state after ~6 h. CPAam hydrogels demonstrated a bit higher swelling ability than the CPHEMA hydrogels. This observation can be explained by the fact that CPAam hydrogels have more well-defined porous morphology than the CPHEMA hydrogels which enhanced the diffusion of water into the CPAam hydrogel networks. In this context, it is reported that the maximum swelling of HEMA-based hydrogel in water is

thermodynamically controlled.[37]As the content of the cross-linker increased from x = 5 to 10 to 15 to 20 wt.%, the %swelling of the hydrogels in water changed significantly but %swelling can hardly be correlated with the content of cross- linkers. The reason of such irregular behaviour can be attributed to two opposite phenomena that may occur simultaneously. The first one is the increase of hydrophilic character of the gels with the increase of ionic IL cross-linker. As a result, the interactions between the hydrogel matrix and water molecules is increased which eventually enhances the swelling ability.[38] The presence of mobile ions in the hydrogel matrix can create an osmotic pressure difference between the matrix polymer and solvent phases, which ultimately leads to enhancement of swelling capacity.[39]. Thus, the increase in the contents of ionic crosslinkers and the concentration of Cl^- ion in the gel matrix increases capability of swelling. On the other hand, one cannot rule out a second phenomenon, i.e., the increase of crosslink density increases the rigidity of the gel due to decreases of the chain length between the cross-linking points, which ultimately hinders the network expansion during the swelling. This phenomenon could result in lowering the swelling ability of gels due the increase of crosslink density in the presence of high content of IL cross-linker.[35, 40] This two synergistic effects result in the irregular trend in % Equilibrium swelling values with increase of wt. % of IL cross-linkers as shown in Figure 11**.** Among acrylamide hydrogels, the highest % of equilibrium swelling (% ES) was observed for CPAam-ILA-5 and CPAam-ILB-10 samples with values of 672 and 928 respectively. For acrylamide hydrogels, the second phenomenon is supposed to predominate over the first one. On the other hand, for CPHEMA hydrogels, the highest %ES was observed for CPHEMA-ILA-15 and CPHEMA-ILB-20 with values of 177 and 143 respectively where the first phenomenon is seemed to have higher effect than the second one.

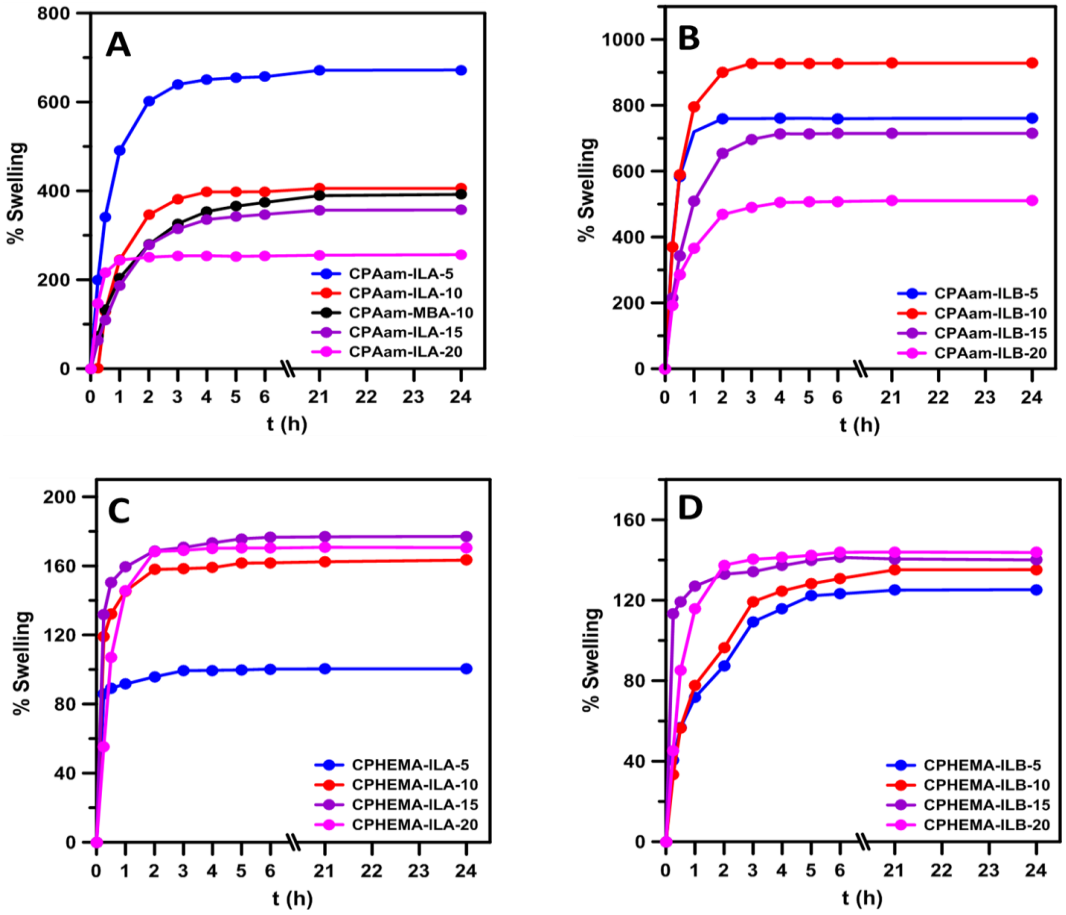

Figure 10. Isothermal time-dependent swelling behaviour of the CPAam (A, B) and CPHEMA (C, D) hydrogels.

It is to be noted that the enhanced swelling ability of CPAam-ILA-10 (%ES = 406) over CPAam-MBA-10 hydrogel (%ES = 392) is attributed to the effect of increase of hydrophilic nature of hydrogel matrix when we use ionic cross-linker (ILA) over non-ionic cross-linker (MBA).

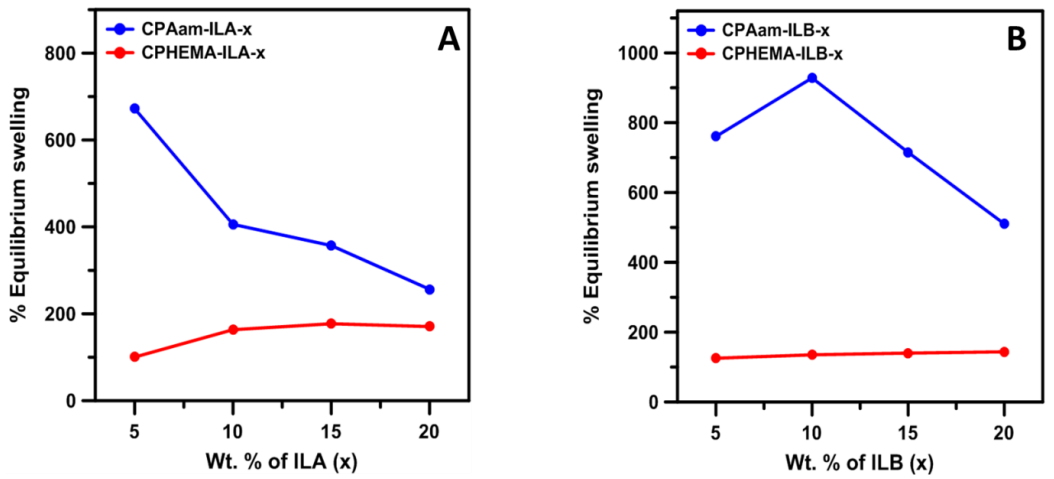

Figure 11. Effect of concentration of IL cross-linker (wt. %) A) ILA and B)ILB on %Equilibrium Swelling for the hydrogels.

For studying the swelling rate, diffusion of water molecules into the hydrogel matrix and consequent relaxation of polymer chain networks, the time dependent water swelling behaviour of the hydrogels has been described by a power law model known as Fickian diffusion model by many groups which is as follows[36, 41] :

$$F=M_t/M_s=Kt^n; \quad (5)$$

and the linear form of equation (5) can be expressed as:

$$\ln F=\ln K+ n \ln t \quad (6)$$

where F is called fractional sorption, K is the diffusion constant related to the structure of the network and permeation medium, n is the swelling exponent and M_t and M_s are the mass of the water uptake at time 't' (min) and at equilibrium condition respectively. The n value (usually ranging from 0.5 to 1) indicates type of transport and the type of diffusion of the water into the gel network. Figure 12 showed the plot of ln F against ln t over a time period of 24 h for some of the representative hydrogels**.** The linear fitting plot gave the value of the exponent n and diffusion constant k from its slope and intercept

respectively. The diffusion parameters (n, k) and the corresponding linear regression correlation coefficient (R^2) are listed in Table 3**.** As can be seen from the plots of Figures 12A-12B**,** that at the initial stage of diffusion (time $\leq$ 3 h) these plots followed linearity with correlation coefficient (R^2) value in the range of 0.972-0.997 and diffusion exponent (n) lies in between 0.13-0.75. It should also be noted that the data points substantially deviated from linearity when the overall diffusion process was considered in the time span of 24 h. Table 3 showed that the values of diffusion exponent (n) were in the range of 0.06-0.34 with R^2 values 0.638-0.813. Hence, the diffusion of water into these crosslinked CPAam and CPHEMA hydrogels is assumed to follow pseudo-Fickian kinetics, which is similar to the Fickian diffusion curves but the final equilibrium is reached very slowly.[42-43]

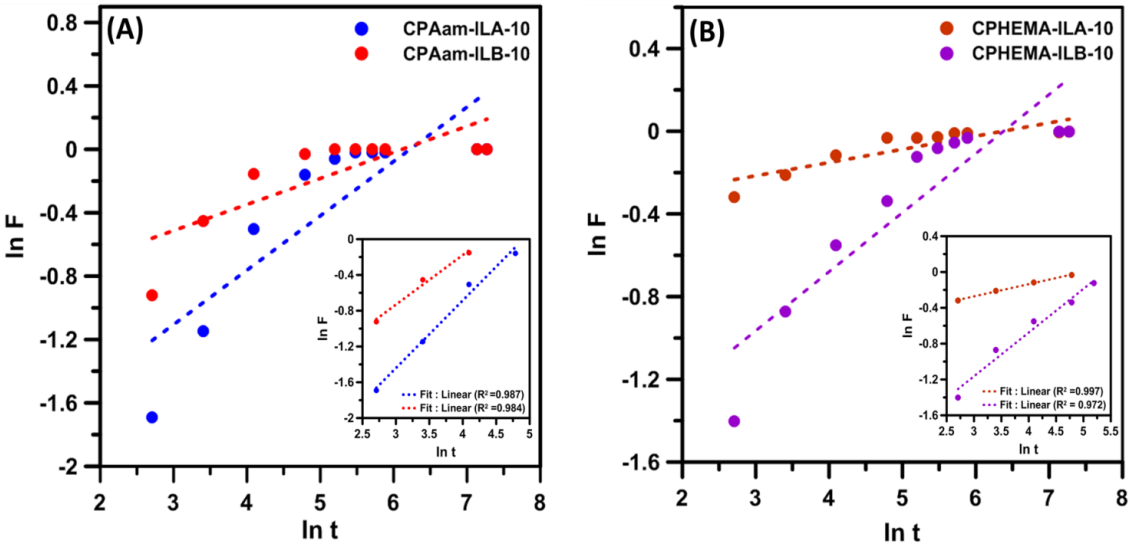

Figure 12. Swelling kinetics for the selected hydrogels in Milli-Q water. The dotted lines are the fitting lines of diffusion mechanism of the hydrogel samples.

Table 3. Diffusion parameter and the correlation coefficients for the selected hydrogels in water.

Hydrogel	n	K (min^{-1})	R^2
CPAam-ILA-10	0.34	11.82×10^{-2}	0.7353
CPAam-ILB-10	0.16	36.56×10^{-2}	0.6380
CPHEMA-ILA-10	0.06	66.56×10^{-2}	0.7743
CPHEMA-ILB-10	0.29	16.20×10^{-2}	0.8133

5.4.5 Dye Uptake Study.

In this present work, Eosin B and Alizarin Red S (ARS) were used as a model dye to check their uptake by these IL-crosslinked hydrogels. The hydrogels prepared in this study are cationic in nature because of the presence of cationic crosslinker in their network structure. As expected, Eosin B and ARS (Scheme 2) both will easily get adsorbed by the hydrogel due to electrostatic force of attraction because dyes were anionic in nature. The concentration of the dye in the solution decreased resulting in the formation of clear solution with time. The probable adsorption mechanism of the dye by the hydrogel will be discussed later in this section. However, there have some inducing factors which have significant effects on the adsorption capacity of the hydrogels which are described in this section. The dye concentrations were chosen in such a way that their initial absorbance values before dye adsorption were near to 1.0 and the change of absorbance values in a time span of 24 h could be monitored well. All adsorption experiments were carried out as follows: 3 mL dye solutions and 20 $\pm$1 mg hydrogel were poured into a 15 mL vial with stirring. After completion of adsorption at each time interval, the absorbance of the supernatant dye solution was measured using UV–Vis spectroscopy at the λ_{max} values of 519 and 423 nm for Eosin B and ARS respectively. From the measured absorbance, the concentration of dye in the external solution was determined.

Four representative IL-crosslinked CPAam and CPHEMA hydrogels namely CPAam-ILA-10, CPAam-ILB-10, CPHEMA-ILA-10 and CPHEMA-ILB-10 were selected for examining their dye uptake capacity by UV-Vis spectroscopy. In Figure 13**,** we have shown how the absorbance value of the 2×10^{-5} M Eosin B dye solution decreased rapidly with time due to continuous uptake of dye molecules by the hydrogels from their aqueous solution. A pictorial representation has also been made to understand the temporal change of colour intensity of the dye solution over a time span of 24 h. From the photographs, it is very clear that all the coloured Eosin B solutions became almost clear after 24 h.

During the sorption of ARS dye, the same type of rapid decrease of absorbance during the initial period of 6 h was observed (Figure 14) and the colour intensities of the ARS dye solutions were also drastically faded away. These observations encouraged us to study the dye adsorption kinetics and mechanism of adsorption by these hydrogels. The effect of concentration of cross-linker, initial concentration of dye solution and adsorbent dosage on the dye uptake ability of these hydrogels will also be discussed later in this section.

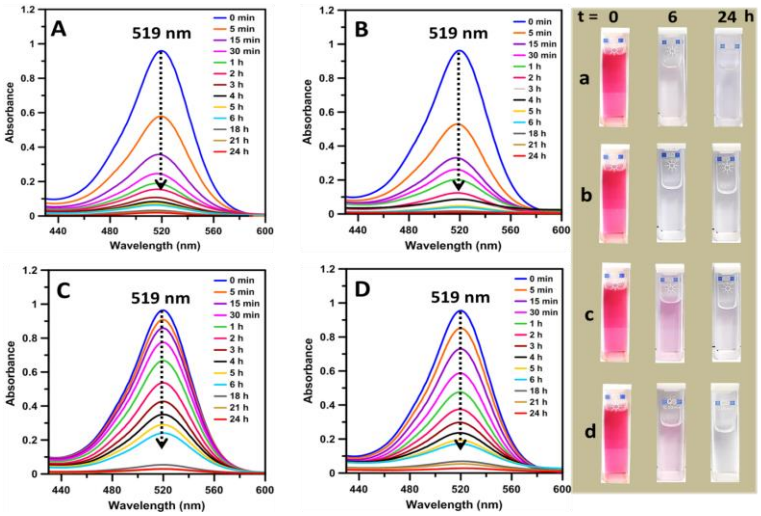

Figure 13. Time dependent UV-Vis spectra and the corresponding photos of dye solution showing the change of colour intensity at different time interval up to

24 h during adsorption of Eosin B from aqueous medium by CPAam-ILA-10 (A, a) , CPAam-ILB-10 (B, b) ,CPHEMA-ILA-10 (C, c) and CPHEMA-ILB-10 (D, d) hydrogels.([Eosin B] = 2×10^{-5} (M) , Hydrogel amount = 20±1 mg, Temperature = 25°C) .The spectra were recorded against water blank.

5.4.6 Adsorption Kinetics.

The adsorption kinetics for the uptake of anionic dyes by the IL cross-linked CPAam and CPHEMA hydrogels were studied and were explained with the help of theoretical models**.** Figure 15 and Figure 16 demonstrated the effect of contact time on the adsorption of Eosin B and ARS dyes respectively onto the series of CPAam and CPHEMA hydrogels by keeping other parameters (adsorbent dose, initial dye concentration and temperature) constant. It is evident from Figures 15-16 that the adsorption capacities (q_t) of the hydrogels increased with the increase of contact time until it reached to the equilibrium value (q_e) at ~24h. The adsorption process for the hydrogels could be divided into three regions: first region where the rate of dye sorption increased rapidly in the initial 6 h, then in the second region it kept increasing in a slower rate up-to ~21 h and then in the third region from 21-24h, there was almost no significant increase in the dye uptake. This indicates that the attainment of equilibrium dye sorption is occurred at ~24 h. The first region where q_t increases rapidly with contact time (up to ~6 h) during the initial stage of adsorption is due to the rapid attachment of dye molecules to the surface of the hydrogels, followed by pore diffusion into the hydrogel matrix.[36, 44] In the second region (6-21 h), q_t increased at a relatively slower rate with contact time. This is because the adsorption takes place in the gel network, which ultimately ended up by reaching the equilibrium approximately in 24 h for all of these hydrogels. It was also very evident that the dye adsorption rate randomly changes when the concentration of IL-crosslinkers increased from 5 to 10, 15 and 20 wt. %. But,

the nature of such change is complex and can be explained by correlating the swelling behaviour and adsorption ability.

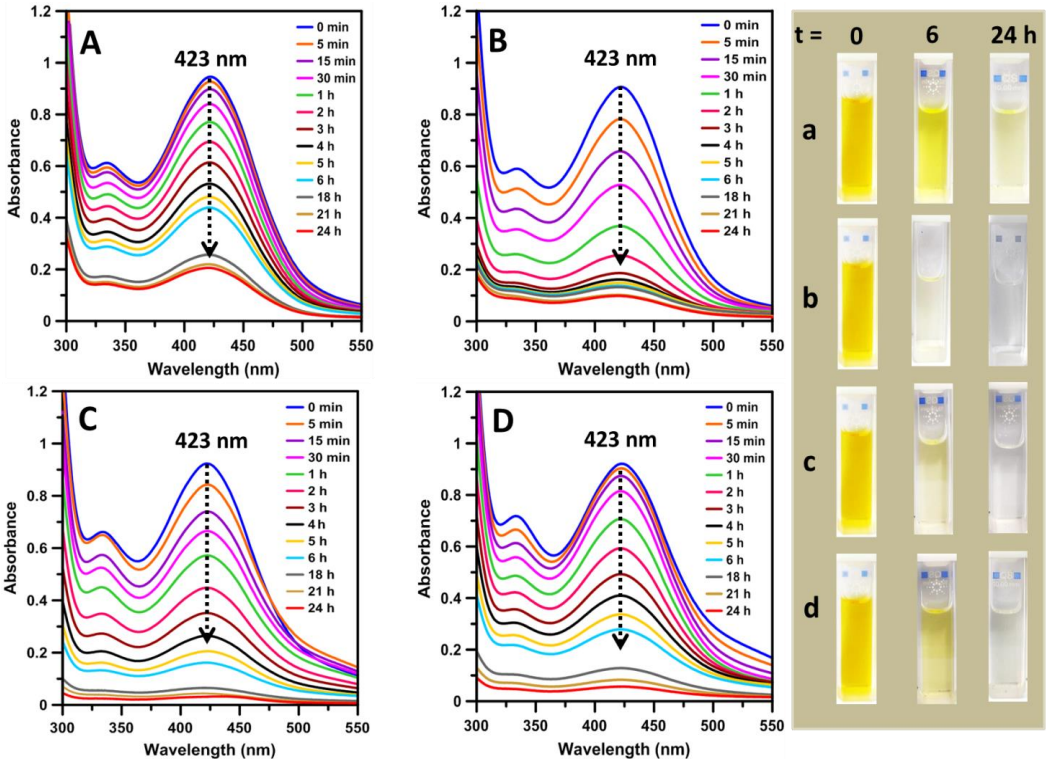

Figure 14. Time dependent UV-Vis spectra and the corresponding photos of dye solution showing the change of colour intensity at different time interval up to 24 h during adsorption of ARS from aqueous medium by CPAam-ILA-10 (A, a) , CPAam-ILB-10 (B, b) ,CPHEMA-ILA-10 (C, c) and CPHEMA-ILB-10 (D, d) hydrogels.([ARS] = 25×10^{-5} (M) , Hydrogel amount = 20±1 mg, Temperature = 25°C) .The spectra were recorded against water blank.

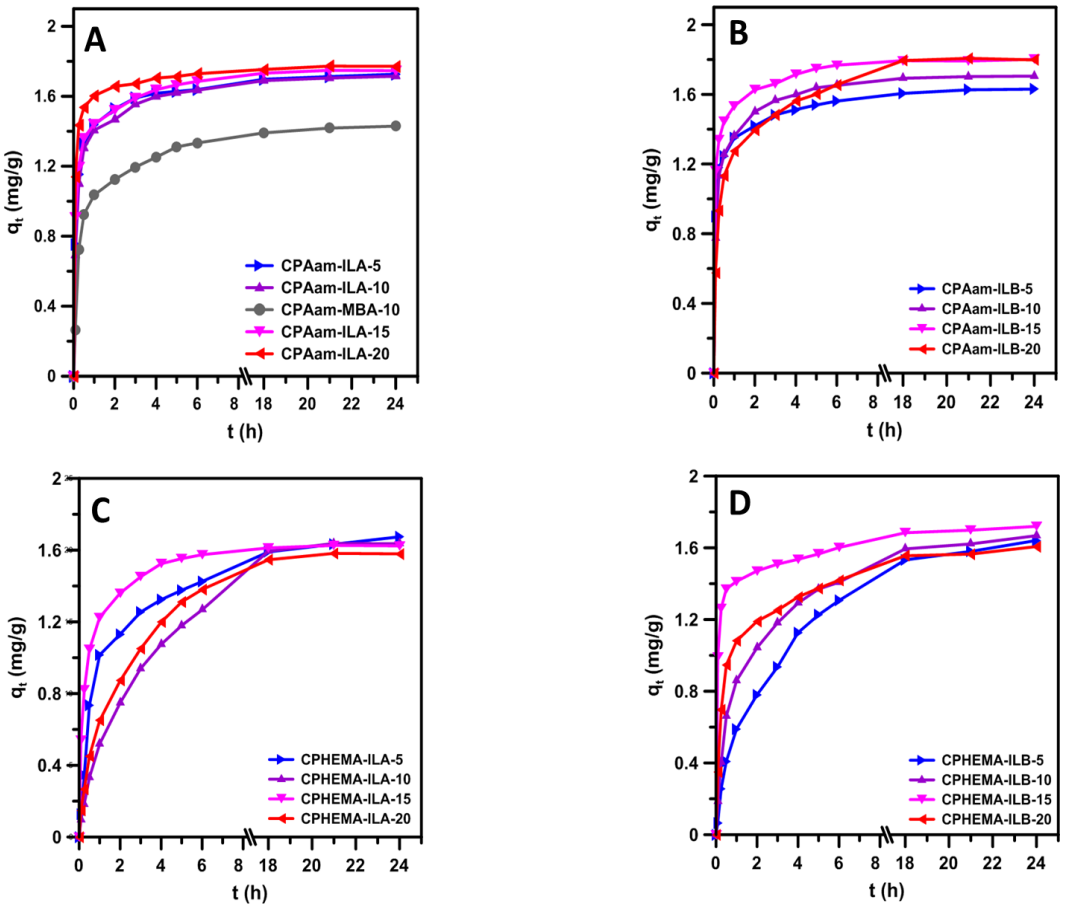

Figure 15. The effect of contact time on the Eosin B dye adsorption of A) CPAam-ILA-x, B) CPAam-ILB-x, C) CPHEMA-ILA-x and D) CPHEMA-ILB-x hydrogels. [x (=5,10,15,20) represents the IL cross-linker content (wt. %)]

As mentioned above, the increase in concentration of IL- crosslinker generates two opposing (synergistic) effects resulting in such abnormal trend. Furthermore, the equilibrium adsorption amount of dye (q_e) was increased with the increase of crosslinker concentration, which can be attributed to the fact that equilibrium process is not a kinetic phenomenon, rather controlled by thermodynamics. That's why q_e increases because of the presence of more cationic adsorption sites in the hydrogel matrix when the concentration of IL cross-linker is increased.

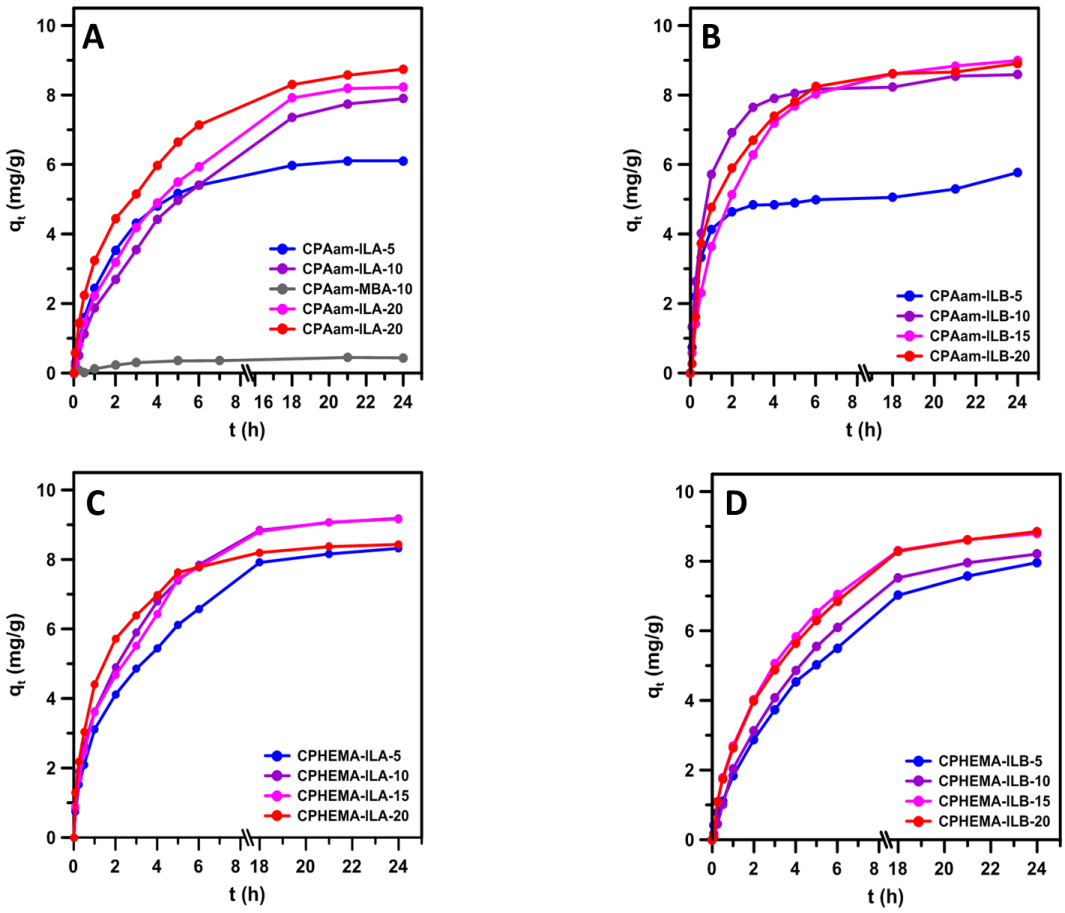

Figure 16. The effect of contact time on the ARS dye adsorption of A) CPAam-ILA-x, B) CPAam-ILB-x, C) CPHEMA-ILA-x and D) CPHEMA-ILB-x hydrogels. [x (=5,10,15,20) represents the IL cross-linker content (wt. %)]

In these cases, to investigate the kinetics of dye adsorption, the experimental data were fitted with the pseudo first-order and a pseudo second-order kinetic model to analyse the experimental data obtained. [36, 45-46] The pseudo first-order kinetic is observed in the polarization-based physisorption process whereas the pseudo second-order kinetic is observed where chemisorption occurs.[47] Note that, the dye adsorption experiments were carried out for 4 different series of hydrogels; however, the kinetic data for CPAam-ILA-10, CPAam-ILB-10, CPHEMA-

ILA-10 and CPHEMA-ILB-10 hydrogels were used for the analysis. It is to be noted that, to assure the adsorption to reach equilibrium, 48 h was chosen in the following experiments.

The Lagergren linear form of the pseudo-first order kinetic model can be expressed as:

$$\ln(q_e - q_t) = \ln q_e - k_1 t \quad , \qquad (7)$$

and the pseudo second-order Ho and Mckay kinetic model can be expressed as:

$$t/q_t = 1/(k_2 q_e^2) + t/q_e \quad , \qquad (8)$$

where q_t (mg g^{-1}) and q_e (mg g^{-1}) are the adsorption capacity at time t (min) and at equilibrium condition respectively; k_1 (min^{-1}), k_2 (g mg^{-1} min^{-1}) are the rate constant of the pseudo first-order and the pseudo second-order adsorption process respectively.

The kinetic parameters of pseudo first-order and pseudo second-order model are listed in Table 4. Note that the actual q_e values found in this experiments ($q_{e,exp}$) were calculated using Equation 4 at time t = 48 h to assure that equilibrium has been reached. The q_e values derived from the models ($q_{e,cal}$) were compared with the $q_{e,exp}$ values. The coefficients of determination (R^2) values were also calculated from the best fit lines of experimental data for both kinetic models. The R^2 values obtained from pseudo first-order kinetic model (Figure 17) during adsorption of Eosin B and ARS dyes by cross-linked CPAam and CPHEMA hydrogels were found to be in a wide range from 0.756–0.979 and 0.919-0.968 respectively. The R^2 values gave an indication that the experimental data points deviated from linearity for the overall process suggesting that the

dye adsorption processes do not fit well with pseudo first-order kinetic model. Moreover, the $q_{e,cal}$ values were not in good agreement with the $q_{e,exp}$ values for

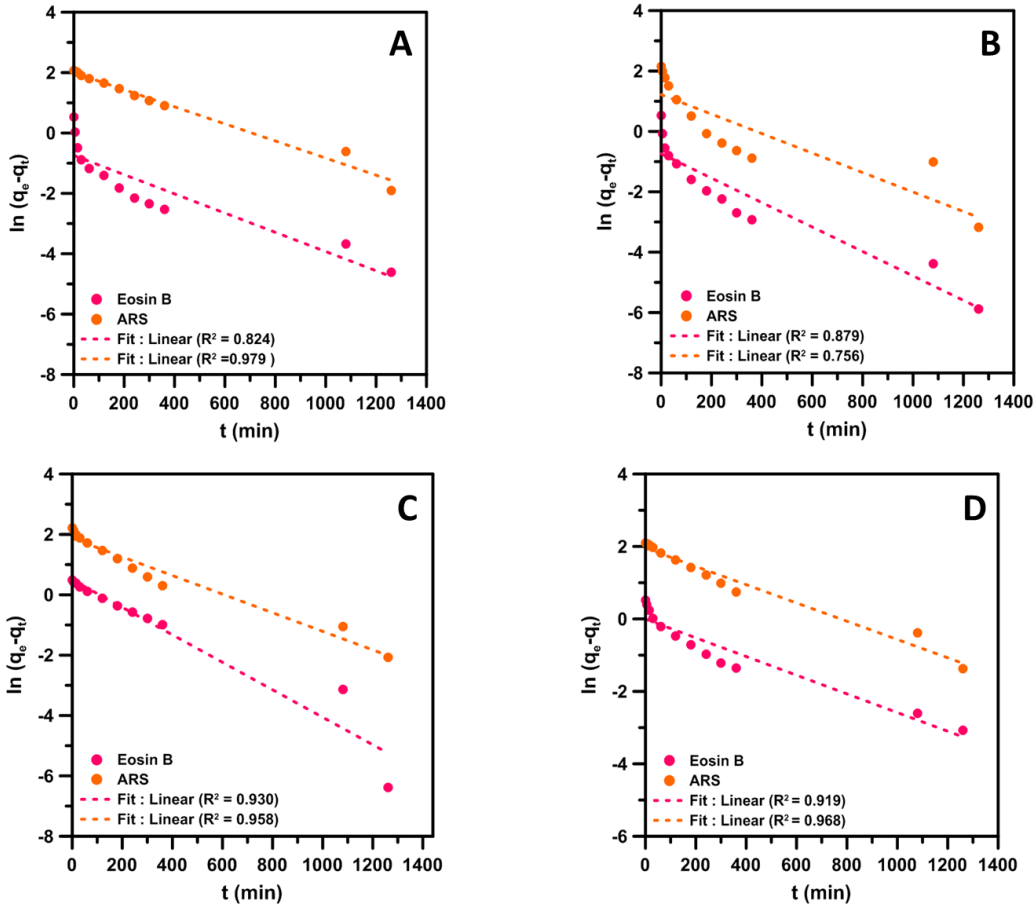

Figure 17. Pseudo first-order kinetics dur A) CPAam-ILA-10 B) CPAam-ILB-10 C) CPHEMA-ILA-10 D) CPHEMA-ILB-10

the pseudo first order kinetics. Therefore, the data did not follow first-order kinetics. This is expected because pseudo the first-order kinetic model generally does not describe the whole adsorption process rather fits well during the initial stage of adsorption (up to 360 min as observed from Figure 17), when the bulk concentration of solute particles is comparatively high.

The pseudo second-order kinetics of Eosin B and ARS dye adsorption onto the representative hydrogels was shown in Figure 18. It can be seen from Table 4, that in contrast to the pseudo first-order kinetic model, the $q_{e,cal}$ values obtained from pseudo second-order kinetic model were in good agreement with the experimental $q_{e,exp}$ values. Moreover, R^2 values (> 0.997) of the pseudo second-order kinetic model were found to have good correlation with experiment values, suggesting that the pseudo second-order kinetic model can be used for explaining the whole adsorption process. This result further reveals that the adsorption behaviour was chemical adsorption (chemisorption).

Along with the pseudo first-order and pseudo second-order kinetic model, the Elovich kinetic model[21] ,which describes a chemisorption process and also assumes that the surface of the solid adsorbent is energetically heterogeneous, was also used to fit the experimental data. The linear form of the Elovich kinetic model can be expressed by the following equation:

$$q_t = \frac{1}{\beta} \ln(\alpha\beta) + \frac{1}{\beta} \ln t \qquad (9)$$

where q_t (mg/g) is the amount of adsorbate adsorbed at time t ; α and β are constants where α (mg g^{-1} min^{-1}) is related to rate of chemisorption and β (g mg^{-1}) which is also termed as desorption coefficient is related to the extent of surface coverage of the adsorbent. Figure. 19 showed the best fit linear plots based on Elovich kinetic model. The constants α and β are obtained from the intercept and slope respectively and were given in Table 4. All the plots are linear with a regression coefficient in the range of 0.891-0.989. From the obtained values of α and β, it can be concluded that in some cases adsorption and desorption processes compete with each other.

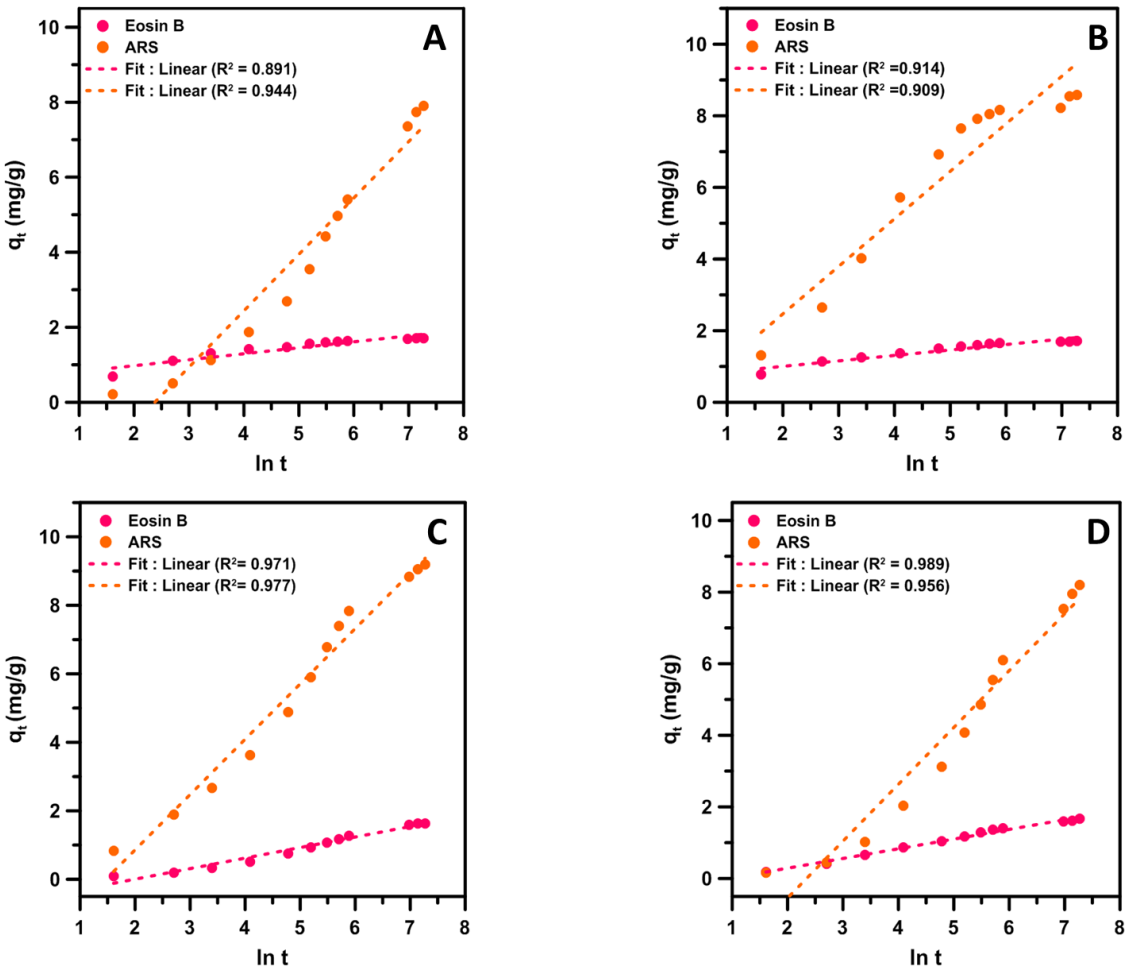

Figure 18. Pseudo second order kinetics of A)CPAam-ILA-10, B) CPAam-ILB-10 ,C) CPHEMA-ILA-10 and D) CPHEMA-ILB-10

Altogether, Figures 17-19 and Table 4 showed that the pseudo second order kinetic model best fits experimental data and consistent with the high R^2 values and the theoretical adsorption capacities ($q_{e,cal}$) calculated from the kinetic model were very close to the experimental values ($q_{e,exp}$). This implies that the adsorption rate is controlled by chemisorption (slow step) which can be

attributed to the chelation between the dye molecules and amine or hydroxyl functional groups present in the IL- crosslinked hydrogels[48-49] whereas interfacial adsorption of anionic dye molecules via cationic sites (cross-linking points of the hydrogel matrix) of the hydrogel matrices through electrostatic force of attraction is the reason of fast dye uptake.

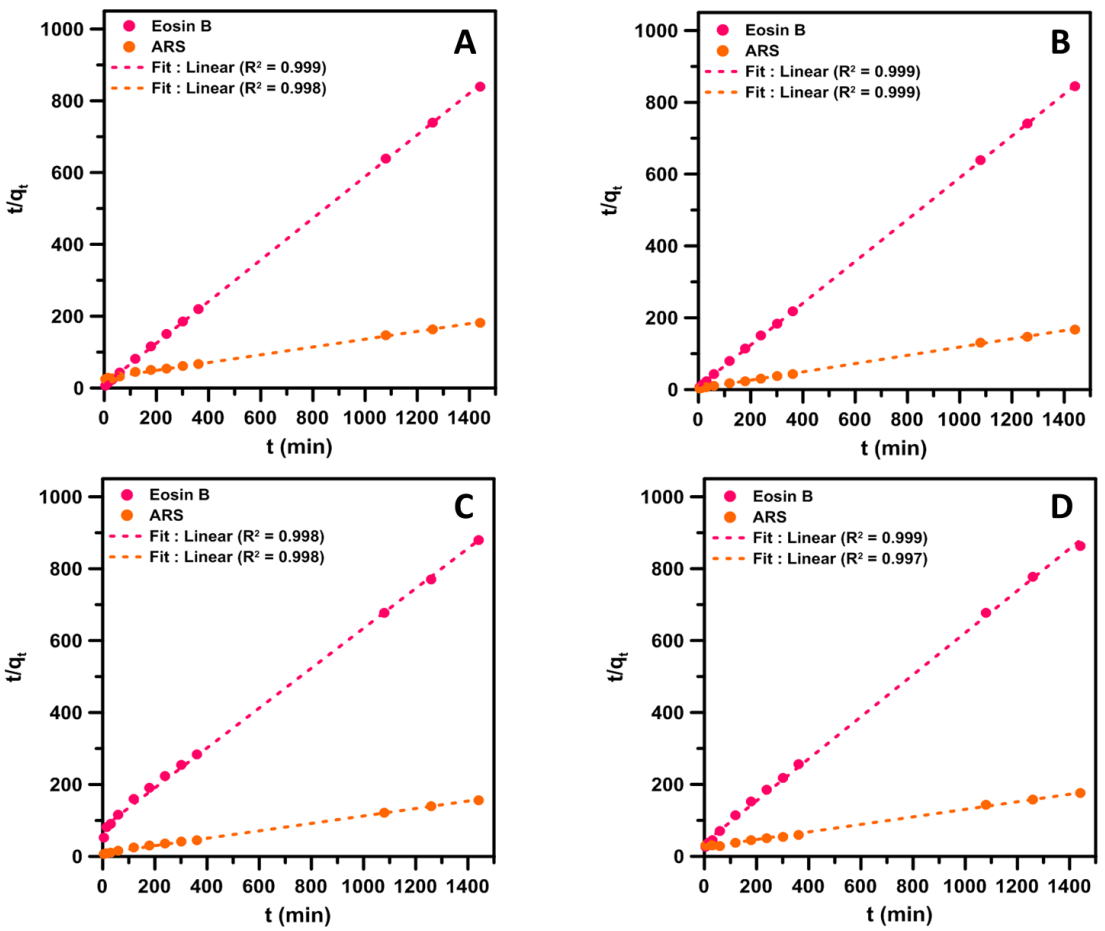

Figure 19. Elovich kinetic model of A)CPAam-ILA-10, B) CPAam-ILB-10 ,C) CPHEMA-ILA-10 and D) CPHEMA-ILB-10.

Table 4. Kinetic parameters for the adsorption of dyes onto hydrogels.

Dye Used	Hydrogel	$q_{e,exp}$ (mg g^{-1})	Pseudo first-order kinetics			Pseudo second-order kinetics			Elovich kinetic model		
			k_1 (min^{-1})	$q_{e,cal}$ (mg g^{-1})	R^2	k_2 (g $mg^{-1}min^{-1}$)	$q_{e,cal}$ (mg g^{-1})	R^2	α (mg g^{-1} min^{-1})	β (g mg^{-1})	R^2
Eosin B	CPAam-ILA-10	1.714	3.18×10^{-3}	0.475	0.8241	0.038	1.723	0.9998	9.82	6.27	0.8907
	CPAam-ILB-10	1.705	4.05×10^{-3}	0.478	0.8795	0.043	1.718	0.9999	14.90	6.56	0.9139
	CPHEMA-ILA-10	1.637	4.55×10^{-3}	1.640	0.9305	3.85×10^{-3}	1.803	0.9982	0.04	3.25	0.9707
	CPHEMA-ILB-10	1.668	2.58×10^{-3}	0.994	0.9186	9.07×10^{-3}	1.712	0.9684	0.11	3.69	0.9890
Alizarin Red S	CPAam-ILA-10	8.799	2.83×10^{-3}	7.384	0.9790	4.31×10^{-4}	9.207	0.9979	0.14	0.66	0.9438
	CPAam-ILB-10	8.586	3.23×10^{-3}	3.382	0.7565	3.92×10^{-3}	8.687	0.9995	1.16	0.75	0.9093
	CPHEMA-ILA-10	9.186	3.08×10^{-3}	6.489	0.9580	1.16×10^{-3}	9.672	0.9985	0.37	0.62	0.9771
	CPHEMA-ILB-10	8.205	2.52×10^{-3}	7.056	0.9684	4.25×10^{-4}	9.535	0.9967	0.15	0.63	0.9556

5.4.7 Adsorption Mechanism.

In the dye adsorption processes, molecular diffusion mechanism also influences the overall adsorption rate on the adsorbent, which cannot be described by the pseudo kinetic models.[47]. As per the literature there are several types of diffusion may occur consecutively during the sorption of adsorbate molecules/ ions on porous adsorbent (solid/liquid phase adsorption process). There is bulk transport and after that, the adsorbate ions start to travel towards the exterior surface of the adsorbent (film diffusion). Then after attachment of small fraction of adsorbate particles onto the external surface of the adsorbent, adsorbate ions start to travel within the pores of the adsorbent (intra-particle diffusion). The final stage (absorption) where adsorbate ions attach themselves inside the inner surface of the adsorbent.[47] Accordingly, a schematic representation of all these mechanisms is shown in Scheme 2 with respect to our case.

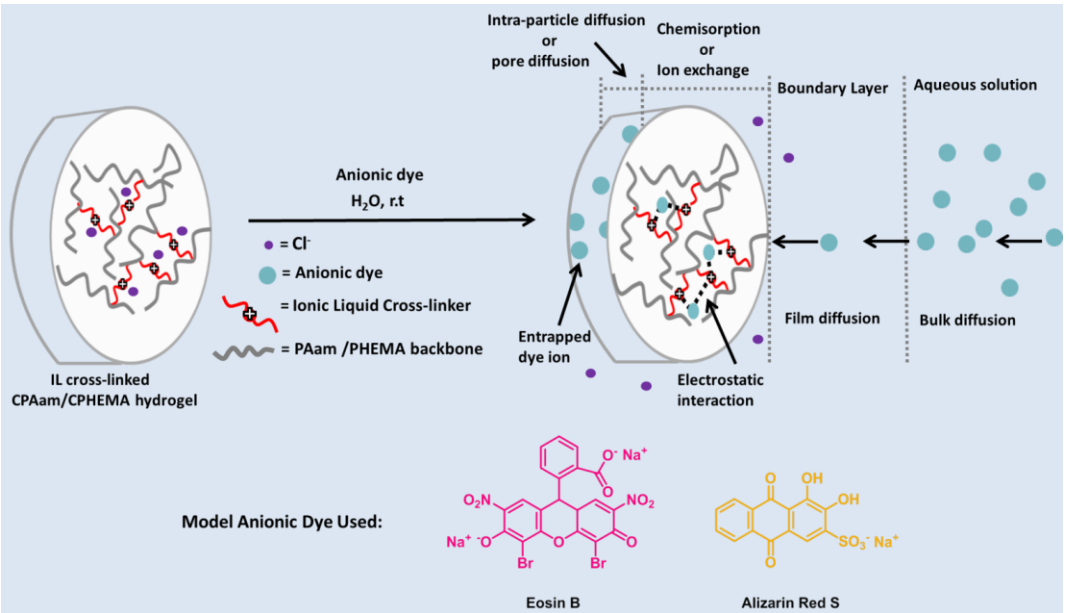

Scheme 2. Schematic representation of anionic dye adsorption onto the cationic hydrogels from aqueous solution.

To describe the diffusion mechanism of the solute dye particles into the interior of the hydrogels, the experimental data were fitted with intra-particle diffusion and film diffusion kinetic model equations. Intra-particle diffusion model is generally used to check whether diffusion is the rate determining step in the sorption process. The intra-particle diffusion model by Weber and Morris[41] is given by the linear equation as;

$$q_t = K_p t^{1/2} + C \qquad (10)$$

where K_p (mg/g $min^{1/2}$) is the rate constant for intra-particle diffusion model where higher value of K_p indicates an enhancement in the rate of adsorption and C(mg/g) is a constant which gives an idea about the thickness of boundary layer where higher the value of C, higher the boundary layer effect.[41] According to this model, if intra-particle diffusion occurs then q_t vs. $t^{1/2}$ plot will be linear. Also, if

the linear plot passes through the origin, which indicates that intra-particle diffusion is the rate-determining step or in other words it gives an indication of sole control of intra-particle diffusion for the whole adsorption period. [47] Whereas the intra-particle diffusion is not the rate-determining step if the linear plot does not pass through the origin for the overall adsorption process. There is possibility of other mechanism to occur along with intra-particle diffusion. The plots of intra-particle diffusion model for the adsorption of Eosin B and ARS dyes onto the representative as-synthesized hydrogels (Figure 20) were not linear but, linear plots can be constructed considering the small region as observed else-where.[21, 41] The values of K_P and C for each linear region were calculated from the slope and intercepts respectively of the linear fit plots of q_t vs. $t^{1/2}$ and were listed in Table 5. The linear fits over the time span of 24 h do not pass through origin which clearly indicate that the adsorption processes do not follow single diffusion mechanism and the only rate-determining step is not intra-particle diffusion.[21 50] Such multiple linear plots indicated the involvement of multi-step process in the adsorption of the dyes by the hydrogels. The first steeper region (Stage I), which has the highest diffusion rate, represented the immediate sorption or external surface sorption of the anionic dye molecules onto the hydrogels through the solution. The sharper slopes (K_{P1}, Table 5) of this first steeper section indicates that a higher rate of ion removal was occurred in the beginning due to boundary layer diffusion of the anions to the immediately available active adsorption sites present on the surface of the hydrogels. The second region (stage II) described the gradual adsorption stage which is the intra-particle diffusion stage. The slopes for this region (K_{P2}, Table 5) were much lesser than that of first stage (K_{P1}). [41] This region can be attributed to the diffusion of the surface adsorbed dye molecules within the porous matrix of the hydrogels.[21] The third region (stage III) revealed lower slopes (K_{P3}, Table 5),

suggesting the final equilibrium stage where intra-particle diffusion starts to slow down due to extremely low concentration of adsorbate particles in the solution. Note that during the adsorption of Eosin B and ARS dyes by the CPHEMA-ILA-10 (Figure 20B) and CPHEMA-ILB-10 hydrogels (Figure 20D) and ARS adsorption by CPAam-ILA-10 hydrogel (Figure 20C**,** purple dotted line), the second linear region got associated with the third linear region final stage, and in these cases the intra-particle diffusion process controls the rate of the process.[41] These observations justified the co-existence of bulk, film and pore/intra-particle diffusions for all the dyes onto the hydrogels.[51] Similar adsorption mechanism has been reported for other cationic hydrogels during dye adsorption processes.[21, 52]

Table 5. Kinetic parameters for intra-particle diffusion model.

Hydrogel	Intra-Particle Diffusion Model								
	Kinetic parameters								
	K_{P1} (mg/g $min^{1/2}$)	C_1 (mg/g)	R^2	K_{P2} (mg/g $min^{1/2}$)	C_2	R^2	K_{P3} (mg/g $min^{1/2}$)	C_3 (mg/g)	R^2
CPAam-ILA-10	0.189	0.303	0.9672	0.029	1.161	0.9822	0.005	1.534	0.9823
CPAam-ILB-10	0.148	0.481	0.9283	0.035	1.085	0.9695	0.004	1.559	0.8978
CPHEMA-ILA-10	0.072	-0.061	0.9967	0.021	0.883	0.9744	--	--	--
CPHEMA-ILB-10	0.075	0.157	0.9554	0.015	1.094	0.9805	--	--	--
CPAam-ILA-10	0.319	-0.634	0.9973	0.135	2.861	0.9953	--	--	--
CPAam-ILB-10	0.652	0.174	0.9714	0.093	6.429	0.9794	0.020	7.745	0.6510
CPHEMA-ILA-10	0.414	0.251	0.9947	0.072	0.251	0.9947	--	--	--
CPHEMA-ILB-10	0.367	-0.852	0.9980	0.111	3.980	0.9955	--	--	--

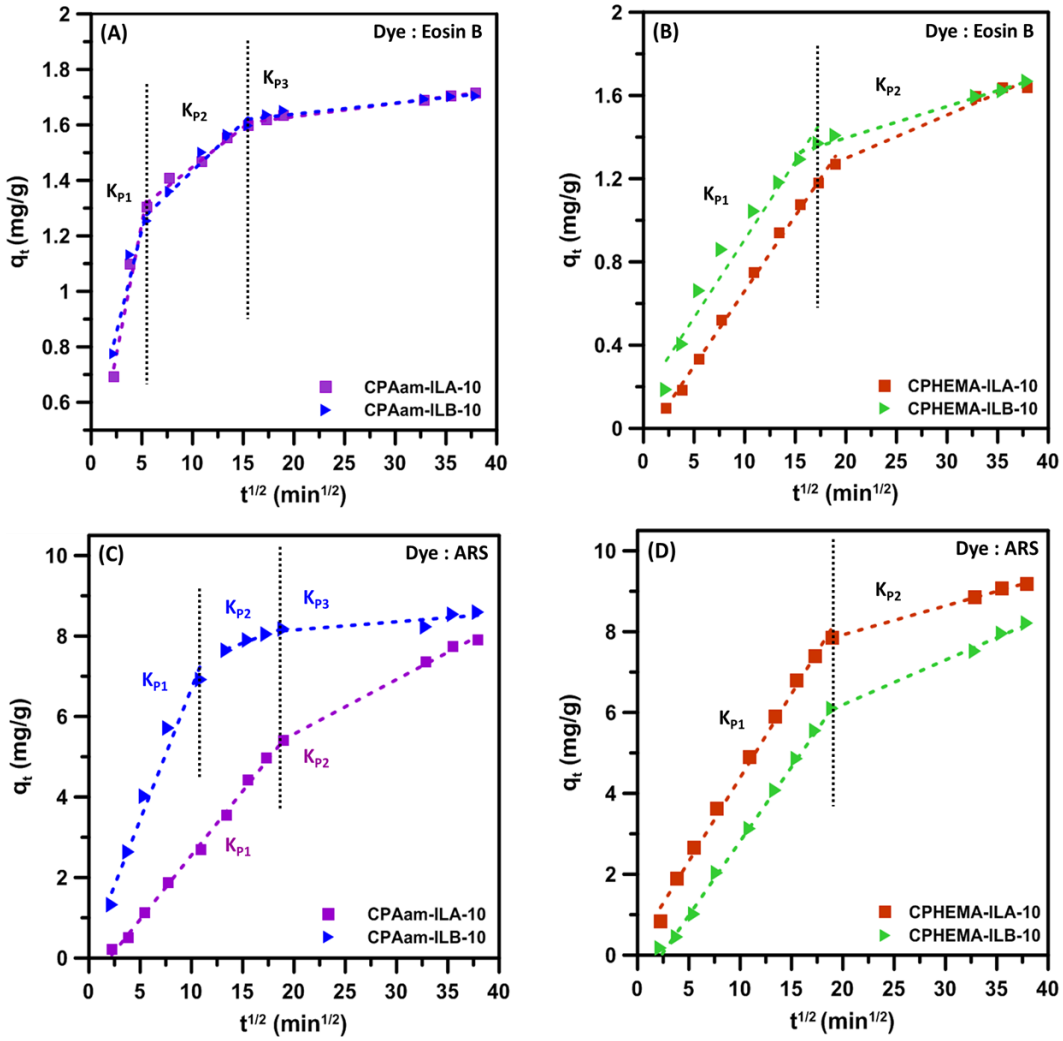

.

Figure 20. Intra-particle diffusion plots for adsorption of Eosin B (A,B) and ARS (C,D) dye on the selected hydrogels at ambient temperature. (Initial concentration of Eosin B and ARS are 12.5 and 85 mg/L respectively)

Thus, it is clear that the adsorption of Eosin B and ARS dyes onto the selected CPAam and CPHEMA hydrogels is a complex and multi-step process. But among particle diffusion and film diffusion, which process actually controls the overall adsorption process still remained unknown. Therefore to identify the actual rate controlling step, the experimental data were also fitted to the Boyd kinetic model[47] as follows:

$$B_t = -0.4977 - \ln(1-F), \quad (11)$$

where $F = q_t/q_e$ represents the fraction of dye adsorbed at any time t and B_t, mathematical function of F, is called Boyd parameter. B_t values have been plotted against corresponding t (min) values to depict the film diffusion model (Figure 21). According to this model, if the kinetic plot 'B_t vs. t' takes a linear form passing through the origin, then it indicates that particle diffusion is the actual rate controlling step in the adsorption process. However in case if the plot is linear but do not pass through the origin then external mass transfer (film diffusion) determines the overall rate of the adsorption process.[53] As shown in Figure 21**,** the values of correlation coefficient (R^2) related to the Boyd kinetic plots for our experimental system are in the region of (0.873-991) and (0.756-0.968) for Eosin B and ARS adsorption respectively. Hence all the plots may broadly be considered as linear but none of the plots passed through the origin indicating that the adsorption of Eosin B and ARS dyes onto the IL cross-linked CPAam and CPHEMA hydrogels was majorly controlled by film diffusion or chemisorption which was later taken over by the intra-particle diffusion at subsequent stages.

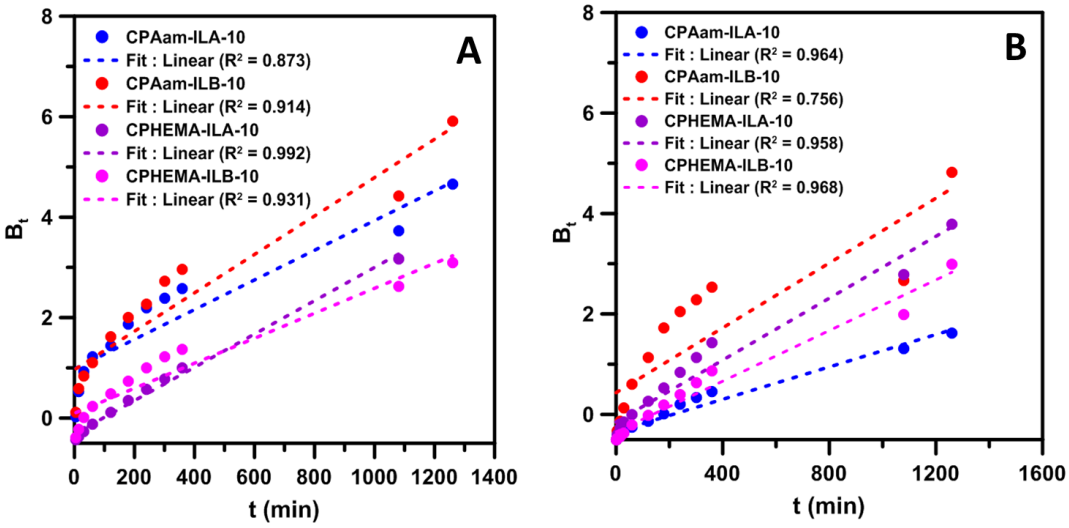

Figure 21. Boyd fitting plot for the adsorption of A) Eosin B and B) ARS dye on the selected hydrogels.

5.5 CONCLUSIONS

Acrylamide and 2-hydroxyethyl methacrylate based hydrogels were prepared using newly synthesized ionic liquid as cross-linkers. The structure of the hydrogels was characterized by different techniques including FTIR and SEM analysis. Thermal stability of the hydrogels was investigated by TGA and DTG analyses. The introduction of ionic liquid into the hydrogel matrix as cross-linkages resulted in the incorporation of cationic binding sites for which further led to electrostatic interaction with anionic dyes. Swelling performance and diffusion mechanism of water within the hydrogels were investigated and pseudo Fickian mechanism is observed to be operated during transportation of water molecules into the hydrogel network. The dye adsorption by these hydrogels was investigated using Eosin B and Alizarin Red S as model dyes. The dye adsorption data of representative hydrogels were fitted with three kinetic models : pseudo first-order, pseudo-second-order and Elovich kinetic models

where pseudo second-order kinetic model gave the best fitting result indicating the adsorption as chemisorption . Further to investigate the dye adsorption mechanism, intra-particle diffusion model used which showed multi-linearity behaviour confirming that the adsorption occurred through different steps. Again the intercepts of the intra-particle diffusion plots did not pass through origin indicating intra-particle diffusion was not only the rate controlling step. Further fitting the experimental data to Boyd kinetic model indicated that film diffusion was rate controlling for a period a time which was taken over by intra-particle diffusion after a certain stage.

5.6 REFERENCES

1. Zagorodni, A. A., *Ion Exchange Materials: Properties and Applications*; Elsevier, 2006.
2. Şolpan, D.; Duran, S.; Torun, M.; chemistry, *Radiat. Phys. Chem.* **2008**, *77*, 447-452.
3. Mondal, S.; Das, S.; Nandi, A. K., *Soft Matter* **2020**, *16*, 1404-1454.
4. Paulino, A. T.; Guilherme, M. R.; Reis, A. V.; Campese, G. M.; Muniz, E. C.; Nozaki, J., *J. Colloid Interface Sci.* **2006**, *301*, 55-62.
5. Imato, K.; Ohishi, T.; Nishihara, M.; Takahara, A.; Otsuka, H., *J. Am. Chem. Soc.* **2014**, *136*, 11839-11845.
6. Weber, J.; Bergström, L., *Langmuir* **2010**, *26*, 10158-10164.
7. Walker, G.; Hansen, L.; Hanna, J.-A.; Allen, S., *Water Res.* **2003**, *37*, 2081-2089.
8. Stylidi, M.; Kondarides, D. I.; Verykios, X. E., *Appl. Catal. Environ.* **2004**, *47*, 189-201.

9. de Menezes, E. W.; Lima, E. C.; Royer, B.; de Souza, F. E.; dos Santos, B. D.; Gregório, J. R.; Costa, T. M.; Gushikem, Y.; Benvenutti, E. V., *J. Colloid Interface Sci.* **2012**, *378*, 10-20.

10. Gupta, V.; Suhas; Ali, I.; Saini, V., *Ind. Eng. Chem. Res.* **2004**, *43*, 1740-1747.

11. Dawood, S.; Sen, T., *J. Chem. Process Eng.* **2014**, *1*, 1-11.

12. Kumar, K. V.; Ramamurthi, V.; Sivanesan, S., *J. Colloid Interface Sci.* **2005**, *284*, 14-21.

13. Silva, J. P.; Sousa, S.; Rodrigues, J.; Antunes, H.; Porter, J. J.; Gonçalves, I.; Ferreira-Dias, S., *Sep. Purif. Technol.* **2004**, *40*, 309-315.

14. Kono, H.; Kusumoto, R., *J. Water Process. Eng.* **2015**, *7*, 83-93.

15. Dafnopatidou, E. K.; Lazaridis, N. K., *Ind. Eng. Chem. Res.* **2008**, *47*, 5594-5601.

16. Khayet, M.; Zahrim, A.; Hilal, N., *Chem. Eng. J.* **2011**, *167*, 77-83.

17. Lu, N.; Zhao, Y.; Liu, H.; Guo, Y.; Yuan, X.; Xu, H.; Peng, H.; Qin, H., *J. Hazard. Mater.* **2012**, *199*, 1-8.

18. Gomes, A. C.; Fernandes, L. R.; Simões, R. M., *Chem. Eng. J.* **2012**, *189*, 175-181.

19. Kwak, N.-S.; Park, H.-M.; Hwang, T. S., *Chem. Eng. J.* **2012**, *191*, 579-587.

20. Mahmoodi, N. M.; Hayati, B.; Arami, M.; Mazaheri, F., *J. Chem. Eng. Data* **2010**, *55*, 4660-4668.

21. Deen, G. R.; Tan, Y. L.; Yalini, M. R.; Mah, C. H.; Teo, T. W., *EJ-CHEM* **2022**, *3*, 12-24.

22. Yagub, M. T.; Sen, T. K.; Afroze, S.; Ang, H. M., *Adv. Colloid Interface Sci.* **2014**, *209*, 172-184.

23. Salleh, M. A. M.; Mahmoud, D. K.; Karim, W. A. W. A.; Idris, A., *Desalination* **2011**, *280*, 1-13.

24. Bolto, B.; Dixon, D.; Eldridge, R., *React. Funct. Polym.* **2004**, *60*, 171-182.

25. Heijman, S.; Van Paassen, A.; Van der Meer, W.; Hopman, R., *Water Sci. Technol.* **1999**, *40*, 183-190.

26. Yuan, C.; Guo, J.; Yan, F., *Polymer* **2014**, *55*, 3431-3435.

27. Zhou, X.; Zhou, Y.; Nie, J.; Ji, Z.; Xu, J.; Zhang, X.; Du, B. J. A. A. M.; Interfaces, *ACS Appl. Mater. Interfaces* **2014**, *6*, 4498-4513.

28. Zhou, X.; Wang, J.; Nie, J.; Du, B., *Polym. J.* **2016**, *48*, 431-438.

29. Das, T.; Paira, T. K.; Biswas, M.; Mandal, T. K., *J. Phys. Chem. C* . **2015**, *119*, 4324-4332.

30. Dumitrescu, A.; Lisa, G.; Iordan, A.; Tudorache, F.; Petrila, I.; Borhan, A.; Palamaru, M.; Mihailescu, C.; Leontie, L.; Munteanu, C., *Mater. Chem. Phys.* **2015**, *156*, 170-179.

31. Saha, S.; Sarkar, P.; Sarkar, M.; Giri, B., *RSC Adv.* **2015**, *5*, 27665-27673.

32. Podhorská, B.; Vetrík, M.; Chylíková-Krumbholcová, E.; Kománková, L.; Rashedi Banafshehvaragh, N.; Šlouf, M.; Dušková-Smrčková, M.; Janoušková, O., *Appl. Sci.* **2020**, *10*, 6672.

33. Zhou, C.; Wu, Q., *Colloids Surf B Biointerfaces* **2011**, *84*, 155-162.

34. Elbedwehy, A. M.; Atta, A. M., *Polymers* **2020**, *12*, 338.

35. Azady, M.; Roman, A.; Alam, M.; Paul, S. C.; Rahaman, M.; Sultana, S.; Hasnine, S. M.; Ahmed, T.; Gafur, M., *J. Polym. Environ.* **2021**, *29*, 520-537.

36. Dalaran, M.; Emik, S.; Güçlü, G.; İyim, T. B.; Özgümüş, S., *Desalination* **2011**, *279*, 170-182.

37. Rapado, M.; Peniche, C., *Polimeros* **2015**, *25*, 547-555.

38. Das, D.; Das, R.; Ghosh, P.; Dhara, S.; Panda, A. B.; Pal, S., *RSC Adv.* **2013**, *3*, 25340-25350.

39. Taleb, M. A.; Hegazy, D. E.; Mahmoud, G. A., *Int. J. Polym. Mater. Polym. Biomater.* **2014**, *63*, 840-845.

40. Chen, B.; Wang, M.; Wang, X.; Zhao, Q.; Wang, Y.; Gao, G., *Polym. Chem.* **2021**, *12*, 2731-2742.

41. Tanan, W.; Panpinit, S.; Saengsuwan, S., *Eur. Polym. J.* **2021**, *143*, 110193.

42. Shi, Y.; Xiong, D.; Liu, Y.; Wang, N.; Zhao, X., *Mater. Sci. Eng. C* **2016**, *65*, 172-180.

43. Xin, F.; Sui, M.; Liu, X.; Zhao, C.; Yu, Y., *Colloid Polym. Sci.* **2019**, *297*, 763-769.

44. Ho, Y.; Chiang, C., *Adsorption* **2001**, *7*, 139-147.

45. Renault, F.; Morin-Crini, N.; Gimbert, F.; Badot, P.-M.; Crini, G., *Bioresour. Technol.* **2008**, *99*, 7573-7586.

46. Chen, H.; Wang, A., *J. Hazard. Mater.* **2009**, *165*, 223-231.

47. Haque, A. N. M. A.; Remadevi, R.; Rojas, O. J.; Wang, X.; Naebe, M., *Cellulose* **2020**, *27*, 6485-6504.

48. Gao, H.; Jiang, J.; Huang, Y.; Wang, H.; Sun, J.; Jin, Z.; Wang, J.; Zhang, J., *SN Appl. Sci.* **2022**, *4*, 1-14.

49. ALSamman, M. T.; Sánchez, J., *Arab. J. Chem.* **2021**, *14*, 103455.

50. Inyinbor, A.; Adekola, F.; Olatunji, G. A., *Water Resour. Ind.* **2016**, *15*, 14-27.

51. Singha, N. R.; Karmakar, M.; Mahapatra, M.; Mondal, H.; Dutta, A.; Roy, C.; Chattopadhyay, P. K., *Polym. Chem.* **2017**, *8*, 3211-3237.

52. Krishnappa, P. B.; Badalamoole, V., *Int. J. Biol. Macromol.* **2019**, *122*, 997-1007.

53. Singh, P. K.; Banerjee, S.; Srivastava, A. L.; Sharma, Y. C., *RSC Adv.* **2015**, *5*, 35365-35376.

SUMMARY

The scientific content of this thesis work covers the development of new types of ionic liquids (ILs) and/or poly (ionic liquids) (PILs), their stimuli-responsive behaviours and explores the role of macromolecular engineering in the development of polymer materials with the desired combination of properties for advanced applications. In particular, a series of new stimuli-responsive ionic liquid-based random copolymers of different architectures were achieved via RAFT polymerization of an ILM with a variety of hydrophilic or hydrophobic monomers. This was accompanied by the investigation of these PILs with regards to their stimuli-responsiveness, particularly in solution under different external stimuli such as temperature and ionic strength. This was followed by the polymerization of an ionic liquid monomer into nonionic-ionic type random copolymers and their ionic conductivities were investigated as a function of different parameters. Development of new photoinitiating ILs and PIL along with the detailed study of the photoinitiation mechanism and comparative photoinitiating abilities in aqueous medium were described. Exploration of PIL as macromolecular photoinitiator towards the development of different types of thermoresponsive graft copolymers was further described. New cross-linkable ILMs and their successive use to fabricate hydrogel adsorbents for the removal of dyes were described.

The introduction section has been described a brief overview on the general aspects of ILs and PILs**.** A broad overview on the design and synthetic strategies for different types of ILs, ionic liquid monomers (ILMs) in particular, the synthesis of PILs via conventional free radical or controlled/living radical polymerization technique (e.g., RAFT) have also been described. Ionic conductivity and stimuli-responsive properties of PILs have been reviewed in detail. Recent developments on water-soluble photoinitiators and polymeric hydrogels have been reviewed in

a systematic way. Finally, the chapter described the various possible applications of ILs/PILs.

A series of PIL, P[VBTP][Cl]- based random copolymers containing conventional polymer segments namely, P[VBTP][Cl]-ran-PMMA, P[VBTP][Cl]-ran-PS, P[VBTP][Cl]-ran-PHEMA and P[VBTP][Cl]-ran-PNIPAM of varying compositions have been synthesized via RAFT polymerization technique. The incorporation of only a very small percentage of ionic P[VBTP][Cl] segment into these copolymers enabled the solubilization of hydrophobic polymer PMMA/PS segments in MeOH/water and hydrophilic PHEMA segment in water regardless of their molecular weights. Further, the copolymeric solutions underwent aggregation resulting in turbidity in the presence of externally added halide ions and experienced phase transitions from turbid suspension to transparent solution upon heating, which revealed the appearance of UCST-type phase behaviours due to the insertion of PIL (P[VBTP][Cl]) segment. The cloud point of UCST transitions in these copolymers were tunable with respect to various parameters such as content of ionic segment (copolymer composition) as well as concentrations of added halide anions. On the other hand, P[VBTP][Cl]-ran-PNIPAM copolymers showed a composition dependent dual thermo- and ion-responsive phase behaviour. The copolymers with low ionic PIL contents showed only inherent LCST behaviour of PNIPAM with tunable cloud points by the addition of varying amount of Cl^- anion. However, the copolymer with moderately high ionic PIL content exhibited both LCST-type behaviour, inherent to PNIPAM segment as well as UCST-type behaviour arising from PIL (P[VBTP][Cl]) segment in the presence of halide anion. Overall, a large variety of dual ion- and thermo-responsive copolymers with tunable cloud point and thermosensitivity were developed by introducing the PIL segment with easily available and cheaper conventional polymer segments, which opens up the

possibility of making varieties of new smart materials towards sensor, drug delivery and other useful applications.

An ionic liquid monomer [VBTP][Cl] has been copolymerized into a series of ionic-nonionic type random copolymers (namely P[VBTP][Cl]-*ran*-PMMA) comprising of ionic PIL, P[VBTP][Cl] segment and non-ionic PMMA segments by using both free radical polymerization as well as reversible addition-fragmentation chain-transfer (RAFT) polymerization methods. The influence of copolymer compositions, counter anions (Cl^- and $TFSI^-$) and molecular weight as well as physical mixing of copolymer segments on ion transport and relaxation were investigated using broadband dielectric spectroscopy followed by analyzing the data using several theoretical models. The free ion diffusivity and ion number density of these random copolymers were obtained by analyzing the contribution of electrode polarization. The temperature dependence of ionic conductivity, relaxation time and ion diffusivity exhibited Vogel-Tammann-Fulcher behavior in these copolymers indicating ion transport controlled by segmental motion of polymer chains. With increasing ionic content of PIL, the ionic conductivity increased in the random copolymers. P[VBTP][Cl]$_{80}$-*ran*-PMMA$_{20}$ copolymer showed the ionic conductivity of 1.95×10^{-7} S cm^{-1} while the neat P[VBTP][Cl] exhibited the high ionic conductivity of 1.96×10^{-6} S cm^{-1} at room temperature. In spite of low ionic conductivity, the applicability of PIL copolymers as energy storage materials is higher because of their less moisture sensitivity due to incorporation of hydrophobic PMMA segment. The ionic conductivity decreased due to the introduction of larger counter anion $TFSI^-$ in the place of Cl^- ion in copolymer. Ionic conductivity increased with decreasing molecular weight. The random PIL copolymers showed a better thermal stability and a faster ion diffusion compared to physically mixing of two homopolymers. In comparison with other reported systems, these PIL copolymers with good

thermal stability, less moisture sensitivity and good ionic conductivity open new opportunities for making advanced materials for energy storage applications.

A series of phosphonium and imidazolium ionic liquids (ILs) with high water-solubility have been synthesized and those have been utilized as efficient photoinitiators (PIs) for the polymerization of vinyl monomers such as N-isopropylacrylamide (NIPAM) and 2-(dimethylamino)ethyl methacrylate (DMAEMA) upon UV irradiation (λ_{max} = 310 nm) in aqueous medium at ambient temperature and pressure. The photopolymerization proceeds through a free radical pathway which has been established by EPR and ^{1}H-NMR spectroscopy, MALDI-TOF-MS, SEC analysis, and other control experiments. The kinetic study demonstrates that this photopolymerization is fast enough to produce high-molecular-weight polymers with ~70% yield even after 30 mins of UV irradiation. Control experiments showed that these IL-based PIs have high water solubility and capability of producing high-molecular-weight polymers compared to other commercially available aqueous PIs. Additionally, poly(NIPAM) and poly(DMAEMA) are grafted from the photoactive pendent IL moiety of the poly(ionic liquid), poly(triphenyl-4-vinylbenzylphosphonium chloride) (P[VBTP][Cl]) backbone by the grafting-from copolymerization. The presence of either poly(NIPAM) or poly(DMAEMA) graft segment induced thermoresponsiveness to their P[VBTP][Cl]-based copolymers.

Two different types of cross-linkable ionic liquid monomers (ILMs) have been successfully synthesized and utilized for the fabrication of acrylamide and 2-hydroxyethyl methacrylate-based hydrogels. The structures of the hydrogels were characterized by different techniques including FTIR and FESEM analyses. Thermal stabilities of the hydrogels were investigated by TGA and DTG analyses. Swelling performance and diffusion mechanism of water within the hydrogels were investigated and pseudo Fickian mechanism was observed to be operated

during transportation of water molecules into the hydrogel network. The introduction of ionic liquid into the hydrogel matrix as cross-linkages resulted in the incorporation of cationic binding sites which further utilized to remove hazardous anionic dyes from water through electrostatic interaction. The dye adsorption abilities of these hydrogels were investigated using Eosin B and Alizarin Red S as model dyes. The dye adsorption data of representative hydrogels were fitted with three kinetic models: pseudo first-order, pseudo-second-order and Elovich kinetic models where pseudo second-order kinetic model gave the best fitting result indicating chemisorption to be the rate controlling step. Further to investigate the dye adsorption mechanism, intra-particle diffusion model was used which showed multi-linearity behaviour confirming that the adsorption occurred through different steps. It was observed that the intercepts of the intra-particle diffusion plots did not pass through origin indicating intra-particle diffusion was not only the rate controlling step. Further fitting the experimental data to Boyd kinetic model showed straight lines which did not pass through the origin, meaning that boundary layer diffusion was involved in the adsorption process and the adsorption system was not solely controlled by intra-particle diffusion. Therefore, neither intra-particle diffusion nor liquid film diffusion was the sole rate-determining step. This indicated that both liquid film diffusion and intra-particle diffusion jointly controlled the removal of anionic dyes from aqueous solution by the macroporous cationic hydrogels.

List of Publications

1. **"Coulomb Interaction-Driven UCST in Poly(ionic liquid) Random Copolymers."**

   Palash Banerjee, Somdeb Jana and Tarun K. Mandal*, *Eur. Polym. J.,* **2020,** *133*, 109747.

2. **"Recent Developments in Stimuli-Responsive Poly(ionic liquid)s."**

   Palash Banerjee[†], Md. Anas[†], Somdeb Jana and Tarun K. Mandal*, *J. Polym. Res.*, **2020,** *27* (7), 1-23. ([†]Equal contributions)

3. **"Ion Transport and Relaxation in Phosphonium Poly(ionic liquid) Homo-and Co-polymers."**

   Palash Banerjee, Pulak Pal, Aswini Ghosh and Tarun K. Mandal*, *J. Polym. Sci.*, **2021,** *59 (14)*, 1556-1570.

4. **"Ionic Liquid-Based Unconventional Photoinitiators for Aqueous Polymerization."**

   Palash Banerjee, Mahuya kar, Priyanka Dinda and Tarun K. Mandal*, *Eur. Polym. J.*, **2022,** *162*, 110870.

5. **"Ionic Liquid Cross-linked Acrylamide and Acrylate-Based Cationic Hydrogels: Adsorption Kinetics and Mechanism for Anionic Dye Removal from Aqueous Solution."**

   Palash Banerjee, Priyanka Dinda, Mahuya Kar and Tarun K. Mandal* (Manuscript under preparation)

6. **"From Polymerizable Ionic Liquids to Poly(ionic liquid)s: Structure-Dependent Thermal, Crystalline, Conductivity, and Solution Thermoresponsive Behaviours."**

   Yajnaseni Biswas, **Palash Banerjee** and Tarun K. Mandal*, *Macromolecules*, **2019,** *52(3)*, 945–958.

7. **"Amphiphilic Perylene Bisimide-Polymer Conjugates by Cysteine-Based Orthogonal Strategy: Vesicular Aggregation, DNA Binding and Cell Imaging**."

   Mahuya Kar, Md. Anas[†], **Palash Banerjee**[†]**,** Arpana Singh, Prasenjit Sen and Tarun K. Mandal*, *ACS Appl. Polym. Mater.*, **2022**, *4 (5),* 3697-3710.

   ([†]Equal contributions)

8. **"Dual Thermoresponsive Boc-Lysine-Based Acryl Polymer: RAFT Kinetics and Anti-Protein-Fouling of Its Zwitterionic Form."**

   Priyanka Dinda, Md. Anas, **Palash Banerjee** and Tarun K. Mandal*, *Macromolecules,* **2022**, *55* (*10)*, 4011–4024.